Vol. 60 JULY, 1956 No. 7

THE JOURNAL OF PHYSICAL CHEMISTRY

(Registered in U. S. Patent Office)

THE JOURNAL OF PHYSICAL CHEMISTRY

(Registered in U. S. Patent Office)

Published monthly by the American Chemical Society at 20th and Northampton Sts., Easton, Pa.

Entered as second-class matter at the Post Office at Easton, Pennsylvania

The *Journal of Physical Chemistry* is devoted to the publication of selected symposia in the broad field of physical chemistry and to other contributed papers.

Manuscripts originating in the British Isles, Europe and Africa should be sent to F. C. Tompkins, The Faraday Society, 6 Gray's Inn Square, London W. C. 1, England.

Manuscripts originating elsewhere should be sent to W. Albert Noyes, Jr., Department of Chemistry, University of Rochester, Rochester 20, N. Y.

Correspondence regarding accepted copy, proofs and reprints should be directed to Assistant Editor, Allen D. Bliss, Department of Chemistry, Simmons College, 300 The Fenway, Boston 15, Mass.

Business Office: Alden H. Emery, Executive Secretary, American Chemical Society, 1155 Sixteenth St., N. W., Washington 6, D. C.

Advertising Office: Reinhold Publishing Corporation, 430 Park Avenue, New York 22, N. Y.

Articles must be submitted in duplicate, typed and double spaced. They should have at the beginning a brief Abstract, in no case exceeding 300 words. Original drawings should accompany the manuscript. Lettering at the sides of graphs (black on white or blue) may be pencilled in and will be typeset. Figures and tables should be held to a minimum consistent with adequate presentation of information. Photographs will not be printed on glossy paper except by special arrangement. All footnotes and references to the literature should be numbered consecutively and placed in the manuscript at the proper places. Initials of authors referred to in citations should be given. Nomenclature should conform to that used in *Chemical Abstracts*, mathematical characters marked for italic, Greek letters carefully made or annotated, and subscripts and superscripts clearly shown. Articles should be written as briefly as possible consistent with clarity and should avoid historical background unnecessary for specialists.

Notes describe fragmentary or less complete studies but do not otherwise differ fundamentally from articles. They are subjected to the same editorial appraisal as are Articles. In their preparation particular attention should be paid to brevity and conciseness.

Communications to the Editor are designed to afford prompt preliminary publication of observations or discoveries whose value to science is so great that immediate publication is imperative. The appearance of related work from other laboratories is in itself not considered sufficient justification for the publication of a Communication, which must in addition meet special requirements of timeliness and significance. Their total length may in no case exceed 500 words or their equivalent. They differ from Articles and Notes in that their subject matter may be republished.

Symposium papers should be sent in all cases to Secretaries of Divisions sponsoring the symposium, who will be responsible for their transmittal to the Editor. The Secretary of the Division by agreement with the Editor will specify a time after which symposium papers cannot be accepted. The Editor reserves the right to refuse to publish symposium articles, for valid scientific reasons. Each symposium paper may not exceed four printed pages (about sixteen double spaced typewritten pages) in length except by prior arrangement with the Editor.

Remittances and orders for subscriptions and for single copies, notices of changes of address and new professional connections, and claims for missing numbers should be sent to the American Chemical Society, 1155 Sixteenth St., N. W., Washington 6, D. C. Changes of address for the *Journal of Physical Chemistry* must be received on or before the 30th of the preceding month.

Claims for missing numbers will not be allowed (1) if received more than sixty days from date of issue (because of delivery hazards, no claims can be honored from subscribers in Central Europe, Asia, or Pacific Islands other than Hawaii), (2) if loss was due to failure of notice of change of address to be received before the date specified in the preceding paragraph, or (3) if the reason for the claim is "missing from files."

Subscription Rates (1956): members of American Chemical Society, $8.00 for 1 year; to non-members, $16.00 for 1 year. Postage free to countries in the Pan American Union; Canada, $0.40; all other countries, $1.20. $12.50 per volume, foreign postage $1.20, Canadian postage $0.40; special rates for A.C.S. members supplied on request. Single copies, current volume, $1.35; foreign postage, $0.15; Canadian postage $0.05. Back issue rates (starting with Vol. 56): $15.00 per volume, foreign postage $1.20, Canadian, $0.40; $1.50 per issue, foreign postage $0.15, Canadian postage $0.05.

The American Chemical Society and the Editors of the *Journal of Physical Chemistry* assume no responsibility for the statements and opinions advanced by contributors to This Journal.

The American Chemical Society also publishes *Journal of the American Chemical Society, Chemical Abstracts, Industrial and Engineering Chemistry, Chemical and Engineering News-Analytical Chemistry, Journal of Agricultural and Food Chemistry* and *Journal of Organic Chemistry*. Rates on request.

THE JOURNAL OF PHYSICAL CHEMISTRY

(Registered in U. S. Patent Office) (© Copyright, 1956, by the American Chemical Society)

VOLUME 60 JULY 23, 1956 NUMBER 7

THE ELECTRICAL CONDUCTIVITY CHANGE CAUSED BY THE CHEMISORPTION OF HYDROGEN ON ZnO, $ZnO \cdot Cr_2O_3$ AND $ZnO \cdot MoO_3$

BY YUTAKA KUBOKAWA AND OSAMU TOYAMA

Department of Applied Chemistry, Naniwa University, Sakai, Japan

Received February 9, 1956

The electrical conductivity change caused by the chemisorption of hydrogen and the rate of chemisorption have been measured with ZnO (not sintered), ZnO (sintered), ZnO (evaporated), ZnO + 1 mole % Al_2O_3, ZnO + 1 mole % Li_2O, $ZnO \cdot Cr_2O_3$ and $ZnO \cdot MoO_3$. In all cases examined, the chemisorption of hydrogen caused an increase in conductivity which was reversible. Chemisorption rate curves show in most cases two types of chemisorption, one predominating at high temperatures and the other at low temperatures. It is concluded from comparison with the conductivity curves that the chemisorption of high temperature type is solely responsible for the observed increase in conductivity. The analysis of the conductivity curves gives about 25 kcal./mole as the activation energy of chemisorption of this type, nearly constant for all adsorbents.

Introduction

Taylor and his co-workers found in their earlier work[1] two types of chemisorption of hydrogen on zinc oxide which, lately, they have confirmed by observing the desorption–readsorption phenomena[2] at varied temperatures. Nevertheless, the natures of these two types of chemisorption are not yet clear. The present study was undertaken to obtain any clue to the problem which might be found by measuring the electrical conductivity change of the adsorbent caused by chemisorption; the approach along this line, *e.g.*, in the work by Garner, *et al.*,[3] on copper oxide, appeared to be promising. The rate of chemisorption of hydrogen, as well as the electrical conductivity change by chemisorption, has been measured on zinc oxide, zinc oxide–chromic oxide, zinc oxide–molybdenum oxide and zinc oxide containing lithium and aluminum oxides which are known to vary the electrical conductivity of zinc oxide. This paper presents the summarized results. Detailed accounts of the work will be given elsewhere.[4]

Experimental

Materials. Zinc Oxide.—Zinc oxalate was precipitated from the solutions of ammonium oxalate and zinc nitrate. The precipitate was washed, filtered and dried at 110°, converted to the oxide by heating in air at 400° and sintered at 520° for 5 hours.

Zinc Oxide (Sintered).—Pure ZnO described above (before sintering at 520°) was sintered at 900° for 4 hours.

Zinc Oxide (Evaporated).—Zinc was evaporated on a glass plate and oxidized as described by E. Mollwo.[5]

ZnO + 1 mole % Al_2O_3 and ZnO + 1 mole % Li_2O.—A solution containing a desired amount of aluminum or lithium nitrate was impregnated with pure zinc oxide described above (before sintering at 520°), dried at 110° and sintered at 530° for 5 hours.

$ZnO–Cr_2O_3$.—This was prepared from zinc nitrate and ammonium chromate by the method described by Taylor and Strother.[1]

$ZnO–MoO_3$.—The preparation from ammonium paramolybdate and zinc nitrate was the same as that described by Taylor and Ogden,[6] except that zinc paramolybdate was decomposed in air at 150–200° in this study.

Gases.—A 30% solution of potassium hydroxide was electrolyzed to obtain hydrogen, which was purified by passing through palladium asbestos and phosphorus pentoxide. Nitrogen was prepared by the thermal decomposition of sodium azide, and purified by passing through phosphorus pentoxide. Pure helium was obtained from commercial sources, and was used without further purification.

Procedures.—Each specimen of the adsorbent for electrical conductivity measurement was, exclusive of evaporated film, shaped by compression into a cylindrical form 10 mm. long and 5 mm. in diameter. The use of too strong a pressure in shaping was avoided in order to prevent the adsorbent conditions from being very different from those in chemisorption rate measurements; the apparent density of the specimens used was of the order of 20–30% of the bulk. The specimen was held between two platinum electrodes

(1) H. S. Taylor and D. V. Sickman, *J. Am. Chem. Soc.*, **54**, 602 (1932); H. S. Taylor and C. O. Strother, *ibid.*, **56**, 586 (1934).

(2) H. S. Taylor and S. C. Liang, *ibid.*, **69**, 1306 (1947).

(3) W. E. Garner, T. J. Gray and F. S. Stone, *Discs. Faraday Soc.*, **8**, 246 (1950); *Proc. Roy. Soc. (London)*, **A197**, 314 (1949).

(4) For a preliminary work carried out on zinc oxide alone, *cf.* Y. Kubokawa and O. Toyama, *Bull. Naniwa Univ.*, **A2**, 103 (1954).

(5) E. Mollwo, *Ann. Physik*, 6] **3**, 230 (1948).

(6) H. S. Taylor and G. Ogden, *Trans. Faraday Soc.*, **30**, 1178 (1934).

and put in a holder with a spring which secured the rigid contact between the specimen and the electrodes. The whole entity was placed in a glass vessel which was connected with the vacuum system and manometer. In the case of an evaporated film, the nickel evaporated only on both ends of the glass plate prior to the evaporation of zinc served as electrodes. Conductivity was measured either by means of a Wheatstone bridge or by reading the current intensity at constant voltage of direct current. Temperature rise of the specimen was avoided by keeping the current through the specimen below 10 ma. In this range Ohm's law was found to be approximately obeyed. Preceding a series of conductivity measurements on a particular specimen, alternating evacuation and exposure to hydrogen at 400° were repeated, until reproducible results were obtained.

The rate of chemisorption was investigated with an ordinary apparatus of constant volume. Except in the case of ZnO-MoO_3, pressure differences were read with a cathetometer to ± 0.02 mm. Hg, corresponding to the accuracy of the amount adsorbed, ± 0.01 cc. The adsorbents were subjected to a pretreatment similar to that in the above-mentioned conductivity measurements. Dead space of the adsorption apparatus was measured either with nitrogen or helium in the usual manner. In both conductivity and chemisorption rate measurements the whole system was evacuated at 420° for 3 hours between each run. An oil-bath was used for temperatures up to 200° and an electric furnace for higher temperatures, the constancy of temperature being ± 1°. Surface area of the adsorbent was determined by the B.E.T. method using nitrogen as an adsorbate.

Results and Discussion

For all the adsorbents examined in this study the conductivity change on the admission of hydrogen was reversible; by evacuating the vessel at 420° after each run, the conductivity was always brought back nearly to the original value. This indicates that the observed changes in conductivity were not due to the reduction of oxides by hydrogen but to the chemisorption of hydrogen on these adsorbents. The results of conductivity measurements are shown in Figs. 1–4. The conductivity change was insignificant below a specified temperature,

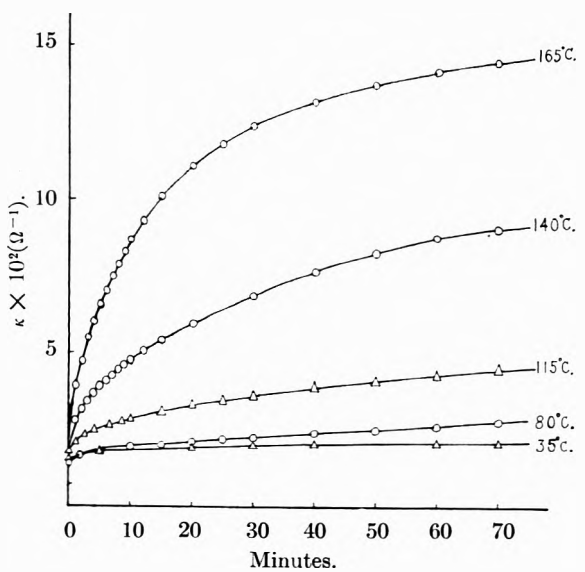

Fig. 1.—Conductivity–time curves for ZnO; pressure, 32–30 mm.

e.g., 80° for zinc oxide and 110° for zinc oxide (sintered), while at higher temperatures the conductivity increased steadily for all the adsorbents with a rate increasing with temperature as seen in the figures.

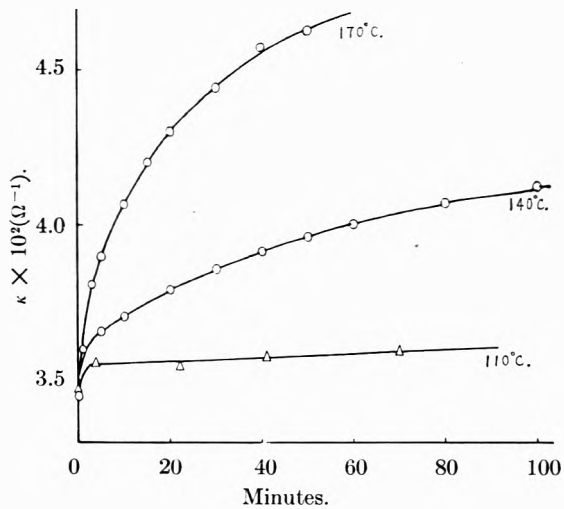

Fig. 2.—Conductivity–time curves for ZnO (sintered); pressure, 65–60 mm.

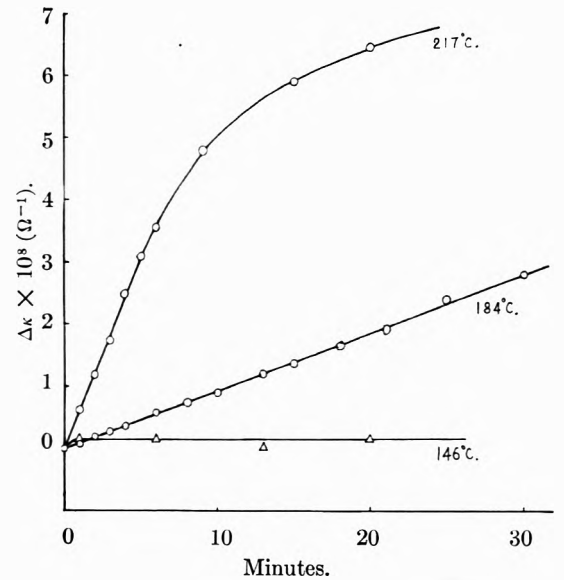

Fig. 3.—Conductivity–time curves for ZnO-Cr_2O_3; pressure, 30 mm. The initial conductivity before the admission of hydrogen was as follows: $1.0 \times 10^{-8}\ \Omega^{-1}$ at 217°, $0.4 \times 10^{-8}\ \Omega^{-1}$ at 184° and $1.5 \times 10^{-8}\ \Omega^{-1}$ at 146°. The data at 146° refer to a sample of different treatment.

The rate of chemisorption was measured at various temperatures and pressures on all the adsorbents used for conductivity measurements, exclusive of zinc oxide (evaporated). Some of the results obtained are given in Figs. 5–7 to show the relation of chemisorption to conductivity change. The kinetics in detail are to be given elsewhere. On zinc oxide (sintered), as shown in Fig. 5, the rate and amount of hydrogen uptake decreased up to 110°, but increased again at higher temperatures. This is to be compared with the results of conductivity measurements on the same adsorbent given in Fig. 2, where the conductivity increase was recognized at temperatures higher than 110°. It may therefore be concluded that two different types of hydrogen chemisorption exist on zinc oxide (sintered): one with a lower heat of adsorption appearing at lower temperatures and the other with a higher

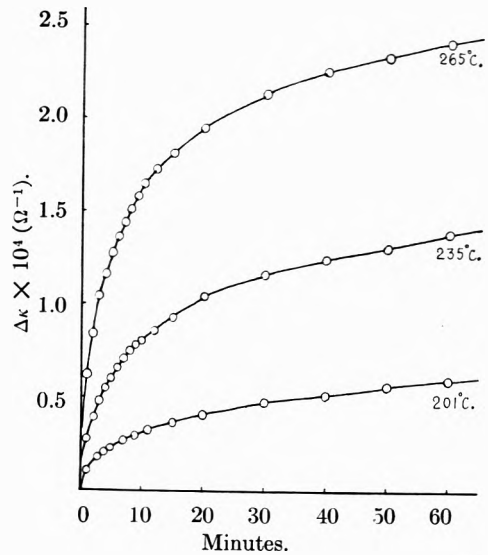

Fig. 4.—Conductivity–time curves for $ZnO{\cdot}MoO_3$; pressure, 18 mm. The initial conductiviy before the admission of hydrogen was as follows: $5.81 \times 10^{-4}\ \Omega^{-1}$ at 265°, $4.40 \times 10^{-4}\ \Omega^{-1}$ at 235° and $2.89 \times 10^{-4}\ \Omega^{-1}$ at 201°.

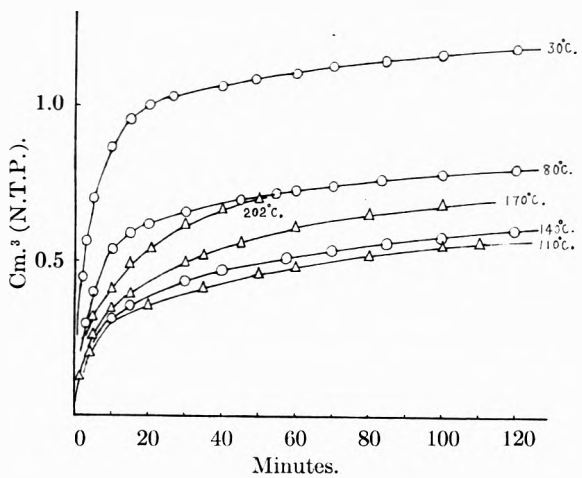

Fig. 5.—Rate of adsorption on ZnO (sintered); initial pressure, 34–30 mm.; surface area, 1.3 m.²/g.; weight of adsorbent, 60.21 g.

heat of adsorption and with a higher activation energy predominating at higher temperatures. It may be further concluded that chemisorption of the high temperature type is responsible for an increase in conductivity, while that of the low temperature type bears little effect on conductivity.

For zinc oxide not sintered the adsorption rate curves are complex and the two types of chemisorption are not clearly discriminated. It is most probable, however, that the same correlation between conductivity and high temperature chemisorption exists in this case too, for a marked increase in conductivity appeared, as shown in Fig. 1, only above 80°, whereas the chemisorption extended to a much lower temperature range, in accordance with the results previously obtained by other workers.[1]

Two types of chemisorption of hydrogen are also recognized in Fig. 6, which shows the adsorption rate curves obtained on $ZnO{\cdot}Cr_2O_3$. The ap-

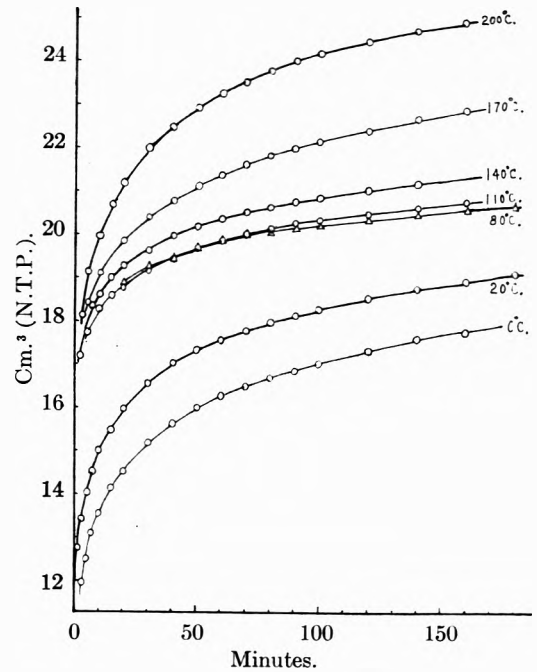

Fig. 6.—Rate of adsorption on $ZnO{\cdot}Cr_2O_3$; initial pressure, 64–60 mm.; surface area, 28 m.²/g.; weight of adsorbent, 12.37 g.

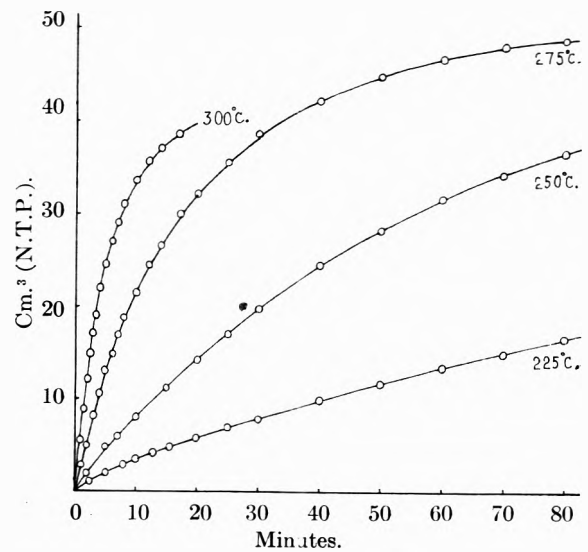

Fig. 7.—Rate of adsorption on $ZnO{\cdot}MoO_3$; initial pressure, 55 cm.; surface area, 13 m.²/g.; weight of adsorbent, 21.83 g.

parent activation energy of adsorption computed from required times for a definite amount of adsorption was about 7 kcal. in the range 0–80°, 13–16 kcal. above 140°, and was negligibly small between 80 and 110°.[7] Figure 3 shows that conductivity increased on this adsorbent at temperatures higher than 140°. Hence the correlation between the conductivity and the high temperature chemisorption here again is evident.

(7) Taylor and Strother investigated the hydrogen adsorption on the same adsorbent with considerably different results from the present work; the adsorption rate monotonously increased with temperature up to 200°, with an activation energy of 3–4 kcal. in the temperature range 80–200°. The reason for the difference is not yet clear.

On $ZnO \cdot MoO_3$ hydrogen chemisorption was recognized only at temperatures higher than 180°. Rate curves at 225–300° are shown in Fig. 7. Conductivity increase was also observed in the same temperature range as shown in Fig. 4. Hence the correspondence between the chemisorption and the conductivity change is very simple and clear in this case. Presumably, the observed chemisorption consisted almost solely of the high temperature type in this case, the contribution of the low temperature type being negligibly small. For this adsorbent, the Zeldovich equation[8] was applicable to the earlier stages of the chemisorption rate curves. The activation energy calculated from the initial rates determined by this equation was found to be 28 kcal.

Except in the last-mentioned case of $ZnO \cdot MoO_3$, the activation energy of chemisorption responsible for the conductivity change cannot be directly obtained from the chemisorption rate curves, since both types of chemisorption are overlapping in them. The activation energies may, however, be estimated from the conductivity measurements in the following manner. We consider here, for simplicity, only the initial stage of the conductivity change. Denoting the initial rate of the conductivity increase and that of the chemisorption by $(d\kappa/dt)_0$ and $(dn/dt)_0$, respectively, we have

$$(dn/dt)_0 = (dn/d\kappa)_0 \times (d\kappa/dt)_0$$

The temperature dependence of $(d\kappa/dn)_0$ may be approximately represented by

$$(d\kappa/dn)_0 = \text{const.} \exp(-E_1/RT)$$

The activation energy of chemisorption E is therefore given by

$$E = E_2 - E_1$$

where E_2 is the activation energy of the conductivity increase in the initial stage. Actually, except in the case of $ZnO \cdot Cr_2O_3$, the conductivity–time curves were well represented by the parabolic rate law $\kappa = \kappa_0 + k\sqrt{t}$ in the earlier stages and E_2 was determined from the temperature dependence of k^2 since $d\kappa/dt = {}^1/_2\, k^2/\Delta\kappa$. E_1 was approximately evaluated from the temperature dependence of the conductivity in the evacuated state. The results thus obtained are given in Table I, and show a roughly constant value of E for all adsorbents, in spite of the marked dispersion in E_1 as well as E_2.

The value of $E = 25$ kcal. for $ZnO \cdot MoO_3$ in Table I is checked by the approximate agreement with 28 kcal. obtained directly from chemisorption rate measurements on the same adsorbent. As another test on the reliability of the activation energies obtained above, some experiments were carried out at various pressures of hydrogen, with the results given in Table II, which show but little pressure effect.

TABLE I[a]

VALUES OF E_2, E_1 AND E FOR VARIOUS SPECIMENS

Adsorbent	E_2 (kcal./mole)	E_1 (kcal./mole)	E, (kcal./mole)
ZnO	26.0	1.7	24.3
ZnO (sintered)	25.8	0.1	25.7
ZnO (evaporated)	24.0	0.1	23.9
ZnO + 1 mole % Al_2O_3	24.8	0.3	24.5
ZnO + 1 mole % Li_2O	31.0	6.5	24.5
$ZnO \cdot MoO_3$	30.0	5.2	24.8

[a] The activation energy of conductivity for $ZnO \cdot Cr_2O_3$ was found to be so much influenced by hydrogen chemisorption that reliable values of E_1 and, consequently, of E were not obtained for this adsorbent.

TABLE II

VALUES OF E FOR EXPERIMENTS AT VARIOUS PRESSURE

Adsorbent	Pressure, mm.	E, (kcal./mole)
ZnO	10–12	25.0
	30–33	24.3
ZnO + 1 mole % Al_2O_3	18–20	24.4
	36–39	24.5

Further study must be made to elucidate the nature of chemisorption responsible for the conductivity change as well as the effect of added substances.

Acknowledgments.—The authors wish to express their best thanks to Prof. H. Kawamura of Osaka City University for valuable advice and discussion in this work. Thanks are also due to Mr. S. Taniguchi for his assistance in the experiments.

(8) Ya. Zeldovich, *Acta Physicochim.* (*U.R.S.S.*), **1**, No. 3/4, 449 (1934); H. A. Taylor and N. Thon, *J. Am. Chem. Soc.*, **74**, 4169 (1952).

HYDROGEN OVERPOTENTIAL AT ELECTRODEPOSITED NICKEL CATHODES IN HYDROCHLORIC ACID SOLUTIONS

BY I. A. AMMAR AND S. A. AWAD

Chemistry Department, Faculty of Science, Cairo University, Cairo, Egypt

Received August 15, 1955

Hydrogen overpotential, η, at electrodeposited Ni cathodes has been measured, under pure conditions, in aqueous HCl solutions (0.01–0.5 N). Measurements have been carried out in the current density range 10^{-6}–10^{-2} a. cm.$^{-2}$ Two Tafel line slopes of b_1 = 0.053–0.063 v. (at the low current density range) and b_2 = 0.105–0.119 v. (at the high current density range) are obtained for the linear logarithmic section of the Tafel line. At lower current densities, dissolution of Ni interferes with the overpotential results. The effect of temperature on η is studied for 0.01, 0.1 and 0.5 N aq. HCl solutions between 25–55°. The heat of activation, ΔH_0^*, at the reversible potential is calculated using two methods: (i) the method employing $\partial \log i_0/\partial(1/T)$ where i_0 is the exchange current, and (ii) the method using $(\partial\eta/\partial T)_i$. The results obtained by the first method are found to be more reproducible than those obtained by the second method. Attempts to fit the results of electrodeposited Ni within the framework of the mechanisms, previously suggested for hydrogen evolution on Ni, have not been successful. For this reason a dual electrochemical catalytic mechanism is suggested to account for the lower slope b_1. The higher slope, b_2, is accounted for by a simple mechanism.

Introduction

Recent advances in the technique of hydrogen overpotential measurements,[1] have made it possible to determine, with certainty, parameters such as slope, exchange current, stoichiometric and electron numbers[2] which are important criteria for establishing the mechanism of the cathodic hydrogen evolution reaction. Existing evidence[1] points out to the fact that the mechanism of the above reaction is dependent, among many other factors, on the nature of the electrode–solution interface and consequently on the nature of the electrode surface.

Few studies[3] have been carried out on the hydrogen overpotential of electrodeposited electrodes, whereas wire electrodes have attracted much attention. The aim of the present investigation is to report on the behavior and characteristics of the Tafel lines on electrodeposited Ni cathodes.

Previous work on Ni, in the wire form, has been carried out by Frumkin and co-workers[4] and also by Bockris and Potter.[5] The results of Frumkin and co-workers correspond to a mechanism in which the reaction is controlled over part of the electrode by a discharge step and over the remaining area by the recombination of atomic hydrogen. Bockris and Potter's results indicate a rate-determining discharge reaction followed by atomic hydrogen recombination. At high current densities a decrease in the rate of the recombination reaction, relative to that of the discharge step, is suggested by the authors.

Experimental Procedure

Electrolytic Cell.—The cell was similar to that of Bockris and Potter,[5] and a diagram of it is shown in Fig. 1. It consisted of three compartments: the anode compartment A, the cathode compartment B and the hydrogen electrode compartment C. A sintered glass disc D was inserted between A and B to minimize the diffusion of gaseous anodic products toward the cathode. The anode E was in the form of a platinum disc, with an area of 1 cm.^{2}. On top of the cathode compartment B, were fixed two barrels of hypodermic syringes F, which enabled the electrodes to be lowered into the solution in B, without allowing any leakage of atmospheric oxygen into the cell. One of the two electrodes (both joined to the pistons of the syringes) was used for preelectrolysis, while the other was used as a test electrode. A platinized platinum hydrogen reference electrode in the same solution was used as a reference. Electrical contact between the reference electrode and the polarized cathode was made through a Luggin capillary G, with an internal diameter of 1 mm. Purified hydrogen was introduced into the cell through H and was divided between the compartments A, B and C. Hydrogen was allowed to escape to the atmosphere through three bubblers I, filled with conductance water. An exit J at the bottom of the cathode compartment was used to empty the cell when required. The electrolytic solution was introduced into the cell through K. In doing so, the anode compartment was separated from the rest of the cell by closing the adjacent taps, and the compartment was completely filled with the solution. This was followed by bubbling purified hydrogen into the solution in A for three hours, to minimize the amount of dissolved oxygen,[6] before the solution was divided between A and B. The compartments B and C were previously washed and completely filled with conductance water and then emptied with a stream of purified hydrogen. The cell was made of arsenic-free glass, technically known as "Hysil." All taps and ground glass joints were of the water-sealed type. After each run, the cell was cleaned with a mixture of Analar HNO_3 and Analar H_2SO_4 followed by washing with equilibrium and conductance water.

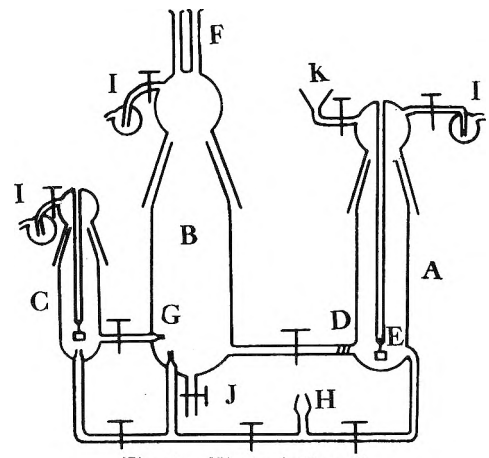

Fig. 1.—Electrolytic cell.

Purification of Hydrogen.—Cylinder hydrogen was purified from O_2 by reduced copper furnaces at 450°, from CO_2 by soda lime, from CO by "Hopcalite" (MnO_2, CuO)[7] at room temperature, and was then dried. The purification

(1) J. O'M. Bockris, *Chem. Revs.*, **43**, 525 (1948).

(2) J. O'M. Bockris and E. C. Potter, *J. Electrochem. Soc.*, **99**, 169 (1952).

(3) J. O'M. Bockris and R. Parsons, *Trans. Faraday Soc.*, **44**, 860 (1948); W. Senett and C. Hiskey, *J. Am. Chem. Soc.*, **74**, 3754 (1952).

(4) P. Lukovzew, S. Lewina and A. Frumkin, *Acta Physicochim. U.R.S.S.*, **11**, 21 (1939).

(5) J. O'M. Bockris and E. C. Potter, *J. Chem. Phys.*, **20**, 614 1952).

(6) With this simple method, no oxygen depolarization was detected in the results.

(7) G. Schwab and G. Drikos, *Z. physik. Chem.*, **185A**, 405 (1940).

apparatus was made of "Hysil" glass. Connections with the cylinder were made with a polythene tube. A movable glass bridge was used to connect the purification apparatus with the cell.

Electrode Preparation.—Electrodeposition of Ni was carried out using the method of Fresenius and Bergmann.[8] The plating bath had the following composition: 30 g. of $NiSO_4$, 10 g. of $(NH_4)_2SO_4$, 150 cc. of conductance H_2O and 100 cc. of concd. NH_4OH. "Analar" grade reagents were used. Electrodeposition was carried out, at a current density of 1 ma. cm.$^{-2}$, on a platinum substrate sealed to glass. The apparent surface area of the electrode was 0.8 cm.^{2}. The electrode was thoroughly washed with equilibrium water, followed by conductance water, and was then immediately introduced into the cell. The pre-electrolysis electrode as well as the test electrode were simultaneously prepared and cleaned in the above manner.

Solution Preparation.—HCl solutions were prepared from the constant boiling acid by addition of the appropriate amounts of conductance water. The constant boiling acid was prepared by a three-stage distillation of a mixture of Analar grade HCl and conductance water in an all glass (Hysil) apparatus. Only the middle fraction of the third stage distillate was used for the solution preparation. The distillation apparatus was cleaned with a mixture of Analar HNO_3 and Analar H_2SO_4, followed by washing with equilibrium and conductance water and was finally steamed. All conductance water used had a specific conductivity of 9×10^{-7} ohm^{-1} cm.$^{-1}$.

Pre-electrolysis.—For the electrolytic purification[9] of the solution a pre-electrolysis electrode of the same material as the test electrode was used. The adequate conditions, current density and time, of pre-electrolysis were determined by trial and error. Sufficient pre-electrolysis was attained when further increase of the extent of pre-electrolysis did not cause more than ±10 mv. change in the overpotential at any current density between 10^{-6} and 10^{-2} a.cm.$^{-2}$ on electrodeposited Ni. Pre-electrolysis was performed at 10^{-2} a.cm.$^{-2}$ for about 20 hours. With these conditions, reproducible results (within ±10 mv.) were obtained in all concentrations studied.

Measurements.—After each run, the cell was cleaned as stated above. The electrodes were fixed in their position in the cell. The cell was completely filled with conductance water and was emptied with a stream of purified hydrogen. The HCl solution was introduced into the compartment A (Fig. 1) as indicated above. After dividing the solution between the anode and the cathode compartments, the pre-electrolysis electrode was lowered into the solution in the cathode compartment, with a p.d. corresponding to a current density of 10^{-2} a.cm.$^{-2}$ imposed on it. At the end of the pre-electrolytic period, the pre-electrolysis electrode was drawn out of the solution with the current still flowing. Part of the pre-electrolyzed solution from B was pushed with a stream of hydrogen into the compartment C. Hydrogen was left to bubble over the platinized platinum electrode for about 20 minutes. The test Ni electrode, with a p.d. corresponding to a current density of *ca.* 10^{-2} a.cm.$^{-2}$ imposed on it, was then lowered into the solution in B. The electrode was adjusted to touch the tip of the Luggin capillary G, and the Tafel line was rapidly traced down to 10^{-6} a.cm.$^{-2}$.

The direct method of measurements was used. The current was measured with a multirange micro-milliammeter and the potential with a valve potentiometer-millivoltmeter. The temperature was kept constant with the help of an air thermostat. The current density was calculated using the apparent surface area.

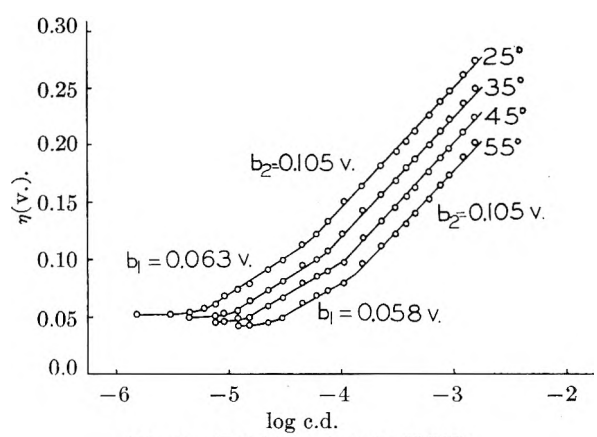

Fig. 2.—Tafel lines in 0.01 *N* HCl.

Results

For each concentration and temperature studied six Tafel lines (on six separate electrodes and in six runs) are measured and the mean line is computed. Tafel lines are reproducible within a maximum limit of ±10 mv., at any current density between 10^{-2} and 10^{-6} a.cm.$^{-2}$ Figures 2, 3 and 4 show the dependence of the mean Tafel lines on

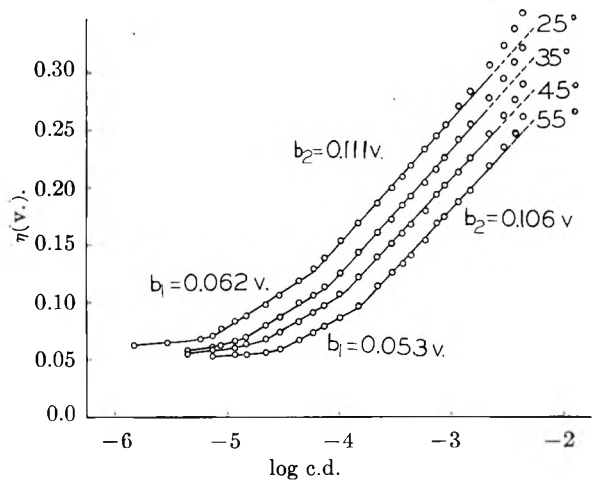

Fig. 3.—Tafel lines in 0.10 *N* HCl.

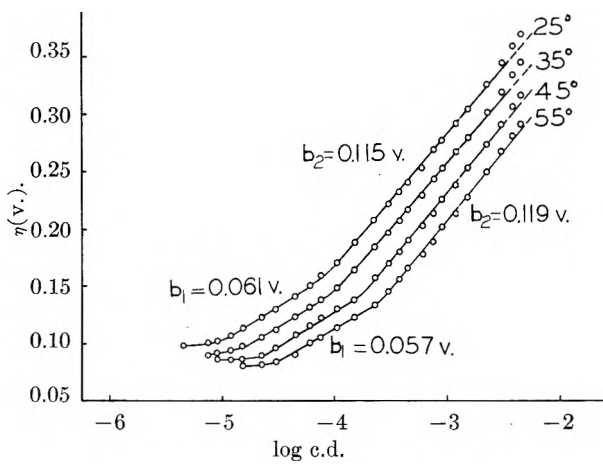

Fig. 4.—Tafel lines in 0.50 *N* HCl.

temperature, in 0.01, 0.10 and 0.50 *N* aq. HCl solutions, respectively. It is clear from these figures that Tafel lines on electrodeposited Ni exhibit two slopes in the linear logarithmic region. At the lowest current density range, the Tafel lines become parallel to the log c.d. axis. At the highest current density range, some lines exhibit a bend-up.

The slopes and exchange currents for the linear logarithmic sections of the mean Tafel lines are calculated by the least square method. The lines

(8) H. Fresenius and F. Bergmann, *Z. Anal. Chem.*, **19**, 314 (1880).

(9) A. Azzam, J. O'M. Bockris, B. Conway and H. Rosenberg, *Trans. Faraday Soc.*, **46**, 918 (1950).

TABLE I

Concn., N	t (°C.)	$(i_0)_1$	b_1[a]	α_1[b]	$(i_0)_2$	b_2[a]	α_2[b]
0.01	25	7.9×10^{-7}	63	0.94	4.0×10^{-6}	105	0.56
	35	1.3×10^{-6}	60	1.02	7.2×10^{-6}	106	.58
	45	2.1×10^{-6}	59	1.07	1.3×10^{-5}	107	.59
	55	3.6×10^{-6}	58	1.12	2.0×10^{-5}	105	.62
0.10	25	5.2×10^{-7}	62	0.95	4.5×10^{-6}	111	0.53
	35	1.0×10^{-6}	60	1.02	7.7×10^{-6}	110	.55
	45	1.5×10^{-6}	57	1.11	1.1×10^{-5}	106	.59
	55	2.3×10^{-6}	53	1.23	2.0×10^{-5}	106	.61
0.50	25	2.1×10^{-7}	61	0.97	3.3×10^{-6}	115	0.51
	35	3.6×10^{-7}	59	1.03	5.2×10^{-6}	114	.54
	45	7.7×10^{-7}	61	1.03	1.1×10^{-5}	118	.53
	55	1.0×10^{-6}	57	1.14	1.8×10^{-5}	119	.55

[a] Values are recorded to the nearest millivolt. Values are recorded to the nearest second decimal figure.

shown in Figs. 2, 3 and 4 are plotted accordingly. In Table I, the values of b_1 (at the low current density range), b_2 (at the high current density range), the corresponding values of α (calculated according to $b = -2.303\ RT/\alpha F$) and i_0 are given for the mean Tafel lines. It is clear from this table that $(i_0)_1$, $(i_0)_2$, α_1 and α_2 numerically increase with temperature.

The heats of activation at the reversible potential, *i.e.*, $(\Delta H)^*_1$ (corresponding to the low current density range) and $(\Delta H_0^*)_2$ (corresponding to the high current density range) are calculated according to[5]

$$\partial \log i_0/\partial \frac{1}{T} = -\frac{\Delta H_0^*}{2.303R} \qquad (1)$$

The values are given in Table II together with their 95% confidence limits. ΔH_0^* has been termed by Bockris[10] as "the virtual heat of activation."

TABLE II[a]

Concn., N	$(\Delta H_0^*)_1$	95% limits	$(\Delta H_0^*)_2$	95% limits
0.01	10.0	±1.0	10.4	±1.4
0.10	11.0	±1.3	9.6	±1.4
0.50	11.6	±0.4	11.6	±1.1

[a] Values of $(\Delta H_0^*)_1$ and $(\Delta H_0^*)_2$ are given to the nearest 0.1 kcal.

ΔH_0^* is also calculated from[2]

$$(\partial\eta/\partial T)_i = (\Delta H_0^* + \alpha\eta F)/\alpha F T \qquad (2)$$

For this reason two current densities of 3.0×10^{-5} a.cm.$^{-2}$ (corresponding to the lower linear segment) and of 9.0×10^{-4} a.cm.$^{-2}$ (corresponding to the higher linear segment) are chosen. $(\Delta H_0^*)_1$ (at 3.0×10^{-5} a.cm.$^{-2}$) and $(\Delta H_0^*)_2$ (at 9.0×10^{-4} a.cm.$^{-2}$) are calculated using the mean values of α, η and T in the expression on the right-hand side of equation 2. The mean values of $(\Delta H_0^*)_1$ and $(\Delta H_0^*)_2$ are given in Table III together with their 95% confidence limits. From Tables II and III, it is clear that the values of ΔH_0^* calculated using $(\partial \log i_0/\partial(1/T))$ are more reproducible than those calculated using $(\partial\eta/\partial T)_i$.

TABLE III[a]

Concn., N	t range (°C.)	(ΔH_0^*)	95% limits	$(\Delta H_0^*)_2$	95% limits
0.01	25–35	14.2	±1.6	13.2	±0.7
	35–45	13.0	±6.2	13.6	±5.2
	45–55	16.7	±3.5	13.5	±5.3
0.10	25–35	14.7	±8.8	13.2	±6.5
	35–45	11.5	±1.1	13.1	±5.1
	45–55	13.2	±2.6	15.3	±6.2
0.50	25–35	14.8	±6.9	12.5	±3.9
	35–45	14.1	±3.3	13.7	±0.7
	45–55	12.7	±6.7	12.9	±4.8

[a] Values of $(\Delta H_0^*)_1$ and $(\Delta H_0^*)_2$ are given to the nearest 0.1 kcal.

(10) J. O'M. Bockris, *Ann. Rep. Phys. Chem.*, **5**, 477 (1954).

The effect of HCl concentration on overpotential is studied by measuring Tafel lines in 0.01, 0.05, 0.10 and 0.50 N HCl solutions at 25°. The results are shown in Fig. 5.

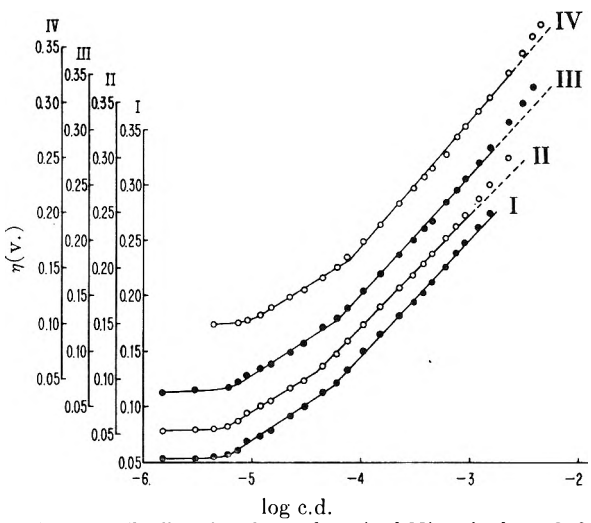

Fig. 5.—pH effect for electrodeposited Ni cathode at 25°: I, 0.01 N HCl; II, 0.05 N HCl; III, 0.10 N HCl; IV, 0.50 N HCl.

The effect of substrate on η is studied by measuring Tafel lines on Ni electrodeposited on a Ni wire. The result is shown in Fig. 6 for 0.10 N HCl at 25°. It is clear from Figs. 2, 3, 4 and 6 that the substrate has no effect on the nature of the results obtained for electrodeposited Ni.

The electron number, λ, defined as the number of electrons necessary to complete one act of the rate-determining step, is calculated using the approximate formula[2]

$$\exp.\left(\frac{\lambda\eta_s F}{RT}\right) = 0.05 \qquad (3)$$

where η_s is the overpotential at which the Tafel line departs from linearity due to the appreciable rate of

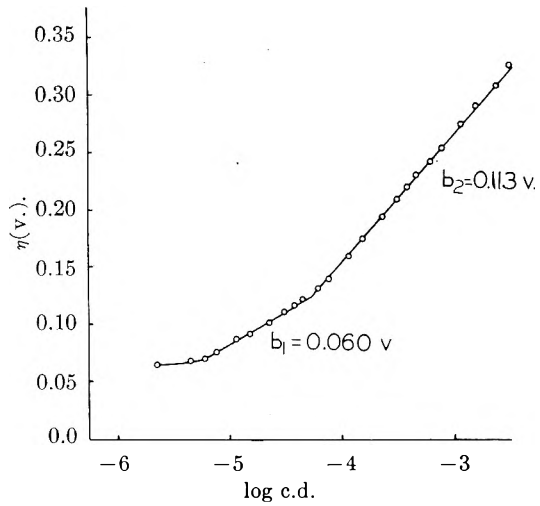

Fig. 6.—Tafel line for Ni electrodeposited on a Ni substrate.

ionization of adsorbed atomic hydrogen. Calculation of λ using the formula[2] could not be done, because η becomes constant at the lowest range of current densities examined. The mean values of λ (calculated according to equation 3) are given in Table IV, together with their 95% confidence limits.

$$\lambda = -(RT/i_0F)(\partial i/\partial \eta)_{\eta \to 0} \qquad (4)$$

TABLE IV[a]

Concn., N	t (°C.)	λ	95% limits
0.01	25	1.2	±0.2
	35	1.3	±0.2
	45	1.5	±0.2
	55	1.8	±0.3
0.05	25	1.3	±0.2
0.10	25	1.0	±0.1
	35	1.1	±0.2
	45	1.2	±0.2
	55	1.4	±0.2
0.50	25	0.7	±0.1
	35	0.8	±0.1
	45	0.9	±0.1
	55	1.0	±0.1

[a] λ is given to the nearest first decimal figure.

Discussion

The mechanism of hydrogen evolution at Ni cathodes in acid solutions has been given by Bockris and Potter[5] as a rate-determining slow discharge step followed by a catalytic desorption. This mechanism is distinguished by: (i) a Tafel line slope of 0.12 v. at 30°, (ii) a value of λ equal to unity, and (iii) by the fact that η is independent of pH in the concentration range where Stern's theory holds, *i.e.*, in dilute solutions.[11] Although most of the values of λ lie near to unity (Table IV), yet the occurrence of two slopes rules out the existence of a simple slow discharge mechanism for electrodeposited Ni. It must be noted that the values of λ given in Table IV are only approximate since equation 3 is an approximate one.

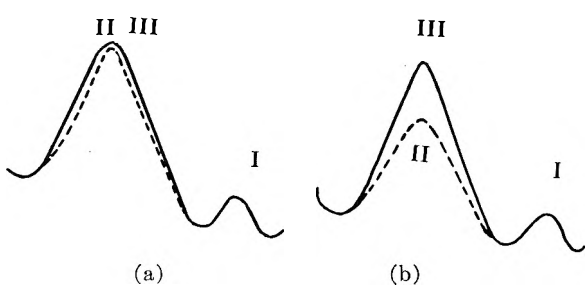

Fig. 7.—(a) Energy barriers for the dual electrochemical-catalytic mechanism; (b) energy barriers for the electrochemical mechanism.

As an attempt to explain the results on electrodeposited Ni, the following scheme may be suggested. If at the low current density range the slow discharge step is fast, and the two desorptive steps (catalytic and electrochemical) have comparable speeds, a dual electrochemical-catalytic mechanism is rate determining when the rate of the discharge step is much greater than the rates of the desorptive steps. A similar mechanism has been discussed before.[12]

The condition for this mechanism may be expressed by

$$V_1 \simeq V_2 \gg V_3 \simeq V_4 \qquad (5)$$

where V_1 is the rate of discharge, V_2 is the rate of ionization of adsorbed atomic hydrogen, V_3 is the rate of the catalytic desorption and V_4 is the rate of the electrochemical desorption. The energy barrier for the discharge step, I (Fig. 7a) corresponds to that of a reversible process, while the barriers II and III for the two desorptive steps are far removed from reversibility and of nearly equal height. For this reason, the reverse rates of the two desorptive steps are neglected in (5). The condition given by (5) can be derived easily when the expression for the steady state is taken as: $(V_1 - V_2) = (V_3 - V_5) + (V_4 - V_6)$, where V_5 and V_6 are the reverse rates for the catalytic and the electrochemical desorption steps, respectively.

The cathodic current V_c is, therefore, proportional to V_3 and to V_4, In fact V_c may be given by

$$V_c \simeq 2V_3 \simeq 2V_4 \qquad (6)$$

The rates V_3 and V_4 (taking $\alpha = 0.5$; *cf.* ref. 2) are given by

$$V_3 = k_3X^2 \qquad (7)$$

$$V_4 = k_4X(a_{H^+})_{d.l.} \exp.\left(-\frac{\Delta\phi F}{2RT}\right) \qquad (8)$$

where $\Delta\phi$ is the p.d. between the Helmholtz double layer (initial state) and the metal, X is the fraction of the surface covered with adsorbed atomic hydrogen and $(a_{H^+})_{d.l.}$ is the activity of hydroxonium ions in the double layer. From (6), (7) and (8), one gets

$$X = (k_4/k_3)(a_{H^+})_{d.l.} \exp.\left(-\frac{\Delta\phi F}{2RT}\right) \qquad (9)$$

for the fraction of the surface covered with adsorbed atomic hydrogen as a function of potential, under the condition given by (5). From (6), (7) and (9) and similarly from (6), (8) and (9), the cathodic current, i, is given by

$$i = \text{const.}\,(a_{H^+})^2_{d.l.} \exp.\left(-\frac{\Delta\phi F}{RT}\right) \qquad (10)$$

(11) S. A. Jofa, *Acta Physicochim., U.R.S.S.*, **10**, 903 (1939).

(12) A. Frumkin, P. Dolin and B. Erschler, *ibid.*, **13**, 779 (1940); B. Conway, Ph.D. Thesis, London, 1949; I. A. Ammar and S. A. Awad, *J. Electrochem. Soc.*, in press (1956).

with the result that the Tafel line slope, at constant $(a_{H^+})_{d.l.}$, becomes

$$(\partial\Delta\phi/\partial \log i) = -\frac{2.303RT}{F} = -0.06 \text{ v. at } 30°$$

Equation 9 indicates that X increases with increase of cathodic polarization till a maximum value of X very near to unity is reached, after which V_3 remains constant while V_4 increases with increase of cathodic potential (*cf.* equations 7 and 8). A condition will, therefore, be reached when $V_4 >> V_3$ (*cf.* Fig. 7b, where II represents the barrier for the electrochemical desorption), and the over-all rate is then governed by the simple electrochemical mechanism, with a Tafel line slope of 0.12 v. at 30°, at high cathodic polarization.[2] It must be noted that the increase of X may not affect the rate of the discharge step, if it is assumed that this reaction takes place on adsorption sites different from those responsible for the desorption reactions. This assumption is reconcilable with the views of Horiuti and Polanyi.[13]

The *p*H effect associated with the dual electrochemical-catalytic mechanism described above can be derived with the help of the Stern theory of the double layer. In dilute solution, under the conditions when specific adsorption of ions is absent and when the electrode potential is far from the potential of the electrocapillary maximum, Stern's theory gives for the zeta potential

$$\xi = \text{const.} + (RT/F) \ln (a_{H^+})_B \qquad (11)$$

where $(a_{H^+})_B$ is the activity of H_3O^+ ions in the bulk of solution. The activity of H_3O^+ ions in the double layer is related to $(a_{H^+})_B$ by

$$(^aH^+)_{d.l.} = (a_{H^+})_B \exp. (-\xi F/RT) \qquad (12)$$

From (10), (11), (12) and substituting for $\Delta\phi$ by $\eta + \Delta\phi_r - \xi$(*cf.* ref. 2), and for $\Delta\phi_r$ (the p.d. for the reversible potential) by $RT/F \ln (^aH^+)_B$, one gets

$$\eta = \text{const.} - (RT/F) \ln i \qquad (13)$$

Equation 13 indicates that η at constant i is independent of *p*H. Similarly the electrochemical mechanism requires that η is independent of *p*H in solutions where Stern's theory applies.[2] Figure 5 shows that this is the case in solutions below 0.5 *N* HCl.

(13) J. Horiuti and M. Polanyi, *Acta Physicochim., U.R.S.S.*, **2**, 505 (1935).

The fact that the lower parts of the Tafel lines become parallel to the log c.d. axis at potentials negative with respect to the hydrogen electrode potential is attributed to the dissolution of Ni in HCl solutions.[14] The bend-up, at high current densities, observed for a number of Tafel lines (*cf.* Figs. 3, 4 and 5) may be attributed (at least in part[5]) to a resistance overpotential effect. The plot of $\Delta\eta$ (difference between the actual Tafel line and the extrapolated line) against i results in a straight line for all cases where the bend-up is observed.

The difference between the results obtained on electrodeposited Ni and those of Bockris and Potter[5] on bulk Ni may be attributed to the difference in the extent of the fractional surface coverage, X, at the start of polarization. The method of electrode preparation employed by Bockris and Potter, *i.e.*, sealing the electrode in a glass bulb under an atmosphere of hydrogen results in a value of X near to unity at the start of polarization. Owing to the fact that the heat of adsorption of hydrogen on Ni is decreased[15] at high values of X, the desorption processes are fast. The slow discharge process taking place on a highly covered surface is, therefore, rate determining with a slope of 0.12 v. at 30°.

For electrodeposited Ni, the value of X at the start of polarization is probably much smaller than unity. The desorption processes are slow by virtue of a decrease in the concentration of the reactants as well as a high value for the heat of adsorption at low values of X. The slow discharge process is fast for a sparsely covered surface and the desorption processes are consequently rate determining. As given above the Tafel line slope b_1 = 0.053–0.063 v. cannot be explained on the basis of either a simple electrochemical or a simple catalytic desorption but may be accounted for by a dual electrochemical-catalytic mechanism.

The author's thanks are due to Prof. A. R. Tourky for the facilities provided and for his interest in the work. Thanks are also due to Prof. J. O'M. Bockris for helpful discussions.

(14) J. Kolotyrkin and A. Frumkin, *Compt. rend. Acad. Sci., U.R.S.S.*, **33**, 445 (1941).

(15) E. Rideal and B. Trapnell, *J. chim. phys.*, **47**, 126 (1950).

A CALORIMETRIC INVESTIGATION OF SOME BINARY AND TERNARY LIQUID ALLOYS RICH IN TIN

BY O. J. KLEPPA

Institute for the Study of Metals, University of Chicago, Chicago, Illinois

Received August 11, 1955

Some new measurements are reported on the heat of solution of indium, antimony, copper and gold in liquid tin. The results are compared with heat data obtained in earlier calorimetric and equilibrium studies. The enthalpy change associated with the formation of the ternary alloys Sn–A–B from the binaries Sn–A (A = Cu, Ag, Au) and Sn–B (B = Cd, In, Sb) was studied by quasi-binary mixing experiments in the tin-rich range. The results are expressed in terms of an interaction parameter characteristic of each quasi-binary system. In all cases studied this parameter was algebraically larger than a corresponding parameter for the pure binary.

Introduction

The introduction of tin solution calorimetry for determination of the heats of formation of solid alloys represents an important development in the field of alloy thermochemistry.[1] This method shows promise of providing far more accurate data on the heats of formation of solid alloys than has been possible by earlier work in this field.

Using this technique the author has initiated a study of the thermochemistry of the alloys of group 1B metals (Cu, Ag, Au; below designated by the letter A) with other group B metals. It is first planned to explore a series of binary alloys where one of the components is changed in a systematic sequence (*i.e.*, Cd, In, Sn, Sb; below designated by B). In this work use is made of a new high-temperature reaction calorimeter developed by the author.[2]

In tin solution calorimetry, as in all non-differential solution calorimetry, the desired heat of formation of the solid alloy is obtained as a difference between two independently observed quantities. One of these is the heat of solution of the alloy in liquid tin to form a ternary liquid alloy. The other is the heat of formation of the same ternary alloy from the pure elements.

A logical first step in the study of these ternary liquid alloys is the exploration of the tin-rich range of the binary systems which are of interest. Previously the author has reported the necessary data for such systems as Sn–Ag[3] and Sn–Cd.[4] In the present communication some new results will be presented on the liquid alloys in the systems Sn–Cu, Sn–Au, Sn–In and Sn–Sb. The reported work was generally carried out at 450°, although some measurements on tin–gold were also performed at 350, 270 and 242°.

If the ternary alloy which is formed when the alloy AB is dissolved in tin contains only very small concentrations of the two solutes, it may be permissible to neglect the interaction between A and B. In this case we may calculate the heat of formation of the ternary alloy Sn–A–B from data relating only to the two binaries Sn–A and Sn–B.

However, in the calorimeter used by the author it is convenient to work with solute concentrations falling in the range 2–4 atomic per cent. Under these conditions the interaction between the solutes cannot be neglected entirely, although it usually will represent only a very small percentage of the total heat of formation. To correct for this interaction a simple formula containing a single interaction parameter for each system was adopted. A series of quasi-binary mixing experiments were performed in order to determine the magnitude of these parameters.

Experimental

General.—The binary solution and mixing experiments reported in the present work did not involve any modification of the previously reported experimental procedures, and readers are referred to earlier papers[2-4] for experimental details. The metals used were generally stock metals of 99.9+% purity. Prior to their use in calorimetric experiments all metals (with the exception of gold) were remelted in graphite crucibles and cast into 1/2" rods. Suitable samples were then cut or machined from the rods. The gold, which was of 99.98% purity, was purchased from Goldsmith Bros. in the form of 2 mm. wire, and was used in this form.

In the quasi-binary mixing experiments one of the binary alloys was always prepared from weighed amounts of the pure components in the crucible of the calorimeter. The other binary alloy containing the same mole fraction of tin was melted down in an evacuated 12 mm. i.d. Pyrex ampoule, and cast into the desired hollow cylindrical shape in one end of this ampoule. After quenching in an air jet, the ampoule was broken and the 1/4" graphite core drilled out. In this manner it was ensured that the two binary alloys maintained their original composition.

Alternative Calibration of Calorimeter.—Numerically the heats of solution of gold in tin given below are 7–8 per cent. lower than those reported in other recent calorimetric investigations. It was considered desirable therefore to check the adopted electrical calibration by a "drop method."

The comparison was carried out as follows. The charging and stirring device[2] which normally connects the center of the calorimeter with the outside of the furnace insulation was replaced by a Pyrex tube of 8 mm. i.d. and about 60 cm. long. Through this tube sections of pure copper and tungsten rod of about 1/4" diameter were dropped from room temperature into the calorimeter. In these experiments the calorimeter temperature was 242 ± 0.4° as measured by a chromel–alumel thermocouple calibrated (before and after the run) at the melting point of tin (231.9°). Prior to each drop experiment the temperature of the rod section was determined to 0.1°. The heat capacities of copper and tungsten were taken from compilations published by Kelley.[5] Before or after the drop calibration a conventional electrical calibration was carried out, and the two results were compared. It was found that the drop method consistently gave about 3% higher calibrations than the electrical method. There was no significant difference between the results obtained with copper and tungsten rods.

Previously the maximum systematic error in the electrical calibration used throughout the present series of calorimetric studies was estimated to be 0.2 to 0.3%.[2] In the light of more recent experience it appears that this estimate may have been too optimistic, and that a figure closer to 1% is more likely. The most probable source of error is that a

(1) L. B. Ticknor and M. B. Bever, *J. Metals*, **4**, 941 (1952).
(2) O. J. Kleppa, THIS JOURNAL, **59**, 175 (1955).
(3) O. J. Kleppa, *Acta Met.*, **3**, 255 (1955).
(4) O. J. Kleppa, THIS JOURNAL, **59**, 354 (1955).
(5) K. K. Kelley, U. S. Bureau of Mines Bull., 476 (1949).

very small fraction ($< 0.5\%$) of the electrical current, which is measured outside the furnace system, may actually bypass the calibrating heater. If this is really the case, the electrical calibrations would tend to be high.

A realistic evaluation of the error involved in the drop calibrations is difficult, particularly because of the unknown amount of heat picked up by the sample during the drop. A very conservative estimate indicates that the uncertainty from this and other sources should be of the order of 1% and may very well be larger. Heat transferred to the sample during the fall would tend to make the calibrations high.

In conclusion it may be stated that at least a significant part of the 3% difference between the two methods of calibration may be accounted for by the assumed experimental uncertainties. It is believed that the electrical method is more reliable than the drop method.

Experiments on Binary Alloys. Comparison with Earlier Data

Tin–Indium.—The results for this system are listed in Table I and are plotted, together with those for the other systems studied, in Fig. 1. The values of $\Delta H^M/x_{In}$ are found to vary linearly with respect to x_{In}, according to the relation

$$\Delta H^M = -595x_{In} + 409x^2_{In} \text{ j./g. atom} \quad (1)$$

TABLE I

MOLAR HEATS OF MIXING FOR INDIUM–TIN ALLOYS AT 450°

Composition x_{In}	Total g. atoms	ΔH^M, joule/g. atom
0.0570	1.8345	− 32.4
.0731	1.3537	− 41.6
.1178	0.9234	− 61.8
.2269	.4555	−115
.3388	.2928	−154

Tin–Antimony.—The results of 13 experiments, in which solid antimony was dissolved in liquid tin, are listed in Table II, and are plotted in Fig. 1. The following linear relation is found between $\Delta H^M/x_{Sb}$ and x_{Sb}

$$\Delta H^M = 15.39x_{Sb} + 1.02x^2_{Sb} \text{ kj./g. atom} \quad (2)$$

TABLE II

MOLAR HEATS OF FORMATION OF LIQUID ANTIMONY–TIN ALLOYS FROM SOLID ANTIMONY AND LIQUID TIN AT 450°

Composition x_{Sb}	Total g. atoms	ΔH^M, joule/g. atom	Composition x_{Sb}	Total g. atoms	ΔH^M, joule/g. atom
0.00882	1.6647	133	0.05344	0.6856	830
.01706	0.9109	266	.07574	.4228	1199
.01736	.8637	267	.08455	.3806	1320
.01953	.8357	307	.1362	.2504	2093
.02755	.8673	420	.1485	.4589	2331
.02852	.8700	434	.2492	.2881	3864
.04080	.8560	619			

The mean deviation of the observed values of $\Delta H^M/x_{Sb}$ from this equation is 0.20 kj.

It is possible to compare these results with heat data obtained calorimetrically at 800° by Kawakami[6] and indirectly from e.m.f. cell work at 632° by Frantik and McDonald.[7] The data reported by Kawakami indicate that the limiting partial molal heat content of liquid antimony in liquid tin ($\bar{L}_{Sb}$) should be of the order of −10 kj./g. atom. Frantik and McDonald, on the other hand, calculate a value of −6.15 kj. If we adopt 19.8 kj. for the heat of fusion of antimony,[8] these earlier investigations yield +10 and +13.65 kj., respectively, for the limiting heat of solution of solid antimony in liquid tin. This should be compared with our value of +15.39 kj. Similarly, Frantik and McDonald give the values −4.2 cal. (18 joule) and −12.0 cal. (50 joule) for the relative partial molal heat content of tin ($\bar{L}_{Sn}$) at $x_{Sn} = 0.9$ and 0.8. In this concentration range we calculate the same quantity from the expression $\bar{L}_{Sn} = -1.02x^2_{Sb}$ kj.[4] For the mentioned compositions we get −10 and −41 joule, respectively. The agreement with the work of Frantik and McDonald must be considered as satisfactory.

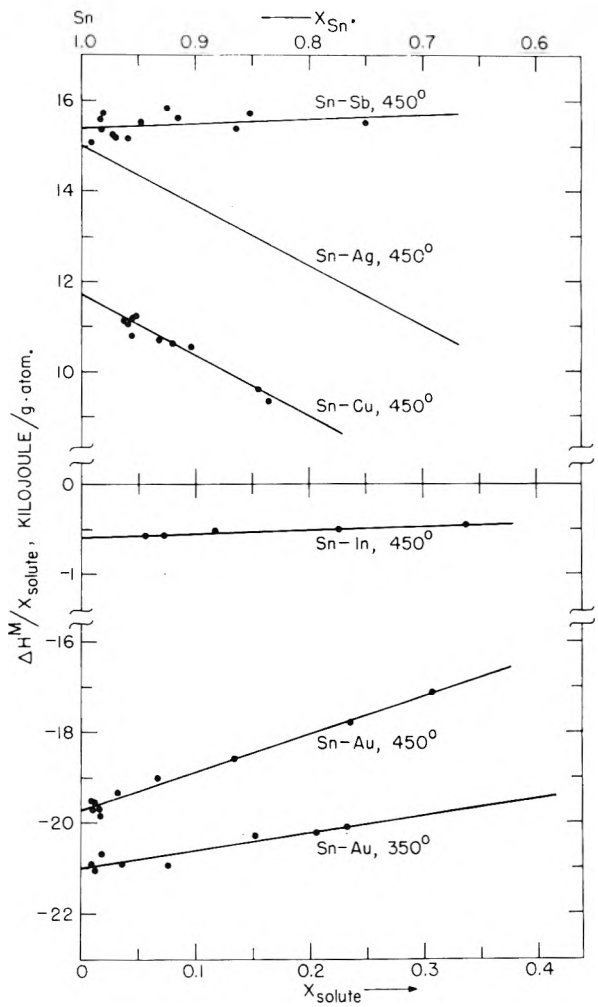

Fig. 1.—Heat of solution of indium, antimony, copper and gold in tin.

Tin–Copper.—The results for this system are given in Table III and plotted ($\Delta H^M/x_{Cu}$ *versus* x_{Cu}) in Fig. 1 along with the data for the other systems.

The following linear relation is found between $\Delta H^M/x_{Cu}$ and x_{Cu}

$$\Delta H^M = 11.68x_{Cu} - 13.66\,x^2_{Cu} \text{ kj./g. atom} \quad (3)$$

The mean deviation of experimental values of $\Delta H^M/x_{Cu}$ from this equation is 0.10 kj.

(6) M. Kawakami, *Sci. Rep. Tôhoku Imp. Univ.* (*I*), **19**, 521 (1930).

(7) R. O. Frantik and H. J. McDonald, *Trans. Electrochem. Soc.*, **88**, 243 (1945).

(8) O. Kubaschewski and E. Ll. Evans, "Metallurgical Thermochemistry," Butterworth-Springer, London, 1951.

TABLE III

MOLAR HEATS OF FORMATION OF LIQUID COPPER–TIN ALLOYS FROM SOLID COPPER AND LIQUID TIN AT 450°

Composition x_{Cu}	Total g. atoms	ΔH^M, joule/g. atom	Composition x_{Cu}	Total g. atoms	ΔH^M, joule/g. atom
0.03855	0.8527	429	0.06871	0.6473	734
.04100	.9132	454	.08051	.8787	854
.04448	.8954	480	.09745	.4190	1028
.04461	.8438	498	.1560	.3694	1495
.04813	.8311	538	.1646	.2555	1535

The present results may be compared with data obtained in earlier calorimetric work. Ticknor and Bever[1] measured the limiting heat of solution of copper in tin at 300°, and report a value of 10.75 kj., with an estimated uncertainty of about 600 joule. This compares with our value 11.68 kj. at 450°. It is estimated that the uncertainty in our figure should be of the order of 2%.

Kawakami[6] and later Körber[9] measured the heat of mixing in liquid copper–tin alloys at 1200 and at 1150°, respectively. From their data we derive the values −8 and ±0 kj. for the relative partial molal heat contents of liquid copper in liquid tin ($\bar{L}_{Cu}$). If we assume, for simplicity, that the heat of fusion of copper[8] is independent of temperature between the melting point (1083°) and 450°, we find from the present work that the corresponding value at 450° is about −1 kj.

It will be noted from Fig. 1 that the slope of the curve for the tin–copper system is very nearly the same as for the previously studied system tin–silver.[3] The negative slope, which corresponds to a negative curvature of the heat of formation in the dilute range, is expected for solutes of lower valence than the solvent, according to theoretical considerations of Friedel.[10] These theoretical aspects will be discussed further in the succeeding paper.[11]

Tin–Gold.—Pure gold was dissolved in liquid tin in 10 experiments at 450°, in 8 experiments at 350°, in 2 experiments at 270°, and in 7 experiments at 242°. The results are recorded in Table IV, and the data for 350 and 450° are plotted, along with the data for the other systems, in Fig. 1.

The following linear relations were derived for the dependence of $\Delta H^M/x_{Au}$ on x_{Au} at 450 and 350°

$$450°: \Delta H^M = -19.73x_{Au} + 8.39x^2_{Au} \text{ kj./g. atom} \quad (4a)$$

$$350°: \Delta H^M = -20.98x_{Au} + 3.70x^2_{Au} \text{ kj./g. atom} \quad (4b)$$

At both temperatures the mean deviation of the experimental values of $\Delta H^M/x_{Au}$ from these equations was 0.10 kj. At 270° the mean value of $\Delta H^M/x_{Au}$ was −22.35 ± 0.15, at 242° − 23.08 ± 0.09 kj. These results may be compared with calorimetric measurements carried out by Ticknor and Bever at 240 and 300°, by Hultgren[12] and co-workers at 243°, and also with heat data for 600° derived indirectly from e.m.f. cell measurements and previously reported by the author.[13] This comparison is presented in Fig. 2, where all available

(9) F. Körber, *Stahl und Eisen*, **56**, 1401 (1936).
(10) J. Friedel, *Advances in Phys.*, **3**, 446 (1954).
(11) O. J. Kleppa, THIS JOURNAL, **60**, 846 (1956).
(12) R. Hultgren, private communication.
(13) O. J. Kleppa, *J. Am. Chem. Soc.*, **72**, 3346 (1950).

TABLE IV

MOLAR HEATS OF FORMATION OF LIQUID GOLD–TIN ALLOYS FROM SOLID GOLD AND LIQUID TIN

Composition x_{Au}	Total g. atoms	$-\Delta H^M$, joule/g. atom
	(a) 450°	
0.00923	1.3673	180
.00994	1.4636	196
.01083	0.8615	212
.01582	.8300	311
.01641	.8019	327
.03213	.4472	621
.06685	.2323	1272
.1346	.1745	2505
.2373	.1979	4222
.3084	.07689	5279
	(b) 350°	
0.00933	0.8385	195
.01116	.8426	235
.01798	.5461	372
.03632	.3047	759
.07606	.1604	1594
.1529	.09196	3104
.2067	.07093	4180
.2339	.07945	4705
	(c) 270°	
0.01142	0.8266	253.5
.01196	.8394	269
	(d) 242°	
0.00932	0.8866	215
.00944	.8454	216.4
.01124	.8784	259
.01133	.8581	262
.01203	.8519	276.6
.01212	.8212	282
.01251	.8709	892.6

data on the limiting heat of solution of gold in tin are plotted against temperature.

It will be noted that the difference between the results of the present work and those of the other calorimetric investigations is of the order of 7–8%. This is considerably more than the uncertainty indicated by the reported experimental precisions, and suggests some systematic error, either in the present work or in the earlier work or in both. The other investigators both calibrate their calorimeters by dropping small pieces of tungsten wire into their tin baths. Therefore a series of similar calibrations were carried out in the author's apparatus. The results are compared with those obtained by the electrical method under "Experimental" above. We here recall that the drop method consistently gave about 3% higher values than the electrical method. Thus even if the drop calibrations were accepted as correct, the agreement with the other calorimetric studies on gold–tin is not entirely satisfactory.

The relatively strong dependence on temperature of the heat of solution of gold in tin is a very interesting phenomenon, which appears to have no clear-cut parallel in the case of solutions of copper and silver in tin. It should be stressed that the change of the limiting heat of solution with temperature represents a change in the strength of the

chemical bond proper, and is not due to a change in the short range order in the solution. An increased short range order is, on the other hand, probably associated with the reduction of the "curvature" of the heat of formation (*i.e.*, the slope of $\Delta H^M/x_{Au}$ *vs.* x_{Au}) as we go from 450 to 350°. In this temperature range the slope is reduced by a factor of two, but remains positive. Thus the system does not obey Friedel's rule.[10,11] However, it is worth noting that the curvature is very small when the strong interaction is taken into account.

Finally it may be pointed out that the increase in ΔH^M with temperature must be associated with a similar increase in the entropy of formation. We may here have at least a partial explanation of the large excess entropy of mixing found in liquid gold–tin alloys at 600°.[13] It should be mentioned, however, that the gold–tin system in this respect is different from certain other liquid alloy systems (*e.g.*, tin–zinc and tin–cadmium) where both the heat and the excess entropy of mixing are reduced as the temperature is increased.[4]

Quasi-binary Mixing Experiments

General.—The molar heat of formation of a ternary tin alloy may be expressed in the following way

$$\Delta H^M_{Sn-A-B} = x_A/(x_A + x_B)\,\Delta H^M_{Sn-A} + x_B/(x_A + x_B)\,\Delta H^M_{Sn-B} + \Delta H^M(x_A, x_B) \quad (5)$$

Here x_A and x_B are the mole fractions of A and B in the ternary alloy, while ΔH^M_{Sn-A} and ΔH^M_{Sn-B} are the molar heats of formation of the two binary alloys which have mole fractions of tin $x_{Sn} = 1 - x_A - x_B$. The term $\Delta H^M(x_A, x_B)$ represents the molar change in enthalpy associated with the quasi-binary mixing process, *i.e.*, when the ternary is formed from the two binaries while x_{Sn} is kept constant. This last term may conveniently be expressed by means of a single interaction parameter, $C_{AB}(x)$, thus

$$\Delta H^M(x_A, x_B) = C_{AB}(x) x_A x_B \quad (6)$$

It is well known that for higher concentrations of A and B this interaction parameter will depend both on the total concentration of A and B and on the relative amounts of A and B in the mixture. However, in moderately dilute solutions, *i.e.*, when $x_A + x_B \leq 0.2$, this dependence is expected to be fairly weak. In this range we may to a good first approximation consider C_{AB} as independent of concentration.[14] This essentially implies the assumption of nearest neighbor interaction between A, B and Sn. Other things being unchanged the number of nearest neighbor contacts or "bonds" in a random mixture is of course proportional to the product of the mole fractions of the two considered species.

For ternary solutions resulting from typical calorimetric solution experiments in the author's apparatus the product $x_A x_B$ usually falls in the range 10^{-3} to 10^{-4}. With values of C_{AB} of the order of 10 kj., the total molar heat effect of quasi-binary mixing experiments in this concentration range will be 1 to 10 joules. These heat effects are too small to be determined with precision in the apparatus. Therefore it was necessary to carry out the quasi-binary experiments in mixtures with total solute concentrations of the order of 10 to 20 atomic per cent. Even so the observed heat effects were quite small, and the values of C_{AB} may very well be in error by as much as 10%. This will be obvious from an examination of Table V where all the results obtained in quasi-binary mixing experiments are recorded.

(14) The independence of C_{AB} on composition was not checked in detail. However, for the system silver–cadmium an increase of $x_{Ag} + x_{Cd}$ from about 0.10 to about 0.34 was found to have only a moderate effect on the value of C_{AB} (see Table V).

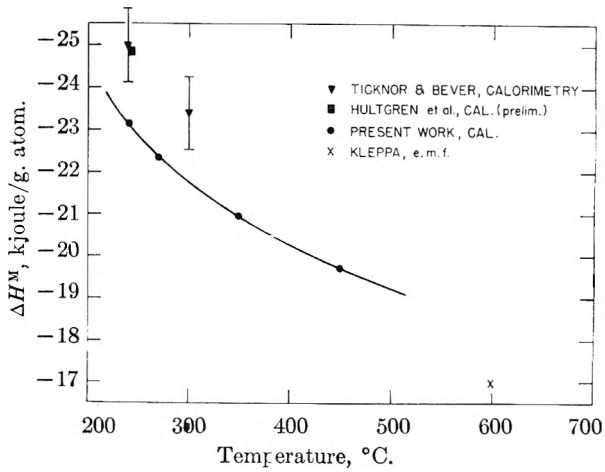

Fig. 2.—The temperature dependence of the limiting heat of solution of gold in tin.

TABLE V

QUASI-BINARY MIXING AT 450° ACCORDING TO FORMAL CHEMICAL EQUATION

$$y\ Sn_xA_{1-x}(l) + (1 - y)Sn_xB_{1-x}(l) = Sn_{xSn}A_{xA}B_{xB}(l)$$

System A–B	Final composition x_{Sn}	x_A	x_B	Total g. atoms	ΔH^M, j./g. atom	$\Delta H^M/x_Ax_B$, kj.
Cu–Cd	0.8424	0.1026	0.0550	0.371	+ 48	+ 8.6
	.8281	.1112	.0607	0.351	+ 63	+ 9.3
Ag–Cd	.8950	.0136	.0914	1.078	− 9.1	− 7.4
	.8330	.0560	1110	0.393	− 46	− 7.4
	.8330	.0717	0953	.382	− 47	− 6.9
	.6588	.2104	.1308	.422	−282	−10.2
Au–Cd	.8785	.0637	.0578	.230	−109	−29.6
	.8962	.0543	0495	.244	− 73	−27.2
Cu–In	.8354	.1123	0523	.375	+ 83	+14.1
	.8466	.0962	0572	.315	+ 73	+13.1
Ag–In	.8330	.0964	0706	.362	+ 33	+ 4.8
	.7638	.0794	1568	.381	+ 65	+ 5.2
Au–In	.8800	.0613	0587	.247	− 86	−23.9
	.8971	.0522	0507	.254	− 55	−20.8
Cu–Sb	.8300	.1032	0668	.338	+100	+14.6
	.8400	.1012	0588	.360	+ 91	+15.3
	.8250	.1073	0677	.340	+126	+17.3
Ag–Sb	.7515	.1656	0829	.374	+305	+22.2
	.8516	.0926	0558	.370	+115	+22.2
Au–Sb	.8978	.0512	0510	.249	+ 25	+ 9.6
	.8501	.0613	0886	.229	+ 48	+ 8.8

Discussion.—It is of considerable interest to compare the quasi-binary interaction parameter $(C_{AB})_{x_{Sn} \approx 1}$ with the corresponding parameter for simple binary interaction. The latter will in general be some function of composition, and we shall presently focus our attention on its value in pure liquid B, $(C_{AB})_{x_B \approx 1}$. We note that this is in fact our old acquaintance, the relative partial molal heat content of liquid A in pure liquid B. The author recently has measured the heat of solution at 450° of copper, silver and gold in liquid cadmium

and indium.[11,15] From these results the desired interaction parameters may be obtained by adopting reasonable values for the heats of fusion of copper, silver and gold. In Table VI these parameters are given along with average values of $(C_{AB})_{x_{Sn} \cong 1}$ obtained from the experimental data recorded in Table V.

TABLE VI

INTERACTION PARAMETERS IN BINARY AND TERNARY LIQUID SYSTEMS AT 450°

System A–B	$(C_{AB})_{x_{Sn}=1}$ kj.	$(C_{AB})_{x_B=1}$ kj.	$C_{x_{Sn}=1} - C_{x_B=1}$ kj.
Cu–Cd	+ 9	−12	21
Cu–In	+14	~ 0	14
Cu–Sn	− 1	− 1	..
Cu–Sb	+16	?	?
Ag–Cd	− 7	−24	17
Ag–In	+ 5	− 4	9
Ag–Sn	+ 4	+ 4	.
Ag–Sb	+22	?	?
Au–Cd	−28	−61	33
Au–In	−22	−46	24
Au–Sn	−33	−33	..
Au–Sb	+ 9	?	?

It will be noted that it is a common feature of the six systems for which full information is available that the binary interaction parameter, C_{AB}, is increased (*i.e.*, interaction weakened) when we go from pure B to nearly pure tin. We also note that the increase in C_{AB} for the cadmium systems is more pronounced than the corresponding increase for the indium systems. There is, however, no clear-cut correlation between the increase in C_{AB} and the magnitude of C_{AB} as we go from one binary system to another.

It is unfortunate that because of the high melting point of antimony there is as yet no reliable information on the heat of solution of copper, silver and gold in liquid antimony. However, a systematic survey of all interaction parameters listed in Table VI suggests that $(C_{ASb})_{x_{Sn} \cong 1}$ probably in all cases will be considerably larger than $(C_{ASb})_{x_{Sb}=1}$. If this is indeed the case, it is tempting to interpret the change in C_{AB} in terms of simple atomic size considerations. It may be postulated that for dilute solutions in any solvent metal there exists a tendency for the nearest neighbor "bonds" to assume the length characteristic of the nearest neighbor distance of that particular metal. On this model it may be argued that the bond lengths which exist, *e.g.*, in pure liquid B, will become compressed or extended (and the bond energies accordingly changed) when they are present in essentially pure liquid tin. We might expect the effect to depend in some manner on the difference in size between A, B and Sn, and to be particularly large if the bonding A–B is strong (or "stiff"). There is a certain amount of semi-quantitative support for this simple picture in the data given in Table VI.

We recall first that the sequence Cd, In, Sn, Sb is one of increasing atomic size, as measured for example by the atomic radii for coördination number 12. For any one of the reference metals, copper, silver and gold, we note that the parameter C_{ACd} is increased more than C_{AIn} in going to liquid tin. We further recall that among the metals copper, silver and gold the two latter have very similar atomic radii, while copper is significantly smaller. If we first consider the alloys formed by silver and gold, where the effect of size should be of the same order of magnitude, we find that C_{AuB} is always more increased than C_{AgB} on going from B to Sn. If we, on the other hand, look at the alloys formed by copper and silver, where the magnitude of the chemical interaction is more nearly equal, while the size effect is different, we note that C_{CuB} is somewhat more increased than is C_{AgB}.

Acknowledgments.—This work was supported in part by the Office of Naval Research through Contract No. N-6ori-02004 with the University of Chicago. The indium metal used was a gift from the Anaconda Copper Company.

(15) O. J. Kleppa, THIS JOURNAL, **60**, 858 (1956).

HEAT OF FORMATION OF SOLID AND LIQUID ALLOYS IN THE SYSTEMS SILVER–CADMIUM, SILVER–INDIUM AND SILVER–ANTIMONY AT 450°

BY O. J. KLEPPA

Institute for the Study of Metals, University of Chicago, Chicago 37, Illinois

Received August 11, 1955

The heats of formation of the liquid alloys of silver with cadmium and indium were determined calorimetrically at 450° by dissolving silver in the low-melting liquid metals. The heats of formation of the solid alloys were obtained by the tin solution technique. The new information is discussed along with data obtained earlier for the system silver–tin. The results are compared with recent theoretical calculations by Varley and by Friedel. Many of the results are in excellent agreement with theoretical predictions advanced by Friedel.

Introduction

In a recent communication the author has published new information on the integral heat of formation of the solid and liquid alloys of silver–tin as determined calorimetrically at 450°.[1] In the present paper equivalent data will be reported for the alloys of silver with cadmium, indium and antimony. A preliminary report on some of this work was given previously.[2] For alloys which are liquid at 450° the desired heat data were obtained di-

(1) O. J. Kleppa, *Acta Met.*, **3**, 255 (1955).

(2) O. J. Kleppa, *J. Am. Chem. Soc.*, **76**, 6028 (1954).

rectly by dissolving silver in the liquid metal in the calorimeter. For solid alloys the heats of formation were calculated from the observed heats of solution of the alloys in pure tin. In evaluating the results use was made of the data on dilute solutions of silver, cadmium, indium and antimony in tin quoted in the preceding paper.[3]

Experimental

The experimental procedure adopted in this study was similar to the one described previously for silver-tin.[1] However, as it was believed that the heat treatment given the alloy during the final stages of preparation might possibly have a noticeable influence on the observed heat of formation (*e.g.*, through the effect of local order), an attempt was made to check this point experimentally. A series of 11 silver-cadmium alloys of the same nominal composition ($x_{Ag} = 0.63_0$) were prepared and annealed for periods of 20 to 150 hours at temperatures from 450 to 675°. The heats of formation of these alloys all fell in the range −8.80 to −9.26 kj./g. atom with a mean of −9.05 and a mean deviation of 0.13. However, no correlation could be established between heat treatment and heat of formation. These results offer a good illustration of the ultimate experimental precision which may be achieved when a large number of calorimetric experiments is performed. Usually only two or three runs were carried out, and the mean deviation of each experiment from the average was larger. It should be stressed that the total error of the data may be somewhat larger than indicated by the precision, due in part to uncertainties in the accepted values of the heats of formation of the ternary liquid alloys and in part to a possible systematic error estimated to be of the order of about 1%.[3]

Preparation of Specimens.—Two different methods were adopted. In the first procedure hollow cylindrical samples of 10–20 g. total weight were prepared according to a method described in the previous paper.[2] Specimens of suitable weight (2–4 g.) and size were then cut from this slug.

A number of silver–cadmium alloys were also prepared in the form of 3 mm. rods of about 2 cm. length by melting the appropriate amounts of metal in evacuated Vycor tubes. In order to facilitate the homogenization of the liquid alloy, one end of the tube was enlarged to form a small bulb. After homogenization above the liquidus the alloys were cast into the cylindrical part of this ampoule, and the heat treatment was completed before the ampoule was broken. As there was essentially 100 per cent. recovery of the samples, they were not subjected to any chemical analysis.

Analysis of Metals and Alloys.—The first method of alloy preparation, while effectively preventing loss of metal, may give differences in composition (segregation) within the slugs. The analytical work (Ag as AgCl) was primarily aimed at establishing the order of magnitude of the segregation. It was generally found that the alloys were uniform in composition to 2–3 parts per thousand.

The metals were stock metals of 99.9+% purity. In the course of the present work a check was carried out of the oxygen content of the silver, which was from the same lot as the metal used for the silver–tin system. By means of vacuum fusion analysis it was established that the granules, as received, contained about 0.010% oxygen by weight. However, after the silver had been melted and cast in graphite, the oxygen content was reduced to about 0.0025%. This oxygen content is too small to cause a significant error in the calorimetric measurements.

Results

Liquid Alloys. Silver–Cadmium.—Measurements on this system are listed in Table I. The lower precision in this case is in part caused by the slowness with which solid silver dissolves in liquid cadmium, in part by the relatively high vapor pressure and reactivity of cadmium at 450°. The mean value of $\Delta H^M/x_{Ag}$ obtained from these 9 experiments is −12.8 kj. with a mean deviation of 0.65.

(3) O. J. Kleppa, THIS JOURNAL, **60**, 842 (1956).

TABLE I

MOLAR HEATS OF FORMATION OF LIQUID SILVER–CADMIUM ALLOYS FROM SOLID SILVER AND LIQUID CADMIUM AT 450°

Composition x_{Ag}	Total g. atoms	$-\Delta H^M$, j./g. atom	Composition x_{Ag}	Total g. atoms	$-\Delta H^M$, j./g. atom
0.0178	1.058	219	0.0315	0.924	379
.0214	1.109	275	.0323	1.096	430
.0241	0.809	312	.0366	1.053	496
.0295	.863	346	.0603	0.411	824
.0304	.912	420			

There are no reliable heat data in the literature on the dilute solutions of silver in cadmium. However, from vapor pressure measurements of Schneider and Schmid[4] at higher silver concentration and higher temperatures, we may estimate a value of about +4 for $\Delta H^M/x_{Ag}$. The agreement is poor, but at the same time not very significant.

Silver–Indium.—The results for this system are listed in Table II. The following linear relation holds for the dependence of $\Delta H^M/x_{Ag}$ on x_{Ag}.

$$\Delta H^M = 7.04x_{Ag} - 11.72x^2_{Ag} \text{ kj./g. atom} \quad (1)$$

The mean deviation of observed values of $\Delta H^M/x_{Ag}$ from this equation is 0.07 kj. There are, to the knowledge of the author, no data in the literature for comparison with these results.

TABLE II

MOLAR HEATS OF FORMATION OF LIQUID SILVER–INDIUM ALLOYS FROM SOLID SILVER AND LIQUID INDIUM AT 450°

Composition x_{Ag}	Total g. atoms	ΔH^M, j./g. atom
0.0555	0.7661	348
.1000	.8040	590
.1320	.4257	740
.1829	.2534	888
.2390	.4856	1028
.3278	.2789	1032

Solid Alloys. Silver–Cadmium.—A survey of the literature shows that there is poor agreement regarding certain details of the silver–cadmium equilibrium phase diagram. Thus, "Metals Handbook"[5] advances a diagram which is based primarily on micrographic studies and which in several respects differs from the diagram recommended by Owen, Rogers and Guthrie.[6] These investigators carried out a careful X-ray study of this system, and from their work one finds that the following phases should be stable at 450°

		Atomic % Cd
α	f.c.c.	0–43
β	b.c.c.	49–56
γ	compl. cub.	59–61
ϵ	c.p. hex.	66–76
L	liquid	88–100

The results obtained in the present work are recorded in Table III, and are plotted, along with the data on liquid silver–cadmium alloys, in Fig. 1.

(4) A. Schneider and H. Schmid, *Z. Elektrochem.*, **48**, 636 (1942).

(5) "Metals Handbook," American Society for Metals, Cleveland, 1948.

(6) E. A. Owen, J. Rogers and J. C. Guthrie, *J. Inst. Metals*, **65**, 457 (1939).

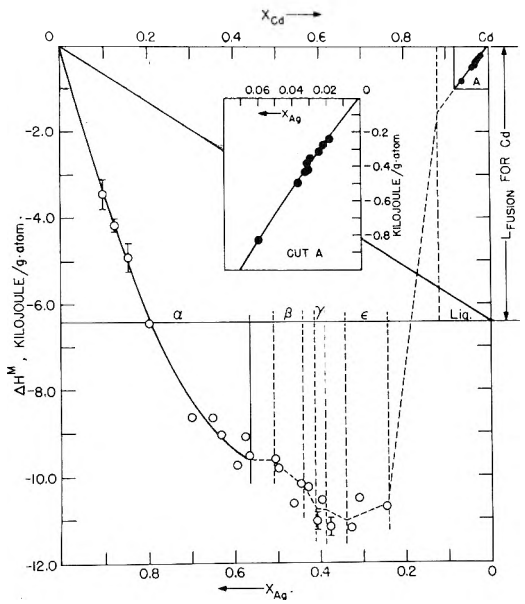

Fig. 1.—Molar heats of formation of solid and liquid silver–cadmium alloys at 450°.

Among the systems covered in the present work silver–cadmium is the only one for which a reasonably comprehensive set of heat data is reported previously. Thus Ölander[7] by means of e.m.f. cell measurements explored solid alloys with silver contents up to 67%, while Cheng and Birchenall[8] studied the vapor pressure of cadmium over three solid silver–cadmium alloys containing about 8, 23 and 34 atomic % cadmium. Very recently Hultgren[9] and co-workers have carried out a few calorimetric determinations of the heat of formation of solid silver–cadmium alloys in the α-solid solution range.

Ölander refrained from calculating integral heat data from his e.m.f. measurements because he had difficulties with getting reproducible potential ob-

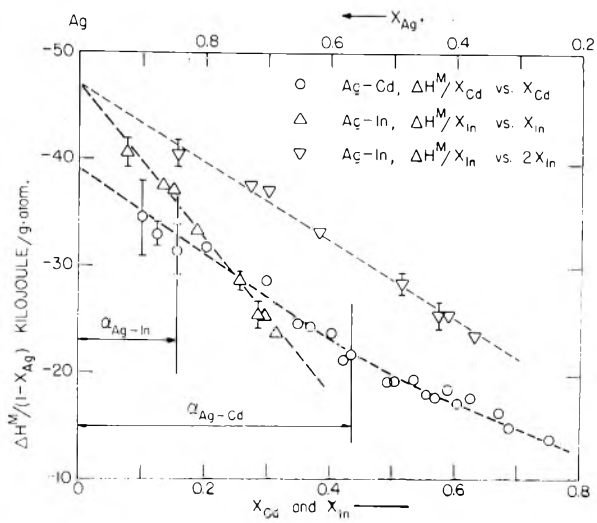

Fig. 2.—Heat of formation for solid alloys of silver–cadmium and silver–indium.

(7) A. Ölander, *Z. physik. Chem.*, **A163**, 107 (1933).
(8) C. H. Cheng and C. E. Birchenall, *J. Metals*, **1**, 420 (1949).
(9) R. Hultgren, private communication.

TABLE III

MOLAR HEATS OF FORMATION OF SILVER–CADMIUM ALLOYS FROM SOLID SILVER AND LIQUID CADMIUM AT 450°

Alloy composition x_{Ag}, phase	Alloy g. atoms	Tin + alloy, g. atoms	Obsd. joule	$-\Delta H^M$ kj./g. atom Result	$-\Delta H^M$ kj./g. atom Av.
0.90_1, α	0.02315	0.8742	391.5	3.06	
	.02295	.8493	403.4	3.74	
	.02301	.8465	389.2	3.08	
	.01798	.8322	219.3	3.85	3.43
$.87_4$, α	.02583	.8890	459.6	4.21	
	.02385	.8389	418.1	3.94	
	.03031	.9264	541.9	4.34	4.16
$.84_4$, α	.03120	.8613	548.8	4.35	
	.02983	.8498	556.5	5.40	
	.01560	.8520	287.9	4.98	4.91
$.79_7$, α	.03054	.8612	592.5	6.54	
	.03135	.8506	601.7	6.34	6.44
$.70_0$, α	.02760	.8499	573.0	8.66	
	.02846	.8842	590.1	8.63	8.65
$.65_0$, α	.01478	.8353	303.1	8.70	
	.01479	.8501[a]	296.6	8.60	8.65
$.63_0$, α	Av. of 11 experiments				9.05
$.59_4$, α	.02735	.9066	578.2	9.88	
	.02723	.8238	567.5	9.61	9.75
$.57_4$, α	.01376	.8419	279.2	9.03	
	.01438	.8661	293.1	9.12	9.08
$.56_5$, α ?	.01583	.8478	327.4	9.51	
	.01633	.8641[a]	331.6	9.57	9.54
$.50_6$, β	.03257	.8843	650.4	9.50	
	.03178	.8908	643.8	9.78	
	.02080	.8479	419.4	9.55	9.61
$.49_5$, β	.01536	.8212	314.3	9.87	
	.01858	.8526	376.6	9.79	9.83
$.46_0$, β	.01848	.8778	388.3	10.73	
	.01776	.8754	370.4	10.57	
	.01952	.8239	406.8	10.59	10.63
$.44_4$, β	.01395	.8459	285.2	10.25	
	.01500	.8609[a]	298.7	10.08	10.17
$.42_9$, β + γ	.01686	.8859	342.6	10.27	
	.01670	.9156	338.3	10.20	10.24
$.40_8$, γ	.02468	.8588	519.1	11.26	
	.03076	.8528	633.0	10.89	11.07
$.39_5$, γ	.01519	.8492	306.9	10.43	
	.01520	.8644[a]	305.2	10.66	10.55
$.37_6$, γ + ε	.01565	.8859	329.4	11.40	
	.01591	.9018[a]	322.1	10.95	11.17
$.32_8$, ε	.03223	.8425	650.7	11.14	
	.02701	.9034	549.5	11.24	11.19
$.31_0$, ε	.01483	.8312	289.3	10.42	
	.01477	.9112	291.0	10.61	10.51
$.24_5$, ε	.03039	.8635	579.4	10.65	
	.02671	.8872	512.5	10.74	10.70

[a] In these cases the alloy was dissolved in the solution formed in the preceding experiment.

servations for alloys with silver contents above 67%. Later on Weibke,[10] noting that Ölander's data showed that the partial molal heat content of cadmium appeared to be independent of composition between 33 and 44% cadmium, calculated a set of integral heat data under the assumption that this would still hold true for lower cadmium con-

(10) F. Weibke, *Z. Metallkunde*, **29**, 79 (1937).

tents. Now we note that there is still a significant curvature in the heat of formation curve between 0 and 33% cadmium (see *e.g.*, Fig. 1). Therefore it is not surprising to find that Weibke's calculations give somewhat low values: For an alloy containing about 43 atomic % cadmium Weibke gives a heat of formation of about −7.8 kj. (from the elements at 350°), while the present work indicates about −9.3 kj. (at 450°). It may here also be mentioned that the still unpublished work by Hultgren indicates a value of about −10.3 kj. at 34° (from solid silver and undercooled liquid cadmium, if we set the heat of fusion of cadmium equal to 6.4 kj.). As it is anticipated that an increase in temperature might lead to a weaker bonding between silver and cadmium, a somewhat more extreme value of ΔH^M at room temperature is expected.

The present data may also be compared directly with the partial molal heat contents reported by Ölander and by Cheng and Birchenall. In order to facilitate this comparison we have in Fig. 2 plotted our experimental values of $\Delta H^M/x_{Cd}$ *vs.* x_{Cd}. It will be noted that the data which cover all solid phases, irrespective of structure, seem to fall in the vicinity of one smooth curve, which in the α-region may be approximated by a straight line. We make use of this to obtain a simple approximate expression for the molar heat of formation of silver–cadmium alloys in the α-range

$$\Delta H^M[\text{Ag(s)} + \text{Cd(l)}, 450°] = -39x_{Cd} + 39x^2_{Cd} \text{ kjoules/g. atom} \quad (2)$$

This gives the following equation for the partial molal heat content of cadmium relative to liquid cadmium of the same temperature

$$\bar{L}_{Cd}\,(\text{Cd(l)}) = -39x^2_{Ag} \text{ kj.} \quad (3)$$

With the aid of this relation we calculate values of $\bar{L}_{Cd}$ ranging from −17.5 kj. at $x_{Ag} = 0.67$ to −12.2 kj. at $x_{Ag} = 0.56$. In same range Ölander's experimental results give a mean value of about −18 kj. Birchenall and Cheng's data allow an evaluation of $\bar{L}_{Cd}$ only for the two alloys containing 8 and 23 atomic % cadmium, and in both cases we find about −28 kj. For these compositions equation 3 gives the values −33 and −23 kj., respectively. As a whole the agreement must be considered as satisfactory.

It was hoped that the calorimetric data obtained in the present study should permit a discussion of the relative stability of the various intermetallic phases in terms of their heats of formation. However, when the difference between the heats of formation of neighboring phases is as small as in the case of silver–cadmium, such a comparison requires more precise heat data. Therefore we have in Fig. 1 given a tentative heat of formation curve only for the alloys in the range 20 to 60 atomic % silver. Better information on the heats of transformation from one phase to another may in this case be obtained from Ölander's work.[7]

Silver–Indium.—The phase diagram for this system was studied by Hellner and Laves[11] and shows that the following phases are stable at 450°

		Atomic % In
α	f.c.c.	0–15.5
γ	c.p. hex.	25–32.5
L	liquid	60–100

The results obtained for this system are given in Table IV and are plotted in Fig. 3. This figure also contains the data on liquid silver–indium alloys given in Table II. The results on solid silver–indium alloys are also found in Fig. 2, along with those for solid silver–cadmium alloys.

TABLE IV

MOLAR HEATS OF FORMATION OF SILVER–INDIUM ALLOYS FROM SOLID SILVER AND LIQUID INDIUM AT 450°

Alloy: composition x_{Ag}, phase	g. atoms	Tin + alloy, g. atoms	Obsd. joule	$-\Delta H^M$, kj./g. atom: Result	Av.
0.92_2, α	0.02871	0.8656	478 7	3.26	
	.03004	.8769	494.7	3 07	3.17
$.86_7$, α	.02062	.8498	363 3	4.95	
	.02369	.8704	419.3	5.06	5.01
$.84_8$, α	.02145	.8520	385.6	5.59	
	.02402	.8718	434.1	5.72	5.66
$.81_0$, $\alpha + \gamma$	.02483	.8242	454.0	6.53	
	.03081	.8630	549.0	6.12	
	.02374	.8877	431.0	6 37	6.34
$.74_2$, γ	.02382	.8697	444.2	7.90	
	.02286	.8718	419 5	7.59	
	.03643	.9017	636.7	6.84	
	.03029	.8616	543.6	7.27	7.40
$.71_3$, γ	.02830	.8469	498.8	7.35	
	.02866	.8932	508.0	7.45	
	.03114	.8723	545.6	7 28	7.36
$.70_4$, γ	.03117	.8806	549.5	7.53	
	.03768	.8852	663.1	7.55	7.54
$.68_4$, γ	.02718	.8898	472.3	7 53	
	.02822	.8554	489.2	7.51	7.52
$.66_4$, $\gamma + L$	.03292	.8737	557.3	7.44	
	.04111	.8788	699.6	7.60	7.52
$.46_5$, $\gamma + L$	.02754	.8708	227.9	1.75	
	.02411	.8769	197.0	1.64	1.70

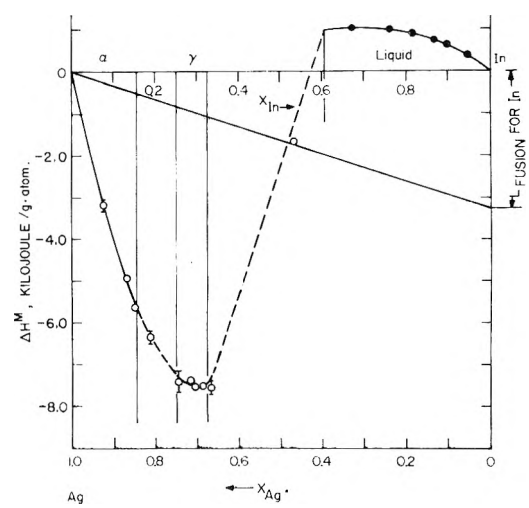

Fig. 3.—Molar heats of formation of solid and liquid silver–indium alloys at 450°.

(11) E. Hellner and F. Laves, *Z. Naturforsch.*, **A2**, 177 (1947); E. Hellner, *Z. Metallkunde*, **42**, 17 (1951).

Silver–Antimony.—The phase diagram for this system was studied by Weibke and Efinger[12] and shows the following phases at 450°

		Atomic % Sb
α	f.c.c.	0–6
β	c.p. hex.	9–15.5
γ	orthorh.	21.5–26.5
η	rhombohedral, 8 − N rule	94–100

The experiments carried out on silver–antimony alloys are listed in Table V and show that the heats of formation of all intermetallic phases in this system are remarkably low.

TABLE V

MOLAR HEATS OF FORMATION OF SOLID SILVER–ANTIMONY ALLOYS AT 450°

Alloy composition x_{Ag}, phase	g. atoms	Tin + alloy, g. atoms	Obsd. joule	ΔH^M, kj./g. atom Result	Av.
0.93_7, α?	0.01808	0.8400	274.4	−0.36	
	.02119	.8541	312.6	+0.02	−0.17
0.90_1, β	.02851	.9178	438.2	−0.62	
	.03709	.8663	534.9	+0.20	−0.21
$.84_6$, β?	.02816	.8312	419.9	−0.15	...
$.79_1$, γ?	.03731	.8845	560.8	−0.21	
	.04037	.8723	598.0	−0.02	−0.11
$.77_2$, γ	.03543	.8723	530.9	−0.14	...
$.74_4$, γ	.02620	.8748	388.4	+0.11	...
$.06_7$, η?	.03136	.8397	478.4	+0.17	
	.03218	.8577	488.6	+0.24	+0.20

No reliable heat data for solid silver–antimony alloys are found in the literature. The origin of the value for "Ag_3Sb" (−6 kj./g. atom) reported by Kubaschewski and Evans[13] is not indicated by the authors.

Discussion

In previous studies of the alloys of copper, silver and gold with metals of groups 2B, 3B, etc, particular attention has been given to the effect of size, chemical interaction and valence on the observed binary phase diagrams.[14] Although it is well known that these factors are not really mutually independent, it is convenient to survey separately their possible influence on the observed thermochemical data.

The Size Effect.—According to the measure of atomic size advanced by the Hume-Rothery school,[14] the "size factors" in the alloys of silver with cadmium, indium, tin and antimony are all small (at most about 5% for silver–indium). However, if one adopts the atomic radii of Goldschmidt[15] or Pauling,[16] the silver to antimony sequence is one of increasing disparity in size with a maximum difference of about 11% (for silver–antimony).[15] We shall not here consider in detail the various attempts to calculate the positive contributions to the heat of formation resulting from lattice misfits.[17] It should suffice to state that one may expect the effect to increase roughly as the square of the "size-factor," and to prevent extensive solid solution formation when the size factor is about 15%.[14]

In the considered series of silver alloys we therefore might expect the influence of the difference in size on the thermochemical data to be either quite small (Hume-Rothery approach) or at least not very pronounced (Goldschmidt–Pauling approach).

In fact we note that for all four systems the experimental results give no indication of significant size effects. We shall therefore assume that these effects are of little importance.

The Chemical Interaction Effect.—Since a long time back it has been customary, for the lack of a better measure of the tendency toward chemical bonding, to assume that the magnitude of the chemical interaction between two metals should be related to the difference in their electrochemical character. This assumption is implied when Hume-Rothery and his school refer to the "electrochemical factor" in alloy formation.

For the four systems considered in the present discussion we find some measure of support for this point of view. We observe, for example, that the chemical interaction as measured by the maximum value of $-\Delta H^M$ (for the solid alloys from the solid elements) increases in the sequence Ag–Sb < Ag–Sn < Ag–In < Ag–Cd. This is also the sequence of increasing difference between the standard oxidation potentials of the two components in aqueous solution. However, it should be noted that for silver–antimony, with $\Delta H^M \sim 0$, the difference between the two oxidation potentials is still about 0.6 volt. Therefore it is apparent that, on this criterion of chemical interaction, a certain minimum difference in oxidation potentials is required before a significant negative heat of formation is to be expected. Similar observations have been made for other systems in the past.

Very recently attempts have been made to calculate the heat of formation of alloys theoretically from suitable physical models. Possibly the most ambitious effort in this direction is that of Varley,[18] and, although we shall not discuss his work in detail, it is of some interest to compare the values calculated by Varley with the results of the present investigation. For the solid alloys of about equiatomic composition Varley calculates the following values of the heat of formation per g. atom (from the elements at 0°): Ag–Cd, −2.0 kcal.; Ag–In, −1.5 kcal. and Ag–Sn, +0.7 kcal. For the first two systems agreement with the present experimental results is good.

However, Varley's calculation fails to show the analogy of silver–tin with the other two systems. This analogy is indicated by the phase diagram and borne out by the calorimetric data. The discrepancy can only in part be explained by the fact that Varley assumes the positive contribution of the size effect to the heat of formation to be quite large.

(12) F. Weibke and I. Efinger, *Z. Elektrochem.*, **46**, 53, 61 (1940).

(13) O. Kubaschewski and E. L. Evans, "Metallurgical Thermochemistry," Butterworth-Springer, London, 1951.

(14) For a recent review see *e.g.*, W. Hume-Rothery and G. V. Raynor, "The Structure of Metals and Alloys," Institute of Metals Monograph, No. 1, Third Edition, London, 1954.

(15) V. M. Goldschmidt, "Geochemistry," Oxford University Press, 1954.

(16) L. Pauling, "The Nature of the Chemical Bond," Cornell University Press, Ithaca, N. Y., 1945.

(17) See *e.g.*, J. Friedel, *Advances in Phys.*, **3**, 446 (1954).

(18) J. H. O. Varley, *Phil. Mag.*, **45**, 887 (1954).

The recent theoretical work of Friedel[15] is of particular interest in a discussion of dilute and moderately dilute alloys. Friedel proposes the following cycle for approximate calculation of the limiting heat of solution of a polyvalent metal (*e.g.*, cadmium, etc.) in a monovalent metal (*e.g.*, silver).

(a) Evaporation and ionization: $Cd(s) = Cd^+(g) + e^-(g)$. The total heat absorbed may be calculated from the heat of sublimation (Q_s) plus the first ionization potential of cadmium, $I_1(Cd)$.

(b) Exchange: $Cd^+(g) + Ag^+(s) = Ag^+(g) + Cd^+(s)$. The singly charged cadmium ion is exchanged with a singly charged silver ion in a very dilute solution of cadmium in silver. As the electronic structures of these two ions differ only by the presence of one more positive charge on the nucleus and one more electron in the cloud of electrons screening the nuclear charge, the energy involved in the exchange process is assumed to be small, and is neglected in the calculations.

(c) Recombination and condensation: $Ag^+(g) + e^-(g) = Ag(s)$. The silver ion is combined with the free electron, and the neutral silver atom is condensed on pure silver. The total heat gained is obtained from the first ionization potential of silver, $I_1(Ag)$, and the heat of sublimation, $Q_s(Ag)$.

Apart from size effects, which we have assumed to be small in this system, the cycle gives $(Q_s + I_1)(Ag) - (Q_s + I_1)(Cd)$ for the limiting heat of solution of cadmium in silver. Similar cycles may be used for the other solute elements.

It should be stressed that Friedel in this calculation assumes that only one of the valence electrons of the solute is given off to the conduction band of the solvent. The other electrons are assumed to remain in bound states associated with the solute ions ("atomic orbital approximation"). This model may or may not be a correct description of the physical situation. What is particularly important from the point of view of the thermochemist is that this approach permits an estimate of the heat of solution without the evaluation of a number of large and uncertain terms (*e.g.*, higher ionization potentials for multivalent ions, correlation energies for electrons, etc.).

A comparison of our experimental data with the values calculated according to Friedel's method is given in Table VI.

TABLE VI

LIMITING HEATS OF SOLUTION OF SOLID METALS IN SILVER (IN ELECTRON VOLTS) CALCULATED ACCORDING TO FRIEDEL, AND EXPERIMENTAL VALUES. IONIZATION POTENTIALS FROM LANDOLT-BÖRNSTEIN HEATS OF SUBLIMATION AND HEATS OF FUSION FROM BREWER[19]

System 1 2	$(Q_s + I_1)(Ag)$	Q_s (2)	I_1 (2)	Limiting heat of soln. Calcd., 25°	Exp., 450°
Ag–Cd	10.58	1.16	8.96	−0.46	−0.34
Ag–In	10.58	2.50	5.76	−2.32	−0.45
Ag–Sn	10.58	3.06	7.30	−0.24	−0.29
Ag–Sb	10.58	2.76	8.35	0.51	−0.02

When one considers that the calculated heats of solution represent differences between two large numbers, each of which is associated with some experimental uncertainty, the agreement is really remarkably good. Only for the system silver–indium can the agreement be considered as unsatisfactory. No really convincing explanation is known to account for this apparent anomaly.

The Valence Effect.—In the work of the Hume-Rothery school the effect of valency on alloy formation has been a central point. Thus when one assumes that copper, silver and gold are monovalent, zinc, cadmium and mercury divalent, and so on, one finds a great deal of analogy in the considered binary phase diagrams. The analogy becomes particularly apparent if certain parts of the phase diagram are plotted in terms of electron concentrations, rather than in terms of molar concentrations. These observations were originally empirical, but were later in large measure explained in theoretical work by Jones.[20]

Of particular interest here is the discussion by Jones of the overlap between the Fermi level and the first Brillouin-zone which in face-centered structures such as copper, silver and gold should set in at about 1.36 electrons per atom. At higher electron concentrations the density of states is supposed to fall off rather steeply, which in turn should give some additional curvature to the corresponding heat of formation curve. This overlap explains the tendency of the α-phases in these alloys not to extend much beyond an electron concentration of about 1.4. The plot of the experimental data for α-Ag–Cd (see Fig. 2) seems to suggest some additional curvature near the phase boundary. However, the data are not sufficiently precise to give strong support to Jones' theory. More definite support possibly may be obtained through electronic heat capacity determinations at very low temperatures.

A survey of the present thermochemical data also shows certain other interesting features which presumably may be attributed to the effect of valence: If we consider first the integral heats of formation of the solid alloys from the solid elements, we note that the maxima of $-\Delta H^M$, at least for silver alloyed with cadmium, indium and tin, appear to fall in the range 1.5 to 1.75 electrons per atom. Thus the energetic asymmetry in these systems tends to increase as the valence difference increases. This effect is even better illustrated by the values of the limiting heats of solution at $x_{Ag} = 1$ and at $x_{Ag} = 0$. We note that while the heats of solution of solid cadmium, indium and tin in silver, are of similar magnitude (about −33, −44 and −28 kj./g. atom, respectively), the corresponding data for liquid silver in the liquid metals differ greatly (−24, −4 and +4 kj.).

Although we do not have the corresponding figures for solid silver in the solid metals, these data must be considered as a very clear thermochemical illustration of Hume-Rothery's relative valence principle: "Other things being equal, a metal of lower valence is more likely to dissolve one of higher valence than *vice versa*." It should be pointed out, however, that silver–antimony does not seem to conform too well to this general picture. For this

(19) L. Brewer, in "The Chemistry and Metallurgy of Miscellaneous Materials," L. L. Quill, Editor, McGraw-Hill Book Co., Inc., New York, N. Y., 1950.

(20) H. Jones, *Proc. Phys. Soc.* (*London*), **49**, 243, 250 (1937).

system the two limiting heats of solution and the two limits of solid solubility are comparable in magnitude.

At this point it should perhaps be pointed out that Varley predicts that the ratio of the two limiting heats of solution, in the absence of size effects, should be related as the third root of the inverse ratio of the two valences.[18] This seems to be in reasonable agreement with the experimental results for silver–cadmium, but is not supported by the other data. However, it is open to question whether we are here entitled to compare quantitatively the data for solid and liquid alloys.

Friedel, in his comprehensive theoretical paper quoted above,[17] also suggests a method by which the curvature of the heat of formation in the moderately dilute range may be calculated. For this purpose he adopts a molecular orbital approach, and the curvature is obtained from a consideration of the screening of the extra charge associated with the solute ions and the displacement of the Fermi level. As a result of detailed calculations Friedel is able to make quantitative predictions, which briefly may be summarized as follows: If the effect of valence is stronger than the complicating effects of size and strong chemical interaction, the limiting curvature of the heat of formation curve will be determined by the difference in valence between solute and solvent. Thus a solute of lower valence than the solvent should give a negative curvature, while one of higher valence should give a positive curvature. Furthermore, for a given solvent metal we may expect the curvatures to be roughly proportional to the difference in valence. Using preliminary data furnished by the author, Friedel (ref. 17) was able to account quantitatively for the observed curvatures in the case of liquid solutions of silver in indium and in tin, and for solid solutions of cadmium in silver. In the present work we are able to illustrate how the theory is confirmed also for the solid alloys of indium in silver. For this purpose we have in Fig. 2 included a plot of $\Delta H^M/x_{In}$ *vs.* $2x_{In}$. We note that the data within experimental precision fall on a straight line, and that the slope of this line is now essentially the same as for the regular silver–cadmium curve.

Unfortunately the data do not permit a similar determination of the curvature for the silver–tin and silver–antimony systems. However, the location of the heat of formation minima for these systems (see above) lends additional qualitative support to the Friedel theory. Similar support may be obtained from the data on solution of silver in liquid cadmium and in solid antimony. In this connection it may also be pointed out that the data on solution of copper in tin given in the preceding paper[3] gives, as it should, essentially the same negative limiting curvature as the data on silver in tin. However, the corresponding data for gold in tin show that in this case the effect of valence is overshadowed by the rather strong chemical interaction. Thus the curvature is positive, but small.

Acknowledgments.—The author wishes to acknowledge discussion with many members of the staff of the Institute for the Study of Metals. The chemical analyses carried out in connection with the present work were performed by Messrs. Louis Trefonas and Morton Kaplan, who were also assisting in the preparation of some of the alloys. The vacuum fusion analysis of silver was carried out by Dr. Patricia Sparrow. The indium metal used was a gift from the Anaconda Copper Co. The work was supported in part by the Office of Naval Research, under contract No. N-6ori-02004 with the University of Chicago.

HEAT OF FORMATION OF SOLID AND LIQUID BINARY ALLOYS OF COPPER WITH CADMIUM, INDIUM, TIN AND ANTIMONY AT 450°

BY O. J. KLEPPA

Institute for the Study of Metals, University of Chicago, Chicago, Illinois

Received December 1, 1955

The heats of formation of solid and liquid binary alloys of copper with cadmium, indium, tin and antimony were determined calorimetrically at 450°. The data are compared with earlier calorimetric work and with heat data calculated from equilibrium studies.

Introduction

In recent communications the author has reported on the heat of formation of alloys of silver with cadmium, indium, tin and antimony.[1,2] In the present work similar results are presented for the copper alloys. The data will be compared with earlier work, and a discussion will be given of the more important features of the results. In a future paper[3] corresponding information will be reported for the alloys involving gold.

(1) O. J. Kleppa, *Acta Met.*, **3**, 255 (1955).
(2) O. J. Kleppa, THIS JOURNAL, **60**, 846 (1956).
(3) O. J. Kleppa, *ibid.*, **60**, 858 (1956).

Experimental

The heats of formation of the alloys which are liquid at 450° were obtained by direct combination of solid copper and liquid solvent metal in the calorimeter. The heat data for the solid alloys were calculated from the heats of solution of the alloys in liquid tin ("tin solution calorimetry"). In these calculations use was made of the previously reported calorimetric data for the dilute solutions of copper, cadmium, indium and antimony in tin.[4]

The metals used were all of 99.9+ % purity and were taken from the lots used in the earlier work. The solid alloys were prepared in the form of hollow cylinders of about 10 g. total weight according to a method described elsewhere.[4] Individual samples, which contained from 0.02 to

(4) O. J. Kleppa, *ibid.*, **60**, 842 (1956).

0.04 g. atom of alloy, were cut from the annealed cylinders for use in the solution experiments. All calorimetric work was performed at 450°. Details of apparatus construction and calorimetric procedure have been given in earlier papers.[1,5]

Results

Liquid Alloys.—Heat data for the liquid alloys of copper–tin in the high tin range were reported previously.[4] In the course of the present work the heat of solution of copper in cadmium and indium was determined. Under the existing conditions the dissolution of copper in these liquid metals was quite slow (40 to 80 minutes reaction periods, the longer period for the higher copper contents). The results are recorded in Table I, and are included in Figs. 1 and 2 (see below). Due largely to the slowness of the reactions and the restricted liquid range at 450°, it was not possible to establish the dependence of $\Delta H^M/x_{Cu}$ on x_{Cu}. The mean values of $\Delta H^M/x_{Cu}$ obtained from the data in Table I are +1.0 and +12.6 kj./g. atom, respectively, for copper in cadmium and indium. The uncertainty in these figures should be of the order of 0.5 kj. or less.

TABLE I

MOLAR HEATS OF FORMATION OF LIQUID COPPER–CADMIUM AND COPPER–INDIUM ALLOYS FROM SOLID COPPER AND LIQUID CADMIUM, RESPECTIVELY, INDIUM AT 450°

Composition x_{Cu}	Total g. atoms	ΔH^M, joule/g. atom	Composition x_{Cu}	Total g. atoms	ΔH^M, joule/g. atom
(a) Cu–Cd			(b) Cu–In		
0.0381	0.8594	48	0.0222	0.7187	280
.0675	.8503	55	..0329	.5179	414
.0890	.7403	79	.0494	.6216	627
			.0789	.3911	760

If the heat of fusion of copper is 13.0 kj.,[6] and if this value is assumed to be independent of temperature between the melting point of copper (1083°) and 450°, the values −12 and −0.4 kj. are obtained for the relative partial molal heat contents of undercooled, liquid copper in cadmium and indium. It is recalled that the corresponding value for liquid copper in tin is −1.3 kj./g. atom.[4]

To the knowledge of the author there is no information in the literature on the heat of formation of copper–indium alloys. However, for the copper–cadmium system there exists a recent investigation by Riccoboni, *et al.*[7] At temperatures up to about 600° these investigators carried out a careful e.m.f. study of liquid copper–cadmium alloys which contained from 40 to 100% cadmium. Based on a tenuous extrapolation of their results into the unexplored high-copper region they calculated integral free energy, heat and entropy data through integration of the appropriate Gibbs–Duhem–Margules relations. It is well known that when extrapolations are carried out over wide ranges in composition, the calculated integral data should be accepted with reservations. Therefore we are not surprised to find that the integral heats of mixing calculated by Riccoboni, *et al.*, differ from the present result: from their data at 602° we obtain a relative partial molal heat content of liquid copper in cadmium of about −3.3 kj./g. atom. This result should be compared with our value −12 kj./g. atom (at 450°).

Another comparison is possible between the calculated data of Riccoboni, *et al.*, and the present results: from Table II (below) we find that the heat of formation of a solid alloy containing 40% copper ("Cu_2Cd_3") is −8.3 kj./g. atom (from solid copper and liquid cadmium, by interpolation of the two results relating to the δ-phase). The phase diagram[8] shows that this alloy melts congruently at 563°, and in Kubaschewski and Evans[6] its heat of fusion is given as 9.6 kj./g. atom. If we adopt the above-mentioned figure for the heat of fusion of copper, we calculate from these data a value of −3.9 kj./g. atom for the integral heat of mixing at 450° (undercooled liquid copper plus liquid cadmium, $x_{Cu} = 0.4$). In this calculation we have assumed, for simplicity, that both the considered heats of fusion are independent of temperature. Therefore the value obtained may be associated with an uncertainty estimated to be of the order of 20% or less. For the same alloy Riccoboni, *et al.*, give an integral heat of mixing of −2.0 kj. at 602°.

TABLE II

MOLAR HEATS OF FORMATION OF SOLID COPPER–CADMIUM ALLOYS FROM SOLID COPPER AND LIQUID CADMIUM AT 450°

Alloy: Composition x_{Cu}, phase	Alloy: G. atoms	Tin + alloy, g. atoms	Obsd. joule	$-\Delta H^M$, kj./g. atom: Result	$-\Delta H^M$, kj./g. atom: Av.
0.665, β	0.03119	0.8235	442.5	4.52	
	.03525	.8596	502.1	4.61	4.57
.657, β + γ	.02719	.8695	395.8	4.89	
	.03429	.8506	492.7	4.77	4.83
.572, γ	.03173	.8432	483.3	6.01	
	.02954	.8317	454.4	6.14	6.07
.560, γ + δ	.02524	.8308	381.2	5.86	
	.03164	.8279	485.2	6.16	6.01
.425, δ	.02282	.8253	369.3	7.57	
	.02187	.8724	348.4	7.31	7.44
.383, δ	.02376	.8323	403.6	8.59	
	.02219	.8716	386.3	8.99	
	.01956	.8707	331.2	8.49	
	.02357	.8470	406.2	8.84	8.73

We may also compare this heat of mixing with the heat involved in the formation of the equivalent solid alloy from the solid elements. If we accept the heat of fusion of cadmium recommended by Kubaschewski and Evans[6] (6.4 kj./g. atom), and assume this value to be independent of temperature between the melting point of cadmium (321°) and 450°, we find for the solid alloy a value of −4.5 kj./g. atom. This figure differs by less than the estimated uncertainty from the corresponding heat of mixing.

In the temperature range 550 to 900° the vapor pressure of cadmium over liquid copper–cadmium alloys was studied by Schneider and Schmid.[9] As a result of this work they concluded that the mix-

(5) O. J. Kleppa, THIS JOURNAL, **59**, 175 (1955).

(6) O. Kubaschewski and E. L. Evans, "Metallurgical Thermochemistry," Butterworth-Springer, London, 1951.

(7) L. Riccoboni, V. Genta, M. Fiorani and V. Valenti, *Gazz. chim. al.*, **84**, 982 (1954).

(8) "Metals Handbook," American Society for Metals, Cleveland, Ohio, 1948.

(9) A. Schneider and H. Schmid, *Z. Elektrochem.*, **48**, 627 (1942).

ing process for liquid alloys in this system should be slightly endothermic. This conclusion is contradicted by the present data and also by the work of Riccoboni, *et al.*

Solid Alloys. Copper–Cadmium.—The phase diagram for this system[8] indicates that the following phases exist at 450°

		Atomic % Cd
α	f.c.c.	0–1
β ("Cu_2Cd")	?; complex	33.3
γ	?; complex	42–43
δ ("Cu_2Cd_3")	complex cubic (γ-brass type)	57–63
L	liquid	88–100

The obtained integral heats of formation for the solid alloys of copper–cadmium are recorded in Table II and are plotted *vs.* composition in Fig. 1.

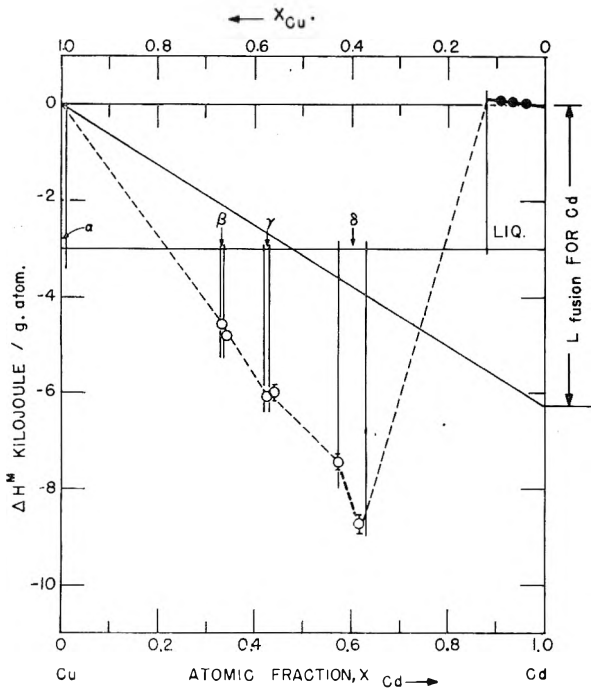

Fig. 1.—Molar heats of formation of solid and liquid copper–cadmium alloys at 450°.

In this figure will be found also the data on liquid copper–cadmium alloys given in Table I.

Previously the heat of formation of the alloy "Cu_2Cd_3" (δ) was determined by solution calorimetry at room temperature by Biltz and co-workers.[10,11] These authors found a heat of formation of about −2.5 kj./g. atom. However, the scattering of the results indicated that this value might be in error by as much as 50%. It is estimated that the uncertainty in the present figure (−4.5 kj./g. atom at 450°) should be of the order of ±0.25 kj.

Copper–Indium.—The phase diagram for this system was studied by Weibke and Eggers,[12] and shows the following phases at 450°

		Atomic % In
α	f.c.c.	0–5
δ	NiAs-type, superstructure (?)[13]	29–31
η'	NiAs-type[13]	34–39
L	Liquid	89–100

The results for this system are recorded in Table III, and are plotted *vs.* composition in Fig. 2. We have included in this figure the observations on liquid alloys given in Table I.

TABLE III

MOLAR HEATS OF FORMATION OF SOLID COPPER–INDIUM ALLOYS FROM SOLID COPPER AND LIQUID INDIUM AT 450°

Alloy: Composition x_{Cu}, phase	Alloy: G. atoms	Tin + alloy, g. atoms	Obsd. joule	$-\Delta H^M$, kj./g. atom: Result	$-\Delta H^M$, kj./g. atom: Av.
0.911, $\alpha + \delta$	0.02985	0.8213	347.7	1.48	
	.02675	.8599	313.6	1.49	1.49
.892, $\alpha + \delta$	.02513	.8684	331.4	3.16	
	.02351	.8796	300.0	2.68	
	.04050	.8497	496.2	2.40	
	.02997	.8798	366.7	2.25	2.62
.706, δ	.02948	.8893	509.4	9.43	
	.02333	.8582	411.9	9.77	9.60
.697, δ	.03099	.8708	532.8	9.46	
	.03382	.8759	576.5	9.33	9.40
.662, η'	.02960	.8599	486.0	9.08	
	.02803	.8813	462.4	9.15	9.12
.625, η'	.02862	.8893	449.3	8.79	
	.02554	.8770	408.3	9.06	
	.03012	.8453	473.6	8.83	8.89

Copper–Tin.—According to Raynor[14] the following phases exist at 450°

		Atomic % Sn
α	f.c.c.	0–8
δ	complex cubic (γ-brass type)	20.5
ϵ (ϵ')	orthorhombic (distorted ϵ-brass)	24.5–25.5
L	liquid	82–100

The results obtained for copper–tin are recorded in Table IV, and are plotted *vs.* composition in Fig. 3. In this figure we have drawn also the previously determined heat of formation curve for liquid copper–tin alloys in the high-tin range.[4]

In the past the solid alloys of copper and tin have been studied by several groups of investigators.[10,11,15,16] Most data refer to the formation of the ϵ-phase ("Cu_3Sn") from the solid elements at or near room temperature. For this alloy Biltz, *et al.*,[10,11] give a ΔH^M of −7.5 and −8.4 kj. at 20°, Körber and Oelsen[15] give −7.5 (at 20°), Cohen, Leach and Bever[16] report −7.82 ± 0.67 (at 0°), while the present work yields −7.61 ± 0.27 kj./g. atom at 450°.

(10) W. Biltz and C. Haase, *Z. anorg. allgem. Chem.*, **129**, 141 (1923).

(11) W. Biltz, W. Wagner, H. Pieper and W. Holverscheit, *ibid.*, **134**, 25 (1924).

(12) F. Weibke and H. Eggers, *ibid.*, **220**, 273 (1934).

(13) See, *e.g.*, E. Hellner and F. Laves, *Z. Naturforschung*, **A2**, 177 (1949).

(14) G. V. Raynor, Annotated Equil. Diagr. #2. Inst. of Metals, London, 1944.

(15) F. Körber and W. Oelsen, *Mitt. Kaiser-Wilhelm Inst. Eisenforschung, Düsseldorf*, **19**, 209 (1937).

(16) J. B. Cohen, J. S. L. Leach and M. Bever, *J. Metals*, **6**, 1257 (1955).

In calculating this value from the data in Table IV we have set the heat of fusion of tin equal to 7.06 kj./g. atom,[6] and we have assumed this value to be independent of temperature between the melting point of tin (232°) and 450°. The quoted result is the average of the six observations on alloys which contain from 24.7 to 25.5 % tin. The given uncertainty represents the mean deviation of individual observations from the unweighted mean, but does not include the possible error in the heat of fusion of tin. It will be noted that the agreement with the earlier work is excellent. The data suggest that the Neumann–Kopp heat capacity rule may be fairly well satisfied for this alloy.

Cohen, Leach and Bever[16] studied also the heat of formation of a copper–tin alloy with 8.1% tin. They dissolved in liquid tin alloys of this composition, which had (a) been quenched to room temperature from the α-field at elevated temperature. These specimens should therefore be supersaturated with respect to δ; (b) been annealed for a period of 219 hr. at 254°; these alloys consisted of the two phases $\alpha + \delta$.

The authors had some difficulty in obtaining reproducible results for the quenched specimens (submicroscopic precipitation of δ?), and give an approximate value of -0.73 kj./g. atom for the apparent heat of formation of the quenched alloy. For the annealed alloy reproducibility was better, and the average of 12 experiments was -1.07 kj./g. atom.

TABLE IV

MOLAR HEATS OF FORMATION OF SOLID COPPER–TIN ALLOYS FROM SOLID COPPER AND LIQUID TIN AT 450°

Alloy: Composition x_{Cu}, phase	G. atoms	Tin + alloy, g. atoms	Obsd. joule	$-\Delta H^M$, kj./g. atom: Result	Av.
0.926, α	0.03519	0.8608	420.0	1.60	
	.03648	.8741	432.7	1.53	1.57
.914, $\alpha + \delta$	.03065	.9184	368.5	1.75	
	.03489	.8384	416.0	1.73	1.74
.798, δ	.03623	.8541	565.3	6.66	
	.02946	.8521	471.3	6.99	6.83
.791, δ	.03917	.8575	615.0	6.86	
	.03133	.8528	485.3	6.58	6.72
.753, ϵ	.03726	.8891	648.4	8.94	
	.03034	.8590	540.3	9.07	9.01
.750, ϵ	.02474	.8590	441.4	9.32	
	.02565	.8687	467.4	9.72	9.52
.745, ϵ	.02370	.9274	426.4	9.51	
	.02282	.8605	415.6	9.74	9.63

The two first alloy compositions listed in Table IV average a tin content of 8.0%. Thus the average is essentially the same as in the alloy used by Cohen, Leach and Bever. The mean of the results listed in Table IV for these alloys is -1.65 ± 0.09 kj./g. atom. If we adopt the mentioned value for the heat of fusion of tin we obtain -1.08 ± 0.09 kj./g. atom for formation of the alloy from the

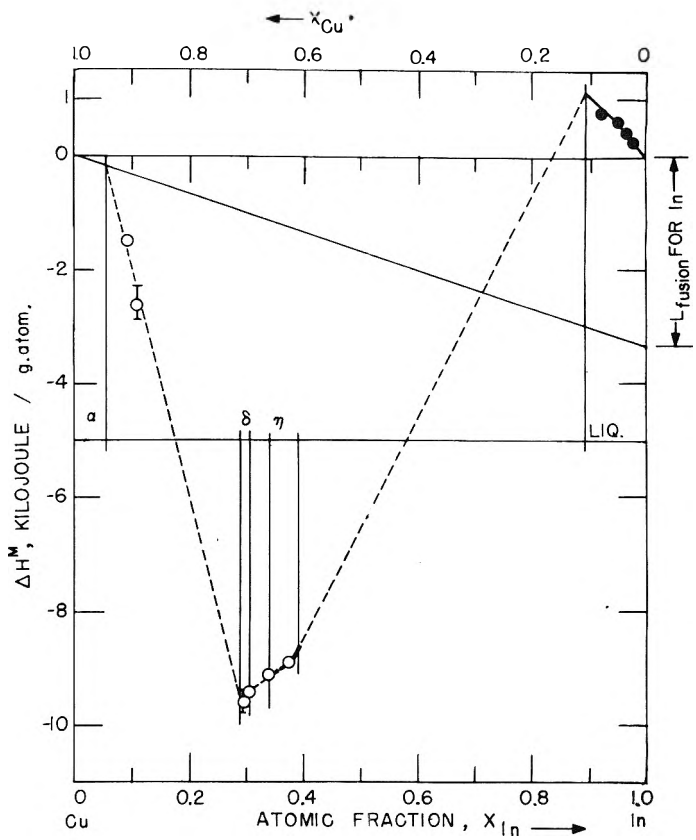

Fig. 2.—Molar heats of formation of solid and liquid copper–indium alloys at 450°.

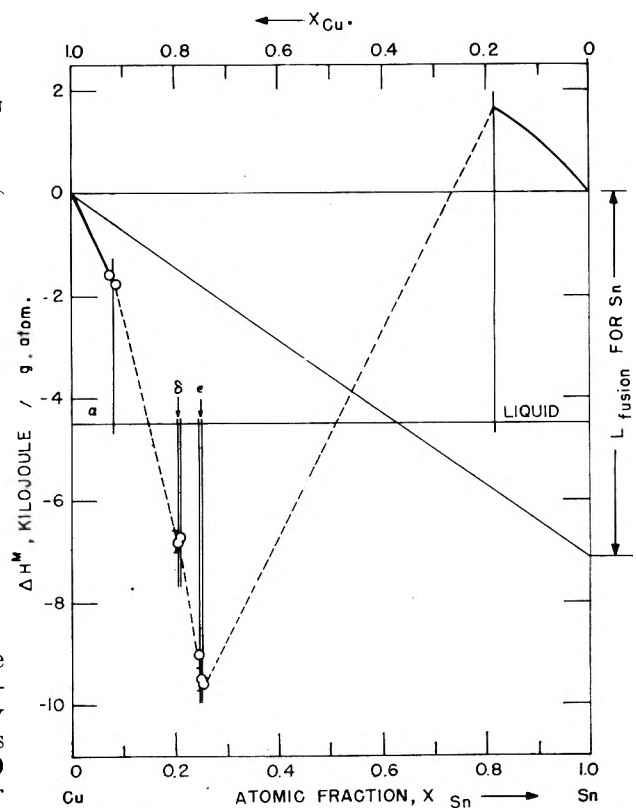

Fig. 3.—Molar heats of formation of solid and liquid copper–tin alloys at 450°.

solid elements at 450°. The agreement with Cohen, Leach and Bever's value for the annealed alloy is excellent.

Copper–Antimony.—According to phase diagram information given by Schubert and Ilschner[17] and by "Metals Handbook,"[8] the following phases, all solid, exist in this system at 450°

		Atomic % Sb
α	f.c.c.	0–5
η	hex. c.p. (ϵ-brass type)	15–16
δ (?)	hex. c.p. (ϵ-brass, ordered ?)	17
κ (?)	orthorhombic (ϵ-brass, distorted)	19
β ("Cu_3Sb")	b.c.c. (?)	23–27
γ ("Cu_2Sb")	Tetr.	32.5–33.5
"Sb"	rhombohedral, 8-N rule	?–100

The calorimetric data for copper–antimony alloys are recorded in Table V, and are plotted *vs.* composition in Fig. 4.

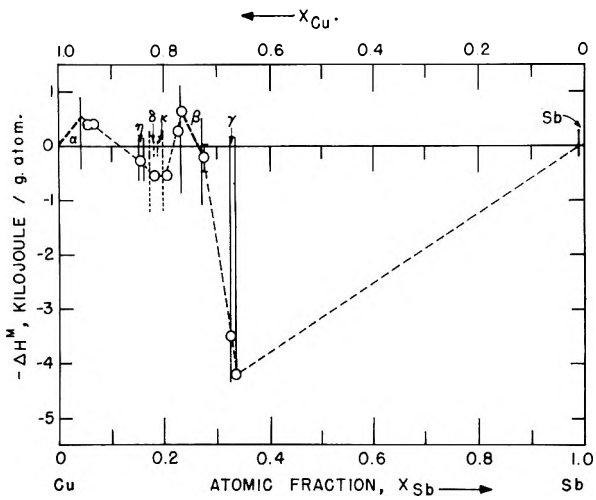

Fig. 4.—Molar heats of formation of copper–antimony alloys at 450°.

The heat of formation of the alloy "Cu_3Sb" (β) was determined previously by Biltz and Haase,[10] who recommend a value for ΔH^M of the order of -2 to -3 kj./g. atom. This is in reasonable agreement with our result -4.23 kj./g. atom for $x_{Sb} = 0.334$. For comparison it may also be pointed out that Kawakami's[18] calorimetric determination of the heat of mixing of liquid copper–antimony alloys at 1200° shows an extreme value of about -3.5 ± 0.5 kj./g. atom (for an alloy with $x_{Sb} \sim 0.4$).

Discussion

The heat data determined for the four systems covered in the present work are given in the form of a composite graph in Fig. 5. The results are plotted *vs.* composition, little attention being given to the location of the various solid–solid phase boundaries. All data refer to formation of the alloys from solid copper and liquid alloying element. As antimony is solid at 450°, the results for copper–antimony are referred to liquid, undercooled antimony of this temperature by adopting 19.8 kj./g. atom for its heat of fusion.[6]

From a fundamental point of view particular interest is attached to the terminal solutions formed when cadmium, indium, tin and antimony are dissolved in copper, and *vice versa*. First we here recall that the solid solubilities of these metals in copper are quite restricted, at 450° ranging from about 1% for cadmium to 8% for tin. Therefore only one calorimetric determination was carried out on alloys in the α-field proper (in Cu–Sn, $x_{Sn} = 0.074$). If we neglect the curvature of the heat of formation between 0 and 8% tin, the result gives about -21 kj./g. atom for the "limiting" heat of solution of liquid tin in solid copper. In principle similar data may be calculated for the other systems if the measured heat data for alloys in the two-phase fields (α + 2nd solid phase) are extrapolated to the known α-phase boundaries. In this way we estimate the heat of solution of liquid antimony in solid copper to be of the order of -10 kj./g. atom. For indium in copper the extrapolation is more uncertain, but a value near 0 is indicated. For cadmium the required data for the two-phase field are not available. However, from the low solid solubility in this system we can deduce that the heat of solution should be positive, although the actual magnitude cannot be established.

It is worth noting that the mentioned heats of solution agree qualitatively with the usual interpretation of the effect of atomic size in the formation of metallic solid solutions: If we adopt the measures of atomic size advanced by the Hume–Rothery school, the "size-factor" for tin in copper is about +9% (*i.e.*, the diameter of the tin atom is assumed to be about 9% larger than that of the copper atom), while the size-factor for antimony in copper is +12, for cadmium in copper +16 and for indium in copper about +18% (?). As the size-factor in-

TABLE V

MOLAR HEATS OF FORMATION OF SOLID COPPER–ANTIMONY ALLOYS AT 450°

Alloy: Composition x_{Cu}, phase	Alloy: G. atoms	Tin + alloy, g. atoms	Obsd. joule	ΔH^M, kj./g. atom: Result	ΔH^M, kj./g. atom: Av.
0.945, $\alpha + \eta$	0.03977	0.8586	436.5	+0.35	
	.03386	.9054	373.1	+0.41	+0.38
.934, $\alpha + \eta$	.03694	.8772	410.3	+0.32	
	.03601	.8774	394.5	+0.50	+0.41
.845, η	.03555	.8946	433.2	−0.31	
	.03816	.8616	460.8	−0.23	−0.27
.817, $\delta + \kappa$	.03424	.8807	423.8	−0.35	
	.03763	.9004	479.6	−0.76	−0.56
.795, $\kappa + \beta$	.03391	.8884	431.8	−0.62	
	.03889	.8452	487.4	−0.49	−0.55
.776, $\kappa + \beta$	.03316	.8636	394.2	+0.33	
	.03310	.8849	395.6	+0.27	+0.30
.765, β	.03353	.8570	391.1	+0.60	
	.03016	.8896	350.7	+0.67	+0.64
.726, $\beta + \gamma$	.03170	.8672	394.3	−0.08	
	.03369	.9034	440.2	−0.61	
	.03278	.8832	406.7	+0.05	−0.21
.675, γ	.03156	.8532	515.6	−3.66	
	.03178	.8869	510.1	−3.36	−3.51
.666, γ	.02761	.8540	469.7	−4.26	
	.02783	.9310	471.9	−4.19	−4.23

(17) K. Schubert and M. Ilschner, *Z. Metallkunde*, **45**, 366 (1954).
(18) M. Kawakami, *Sci. Rep. Tohoku Imp. Univ.*, **19**, 521 (1930).

creases, so does presumably the (positive) contribution of the lattice "misfit" energy to the over-all heat of formation of the solid solution. At first it is somewhat surprising to find that copper–cadmium, in spite of the slightly more favorable size-factor, appears to have a more positive heat of solution than copper-indium. A possible explanation may rest in the fact that the chemical "bonding" between copper and indium at high copper contents is stronger. Thus the larger positive misfit energy for copper–indium may be more than balanced by the stronger interaction. The present data for the copper–antimony and copper–tin systems indicate that size factors as low as 12 and 9% may be associated with significant positive contributions to the heat of formation. Thus we note that even for copper–tin the over-all heat of formation curve has a characteristic re-entrant shape at the boundary of the α-phase. This shape presumably arises from the misfit energy being higher in the α-phase than in the neighboring phases. It is worth recalling that for the corresponding silver systems, which all have much smaller size factors, re-entrant heat of formation curves were not observed at the boundaries of the α-phases.

While the heats of solution of the liquid metals in copper show both positive and negative values, we note that the corresponding figures for solid copper in liquid cadmium, indium and tin are all positive. The values range from +1.0 kj./g. atom in cadmium to +11.7 in tin and +12.6 in indium. However, if we correct for the heat of fusion of copper by subtracting 13.0 kj. from these values,[5] the figures change from positive to negative, although in tin and indium barely so.

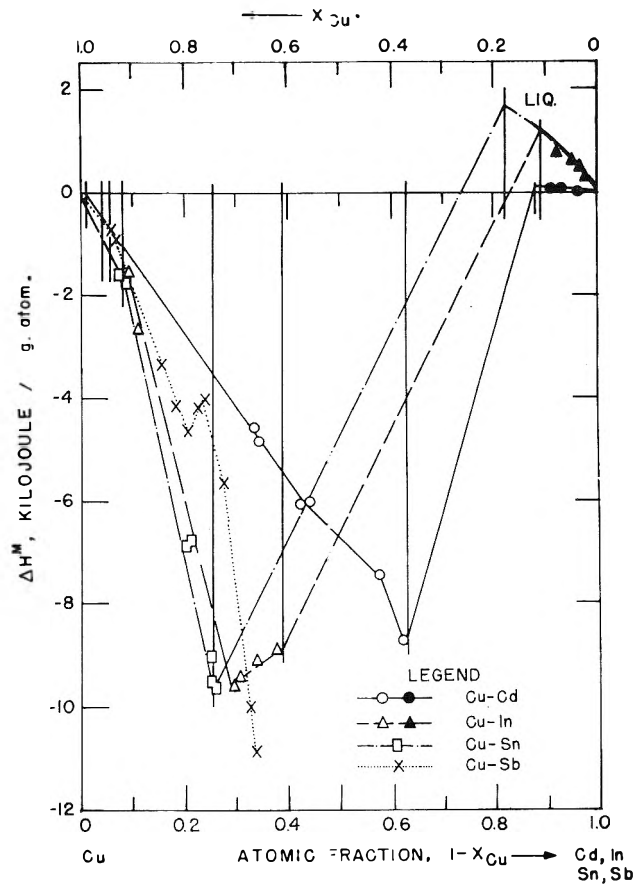

Fig. 5.—Composite graph of heats of formation of alloys of copper with cadmium, indium tin and antimony from solid copper and liquid alloying components.

Among the eight terminal solutions considered in the present work a reasonably reliable value for the limiting "curvature" of the heat of formation actually $^1/_2(d^2\Delta H^M/dx^2)$ for small values of x is available only for copper dissolved in liquid tin, −13.7 kj./g.atom.[4] However, for copper in liquid cadmium, an approximate value may be obtained from the above-mentioned work of Riccoboni, *et al.*,[7] namely, −5 to −10 kj./g. atom at 600°. Similarly there can be little doubt that a negative "curvature" exists for moderately dilute solutions of copper in indium. This may be inferred from a comparison of the strong interaction between copper and indium at moderate indium contents with the weak interaction at high indium concentrations. A value of −10 to −20 kj. for the "curvature" is indicated. From this we may conclude that our present data for the solutions of copper in liquid cadmium, indium and tin provide semi-quantitative confirmation of Friedel's "valence rule."[2,19]

Let us next consider the compositions at which $-\Delta H^M$ reaches extreme values (for the solid alloys formed from the solid elements). If copper is assumed to be monovalent, cadmium divalent and so on, the maxima, with one exception, occur at electron concentrations between 1.6 and 1.8 electrons per atom. It is here recalled that similar observations were made previously for the corresponding silver alloys. The analogy is particularly clear-cut for the systems involving indium and tin, which with both copper and silver show maxima at 1.6 (indium systems) and 1.75 electrons per atom (tin systems). It also is suggestive that if antimony is assumed to be trivalent in the "exceptional" alloy "Cu_2Sb," its composition corresponds to 1.66 electrons per atom.

It finally is interesting to note that while the silver systems showed increasing chemical interaction between the two components (as indicated by the magnitude of the maximum value of $-\Delta H^M$) in the sequence Ag–Sb < Ag–Sn < Ag–In < Ag–Cd, the corresponding sequence for the copper alloys is Cu–Sb < Cu–Cd(!) < Cu–Sn < Cu–In.

Copper and silver both show exceptionally weak "bonding" to antimony in the phases at $x_{Sb} \sim 0.15$ to 0.20. However, in 'Cu_2Sb" the magnitude of the interaction appears to fall in line with that of the other copper systems. It is particularly surprising to note that cadmium, which shows the strongest interaction in the silver series, has dropped to second lowest place among the copper alloys. Previously we noted for the silver alloys a crude correlation between the magnitude of the heat of formation and the difference between the standard oxidation potentials of the component metals in aqueous solutions. The observed change in sequence for the copper alloys illustrates the

(19) J. Friedel, *Advances in Phys.*, **3**, 446 (1954).

crudeness of the concept of "the electrochemical factor" in alloy formation.

Acknowledgments.—The author is indebted to Dr. K. Anderko for a preview of the manuscript of the new edition of "Hansen."

The indium metal used in the present work was a gift from the Anaconda Copper Company Some of the solid alloys were prepared with the help of Messrs. Louis Trefonas and Morton Kaplan.

The reported work was supported in part by the Office of Naval Research through contract No. N-6ori-02004 with the University of Chicago.

HEAT OF FORMATION OF SOME SOLID AND LIQUID BINARY ALLOYS OF GOLD WITH CADMIUM, INDIUM, TIN AND ANTIMONY

BY O. J. KLEPPA

Institute for the Study of Metals, University of Chicago, Chicago, Illinois

Received December 10, 1955

The heats of solution of gold in liquid cadmium and indium were determined at 450°. The heats of formation of the solid alloys of gold with cadmium, indium, tin and antimony were determined by the tin solution technique. The results are discussed and compared with the previously reported data for the copper and silver alloys.

Introduction

The present report completes an experimental survey of the thermochemistry of the binary alloys of copper, silver and gold with cadmium, indium, tin and antimony. The results for the copper and silver systems were presented recently.[1-3] For these alloys all calorimetric determinations were carried out at one common reference temperature, 450°. Similarly most of the data on the gold alloys were obtained at this temperature. However, for the low-melting intermetallic phases in the gold–tin system the heats of formation were determined at 350° ("AuSn") and 242° ("$AuSn_2$" and "$AuSn_4$").

Experimental

All solid gold alloys were prepared in the form of 3 mm. rods of about 2–3 g. total weight according to a method described previously.[2] In other respects the experimental procedures were similar to those described for copper and silver alloys. All metals were taken from the lots used in the earlier work.

Results

Comparison with Earlier Data. Liquid Alloys.—At 450° the liquid range of the system gold–cadmium extends to about 16 atomic % gold, of gold–indium to about 14% and of gold–tin to about 76% gold. Data on the heat of solution of gold in tin at 450, 350 and 242° have been presented elsewhere.[4] In the present work similar data are reported for gold in cadmium and indium at 450°. While the solution process for silver and copper in these metals was quite sluggish, gold dissolved rapidly (reaction periods of 15–20 minutes). The results obtained are given in Table I. It was found that within experimental precision $\Delta H^M/x_{Au}$ does not vary with x_{Au} in the explored concentration range.

The average heats of solution are −48.4 ± 0.4 for gold in cadmium and −33.05 ± 0.17 kj./g. atom for gold in indium. We recall that at 450° the limiting heat of solution for gold in tin is −19.73 kj.[4]

TABLE I

MOLAR HEATS OF FORMATION OF LIQUID GOLD–CADMIUM AND GOLD–INDIUM ALLOYS FROM SOLID GOLD AND LIQUID CADMIUM, RESPECTIVELY, INDIUM AT 450°

Composition x_{Au}	Total g. atoms	$-\Delta H^M$, j./g. atom	Composition x_{Au}	Total g. atoms	$-\Delta H^M$, j./g. atom
(a) Au–Cd			(b) Au–In		
0.00785	0.9586	380	0.02110	0.4019	692
.01047	.6998	507	.03436	.2754	1145
.01550	.5283	794	.04474	.1960	1486
.02194	.3495	1049	.07498	.1448	2472
.04217	.1910	2086	.1217	.0795	4013
.06893	.1279	3329	.1621[a]	.0822	8320
.1225	.1504	5890			

[a] At 450° this composition consists of a mixture of "$AuIn_2$" and liquid.

If we set the heat of fusion of gold equal to 12.8 kj.,[5] and assume this value to be independent of temperature between the m.p. of gold (1063°) and 450°, we obtain about −61, −46 and −33.5 kj./g. atom for the relative partial molal heat content of (undercooled) liquid gold in cadmium, indium and tin, respectively.

The vapor pressure of cadmium over liquid gold–cadmium alloys at higher temperatures and higher gold contents was studied by Schneider and Schmid.[6] For an equiatomic mixture of gold and cadmium these authors calculated an integral heat of mixing ($-\Delta H$) of about 4 kj./g. atom. A conservative estimate based on extrapolation of the present data shows that this figure is much too low. This is confirmed by a calculation based on the data for solid gold–cadmium alloys given below (Table II).

The equilibrium phase diagram for the gold–cadmium system[7] shows that a solid alloy of approximately equiatomic composition has a congruent melting point at 627°. According to Kubaschewski and Evans[5] the heat of fusion of this alloy is 9.0 ± 0.6 kj./g. atom. We may use this information to calculate the heat of mixing of the equi-

(1) O. J. Kleppa, *Acta Met.*, **3**, 255 (1955).
(2) O. J. Kleppa, THIS JOURNAL, **60**, 846 (1956).
(3) O. J. Kleppa, *ibid.*, **60**, 852 (1956).
(4) O. J. Kleppa, *ibid.*, **60**, 842 (1956).
(5) O. Kubaschewski and E. Ll. Evans, "Metallurgical Thermochemistry," Butterworth-Springer, London, 1951.
(6) A. Schneider and H. Schmid, *Z. Elektrochem.*, **48**, 627 (1952).
(7) M. Hansen, "Aufbau der Zweistofflegierungen," Berlin, 1936.

TABLE II

MOLAR HEATS OF FORMATION OF SOLID GOLD–INDIUM ALLOYS FROM SOLID GOLD AND LIQUID CADMIUM AT 450°

Alloy: Composition x_{Au}, phase	Alloy: G. atoms	Tin + alloy, g. atoms	Obsd. joule	$-\Delta H^M$, kj./g. atom: Result	$-\Delta H^M$, kj./g. atom: Av.
0.928, α	0.01074	0.8035	−144.2	4.33	
	.01096	.8517	−141.5	4.83	4.58
.897, α	.00931$_5$	.8686	−101.1	6.11	
	.00946$_6$	.7845	−98.3	6.58	6.35
.838, α	01081	.7766	−60.4	9.81	
	.01098	.8265	−67.3	9.30	9.56
.786, α	.01130	.8142	−20.3	12.28	
	.01141	.8585	−18.9	12.40	12.34
.736, α_2	.00933	.8097	+16.1	14.51	
	.00905	.8338	+18.5	14.80	14.66
.682, α_2	.00978	.8573	53.9	16.86	
	.00979$_5$	.8615	52.2	16.68	16.77
.561, β	.01167	.8752	136.9	19.93	
	.01185	.8164	137.9	19.86	19.90
.533, β	.01256	.8112	166.3	20.71	
	.01248	.8217	160.7	20.35	20.53
.470, β	.01452	.8941	216.8	20.79	
	.01457	.8486	225.2	21.28	21.04
.449, β	.01423	.8609	225.7	21.17	
	.01434	.8812	221.9	20.77	20.97
.372, γ	.01483	.8341	229.8	18.78	
	.01402	.8468	227.0	19.47	
	.01508	.8601	236.2	18.94	19.06
.354, γ	.01379	.8360	221.3	18.83	
	.01321	.8906	210.5	18.72	18.78
.303, ϵ	.01228	.8669	219.2	19.28	
	.01168	.8327	207.8	19.21	19.25
.250, ϵ	.01135	.8631	223.6	19.74	
	.01063	.8674	202.7	19.12	19.43

atomic liquid mixture, form the heat of formation of the solid alloy (~ -21 kj./g. atom). If we neglect the possible temperature dependence of the heats of fusion of gold and of "AuCd," we arrive at a value of -18.4 kj./g. atom at 450°. It is estimated that the uncertainty in this figure may be of the order of 10% or less.

It is of interest to compare this result with the heat of formation of the solid alloy from the solid components. With a heat of fusion of cadmium equal to 6.4 kj.,[5] we obtain for "AuCd" a value of -17.8 kj./g. atom.

There are, to the knowledge of the author, no heat data in the literature for gold–indium alloys.

Solid Alloys. Gold–Cadmium.—There is some disagreement in the literature regarding the details of the gold–cadmium phase diagram. According to information given by Hansen[7] and by Owen and co-workers,[8] supplemented by data of Byström and Almin,[9] several phases should be stable at 450°, as listed in the tabulation given in the next column. The results for solid alloys of gold–cadmium are recorded in Table II and are plotted *vs.* composition in Fig. 1. In this figure we have included also the

		Atomic % Cd
α	f.c.c.	0–23
α''	cubic, ordered	~23
α_2	c.p. hex.	25–35
β	b.c.c., ordered	43–57
γ (δ')	?	62–65
ϵ	?	70–76
L	Liquid	84–100

data on liquid gold–cadmium alloys recorded in Table I.

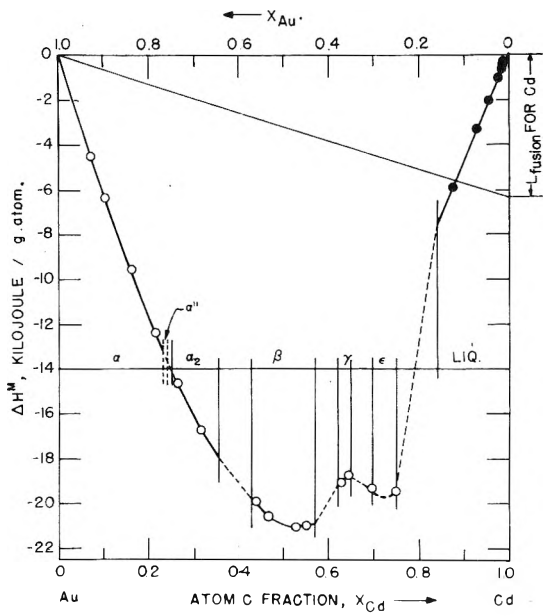

Fig. 1.—Molar heats of formation for solid and liquid gold–cadmium alloys at 450°.

Previously Ölander[10] studied the solid gold–cadmium alloys containing more than about 20 atomic % cadmium by the e.m.f. method. For alloys with lower cadmium contents the observed e.m.f.'s were not quite reproducible, presumably due to low rates of diffusion at the measuring temperatures (250–500°). Therefore Ölander refrained from calculating integral thermodynamic quantities from his equilibrium measurements. Later Weibke[11] noted that Ölander's data for alloys with 20 to 30% cadmium indicated little or no dependence of the relative partial molal heat content of cadmium ($\bar{L}_{Cd}$) on composition. Thus all values of $\bar{L}_{Cd}$ fell between -36 and -40 kj./g. atom (referred to liquid cadmium), and the data showed no definite trend with changing composition. Weibke went on to assume that this would still hold true for lower cadmium contents. On this assumption he calculated a set of integral heat data from Ölander's experimental results.

Weibke's assumption should be considered as a crude approximation only. Therefore it is not surprising to find that his integral heat data numerically are somewhat too low: For an alloy with $x_{Au} = 0.77$ (α) Weibke calculated a ΔH^M (from the solid elements at 350°) of -7.6 kj. From the present work we obtain the corresponding value -11.4 at 450°.

(8) E. A. Owen and E. A. O'Donnel Roberts, *J. Inst. Metals*, **66**, 389 (1940); E. A. Owen and W. H. Rees, *ibid.*, **67**, 141 (1941).

(9) A. Byström and K. E. Almin, *Acta Chem. Scand.*, **1**, 76 (1947).

(10) A. Ölander, *J. Am. Chem. Soc.*, **54**, 3819 (1932).

(11) F. Weibke, *Z. Metallkunde*, **29**, 79 (1937).

Another comparison is possible between Ölander's $\bar{L}_{Cd}$ for the α-phases and the present work: to facilitate this comparison we have in Fig. 2 plotted

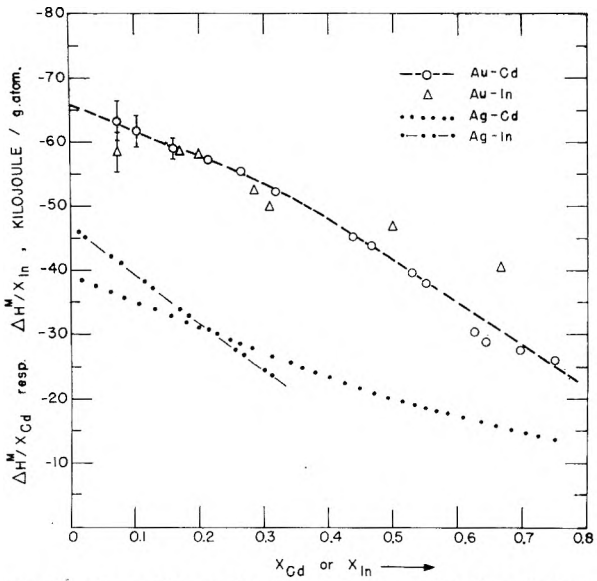

Fig. 2.—Heat of formation for solid alloys of gold–cadmium, gold–indium, silver–cadmium and silver–indium.

our experimental values of $\Delta H^M/x_{Cd}$ *vs.* x_{Cd}. It will be noted that practically all the results fall on a smooth curve, which in the α–α_2-range may be approximated by the straight line.

$$\Delta H^M/x_{Cd} = -66 + 40x_{Cd} \text{ kjoule} \qquad (1)$$

From this expression we get

$$\bar{L}_{Cd} = -26 - 40x^2_{Au} \text{ kjoule} \qquad (2)$$

At $x_{Au} = 0.2$ and 0.3 this gives $\bar{L}_{Cd} = -51.6$ and -45.6 kj., respectively. We recall that Ölander's experiments gave values from -36 to -40 kj. The agreement must be considered satisfactory.

From his e.m.f. study Ölander was able to obtain important information on the heats and entropies associated with several solid state transformations occurring in this system. It is evident that the present work, which is restricted to a study of phases which are stable at 450°, only to a limited extent can add to this information. However, from our Fig. 1 it is apparent that the $\gamma(\delta')$-phase has a higher enthalpy than a mixture of the neighboring β- and ϵ-phases. From the quoted results we obtain for the hypothetical process

$$\gamma\,(x_{Cd} = 0.625) = {}^1/_2\beta\,(x_{Cd} = 0.55) + {}^1/_2\epsilon\,(x_{Cd} = 0.70)\,(450°)$$

a heat of transformation of about -1.1 kj./g. atom.[12] It should be stressed that because this number represents the difference between two much larger quantities, the uncertainty in this figure is quite large, perhaps 30–40%. However, the result is in excellent agreement with the value which is obtained from Ölander–Weibke, namely, about -1 kj./g. atom.

Gold–Indium.—According to Pfisterer,[13] the following phases are stable in gold–indium at 450°

		Atomic % In
α	f.c.c.	0–7
β	c.p. hex	16–21
δ	complex cubic (γ-brass type)	28.5–31.5
"AuIn"	triclinic[14]	49–50
"$AuIn_2$"	cubic (CaF_2-type)	66.7
L	liquid	86–100

The results of the experiments on gold–indium alloys are recorded in Table III, and are plotted *vs.* composition in Fig. 3. In this figure we have included also the data on liquid gold–indium alloys given in Table I. A plot of the experimental values of $\Delta H^M/x_{In}$ *vs.* x_{In} for the solid gold–indium alloys is found in Fig. 2 along with the corresponding

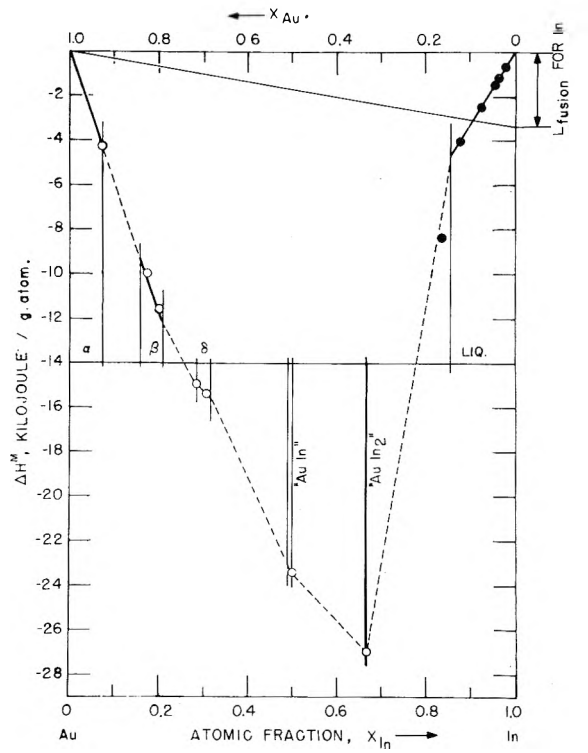

Fig. 3.—Molar heats of formation for solid and liquid gold–indium alloys at 450°.

curve for gold–cadmium. It will be seen that while the heats of formation of "AuIn" and "$AuIn_2$" numerically are significantly larger than the heats of formation of the corresponding gold–cadmium alloys, the results for lower indium contents are very similar indeed. We note in particular that within experimental precision the limiting heat of solution of liquid indium in gold is about the same as for liquid cadmium.

Gold–Tin.—According to Hansen,[7] three phases are stable in this alloy system at 450°

		Atomic % Sn
α	f.c.c.	0–7
β	c.p. hex.	12–14
L	Liquid	24–100

(12) When the transformation does not occur spontaneously at 450° it is of course because of the higher entropy of the γ-phase. This is borne out by the appearance of the phase diagram.[7]

(13) H. Pfisterer, *Z. Metallkunde*, **41**, 95 (1950).

(14) K. Schubert and U. Rösler, *Z. Metallkunde*, **41**, 298 (1950); *Naturwissenschaften*, **40**, 437 (1953).

TABLE III

MOLAR HEATS OF FORMATION OF SOLID GOLD-INDIUM ALLOYS FROM SOLID GOLD AND LIQUID INDIUM AT 450°

Alloy: Composition x_{Au}, phase	G. atoms	Tin + alloy, g. atoms	Obsd. joule	$-\Delta H^M$, kj./g. atom: Result	Av.
0.928, α	0.00976	0.8800	−134.9	4.47	
	.00981	.8481	−139.9	4.02	4.25
.830, β	.00735	.8304	− 46.8	10.07	
	.00730[a]	.8377[a]	− 47.8	9.84	9.96
.800, β	.00752	.8289	− 32.7	11.52	
	.00780	.8367[a]	− 32.2	11.68	11.60
.715, δ	.00837	.8854	+ 5.8	14.90	
	.00875	.8941[a]	+ 6.2	15.00	14.95
.692, δ	.00915	.8263	+ 16.1	15.59	
	.00924	.8356[a]	+ 12.4	15.15	15.37
.500, "AuIn"	.00910	.8861	124.7	23.88	
	.00746	.8322	96.3	23.08	23.42
	.01676	.8954	220.0	23.31	
.333, "$AuIn_2$"	.01036	.8907	209.3	27.20	
	.00969	.8648	191.0	26.71	26.96

[a] In these cases the solid alloy was dissolved in the liquid solution formed in the previous experiment.

At lower temperatures the following phases, which all have very narrow ranges of homogeneity, also exist

"AuSn"	NiAs-type	50 at. % Sn, congruent m.p. at 418°
"$AuSn_2$"	orthorhombic[14]	66.7 at. % Sn, peritectic dec. at 309°
"$AuSn_4$"	orthorhombic[14]	80 at. % Sn, peritectic dec. at 252°

The heat of formation of two alloys in the α and β regions was determined at 450°, that of "AuSn" at 350°, while the alloys "$AuSn_2$" and "$AuSn_4$" were studied at 242°. The results of all experiments are recorded in Table IV and are plotted *vs.* composition in Fig. 4. This figure also includes the previously determined heat of formation curve for liquid gold–tin alloys at 450°.[4]

TABLE IV

MOLAR HEATS OF FORMATION OF SOLID GOLD-TIN ALLOYS FROM SOLID GOLD AND LIQUID TIN

Temp., °C.	Alloy: Composition x_{Au}, phase	G. atoms	Tin + alloy, g. atoms	Obsd. joule	$-\Delta H^M$, kj./g. atom: Result	Av.
450	0.940, α	0.01002	0.9005	−169.5	1.56	
		.00988	.8776	−168.3	1.43	1.50
450	.870, β	.01109	.8519	−167.0	2.03	
		.01101	.8629[a]	−166.8	1.78	1.91
350	.500, "AuSn"	.01133	.8538	82 6	17.76	
		.01181	.8656[a]	86.9	17.81	17.78
242	.333, "$AuSn_2$"	.01419	.8352	142.6	17 74	
		.00966	.8448	97.2	17.75	17.74
242	.200, "$AuSn_4$"	.01092	.8374	85.0	12.39	
		.01120	.8485	90.8	12.71	12.55

[a] In these cases the solid alloy was dissolved in the liquid solution formed in the previous experiment.

In the past the heats of formation (from the solid elements) of "AuSn" and "$AuSn_2$" were reported by Biltz, Rohlffs and Vogel.[15] At 90° they found −17.1 kj./g. atom for "AuSn" and −7.7 for "$AuSn_2$." If we set the heat of fusion of tin equal to 7.06 kj.,[5] and assume this value to be independent

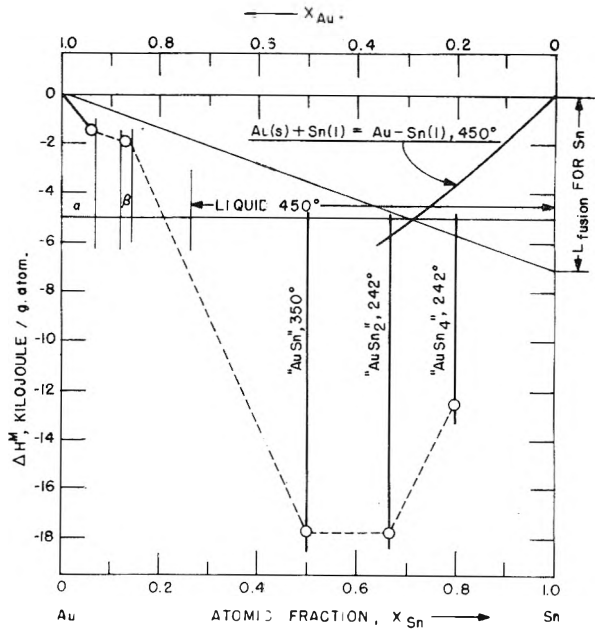

Fig. 4.—Molar heats of formation for solid and liquid gold–tin alloys.

of temperature between the melting point of tin (232°) and the temperatures of our measurements, we obtain from the present work the corresponding values −14.3 kj. (for "AuSn" at 350°) and −13.1 kj. (for "$AuSn_2$" at 242°). It is possible that part of the discrepancy between the data of Biltz, *et al.*, and those of the present work could be due to the temperature dependence of the heat of formation. For the alloy "AuSn" this was checked by use of the heat capacity data reported by Kelley.[16] It was found that the heat of formation should change by about 0.1 kj. only on going from 90 to 350°. This is less than the uncertainty of our reported value.

A value for the heat of formation of "AuSn" may also be derived from the e.m.f. study of liquid gold–tin alloys previously published by the author.[17] When the heat data for 600° obtained in this work are combined with the heat of fusion for "AuSn" given by Kubaschewski and Evans[5] (12.8 ± 0.35 kj./g. atom), we obtain for "AuSn" (from the solid elements at 418°) a ΔH^M of −12.4 kj./g. atom. In this calculation we neglected the possible temperature dependence of the heats of fusion of gold and tin, and of the heat of mixing of the liquid alloy between 600 and 418°. Now we know that liquid gold–tin alloys show considerable positive deviations from the Neumann–Kopp heat capacity rule in alloys with gold contents up to 30%.[4] If this could be taken into account for the equiatomic mixture, an even better agreement with the present work should result.

The two results on solid gold–tin alloys in the α- and β-phases given in Table IV indicate that the heat of solution of liquid tin in gold should be of the order of −30 kj./g. atom at 450°. Numerically this is roughly one-half of what we found above for liquid cadmium and indium.

(15) W. Biltz, G. Rohlffs and H. U. v. Vogel, *Z. anorg. allgem. Chem.*, **220**, 113 (1934).

(16) K. K. Kelley, U. S. Bureau of Mines, Bull. 476, 1949.

(17) O. J. Kleppa, *J. Am. Chem. Soc.*, **72**, 3346 (1950).

Gold–Antimony.—According to the equilibrium diagram given by Hansen[7] the following phases are stable at 450°

		Atomic % Sb
α	f.c.c.	0–1 (?)
L	Liquid	30–55
"$AuSb_2$"	Cubic, FeS_2-type	66.7
"Sb"	Rhombohedral, 8-N rule	?–100

Calorimetric experiments were performed with alloys of nominal composition 6, 66.7 and 95 atomic % antimony. The results are recorded in Table V.

TABLE V

MOLAR HEATS OF FORMATION OF GOLD–ANTIMONY ALLOYS AT 450°

Alloy: Composition x_{Au}, phase	Alloy: G. atoms	Tin + alloy, g. atoms	Obsd. joule	ΔH^M, kj./g. atom: Result	ΔH^M, kj./g. atom: Av.
0.939, α + L	0.01001	0.8681	197.6	+2.24	
	.01003	.8272	199.8	+2.41	
	.01004	.8200	213.8	+3.13	+2.59
.333, "$AuSb_2$"	.01075	.8052	74.3	−3.15	
	.00680	.8290	46.5	−3.12	−3.14
.050, "Sb"	.01328	.8022	180.7	+0.06	
	.01440	.8628	196.3	+0.03	+0.05

It will be noted that the alloy which contains 95% antimony shows essentially zero heat of formation. Although we have no definite information on the extent of the (small) solid solubility of gold in antimony at 450°, this confirms the positive sign of the limiting heat of solution of gold in antimony. It should be noted, however, that the alloy containing 6% Sb at 450° is $^4/_5$ α-phase and $^1/_5$ liquid alloy of $x_{Sb} \sim 0.3$. Therefore the observed positive ΔH^M for this alloy is due largely to the presence of the liquid phase.

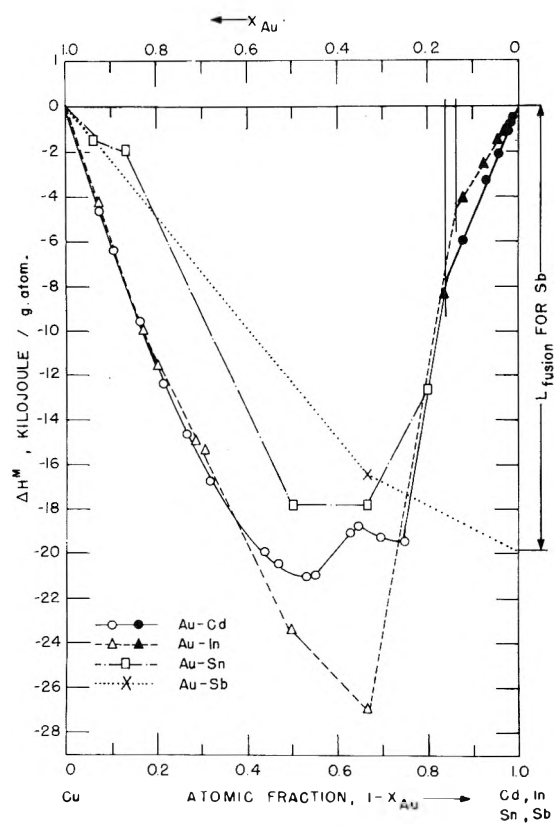

Fig. 5.—Composite graph of heats of formation for alloys of gold with cadmium, indium, tin and antimony from solid gold and liquid alloying components.

More interest is attached to the data for "$AuSb_2$," where the present investigation shows a value of −3.14 kj./g. atom at 450°. This alloy was previously studied by Biltz, *et al.*,[15] who at 90° found a ΔH^M of −4.9 kj./g. atom. Later a value of −6.7 kj. was calculated from e.m.f. work by Weibke and Schrag.[18] However, due to difficulties with operation of their gold-antimony cells, they stressed that this result was an "upper" value, and recommended a figure intermediate between their own and that of Biltz, *et al.*

We may, as we did for "AuSn," refer our heat of formation of "$AuSb_2$" to 90° by adopting heat capacity data for Au, Sb and "$AuSb_2$" recommended by Kelley.[16] As a result we find at 90° a ΔH^M of −3.9 kj./g. atom. Thus the agreement with Biltz *et al.*, is improved and must be considered as satisfactory.

Discussion

The previous papers, covering the binary alloys of copper and silver with cadmium, indium, tin and antimony,[1–3] presented a good deal of new information regarding the thermochemical properties of these alloys. As a whole this information, although restricted to the alloys stable at 450°, tended to confirm earlier conclusions which had been based almost exclusively on the appearance of the various binary phase diagrams.

(a) It was observed that the "size-effect," while very pronounced in the copper systems, seemed to be of little significance in the silver alloys.

(b) It was confirmed that the chemical interaction is of similar magnitude in the silver and copper systems, although differing significantly from one system to another.

(c) Finally it was noted that the difference in valence between the monovalent silver and copper on the one hand and the divalent cadmium, trivalent indium, etc., on the other, gives rise to interesting thermochemical similarities. In particular it was observed that the maximum values of $-\Delta H^M$ (for the solid alloys from solid components) tended to be found at electron concentrations in the range 1.5 to 1.75 electrons per atom, and that the "curvatures" of the heats of formation in the dilute regions frequently were in reasonable agreement with Friedel's predictions.[19]

As we now go on to consider the corresponding binary alloys involving gold interesting differences appear. In order to facilitate the present discussion we give in Fig. 5 a composite graph of most of the heat data for gold alloys reported above. All data in this figure relate to the formation of the alloys from solid gold and liquid alloying elements, and the curves have been drawn without regard for the many solid–solid phase boundaries in these alloy systems. As antimony is solid at 450°, the data for "$AuSb_2$" are referred to undercooled liquid antimony by adopting 19.8 kj. for its heat of fusion.

(18) F. Weibke and G. Schrag, *Z. Elektrochem.*, **46**, 658 (1940).
(19) J. Friedel, *Advances in Phys.*, **3**, 446 (1954).

The atomic radii of gold and silver are very similar. Since we observed no pronounced size effects (*i.e.*, re-entrant heat curves centered on the α-boundaries[3]) in the silver systems, it was anticipated that the same should hold true for the gold alloys. With the exception of the gold–antimony system, for which we do not have heat data in the α-field proper, this appears to be confirmed by the experimental data.

If we consider next the strength of the chemical bonding we note for gold–cadmium, gold–indium and gold–tin that the heats of formation ($-\Delta H^M$) are substantially increased compared to the silver and copper systems. However, this is not the case for gold–antimony. In a qualitative sense we may correlate the increased interaction for the three gold alloys with the increased "electrochemical factor." It should be stressed that this stronger bonding is apparent both for the heat of solution of cadmium and indium in solid gold, for the heat of solution of gold in liquid cadmium, indium and tin, and for the maximum values of $-\Delta H^M$.

Finally we observe that the valence effects which were so pronounced in the silver and copper systems have all but disappeared in the gold alloys. We find, for example, that the heats of solution of solid cadmium, indium and tin in gold (~ -60, -63 and -23 (?) kj./g. atom, respectively) are comparable in magnitude to the heats of solution of liquid gold in the three liquid metals (~ -61, -46 and -33 kj.). Similarly we find no correlations between the maxima for $-\Delta H^M$ and the electron concentrations, and no clear-cut confirmation of Friedel's curvature predictions. In fact, the observed curvatures for solutions of gold in cadmium, indium and tin appear to be positive or near zero, rather than negative (as one might have expected according to Friedel). We note also from Fig. 2 that the curvature (*i.e.*, the slope) indicated for indium in gold is not significantly larger than for cadmium in gold. We do find, however, that the curvature for cadmium in gold is very similar to the one previously obtained for cadmium in silver.[2] This may possibly be a significant point. It should finally be stressed that it is of course possible that the apparent non-applicability of Friedel's valence "rule" in the gold systems may be due to the strong interaction.[2]

Acknowledgments.—The author is indebted to Dr. K. Anderko for a preview of the manuscript for the new edition of "Hansen."[7] Many of the gold alloys were prepared with the help of Mr. Morton Kaplan. The indium metal used was a gift from the Anaconda Copper Company. The work was supported in part by the Office of Naval Research through contract No. N-6ori-02004 with the University of Chicago.

POLYMERIZATION AND DEPOLYMERIZATION PHENOMENA IN PHOSPHATE–METAPHOSPHATE SYSTEMS AT HIGHER TEMPERATURES. IV. CONDENSATION REACTIONS OF ALKALI METAL HYDROGEN PHOSPHATES[1,2]

BY R. K. OSTERHELD[3] AND M. M. MARKOWITZ

Department of Chemistry, Cornell University, Ithaca, New York

Received September 19, 1955

The reactions occurring when lithium dihydrogen orthophosphate, cesium dihydrogen orthophosphate and cesium monohydrogen orthophosphate are individually heated were studied with the use of thermal analyses, X-ray and chemical analyses, and weight loss data. Lithium dihydrogen orthophosphate decomposed at about 189° to form the dihydrogen pyrophosphate as an intermediate thermally stable at that temperature. At about 277° the rate of decomposition of the dihydrogen pyrophosphate to lithium metaphosphate became rapid. Cesium dihydrogen orthophosphate was converted at about 233° to a long-chain metaphosphate. Cesium dihydrogen pyrophosphate was an intermediate in the reaction. The conversion of cesium monohydrogen orthophosphate to cesium pyrophosphate became rapid at about 339°. These data were correlated with existing information on the alkali metal hydrogen phosphates. The relative thermal stabilities of these materials appear to depend upon the relative effects of the cations upon the hydrogen-bonding in the crystalline reactants.

The literature concerning the molecular dehydration of the alkali metal hydrogen phosphates mainly describes the ultimate products of condensation and deals principally with the sodium and potassium compounds. Little has been done to elucidate the paths of the hydrogen phosphate aggregation reactions. Extending the previous studies of this series,[4-6] investigations have been carried out on the high temperature condensation reactions of the lithium and of the cesium hydrogen phosphates. Prior work on these compounds largely neglected the reaction course.[7-10] The additional information provided by the present investi-

(1) Abstracted from a thesis submitted by M. M. Markowitz in partial fulfillment of the requirements for the degree of Doctor of Philosophy, 1953, Cornell University.

(2) This work was supported by the Office of Naval Research.

(3) Department of Chemistry, Montana State University, Missoula, Montana.

(4) R. K. Osterheld and L. F. Audrieth, THIS JOURNAL, **56**, 38 (1952).

(5) L. F. Audrieth, J. R. Mills and L. E. Netherton, *ibid.*, **58**, 482 (1954).

(6) R. K. Osterheld and R. P. Langguth, *ibid.*, **59**, 76 (1955).

(7) G. Tammann, *J. prakt. Chem.*, **45**, 417 (1892).

(8) L. Hackspill and R. Laffenberger, *Compt. rend.*, **193**, 399 (1933).

(9) H. N. Terem and S. Akalan, *Rev. faculte sci. univ. Istanbul*, **16A**, 14 (1951); *C.A.*, **46**, 4408*h* (1952).

(10) E. von Berg, *Ber.*, **34**, 4181 (1901).

gation permitted some correlation of the thermal behavior of the various alkali metal hydrogen phosphates.

Experimental Procedures

Descriptions of the experimental methods were presented in the earlier papers of this series.[4-6] All differential thermal analyses and thermal treatments in this work were carried out under low humidity conditions obtained by continuously sweeping out the furnace cavity (about 1 liter) with preheated dry air at a flow rate of about 100 ml. per minute. This procedure was adopted as a result of an observation reported below (see the beginning of the section on the thermal decomposition of lithium dihydrogen orthophosphate). Use was made of differential thermal analyses to fix the temperatures of phase changes and the temperatures at which chemical reactions became appreciable in rate. The behavior of samples at or near these temperatures was then studied by means of weight loss measurements and by chemical and X-ray analyses of the initial, intermediate and final products. The temperature measurements are considered reliable to within 3°. A reaction temperature determined by thermal analysis is the temperature at which the rate of the reaction became appreciable in a steadily heated sample and is generally not the lowest temperature at which the reaction will occur.

Orthophosphate, total phosphorus content, long-chain metaphosphate and cyclic metaphosphate contents were determined by the Jones procedure.[11] Analyses for pyrophosphate and triphosphate were by the Bell method.[12]

Lithium dihydrogen orthophosphate was prepared by treating a slurry of lithium carbonate in water with a 50% excess of orthophosphoric acid. The solution was evaporated until it became viscous. After cooling the solution, the salt was precipitated by addition of acetone. The salt thus obtained was heated with glacial acetic acid for two hours on a water-bath. The product was recovered by filtration, washed with acetone and dried to constant weight at 150°. *Anal.* of product: PO_4^{-3}, 90.6% (calcd., 91.4%).

Cesium dihydrogen orthophosphate was prepared by neutralization of a solution of 55 g. of cesium hydroxide in 200 ml. of water with 3 *N* orthophosphoric acid to the methyl orange end-point. The resulting solution was concentrated by evaporation to half its original volume, cooled, and the salt precipitated by the addition of ethanol. *Anal.* of product: PO_4^{-3}, 41.0% (calcd., 41.3%). The quantity of standard base required for titration of a sample of the product to the phenolphthalein end-point was 99.9% of the theoretical.

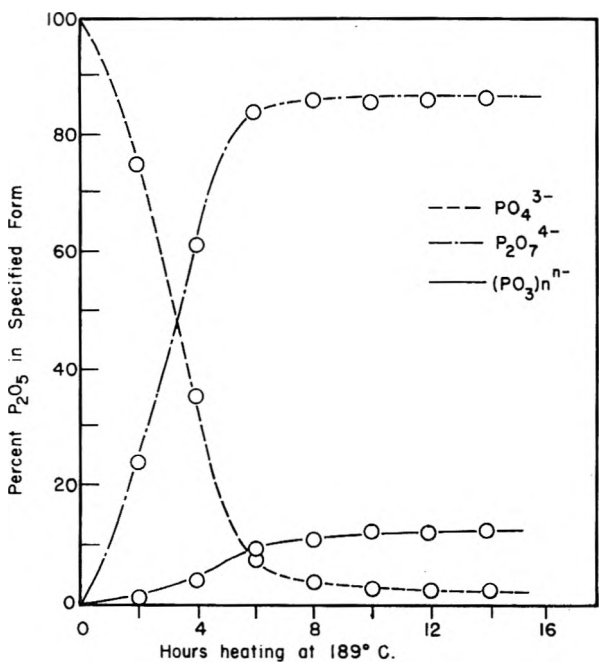

Fig. 1.—Progress of the reaction: $2LiH_2PO_4 \rightarrow Li_2H_2P_2O_7 + H_2O$.

For the preparation of cesium monohydrogen orthophosphate 3 *N* orthophosphoric acid was added to a solution of 100 g. of cesium hydroxide in 300 ml. of water until the phenolphthalein end-point was reached. The solution was evaporated until crystals appeared on the surface of the liquid. The addition of absolute ethanol to the vigorously stirred, cooled solution caused separation of an oily layer. Further heating and stirring of this layer with absolute ethanol brought about crystallization of cesium monohydrogen orthophosphate monohydrate. The crystallized product was dried at 100° for eight hours. *Anal.* of product: PO_4^{-3}, 25.0% (calcd. for the monohydrate, 25.0%). Titration of a sample of the product to the methyl orange end-point required 100.3% of the theoretical quantity of standard acid. Dehydration of the monohydrate was carried out at 145°. *Anal.* of product: PO_4^{-3}, 26.3% (calcd. for anhydrous salt, 26.3%). Both the monohydrate and the anhydrous salt were highly deliquescent.

Cesium dihydrogen pyrophosphate was prepared by heating cesium pyrophosphate with 1:1 acetic acid–water at 50° for two hours. The product was precipitated from the cooled solution by adding ethanol. It was washed with ether and dried for three hours at 60°. *Anal.* of product: $P_2O_7^{-4}$, 38.5%; total P_2O_5, 31.7% (calcd., 39.4 and 32.1%, resp.).

Thermal Decomposition of Lithium Dihydrogen Orthophosphate.—Preliminary differential thermal analyses of lithium dihydrogen orthophosphate showed the irregular appearance of an exothermic break at temperatures within the range 331–403°. This erratic behavior was found to be due to variations in the water vapor pressure within the furnace muffle. The exothermic process was found to be reproducibly absent from the thermal analysis curves when run under the low humidity conditions provided by sweeping out the furnace cavity with preheated dry air. On the other hand, the presence of a crucible of water in the furnace caused the regular appearance of the exothermic process.

Differential thermal analyses of lithium dihydrogen orthophosphate when carried out under low humidity conditions exhibited breaks at 189, 277 and 656°, all corresponding to endothermic processes. Four samples of lithium dihydrogen orthophosphate heated to constant weight at 189, 205, 225 and 230°, respectively, lost 0.550, 0.597, 0.532 and 0.537 mole of water per gram formula weight of lithium dihydrogen orthophosphate. Analytical data for the constant weight samples appear in Table IA. Analyses of samples withdrawn at regular intervals from the run at 189° are presented graphically in Fig. 1. The principal reaction at these temperatures was

$$2LiH_2PO_4 \longrightarrow Li_2H_2P_2O_7 + H_2O$$

Although considerable lithium metaphosphate was produced in a side reaction, the lithium dihydrogen pyrophosphate, once formed, was converted to lithium metaphosphate only very slowly. The 189° break was absent from the thermal analysis curves of the four constant weight materials. An X-ray diffraction pattern of the product obtained at 205° contained new lines which were attributed to lithium dihydrogen pyrophosphate.

Investigation of the processes corresponding to the 277 and 656° breaks was carried out on samples of lithium dihydrogen orthophosphate previously heated to constant weight at 230°, *i.e.*, on samples

(11) L. T. Jones, *Ind. Eng. Chem., Anal. Ed.*, **14**, 536 (1942).
(12) R. N. Bell, *Anal. Chem.*, **19**, 97 (1947).

of lithium dihydrogen pyrophosphate containing significant quantities of metaphosphate. Attempts to prepare pure lithium dihydrogen pyrophosphate by a method analogous to that used for cesium dihydrogen pyrophosphate were unsuccessful. Analytical data for the products obtained by heating lithium dihydrogen pyrophosphate samples to constant weight at 275, 280 and 285° appear in Table IB. The reaction becoming rapid at 277° must be

$$n\mathrm{Li_2H_2P_2O_7} \longrightarrow 2(\mathrm{LiPO_3})n + n\mathrm{H_2O}$$

X-Ray diffraction patterns for the analytical samples removed from the material heated at 275° showed a steady disappearance of the lines attributed to lithium dihydrogen pyrophosphate and a regular increase in the strength of a new set of lines attributed to lithium metaphosphate. There was no indication in the chemical or X-ray analyses of the formation of any stable intermediates.

The lithium metaphosphate melted at 656°, and it recrystallized on slow cooling. Quenching of the melt produced a clear water-soluble glass. End-group analyses[13] of the glass produced by quenching from 800° showed a number average chain length of twenty PO_3^- units. For the glass quenched from 1000° a chain length of eighteen units was found. The powdered lithium metaphosphate glass crystallized exothermically at 359° to produce the original metaphosphate, verified by the X-ray diffraction pattern. The crystalline lithium metaphosphate was a white, water-insoluble substance. In common with a number of insoluble metaphosphates, it was slightly soluble in pyrophosphate solutions.

Thermal Decomposition of Lithium Monohydrogen Orthophosphate.—Inability to prepare lithium monohydrogen orthophosphate prevented the investigation of its thermal decomposition. Although titration studies indicate the formation of monohydrogen orthophosphate in solution in the neutralization of orthophosphoric acid with lithium hydroxide,[14] a solid phase of lithium monohydrogen orthophosphate does not appear in the system Li_2O–P_2O_5–H_2O at 0 or 20°.[15] Attempts to crystallize the monohydrogen orthophosphate from solution produce instead the less soluble hydrated trilithium orthophosphate. For this investigation preparation by the following reactions between solids was also attempted without success

$$\mathrm{Li_3PO_4} + \mathrm{LiH_2PO_4} \longrightarrow 2\mathrm{Li_2HPO_4} \quad (a)$$

$$2\mathrm{LiH_2PO_4} + \mathrm{Li_2CO_3} \longrightarrow 2\mathrm{Li_2HPO_4} + \mathrm{CO_2} + \mathrm{H_2O} \quad (b)$$

Thermal Decomposition of Cesium Dihydrogen Orthophosphate.—Differential thermal analyses of cesium dihydrogen orthophosphate exhibited five endothermic breaks appearing at 233, 263, 330, 480 and 735°. The last two were reversible, appearing also on cooling curves. Samples of cesium dihydrogen orthophosphate heated to constant weight at 234° and at 250° each lost 1.01 moles of water per gram formula weight of the orthophosphate. Analyses of the constant weight samples are presented in Table IIA. Analytical data for samples withdrawn at regular intervals during the run at 234° appear in Fig. 2. At both temperatures the pyrophosphate content built up and then decreased, the samples finally being converted to cesium metaphosphate. The breaks at 233, 263 and 330° were absent from the thermal analysis curves for the constant weight products. On the other hand, the breaks at 263 and 330° were exhibited strongly in thermal analyses of pure cesium dihydrogen pyrophosphate prepared as stated under Experimental

(13) J. R. Van Wazer, *J. Am. Chem. Soc.*, **72**, 639, 647 (1950).
(14) Travers and Perron, *Ann. chim.*, [10] **1**, 135 (1924).
(15) A. P. Rollet and R. Lauffenberger, *Bull. soc. chim.*, [5] **1**, 146 (1934).

TABLE I

THERMAL DECOMPOSITION OF LITHIUM HYDROGEN PHOSPHATES

Temp., °C.	Heating time, hr.	% of total P as PO_4^{-3}	$P_2O_7^{-4}$	$P_3O_{10}^{-5}$	$(PO_3^-)n$[a]
A. Lithium dihydrogen orthophosphate					
189	14	2.5	86.4	0.0	11.1
205	12	1.6	82.4	0.0	16.0
225	3	0.9	91.8	0.0	7.3
230	6	0.7	89.2	0.0	10.1
B. Lithium dihydrogen pyrophosphate					
275	0[c]	0.0	93.5	0.0	6.5
	2	0.0	71.8	0.0	28.2
	4	0.0	38.6	0.0	61.4
	6	0.0	19.9	0.0	81.1
	8	0.0	13.4	0.0	86.6
	10	0.0	10.3	0.0	89.7
280	0[c]	0.0	90.7	0.0	9.3
	8	0.0	4.1	*b*	95.9
285	0[c]	0.0	89.2	0.0	10.8
	10	0.0	3.2	*b*	96.8

[a] By difference, due to solubility in presence of pyrophosphate. $(PO_3^-)_n$ refers to linear polymetaphosphate. [b] Entire titration value assigned to pyrophosphate since coprecipitation of metaphosphate with zinc pyrophosphate prevented independent determination of pyrophosphate. [c] The 0 hr. sample is the product obtained by heating lithium dihydrogen orthophosphate to constant weight at 230°.

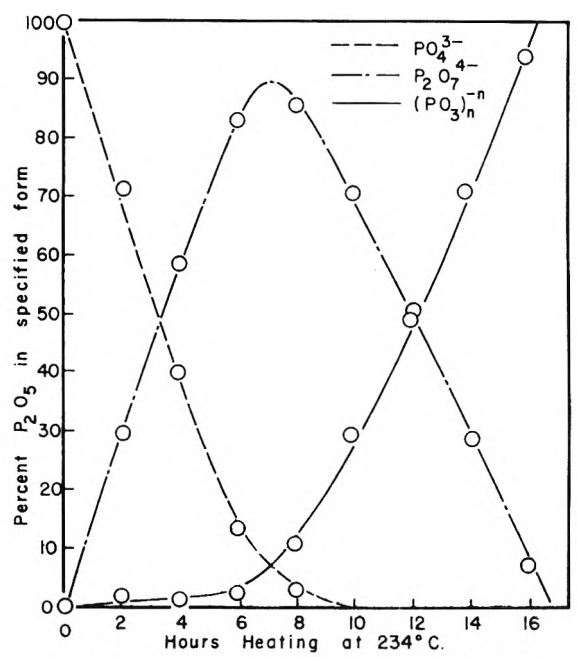

Fig. 2.—Progress of the over-all reaction: $n\mathrm{CsH_2PO_4} \rightarrow (\mathrm{CsPO_3})_n + n\mathrm{H_2O}$.

Procedures and of impure samples of cesium dihydrogen pyrophosphate prepared by heating cesium dihydrogen orthophosphate at temperatures from 234 to 300° to the loss of from half to three-quarters of the constitutional water. The 233° break was attributed to the attainment of an appreciable rate by the process

$$2CsH_2PO_4 \longrightarrow Cs_2H_2P_2O_7 + H_2O$$

The 263 and 330° breaks were associated with the cesium dihydrogen pyrophosphate and its conversion to metaphosphate, although the reaction could be carried essentially to completion at lower temperatures. Data for the conversion of cesium dihydrogen pyrophosphate to cesium metaphosphate at 250 and at 275° appear in Table IIB.

TABLE II

THERMAL DECOMPOSITION OF CESIUM HYDROGEN PHOSPHATES

Temp., °C.	Heating time, hr.	% of total P as PO_4^{-3}	$P_2O_7^{-4}$	Linear $(PO_3^-)_n$	Cyclic $(PO_3^-)_n$
	A. Cesium dihydrogen orthophosphate				
234	16	0.0	6.7	89.6	0.0
250	18	0.0	2.2	94.9	..
	B. Cesium dihydrogen pyrophosphate				
250	0	..	100.0	0.0	0.0
	22	..	3.1	95.3	0.0
275	0	..	100.0	0.0	0.0
	6	..	1.8	93.7	0.0

[a] See note *b*, Table I.

Two possible interpretations of the 263 and 330° breaks among those considered were: that a phase change or changes occurred in unreacted cesium dihydrogen pyrophosphate or that there was a change or changes in a rate controlling aspect of the process (*e.g.*, assuming the reaction to be controlled by diffusion of water away from the reaction site, an increase in the diffusion rate as the result of recrystallization of the diffusion barrier). Considerably more work will be necessary before these interpretations can be assessed. The breaks could not be attributed to changes in the molecular or crystal structure of the metaphosphate product since they did not appear in thermal analyses of cesium metaphosphate prepared at 234 or 250°. It was possible that the breaks corresponded to processes involving a reaction intermediate or side-product although any such material must have been present only in small amount. The chemical analyses generally did not account for all the phosphorus content; however, the unaccounted for portion in samples heated at 234, 250 and 275° was small (less than 5% of the phosphorus content), and X-ray patterns for the analytical samples showed no lines other than those attributable to cesium dihydrogen orthophosphate, cesium dihydrogen pyrophosphate and cesium metaphosphate. On the other hand, a sample of cesium dihydrogen pyrophosphate heated at 300° (between the temperatures of the two unaccounted for breaks) to a loss of 0.467 mole of water per mole of cesium dihydrogen pyrophosphate showed the largest amount of unaccounted for material, analyzed as: % of total P as: PO_4^{-3}, 0.0; $P_2O_7^{-4}$, 47.9; $(PO_3^-)_n$, 43.5; cyclic $(PO_3^-)_n$, 0.0; unaccounted for, 8.6%.

The cesium metaphosphate produced by the thermal decomposition of cesium dihydrogen orthophosphate or of cesium dihydrogen pyrophosphate underwent a crystallographic transition at 480° and melted at 735°. Even rapid quenching of the melt from 1000° (by dropping it into chloroform at −70°) failed to produce any glassy metaphosphate. However, the quenched material consisted of shorter metaphosphate chains than material cooled slowly from 1000°. Analyses showed the quenched material contained 5.4 wt. % of cyclic metaphosphates; the slowly cooled material contained none. End-group analyses[13] showed a number average chain length of 40 PO_3^- units for the quenched material (corrected for cyclic metaphosphate content) compared to 112 units for the slowly cooled material. The X-ray diffraction patterns of the two products were the same within the precision of the 57.3 mm. diameter camera used. The quenched cesium metaphosphate was readily soluble in water; the slowly cooled product gelled in water, dissolving slowly to give a very viscous solution.

Thermal Decomposition of Cesium Monohydrogen Orthophosphate.—An endothermic break appeared at 339° in the differential thermal analyses of cesium monohydrogen orthophosphate. Analyses of the product showed the process to be the conversion of the monohydrogen orthophosphate to cesium pyrophosphate

$$2Cs_2HPO_4 \longrightarrow Cs_3P_2O_7 + H_2O$$

The cesium pyrophosphate underwent a reversible crystallographic transition at 238° and melted at 965°.

Discussion of Results

The data reported in this paper are compared in Table III with information from previous papers of this series. The range of the reaction temperatures listed is surprisingly small (compare the thermal decomposition of carbonates: $PbCO_3$, dec. 315°; $BaCO_3$, dec. above 1000°). It is known that the $H_2PO_4^-$ anions of solid KH_2PO_4 are hydrogen-bonded into a three-dimensional network, all of the oxygen and hydrogen atoms being involved in the hydrogen bonds.[16] It may be assumed that the other dihydrogen orthophosphates listed possess structures with comparable hydrogen-bonding. The thermal decompositions of the dihydrogen orthophosphates then may all be viewed as the conversion of one type of anionic condensation (hydrogen bonding) to another (oxygen bridging). The actual details of each reaction, at least of the initiation of reaction, and of the immediate surroundings of the reaction site are probably quite similar throughout the series of reactants. This would account for the small range of reaction temperatures. The contribution of the hydrogen bonding to properties of these compounds has already been noted by Ubbelohde and co-workers. On the basis of experiments on the effects of the replacement of hydrogen by deuterium and of potassium by ammonium in potassium dihydrogen orthophosphate, it was suggested that ". . . in the acid phosphates the hydrogen bonds must make a

(16) J. West, *Z. Krist.*, **74**, 306 (1930).

TABLE III

THERMAL DECOMPOSITION OF DIHYDROGEN ORTHOPHOSPHATES

Reactant	Cation radius,[a] Å.	Reaction rate appreciable at temp., °C.	Principal initial product[b]
LiH_2PO_4	0.68	189	$Li_2H_2P_2O_7$
NaH_2PO_4	0.97	200	$Na_2H_2P_2O_7$
KH_2PO_4	1.33	208	$[K_2H_2P_2O_7]$
CsH_2PO_4	1.67	233	$[Cs_2H_2P_2O_7]$
$Pb(H_2PO_4)_2$	1.20	208	$[PbH_2P_2O_7]$
$Ba(H_2PO_4)_2$	1.34	243	$[BaH_2P_2O_7]$

[a] From L. H. Ahrens, *Geochim. Cosmochim. Acta*, **2**, 155 (1952). [b] Brackets indicate the product undergoes further decomposition at the temperature listed.

contribution to the lattice structure such that quite different arrangements of atoms can have much the same stability and lattice free energy."[17] A trend is apparent toward lower reaction temperatures with the smaller cations. This is the usual trend for the thermal decomposition of a series of salts of an oxy-acid. It is likely here that polarization of the oxygen atoms by the smaller cations weakens the oxygen-hydrogen bonds and the oxygen-phosphorus bonds, rendering them more liable to thermal rupture and also that the lighter atoms have a greater amplitude of thermal vibration leading to decomposition at lower temperatures.

(17) A. R. Ubbelohde and I. Woodward, *Proc. Roy. Soc.* (*London*), **A179**, 399 (1942).

TABLE IV

THERMAL DECOMPOSITION OF MONOHYDROGEN ORTHOPHOSPHATES

Reactant	Cation radius, Å.	Reaction rate appreciable at temp., °C.	Product
Na_2HPO_4	0.97	240	$Na_4P_2O_7$
K_2HPO_4	1.33	282	$K_4P_2O_7$
Cs_2HPO_4	1.67	339	$Cs_4P_2O_7$

The degree of hydrogen bonding in the monohydrogen orthophosphates, from purely stoichiometric considerations, must be less than in the dihydrogen orthophosphates. In the monohydrogen orthophosphates hydrogen bonding can then be expected to make a smaller contribution to the crystal properties. For a smaller range of cations, a greater range of decomposition temperatures is noted (Table IV). The trend in reaction temperature with cation size is the same as for the dihydrogen orthophosphates and for salts of oxy-acids in general.

THE APPLICATION OF THE ABSOLUTE RATE THEORY TO THE IGNITION OF PROPAGATIVELY REACTING SYSTEMS. THE THERMAL IGNITION OF THE SYSTEMS LITHIUM NITRATE–MAGNESIUM, SODIUM NITRATE–MAGNESIUM[1]

BY ELI S. FREEMAN AND SAUL GORDON

Pyrotechnics Chemical Research Laboratory, Picatinny Arsenal, Dover, N. J.

Received September 21, 1955

Upon heating intimate mixtures of finely divided alkali nitrates with powdered magnesium at temperatures greater than 480°, ignition ensues, accompanied by a highly exothermal self-propagating reaction. In this investigation, the thermal ignition of the binary systems, lithium nitrate–magnesium and sodium nitrate–magnesium, was studied by measuring the time to ignition as a function of temperature. The experimental data indicate that, to a first approximation, the duration of the induction period prior to ignition, depends upon the accumulation of a specific minimum amount of heat. By the application of the technique of differential thermal analysis, it was shown that the increase in temperature during the induction or pre-ignition stage of the reaction is relatively small. The data appear to support a proposed theory for self-propagating exothermal reactions, expressed in terms of the absolute rate theory. The derived expressions relate the time to ignition, to the specific rate, free energy, entropy and energy of activation of the pre-ignition reaction. The calculated and observed ignition times are in relatively good agreement.

Introduction

The concept of pre-ignition reactions was formulated during the latter part of the 19th century.[2] Semenov[3] expressed the relationship between the time for ignition and the temperature of the system as

$$t = A'e^{E/RT}$$

(definition of symbols in Appendix). The form of this equation is followed by a large number of propagatively reacting systems, such as explosives,[4] propellants and pyrotechnic compositions. The validity of applying this empirical relationship appears to be independently corroborated by the derivation presented in this paper, which is based upon the application of modern rate theory. The derivation also gives a physical significance to the coefficient, A, which is not apparent in the Semenov relationship. Eyring and Zwolinski[5] used the absolute rate theory to predict the minimum ignition temperature of magnesium in oxygen, but did not consider the time to ignition.

(1) This paper was presented in part, before the Division of Physical and Inorganic Chemistry at the National Meeting of the American Chemical Society in New York, Sept., 1954.

(2) Van't Hoff, "Études de Dynamique Chimique," 1884.

(3) N. Semenov, "Chemical Kinetics and Chain Reactions," Oxford, Ch. 18, 1935.

(4) H. Henkin and R. McGill, *Ind. Eng. Chem.*, **44**, 1391 (1952).

(5) H. Eyring and B. J. Zwolinski, *Rec. Chem. Prog.*, **8**, 87 (1947).

Due to the importance of this factor, expressions have been derived relating the time to ignition to the specific rate, the energy of activation, the free energy of activation and the entropy of activation of the preignition reaction. The systems lithium nitrate–magnesium and sodium nitrate–magnesium were studied by measuring the time to ignition as a function of temperature. The theoretical and experimental times to ignition are presented.

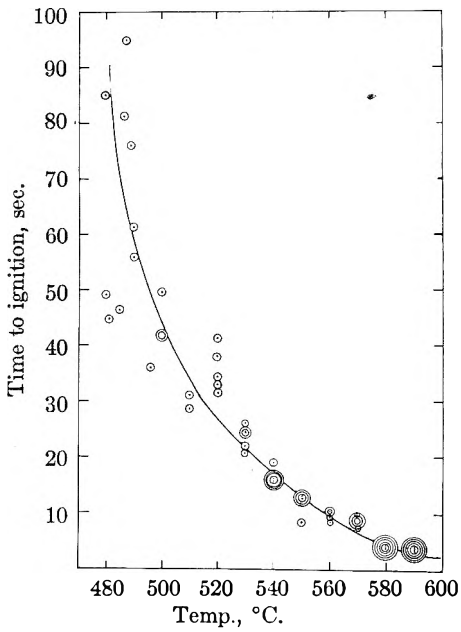

Fig. 1.—Time to ignition of mixture of 250 mg. of lithium nitrate and 25 mg. of magnesium as a function of temperature.

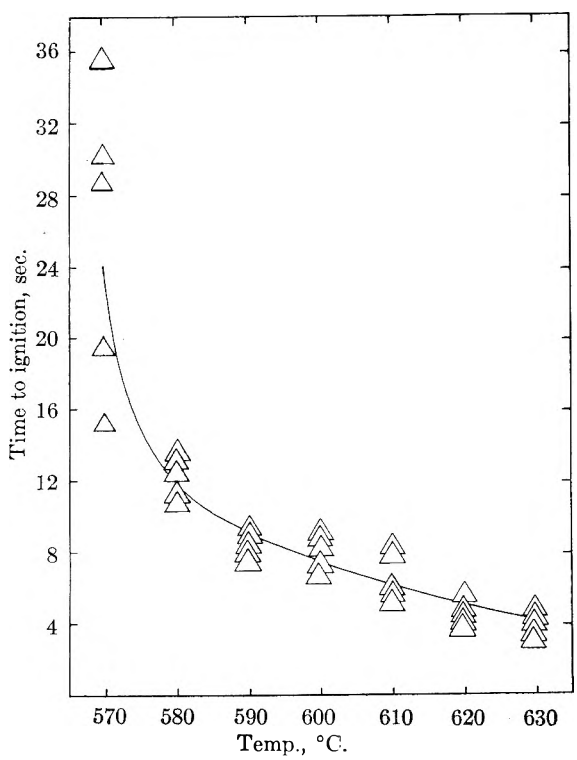

Fig. 2.—Time to ignition of mixture of 200 mg. of sodium nitrate and 100 mg. of magnesium as a function of temperature.

Experimental

The atomized (spherical) magnesium powder, 60/80 U. S. Standard Sieve fraction, specific surface 176 cm.²/g., was obtained from the Golwynne Chemical Corporation. The specific surface was measured by the air permeability method using the Picatinny Arsenal Particle Size Apparatus.[6] The lithium and sodium nitrate were purchased from the Fisher Chemical Company and are of C.P. grade. Mixtures of 200 mg. of ground sodium nitrate and 100 mg. of magnesium and 250 mg. of lithium nitrate and 25 mg. of magnesium were weighed, placed in small copper blasting caps (Special, Type 2), No. 33 B & S gauge, 5 mm. in diameter and 3 cm. long, and kept in a desiccator prior to use. The blasting caps containing the composition were plunged into a molten lead bath maintained at the desired temperature to ±2°.[7] The moment the sample entered the bath, a circuit was closed by means of a microswitch, automatically starting a timer. At the first appearance of light resulting from the reaction, the clock was stopped manually. The over-all timing error for these operations is estimated to be ±0.2 second, and is negligible with respect to the measured times. By determining the time required to melt barium nitrate crystals, it was found that when the bath temperature is 600°, it takes 0.2 second for the crystals at the inner surface of the blasting cap to attain a temperature of 590°. The equipment used for the differential thermal analyses (DTA) of the compositions, has been previously described.[8] The differential temperatures of the samples were recorded with respect to an inert substance, aluminum oxide, as the temperature of the furnace was increased at a rate of approximately 15° per minute. The compositions studied by DTA were, 5 g. of lithium nitrate–1 g. of magnesium and 5 g. of sodium nitrate–1 g. of magnesium.

Results and Discussion

From graphs of the time to ignition *vs.* temperatures, Figs. 1 and 2, it is seen that the minimum ignition temperatures of the lithium nitrate–magnesium and sodium nitrate–magnesium systems are 480 and 570°, respectively. The largest dispersion of points occurs at these values, where changes in temperature as small as 1 to 2° result in either relatively large changes in ignition time or ignition failure. This illustrates the sensitivity of the systems to the heat balance boundary condition which, when exceeded, results in ignition. The condition is that the rate of heat produced by the pre-ignition reaction equals the rate of heat dissipation.

A considerable amount of information concerning the thermal behavior of the systems during the pre-ignition reaction may be obtained from the differential thermal analyses (see Figs. 3 and 4). Figure 3, represents the reaction of sodium nitrate and magnesium. At approximately 280° an endotherm is observed, which is attributed to the rotation of the nitrate ion in the crystal followed by a lattic expansion.[9] The endotherm, at 315°, results from the melting of the sodium nitrate crystals, after which a new reference level is attained due to the greater thermal conductivity of the melt with respect to the solid.[8] No other prominent thermal effects are noted until a temperature of 550° is attained, at which point there is a sharp increase in temperature, due to a highly exothermal self-propagating reaction which is accompanied by ignition. Figure 4 shows a similar curve for lith-

(6) B. Dubrow and M. Nieradka, *Anal. Chem.*, **27**, 302 (1955).

(7) S. Gordon and C. Campbell, "Fifth Symposium (International) on Combustion," Reinhold Publ. Corp., New York, N. Y., 1954, p. 277.

(8) S. Gordon and C. Campbell, *Anal. Chem.*, **27**, 1102 (1955).

(9) S. Glasstone, "Textbook of Physical Chemistry," D. Van Nostrand Co., Inc., New York, N. Y., 1946, p. 423.

ium nitrate–magnesium. An endotherm representing a fusion is observed at approximately 268°, and at 457° there is a rapid increase in temperature, accompanied by ignition. For both compositions there is only a small increase in temperature (about 3°) prior to the rapid exothermal reaction, at which point, within several tenths of a second, ignition is observed.

Considering the time to ignition as a function of temperature, where the induction period was found to vary from 4 to 95 seconds, it appears that a relatively long, slow pre-ignition reaction occurs prior to ignition (see Figs. 1 and 2). The thermal energy accumulated by the system as the pre-ignition reaction proceeds results in a small increase in temperature. During this induction period, the rate of the pre-ignition reaction increases to a relatively small extent with the increase in temperature. As the reaction proceeds a critical region is reached in which further small changes in the temperature produce relatively large changes in the reaction rate, which is accompanied by a corresponding increase in the rate of heat evolution. At this point, the temperature and the rate of reaction accelerate rapidly and ignition ensues. This behavior may be expected since the rate of reaction is an exponential function of temperature.

A possible explanation for the relatively small increase in temperature just prior to the rapid reaction leading to ignition may be that the heat produced by the pre-ignition reaction goes into raising the surface of the metal particles to the activated state, and that the rate of formation of activated molecules is more rapid than the rate at which the activated complexes decompose to the final products. On this basis the net amount of heat evolved may be expected to be relatively small. However, since the rate of decomposition is accelerated as the concentration of activated molecules increases, it is reasonable to assume that a time will be attained when the rate of decomposition of the activated molecules to products will be comparable to that of the rate of formation of the activated state. This results in a relatively rapid evolution of heat, and an increase in surface temperature.

In order to have a self-propagating reaction the reaction rate must be rapid enough so that the net amount of heat gained due to the decomposition of an activated complex and the thermal conductivity of the composition is greater than that required to activate an adjacent molecule. Therefore, the duration of the induction period depends upon the time required to attain this condition.

Since there is only a relatively small increase in temperature during the induction period, it is assumed in the following derivation that the pre-ignition reaction occurs at a constant temperature. Consider the general pre-ignition reaction

$$aA + bB = [aA \ldots bB]^* \longrightarrow \text{products} \qquad (1)$$

The rate of reaction is given by the expression

$$v = k_s \mathcal{C}_A^a \mathcal{C}_B^b = \mathcal{C}^*_{AB} \sqrt{\frac{kT}{2\pi m^*}} \frac{K}{l} \qquad (2)$$

(see Appendix for definition of symbols).

By the appropriate substitutions[10] in equation 2,

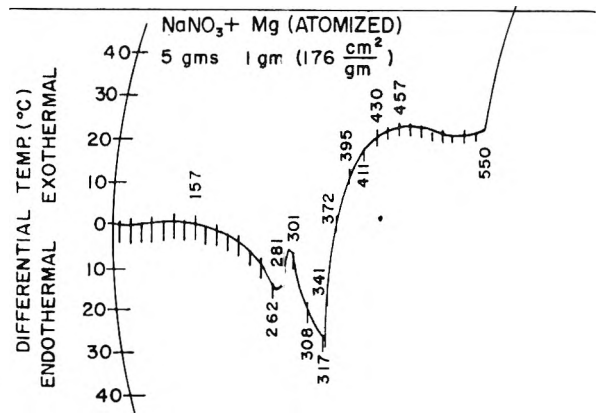

Fig. 3.—Differential thermal analysis: marks on curve appear at 1 min. intervals; temp. °C. indicated at timing marks.

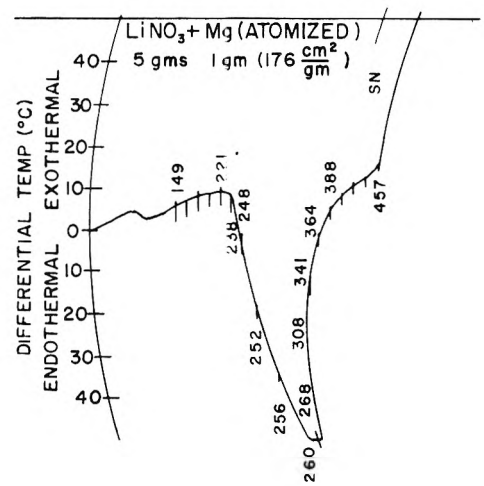

Fig. 4.—Differential thermal analysis: marks on curve appear at 1 min. intervals; temp. °C., indicated at timing marks; SN slight NO_2 fumes.

equation 3 is obtained

$$v = K \mathcal{C}_A^a \mathcal{C}_B^b \frac{kT}{h} \frac{Q^*_{AB}}{Q_A^a Q_B^b} e^{-\Delta E^*/RT} = \frac{dn}{dt} \qquad (3)$$

Multiplication of the rate of reaction and the heat of reaction gives the amount of heat evolved per unit time

$$\frac{dn}{dt} \times \Delta H_r = \frac{dH}{dt} \qquad (4)$$

Substituting equation 3 in equation 4

$$K \mathcal{C}_A^a \mathcal{C}_B^b \frac{kT}{h} \frac{Q^*_{AB}}{Q_A^a Q_B^b} e^{-\Delta E^*/RT} \Delta H_r = \frac{dH}{dt} \qquad (5)$$

The net rate of heat gain in the system dQ_H/dt is the difference between the rate of heat produced, as a result of the pre-ignition reaction, dH/dt, and the rate of heat dissipation dq/dt.

$$\frac{dQ_H}{dt} = \frac{dH}{dt} - \frac{dq}{dt} \qquad (6)$$

Separating the variables in equation 5 and integrating from time equals zero to the time for ignition, equation 7 results

$$K \mathcal{C}_A^a \mathcal{C}_B^b \frac{kT}{h} \frac{Q^*_{AB}}{Q_A^a Q_B^b} e^{-\Delta E^*/RT} \Delta H_r t = H \qquad (7)$$

(10) S. Glasstone, K. J. Laidler and H. Eyring, "The Theory of Rate Processes," McGraw-Hill Book Co., New York, N. Y., 1941, p. 187.

where H is the total heat produced by the pre-ignition reaction in the time interval zero to t.

It is assumed, for reasons previously mentioned, that ignition occurs, when

$$Q_H = H' \quad (8)$$

From equation 6 it may be seen that

$$Q_H = H - q \quad (9)$$

The condition for ignition, then, is

$$\text{If } H - q \geq H'; \text{ ignition will occur} \quad (10)$$
$$\text{If } H - q < H'; \text{ ignition will not occur} \quad (11)$$

The total heat produced by the pre-ignition reaction must be greater than H' by the amount of heat dissipated

$$H = H' + q \quad (12)$$

Transposing and solving for time in equation 7

$$t = \frac{(H' + q)h}{K\Delta H_r kT \mathfrak{A}_A^a \mathfrak{A}_B^b} \times \frac{Q_A^a Q_B^b}{Q^*_{AB}} e^{\Delta E^*/RT} \quad (13)$$

$$k_s = K \frac{kT}{h} \frac{Q^*_{AB}}{Q_A^a Q_B^b} e^{-\Delta E^*/RT} \quad (14)$$

Substituting in equation 13

$$t = \frac{H' + q}{\Delta H_r \mathfrak{A}_A^a \mathfrak{A}_B^b k_s} \quad (15)$$

Let

$$B = \frac{H' + q}{\Delta H_r \mathfrak{A}_A^a \mathfrak{A}_B^b} \quad (16)$$

$$t = B/k_s \quad (17)$$

Substituting the expression for the equilibrium constant

$$K^*_{eq} = \frac{Q^*_{AB}}{Q_A^a Q_B^b} e^{-\Delta E^*/RT} \quad (18)$$

between the activated and normal states in equation 13, equation 19 results

$$t = \frac{(H' + q)h}{K\Delta H_r \mathfrak{A}_A^a \mathfrak{A}_B^b kTK^*_{eq}} \quad (19)$$

$$K^*_{eq} = e^{-\Delta F^*/RT} \quad (20)$$

substituting in equation 19

$$t = \frac{(H' + q)h}{K\Delta H_r kT \mathfrak{A}_A^a \mathfrak{A}_B^b} e^{\Delta F^*/RT} \quad (21)$$

$$\Delta F^* = \Delta H^* - T\Delta S^* \quad (22)$$

Substituting in equation 21

$$t = \frac{(H' + q)h}{K\Delta H_r kT \mathfrak{A}_A^a \mathfrak{A}_B^b} e^{-\Delta S^*/R} e^{\Delta H^*/RT} \quad (23)$$

Let

$$A = \frac{(H' + q)h}{K\Delta H_r kT \mathfrak{A}_A^a \mathfrak{A}_B^b} e^{-\Delta S^*/R} \quad (24)$$

Substituting in equation 24

$$t = Ae^{\Delta H^*/RT} \quad (25)$$

The coefficient A is a function of the activity of the reactants and the absolute temperature. If the activities of the reactants do not change significantly during the pre-ignition reaction, the logarithm of the time to ignition should be a linear function of the reciprocal of the absolute temperature over relatively short temperature ranges. It is also apparent from the relationship that the heat of activation may be calculated from the slope of the line.

A plot of $\log t$ *vs.* T^{-1} shows this linear relationship for the sodium nitrate–magnesium system. The heat of activation, which is approximately equal to the activation energy, was calculated to be 32 kcal. per mole. A linear relationship is also observed for the lithium nitrate–magnesium system and the heat of activation was calculated to be 34 kcal. per mole.

Using equation 13, theoretical values for the time to ignition were calculated and compared with the observed results (see Table I). The values of $(H' + q)$ are approximately equal to the heats of activation, 32 kcal. per mole and 34 kcal. per mole for the sodium nitrate–magnesium and lithium nitrate–magnesium systems, respectively. The transmission coefficient, K, was taken to be unity. Since the oxidant is in the molten state, the activity of the magnesium surface was taken as the number of moles of oxidant on the surface of a particle per mole of magnesium (bulk), and were calculated to be 3.94×10^{-7} and 5.91×10^{-7} for the sodium nitrate–magnesium and lithium nitrate–magnesium systems. The activity of the sodium nitrate, which is in excess, is assumed to be unity. The calculations of the heats of reaction, ΔH_r, at 25° were based upon the reaction between metal and oxidants to form magnesium oxide and sodium or lithium nitrite. The values are 125 kcal. per mole magnesium or oxidant and 117 kcal. per mole magnesium or oxidant for the reactions between sodium nitrate and magnesium and lithium nitrate and magnesium, respectively. Since the difference between the activated and normal states of a molecule is the conversion of a vibrational degree of freedom to a translational degree of freedom, the partition function term (Q/Q^*) was calculated to be approximately unity. The values for Planck's and Boltzman's constants are 6.62×10^{-27} erg sec. and 1.38×10^{-16} erg per °K. The calculated results are in good agreement with the observed data considering the magnitude of the numbers and assumptions involved.

TABLE I

COMPARISON BETWEEN CALCULATED AND OBSERVED TIMES TO IGNITION

System	Temp., °C.	Time, sec. Calcd.	Time, sec. Obsd. (Range)
$NaNO_3$–Mg	570	8	15–36
	580	6	11–14
	600	4	7–9
	630	2	4
$LiNO_3$–Mg	480	282	45–95
	520	83	32–41
	590	13	3–5

The logarithms of the times to ignition for mixtures varying in composition from 20 to 50% magnesium having specific surfaces from 176 to 650 cm.^{2}/g. were also found to be linear functions of T^{-1}. The ignition times were effected to a relatively small extent, considering the type of measurement, increasing by 10 to 30%, with increases in magnesiun concentration and specific surface. The slopes remained essentially unchanged.

Acknowledgment.—Acknowledgment is made to A. Tomichek for obtaining the ignition temperature data presented in this investigation. The authors wish to express their gratitude to D. Hart for reviewing this manuscript.

Appendix

A' = constant
A = constant
$\mathfrak{A}$ = activity
ΔE^* = energy of activation
ΔH^* = heat of activation
h = Planck's constant
H = total heat produced by pre-ignition reaction
H' = min. amount of heat required to raise the temp. of system to the point of ignition
k_s = specific rate
k = Boltzmann's constant
K = transmission coefficient
l = length of coördinate of decomposition
m^* = mass of activated complex
Q = partition function
R = gas constant
ΔS^* = entropy of activation
T = absolute temp.
t = time
ΔH_r = heat of reaction per mole magnesium
dH/dt = rate of heat produced by pre-ignition reaction
dQ_H/dt = net rate of heat gain in system
dn/dt = no. of moles of activated complex traveling over the potential energy barrier per unit length of the decomposition coördinate per unit time
dq/dt = rate of heat dissipation
* = designates activated state

THE EFFECT OF SOME CORROSION INHIBITORS AND ACTIVATORS ON THE HYDROGEN OVERPOTENTIAL AT Fe CATHODES IN NaOH SOLUTIONS

BY I. A. AMMAR AND S. A. AWAD

Chemistry Department, Faculty of Science, Cairo University, Cairo, Egypt

Received October 10, 1955

Hydrogen overpotential, η, at Fe cathodes is measured in pure NaOH solutions at 25°. Measurements are also carried out in 0.2 *N* NaOH solutions to which the following organic substances have been added: ethylamine, *n*-butylamine, dimethylamine, tri-*n*-propylamine, benzylamine, pyridine, quinoline, picric acid, *p*-benzoquinone and *m*-dinitrobenzene. The numerical increase of η upon addition of the organic substance is explained on the basis of a decrease in the available surface area for hydrogen discharge. On the other hand, the numerical decrease of η is probably caused by the depolarization of the hydrogen evolution reaction. An alternative explanation of the results is based on the assumption that either an attraction or a repulsion, between the adsorbed atomic hydrogen and the organic molecules, take place.

Introduction

The inhibition, by organic compounds, of the corrosion of iron in acid solutions was studied by Mann, Lauer and Hultin.[1] They observed that with mono-aliphatic amines, the efficiency of corrosion inhibition increased with the length of the aliphatic chain. Furthermore, the efficiency increased as the number of radicals attached to the nitrogen increased to three. With aromatic amines the efficiency was dependent on the nature and the size of the inhibitor.

Various theories were put forward to explain the action of organic inhibitors. Thus Chappell, Roetheli and McCarthy[2] concluded that the inhibition of corrosion was caused by a resistive film on the surface of iron. Bockris and Conway[3] measured the hydrogen overpotential, η, at an iron cathode, in the presence and absence of corrosion inhibitors and activators, in acid solutions. They observed a rise in η toward more negative values in the presence of inhibitors. In the presence of activators η was numerically decreased. Furthermore, they observed that the direct and the indirect methods of measuring overpotential gave the same results. From this they concluded that the inhibition and activation of corrosion were directly related to the hydrogen activation overpotential rather than to the formation of a surface film. Hackerman and Makrides[4] explained the effect of inhibitors on the basis of general adsorption, *i.e.*, weak physical adsorption, electrostatic attraction between the inhibitor ion and the metal and chemisorption resulting in the formation of a dative bond between the inhibitor and the metal.

The aim of the present investigation is to study the effect of corrosion inhibitors and activators on the hydrogen overpotential at iron cathodes in NaOH solutions.

Experimental

Hydrogen overpotential was measured in an electrolytic cell similar to that described by Bockris.[5] The cell consisted of four compartments: the anode compartment, the cathode compartment, the hydrogen electrode compartment and the inhibitor (or activator) compartment. A sintered glass disc was inserted between the first two compartments to minimize the diffusion of gaseous anodic products toward the cathode. Diffusion of atmospheric oxygen into the cell was hindered by the use of water-sealed taps and ground glass joints for the construction of the cell. Electrical contact between the cathode and the reference hydrogen electrode was made through a Luggin capillary (internal diameter 1 mm.). Hydrogen, previously purified by passing it over hot copper (450°) and then over soda lime, was introduced into the cell and was divided between the four compartments.

The iron electrode, in the form of a pure iron strip[6] sealed to glass, was introduced into the cathode compart-

(1) C. A. Mann, B. E. Lauer and C. T. Hultin, *Ind. Eng. Chem.*, **28**, 159 (1936).

(2) E. L. Chappell, B. E. Roetheli and B. Y. McCarthy, *Ind. Eng. Chem.*, **20**, 582 (1928).

(3) J. O'M. Bockris and B. Conway, THIS JOURNAL, **53**, 527 (1949).

(4) N. Hackerman and A. C. Makrides, *Ind. Eng. Chem.*, **46**, 523 (1954).

(5) J. O'M. Bockris, *Chem. Revs.*, **43**, 525 (1948).

(6) A "Hilger" pure iron strip, prepared by Hilger and Co., London, England.

ment through a ground glass tube sealed to the top of this compartment. Two electrodes were used: one as a pre-electrolysis electrode and the other as a test electrode. The test electrode was adjusted to touch the tip of the Luggin capillary.

The cell was cleaned with a mixture of pure chromic and sulfuric acids. This was followed by washing with distilled water and then with conductance water. The electrodes, previously washed with conductance water, were then fixed in their positions in the cell. The cell was filled completely with conductance water and this water was completely displaced by pure hydrogen before the NaOH solution and the inhibitor (or the activator) were introduced.

NaOH solutions were pre-electrolyzed[6] for 12 hours at 10^{-2} a.cm.$^{-2}$, on the pre-electrolysis iron electrode. After pre-electrolysis, the test iron electrode was lowered into the solution and the Tafel line was traced between 10^{-2} and 10^{-6} a.cm.$^{-2}$. The electrode was then drawn out of the solution and the polarizing potential was adjusted such that a current of 2 ma. (2.5×10^{-3} a.cm.$^{-2}$) would flow through the electrode–solution interface when the electrode was again introduced into the solution. The electrode potential was then traced as a function of time till a constant value of η was attained. The previously de-oxygenated corrosion inhibitor or activator was then added to the solution in the cathode compartment to prepare a solution of known strength. The cathode potential was again traced as a function of time till a constant value was again attained. All measurements were carried out at 25° using the direct method. The potential was measured with a valve *p*H meter-millivoltmeter and the current with a multirange micro milli-ammeter. The current densities were calculated using the apparent surface areas.

The following amines were used: ethylamine, dimethylamine, *n*-butylamine, tri-*n*-propylamine, benzylamine, pyridine and quinoline. Pyridine and quinoline were used as liquids. The other amines were used as hydrochlorides. The hydrochlorides were twice crystallized before the solution was prepared. The effect of the addition of picric acid, *p*-benzoquinone and *m*-dinitrobenzene on η also was studied. The first two were dissolved in water and the third was dissolved in ethyl alcohol.

Results

Figure 1 shows three typical Tafel lines for hydrogen overpotential at iron cathodes in pure 0.2, 0.5 and 1.0 *N* aq. NaOH solutions at 25°. Each of these three Tafel lines is the mean of six individual lines. It is clear from this figure that at the low current density range, dissolution of iron causes the Tafel lines to become parallel to the log c.d. axis at potentials negative with respect to the potential of the reversible hydrogen electrode. The Tafel line slope varies between 0.120 and 0.130 v.

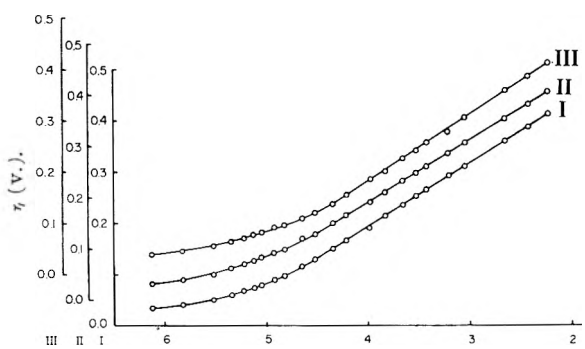

Fig. 1.—I, 0.2 *N* NaOH, b = 0.125 v.; II, 0.5 *N* NaOH, b = 0.120 v.; III, 1.0 *N* NaOH, b = 0.130 v.

Figure 2 shows the effect of the addition of ethylamine and *n*-butylamine on the steady-state value of η at 2.5×10^{-3} a.cm.$^{-2}$, in 0.2 *N* NaOH solution. Thus, the numerical increase of η in the case of 0.1 *M* ethylamine is 40 mv., whereas for 0.1 *M* *n*-butylamine it is 120 mv. The time at which the amine is added is marked by a cross. The time is reckoned from the start of polarization.

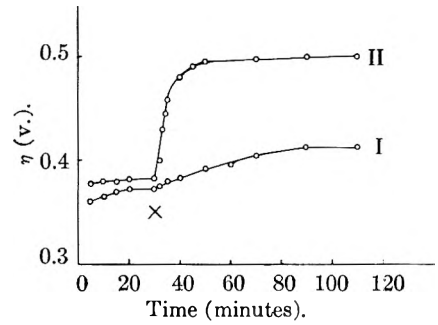

Fig. 2.—I, 0.1 *M* ethylamine; II, 0.1 *M* *n*-butylamine.

Figure 3 shows the effect of dimethyl- and tri-*n*-propylamine on η. Thus, 0.1 *M* dimethylamine causes a numerical decrease of about 7 mv. in the steady-state value of η, while 0.01 *M* tri-*n*-propylamine decreases η by 40 mv.

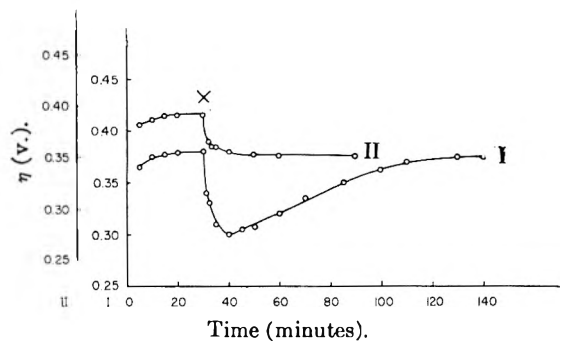

Fig. 3.—I, 0.1 *M* dimethylamine; II, 0.01 *M* tri-*n*-propylamine.

The effect of aromatic amines is shown in Fig. 4. Benzylamine (0.1 *M*) increases η numerically by about 18 mv., whereas 0.1 *M* pyridine causes an increase of 30 mv. A saturated solution of quinoline increases η by 70 mv.

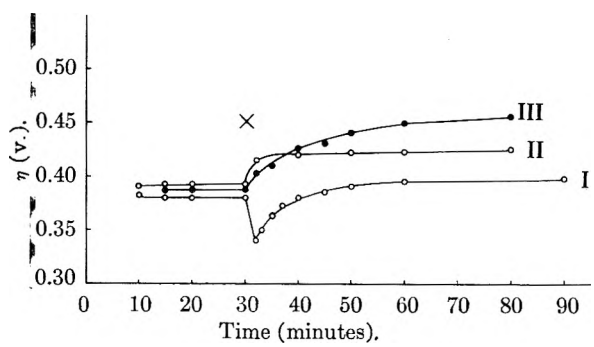

Fig. 4.—I, 0.1 *M* benzylamine; II, 0.1 *M* pyridine; III, satd. quinoline.

Figure 5 shows the effect on η of the corrosion activators: *p*-benzoquinone, picric acid and *m*-dinitrobenzene. For 0.01 *M* *p*-benzoquinone η numerically decreases by 20 mv. For the same concentration of *m*-dinitrobenzene and picric acid

the decrease in η is 100 and 200 mv., respectively. The dotted line in Fig. 5 indicates that η becomes positive between 30 and 38 minutes.

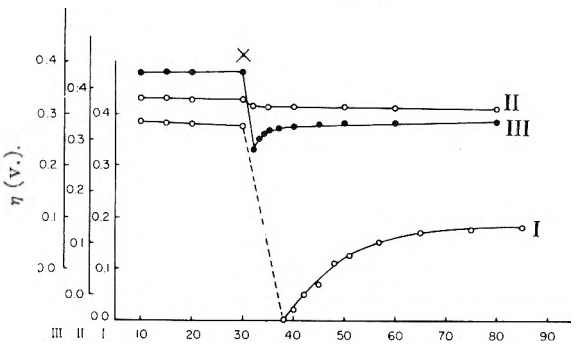

Fig. 5.—I, 0.01 *M* picric acid; II, 0.01 *M* *p*-benzoquinone; II, 0.01 *M* *m*-dinitrobenzene.

The effect of the concentration, C, of corrosion inhibitors or activators on η is given in Table I. Thus, for amines, η numerically increases with increase of concentration. For corrosion activators such as picric acid η numerically decreases with increase of concentration.

TABLE I

Substance	Concn., moles/l.	η (mv.)
Ethylamine	10^{-1}	417
	10^{-2}	382
	10^{-3}	350
Dimethylamine	10^{-1}	375
	2×10^{-2}	355
	10^{-3}	313
n-Butylamine	10^{-1}	500
	10^{-2}	398
	10^{-3}	293
Picric acid	10^{-2}	180
	10^{-3}	325

Discussion[7]

The mechanism of the cathodic hydrogen evolution at iron electrodes in pure NaOH solutions is probably governed by a rate-determining slow discharge step. This conclusion is based upon the value of the Tafel line slope (*cf.* Fig. 1). The facts that the Tafel line slope lies between 0.120 and 0.130 v. and that only one slope is observed in the linear logarithmic section of the line indicates a rate-determining slow discharge process.[8] In alkaline solutions, it is probable that the discharge takes place from water molecules.[9] It has been suggested by Bockris and Conway[3] that the inhibition and activation of corrosion are caused by changes in the activation overpotential. The reason for the fact that some substances numerically increase η while some others decrease η is not clear.

The numerical increase of η upon addition of some organic substances may be attributed to a decrease in the available surface area for hydrogen discharge, thus increasing the current density. The fact that η is numerically greater in the case of 0.1 *M* *n*-butylamine than in the case of 0.1 *M* ethylamine (*cf.* Fig. 2) may be ascribed to a stronger adsorption in the former than in the latter case. Similar observations have been reported by Swearingen and Schram.[10] The increase in the efficiency of corrosion inhibition in the case of *n*-propylamine than in the case of ethylamine has been attributed by the above authors to a stronger adsorption in the case of *n*-propylamine than in the case of ethylamine. The results obtained for benzylamine, pyridine and quinoline (Fig. 4) may also be explained on the basis of a decrease in the available surface area for hydrogen discharge.

It has been pointed out by Hackerman and Sudbury[11] that amines are incapable of undergoing cathodic reduction under conditions existing in corrosion. For this reason it is difficult to explain the decrease of η in the case of dimethylamine and tri-*n*-propylamine on the assumption that such amines depolarize the hydrogen evolution reaction. On the other hand the results of Fig. 5 may be attributed to the depolarization of the hydrogen evolution reaction by reducible substances such as picric acid, *p*-benzoquinone and *m*-dinitrobenzene.

The fact that in some cases (*cf.* Fig. 3, 4 and 5) the decrease of η after the addition of the organic substance is followed by an increase of η cannot be explained on the basis given above. In the following discussion an alternative explanation of the results obtained in the present investigation is given.

At the steady state, before the organic substance is added, the cathode surface is covered to a certain extent with adsorbed atomic hydrogen. Upon addition of the organic substance, part of this substance is transferred to the electrode surface by diffusion. Assuming for simplicity that the adsorbed hydrogen is then surrounded by organic molecules, also adsorbed on the surface, one of the following two processes may take place: (1) a repulsion between the adsorbed atomic hydrogen and the organic molecules, or (ii) an attraction, or even a chemical reaction, between the above two entities. If the heat evolved for the adsorption of one atom of hydrogen on a bare metal surface is designated by ϵ, the heat of adsorption ϵ', also for one atom of hydrogen, on a surface partly covered with the organic substance is given by [12]

$$\epsilon' = \epsilon \pm S\theta E \qquad (1)$$

where S is the number of adsorption sites, occupied by the organic molecules, in the near neighborhood of the site occupied by adsorbed atomic hydrogen, θ is the surface coverage and E is the interaction energy per molecule of the organic substance. The plus and minus signs refer to attraction and repulsion interactions, respectively. For the adsorption of one gram atom of hydrogen, equation 1 becomes

$$A = \epsilon' N = \epsilon N \pm S\theta NE \qquad (2)$$

where N is Avogadro's number.

(7) The European convention of sign of potential is used.

(8) J. O'M. Bockris and E. C. Potter, *J. Electrochem. Soc.*, **99**, 169 (1952).

(9) J. O'M. Bockris and E. C. Potter, *J. Chem. Phys.*, **20**, 614 (1952).

(10) L. E. Swearingen and A. Schram, THIS JOURNAL, **55**, 180 (1951).

(11) N. Hackerman and J. D. Sudbury, *J. Electrochem. Soc.*, **97**, 109 (1950).

(12) S. Glasstone, K. Laidler and H. Eyring, "The Theory of Rate Processes," McGraw-Hill Book Co., New York, N. Y., 1941, p. 364.

The relation between η and the heat of adsorption, A, has been given as[13]

$$(d\eta/dA) = (1/\alpha F) \quad (3)$$

where α is the transfer coefficient. From (2) and (5) one gets

$$\eta = \frac{\epsilon N \pm S\theta NE}{\alpha F} + C \quad (4)$$

where C is an integration constant. ϵ and S may be taken as constants for a constant surface structure, and E is a constant for each organic substance. Differentiating η with respect to θ one gets

$$(d\eta/d\theta) = \pm \frac{SNE}{\alpha F} \quad (5)$$

The increase of θ with time (after the addition of the organic substance) is directly proportional to the rate, V, of the diffusion of this substance to the electrode surface, thus

$$(d\theta/dt) = C'V \quad (6)$$

where C' is a proportionality constant. From (5) and (6) one gets

$$(d\eta/dt) = \pm \frac{SNE}{\alpha F} C'V \quad (7)$$

Equation 7 indicates that for an attraction, or a chemical reaction, between the adsorbed hydrogen and the organic substance, *i.e.*, when E is positive η increases with time. In other words η numerically decreases with time. On the other hand a repulsion interaction results in a numerical increase of η with time. The fact that $(d\eta/dt)$ is not always linear (*cf.* Figs. 2, 3, 4 and 5) after the addition of the organic substance may be attributed to the change of V with time. As the rate of diffusion decreases with time, $(d\eta/dt)$ numerically decreases until η is almost constant at a comparatively large time of polarization.

On the basis of the above discussion, the results obtained for ethylamine, *n*-butylamine (Fig. 2), pyridine and quinoline (Fig. 4) indicate a repulsion between the adsorbed hydrogen and the organic molecules. On the other hand, the results for tri-*n*-propylamine (Fig. 3) and *p*-benzoquinone (Fig. 5) indicate an attraction between the organic substance and the adsorbed hydrogen. Although the assumption of attraction and repulsion may explain some of the results obtained in this investigation, yet it fails to account for the fact that in some cases (*cf.* Figs. 3, 4 and 5) the numerical decrease of η observed after the addition of the organic substance is followed by a numerical increase of η at a comparatively large time of polarization. Similar observations have been reported by Bockris and Conway[3] for nitrobenzene.

The time effect may be that caused solely by the displacement of hydrogen atoms (or some other sorbed material) by the inhibitor. With activators the displacement could occur either simultaneously or prior to the depolarization, but the final step in each case is adsorption of the organic substance.

The authors wish to express their thanks to Prof. A. R. Tourky for helpful discussion.

(13) P. Ruetschi and P. Delahay, *J. Chem. Phys.*, **23**, 195 (1955).

A KINETIC STUDY OF METHYL CHLORIDE COMBUSTION

BY HUBERT T. HENDERSON AND GEORGE RICHARD HILL

Department of Fuel Technology, University of Utah, Salt Lake City, Utah

Received October 31, 1955

A study of the burning of methyl chloride has been carried out by the tube method of Gerstein, Levine and Wong.[1] Burning velocity data have been taken in air and in oxygen. The burning velocity and limit data for methyl chloride are compared with methane and methyl alcohol and with some other chlorinated hydrocarbons. In addition, the influence of tube diameter for the Gerstein, *et al.*, tube method has been studied and found to be much the same as for the Coward-Hartwell[2] method. A new generalized procedure for calculating flame front areas has been used.

Introduction

The work presented here is a part of an over-all program to determine the effect of substituent groups in the fuel molecule on the rate of burning. For this work the simplest member of the paraffin series, methane, has been chosen as a reference. The effect of the substitution of an OH group for an H atom in methane has been studied and previously reported.[3,4] The work reported here concerns itself with the effects of substituting a Cl for an H atom in methane. It is believed that such studies as these will assist in gaining a better understanding of the mechanism of hydrocarbon burning.

(1) M. Gerstein, O. Levine and E. L. Wong, *J. Am. Chem. Soc.*, **73**, 418 (1951).

(2) H. F. Coward and F. J. Hartwell, *J. Chem. Soc.*, Pt. 2, 2676 (1932).

(3) W. H. Wiser and G. R. Hill, "The Kinetics of Combustion of Methyl Alcohol," Tech. Rpt. No. 4, Air Force Combustion Contract No. AF 33 (038) (20839), University of Utah, 1952.

(4) W. H. Wiser and G. R. Hill, "A Kinetic Comparison of the Combustion of Methyl Alcohol and Methane," Fifth Symposium on Combustion, Williams and Wilkins, Baltimore, Md., 1955.

Experimental Apparatus and Procedure

The apparatus used for determining burning velocities has been patterned after Gerstein, *et al.*[1] Pyrex combustion tubes, open at both ends, were used in a horizontal position. Mixtures were ignited in all cases by a methyl chloride–oxygen flame seated on a porous glass plug burner tip. Burning mixtures were prepared by a partial pressure method and thoroughly mixed prior to introduction into the combustion tube. The combustion tubes were fitted with the appropriate orifices to give stable, constant burning rates. Observed flame velocities were measured by means of balanced photomultiplier tubes placed behind collimating slits spaced 15.22 cm. apart near the end opposite the point of ignition. The time between impulses from these tubes as the flame front passed gave the flame velocity, U_0.

The flame fronts were photographed by means of an electronically actuated Speedgraphic camera at a shutter speed of $^1/_{400}$ second. Flame areas, A_f, were calculated by a method which will be discussed.

The translation velocity of the gas, U_g, in which the flame front propagates was measured by the soap bubble technique described by Gerstein.[1]

If the burning rate is assumed constant over the entire flame front, then the burning velocity may be expressed as

$$U_f = (U_0 - U_g)\frac{A_t}{A_f} \qquad (1)$$

where A_t is the tube cross sectional area. Since the burning rate decreased to zero near the tube wall, this expression actually gives an average burning rate, slightly lower than exists over most of the flame front.

All data were obtained at room temperature, 25°, and atmospheric pressure, 650 mm.

To check the influence of tube diameter three standard Pyrex tube sizes were used. The dimensions of these are given in Table I.

TABLE I

COMBUSTION TUBE DIMENSIONS

Pyrex tube size, cm.	Inside diameter, cm.	Distance between orifices, cm.
3.2	2.8	64
2.8	2.4	64
2.5	2.14	64

Results and Discussion

The burning velocity–composition curves for methyl chloride, methanol, and methane in air are shown in Fig. 1, and the corresponding calculated equilibrium flame temperatures are shown in Fig. 2. It is interesting that while the flame temperatures for methyl chloride are slightly higher than for methane, the burning velocities are much lower. In fact, for methyl alcohol, methane and methyl chloride the relative maximum burning velocities are 4.14, 3.31, 1, respectively. The very low burning velocities of methyl chloride indicate self-inhibition by Cl atoms or chlorine compounds, *e.g.*, HCl.

If the slow rate of burning is due to inhibition by chlorine, then one might expect the slowing effect to be greatest where the population of Cl atoms in the fuel molecule is highest. The burning velocities of the straight chain paraffin hydrocarbons differ but little. The burning velocity of methyl chloride is compared with similar values from the literature for some chlorinated hydrocarbons in Table II. The values of the ordinary paraffin hydrocarbons also are shown.

If the simplified assumptions are made that (1) the concentration of free radical chain carriers is proportional to the carbon and hydrogen atom population in the fuel molecule, and that (2) the chain inhibition is proportional to the population of chlorine atoms in the fuel molecule, then the burning velocity may be assumed to be roughly inversely proportional to the chlorine atom population in the fuel molecule. If it is assumed further that methane, propane and butane burn by similar mechanisms, each inhibited in the corresponding chlorinated fuels, then the ratio of the burning velocities of the chlorinated hydrocarbons should be approximately the same as the ratio of the reciprocals of the Cl/total atoms in the fuel molecule.

$$K = C/N_{Cl}$$

where

K = rate constant
C = proportionality constant, dependent on the uninhibited mechanism and transport properties
N = mole fraction of chlorine in the fuel molecule

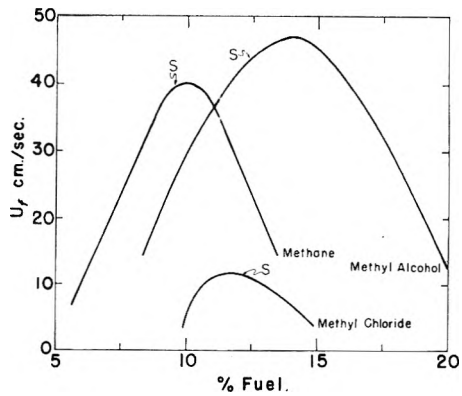

Fig. 1.—Burning rate *versus* composition for fuel-air systems: S, stoichiometric; methane data = bunsen burner[37]; methyl alcohol data = horizontal tube 2.74 cm. i.d.; methyl chloride data = horizontal tube 2.8 cm. i.d.

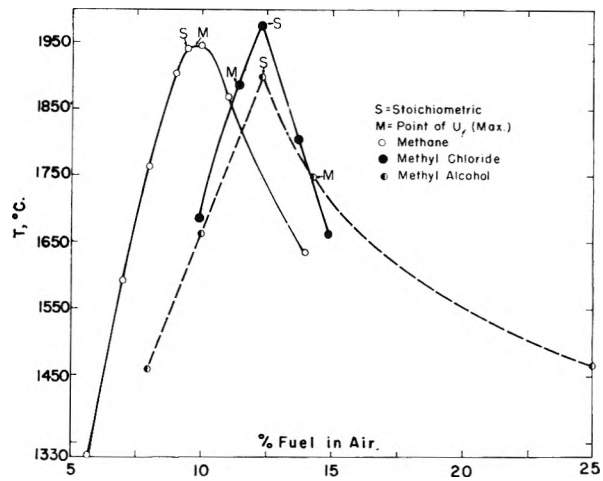

Fig. 2.—Equilibrium flame temperatures for fuel-air systems.

TABLE II

BURNING VELOCITIES OF STOICHIOMETRIC MIXTURES OF SOME PARAFFIN AND CHLORINATED HYDROCARBONS

Compound	Exptl. method	U_f, cm./sec.
CH_3Cl	Horizontal tube	10.9[a]
$CH_3CH_2CH_2Cl$	Bunsen burner	27.5[b]
$CH_3CHClCH_3$	Bunsen burner	27.4[b]
$CH_3CH_2CH_2CH_2Cl$	Bunsen burner	31.6[b]
CH_4	Bunsen burner	38.9[b]
CH_4	Bunsen burner	36.3[c]
$CH_3CH_2CH_3$	Bunsen burner	44.0[b]
$CH_3(CH_2)_2CH_3$	Bunsen burner	44.8[b]

[a] This research. [b] From Calcote and Gibbs.[5] [c] From Wiser and Hill.[3]

The ratio of burning velocities for stoichiometric mixtures in air of methyl, propyl and butyl chloride is 1.0, 2.35, 2.7. The corresponding ratio of K values from equation 2 is 1.0, 2.2, 2.8. The correspondence between actual burning velocities and the relative predictions from such an over-simplified theory is rather remarkable. A burning velocity for ethyl chloride could not be found in the literature, but from the foregoing analysis would be

(5) H. F. Calcote and G. Gibbs; J. B. Fenn and H. F. Calcote, Fourth Symposium on Combustion, Williams and Wilkins, Baltimore, Md., 1953, p. 231.

predicted to be about 19 cm./sec. for a stoichiometric fuel–air mixture.

Similar evidence for chlorine inhibition exists in the comparison of the flammability limit data of methyl chloride with other chlorinated hydrocarbons and their respective hydrocarbons. Some of these lower limit data are shown in Table III.

TABLE III

LOWER LIMITS AND CORRESPONDING CALORIFIC VALUES OF FUEL-AIR MIXTURES

Fue	Lower limit % fuel	Heat of combustion of gaseous fuel, kcal./g. mole[a]	Relative calorific value, lower limit mixt., kcal./g. mole
CH_4	5.64[7]	210.8	11.9
CH_3Cl	9.7[a]	164.2	15.9
CH_3CH_3	3.2[8]	368.4	11.7
CH_3CH_2Cl	4.25[8]	316.7	13.4
$CH_3CH_2CH_3$	2.4[8]	526.3	12.6
$CH_3CH_2CH_2Cl$	2.6[9]	478.3	12.4

[a] Data of this research.

The more fuel-rich lower limit for methyl chloride than for methane again harmonizes with the chlorine inhibition theory, but it will be noticed from Figs. 1 and 2 that methyl chloride has a more fuel-rich upper limit than methane, which might seem inconsistent with the chlorine inhibition argument. Upper limits are usually governed by the composition at which a critical concentration of oxygen is reached. In this connection it will be noted that only 3/2 O_2 are required to burn completely a CH_3Cl molecule. Thus, one would expect the upper limit, neglecting inhibition effects, to be richer in fuel for methyl chloride than for methane. The upper limit for methane–air mixtures is at 95.8% of stoichiometric oxygen, while methyl chloride burning appears to be inhibited also at upper limit mixtures. It should also be noted that the flame temperature at the upper limit is higher for methyl chloride–air than for methane–air flames (Fig. 2).

It is well known that the lower limit mixtures of many fuel–air systems are characterized by nearly identical calorific values.[10-12] This is especially true of the lower members of the paraffin series. The unit mixture calorific value is proportional to both the heat of combustion and the per cent. of fuel at the lower limit. The effect of chlorine inhibition is to increase the lower limit values, but would be expected to have decreasing effect with decreasing population of chlorine atoms in the fuel molecule. Qualitative agreement with chlorine inhibition theory is seen in the convergence of the calorific values of lower limit mixtures of chlorinated paraffins toward that for methane as chlorine atom population in the fuel molecule decreases (Table III).

The experimental evidence for both flame velocities and lower limits suggests that the burning mechanism for the CH_3 group in methyl chloride is similar to that for methane, but that it is inhibited by chlorine. Further evidence for this conclusion lies in the intermediate and final products identified in these flames. Simmons and Wolfhard make a similar suggestion for inhibition by bromine atoms in methyl bromide inhibited flames.[13]

Both methyl chloride and methane burn with characteristic green flames associated with the green C_2 Swan Bands,[14,15] and in general show the same spectroscopically identified species, except for those involving chlorine.[14-17] In addition, both of these flames produce soot in fuel-rich mixtures.[18] Significantly, methyl alcohol flames never produce soot nor show C_2 bands. Also, the strong CO bands in methyl alcohol[19] combustion have not been reported for methane and methyl chloride. The foregoing evidence indicates a different burning mechanism for methyl alcohol and reflects the influence of the strong attachment of the oxygen to the carbon atom.

Three mechanisms of chlorine inhibition have been considered: (1) chain breaking, (2) deactivation in a mechanism involving some sort of excited radicals, and (3) kinetic "short circuiting." It is somewhat difficult to realize how chlorine chain breaking could account for such a remarkable reduction in burning rate as exists between methane and methyl chloride since nearly every reaction producing Cl atoms also produces other free radicals. It is possible that electronically excited radicals have an important role in the chain combustion mechanism, in which case chlorine atoms might on collision "deactivate" them. This is not a likely possibility due to the low population of these electronically excited states at these temperatures.

Kinetic "short circuiting" may be illustrated by the reaction

$$CH_3 + HCl \longrightarrow CH_4 + Cl, E_{act} = 5 \text{ kcal.} \quad (a)$$

An alternative short circuiting mechanism might be

$$Cl + CO \longrightarrow CO + Cl, E_{act} = \text{small}^{19} \quad (b)$$

$$CO\,Cl + Cl \longrightarrow CO + Cl_2, E_{act} = 1.9 \text{ kcal.}^{19} \quad (c)$$

$$CH_3 + Cl_2 \longrightarrow CH_3Cl + Cl, E_{act} < 5 \text{ kcal.}^{19} \quad (d)$$

These are examples of very low energy paths which may be responsible for re-forming reactant molecules by means of Cl atoms and product molecules, thereby greatly slowing the rate of burning.

(6) C. D. Hodgman (Editor), "Handbook of Chemistry and Physics," 33rd Ed., Chemical Rubber Publishing Co., Cleveland, Ohio, 1951, p. 1579.

(7) F. Leprince-Ringuet, *Compt. rend.*, **158**, 1793 (1914).

(8) G. W. Jones, *Ind. Eng. Chem.*, **20**, 367 (1928).

(9) G. W. Jones, H. F. Coward and G. W. Jones, "Limits of Flammability of Gases and Vapors," Bulletin 503, Bur. Mines, 1938.

(10) H. LeChatelier and O. Boudouard, *Compt. rend.*, **126**, 1510 (1898).

(11) H. LeChatelier, *Bull. soc. chim.*, **19**, 483 (1898).

(12) M. J. Burgess and R. V. Wheeler, *J. Chem. Soc.*, **105**, 2591 (1914).

(13) R. F. Simmons and H. G. Wolfhard, *Trans. Faraday Soc.*, **51**, 1211 (1955).

(14) A. G. Gaydon and H. G. Wolfhard, "Third Symposium on Combustion, Flame and Explosion Phenomena," Williams and Wilkins, Baltimore, Md., 1949, p. 504.

(15) V. M. Vaidya, *Proc. Roy. Soc.*, (*London*), **A178**, 356 (1941).

(16) A. G. Gaydon and H. G. Wolfhard, "Fourth Symposium on Combustion," Williams and Wilkins, Baltimore, Md., 1953, p. 211.

(17) G. Pannetier and A. G. Gaydon, *Compt. rend.*, **225**, 1139 (1947).

(18) A. G. Gaydon and H. G. Wolfhard, "Flames, Their Structure, Radiation and Temperature," Chapman and Hall, London, 1953.

(19) E. W. R. Steacie, "Atomic and Free Radical Reactions," Reinhold Publ. Corp., New York, N. Y., 1946.

Calculations by the authors have shown dissociation of methyl chloride according to the reaction

$$CH_3Cl \longrightarrow CH_3 + Cl \qquad (3)$$

to be essentially complete at 1400°. Reference to Fig. 2 shows that Cl atoms could be produced easily by dissociation; or, reactions of the type (a) may be most important.

Evaluation of the Experimental Method

For the purpose of evaluating the influence of tube diameter on burning velocity three different tube diameters were used. A similar study had been made by Coward and Hartwell[2] for their tube method, but tube diameter effects for the Gerstein, Levine and Wong tube method have not been reported.[20] Tube diameters for the present study were chosen in the critical region indicated by the investigations of Coward and Hartwell.[2]

The results for the tube method of Gerstein, *et al.*, are shown in Figs. 3 and 4 for observed flame and burning velocities Analysis of these curves shows the burning velocities determined by the two larger tubes to be within experimental error up to nearly 16% methyl chloride, while values for the 2.14 cm. i.d. tube are low in all cases.

Photographs of flames in the larger tubes for mixtures above 20% methyl chloride showed multiple and very distorted flame fronts. This accounts in part for the spread in observed flame velocities at higher fuel percentages, although analysis of the data indicates some surface effects even at higher velocities. The evaluations of flame areas were made on the basis of a simple geometrical solid, obviously giving values of flame area that were too low (perhaps by factor of 2) where irregular and multiple burning surfaces appeared. The use of low values of flame area, A_f, in equation 1 results in even more exaggerated burning rates. Thus, the amount of upward curvature in the right-hand portion of the curves of Fig. 4 is an indication of the relative amount of flame front distortion due to turbulence.

The data presented indicate the importance in selecting tube diameters for the velocity range to be measured. For high velocity measurements the tube diameter probably should not be above about 2.4 cm. i.d. if turbulent flame fronts are to be avoided. For slow burning mixtures (fuel–air) the tube diameter probably should be 2.8 cm. i.d. or greater to avoid excessive surface effects. From the present study a tube diameter of 2.4 cm. appears to be the best over-all compromise.

The general method of evaluating flame front areas introduced by Coward and Hartwell[2] has been revised in the present work.

In Fig. 5 are shown tracings of typical flame fronts fitted to their mirror images. The completed solid still approximates an ellipsoid but for leaning flames the line joining the points where the flame touches the top and bottom of the tube is not an axis. Using the mid-point of this line, however, the three semi-axes may be measured as (1) the distance from the reference mid-point to the

(20) J. W. Linnett, "Methods of Measuring Burning Velocities, Fourth Symposium on Combustion," Williams and Wilkins, Baltimore, Md., 1953, p. 20.

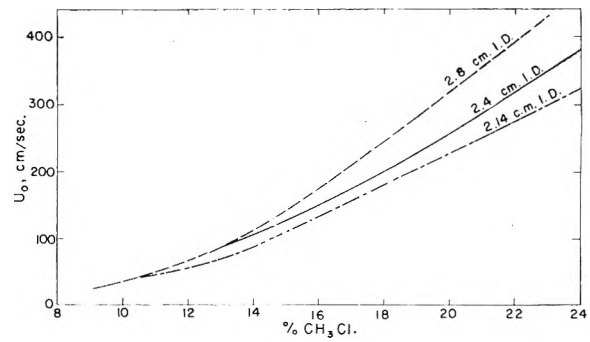

Fig. 3.—Flame velocity as a function of composition and tube diameter for CH_3Cl–O_2.

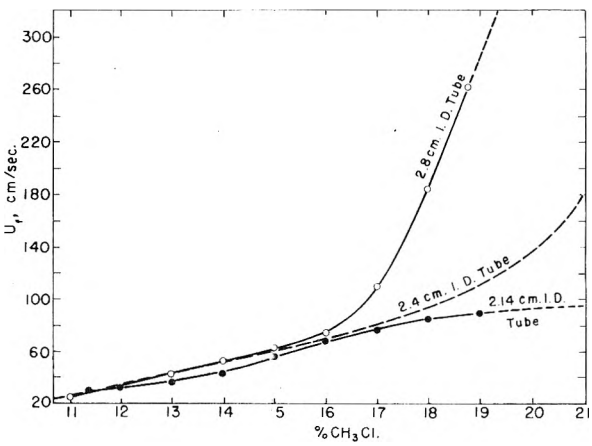

Fig. 4.—Burning velocity of CH_3Cl–O_2 as a function of tube diameter.

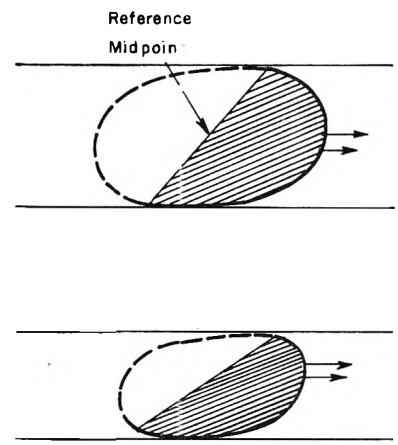

Fig. 5.—Tracings of typical flame fronts (shaded) forming complete figures with their mirror images. Arrows show direction of flame travel.

point most remote from it on the flame front, (2) the vertical distance from the axis just measured to the bottom edge of the flame from the reference mid-point, and (3) the radius of the tube. It is seen from Fig. 5 that the ellipsoid so described still lies nearly parallel to the tube axis but has its major axis slightly rotated in the vertical plane.[21]

The flame areas calculated from these revised measurements are several per cent. smaller than those obtained by the conventional Coward–Hart-

(21) H. Guenoche and M. Jouy, "Fourth Symposium on Combustion," Williams and Wilkins, Baltimore, Md., 1953, p. 403.

well formula, except where the flames are essentially up-right in the tube. For the slower fuel–air flames the flame areas were calculated as much as 18.5% lower than by the conventional method. Maximum burning velocities are increased by as much as 9% by this improvement, with increases of 4 to 18% over the composition range of ignitability. Since burning velocities measured by the tube method have been generally a little lower than the most acceptable burner methods, this represents a rather significant improvement.

With the foregoing improvements the maximum burning velocity determined for methane was 37.8 cm./sec., which is still low compared to the value of 39 cm./sec. obtained by Smith[22], and 40 cm./sec. obtained by Singer and Heimel.[23] Gerstein, *et al.*, obtained 33.8 cm./sec. It is believed that the calculated flame areas are still as much as 5% too large due to the assumption that one axis of the ellipsoid is the diameter of the tube. If the quenching distance for each mixture were taken as a correction to this measurement it is believed that the results would be in even better agreement with the frustrum method of the bunsen burner (Singer and Heimel).[23]

(22) F. A. Smith, *Chem. Revs.*, **21**, 389 (1937).

(23) J. M. Singer, S. Heimel, B. Lewis and G. von Elbe, "Combustion, Flames, and Explosion of Gases," Academic Press, New York, N. Y., 1951, p. 467.

Conclusions

1. The experimental data of this research together with kinetic and spectroscopic data from the literature support the hypothesis that methyl chloride burns by a chlorine inhibited paraffin burning mechanism.
2. An evaluation of the influence of tube diameter by the Gerstein, *et al.*, tube method shows both upper and lower limits on tube size imposed by turbulence and pressure effects and by surface effects, respectively. The proper tube size for use depends on the velocity range to be studied.
3. An improvement is suggested in the method of Coward and Hartwell for evaluating flame areas which results in significantly higher burning velocities and better agreement with the improved bunsen burner techniques.

This research was supported by the United States Air Force under contract No. AF 33(038) 20839 monitored by the Office of Scientific Research of the Air Research and Development Command.

A SPECTROPHOTOMETRIC INVESTIGATION OF URANYL PHOSPHATE COMPLEX FORMATION IN PERCHLORIC ACID SOLUTION

BY C. F. BAES, JR.

Oak Ridge National Laboratory, Oak Ridge, Tennessee

Received November 11, 1955

A spectrophotometric investigation of uranium(VI)–orthophosphate complex formation in 1 and 0.1 M perchloric acid solutions has been carried out. Continuous variation results indicate the presence of 1:1 complexes in these solutions, while detailed analysis of absorbancy results at constant uranium(VI) perchlorate formal concentrations indicate that 2:1 complexes also are formed. The acidity dependence of the formation quotients $K_1 = C_1/C_U C_P$ and $K_2 = C_2/C_U C_P^2$ (in which C_1 and C_2 are the total concentrations of 1:1 and 2:1 phosphate–uranium complexes, C_U and C_P are the concentrations of uncomplexed uranium(VI) and phosphoric acid) can be accounted for in terms of the complex species $UO_2H_2PO_4^+$, $UO_2H_3PO_4^{++}$, $UO_2(H_2PO_4)_2$ and $UO_2(H_2PO_4)(H_3PO_4)^+$.

From measurements of uranium(VI) monohydrogen phosphate solubility behavior in acidic nitrate solutions, Leader[1] suggested the formation of the complex $UO_2H_2PO_4^+$ at moderate phosphoric acid concentrations and the formation of higher complexes in more concentrated phosphoric acid. Similar measurements by Schreyer and Baes[2] in phosphoric acid and acidic perchlorate solutions confirmed extensive complexing between uranium (VI) and various orthophosphate species in aqueous solution.

The present publication describes a spectrophotometric investigation of such complexing in acidic perchlorate solutions. While some use was made of the method of continuous variations, most of the absorbancy measurements were made at constant total uranium(VI) concentration and constant acidity, the phosphoric acid concentration being varied. The results were interpreted in terms of complexing equilibria of the type

$$UO_2^{++} + nH_3PO_4 = UO_2H_x(PO_4)_n^{+(2-3n+x)} + (3n - x)H^+ \quad (1)$$

wherein the various complexes which may be formed are characterized by $n = 1, 2, 3, \ldots$ and $x = 0, 1, 2 \ldots$. It has been assumed that polynuclear uranium(VI) complexes are not formed in appreciable amounts.

Theoretical

If the molar concentrations of the reactants and products in equation 1 are designated, respectively, as C_U, C_P, $C_{n,x}$ and C_H, then the concentration equilibrium quotient of formation for a single complex species, $UO_2H_x(PO_4)_n^{+(2-3n+x)}$ is

$$K_{n,x} = \frac{C_{n,x}C_H^{3n-x}}{C_U C_P^n} \quad (2)$$

From the measurements which were performed at constant acidity, complex formation quotients

$$K_n = \frac{C_n}{C_U C_P^n} \quad (3)$$

were determined in which C_n is the total molarity of all complexes with a PO_4/UO_2 ratio of n, *i.e.*,

(1) G. R. Leader, Report CN-2195 (1944).

(2) J. M. Schreyer and C. F. Baes, Jr., *J. Am. Chem. Soc.*, **76**, 354 (1954); THIS JOURNAL, **59**, 1179 (1955).

$\sum_{x=0}^{x} C_{n,x}$. K_n is related to the individual formation quotients $K_{n,x}$ by

$$K_n = \frac{K_{n,0}}{C_H^{3n}} + \frac{K_{n,1}}{C_H^{3n-1}} + \frac{K_{n,2}}{C_H^{3n-2}} + \ldots = \sum_{x=0}^{x} \frac{K_{n,x}}{C_H^{3n-x}} \quad (4)$$

The observed absorbancy difference D (corrected for any phosphoric acid absorption) between an acidic uranium(VI) phosphate solution and a reference solution of the same composition, except that it contains no phosphoric acid, may be related to C_U, C_n and the corresponding molar extinction coefficients ϵ_U, ϵ_n by

$$D = \epsilon_U C_U + \sum_{n=1}^{n} \epsilon_n C_n - \epsilon_U \Sigma C_U \quad (5)$$

In this equation ΣC_U denotes the total concentration of uranium(VI) in solution. The molar extinction coefficient term ϵ_n is equal to $\left[\sum_{n=1}^{n} \epsilon_{n,x} C_{n,x}\right] / C_n$; *i.e.*, the sum of the absorbancies of all complex species of the same PO_4^{-3}/UO_2^{++} mole ratio n, divided by their total molarity. Upon introducing the material balance relation, $\Sigma C_U = C_U + \sum_{n=1}^{n} C_n$, and combining equations 3 and 5

$$D = \frac{\sum_{n=1}^{n} A_n K_n C_P^n}{1 + \sum_{n=1}^{n} K_n C_P^n} \quad (6)$$

wherein $A_n = (\epsilon_n - \epsilon_U)\Sigma C_U$. This equation provides a relationship between the observed absorbancy difference and the phosphoric acid concentration in terms of a set of $A_n K_n$ values and a set of K_n values.

In applying equation 6 to each series of measurements in which ΣC_U, the ionic strength, and the acidity were constant, it was assumed that the A_n and K_n terms were constant.

Experimental

Uranium(VI) perchlorate stock solutions were prepared by dissolving purified UO_3 (free of nitrate) in slightly less than the equivalent amount of perchloric acid. An aliquot portion of the resulting solution was analyzed for uranium by a volumetric dichromate method,[3] and the required amount of perchloric acid was added to the remainder to produce a stoichiometric uranyl perchlorate solution. Stock solutions of phosphoric acid, perchloric acid and sodium perchlorate were prepared from reagent grade materials.

The purification of UO_3 was accomplished by the peroxide method[4,5]; Mallinckrodt UO_3 was dissolved in a perchloric acid solution and diluted to a uranium concentration of 5%. The solution was adjusted to *p*H 2 with dilute ammonia and 30% hydrogen peroxide was added dropwise with rapid stirring, resulting in the precipitation of uranium(VI) peroxide. The *p*H was held constant during the precipitation by the addition of small amounts of ammonia solution. Hydrogen peroxide was added until further addition caused no change in *p*H. The slurry was stirred for one hour, then filtered through coarse filter paper in a buchner funnel. The precipitate was washed first with 1% peroxide acidified to *p*H 2 with perchloric acid, then with 1% hydrogen peroxide, and dried at 110°. The cake was ground, placed in a large platinum dish, and heated at 350° for 3 days. Solutions prepared from this purified UO_3 gave negative tests for nitrate and peroxide.

All absorbancies were measured with a Beckman Model DU spectrophotometer, using 1-cm. and 5-cm. silica cells in the ultraviolet, and 1-cm. Corex cells in the visible range. Cell blank determinations were made in all cases, and the results were corrected accordingly. A hydrogen discharge lamp was used in all ultraviolet measurements.

In the ultraviolet, the absorbancy of phosphoric acid in 1 *M* perchlorate solutions was found to be large enough to require correction of some of the measurements. The observed molar extinction coefficients at 290, 300, 310 and 318 mμ were, respectively, 0.058, 0.037, 0.021 and 0.014.

Continuous Variation Measurements.—The absorbancies of two series of uranium(VI) phosphate solutions, 1 and 0.1 *M* in perchloric acid, were determined at 25 ± 2°, using water in the reference cell. In the 1 *M* acid solutions, wherein the sum of the uranium(VI) and phosphoric acid concentrations was 0.137 *M*, measurements were made in the visible range. In the 0.1 *M* acid solutions, adjusted to an ionic strength of approximately 0.14 *M* with sodium perchlorate, it was necessary to reduce the total uranium(VI)–phosphoric acid concentration to 0.014 *M* in order to avoid the precipitation of uranium(VI) monohydrogen phosphate. As a result, the latter measurements were made in the ultraviolet at wave lengths where absorbancies were conveniently high.

Measurements at Constant Formal Concentration of Uranium(VI) Perchlorate.—The absorbancies of two series of solutions, 0.000943 *M* in uranium(VI) perchlorate, 1 and 0.1 *M* in perchloric acid, and containing various amounts of phosphoric acid, were determined in the ultraviolet. The ionic strength of the 0.1 *M* acid solutions was adjusted to 1 *M* by the addition of sodium perchlorate. A third series of solutions, 0.0377 *M* in uranium(VI) perchlorate and 1 *M* in perchloric acid, was run in the visible range. The absorbancy, D, of each sample was measured at 25 ± 1°, against a reference solution otherwise of the same composition, but free of phosphoric acid. As a result, wider slit widths were required than for the continuous variation measurements. Care was taken to keep the slit width the same for all measurements at a single wave length.

Results

The continuous variation plots of D, the difference in absorbancy between the uranium(VI) phosphate solution and a similar solution of free phosphate, *vs.* x, the ratio of uranium(VI) molarity to the sum of the formal concentrations of uranium(VI) and phosphoric acid, are presented in Fig. 1. These curves clearly indicate the presence both in 1 and 0.1 *M* acid of complex species in which the ratio of uranium to phosphate is unity.

Plots of D *vs.* C_P (the equilibrium concentration of free, undissociated phosphoric acid) for the two series of measurements at 0.000943 $M\Sigma C_U$ are presented in Fig. 2. In the case of the 1 *M* acid data, C_P was assumed to be equal to the total concentration of phosphoric acid, ΣC_P, since the amount consumed in complex formation may be neglected and the primary dissociation

$$H_3PO_4 = H^+ + H_2PO_4^-, K = 0.021 \text{ mole/l.}^6 \quad (7)$$

is only about 2%. In the case of the 0.1 *M* acid data, however, the dissociation of phosphoric acid becomes appreciable, not only decreasing C_P, but also increasing the hydrogen ion concentration, C_H. A simple correction can be made for these two effects by the assumption that $UO_2H_2PO_4^+$ and UO_2-

(3) J. M. Schreyer and C. F. Baes, Jr., *Anal. Chem.*, **25**, 644 (1953).
(4) D. W. Mogg and C. E. Larson, Report C-0.375.5, 1946.
(5) K. B. Brown and C. E. Larson, Report C-0.375.7, 1946.

(6) This concentration equilibrium quotient value was estimated from as yet unpublished potential measurements of the cell: Pt, Quinhyd; $NaClO_4$ (0.9 *M*), $HClO_4$ (0.1 *M*); $NaClO_4$ (0.9 *M*), $HClO_4$ (0.1 *M*), H_3PO_4 (*c*); Quinhyd., Pt. It may be compared with 0.016 mole/l. (30°, μ = 0.56), R. Griffith and A. McKeown, *Trans. Faraday Soc.*, **36**, 776 (1940); 0.030 mole/l. (30°, μ = 0.665), O. Lanford and S. Kiehl, *J. Am. Chem. Soc.*, **64** 292 (1942); 0.020 (30°, μ = 1.0–1.1), M. Cher and N. Davidson, *ibid.*, **77**, 793 (1955).

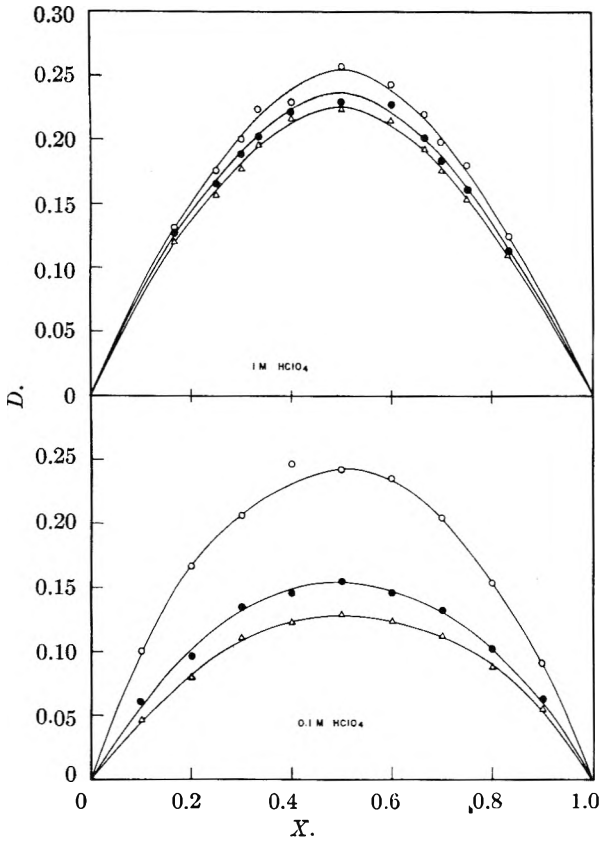

Fig. 1.—Continuous variation results: in 1 M acid: △, 410 mμ; ●, 420 mμ; ○, 424 mμ; in 0.1 M acid: ○, 290 mμ; ●, 300 mμ; △, 310 mμ.

$(H_2PO_4)_2$ are the only complex species in solution which need be considered at this acidity and range of phosphoric acid concentration.[7] The corresponding formation quotients (*cf.* equation 2) are

$$K_{1,2} = C_{1,2}C_H/C_UC_P \text{ and } K_{2,4} = C_{2,4}C_H^2/C_UC_P^2$$

which may be rewritten

$$K_{1,2} = \frac{C_{1,2}(0.1)}{C_U(0.1C_P/C_H)};\ K_{2,4} = \frac{C_{2,4}(0.1)^2}{C_U(0.1C_P/C_H)^2} \quad (8)$$

From these expressions it is clear that the term $(0.1\ C_P/C_H)$ represents the equilibrium concentration of undissociated phosphoric acid at an equilibrium acidity of exactly 0.1 M for the same values of the ratios $C_{1,2}/C_U$ and $C_{2,4}/C_U$ that existed in actual solutions. Accordingly, equilibrium values of $(0.1\ C_P/C_H)$ were calculated from the initial solution composition using $K = 0.021$ (neglecting the small changes produced by complex formation). These corrected values for C_P were plotted for the 0.1 M acid results in Fig. 2 and were used in the subsequent calculations. The magnitude of this correction is indicated in Table I.

The absorbancy results at 0.0377 M ΣC_U in 1 M acid are plotted *vs.* ΣC_P in Fig. 3. Here C_P is not known directly from ΣC_P since, at this higher uranium concentration, an appreciable amount of phosphoric acid is consumed in complex formation.

(7) While the $K_{n,z}$ values estimated in the discussion indicate that in 0.1 M acid three complexes—$UO_2H_2PO_4^+$, $UO_2(H_2PO_4)_2$ and $UO_2(H_2PO_4)(H_3PO_4)^+$—should be considered, the fairly small effect of this correction procedure on K_1 and K_2 values (*cf.* footnote *b*, Table III) suggests that no serious error is introduced by neglecting $UO_2(H_2PO_4)(H_3PO_4)^+$.

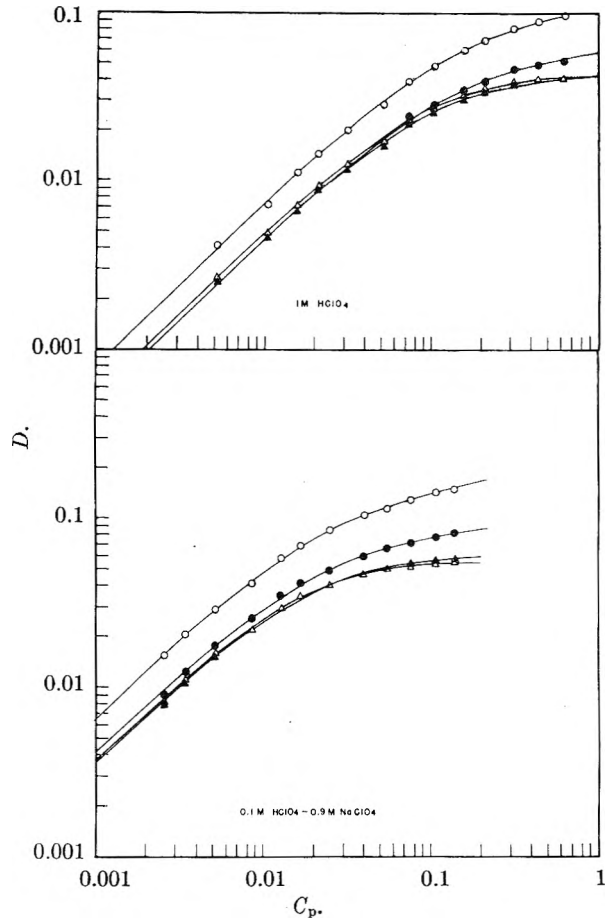

Fig. 2.—Absorbancy results at $\Sigma C_U = 0.000943$ M: ○, 290 mμ; ●, 300 mμ; ▲, 310 mμ; △, 318 mμ. The points are the measured absorbancies; the curves were calculated from equation 9 using appropriate values of A_nK_n and K_n (Tables II and III).

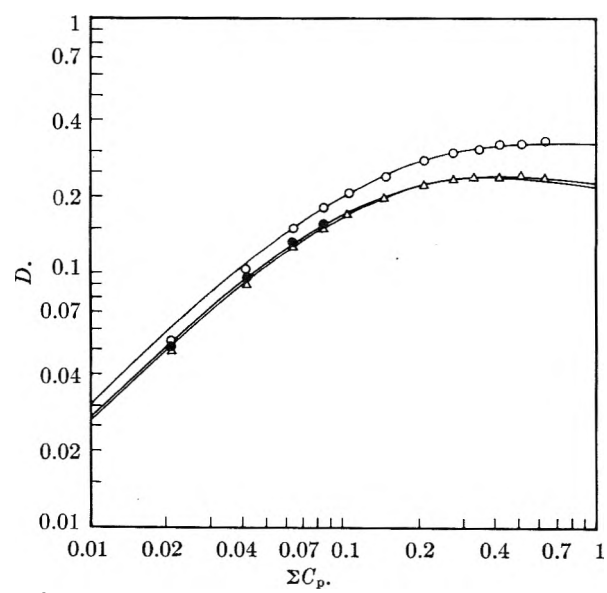

Fig. 3.—Absorbancy results in 1 M perchloric acid at $\Sigma C_U = 0.0377$ M: △, 410 mμ; ●, 420 mμ; ○, 424 mμ. The points are the measured absorbancies; the curves were calculated from equation 9 using $K_1 = 11$ and $K_2 = 24$, along with the following A_n values (obtained by solutions of equation 13): at 410 mμ, $A_1 = 0.358$, $A_2 = 0.171$; at 420 mμ, $A_1 = 0.371$, $A_2 = 0.152$; at 424 mμ, $A_1 = 0.422$, $A_2 = 0.282$.

TABLE I

EFFECT OF THE DISSOCIATION OF PHOSPHORIC ACID IN 0.1 *M* PERCHLORIC ACID

K = 0.021 mole/l.; μ = 1.0.

ΣC_P, *M*	C_P, *M*	$0.1C_P/C_H$%, *M*
0.00417	0.00345	0.00343
.01043	.00865	.00849
.02086	.01734	.01675
.0522	.0437	.0403
.1043	.0883	.0761
.2086	.1794	.1389

Determination of K_n Values.—The first step in the analysis of the D *vs.* C_P data in Fig. 2 was to plot D/C_P *vs.* D for each wave length at each acidity.[8] From equation 6 it can be shown that for a series of mononuclear complexes in which n = 1, 2, 3, ..., the intercept of such a plot at $D = 0$ is A_1K_1. As $D \rightarrow 0$ the limiting slope, $d(D/C_P)/dD = -K_1 + A_2K_2/A_1K_1$. For the special case in which only 1:1 complexes are formed, the plots will be linear with slope $-K_1$.[9]

The D/C_P *vs.* D plot obtained from the present results were linear up to fairly high values of D in all cases, permitting good extrapolations to $D = 0$. The A_1K_1 values so obtained, along with the limiting slopes are listed in Table II. Since these limiting slopes are not the same for all four wave lengths at each acidity, and since systematic deviations from linearity occurred at high D (high C_P) values it was assumed that in addition to the 1:1 complexes indicated by the continuous variation curves (Fig. 1), 2:1 complexes also are formed.

TABLE II

SUMMARY OF A_1K_1 AND A_2K_2 VALUES

λ, mμ	$[d(D/C_P)/dD]_{D\rightarrow 0}$, M^{-1}	A_1K_1, M^{-1}	A_2K_2, M^{-2}
	1 *M* $HClO_4$		
290	− 6.91	0.794	3.00
300	− 7.62	.489	1.58
310	− 9.66	.491	1.01
318	−10.0	.532	0.98
	0.1 *M* $HClO_4$-0.9 *M* $NaClO_4$		
290	−41.0	6.85	90.3
300	−45.1	4.22	45.0
310	−48.6	3.67	26.8
318	−51.6	3.81	22.8

(8) This kind of plot was first proposed by W. B. Lewis (Thesis, University of California at Los Angeles, 1942, described by T. W. Newton and G. M. Arcand, *J. Am. Chem. Soc.*, **75**, 2449 (1953)).

(9) Upon rearranging equation 6 to

$$\frac{D}{C_P} = \sum_{n=1}^{n} (A_n - D)K_nCP^{n-1}$$

it is evident that as C_P and D approach zero, D/C_P approaches A_1K_1. Upon differentiating this equation with respect to D and letting D and C_P approach zero

$$\frac{d(D/C_P)}{dD} = -K_1 + A_2K_2\frac{dC_P}{dD}$$

and since the limiting value of dC_P/dD is $1/A_1K_1$, the limiting slope $d(D/C_P)/dD$ is $-K_1 + A_2K_2/A_1K_1$.

While this kind of plot has been used by several investigators for analysis of 1:1 complex formation, to the author's knowledge it has not been emphasized previously that if appreciable 2:1 complex formation occurs, the limiting slope of such a plot will not be the expected simple function of K_1.

In such a case equation 6 becomes

$$D = \frac{A_1K_1C_P + A_2K_2C_P^2}{1 + K_1C_P + K_2C_P^2} \qquad (9)$$

Besides K_1 and K_2, the only unknown constant in this equation is A_2K_2. Values for this quantity were estimated by a graphical method based on the equation

$$\frac{1 - R_0/R}{C_P} = \frac{A_2'K_2}{A_1'K_1}(R_0/R) - \frac{A_2''K_2}{A_1''K_1} \qquad (10)$$

Here, $R = D'/D''$ for two wave lengths, λ' and λ'', at the same C_P value; $R_0 = A_1'K_1/A_1''K_1$ (the limiting value of R as $C_P \rightarrow 0$). This equation is derived directly from equation 9.[10] Plots of $(1 - R_0/R)/C_P$ *vs.* R_0/R were made for the following pairs of wave lengths

(1) λ' = 290, λ'' = 318 (3) λ' = 300, λ'' = 318
(2) λ' = 290, λ'' = 310 (4) λ' = 300, λ'' = 310

The points conformed sufficiently well to straight lines so that individual slopes and intercepts could be estimated to ±10% and ±15%, respectively.[11] These uncertainties were improved somewhat by making the fitted lines also conform to the following relationships, as required by equation 10

Slope (1) = slope (2), Slope (3) = slope (4)
Intercept (1) = intercept (3), Intercept (2) = intercept (4)

The ratios A_2K_2/A_1K_1, so determined, give the A_2K_2 values listed in Table II.

From these values of A_1K_1 and A_2K_2 it was possible to determine the formation quotients K_1 and K_2 by means of the following rearrangement of equation 9.

$$\frac{A_1K_1 - A_2K_2C_P}{D} - \frac{1}{C_P} = K_2C_P + K_1 \qquad (11)$$

A plot of the left-side of this equation *vs.* C_P is shown in Fig. 4. The single straight lines at each acidity, of slope K_2 and intercept K_1 (Table III),

TABLE III

FORMATION QUOTIENTS FOR URANIUM(VI)-ORTHOPHOSPHATE COMPLEXES AT 25°.

Formation quotient[a]	1 *M* $HClO_4$	0.1 *M* $HClO_4$-0.9 *M* $NaClO_4$[b]
K_1, M^{-1}	11 ± 2	58 ± 4
K_2, M^{-2}	24 ± 5	470 ± 50

[a] *Cf.* equation 3. [b] If no corrections were made for the dissociation of phosphoric acid, the resulting K_n values would be K_1 = 50; K_2 = 400.

indicate that the data in Fig. 2 may be accounted for by assuming 1:1 and 2:1 phosphate–uranium complexes only. This is apparent (Fig. 2) from the conformity between the measured points and the calculated D *vs.* C_P curves, which were obtained by substituting appropriate values of A_1K_1,

(10) Equation 10 is obtained by rearranging

$$\frac{D'}{D''} = \frac{A_1'K_1 + A_2'K_2C_P}{A_1''K_1 + A_2''K_2C_P}$$

(11) For these plots only the measurements at the five highest C_P values were used since, at the lower C_P (lower D) values, the experimental error led to excessive scatter.

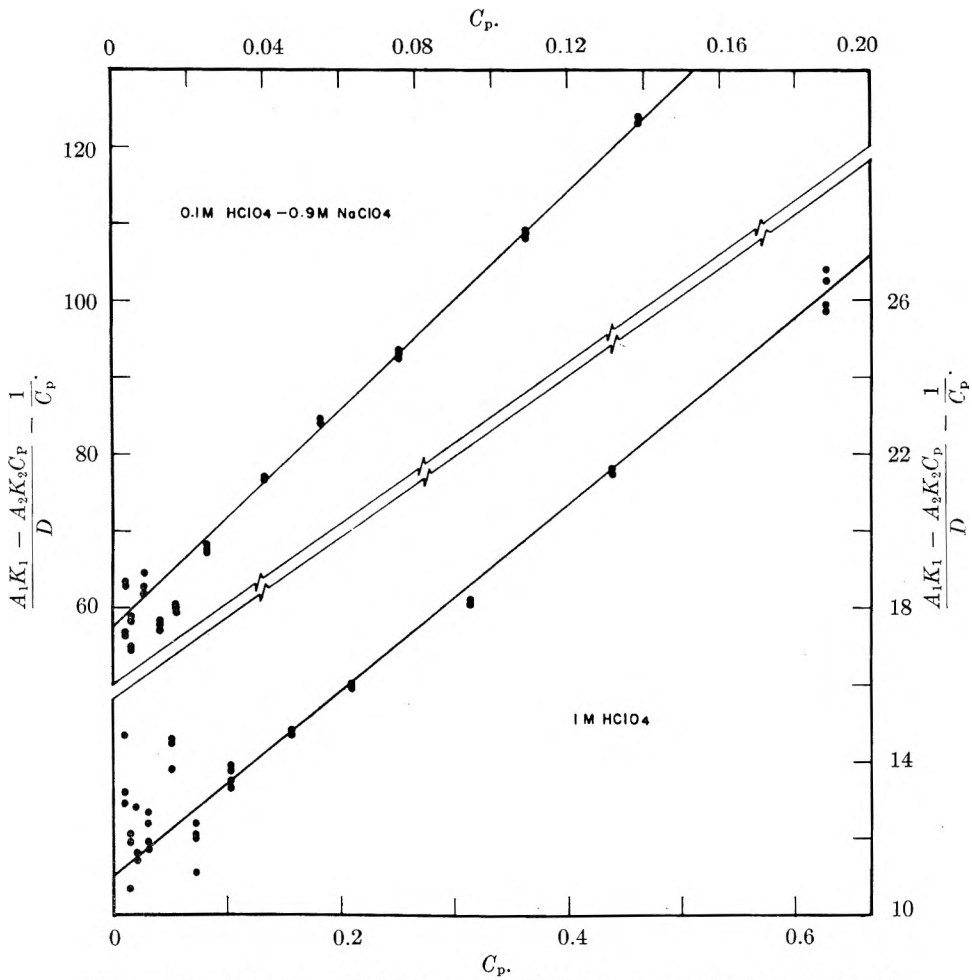

Fig. 4.—The evaluation of K_1 (intercept) and K_2 (slope) according to equation 11.

A_2K_2, K_1 and K_2 into equation 9.[12] The scatter of points at low C_P values in Fig. 4 results from the increased sensitivity of the $A_1K_1 - A_2K_2$ function to errors in D.

Similar determinations of K_1 and K_2 could not be made from the data at $0.0377M\Sigma C_U$ (Fig. 3) since here the equilibrium concentration of phosphoric acid C_P was not known from ΣC_P with sufficient accuracy. However, the conformity of these results to $K_1 = 11$ and $K_2 = 24$ was established as follows. The concentration of uncomplexed phosphoric acid C_P was first calculated for each ΣC_P value from the equation[13]

$$C_P = \Sigma C_P - \Sigma C_U \left[\frac{K_1C_P + 2K_2C_P^2}{1 + K_1C_P + K_2C_P^2}\right] \quad (12)$$

Using these same K_n values, A_1 and A_2 were then evaluated at $\lambda = 410$, 420 and 424 mμ from graphical solutions of the equation

$$\frac{D}{C_P}(1 + K_1C_P + K_2C_P^2) = A_2K_2C_P + A_1K_1 \quad (13)$$

(a rearranged form of equation 9). The resulting A_n values along with these K_n values lead to the calculated D *vs.* ΣC_P curves drawn in Fig. 3.

Discussion

From the continuous variation results, it is evident that equilibria of the type

$$UO_2^{++} + H_3PO_4 = UO_2H_xPO_4^{+(x-1)} + (3 - x)H^+ \quad (14)$$

are important complex-forming reactions in both 1 and 0.1 M acid. In the analysis of the results in Figs. 2 and 3, it has been found necessary to assume the formation of 2:1 complexes as well, corresponding to the general reaction

$$UO_2^{++} + 2H_3PO_4 = UO_2H_x(PO_4)_2^{+(x-4)} + (6 - x)H^+ \quad (15)$$

The conformity of the results for 0.0377 M uranium(VI) solutions to the K_1 and K_2 values derived from the 0.000943 M uranium(VI) data (Table III) provides strong evidence that the neglect of polynuclear complex formation in the pres-

(12) The following additional observations can be made from the A_nK_n and K_n values in Tables II and III. The calculated limiting slopes for the D/C_P *vs.* D plots $(-K_1 + (A_2K_2/A_1K_1))$ agree with the observed values with an average deviation of *ca.* 5%. Because of the wide range of linearity of these D/C_P *vs.* D plots, equation 9 was examined for a condition which would yield perfectly linear plots. This condition was found to be

$$K_2 = \frac{A_2K_2}{A_1K_1}\left[K_1 - \frac{A_2K_2}{A_1K_1}\right]$$

It is approximately true for each set of A_nK_n and K_n values in Tables II and III.

(13) Equation 12 is obtained by combination of the material balance relations

$$\Sigma C_P = C_P + C_1 + 2C_2 = C_P + K_1C_UC_P + K_2C_UC_P^2$$
$$\Sigma C_U = C_U + C_1 + C_2 = C_U + K_1C_UC_P + K_2C_UC_P^2$$

The dissociation of phosphoric acid in 1 M perchloric acid is again neglected.

ent treatment is justified. If such complexes were formed to an appreciable extent in the dilute uranium(VI) solutions, their contribution would be much higher in the more concentrated solutions and would be expected to produce inconsistencies in the latter case.

The uncertainties assigned to K_1 and K_2 are valid only within the assumptions which have been made. As discussed elsewhere,[2] the solubility behavior of uranium(VI) phosphates in phosphoric acid indicates the formation of 3:1 complexes. If 3:1 complexes are formed to an appreciable extent in the present 1 and 0.1 M solutions, the corresponding A_3 term in equation 6 must be such that the resulting effect on D is not apparent. Accordingly, the value of K_2 should be regarded as less certain than K_1, which would be relatively unaffected by such a complication.

From the values listed in Table III, it appears that the acidity dependence of K_1 is less than first power, while that of K_2 lies between first and second power. Considering the general relationship between K_n and the individual formation quotients $K_{n,x}$, given by equation 4, these acid dependencies may be accounted for most simply by

$$K_1 = K_{1,2}/C_H + K_{1,3}; \quad K_2 = K_{2,4}/C_H^2 + K_{2,5}/C_H \quad (16)$$

This corresponds to the formation of the following complex species

$UO_2H_2PO_4^+$	$UO_2(H_2PO_4)_2$
$UO_2H_3PO_4^{++}$	$UO_2(H_2PO_4)(H_3PO_4)^+$

Acknowledgment.—The author is grateful to Dr. J. M. Schreyer and Mr. J. M. Lesser for their collaboration in the continuous variation measurements. He also wishes to express his appreciation to Dr. K. A. Allen for his participation in many valuable discussions concerned with the present investigation, and to Dr. C. F. Coleman for his critical and comprehensive reading of the manuscript.

THE INFLUENCE OF STRUCTURE UPON THE VISCOUS BEHAVIOR OF SOME CARBOXYMETHYL POLYSACCHARIDES[1]

BY STEPHEN S. WINTER[2] AND CHARLES O. BECKMANN

Department of Chemistry, Columbia University, New York 27, New York

Received November 17, 1955

An investigation of the viscosity of aqueous solutions of carboxymethyl polysaccharides showed that the reduced viscosity of polyelectrolytes depends upon the normal conformation of the polymer chain, the density of attached ions, structural limitations to deformation and the concentration of the polymer. The variation of the viscosity with charge was found to be independent of the concentration, so that one can describe the reduced viscosity in terms of an equation containing four independent terms: $\eta_{sp}/c = [\eta]R_m f(\gamma)f(c)$. In this equation, $[\eta]$ is the intrinsic viscosity of the uncharged polyelectrolyte, R_m is a constant describing its extensibility, $f(\gamma)$ is a quadratic function of the charge and is identical for all the polysaccharides studied, but does contain the parameter R_m, and $f(c)$ is given by the Fuoss equation, and is identical for all samples. Both amyloses and amylopectins were used in this work and it was shown that for samples of equal molecular weight, the constant R_m is larger for the linear amyloses than for the branched amylopectins. From the value of R_m of dextran samples it was inferred that these must be essentially linear with short branches attached to a main chain.

An investigation of polyelectrolyte viscosity derives a number of advantages from the use of carboxymethyl polysaccharides (CMP). The carbohydrate polymers allow the independent determination of structure and molecular weight on the parent polymer; they permit the formation of well-defined, branched polyelectrolytes; and they permit control of the extent of substitution. In this manner, polyelectrolytes of identical structure, but with different charge densities are produced. The latter property, particularly, distinguishes this group of compounds and adds an exceedingly useful variable.

The experiments reported here make use of the properties peculiar to CMP. The work is limited to the study of viscosity as a function of the number of charged groups on the various molecular skeletons available, a variable which can be changed by both a variation of the degree of substitution and a variation of the degree of neutralization. At the same time, the influence of the degree of substitution on the acid strength was studied to determine any possible electrostatic effects due to the spatial arrangements of the charged groups.

A number of theoretical developments on the viscosity of polyelectrolytes have been published[3-9]; but only one of these[3] is applicable to salt-free solutions, and its assumptions break down at quite low degrees of neutralization and at small concentrations. Elucidation of the observed behavior must, therefore, rest upon an empirical approach.

Fuoss and co-workers[10,11] have studied the problem extensively, and have proposed the equation

$$\eta_{sp}/c = A/(1 + Bc^{1/2}) + D \quad (1)$$

for the concentration dependence of the viscosity

(1) Presented at the 125th meeting of the American Chemical Society, Kansas City, April, 1954.

(2) Department of Chemistry, Northeastern University, Boston 15, Massachusetts.

(3) A. Katchalsky, O. Künzle and W. Kuhn, *J. Polymer Sci.*, **5**, 283 (1950).

(4) W. Kuhn, O. Künzle and A. Katchalsky, *Helv. Chim. Acta*, **31**, 1994 (1948).

(5) O. Künzle, *Rec. trav. chim.*, **68**, 699 (1949).

(6) J. J. Hermans and J. T. G. Overbeek, *ibia.*, **67**, 761 (1948); *Bull. soc. chim. belg.*, **57**, 154 (1948).

(7) G. E. Kimball, M. Cutler and H. Samelson, THIS JOURNAL, **56**, 57 (1952).

(8) P. J. Flory, *J. Chem. Phys.*, **21**, 162 (1953).

(9) A. Katchalsky and S. Lifson, *J. Polymer Sci.*, **11**, 409 (1953).

(10) R. M. Fuoss and U. P. Strauss, (a) *Ann. N. Y. Acad. Sci.*, **51**, 836 (1949); (b) *J. Polymer Sci.*, **3**, 246 (1948); (c) **3**, 602 (1948); (d) **3**, 603 (1948).

(11) R. M. Fuoss and G. I. Cathers, *ibid.*, **4**, 97 (1949).

at a fixed degree of neutralization. In this equation, A, B and D are empirical constants, c is the concentration of the polyelectrolyte, and η_{sp}/c, the reduced viscosity. Only one attempt has been made to correlate the parameters of equation 1 with experimental variables[10d]; in another study,[12] the equation has been reported to fail, yielding negative quantities for the extrapolated value of the reduced viscosity at zero concentration, and thereby indicating a lack of correspondence between equation 1 and the Huggins[13] equation for the intrinsic viscosity of an uncharged polymer.

Katchalsky[14] has shown that the viscosity of polyacrylic acids (PAA) of different degree of polymerization in solution of *p*H 6 increases greatly with degree of polymerization, whereas acidified solutions of the same substances show only slight increases similar to those observed with uncharged polymers. The explanation for this behavior is that the acidified polymer is uncharged and in a random coil configuration, and shows a molecular weight dependence of viscosity similar to that of uncharged polymers. The partially neutralized PAA, on the other hand, is distorted toward a rigid rod, with the axial ratio increasing as the number of segments becomes larger.

In the present investigation, the conclusions of Katchalsky are tested further by a comparison of the changes in viscosity of some polymer homologous, branched polyelectrolytes (carboxymethylamylopectins) and some linear, polymer homologous polyelectrolytes (carboxymethylamyloses) consisting of identical monomer units.

The factors which must be considered in a study of the viscosity of polyelectrolytes are the concentration, the degree of charge and the degree of polymerization. In addition, for comparison of branched and linear polyelectrolytes, the spacing of the charges and the polymer structure also are of importance. All these were treated in the following manner.

Relative molecular weights could be obtained from the intrinsic viscosities of the acid forms of the CMP in dilute HCl solution. Concentration and degree of charge effects could be investigated separately because it was discovered that these are independent of each other. Furthermore, it was found that the functions of the reduced viscosity with respect to the concentration and with respect to the degree of charge are identical for all polymers investigated. Measurements of *p*H showed that there is no difference in the hydrogen ion binding between linear and branched series. It could, therefore, be inferred that the different spatial distribution of charges on linear and branched CMP does not change the interionic repulsions. Any difference in the viscosity between branched and linear CMP, after the above factors are taken into consideration, may then be attributed to the structure, and to the structural limitations to extension.

Experimental

CM derivatives were prepared from samples of amylose, amylopectin and dextran described in Table I. It must be noted that the conditions of the substitution reaction are sufficiently drastic to cause slight changes in molecular weight distribution and average molecular weights.[15] The reaction, for which the over-all equation

$$(C_6H_{10}O_5)_n + xClCH_2COOH \xrightarrow{20\%\ NaOH} (C_6H_{10}O_5)_{n-x}(C_6H_9O_6CH_2COOH)_x$$

can be written, involves the solution of the polysaccharide in 20% NaOH solution to which the required amount of monochloroacetic acid was then added.[16] The reaction mixture was left at room temperature overnight. Substitution occurred to about 30–60% of theoretical monochloroacetic acid addition. The CM derivative was then precipitated from the alkali solution by the addition of three volumes of 95% ethanol. The gummy mass was redissolved, then dialyzed for two days against frequently changed distilled water. The purified solution was concentrated and converted to the acid form by passing through a column of cationic ion exchange resin IR-120-H. The remaining anions were removed by passing the acid through a bed of Amberlite IR-4-B.

TABLE I

THE PARENT POLYSACCHARIDES

Polysaccharide	Branching, %	Source
Native Amylose	None	Whole potato starch
L.S. 96 Amylose	None	Defatted corn starch in 2 *M* HCl at room temp., 96 hr.
Native Amylopectin	5[31]	Whole potato starch
L.S. 96 Amylopectin	5	Same as L.S. 96 Amylose
L.S. 648 Amylopectin	5	Whole potato starch in 2 *M* HCl at room temp., 648 hr.
Limit Dextrin, L.S. 96	5	L.S. Amylopectin treated with β-amylase for 60 hr.
Dextran 1028	20[35]	*Leuconostoc mesenteroides* 1028, hydrolyzate
Dextran 1041 C	20[35]	*Leuconostoc mesenteroides* 1041 C, hydrolyzate
Dextran B 512	4[35]	*Leuconostoc mesenteroides* B 512, hydrolyzate

The samples prepared and their degree of substitution are listed in Table II. The reaction by which they were prepared was not carefully controlled, and the average extent of substitution of each sample was determined by titration of the sample with base, and dry weight analysis. The degree of substitution of a sample, β, in –COOH groups per glucose unit can be obtained from the above data by the equation

$$\text{milliequiv. base} = \text{mg. of sample}/(58 + 162/\beta) \quad (2)$$

All the CM derivatives prepared in this work showed enhanced solubility over their parent polymers. Because of the experience of Roger,[16] who found that dried samples of CMP would not readily redissolve, the samples were never dried, but were stored in a refrigerator.

The viscosities were measured with a Bingham[17] viscometer set up for operation with an external pressure of 30–90 cm. water. This arrangement was necessary because all but the lowest molecular weight samples showed a definite shear dependence of viscosity. A precision of ±0.3% could be attained for any one reading. The viscometers were calibrated with distilled water and with National Bureau of Standards Oil H-6. Measurements were made in a constant temperature bath at 30 ± 0.02°, and 20 minutes were allowed for temperature equilibration. Four readings were taken at each of at least three different pressures, and the averages of the four readings were taken for a single point. The viscosity at zero shear stress was determined from plots

(12) J. R. Schaefgen and C. F. Trivisonno, *J. Am. Chem. Soc.*, **74**, 2715 (1952).

(13) M. L. Huggins, *ibid.*, **64**, 2716 (1942).

(14) A. Katchalsky, *J. Polymer Sci.*, **7**, 393 (1951).

(15) P. M. Willis, Dissertation, Columbia University, 1946.

(16) M. Roger, Dissertation, Columbia University, 1952.

(17) E. C. Bingham, "Fluidity and Plasticity," McGraw-Hill Book Co., New York, N. Y., 1922.

TABLE II
DESCRIPTION OF SAMPLES

Parent material	Type	Av. mol. wt.	Sample code	Degree of substitution
Native amylose	linear	*ca.* 10^5	CMHAa	0.794
			CMHAa-2	.600
			CMHAb	.152
			CMHAc	.170
Lintner starch 96 Amylose	linear	...	CMMAa	.750
			CMMAb	.275
Native amylopectin	branched	*ca.* 10^7	CMHBa	.746
Lintner starch 96 amylopectin	branched	...	CMMBa	.746
			CMMBb	.172
Lintner starch 648 amylopectin	branched	5000	CMLBa	.821
Limit dextrin from L.S. 96 amylopectin	branched	...	CMMDf	.485
			CMMDg	.270
			CMMDh	.132
Dextran from B 512		3×10^4	CM512a	.690
			CM512b	.467
Dextran from 1028		2×10^5	CM28a	.505
			CM28b	.499
Dextran from 1041 C		2×10^5	CM41a	.763
			CM41b	.407

of the viscosity at the various pressures against the pressure.[18] Fox, Fox and Flory[19] have suggested another method which was also used in a few cases. Agreement between the zero shear stress values obtained by the two methods was better than 1%.

Intrinsic viscosities to characterize each of the samples were first determined in 0.0869 *M* HCl at concentrations up to about 0.05 grundmolar.[20] The remaining data were taken in water solution. The correct degree of ionization in these determinations was found by adding the number of carboxyl groups which dissociated by self-ionization to the number neutralized by base. The former quantity was calculated from *p*H measurements.

A Beckman laboratory model *p*H meter was employed for the *p*H measurements. In addition, a few determinations were checked with a quinhydrone electrode.[21] Agreement between the two methods was to ±0.03 *p*H unit, which was also the limit of reproducibility.

Results

Viscosity.—The intrinsic viscosity of the uncharged CMP can be measured directly because of their solubility in dilute HCl solutions in which only about 0.1% of the carboxyl groups are ionized. The values vary slightly with substitution, but agree closely with the values of the intrinsic viscosity of the parent polymers in the case of the dextrans, for which the latter quantity is easily obtainable (Table III). The concentration in all cases is given in terms of grundmole[20] since this unit is related to the kinetic segments upon which theoretical developments of the viscosity[22,23] are based. For the partially substituted CMP, the monomer is either the glucose residue, or the glucose glycolic acid ether, and thus the average molecular weight of the monomer unit varies with the extent of substitution.

TABLE III
COMPARISON OF THE INTRINSIC VISCOSITIES OF DEXTRANS AND CARBOXYMETHYL DEXTRANS

Sample	Degree of substitution	Intrinsic viscosity
Dextran 1028	...	4.5 ± 0.1
CM28a	0.505	5.0
CM28b	.499	4.8
Dextran 1041 C	...	4.2
CM41a	.763	4.2
CM41b	.407	4.2
Dextran B 512	...	3.4
CM512a	.690	3.6
CM512b	.467	3.4

The viscosities of the aqueous solutions of the pure acid, or the partially neutralized CMP showed the usual increase in reduced viscosity with decreasing concentration. In many instances, when the reciprocal of the reduced viscosity was plotted against the square root of the concentration, according to equation 1, negative values were obtained for the constants which, therefore, could have no physical significance in terms of a model of the molecules. Schaefgen and Trivisonno[12] had found similar behavior in the case of polyamides in formic acid, and modified the equation to ensure positive constants. It became apparent that an explanation of the extension of the CMP molecules could not be based upon an equation which failed in several instances.

To avoid this difficulty another approach was pursued. It was discovered that the ratio of the viscosity of a sample of a partially neutralized CMP to the viscosity of its pure acid form in water at the same concentration remains approximately constant, irrespective of the concentration (Table IV—Experimental Data). The constancy of this ratio can be improved somewhat (Table IV—Corrected Data) by taking into consideration that the carboxymethyl polysaccharides are fairly strong acids, with pK values of about 5. In solution, the polyelectrolyte molecules will therefore dissociate to an extent which depends upon the concentration. Consequently, the values of the reduced viscosity that appear in the denominator of the ratios in Table IV refer to solutions which are not at the same degree of ionization.

The correction that can be applied can be illustrated with reference to Fig. 1, which shows the concentration dependence of the reduced viscosity of sample CMHAb. The upper curves represent experiments in which the acid groups of the polyelectrolyte molecules have been neutralized with base to the extent shown. Because of the large amount of ionization by base, self-ionization is negligible in these solutions. The lowest curve, on the other hand, represents points that were charged only by self-ionization, which quantity varies from 0.037 to 0.062 in the concentration range shown. Since it was found that, to a good approximation, one can treat the charge dependence of the reduced viscosity independently of all other factors by means of equation 5, one can correct the viscosities of the lowest curve to a common value

(18) H. T. Hall and R. M. Fuoss, *J. Am. Chem. Soc.*, **73**, 265 (1951).
(19) T. G. Fox, Jr., J. C. Fox and P. J. Flory, *ibid.*, **73**, 1901 (1951).
(20) Grundmolarity is defined as the molarity of monomer units. H. Staudinger, "Die Hochmolekularen Organischen Verbindungen," Julius Springer, Berlin, 1932.
(21) F. Daniels, J. H. Mathews and J. W. Williams, "Experimental Physical Chemistry," 3rd Ed., McGraw-Hill Book Co., New York, N. Y., 1941.
(22) J. G. Kirkwood and J. Riseman, *J. Chem. Phys.*, **16**, 565 (1948).
(23) P. Debye and A. M. Bueche, *ibid.*, **16**, 573 (1948).

TABLE IV

RATIO OF THE VISCOSITY OF A PARTIALLY NEUTRALIZED CARBOXYMETHYL POLYSACCHARIDE TO THE VISCOSITY OF ITS PURE ACID FORM

Sample	Concn.	$\eta(\alpha)/\eta$ in water: Exp.	Cor.	Exp.	Cor.	Exp.	Cor.
CMHAa		$\alpha = 0.322$		$\alpha = 0.638$		$\alpha = 0.925$	
	0.01	2.77	6.18	4.35	10.6	5.60	12.7
	.02	3.41	6.56	5.80	11.0	7.70	14.0
	.03	3.51	6.85	6.30	11.6	7.94	15.3
	.04	3.63	6.79	6.72	12.4	10.0	17.0
CMHAb		$\alpha = 0.277$		$\alpha = 0.587$		$\alpha = 0.950$	
	0.01	1.57	2.28	2.32	3.36	3.18	4.60
	.02	1.34	1.51	2.06	2.32	2.88	3.25
	.03	1.69	1.69	2.65	2.65	3.24	3.24
	.04	1.75	1.57	2.70	2.43	4.00	3.60
CMMBa		$\alpha = 0.314$		$\alpha = 0.605$		$\alpha = 0.950$	
	0.01	2.55	3.44	3.82	5.16	4.58	6.18
	.02	2.58	3.04	3.85	4.54	4.78	5.64
	.03	2.60	2.83	3.85	4.14	4.83	5.18
	.04	2.54	2.54	3.87	3.87	4.85	4.85
CMMBb		$\alpha = 0.305$		$\alpha = 0.615$		$\alpha = 0.950$	
	0.01	1.60	1.94	2.50	3.03	3.65	4.42
	.02	1.68	1.81	2.59	2.80	3.88	4.19
	.03	1.61	1.61	2.56	2.56	3.64	3.64
	.04	1.62	1.46	2.50	2.25	3.41	3.07
CMMDf		$\alpha = 0.300$		$\alpha = 0.607$		$\alpha = 0.968$	
	0.01	2.40	2.71	3.87	4.37	4.91	5.55
	.015	2.39	2.53	3.96	4.20	4.80	5.09
	.02	2.54	2.54	3.77	3.77	5.00	5.00

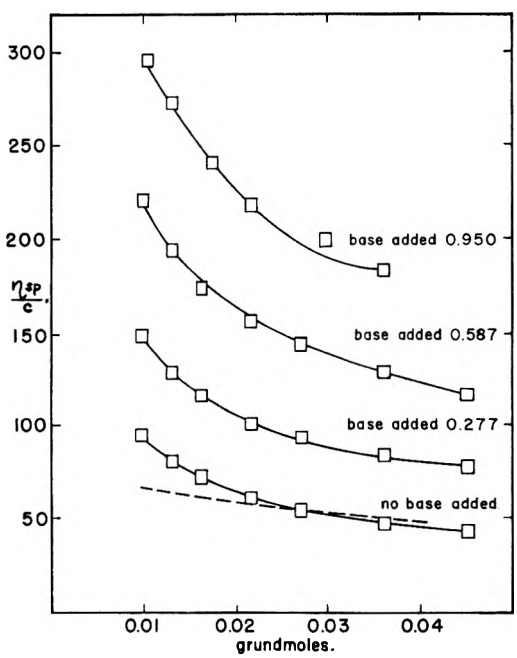

Fig. 1.—Variation of reduced viscosity with concentration sample CMHAb.

of the degree of charge (dotted line in Fig. 1) by evaluating $f(\gamma)$ for the common value of the degree of charge, evaluating it for the experimentally determined degree of charge, and multiplying the experimental reduced viscosities of the acid form by their ratio. The corrected values of the reduced viscosity are then used to determine the corrected ratios in Table IV.

The above approximation regarding the independence of the effects of the concentration and the charge permits the measurement of the increase of the reduced viscosity due to charge alone and, therefrom, the extension of the hydrodynamic volumes of the molecules under the influence of electrostatic repulsions. To simplify the representation of these effects, the stretching ratio, R, is defined as the ratio of the reduced viscosity of the ionized polyelectrolyte in 0.01 gdm. solution to its intrinsic viscosity as measured in strong acid. R is then a measure of the additional hydrodynamic volume of the partially charged molecules, and a comparison of R values for various structural types gives some information about their susceptibility to deformation. The arbitrary concentration of 0.01 gdm. was chosen because of the ease of measurement with the desired precision.

If the substitution of carboxymethyl groups on the polysaccharide as well as the subsequent ionization of these groups are random, the extensibility of the molecule, as measured by R, should depend only on the average number of ionic groups per glucose monomer which will be designated by γ. The quantity γ is obviously the product of α, the degree of neutralization, and β, the degree of substitution. For a given structure, the average interionic distance along a polymer chain is the same for various samples with the same value of γ although the individual values of α and β may differ. In addition, at constant γ the concentration of ions in solution is the same. Thus, since the ionic relationships in the solution are the same, one may neglect the ionic effects by comparing materials under these conditions.

Figures 2–5 show the stretching ratios, R, of the various CMP as a function of γ. The degrees of dissociation, α, which entered into the calculations of γ were corrected for self-ionization as determined by pH measurements. In the pure acid form of the polymer, self-ionization was the sole source of charges, and it contributed as much as 20% at the lower degrees of neutralization.

It is evident from the curves of Figs. 2–5 that all the points corresponding to derivatives stemming from a single parent polymer fall on the same curve even though the degree of substitution of the derivatives may be different. It is apparent that the extension of the molecule is determined by the size, shape and ionic charge of the skeleton of the molecule and is not appreciably affected by the substituent —CH_2COOH groups.

The data permit the comparison of the extensibility of the various structures studied as a function of the charge (Table V). The values of the intrinsic viscosity listed in the table were those estimated for an unsubstituted sample by extrapolation of the intrinsic viscosities of the samples of different degrees of substitution. This value is characteristic of a particular polymer skeleton. To express the extensibility of a given structure by a single parameter, the value of R at $\gamma = 0.7$ was chosen, designated as R_m and so reported in the table.

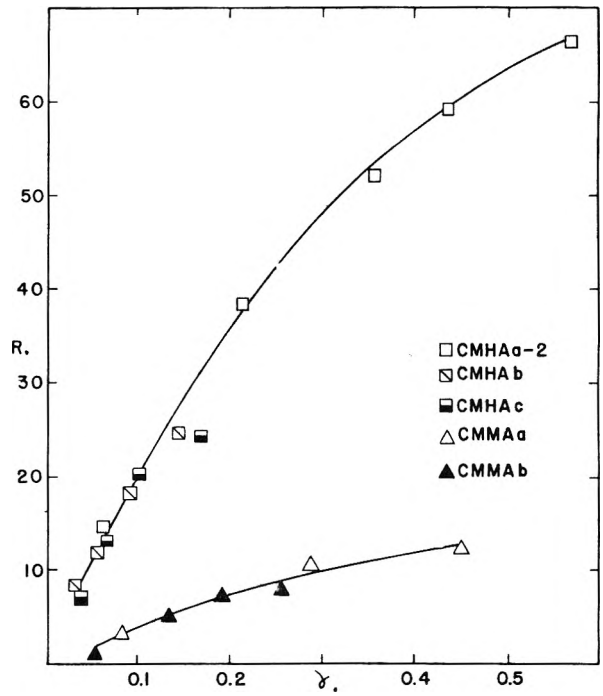

Fig. 2.—Variation of stretching ratio with degree of charge amylose derivatives.

TABLE V

SOME PHYSICAL CONSTANTS OF THE CARBOXYMETHYL POLYSACCHARIDES

Structural type	Sample	[η] extrapd., 1/gdm.	R_m	Mol. wt.	Method
Linear	CMHA	12	70	10^5	End group[33]
	CMMA	3.5	14.7	...	
Branched	CMHB	8	157	10^7	Sedimentation[26]
	CMMB	2	17.7	...	
	CMMD	2	16.6	...	
	CMLB	1.5	5.1	5000	End group[25]
Dextrans	CM41	4.2	22.7	2×10^6	Viscosity[24]
	CM28	4.8	20.7	2×10^6	Viscosity[24]
	CM512	3.4	15.3	3×10^4	Viscosity[26]

For those derivatives for which experimental data at $\gamma = 0.7$ were not available, equation 4 had to be used to determine the value of R_m. The experimental values of the other parameters at a concentration of 0.01 gdm., ($f(c) = 1$), were inserted, and that value of R_m chosen which gave the best agreement between the experimental and calculated reduced viscosities for the particular sample.

Hydrogen Ion Binding.—Table VI lists the pK values of all samples in solution which is 0.001 M in –COOH groups. The ionization constants increase slightly with increasing degree of substitution of the sample, but no regular shift in the constant occurs between linear and branched carboxymethyl polysaccharides. The values of the pK constants were determined from pH data using the modified Henderson–Hasselbalch equation of Kern[27,28]

$$pH = pK + n \log \alpha/(1 - \alpha) \qquad (3)$$

at several concentrations for each sample. The pK values varied linearly with the logarithm of the concentration, and were interpolated to permit comparison at one concentration. In view of the fact that the ionization constants are not affected by the structural type of the polyelectrolytes, one may conclude that the electrostatic interactions are identical in both branched and linear series, and that the repulsions which cause the extension of the polymers are likewise identical, irrespective of the somewhat differing spatial locations of the charged groups in the two series

Discussion

Concentration, Charge and Viscosity.—The near constancy of the ratios given in Table IV suggests that the concentration of the solution of polyelectrolyte does not greatly influence the extension of the molecules caused by interionic repulsions. Unless other, exactly compensating factors enter, this conclusion is inevitable.

Such behavior can be explained in terms of a model of the molecules in the following manner. The concentration dependence of viscosity is an

(24) B. Ingelman and M. S. Halling, *Arkiv Kemi*, **1**, 61 (1949).
(25) F. E. Horan, Dissertation, Columbia University, 1944.
(26) M. Wales, P. A. Marshall and S. G. Weissberg, *J. Polymer Sci.*, **10**, 229 (1953).
(27) W. Kern, *Z. physik. Chem.*, **181**, 249 (1938).
(28) A. Katchalsky and P. Spitnik, *J. Polymer Sci.*, **2**, 432 (1947).

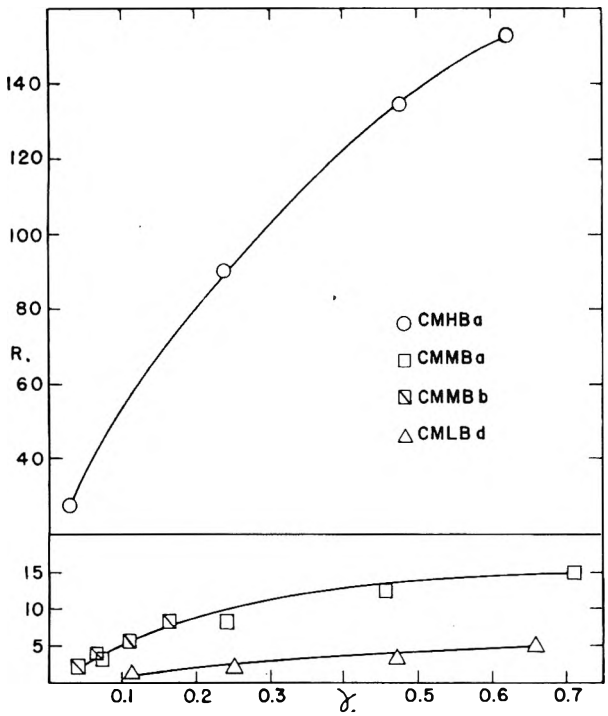

Fig. 3.—Variation of stretching ratio with degree of charge amylopectin derivatives.

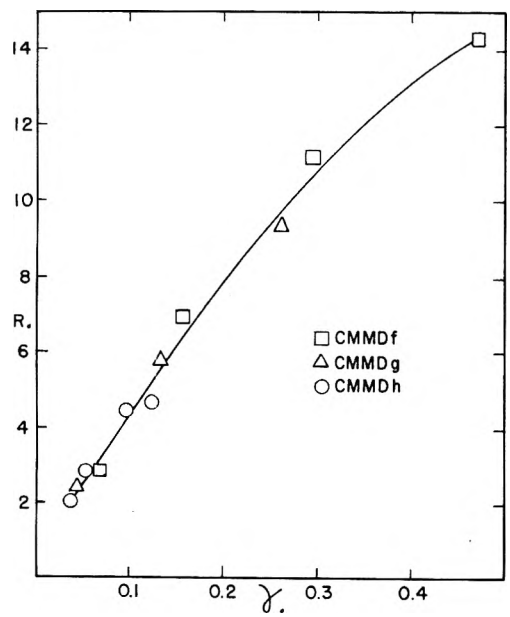

Fig. 4.—Variation of stretching ratio with degree of charge limit dextrin derivatives.

inter-molecular effect. It is governed by the freedom of the individual molecules in the hydrodynamic and electrostatic fields of the remainder of the solution, and is responsible for the observed decrease of the reduced viscosity with increased concentration. The charge dependence is intra-molecular in character. It is the result of the changes in the conformation of the individual molecules which arise as electrostatic repulsions between the ionic groups of the same molecule change its shape. The extensions of the individual molecules are responsible for the observed increase in the reduced viscosity with an increase in the degree of charge.

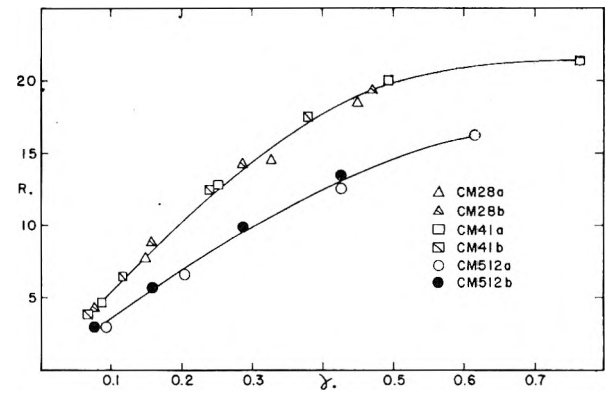

Fig. 5.—Variation of stretching ratio with degree of charge dextran derivatives.

The existence of the inter-molecular and intra-molecular effects has been suggested by Aten[29]; however their relation to measured values had not been established prior to the present work, nor has it been shown, heretofore, that there are only minor interactions between these two effects.

TABLE VI

pK VALUES OF CARBOXYMETHYL POLYSACCHARIDES AT —COOH CONCENTRATION OF 0.001 *M*

Sample	Degree of substitution	*pK*
CMLBa	0.821	4.85
CMHAa	.794	4.80
CM41a	.763	5.22
CMMBa	.746	5.47
CM512a	.690	4.88
CMHAa-2	.600	5.22
CM28a	.505	4.75
CM28b	.499	4.74
CMMDf	.485	4.96
CM512b	.467	4.49
CM41b	.407	4.72
CMMAb	.275	4.45
CMMDg	.270	4.53
CMMBb	.172	4.41
CMHAc	.170	4.15
CMHAb	.152	4.08
CMMDh	.132	4.25

The fact that the inter-molecular interactions seem only slightly affected by the charges upon the molecules indicates that inter-molecular electrostatic interactions are small. This supports the suggestion made by Schneider and Doty[30] that each polyelectrolyte molecule, because of its counterions, has a smaller effective charge than would be inferred from its degree of neutralization.

Structure and Viscosity.—The CM starch fractions were chosen for this work because the structures of both amylose and amylopectin are known with considerable certainty. These materials may therefore serve as prototypes for linear and branched polymers. Larner, Illingworth, Cori and Cori have shown that amylopectins have a highly branched, tree-like structure, with branches of about ten glucose units.[31,32] The linear structure

(29) A. H. W. Aten, Jr., *J. Chem. Phys.*, **16**, 636 (1948).
(30) N. S. Schneider and P. Doty, THIS JOURNAL, **53**, 762 (1954).
(31) J. Larner, B. A. Illingworth, G. T. Cori and C. F. Cori, *J. Biol. Chem.*, **199**, 641 (1952).
(32) C. O. Beckmann, *Ann. N. Y. Acad. Sci.*, **57**, 384 (1953).

of amyloses was found chemically by Meyer,[33] and has been confirmed by many physical methods. These substances have the further advantage of having identical monomer units.

The accurate knowledge of the structure of the starch fractions is balanced, however, by the difficulty of obtaining samples of identical molecular weight which are required for an accurate evaluation of the influence of structure upon the stretching ratio. Four of the samples used here are of approximately equal molecular weight. The molecular weights of the dextrans CM28 and CM41 were obtained from the viscosity equation of Ingelman and Halling.[24] The molecular weight of the amylose was determined by Meyer[33] from an end group analysis. Since the two methods give different averages, the molecular weights of the samples used here may differ by as much as a factor of 10. The molecular weight of the amylopectin limit dextrin (CMMD) had to be inferred from Horan's[25] sedimentation data on Lintner Starch 96, and the fact that β-amylase action reduces the molecular weight by approximately one-half. These data suggest a molecular weight of the same order of magnitude for CMMD.

The intrinsic viscosities of these four samples show the expected variation with structure type, the linear amylose showing the highest, and the limit dextrin the lowest value in accordance with the theoretical interpretation of the intrinsic viscosity as a function of molecular shape.[34] The stretching ratios, likewise, are in accord with expectation. This is evident when one considers amylose and amylopectin as being composed of unit chains of 20 glucose residues. In the case of amylose these unit chains are combined end to end so that the extension of the whole is the sum of the extensions of the unit chains and results in a large change in axial ratio. In the case of amylopectin, the end of one unit chain is linked to a branch point located at approximately the mid-point of another unit chain and at some angle to the main axis of the chain. The extension of the whole amylopectin molecule is obviously no longer the sum of the extensions of the unit chains but much less than the sum; and because the unit chains will be pointing in many directions, it will result in a small change in axial ratio. In fact, the mechanism probably approximates more closely the swelling of a sphere.

The dextrans appear intermediate in structure, although determination of branch points yields a high value, 20% of the monomer units.[35] To reconcile these findings, one must postulate a structure consisting of a linear core to which short, highly sub-branched branches are attached. Such a conformation permits a large distortion of the axial ratio which then appears as a large stretching factor. The third sample of dextran, CM512, has fewer branch points (4%).[35] If one considers its lower molecular weight,[25] its constants indicate that it too has a well defined skeletal axis. The data for dextran B512, therefore, serve to support the conclusions of the workers at the National Bureau of Standards[36] regarding its structure.

The importance of the molecular weight in this work can be seen from sample CMHB which according to the best estimates[25] has a molecular weight of between 20 and 80 times that of the samples discussed above. As a consequence, both its intrinsic viscosity and maximum stretching ratio are larger than those of the smaller polymers, but the per cent. difference between the values of its constants and those of the amylose (CMHA) is not as great as the per cent. difference between the constants of amylose and amylopectin limit dextrin of approximately equal molecular weight.

A General Equation for the Viscous Behavior of CMP.—On the basis of the data obtained in this investigation, it is possible to write for the reduced viscosity of any CMP the equation

$$\eta_{sp}/c = [\eta]R_m f(\gamma)f(c) \qquad (4)$$

where η_{sp}/c is the reduced viscosity of the polymer, $[\eta]$ is the intrinsic viscosity of the uncharged polymer measured in 0.0869 M HCl, R_m is the previously defined extensibility, $f(\gamma)$ is a function of the number of charges only, and $f(c)$ is a function of the concentration only, and takes the form of equation 1. In equation 4 the first two variables are characteristic of the particular polymer, whereas the latter two are identical for all the carboxymethyl polysaccharides investigated.

The numerical values of the functions are obtained from the following considerations. Figures 2–5 show that $f(\gamma)$ is a quadratic function with a maximum at $\gamma = 0.7$. The definition of R_m requires that $f(\gamma) = 1$ at the maximum. Furthermore, the terms in equation 4 which relate to the extension of the polyelectrolyte with charge must become equal to unity when the degree of charge becomes zero. At the limit of $\gamma = 0$, $f(\gamma)$ must therefore be $1/R_m$. These requirements lead to

$$f(\gamma) = 2.86\gamma - 2.04\gamma^2 - (2.86\gamma - 2.04\gamma^2 - 1)/R_m \qquad (5)$$

The best agreement for the experimentally determined variation of the reduced viscosity with the concentration was found for

$$f(c) = 3.16/(1 + 21.6c^{1/2}) \qquad (6)$$

This leads to $f(c) = 1$ when $c = 0.01$ gdm. as required by the definition of the extensibility, R_m.

The applicability of equation 4 was checked by a comparison of the experimental and calculated reduced viscosities, using equations 5 and 6, and the values $[\eta]$ and R_m in Table V. For 140 data of all the polyelectrolytes used in this work, the average deviation is 11.1%. If points of low γ are omitted (at γ less than *ca.* 0.1, $f(\gamma)$ changes most rapidly and γ itself is known with the least precision) the average per cent. deviation is reduced to 8.5% for 90 points.[37]

The applicability of equation 4 to all data indicates that in a consideration of polyelectrolyte vis-

(33) K. H. Meyer, M. Wertheim and P. Bernfeld, *Helv. Chim. Acta*, **23**, 865 (1940); **24**, 378 (1941).

(34) R. Simha, THIS JOURNAL, **44**, 25 (1940).

(35) Dr. L. L. Phillips, private communication.

(36) M. Wales, P. A. Marshall, S. Rothman and S. G. Weissberg, *Ann. N. Y. Acad. Sci.*, **57**, 353 (1953).

(37) Complete data are available in the dissertation by S. S. Winter from University Microfilms, Ann Arbor, Mich.

cosities the following factors are of paramount importance: (1) the structure of the polymer and its extensibility, (2) its concentration in solution, and (3) intra-molecular electrostatic interaction.

Acknowledgments.—The authors are indebted to the Dextran Corporation of Yonkers, New York, and to the Corn Industries Research Foundation for partial support of this work.

EQUILIBRIUM AND KINETICS OF DETERGENT ADSORPTION— A GENERALIZED EQUILIBRATION THEORY

BY ANTONINO FAVA[1] AND HENRY EYRING

Department of Chemistry, University of Utah, Salt Lake City, Utah

Received November 19, 1955

As a result of the study of the adsorption of detergents a new theory of detergent action is proposed which postulates that in addition to the usual stabilizing of dirt in the solvent by micelle formation, adsorption of detergent on the fabric surface weakens the bond of dirt to fabric and so speeds up the dissolution of such bonds. The peculiar break and the maximum in the adsorption *versus* concentration curves are shown to arise from the anomalous properties of the solution rather than from peculiarities of the adsorbate–surface system. The rates of adsorption and desorption of detergent are found to follow a very simple non-linear reduced equation which has general applicability to condensed systems approaching equilibrium. Irreversible thermodynamics suffices to represent only the final part of this equilibration process which is, however, readily formulated in terms of reaction rate theory.

Introduction

It is a widely accepted opinion that in the mechanism of detergent action, adsorption plays an important role. However, no clear mechanism supported by experimental evidence has been developed and no simple relation between detergency and adsorption is as yet established.

An interesting study recently was carried out by Meader and Fries[2] who investigated in detail the adsorption on cotton and wool of a sodium alkyl-aryl-sulfonate and of potassium palmitate. In their article reference is also made to other papers concerned with adsorption of detergents on textile fibers. A few other papers have appeared in the meantime.[3] The adsorption of detergents on surfaces other than textile fibers has also been studied. Activated carbon,[4] latex particles,[5] polystyrene,[4a] bacteria,[6] sand,[7] cassiterite,[8] and metals,[9] were also used as adsorbents. The adsorption of detergents at liquid/liquid and liquid/gas interfaces has been also widely investigated, often by means of interfacial tension,[10] or more recently by means of a clever technique introduced by Dixon, Weith, Argyle and Salley.[11]

Despite the considerable amount of work done, very little attention has been paid to the kinetic aspect of the problem. Actually the only kinetic data are those of Wolstenholme and Shulmann,[9] and those concerning the so-called time effect in surface tension.[12] The present study deals with adsorption of detergents from the point of view of equilibrium, and of rates of adsorption and desorption. Most of the experimental data were taken using cotton as adsorbent. Some results concerning metals, particularly nickel and lead were also obtained. The technique used to detect adsorption has been a radiochemical one. The procedure introduced by Meader and Fries was used throughout this work. Because of its sensitivity this technique permits the measure of the adsorption directly. This makes the measurements fairly accurate even at the large concentrations where indirect methods become impractical.

Experimental

Materials.—Sodium dodecylbenzene sulfonate (DBSNa) was employed as the detergent. S^{35} was used for labelling purposes. To a solution of $H_2S^{35}O_4$ carrier free (obtained from Oak Ridge) about 1 mg. of Na_2SO_4 was added and the solution evaporated to dryness in a centrifuge tube. This highly radioactive Na_2SO_4 is now diluted to a proper level by adding sulfuric acid with a content of about 15% of free SO_3. This is then used to sulfonate the hydrocarbon. The sulfonation is carried out at 0°. The temperature is then gradually raised and finally held for one hour at 60°. Thereafter an amount of alcoholic NaOH just insufficient to neutralize it is added to the mixture. Sodium bicarbonate is next added and the slurry stirred until no more CO_2 is evolved. The slurry is centrifuged and the alcoholic solution yields the sulfonate on evaporation. To eliminate

(1) We wish to thank the Foreign Operation Administration and the National Academy of Sciences for a fellowship and the Purex Corporation for financial support.

(2) A. L. Meader and B. A. Fries, *Ind. Eng. Chem.*, **44**, 1636 (1952).

(3) (a) L. H. Flett, L. F. Hoyt and J. E. Walter, *J. Am. Oil Chemists' Soc.*, **32**, 166 (1954); (b) L. H. Flett and L. F. Hoyt, Am. Dyestuff Reptr. **43**, Proc. Am. Assoc. Textile Chemists Colorists, p. 335 (1954).

(4) (a) M. L. Corrin, E. L. Lind, A. Roginsky and W. D. Harkins, *J. Colloid Sci.*, **4**, 485 (1949); (b) A. S. Weatherburn, G. R. F. Rose and C. H. Bagley, *Can. J. Research*, **27F**, 179 (1949); (c) R. Cavier, *Compt. rend.*, **216**, 255 (1943).

(5) E. A. Willson, J. R. Miller and E. H. Rowe, THIS JOURNAL, **53**, 357 (1949).

(6) A. E. Alexander and A. I. McMullen, "Surface Chemistry (Special Supplement to *Research*)," Butterworths, London, 1949, p. 309.

(7) Lun Hsiao and H. N. Dunning, THIS JOURNAL, **59**, 362 (1955).

(8) G. R. Edwards and W. E. Ewers, *Australian J. Sci. Research*, **A4**, 627 (1951).

(9) G. A. Wolstenholme and J. H. Shulmann, *Trans. Faraday Soc.*, **46**, 489 (1950).

(10) (a) C. P. Roe and P. D. Brass, *J. Am. Chem. Soc.*, **76**, 4703 (1954); (b) E. G. Cockbain, *Trans. Faraday Soc.*, **50**, 874 (1954); (c) B. A. Pethica, *ibid.*, **50**, 413 (1954).

(11) (a) J. K. Dixon, A. J. Weith, A. A. Argyle and D. J. Salley, *Nature*, **163**, 845 (1949); (b) G. Aniansson and O. Lamm, *ibid.*, **165**, 357 (1950); (c) G. Aniansson, THIS JOURNAL, **55**, 1286 (1951); (d) R. Loos, *Medel. Konickl. Vlaam. Acad. Wetenschap. Belg. Klasse Vetenschap*, **13**, 3 (1951); (e) G. Nielsson and O. Lamm, *Acta Chem. Scand.*, **6**, 1175 (1952); (f) R. Ruyssen, *Bull. soc. chim. Belges*, **62**, 97 (1953).

(12) G. C. Nutting, F. A. Long and W. D. Harkins *J. Am. Chem. Soc.*, **62**, 1496 (1940).

traces of radioactive sulfate, the sulfonate is now dissolved in a few drops of water and sodium sulfate is added. The solution is then diluted with a large excess of alcohol, and the sodium sulfate centrifuged. The solution is finally evaporated and the product is dried *in vacuo* at 90°. This last operation is intended to eliminate traces of unreacted hydrocarbon. The purity of the product was tested by running a series of measurements of surface tension at various concentrations of the detergent. Surface tension was measured by the ring method. As shown in Fig. 3, no minimum in surface tension was found.[13] The final product weighed 232 mg., with a total activity of 4 mc. In our condition of counting, this activity permitted the detection of an amount of detergent as low as 10^{-8} g. A thin mica window Geiger–Mueller counter was used. Most of our measurements were made on cotton cloth. "Indian Head" cotton was employed and pretreated as follows.

A single piece of cotton was washed several times in hot distilled water and dried at room temperature in the air. From this piece of cloth, the different samples were cut. These were dried in an evacuated vessel at room temperature for 5 minutes before the counting operation. The loss of bound water in such a short time was considered negligible since the vacuum was not better than a few mm. In any case, the drying time was the same for all samples.

The value of the correction to be applied to the measured value of the radioactivity varies according to the concentration of the solution from about 5% for the most dilute to about 50% for the most concentrated solutions.

Procedure.—In the case of cotton the adsorption is measured on samples of cloth of about 2 cm.^{2} of apparent area. The activity of the solutions was measured by pipetting a known volume onto a circular support, one inch in diameter, evaporating the solvent and counting. The volumes of the solution were always chosen in order to contain between 0.01 and 0.1 mg. of solute. With such a tiny amount spread on about 4 cm.^{2} of area, no correction for self-adsorption was necessary. The correction made for the radioactivity absorbed by the cloth was a purely empirical one. On one of the cotton samples, which were about 2 cm.^{2} in area, a known volume (~0.05 cc.) of a solution of known radioactivity was placed in such a way that it was absorbed by the cloth. The cloth was then dried. A few drops of water were next added to the cloth in order to better distribute the solute, after which the cloth was dried a second time. This last addition of water and drying was repeated, and finally the sample was counted for radioactivity. Since the amount of solution put on the cloth was known, as well as the total radioactivity, the fraction of radioactivity adsorbed by the fibers is easily evaluated. By repeating this procedure several times with different samples and with different amounts of radioactivity, it was found that absorption by the cloth reduced the radioactivity by a factor of between 2.6 and 3.0. Actually the average of many experiments gave 2.8, and this number was used in all experiments. Thus, in order to obtain the true radioactivity of a sample in the adsorption experiments, the measured activity was multiplied by 2.8. No further correction for self-absorption was necessary. Consider, for instance, the case in which the maximum of radioactive material was absorbed (Fig. 1, curve II). The amount adsorbed was 140×10^{-7} mole/g. of cotton. Since the molecular weight is about 300 and the cotton sample weighed 30 mg., the amount adsorbed was calculated as $140 \times 10^{-7} \times 300 \times 30 \times 10^{-3} = 1.3 \times 10^{-4}$ g. With such a small amount uniformly distributed over the surface of the cotton, no correction for self-absorption need be made.

To the measured activity a correction must be made to account for the amount of solution still held by the cloth after blotting. This amount is determined by weighing the sample wet and dry. In case of metals no correction is necessary, the amount adsorbed being usually so small that self-absorption of the β-rays can be neglected.

In rate experiments the volume of solution used was always such that the amount actually adsorbed by the sample was negligible compared with the total amount present and therefore the concentration of the solution remained practically constant throughout the experiment. Analogously in desorption experiments the water was continuously renewed so that the concentration of detergent in solution was always very close to zero. The concentration of the various solutions used was determined by measuring the activity of a known volume of solution. A reference standard was prepared by weight.

In order to obtain more consistent results each adsorption isotherm was determined using one sample, with the following procedure: the sample is put in the solution of lowest concentration and left there for 6 hours.[14] After being blotted and dried, the sample is counted to determine the radioactivity. The same sample is then used with the same procedure for all the successively more concentrated solutions.

Also in rate experiments one sample was used for each adsorption or desorption curve. In fact the use of a different sample for each point introduces such scattering that it becomes very difficult to handle the data, unless one determines a much larger number of points.

Results

Adsorption isotherms for cotton were determined in the range 1.5×10^{-5} to 6.0×10^{-3} mole/l. A typical curve is shown in Fig. 1. Two distinct features characterize the isotherm, (1) a sudden increase in adsorption at a concentration of about 1×10^{-3} (point A); (2) a maximum in adsorption at about 3.0×10^{-3}. These features are common to all isotherms we determined. The concentrations corresponding to these characteristic points remain sensibly the same at different temperatures (Fig. 1, curve II), only the amount adsorbed is higher at lower temperature.

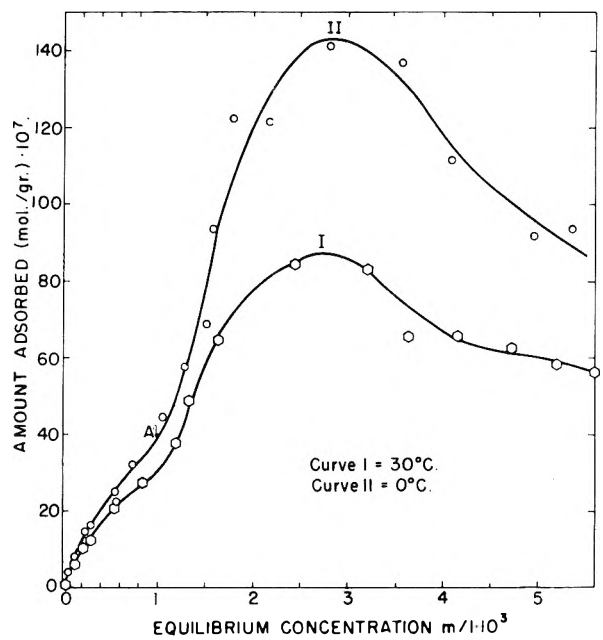

Fig. 1.—Adsorption isotherms of DBSNa on cotton.

The effect of the concentration of H^+ ions is shown in Fig. 2. The increase in adsorption in the HCl solution and the decrease in the NaOH solution with respect to a neutral solution of the same concentration in electrolytes, points out that the hydrogen ions play an important role in the adsorption process. Figure 2 shows also that the increase in adsorption is accompanied by a shift of the maximum toward lower concentrations.

It is interesting to correlate the adsorption isotherm with the formation of aggregates in solution, *i.e.*, with the critical micelle concentration (cmc.). We determined the cmc. with the dye method using

(13) G. D. Miles and L. Shedlovsky, THIS JOURNAL, **48**, 57 (1944).

(14) A 6-hour period is long enough to practically reach an equilibrium condition at all temperatures and concentrations.

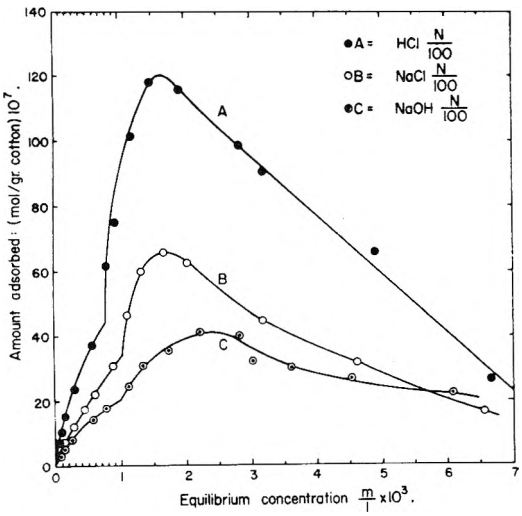

Fig. 2.—Adsorption isotherms of DBSNa on cotton at 30°.

pynacyanole in a set of experiments and Rhodamine 6G in another. Both dyes located the cmc. for the pure soap in the range 2.5×10^{-3} to 3.0×10^{-3}, about at the maximum of the isotherm. However the determination of the surface tension of the soap solutions as a function of concentration (Fig. 3) showed that a constant value of the surface tension is reached at about 1.0×10^{-3} corresponding to the first break in the isotherm. It is generally agreed (see for instance ref. 10a) that the concentration at which the surface tension no longer varies corresponds to the cmc. It is not very surprising that two different methods give somewhat different values of the cmc. Here however the disagreement seems to be larger than is usually found.

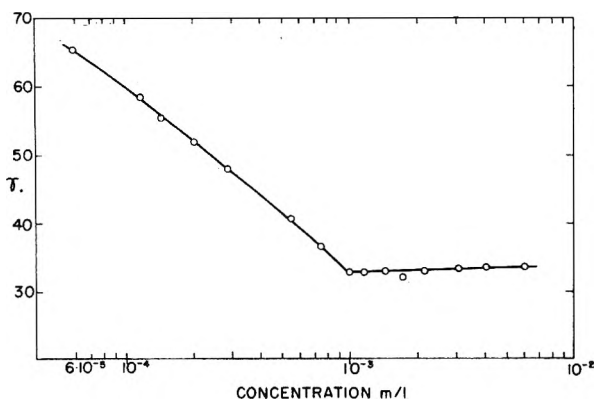

Fig. 3.—Variation of surface tension with concentration.

The difference in the amount adsorbed at different temperatures permits us to calculate the heat of adsorption. We calculated ΔH in the conventional way from two pairs of isotherms, obtaining 1700 and 1100 cal., respectively. The last figure is obtained from the two isotherms reproduced in the paper. We believe these values are less reliable than the 800 cal. obtained by the method described below. Because of the peculiar form of the isotherm, it seemed more nearly correct to determine the heat of adsorption from the ratio of the amount adsorbed by a given sample at two different temperatures. In practice this analysis was carried out as follows. Adsorption is allowed to take place on a sample at the higher of two temperatures at a given concentration. After the adsorption has been measured, the same sample is placed again in the same solution but at a lower temperature. The heat of adsorption is then calculated from the ratio of the amounts adsorbed at the two temperatures. The results of this analysis are shown in Table I. It can be seen the ΔH_a varies widely from experiment to experiment, but since its absolute value is very small (0.8 kcal.), these variations are probably due to experimental error. Anyway, no definite variation of ΔH_a with coverage before and after point A (Fig. 1) is apparent. This fact justifies the procedure used in determining ΔH_a.

TABLE I

ADSORPTION OF DBSNa ON COTTON AT 38 AND 2°

Concn., mole/l.	Amount ads. (mole/g.) × 10⁷ 38°	2°	ΔH_a, cal.
5.6×10^{-4}	16.30	19.75	848
6.02	18.25	21.90	807
7.63	17.7	21.45	850
1.14×10^{-3}	28.8	31.3	368
1.45	34.7	41.9	840
2.16	62.2	69.7	509
3.13	62.1	70.0	532
4.28	53.6	57.5	306
5.17	42.8	52.2	880
5.60	28.3	42.9	1840
		Av.	778

Adsorption Isotherms on Nickel and Lead.—Several metals were tested for adsorption. For some (silver, copper) the amount adsorbed was very small and for practical purposes undetectable with our method. For others (zinc, tin, aluminum) it was evident that corrosion took place. For lead, and particularly for nickel the adsorption was measurable and yet corrosion was not evident from a visual examination of the surface. Coleman and Bell nickel foil, and Fisher Reagent lead foil were used in a series of experiments. Since no particular precautions were taken to exclude air from the detergent solution nor to prepare a bare surface, these results must not be considered as giving a precise measure of the adsorption. The data obtained with lead were not very reproducible; nickel on the contrary showed good reproducibility. The samples were prepared for the adsorption experiments, cleaning them as follows:

Nickel was successively washed in hot alcohol, in water, in 0.1 *N* HCl and finally in water again. After the last rinsing the samples were blotted and immediately used for the adsorption experiments. For lead the same procedure was followed with acetic acid instead of hydrochloric.

A preliminary study of the rate at which adsorption on these metals takes place showed that the adsorption is immeasurably fast. However if the sample is left in the solution a long time, more detergent is adsorbed. This second step is very slow. Moreover, the adsorption seems not to reach an equilibrium value but increases steadily. It is very likely that only the first part of this process represents adsorption, whereas the second is merely a corrosion phenomenon.

In view of these considerations, the sample was left in solution 5 minutes to determine the adsorption isotherm. This time is long enough to be sure that the first fast process takes place and yet so short that the slow one would not critically interfere. The isotherm obtained with nickel is shown in Fig. 4. A striking resemblance of this curve

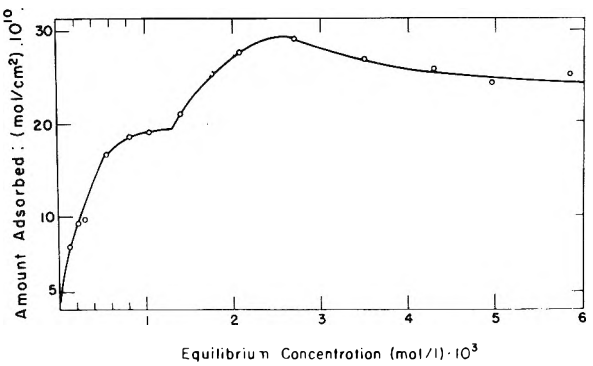

Fig. 4.—Adsorption isotherm of DBSNa on nickel.

with those obtained with cotton is apparent. Both the characteristic points are present and the concentrations corresponding to them are practically the same as for cotton. With lead substantially analogous results were obtained. Reproducibility however was too poor to draw definite conclusions.

Rate of Adsorption and Desorption (Cotton).—Figure 5 shows how the amount adsorbed varies

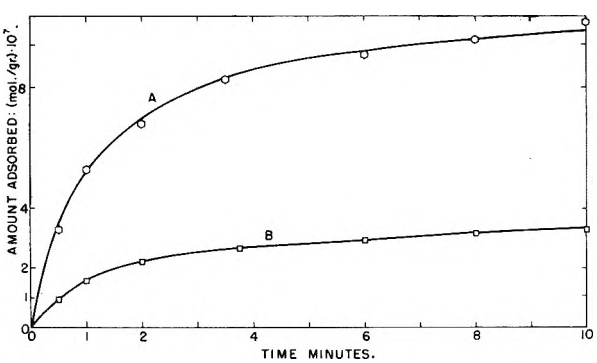

Fig. 5.—Adsorption of DBSNa on cotton at 29.5°: curve A, 2.98×10^{-4} mole/l.; curve B, 5.6×10^{-5}.

with time for two different concentrations. Since it proved difficult to fit these data in a simple predictable kinetic equation, an attempt was made to simplify the problem, studying first how the detergent concentration affects the rate. For this purpose the initial rate, extrapolated graphically, was measured for a number of solutions in the range of concentration 5×10^{-5} to 3.0×10^{-3}. The results of these experiments are collected in Fig. 6. At very low concentrations the initial rate varies almost linearly with the concentration in solution (actually the measured order is 0.8) until at about 9.0×10^{-4} a sudden rise in the initial rate is observed. Gradually the slope of the curve decreases and the rate becomes practically constant at a concentration of about 2.0×10^{-3}. At concentrations above 3×10^{-3} the measure of the initial rate becomes very inaccurate because the correction for the "liquid holdup" becomes more and

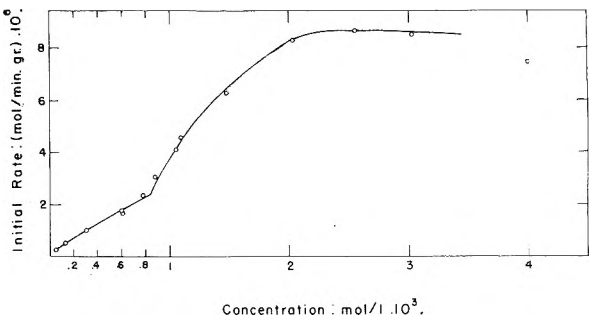

Fig. 6.—Initial adsorption rate of DBSNa on cotton *vs* concentration.

more important. Consequently we cannot be sure as to whether above this concentration the rate remains constant, decreases or even increases a little.

These results instead of clarifying the problem obscure it. However from the many experiments carried out at different concentrations a very important and unexpected result came to light. The rate of adsorption for all the experiments may be represented by the same reduced curve provided that, instead of the amount adsorbed, the ratio (φ) of it to the amount that will be adsorbed at equilibrium is plotted against time. This behavior is exemplified in Fig. 7 where the points of Fig. 5 are

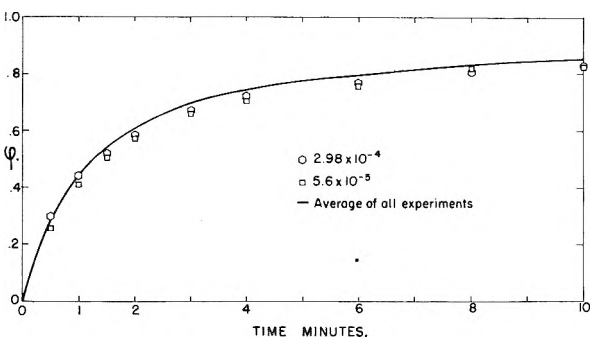

Fig. 7.—Adsorption of DBSNa on cotton at 29.5°.

replotted in this fashion. The solid curve is drawn from the average of 13 different experiments in which the amount adsorbed at equilibrium varied from 3.55×10^{-7} to 77×10^{-7} mole/g. The conclusion is that whatever kinetic equation represents the adsorption with time, it is a reduced equation.

Before trying to analyze more closely these data it is helpful to investigate the desorption.[15] The curve giving the amount still remaining on the surface *versus* the time is one which reaches zero asymptotically. When a number of desorption curves, corresponding to different amounts initially adsorbed, are analyzed, a most interesting result is found. If the ratio of the amount adsorbed at time t to the amount initially adsorbed is plotted against time, all the desorption experiments may be expressed by the same reduced curve (Fig. 8). Thus in desorption it is again a reduced equation that holds.

Since a reduced equation holds both in adsorption and desorption, it might be deduced that both

(15) The desorption experiments are in fact more simple and accurate than those of adsorption because, except for the value at the time zero, no corrections for liquid holdup are necessary. This circumstance makes the adsorption experiments very inaccurate in the region where $\varphi > 0.8$.

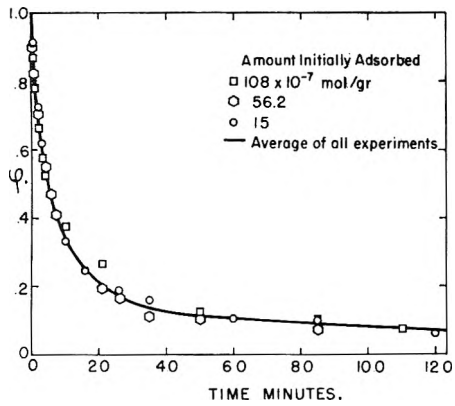

Fig. 8.—Desorption of DBSNa from cotton at 29.5°.

processes are first order. However the integrated form of a first-order kinetic law is completely inapplicable. A careful analysis of all the data establishes the fact that the following kinetic equation applies both in adsorption and desorption

$$-\frac{d\varphi}{dt} = 2k'\varphi \sinh b\varphi \qquad (1)$$

where φ is defined as distance from equilibrium over initial distance from equilibrium, in these cases measured in terms of concentrations. Thus

$$\varphi = \frac{a - a_f}{a_i - a_f} \qquad (2)$$

in which a_i, a, a_f are the amounts adsorbed at the times zero, t and ∞, respectively. The agreement between experiment and an equation of this type is shown in Figs. 8, 9 and 10. It is remarkable that

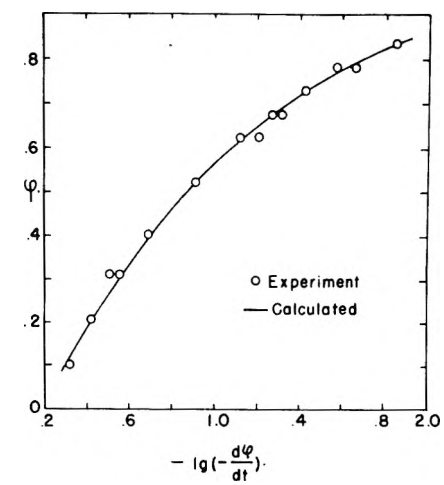

Fig. 9.—Adsorption rate of DBSNa on cotton at 3°.

exactly the same equation expresses both the data for adsorption and desorption, *the constant b having the same numerical value* (1.26). Only the constant k' differs in adsorption and desorption. Moreover, a study of adsorption and desorption at different temperatures shows that the constant b is temperature independent. The two constants k' are temperature dependent. They are the true rate constants for adsorption and desorption, respectively, at $\varphi = 0$. From the values of these constants at different temperatures the heat of activation for

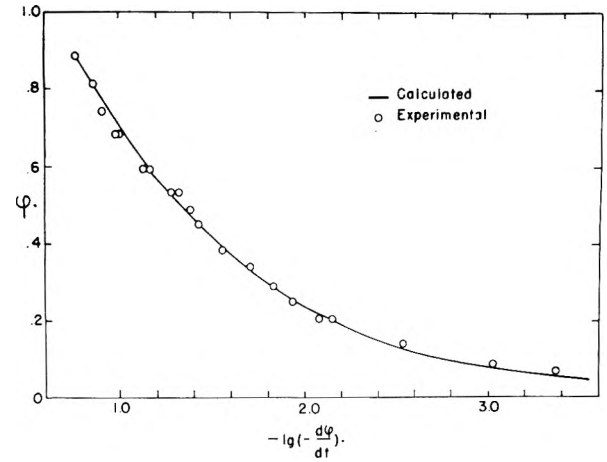

Fig. 10.—Desorption rate of DBSNa from cotton at 29.5°.

adsorption ($\Delta H_a^{\pm}$) and for desorption ($\Delta H_d^{\pm}$) may be obtained. The following values were found

$k'_{3°} = 3.35 \times 10^{-3}$ sec.$^{-1}$ $\quad k'_{29.5°} = 4.65 \times 10^{-3}$ sec.$^{-1}$
$k''_{2°} = 7.37 \times 10^{-4}$ sec.$^{-1}$ $\quad k''_{29.5°} = 1.17 \times 10^{-3}$ sec.$^{-1}$

We have used a double prime for desorption.

From these values one obtains: $\Delta H_a^{\pm} = 2075$ cal., and $\Delta H_d^{\pm} = 2720$ cal. The difference gives $\Delta H_a^{\pm} = 645$ cal. From the equilibrium values (see Table I) we obtained 778 cal. Considering the smallness of these numbers the agreement must be considered good.

Applying the absolute reaction rate theory we can calculate the entropies of activation for adsorption and desorption. The resulting values are: $\Delta S_a^{\pm} = -62.3$ e.u., $\Delta S_d^{\pm} = -62.9$ e.u. Therefore, at all temperatures the specific rate constants have the values

$$k' = \frac{kT}{h} \exp\left(-\frac{62.3}{R}\right) \exp\left(-\frac{2075}{RT}\right)$$

$$k'' = \frac{kT}{h} \exp\left(-\frac{63.9}{R}\right) \exp\left(-\frac{2,730}{RT}\right)$$

Discussion

Adsorption Isotherms.—Among all the investigators who have studied the adsorption of detergents, only two groups have fully recognized the features characterizing the isotherm of adsorption: Corrin, Lind, Roginsky and Harkins[16a] for adsorption of dodecyl sulfate on ashless graphite, and Meader and Fries[2] for adsorption of an alkyl-aryl-sulfonate on cotton. Both these groups determined the cmc. with the dye method[16] and found a value corresponding to the first kink (A in our Fig. 1). We have already mentioned that using the same method we found the cmc. to correspond with the maximum, whereas surface tension measurement gave the cmc. at A. We do not know how to explain this disagreement, and we will suppose that actually the concentration corresponding to point A is the value at which aggregates start to form in solution.

A complete interpretation of the adsorption isotherm is not easy. The rise in adsorption at A

(16) (a) M. L. Corrin, H. B. Klevens and W. D. Harkins, *J. Chem. Phys.*, **14**, 480 (1946); (b) M. L. Corrin and W. D. Harkins, *J. Am. Chem. Soc.*, **69**, 679 (1947).

could be due either to a phase transition of the adsorbate or multilayer adsorption, or be related in some way to the formation of aggregates. The first two possibilities seem improbable for the following reasons: (a) **Surface area:** although we did not measure it, the values given in the literature[17] for surface area of cotton as determined by adsorption of polar substances lie between 0.9 to 2.3 $\times$ 10^6 cm.^{2}/g. Since the amount adsorbed at A is about 30 $\times$ 10^{-7} mole/g. it means that each molecule occupies about 9 $\times$ 10^3 Å^2. It is therefore hard to believe that on such a sparsely covered surface a phase transformation or multilayer adsorption can take place. (b) **Temperature effect:** temperature has no effect in shifting the characteristic point, as would be expected if a phase transition were involved. On the other hand it is an experimental fact that micelle formation is but little affected by temperature. (c) **The characteristic point** happens to be at the same concentration for both cotton and nickel. This shows that the cause for it lies in the solution and not in the nature of the surface. (d) **Rate of adsorption and desorption:** if the adsorption below A represents the formation of one phase (or layer) and above A of another phase (or layer) we should observe different specific rates of adsorption and desorption according to whether the final (or initial) value lies below or above A (see Fig. 1). (e) **The initial rate of adsorption:** we saw (Fig. 6) that at the same concentration at which the isotherm shows a kink the initial rate rises suddenly. Since by definition the initial rate is the rate on a bare surface it is evident that the rise is due to an increase of activity of adsorbable species in the solution.

From the above considerations we must reject the idea that a phase transformation or multilayer adsorption is responsible for the kink at A, and admit it is related to the formation of aggregates in solution. In order to explain this point Meader and Fries[2] postulated that the adsorption of micelles occur from this concentration. If this simple hypothesis were to account for the break at A, it is hard to visualize how, when the concentration increases and the number of micelles consequently increases, the amount adsorbed decreases. Meader and Fries suggest that "at higher concentrations the adsorption of micelles begins to level off, while the adsorption of single ions may be expected to decrease somewhat. Consequently the total amount reaches a maximum." It seems to us that if micelles as such are adsorbable, no decrease in adsorption can be expected if the number of micelles continuously increases. One way to overcome this difficulty is to consider the possibility of the existence of a range of aggregates and admit that only the smallest of these aggregates are capable of being adsorbed.

The process of building up aggregates cannot be an abrupt one. If in a detergent solution there exist, in equilibrium with the monomer, micelles containing n single anions, all the series of intermediates containing from $n - 1$ to 2 ions must necessarily be present. Since, because of electroneutrality the adsorbate must be neutral, it is understandable that the smallest aggregates are more easily adsorbed than the larger ones. This statement may be supported from the consideration of the factors determining the equilibrium between an aggregate and the single ions: (a) the decrease in free energy due to the decrease of interface water/hydrocarbon chains (b) molecular motion, (c) ionic repulsion. Of these factors, (a) tends to stabilize the aggregate, (b) and (c) tend to destroy it. Of the latter two, (b) may be considered only of secondary importance. In fact temperature is known to be of little effect on micelle formation and that means that the energies involved in the formation of these aggregates are small. (a) and (c) are therefore the tendencies whose balance determines the *size and the charge of the aggregate.* In fact for a very small aggregate, the decrease in free energy per ion is very small, and therefore the aggregate may stay together only if the charge is very small. Hence at equilibrium the smallest aggregate must have the lowest charge (above unity). The net consequence of this will probably be a scarcity of these aggregates, but at concentrations just above the cmc., when the larger aggregates are not yet present, they are the only aggregates in solution. If we postulate that besides the monomer, these small aggregates are adsorbable on the surface, the sudden rise in the adsorption isotherm as well as in the initial rate of adsorption can be explained. If the adsorbed radioactive species is any derivative of DBSNa, say the acid, then it might eventually decrease in activity with increasing DBSNa because of hydrolysis accompanying micelle formation thus accounting for the maximum in the adsorption. An impurity more tightly adsorbed than DBSH seems ruled out experimentally as an explanation of the maximum. The competitive adsorption of a hydrolysis product such as NaOH may also play a role.

Yet another difficulty must be considered. If it is true that small aggregates are adsorbable as such, in the desorption process we should be able to find differences in the specific rate according as the initial adsorption is larger or smaller than A (see Fig. 1). The experiments, however, show that no difference is detectable, so that one kind only of adsorbate seems to be present. Therefore, if we have to maintain the idea of the adsorption of small aggregates we must admit that, once on the surface these small aggregates dissociate into single molecules so that the final adsorbate is distributed over the surface in the same way whether the molecule arrived on the surface alone or as an aggregate.

Effect of Hydrogen Ions.—We have seen (Fig. 2) that an increase in the concentration of hydrogen ions, causes an increase in adsorption. This could be due to: (a) increase in the activity of the adsorbable species, (b) formation of a new adsorbable species in considerable amount, (c) modification of the surface which results in an increase of available sites. Point (b) may be ruled out on the basis of desorption experiments which showed no difference in the specific rate between samples that were adsorbed in acid media and samples adsorbed in neutral media. We should therefore conclude

(17) A. J. Stamm and M. A. Millet, THIS JOURNAL, **45**, 43 (1941).

that the adsorbate is the acid soap. However, a simple application of the mass law shows that the increase in adsorption from *p*H 7 to *p*H 2 is too small to be accounted for by the relative increase of acid soap. A possible explanation could be found, assuming that the acidity affects not only the equilibrium between soap anions and acid soap, but also a dissociation equilibrium taking place on the cellulose surface such as: C–OH $\rightleftarrows$ C–O$^-$ . . . H$^+$ and assuming that only the "dissociated" sites are suitable for adsorption. Obviously the number of these sites is a function of the acidity, and their number decreases with increasing [H$^+$]. The combined effects of the increase of the acid soap concentration and the decrease of the number of available sites, both caused by an increase in [H$^+$], could result in a relatively small increase of the total amount adsorbed.

We realize that this explanation of the hydrogen ion effect is only a tentative one, and much more quantitative data should be taken in order to draw more definite conclusions.

Rate of Adsorption and Desorption—Equilibration Theory.—In discussing systems far removed from equilibrium, one can usually neglect the back reaction. This is, however, no longer true as

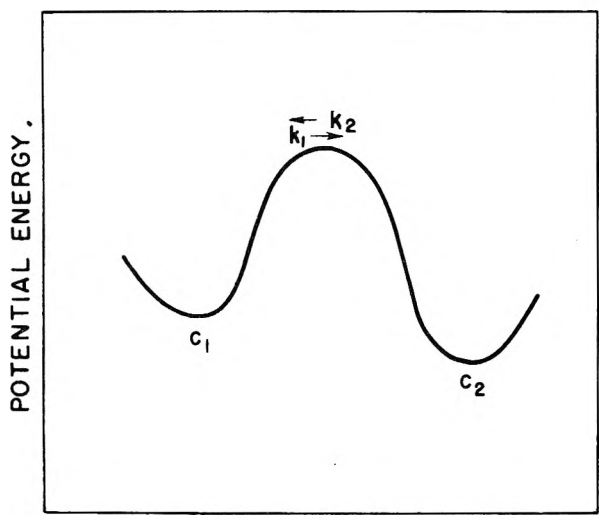

Fig. 11.

equilibrium is approached. If we discuss (Fig. 11) the passage to equilibrium across a single barrier of some system we can write

$$-\frac{dc}{dt} = c_1k_1e^{w_1/kT} - c_2k_2e^{-w_2/kT} \qquad (3)$$

Here we have subtracted the back reaction from the forward reaction to get the net rate of the approach to equilibrium. In (3) $(w_1 + w_2)$ is the total irreversible work degraded per unit reacting. The concentrations c_1 and c_2 on the right side of (3) would be replaced by the appropriate products of concentrations for multimolecular reactions. From the principle of detailed balance we must have

$$c_1k_1 = c_2k_2 \qquad (4)$$

since upon the vanishing of the irreversible work $(w_1 + w_2)$ we must have $-dc_1/dt = 0$. It follows that (3) can be rewritten as

$$-\frac{dc}{dt} = c_1k_1(e^{w_1/kT} - e^{-w_2/kT}) \qquad (5)$$

It is important to notice that even when the reaction passes through a sequence of intermediate states rather than over a single barrier an equation of the form (5) is to be anticipated.[18]

Suppose the standard free energy change in passing from the initial to the activated state is $\Delta F_i^{\ddagger}$ and that $\Delta F_i^{\ddagger}$ depends on a set of parameters which have the values $q_{1)}\ q_{2)}$ . . . . at equilibrium, but that a constraint is applied which changes these parameters to $q_1 + \delta q_1,\ q_2 + \delta q_2$ - - - - -. Then

$$\Delta F_i^{\ddagger} = \Delta F_e^{\ddagger} + \frac{\partial \Delta F^{\ddagger}}{\partial q_1}\delta q_1 + \frac{\partial \Delta F^{\ddagger}}{\partial q_2}\delta q_2 + \ldots$$

Hence $k_1 = \kappa kT/h \exp(-\Delta F_e^{\ddagger}/kT)$ and $w_1 = (\partial \Delta F^{\ddagger}/\partial q_1)\delta q_1 + (\partial \Delta F^{\ddagger}/\partial q_2)\delta q_2 +$ . . . plus higher order terms in the Fourier expansion. Analogously we write

$$w_2 = \frac{\partial \Delta F^{\ddagger}}{\partial q_1}\delta q'_1 + \frac{\partial \Delta F^{\ddagger}}{\partial q_2}\delta q'_2 + \ldots$$

where for a symmetrical barrier

$$\delta q'_1 = \delta q_1,\ \delta q'_2 = \delta q_2, \text{ etc.}$$

Now if the constraint applied is measured by the divergence y from equilibrium of some property such as the concentration, the shear stress, or the viscosity, we can write

$$w_1 = w_2 = \left(\frac{\partial \Delta F^{\ddagger}}{\partial q_1}\frac{\partial q_1}{\partial y} + \frac{\partial \Delta F^{\ddagger}}{\partial q_2}\frac{\partial q_2}{\partial y} + \ldots\right)y = ay$$

and (5) becomes

$$-\frac{dc}{dt} = c_1k_1(e^{ay/kT} - e^{-ay/kT}) \qquad (6)$$

Now if the concentration c_1 of systems which can relax is proportional to the stress y, we write $c_1 = ly$ which leads to the result

$$-\frac{dy}{dt} = yk_1^2 \sinh\left(\frac{ay}{kT}\right) \qquad (7)$$

Equation 7 is still not a reduced equation as is required in the experiments here reported on the adsorption and desorption of dodecylbenzene sulfonate on cotton cloth. The quantity ay/kT is dimensionless and the virial theorem[19] provides an alternative way of expressing twice the kinetic energy, kT, of an oscillator. If, as in the usual case, we start with the identity $d/dt\ (m\dot{x}x) \equiv m\ddot{x}x + m\dot{x}^2$ and integrate both sides over a long period of time from $t = 0$ to t, we obtain by taking averages, the result

$$\int_{t=0}^{t}\frac{d}{dt}(m\dot{x}x)\,dt = \int_{t=0}^{t}(m\ddot{x}x + m\dot{x}^2)\,dt = \overline{(m\ddot{x}x + m\dot{x}^2)}t$$

$$\frac{1}{t}\{(m\dot{x}x)_t - (m\dot{x}x)_0\} = \overline{m\ddot{x}x} + \overline{m\dot{x}^2}$$

Now as t becomes long the quantity on the left approaches zero and we obtain the usual virial expression

$$0 = \overline{m\ddot{x}x} + \overline{m\dot{x}^2} = \overline{Xx} + \overline{m\dot{x}^2}$$

(18) See equation 15 of the paper by R. B. Parlin and H. Eyring, "Ion Transport Across Membranes," Academic Press, Inc., New York, N. Y., 1954, p. 103.

(19) H. Eyring and T. Ree, *Proc. Nat. Acad. Sci., U. S.*, **41**, 118 (1955).

Here $\overline{Xx}$ is the product of the mean force acting on a system times the mean positional coördinate x and $\overline{mx^2}$ is twice the mean kinetic energy per oscillator and has the value kT. If as an example we use the virial theorem to discuss ay/kT in (7) where the constraint y is the shear stress f, then ax has the value $\lambda_2\lambda_3\lambda f/2$, and in the virial expression $\overline{X} = f_0\lambda_2\lambda_3$ where f_0 is the local stress on the flow unit, $\lambda_2\lambda_3$ is the area of the flow unit in the shear plane and λ is the distance jumped. The length $\bar{x}$ is then the free length of the vibrating flow unit in the direction of flow and has the value $\bar{x} = g\lambda$ where λ probably approximates a lattice distance in this direction. The quantity g should then be approximately the velocity of sound in the gas phase divided by its velocity in the phase in question. The virial theorem thus yields the result

$$-f_0\lambda_2\lambda_3 g\lambda + kT = 0$$

and

$$\frac{ay}{kT} = \frac{\lambda_2\lambda_3\lambda f}{2\lambda_2\lambda_3\lambda g f} = \frac{f}{2gf_0}$$

In certain cases f_0 can be identified with the initial largest constraint whence $f/f_0 = \varphi$ is the fractional approach toward equilibrium. Thus if we substitute $ay/kT = b\varphi$ in (7) it will be seen to take the familiar form

$$-\frac{d\varphi}{dt} = 2k'\varphi \sinh b\varphi \qquad (8)$$

which describes accurately the data on adsorption and desorption of detergents and apparently has quite general validity.[20]

The kinetics of unimolecular processes in the condensed phase has been treated recently by Eley[21] who deduced an equation for a unimolecular process which, as a result of molecular interaction, possesses a free energy of activation that increases during the course of the reaction. He showed how certain data on elastic, magnetic and volume creep in solids, and adsorption and desorption processes fit the equation. Eley's treatment considers a reaction in which the concentration of a single reactant varies under the action of a driving force from a value $c(t)$ to $c(\infty)$. If $x = c(t) - c(\infty)$, then the first-order equation is

$$-\frac{dx}{dt} = k'x \qquad (9)$$

where

$$k' = \frac{kt}{h}\exp(-\Delta F^{\ddagger}/RT) \qquad (10)$$

The hypothesis is then made that: $\Delta F^{\ddagger} = \Delta F^{\ddagger}_{\infty} - \gamma x$.

It is clear that k' has the value given by (10) only if $c(\infty)$ is zero, that is only if the back reaction is so slow that it can actually be neglected. Therefore a process may be adequately described by Eley's equation only in the range in which the back reaction is negligible with respect to the forward one.

We have carried out an analysis of some of the data treated by Eley and we have found that in all the cases for which the Eley treatment is satisfactory, the argument of the exponential is so large that our equation and Eley's practically coincide even for fairly small values of φ. In these instances in order to test the equations it should be necessary to study the rate in a region very close to equilibrium where unfortunately the relative errors are very large and where there is also a lack of experimental data. We therefore must expect that our equation applies also in those cases in which the argument of the exponential is fairly small even for relatively large value of φ, that is, in a region where the experimental errors are still relatively small. This is the case for the experiments described by Berger[22] on the variation of the index of refraction during the annealing of glass, for which Eley's equation was inapplicable. In this instance the constant b of equation 8 has the value 1.2; it is therefore small enough for $e^{-b\varphi}$ to be significant even for larger value of φ. The Fig. 12 shows the

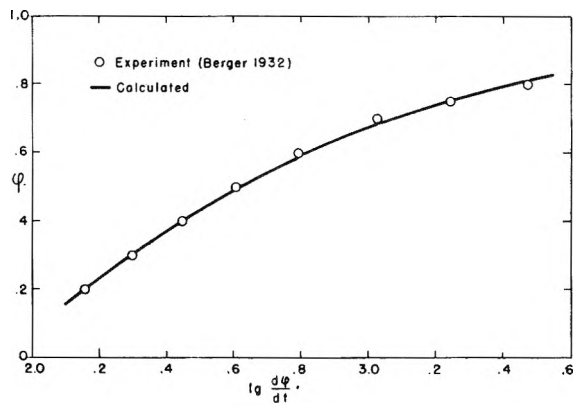

Fig. 12.—Rate of variation of index of refraction.

agreement of the experimental data with the value calculated from equation 8 using the parameters: $k' = 3.8 \times 10^{-3}$ and $b = 1.2$.

Cagle and Eyring[23] considered the applicability of (7) for the annealing of glass, in which case the constant a/kT is so small that the hyperbolic sine may be expanded in the following way

$$-\frac{dy}{dt} = \frac{k'a}{kT}y^2$$

Another case in which the equation 7 has been shown applicable is given by the variation of viscosity with time.[20] Moreover the complete equation 8 was shown[24] to apply to the stress relaxation of polyisobutylenes.

Returning now to equation 5 if we expand the exponentials we obtain the equation

$$-\frac{dc}{dt} = c_1k_1\frac{w_1 + w_2}{kT} \qquad (11)$$

which is the irreversible thermodynamic approximation for the case under consideration. $(w_1 + w_2)/kT$ may be a function of many gradients such as those of concentration, potential, temperature, etc. Comparing (11) and (5) we see that the extension of the limiting irreversible thermodynamic

(20) T. Ree, A. Fava, I. Higuchi and H. Eyring, to be published.
(21) D. D. Eley, *Trans. Faraday Soc.*, **49**, 643 (1953).
(22) E. Berger, *Kolloid Beih.*, **36**, 1 (1932).
(23) F. W. Cagle and H. Eyring, *J. Appl. Phys.*, **22**, 771 (1951).
(24) T. Ree and H. Eyring, Tech. Report Univ. of Utah No. 38 O.N.R. (1952).

rate expression is generalized by multiplying the expression on the right of equation 11 by the factor

$$\left\{(e^{w_1/kT} - e^{-w_2/kT})\frac{kT}{w_1 + w_2}\right\}$$

When $w_1 = w_2$, as frequently happens, this factor becomes $\{(\sinh w/kT)\ kT/w\}$ which approaches unity for small values of the argument (w/kT) and rapidly increases for large arguments. Our considerations here are eloquent evidence of the slight utility of the irreversible thermodynamic approach in most molecular equilibrations.[25]

Mechanism of Detergency.—As we said at the beginning of this paper, adsorption of the detergent is usually postulated as a necessary step in the mechanism of detergent action. To the detergent is often attributed the possibility of displacing the dirt adsorbed on a soiled cloth by forming soil-detergent and cloth-detergent complexes, according to the so called soil equation

fabric–dirt + detergent =
fabric–detergent + soil–detergent

Nothing, however, could be inferred about the nature of the displacement process. In view of what we have learned from the rate of the adsorption and desorption processes a tentative interpretation of the detergent action may be advanced.

A measure of the efficiency of a detergent as cleansing agent is given by the detergency curve. A typical detergency curve[26] is shown in Fig. 13.

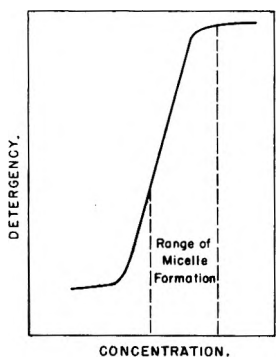

Fig. 13

The similarity of this curve with the adsorption isotherms and the initial rate curve is evident. A noteworthy feature of the detergency curve is that the detergency does not increase with increasing concentration, but reaches a maximum, as adsorption does. However the detergency must be directly related to the desorption rate. Since a reduced equation holds for desorption, the rate of desorption is solely determined by the amount adsorbed. In particular if we plot the initial rate of desorption (equal to the rate of adsorption at equilibrium) as a function of the concentration of detergent in solution, we would obtain a curve that matches exactly the adsorption isotherm. Therefore the same similarities observed between detergency and the isotherm, necessarily exist between detergency and the rate of desorption at equilibrium. We have seen that the rate of desorption of a detergent may be written

$$-\frac{dD}{dt} = 2Dk_D \sinh b_D D$$

in which D is the amount of detergent adsorbed. A similar equation should hold for the desorption of the "dirt" provided that new constants are used. (Actually a set of constants for each constituent of the dirt should be used, but for simplicity we can assume that only one "dirt substance" is present)

$$-\frac{dS}{dt} = 2Sk_S \sinh b_S S$$

where S is the amount of "dirt substance" adsorbed.

If several substances (dirt and detergent) are adsorbed on the cloth at the same time, the contributions to the rate of desorption, of the stresses due to each substance should be additive. In particular the rate of desorption for dirt becomes

$$-\frac{dS}{dt} = 2Sk_S \sinh (b_S S + b_D D)$$

Hence for a given value of S the rate of desorption of the dirt is maximum when D is maximum and therefore the detergency is also maximum at that point.

According to this hypothesis the fundamental operation of the detergent would be to accelerate the desorption of dirt by increasing the stress on the adsorbent material. If this hypothesis is correct it should be possible to improve the efficiency of a detergent by changing conditions or by adding substances capable of increasing the adsorption of the detergent itself, *or even by adding substances that are by themselves liable to be highly adsorbed on the cloth, whether or not they are detergents.* It must be emphasized, however, that actually the detergents, because of their capacity for the formation of aggregates, play another essential role, which, however, is not rate determining. They prevent the readsorption of the "dirt" by solubilizing and dispersing it in the water medium.

(25) R. B. Parlin, R. J. Marcus and H. Eyring, *Proc. Nat. Acad. Sci.*, **41**, in press (1955).

(26) W. C. Preston, THIS JOURNAL, **52**, 84 (1948).

CRITICAL MICELLE CONCENTRATIONS OF α-SULFONATED FATTY ACIDS AND THEIR ESTERS[1]

BY J. K. WEIL AND A. J. STIRTON

Eastern Regional Research Laboratory,[2] Philadelphia 18, Pennsylvania

Received December 5, 1955

Conductance, surface tension and dye titration methods have been used to determine the c.m.c. of α-sulfomyristic acid, α-sulfopalmitic acid, α-sulfostearic acid and sodium salts of methyl, ethyl, propyl and 2-sulfoethyl esters of α-sulfonated palmitic and stearic acids. Increase in length of the carbon chain of the fatty acid results in a decrease in c.m.c. in accordance with the usual logarithmic relationship. Disodium 2-sulfoethyl α-sulfopalmitate has a c.m.c. which is a little greater than that reported for sodium dodecyl sulfate. Disodium 2-sulfoethyl α-sulfostearate has a c.m.c. which is about midway between that reported for sodium dodecyl sulfate and sodium tetradecyl sulfate. This may account for the similarity of these compounds in detergency and response to building.

Sodium salts of α-sulfonated fatty acids [$RCH(SO_3Na)COOH$ and $RCH(SO_3Na)COONa$] and their esters [$RCH(SO_3Na)COOR'$ where R' is alkyl or $-CH_2CH_2SO_3Na$] have been prepared in high purity[3,4] and their detergent properties have been evaluated.[4,5] It is of interest to study the micellar properties of solutions of these compounds in order to correlate their surface active properties with critical micelle concentration (c.m.c.). The esters are of particular interest because their structure can be varied at both the fatty acid and the alcohol portion of the molecule. The disodium salts of 2-sulfoethyl esters and the simple disodium salts of α-sulfonated fatty acids are interesting examples of surfactants with two hydrophilic groups.

There are sources of error in the methods used for these studies. Impurities affect the accuracy of the surface tension method; in the dye titration method, dyes have been shown[6] to initiate the formation of micelles at slightly lower concentrations; and in the conductance method difficulties are encountered when the conductivities are low. Therefore all three methods were used whenever applicable and an attempt was made to correlate them.

Experimental

Surfactants used were those described in earlier publications.[3,4] In all cases an attempt was made to purify the compounds until the surface tension *versus* concentration curve of the aqueous solutions did not show a minimum. α-Sulfomyristic acid and α-sulfopalmitic acid were found to be free of surface tension minima after five crystallizations from chloroform. Crystallization from chloroform did not purify α-sulfostearic acid to this degree.

Simple esters such as sodium ethyl α-sulfopalmitate were extracted with ether in a Soxhlet extractor for six to eight hours and found to be free of surface tension minima. Ether extraction failed to remove the minimum from disodium 2-sulfoethyl α-sulfostearate but foam fractionation[7] followed by freeze drying was found to be successful.

Surface Tension.—The du Noüy tensiometer was used for all surface tension measurements. Since little change in surface tension with temperature was observed with these compounds, and since it has been shown that the c.m.c. is nearly independent of temperature,[8] all surface tension measurements were made at room temperature, 28 ± 1°. Appropriate corrections were applied to the tensiometer readings to give surface tension in dynes per centimeter.

Conductance.—A Leeds and Northrup conductivity bridge operating at 1,000 cycles was used to measure conductance. The bridge was capable of measuring resistance up to 20,000 ohms with an error of 0.1% or less. Measurements were made at 25.00 ± 0.05° in a cell with a constant of 2.26 ± 0.02. Variations in conductance due to temperature were thus found to be less than one part in five thousand. Surfactants were dissolved in a redistilled water with a specific conductance of 2.53×10^{-6} mho and correction made for the conductance of the solvent in all cases.

Dye Titration.—Determinations of c.m.c. by the pinacyanole method were carried out as described by Corrin, Klevens and Harkins.[9] A solution of surfactant in 10^{-5} *M* pinacyanole chloride (0.0005%) solution was made up at a concentration well above the c.m.c. of the surfactant and diluted with 10^{-5} *M* dye solution. Critical micelle concentrations were determined both by visual observation of the color change and from a plot of the light absorbance at the maxima: 480, 557 and 608 mμ, as measured in a Beckman model DU spectrophotometer.

Solubility.—The solubility of the more readily soluble surfactants was determined by filtering insoluble matter from an equilibrated mixture of solid and water.[5] Lower solubilities were determined by a trial and error method to determine the limiting concentration capable of producing a clear solution.

Discussion of Results

Table I lists the c.m.c. values determined by the surface tension, conductance and dye titration methods for α-sulfomyristic, α-sulfopalmitic and α-sulfostearic acids and some of their esters. The conductance method has an advantage over the other methods in that it is not affected either by small amounts of impurities, as is the surface tension method, or by the presence of dye particles, as is the dye titration method.[6] The conductance values reported have been found to have a normal Onsager slope below the c.m.c. Figure 1 shows the conductance curve for α-sulfomyristic acid, in the upper part; and the conductance curves for disodium 2-sulfoethyl α-sulfopalmitate (A) and disodium 2-sulfoethyl α-sulfostearate (B), in the lower part.

Figure 2 shows surface tension curves for solutions of disodium 2-sulfoethyl α-sulfostearate after ether extraction as the only purification, and after foam fractionation of the same material. Ether extraction of the ester resulted in a surface tension curve with a broad minimum but foam fractiona-

(1) Presented at the Delaware Valley Regional Meeting, at Philadelphia, February 16, 1956, and the 129th National Meeting of the American Chemical Society, Dallas, Texas, April 8–13, 1956.

(2) A laboratory of the Eastern Utilization Research Branch, Agricultural Research Service, U. S. Department of Agriculture.

(3) J. K. Weil, R. G. Bistline, Jr., and A. J. Stirton, *J. Am. Chem. Soc.*, **75**, 4859 (1953).

(4) J. K. Weil, R. G. Bistline, Jr., and A. J. Stirton, *J. Am. Oil Chemists' Soc.*, **32**, 370 (1955).

(5) A. J. Stirton, J. K. Weil and R. G. Bistline, Jr., *ibid.*, **31**, 13 (1954).

(6) P. Mukerjee and K. J. Mysels, *J. Am. Chem. Soc.*, **77**, 2937 (1955).

(7) L. Shedlovsky, J. Ross and C. W. Jakob, *J. Colloid Sci.*, **4**, 25 (1949).

(8) A. P. Brady and H. Huff, *ibid.*, **3**, 511 (1948).

(9) M. L. Corrin, H. B. Klevens and W. D. Harkins, *J. Chem. Phys.*, **14**, 480 (1946).

Table I

Critical Micelle Concentration

Per Cent. at Room Temperature

	Surface tension method	Dye Method		Conductance method (25°)
		Spectrophotometer	Visual	
α-Sulfomyristic acid	0.07	0.075	0.08	0.13
α-Sulfopalmitic acid	.02	.023	.017	
α-Sulfostearic acid	.005	.004	.005	
Sodium methyl α-sulfopalmitate	.012	.014	.015	
Sodium ethyl α-sulfopalmitate	.009	.013		
Sodium propyl α-sulfopalmitate	.004			
Sodium methyl α-sulfostearate	.004	.004	.003	
Sodium ethyl α-sulfostearate	.005	.002	.002	
Sodium propyl α-sulfostearate	.0005			
Sodium isopropyl α-sulfostearate	.001			
Disodium 2-sulfoethyl α-sulfopalmitate		.3	.4	.53
Disodium 2-sulfoethyl α-sulfostearate	.13	.10		.16

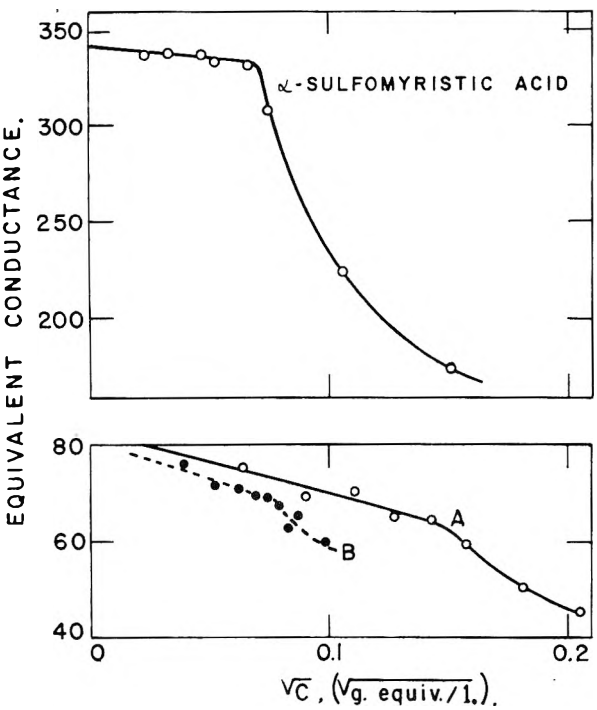

Fig. 1.—Variation of equivalent conductance with concentration for α-sulfonated fatty acids and esters, 25.00 ± 0.05°: A, disodium 2-sulfoethyl α-sulfopalmitate; B, disodium 2-sulfoethyl α-sulfostearate.

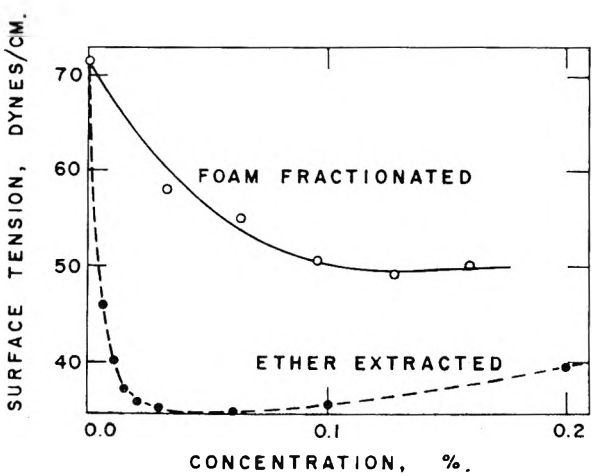

Fig. 2.—Variation of surface tension with concentration for disodium 2-sulfoethyl α-sulfostearate, 28°.

tion was able to remove it completely. Miles and Shedlovsky[10] have illustrated the effect of adding a material of lower c.m.c. such as sodium cetyl sulfate to sodium lauryl sulfate. Their curves were similar to those shown here. Small amounts of suspected ether-insoluble impurities such as sodium ethyl α-sulfostearate and sodium 2-sulfoethyl stearate, which have lower c.m.c. values, may be expected to be responsible for this effect. Critical micelle concentrations of foam fractionated and non-foam fractionated disodium 2-sulfoethyl α-sulfostearate by the dye titration method were in agreement with c.m.c. values shown in Fig. 2.

Table II lists the solubility of some mono- and disodium salts of α-sulfonated fatty acids. When pinacyanole chloride was added to solutions of these surfactants at the concentrations shown in Table II, micelles were found to be absent in all cases. The c.m.c., accordingly, is not less than the concentration of a saturated solution. Little difference is observed in comparing the solubility of sodium α-sulfostearic acid, sodium α-sulfopalmitic acid and sodium α-sulfomyristic acid (Table II) with the c.m.c. values of α-sulfostearic acid, α-sulfopalmitic acid and α-sulfomyristic acid (Table I), respectively.

Table II

Solubility of Sodium Salts of α-Sulfonated Fatty Acids in Per Cent. at 25°

Disodium α-sulfomyristate	1.50
Disodium α-sulfopalmitate	0.25
Disodium α-sulfostearate	0.10
Sodium α-sulfolauric acid	0.42
Sodium α-sulfomyristic acid	0.11
Sodium α-sulfopalmitic acid	0.02
Sodium α-sulfostearic acid	<0.01

Increase in the length of the fatty acid chain of these compounds results in a decrease in c.m.c. in the usual logarithmic relationship shown for other homologous series.[11,12] There is also a general decrease in the c.m.c. with increase in number of carbon atoms in the alcohol portion of the esters but no consistent relationship is shown over this limited range. Only a slight decrease in c.m.c. is observed on esterifying the diacid or monosodium salt with methyl alcohol.

(10) G. D. Miles and L. Shedlovsky, This Journal, **48**, 57 (1944).
(11) S. H. Herzfeld, *ibid.*, **56**, 953 (1952).
(12) P. Debye, *J. Colloid Sci.*, **3**, 407 (1948).

Some interesting observations may be made on the effect of adding a second hydrophilic group to a long hydrophobic chain. The solubility of disodium α-sulfostearate and the c.m.c. of disodium 2-sulfoethyl α-sulfostearate are not what one might expect from half the number of carbon atoms attached to one hydrophilic group but rather their ion solubilities are about midway between those reported[13] for sodium dodecyl sulfate and sodium tetradecyl sulfate. Likewise, disodium α-sulfopalmitate and disodium 2-sulfoethyl α-sulfopalmitate have a little higher ion solubility than sodium dodecyl sulfate. Disodium 2-sulfoethyl α-sulfostearate has been found to have good detergency and shows a response to building[4] similar to that of surfactants with twelve and fourteen carbon atoms. The c.m.c. values given here are only slightly lower than those reported by Shinoda[14] for corresponding alkyl malonates: $C_{12}H_{25}CH(COOK)_2$, 1.7%; $C_{14}H_{29}CH(COOK)_2$, 0.7%; $C_{16}H_{33}CH(COOK)_2$, 0.2–0.4%.

(13) J. Powney and C. C. Addison, *Trans. Faraday Soc.*, **33**, 1243 (1937).

(14) K. Shinoda, THIS JOURNAL, **59**, 432 (1955).

Conclusions

The conductance method is preferred for measurement of critical micelle concentrations of α-sulfonated acids and esters when the value obtained is above 0.05% (0.001 *M*). The surface tension and dye titration methods were used for those having lower c.m.c. values.

α-Sulfonated acids and their alkyl esters have c.m.c. values in the same region as other surfactants of equal carbon chain length. Disodium 2-sulfoethyl α-sulfostearate has a c.m.c. between that of sodium dodecyl sulfate and sodium tetradecyl sulfate. Simple monosodium and disodium salts of α-sulfonated acids do not form micelles at room temperature but have solubilities which are very close to the c.m.c. values of other materials having the same length of alkyl chain and the same number of hydrophilic groups.

Acknowledgment.—The authors wish to express their appreciation to Serge N. Timasheff for his helpful suggestions in carrying out this work and to Raymond G. Bistline, Jr., for making some of the surface tension measurements.

THE EXTRACTION OF FERRIC CHLORIDE BY ISOPROPYL ETHER. PART I. THE SIGNIFICANCE OF WATER IN THE EXTRACTED IRON COMPLEX

BY A. H. LAURENE, D. E. CAMPBELL, S. E. WIBERLEY AND H. M. CLARK

Department of Chemistry, Walker Laboratory, Rensselaer Polytechnic Institute, Troy, New York

Received December 9, 1955

The crystalline anhydrous dietherate of tetrachloroferric acid has been prepared and its behavior with water has been studied. The hydrated acid was shown by spectro-chemical means to be identical with the complex which is extracted by isopropyl ether from hydrochloric acid containing ferric chloride. It has been found that water is essential for the extraction of the ferric chloride complex and that water is the controlling factor in the formation of a third phase in the extraction system.

Introduction

Several investigators[1–7] have displayed interest in the possible significance of the water found in the ether layer when ferric chloride is extracted from hydrochloric acid solution by ether. It is generally believed that most of this water is associated with the extracted material.[1,2,5–7] By means of analyses for hydrogen, iron, chloride and water in the ether layer, previous workers[1,2] have assigned the empirical formula $HFeCl_4 \cdot 4\text{–}5H_2O$ to the material which extracts.

Hydrogen chloride and water are normally distributed between isopropyl ether and hydrochloric acid.[3,6] It may be expected that these compounds will also exist in the ether layer of the ferric chloride extraction system apart from that associated with the extracted material. The amounts of free hydrogen chloride and water in the ether layer depend on the concentration of hydrochloric acid in the aqueous layer and on the effect of ferric chloride on their distribution. Because the latter effect has not been determined, it is difficult to establish the exact amount of water which is associated with the extracted iron complex from analyses alone. The problem has been approached, therefore, by studying the action of water on anhydrous $HFeCl_4$ and ether.

(1) S. Kato and R. Ishii, *Sci. Papers Inst. Phys. Chem. Research, Tokyo*, **36**, 82 (1939).

(2) J. Axelrod and E. H. Swift, *J. Am. Chem. Soc.*, **62**, 33 (1940).

(3) N. H. Nachtrieb and J. G. Conway, *ibid.*, **70**, 3547 (1948).

(4) N. H. Nachtrieb and R. E. Fryxell, *ibid.*, **70**, 3552 (1946).

(5) R. J. Myers and D. E. Metzler, *ibid.*, **72**, 3772 (1950).

(6) R. J. Myers, D. E. Metzler and E. H. Swift, *ibid.*, **72**, 3767 (1950).

(7) H. L. Friedman, *ibid.*, **74**, 5 (1952).

Experimental

Materials.—The isopropyl ether, ferric chloride and hydrogen chloride used in the preparation of tetrachloroferric acid, $HFeCl_4$, were anhydrous. All operations were carried out in a dry box which was charged with phosphoric anhydride. The drying agent was stirred frequently to expose a fresh surface and was replaced as soon as its efficiency appeared doubtful.

The isopropyl ether was purified by treatment with acidified, saturated ferrous sulfate solution followed by sodium hydroxide solution. It was rinsed with distilled water, dried with silica gel and distilled twice over calcium hydride. The fraction of the purified ether which boiled between 67.4 and 67.9° (uncor.) was collected for use. Commercial C.P. anhydrous ferric chloride was found to be entirely satisfactory for this preparation. The hydrogen chloride was taken from a cylinder of the anhydrous gas.

Analyses.—Iron was determined on the aqueous extracts of the samples after the ether had been removed by evaporation. The aqueous solutions were made two molar in hydrochloric acid, passed through a silver reductor and titrated with standard ceric sulfate to the ferrous-*o*-phenanthroline end-point. Chlorine was determined by the Volhard method (the silver chloride precipitate being filtered off). Analysis for hydrogen was carried out on aqueous extracts of the samples without removal of the ether. The aqueous solution was titrated with standard sodium hydroxide solution to the phenolphthalein end-point. The hydrogen was computed by subtracting the volume of reagent required for the known quantity of iron present from the total volume of reagent used. The isopropyl ether content of solid etherate samples was determined by difference after the amounts of all other constituents had been determined.

Spectra.—A Beckman model D.U. quartz spectrophotometer, equipped with a Beckman hydrogen discharge lamp and a constant voltage power pack, was used to obtain ultraviolet absorption spectra. A Model B Beckman spectrophotometer was employed for obtaining spectra in the visible region. Matched glass-stoppered cells with quartz windows and ten millimeter inside thickness served to contain the samples for both of these instruments. Infrared absorption spectra were run on a Model 12B Perkin–Elmer Infrared Spectrometer using a rock salt prism and cells with fixed and demountable rock salt windows. The spectroscopic nomenclature recommended by Hughes[8] was used in reporting data.

The Preparation of Anhydrous Tetrachloroferric Acid Dietherate.—Isopropyl ether was dried by allowing it to react for two days with extruded sodium. It was then filtered into a large bottle and a few grams of calcium hydride added. The bottle was fitted with a syphon so that ether could be removed by increasing the air pressure within the apparatus. A fine sintered glass filter was sealed to the lower end of the siphon to prevent small particles of calcium hydride from being withdrawn along with ether. This dispensing apparatus was kept in the dry box throughout its use.

One liter of the dry isopropyl ether was saturated with anhydrous ferric chloride and the solution filtered into a one-liter flask provided with a male 24/40 ground joint. Samples of this solution were taken for iron analysis. The ether solution was found to be 0.367 molar in ferric chloride.

The flask containing the anhydrous solution of isopropyl ether and ferric chloride was fitted with a bubbling device which consisted of a female 24/40 joint with a side arm and a ring-sealed tube. A coarse, sintered glass, gas bubbler was sealed to the bottom of the tube. This apparatus was removed from the dry box and connected *via* a Dry Ice–acetone cold trap to a cylinder of hydrogen chloride gas. Care was taken to prevent the introduction of atmospheric moisture.

Hydrogen chloride gas was passed slowly through the system and a solid began to separate from the solution immediately. No increase in the temperature of the solution was noted at this stage. When it was apparent that all the ferric chloride had been precipitated by the reaction taking place, continued passage of gas through the solution caused a sharp rise in temperature. The flow of hydrogen chloride was stopped at this point, the hose connections clamped off, and the flask with its gas bubbler removed to the dry box.

The solid material was separated, first by decanting the bulk of the ether, and finally by suction filtering. While on the sintered glass filter, the solid was washed several times with dry ether from the dispensing bottle. After a brief drying by suction, the crystalline material was collected and samples were taken for analysis.

The solid is light yellow-green in color, crystalline, voluminous in bulk and adheres to glass and metal even after thorough drying between pieces of filter paper. It is extremely hygroscopic and forms a dark green sirupy liquid immediately upon exposure to atmospheric moisture. It is only very slightly soluble in isopropyl ether (0.0025 mole per liter, obtained by iron and chloride analysis). The composition of the crystalline solid was found to be 14.25% iron, 36.09% chlorine, 0.255% hydrogen and 49.4% isopropyl ether. The atomic ratios of the constituents are 1.00 Fe:3.98 Cl; 1.00 H:1.89 i-Pr_2O giving the empirical formula $HFeCl_4 \cdot 2$ isopropyl ether.

The Action of Water on Anhydrous $HFeCl_4 \cdot 2$-i-Pr_2O.—As stated previously, anhydrous tetrachloroferric acid is extremely hygroscopic. When hydrated, the acid becomes soluble in isopropyl ether. In order to determine quantitatively the amount of water necessary to make the anhydrous material soluble in ether, the compound, in the presence of isopropyl ether, was titrated with water.

Arbitrary amounts of the anhydrous acid were placed in 100-ml. volumetric flasks. About 75 ml. of dry isopropyl ether was added to each flask which was then stoppered and removed from the dry box. Each mixture was titrated with water from a micro-buret. During the titration two ether phases formed and the denser phase, containing most of the iron, was observed to grow at the expense of the light phase. In the systems which contained small amounts of tetrachloroferric acid the dense ether layer reached a maximum volume which then began to decrease as the titration proceeded and suddenly disappeared. The disappearance of the two layers which produced a clear homogeneous solution, was considered the "end-point" of the titration. The systems containing large quantities of the acid exhibited a continuous expansion of the dense phase at the expense of the light ether layer above it. The "end-point" in these cases was the disappearance of opalescence in the solution which indicated that no more light ether layer existed. It was noted that just at the end-point each solution foamed very readily.

Following the preliminary titrations with water, each flask was returned to the dry box and filled to the mark with dry ether. The solutions which contained large amounts of the tetrachloroferric acid again formed two liquid phases. These were titrated to homogeneous solutions by a few drops of water.

TABLE I

THE DEGREE OF HYDRATION OF ETHER-SOLUBLE TETRACHLOROFERRIC ACID

No.	Type of soln.	Molar concn. of Fe	Cl	H_2O	Ratios of constituents Fe	Cl	H_2O
1	Light ether phase	0.0130	0.0529	0.0655	1	4.06	5.04
2	Light ether phase	.1544	0.609	.749	1	3.94	4.85
3	Light ether phase	.0980	...	.493	1	...	5.03
4	Light ether phase	.0483	...	.252	1	...	5.22
5	Light ether phase	.0439	...	.221	1	...	5.02
6	Light ether phase	.0211	...	.103	1	...	4.88
7	Light ether phase	.0202	...	.105	1	...	5.19
8	Light ether phase	.0111	...	.0595	1	...	5.37
9	Light ether phase	.00854	...	.0481	1	...	5.63
10	Light ether phase	.00569	...	.0262	1	...	4.61
11	Light ether phase	.00261	...	.0135	1	...	5.18
12	Heavy ether phase	.2381	0.957	1.067	1	4.02	4.48
13	Heavy ether phase	.2463	0.973	1.106	1	3.96	4.49
14	Heavy ether phase	.2829	1.126	1.265	1	3.99	4.47
15	Heavy ether phase	.3116	1.239	1.363	1	3.98	4.37

(8) H. K. Hughes, *Anal. Chem.*, **24**, 1349 (1952).

After the titrations with water were complete, each solution was analyzed for iron and chloride. The results of the analyses, and the water titrations are summarized in Table I.

The light ether layers appeared to be entirely miscible with isopropyl ether while the heavy ether solutions were immiscible. As was shown by this experiment, the immiscible layers could be made to dissolve isopropyl ether by adding small amounts of water.

The average value (taken over all the solutions considered to be light ether phases) of the number of molecules of water necessary to make the anhydrous tetrachloroferric acid completely soluble in isopropyl ether is 5.09 with an average deviation of a single observation of ±0.21. For the heavy ether solutions this ratio of water to iron appears to fall off with increasing iron concentration.

Comparison of Spectra.—The solution indicated no. 1 in Table I was diluted with isopropyl ether to 1.3×10^{-4} and its ultraviolet spectrum measured. The spectrum was found to be identical with that observed for an ether layer obtained by extracting iron from an aqueous solution of ferric chloride and hydrochloric acid with isopropyl ether. A markedly different ultraviolet spectrum was observed for an anhydrous solution of ferric chloride in isopropyl ether. Both the spectrum for the ether extract and that for the anhydrous solution were in agreement with those reported by Metzler and Meyers.[9]

The visible spectrum of the solution indicated no. 14 in Table I was found to be identical with that of an ether layer from a ferric chloride–isopropyl ether extraction system and unlike that of anhydrous ether solution of ferric chloride. The latter two spectra were in agreement with those reported by Nachtrieb and Conway.[3]

Two bands appear at 757 and 827 cm.$^{-1}$ in the infrared spectrum of the saturated anhydrous solution of ferric chloride and isopropyl ether. These bands are not present in the isopropyl ether spectrum. A thin section (0.001 mm.) of the ether layer obtained by extracting with isopropyl ether from 7.0 *M* hydrochloric acid saturated with ferric chloride was run in the infrared. The 1015 cm.$^{-1}$ band of the isopropyl ether spectrum was shifted to 1000 cm.$^{-1}$. The same shift was noted in the infrared spectrum of hydrated tetrachloroferric acid in isopropyl ether. A thin section (0.001 mm.) of this solution, which was 2.8 *M* in $HFeCl_4$, was run in the infrared and the 1015 cm.$^{-1}$ band was shifted to 990 cm.$^{-1}$.

The ultraviolet spectrum of an anhydrous solution of isopropyl ether, ferric chloride and hydrogen chloride was obtained. This solution was 1.38×10^{-4} *M* in ferric chloride and 1.4×10^{-3} *M* in hydrogen chloride. The spectrum was identical with that of the hydrated tetrachloroferric acid in isopropyl ether.

Discussion

The absorption spectrum of hydrated tetrachloroferric acid, from the ultraviolet through the infrared regions, is different from the spectrum of anhydrous ferric chloride in isopropyl ether. It is identical with the spectrum of the ether layer from the ferric chloride–isopropyl ether extraction system. This is considered evidence that the complex in the ether layer of the ferric chloride extraction system is hydrated tetrachloroferric acid.

The significance of associated water in the extracted complex is quite apparent from the fact that the anhydrous tetrachloroferric acid is insoluble in isopropyl ether. Moreover, when the mole ratio of water to iron in a solution of isopropyl ether and tetrachloroferric acid is less than *five* the solution is immiscible with dry ether. The complex becomes *completely* soluble in ether when sufficient water is present to form the pentahydrated acid.

The manner in which water is associated with the complex acid in ethereal solution has not been determined. Results from studies of the electrolysis of ether extracts[10] indicate that all of the water is combined with the hydrogen of the acid. Additional evidence for this is given by the work of Friedman[7] who has shown that the absorbing species in tetrachloroferrate compounds is the anion and that the anhydrous compounds give spectra identical with the hydrated tetrachloroferric acid. Furthermore, the ultraviolet spectrum of the anhydrous isopropyl ether–tetrachloroferric acid solution in this study is the same as that of the hydrated acid in ethereal solution. Ordinarily, when an absorbing complex becomes hydrated by coördinated water its spectrum is altered quite noticeably.[11,12] The above evidence indicates that the material which is extracted by isopropyl ether from hydrochloric acid containing ferric chloride is $(H_3O^+ \cdot 4H_2O)FeCl_4^-$.

A possible explanation for the occurrence of two ether phases in the ferric chloride extraction system[13,14] is found in these studies. The two ether phases of this system are analogous to a heterogeneous $HFeCl_4$–ether system which has insufficient water to bring about a homogeneous ethereal solution. The two ether-phase extraction system occurs when the over-all concentration of hydrochloric acid is very high (above eight molar initial concentration).

Stokes and Robinson[15] indicate that very little "free water" exists in hydrochloric acid at a concentration of seven molar. Almost all the water present serves to hydrate the ions and very little, if any, acts as solvent. When the concentration exceeds seven molar a deficiency of water may be considered to exist. Thus, concentrated hydrochloric acid may act as a dehydrating agent upon a substance possessing loosely-bound water.

That some of the water associated with the extracted complex is loosely-bound is illustrated by the effect of sodium chloride on an ether extract. When the salt is added to the ether phase (separated from the aqueous phase) a layer of brine and two ether layers are formed.[16] Dehydrating agents stronger than sodium chloride will of course give the same effect.

Under no circumstances have two ether phases been observed in the isopropyl ether–HCl–H_2O ternary systems.[17] A study of this system has, however, disclosed that when the initial hydrochloric acid concentration is increased the concentration of water in the ether layer decreases. When the over-all concentration of hydrochloric acid in the ferric chloride extraction system exceeds eight molar the aqueous layer may exert a dehydrating influence upon material in the ether layer. Part of the extracted tetrachloroferric acid may be deprived

(9) D. E. Metzler and R. J. Meyers, *J. Am. Chem. Soc.*, **72**, 3776 (1950).

(10) J. E. Savolainen, unpublished results from this Laboratory.

(11) W. R. Brode, THIS JOURNAL, **30**, 56 (1926).

(12) W. R. Brode, "Chemical Spectroscopy," John Wiley and Sons, Inc., New York, N. Y., 1943, p. 205, 246, 267.

(13) R. W. Dodson, G. J. Forney and E. H. Swift, *J. Am. Chem. Soc.*, **58**, 2573 (1936).

(14) N. H. Nachtrieb and R. E. Fryxell, *ibid.*, **74**, 897 (1952).

(15) R. H. Stokes and R. A. Robinson, *ibid.*, **70**, 1870 (1948).

(16) Unpublished results from this Laboratory.

(17) D. E. Campbell, A. H. Laurene and H. M. Clark, *J. Am. Chem. Soc.*, **75**, 6193 (1952).

of some associated water with the consequent formation of a heavy ether phase which has a water to iron mole ratio of less than *five*.

Acknowledgment.—This work was partially supported by the Atomic Energy Commission under Contract No. AT(30-1)-562.

BURNING RATE STUDIES. 4. EFFECT OF EXPERIMENTAL CONDITIONS ON THE CONSUMPTION RATE OF THE LIQUID SYSTEM 2-NITROPROPANE–NITRIC ACID

BY A. GREENVILLE WHITTAKER, HARRY WILLIAMS AND PENNIMAN M. RUST

Contribution from the Chemistry Division, Research Department, U. S. Naval Ordnance Test Station, China Lake, California

Received December 9, 1955

An apparatus and experimental technique for measuring the consumption rate of burning liquid systems are described. The effect of such experimental parameters as pressure, igniter size, tube diameter and tube material on consumption rate was investigated. The consumption rate curve for the system 2-nitropropane–nitric acid shows abrupt changes in slope at various pressures. Two of these regions of abrupt change in slope were studied in some detail by means of moderately high-speed motion-picture photography. The resolution obtained in these photographs was good enough to show many features of the burning process that could not be seen by direct observation.

Introduction

Studies of temperature profiles in burning liquids[1,2] were made after a study of the effect of experimental conditions on consumption rate had been completed. These results are given here along with a description of the liquid burning rate apparatus. This work was to test a method of measuring liquid consumption rate, and to determine how certain physical parameters affect the consumption rate. The apparatus might introduce spurious effects which would give rise to erroneous rate data. Therefore it was desirable to determine effects (if any) characteristic of the apparatus so that they could be distinguished from those characteristic of the burning liquid. A short study was made of the effect of bomb pressure, igniter energy, combustion tube size and combustion tube material since these factors most likely affect observed consumption rates. An effort was made to determine the relationship between observed rate and fundamental burning rate. Many side observations were made. The more important ones are described. Although some 20 different combustible liquids (both single and two-component systems) were investigated to some extent, the system 2-nitropropane–nitric acid was chosen to illustrate the behavior of liquids burning under pressure because it was studied in most detail.

Materials

Commercial Solvents Corporation commercial grade 2-nitropropane was distilled once and the center constant boiling fraction was used in these studies. The starting material, however, gave consumption rates essentially identical with those obtained with the purified material. Nitric acid was obtained by two different methods. Anhydrous nitric acid was prepared from concentrated sulfuric acid and potassium nitrate. The anhydrous nitric acid was distilled from the mixture at about 30° and 1 mm. Larger quantities of anhydrous nitric acid were prepared by distilling a mixture of C.P. white fuming nitric acid in the presence of a large excess of concentrated sulfuric acid at a pressure of about 1 mm. This process also reduced the NO_2 content to about 0.1% or less. The anhydrous acid obtained by either method was then analyzed and diluted to desired concentration with distilled water.

Apparatus and Procedure

Description of Apparatus.—The apparatus used was similar to that described by Crawford and co-workers,[3] to measure the consumption rate of solid propellants. In this work the rate was measured according to a principle described by Muraour and Schumacher[4] in which a direct determination was made of the time required to burn a given length of combustible material of uniform cross section. The liquid was contained in Pyrex combustion tubes 4 mm. i.d., 6 mm. o.d., and 17.8 cm. long. The tubes were sealed at the bottom end. Unless otherwise indicated all rates were measured in tubes of this size. The bomb was a stainless steel vessel having a concentric cavity approximately 23 cm. deep and 6.4 cm. in diameter. The bomb had two diametrically opposite windows of Lucite approximately 1.9 cm. wide, 17.8 cm. long, and 3.2 cm. thick. These windows showed no signs of failure after considerable use up to pressures as high as 307 atm. The bomb head threaded into the top of the bomb and the seal was made by using the unsupported area principle. The combustion tube holder, which contained electric contacts for the igniter and fuse wires, was firmly fastened to the bomb head. Horizontal metal bars, spaced exactly 1 or 2 in. apart with respect to their top edges, were used to measure distances. Electric leads from the contacts on the strand holder were brought out through the bomb head.

Ignition of the liquid was achieved by passing current through a short length of No. 30 iron wire with a small piece of ballistite threaded onto the wire. This wire was bent in a sharp "U" around the ballistite bead so that it would fit inside the top of the combustion tube. The position of the ballistite was adjusted so that it just touched the surface of the liquid in the combustion tube.

The bomb was pressurized by two methods. For pressures up to 125 atm. the bomb was pressurized from commercial cylinders of dry nitrogen; pressures above 125 atm. were obtained by means of a three-cylinder cascade system and a high-pressure reaction vessel. Liquid nitrogen was pumped into the reaction vessel and permitted to vaporize which resulted in pressures of about 475 atm. This high-pressure source was used to pressurize the bomb to 307 atm. During combustion a 3-liter surge tank maintained the pressure constant to within 3% in the low pressure range. Adjustable relief valves gave additional control. This combination permitted control to about 5% at pressures above 70 atm. The bomb pressure was measured on a 16-in. Heise gage of 410 atm. total range.

(1) D. L. Hildenbrand, A. G. Whittaker and C. B. Euston, THIS JOURNAL, **58**, 1130 (1954).

(2) D. L. Hildenbrand and A. G. Whittaker, *ibid.*, **59**, 1024 (1955).

(3) B. L. Crawford, Jr., C. Huggett, F. Daniels and R. E. Wilfong, *Anal. Chem.*, **19**, 630 (1947).

(4) H. Muraour and W. Schumacher, *Mém. Poudres*, **37**, 87 (1937).

Movement of the combustion wave down the tube was timed by several methods. Fuse wires and electrically actuated clocks[3] were used, and are still used when opaque combustion tubes are required. For this purpose 0.5-amp. fuse wires were threaded through the combustion tube at 5.08 cm. intervals and were sealed in place. The igniter was fired by means of a 6-volt source which also supplied about 300 ma. of current through the fuse wires to the timing clocks after the clock-starting fuse wire was burned through. The clocks were stopped as successive fuse wires were burned through.

When the rate was less than 1.3 cm. per second hand-timing was used. For this a circuit was set up in which switches external to the bomb replaced the fuse wires. As the combustion wave passed the fiducial marks, the clocks were stopped by manually throwing the appropriate switches Intervals of 5.08 cm. were used at the lower rates, and 2.54-cm. intervals were used at higher rates.

Photographic timing, as described by Williams and Whittaker,[5] was made of the combustion wave through the bomb window. Timing marks were made on the film by suitably pulsed light from either inside or outside the camera. The distance was scaled by the fiducial marks located inside the bomb. Usually silhouette lighting was used.

Preparation of Mixture

Mixtures of 2-nitropropane–nitric acid in stoichiometric proportions were studied. Stoichiometric proportions were defined by the equation

$$5C_3H_7NO_2 + 15HNO_3 \longrightarrow 15CO_2 + 25H_2O + 10N_2 \quad (1)$$

Although the mixtures were prepared according to the proportions indicated in eq. 1, allowance was made for the fact that the nitric acid was not 100% HNO_3; the density of 2-nitropropane was taken as 1.00 g./cc.

Results and Discussion

Burning Rate *vs.* Consumption Rate.—When the surface of the burning liquid appears to be oriented perpendicular to the axis of a vertical combustion tube and all points in the surface move parallel to the walls of the tube at the same rate, the liquid is said to burn smoothly; its surface has a meniscus shape. Therefore, the observed linear consumption rate along the tube is not identical with the true linear burning rate. This difference can be treated quantitatively as follows: let M be the true mass burning rate in g./cm.^{2} sec., then the mass of liquid consumed per second is MA, where A is the area of the burning surface. The true mass burning rate, M, and the true linear burning rate L are related by $M = \rho L$, where ρ is the liquid density. The mass of liquid consumed per second can also be given by $C\pi r^2\rho$, where r is the radius of the combustion tube and C is the observed consumption rate. Equating equivalent expressions and replacing M by ρL gives

$$L\rho A = C\pi r^2\rho$$

$$L = C\frac{\pi r^2}{A} \quad (2)$$

Since $A \geqq \pi r^2$ the true linear burning rate will always be equal to or less than the observed consumption rate. The surface correction values in Table I are actually $A/\pi r^2$, thus giving numbers greater than unity. The value of A was estimated as follows: From the photographs the image of the combustion tube was projected to about 10 cm. in diameter. The surface shape was then traced on a piece of paper and the meniscus depth measured.[6] The projected external diameter of the tube was measured to give a scaling factor. From these measurements and the assumption that the surface of the liquid had the shape of a spherical cap, A was calculated. This procedure was repeated on widely separated frames to get an average value for a given system and pressure.

The surface correction for the system 2-nitropropane–nitric acid was quite large at low pressure and decreased with increasing pressure. The results of a detailed study of this effect are given in Table I. Within the accuracy of the method the data show that surface correction for the burning system decreased linearly with pressure; for the non-burning system it was independent of pressure.

TABLE I

VARIATION OF SURFACE CORRECTION WITH PRESSURE FOR THE SYSTEM 2-NITROPROPANE–95% HNO_3 IN 4 MM. I.D. PYREX TUBES

Surface correction			Surface correction		
Burning	Not burning	Pressure (atm.)	Burning	Not burning	Pressure (atm.)
...	1.18	1.0	1.40	1.18	48.6
1.70	1.18	14.6	1.36	1.18	55.4
1.67	1.18	21.4	1.35	1.18	62.2
1.63	1.18	28.2	1.33	1.18	69.0
1.52	1.18	35.0	1.25	1.18	75.8
1.45	1.18	41.8			

Effects of Pressure.—Data on the consumption rate as a function of bomb pressure for a stoichiometric mixture of 2-nitropropane with both 100% and 97% nitric acid are plotted in Fig. 1 to show

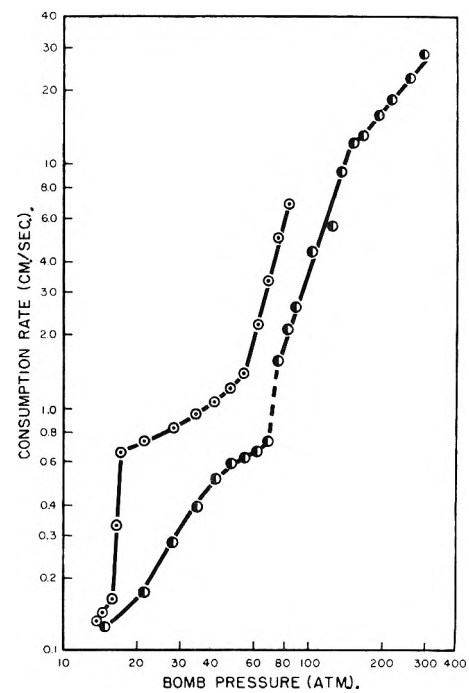

Fig. 1.—Consumption rate curves for the system 2-nitropropane–nitric acid: ⊙, 2-nitropropane–100% nitric acid; ◐, 2-nitropropane–97% nitric acid.

log consumption *vs.* log pressure. Some theoretical treatments (*e.g.*, Boys and Corner[7] and Rice and

(5) H. Williams and A. Greenville Whittaker, *Photographic Soc. America*, **19B**, No. 4, 161 (1953).

(6) Special illumination of the combustion wave is required to clearly define the upper and lower limits of the meniscus. Otherwise large errors would be made in the value of A.

(7) S. F. Boys and J. Corner, *Proc. Roy. Soc.* (*London*), **A197**, 90 (1949).

Ginell[8]) show that the slope of the curve may have some theoretical significance. Unfortunately, they do not agree on what fundamental information can be obtained.

In discussing the results, it is convenient to define the various features of the curves. The system prepared with 97% nitric acid shows a gradually changing slope for low pressure, followed by a sharp change ("turbulence break") in slope at about 70 atm. This break is followed by a region of high slope, and then another fairly sharp change ("high-pressure break") occurs. This break is followed by a region of intermediate slope up to the highest pressure studied. When 100% nitric acid is used, the consumption rate is increased at all pressures; but more important, the low pressure region develops a new structure. The region of slowly changing slope becomes a region of additional sharp changes in slope. This feature is called the "low pressure step." The various features of the curve are doubtless the result of both chemical and physical phenomena which take place in the liquid and in the flame just above the liquid.

Further evidence of these phenomena is given by direct observation of the burning liquid throughout the entire pressure range. There is a reddish-brown layer just beneath the liquid surface which apparently contains nitrogen dioxide. This layer consists of many small regions in rather active random motion due, perhaps, to convection currents. Its thickness (about 1 mm. at 20 atm.) decreases as the pressure increases. Around 35 atm. the flame has two distinguishable zones: first, a small, very dense, blue-white cone just above the surface; and second, a fairly transparent blue-white cone extending about 2 cm. above the liquid. Above the turbulent break the flame has only one discernible zone—a rather opaque whitish-blue cone about 4 cm. long. Throughout the entire pressure range it appeared that the flame volume increased with the pressure. There was no observable fizz zone (as in the case of burning solids) at any pressure above 20 atm. When the pressure was reduced to 14 atm. a fizz zone formed; and it increased in size as the pressure decreased further. However, this liquid does not maintain a fizz zone of even thickness at any pressure. At the low pressure limit for sustained combustion (about 9.5 atm.) the system burns alternately with and without flame in a random fashion; the brown zone is fairly wide, and bubbles form in the liquid surface.

Studies of the temperature distribution in burning liquids[1] showed that a small fraction of Lucite altered the behavior of the liquid phase and had a marked effect on the behavior of the vapor phase. Addition of 0.5% Lucite gave rise to a very stable fizz zone which was measured. A log–log plot of the data was very close to a straight line which was fitted by the empirical equation

$$D = \frac{3.77 \times 10^2}{P^2} \qquad (18 \text{ to } 35 \text{ atm.}) \quad (3)$$

where D is the fizz zone thickness in cm. and P is the bomb pressure in atm. It is interesting to note that eq. 3 differs from the $1/P^3$ function as reported by Crawford, Huggett and McBrady[9] for solid propellant combustion. However, it is similar to the equation relating distance from the burning surface to the position of maximum gas phase temperature and bomb pressure for nitrate esters obtained by Hildenbrand and Whittaker.[2]

Although no significant analytical results were obtained on the composition of the combustion products, there was no evidence (*e.g.*, appearance of NO, NO_2 or carbon in the combustion products) of incomplete combustion at any pressure as long as there was visible flame. When the flame was intermittent there was evidence of either NO or NO_2 in the combustion products.

Heat transfer to the combustion tube went through a peculiar cycle as the bomb pressure was increased. For pressures up to about 28 atm. the combustion tube would be quite hot when an experiment was completed. As the pressure increased (from 28 to 55 atm.) the final temperature of the tube decreased. Above 55 atm. the combustion tube became hotter again. This phenomenon was demonstrated in another way. If the mix were made slightly fuel rich, combustion tubes used for measurements at a set of increasing pressures would show gradations of carbon deposits. At 14 atm. there would be essentially no deposit; as the pressure increased the deposit would extend further up the tube; when about 55 atm. was reached the carbon deposit would decrease in extent; and at about 69 atm. there would be no deposit in the tube. In all cases the carbon deposit was very thin and represented only a very small fraction of the combustion products.

Turbulent Combustion.—The most striking effect of pressure is the onset of surface turbulence at a particular pressure. High-speed photographs of the combustion showed that the liquid burned smoothly at all pressures below 69 atm. when 97% nitric acid was used. Above this pressure the surface became very turbulent. Twenty liquid systems have been studied so far, and the appearance of turbulent combustion and the corresponding turbulence break in the consumption rate curve was common to all liquids. Of many different types of surface turbulence, three occurred rather frequently. One was an oscillatory type in which the surface liquid oscillated across the tube diameter and each time that the material changed direction a shower of droplets was thrown free from the major body of liquid. This was accompanied by flash burning of the liquid droplets which seemed to develop sufficient pressure transient to maintain the oscillation. Another was helical turbulence in which an inclined meniscus was formed and propagated down the tube along a helical path as the liquid burned. The trailing edge of the inclined surface was broken; from this broken edge many droplets were released into the flame zone. In the third type a large filament of liquid extended up the tube wall. The surface of the filament seemed to show wave motion and the liquid appeared to stream upward along the filament and again droplets were thrown into the flame zone from the

(8) O. K. Rice and R. Ginell, THIS JOURNAL, **54**, 885 (1950).

(9) B. L. Crawford, C. Huggett and J. J. McBrady, *ibid.*, **54**, 854 (1950).

trailing edge. All types of turbulence produced an excessive burning surface and much, if not all, of the sharp increase in consumption rate at the turbulence break was probably due to this sudden increase in burning surface. It was observed that oscillatory burning can change to helical burning, but the reverse process was never observed. During helical burning the helix pitch may change at a random location in the tube, but the change was always from high to low pitch. If the pitch was low (say 20 turns per inch) helical burning could not be distinguished from smooth burning insofar as overall rate was concerned. No easily recognizable relationship between helix pitch and tube diameter was found. However, there appeared to be a relationship between the helix angular velocity and the bomb pressure. Most of the data gave points falling very close to the linear relation

$$V = -0.132B + 17.3 \qquad (4)$$

where V is the angular velocity in revolutions per second and B is the bomb pressure in atmospheres. Although there were insufficient data to confirm it, there was an indication that there were several different modes of helical burning and that each mode may follow an equation similar to eq. 4. According to eq. 4 the angular velocity goes to zero at a pressure of 131 atm. This is close to the pressure region above which helical burning was not observed. Above 131 atm. only filament type turbulence was found, and this type always had zero angular velocity.

Close study shows that the onset of turbulence does not occur sharply at a particular pressure. The system 2-nitropropane–nitric acid was studied at 1.33-atm. intervals (using special pressure control apparatus) over a pressure range of 81.22 to 94.83 atm., which bracketed the turbulence break. Very close to the break 0.33-atm. intervals were used. From observation of high-speed photographs of the combustion it was estimated that the pressure for the onset of turbulence could not be defined more closely than 89.4 ± 1.33 atm. As the turbulence threshold was approached the actual oscillation of the liquid surface was very slight. Consequently, the consumption rate was not significantly different from that of a corresponding smooth combustion. This held true until about 1.3 atm. above the turbulence pressure and then the turbulence becomes so violent that it could be detected readily by any method. Because of this situation the pressure of 89.4 atm. was chosen close to the middle of the pressure range which included the first perceptible oscillation of the burning surface and the first occurrence of violent oscillations. Also, as the turbulence break was approached from the low pressure side, the time required for the igniter-excited turbulence to die out increased. Consequently, if the combustion tube was not long enough it could be concluded that the turbulence region had been reached, whereas actually the system would have gone to smooth burning had the tube been longer. Therefore, it was difficult to tell whether turbulence or smooth burning was the stable state as the turbulence pressure was approached.

High-speed photographs clearly show that the second break is accompanied by the onset of turbulence. Why turbulence starts at a particular consumption rate or pressure is still not answered. What happens to the true burning rate in the pressure region above the turbulence break should be known before attempting to answer this. Unfortunately, the turbulence, itself, makes it impossible to obtain this information. Surface correction, as applied in the smooth burning region, cannot be applied in the turbulent burning region because of the highly irregular and rapidly changing surface shape. However, two hypotheses are suggested to describe a mechanism for the onset of turbulent combustion. Turbulence may be generated within the liquid near the burning surface. The existence of the brown layer just below the liquid surface shows that there are some liquid phase reactions. Also, the rather rapid motion observed in this layer indicates that these reactions may be fairly energetic, and that their net heat effect may be exothermic. These subsurface reactions could increase in intensity as burning rate increases and at some particular rate the surface of the liquid could be upset either by thermal disturbance or by the evolution of gas bubbles or both. Observations on the vertical component of velocity of the free droplets broken from the liquid surface indicate that there is a turbulent region in the gas phase just above the liquid surface. Therefore, it is possible that at some pressure the products of combustion change from laminar to turbulent flow. This gas turbulence could then react on the liquid surface, causing it to oscillate and break up.

For some reason some of the droplets thrown into the flame do not even start to burn. These droplets (approximately 0.8 mm. dia.) make it possible to estimate the average gas velocity of the combustion products, which was approximately 150 cm./sec. If perfect gas behavior, a flame temperature of about 3000°K., and complete combustion, are assumed, a theoretical gas velocity for the combustion products can be calculated. At 69 atm. this calculated velocity is about 120 cm./sec. which is in fair agreement with the observed velocity. This yields a Reynolds number of approximately 600. While this is below the critical value for tube flow it may not be too low for the onset of turbulence in the gas under combustion conditions. The relationship between Reynolds number of the combustion products and the onset of liquid turbulence has been studied and will be reported in a separate paper.

It is possible that turbulence is really igniter excited, but in the following experiments it was shown that this is not the case. The liquid was ignited in the smooth burning region and steady-state combustion established. When the pressure in the bomb was increased beyond the turbulence pressure, the liquid would burn turbulent immediately as the pressure passed through the turbulence break. When the strand was ignited in the turbulent region and the bomb depressurized to the smooth burning region, however, the combustion went from turbulent to smooth burning as it passed through the turbulence break. These experiments indicate that there is no relationship between the onset of liquid turbulence and the igniter used to start the liquid burning.

Effect of Igniter Energy.—Since it was conceivable that igniters could effect the measurement of rate in ways other than by excitation of turbulent combustion, igniters of different types and energy were tried. Although hot-wire ignition was found to be possible, this method was not convenient because the energy required for ignition was a function of pressure, and had to be held within close limits. If the energy was too high or too low, ignition would not occur. Since the hot-wire igniter and the ballistite igniter gave similar results, and since more variations were possible with the ballistite igniters, only these results were considered. The energy of the igniters was changed by varying the weight of the ballistite bead. The measured rate over three successive intervals was compared to see if the rate changed over these intervals in the turbulent burning. The data in Table II show that over a fivefold range in igniter energy there is no evidence of an overdrive of the combustion wave by the larger igniters. The data also show that there is not sufficient pressure built up in the tubes during combustion to cause an acceleration of the combustion wave as it passes down the tube.

Effect of Combustion Tube Diameter.—To establish the effect of combustion tube diameter on consumption and burning rates, consumption rate and surface correction measurements were made for tubes with inside diameters from 0.5 to 10.5 mm. Because the reproducibility of consumption rate measurements is better at lower acid concentration, the system 2-nitropropane–95% nitric acid was used. Rate measurements were made in the smooth and turbulent burning regions (the turbulence break for this system was 82.6 atm.). The results obtained at 69 atm. are shown in Fig. 2.

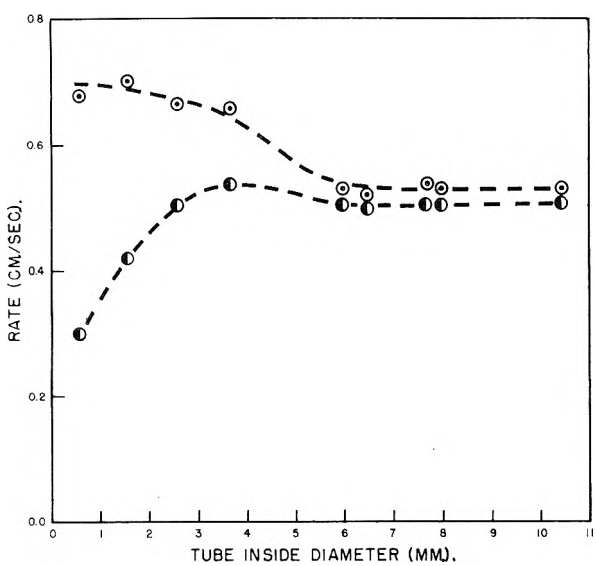

Fig. 2.—Effect of tube diameter on consumption rate and burning rate at 69 atm.: ○, consumption rate; ◐, burning rate.

The curve in Fig. 2 shows that the consumption rate decreased as tube diameter increased. Qualitatively this was expected since it was compatible with the fact that the meniscus becomes flatter as tube diameter increases. When surface corrections were applied to the data, burning rates increased as tube diameter increased because the surface correction for small tubes was appreciable and approached unity for large tubes. The effect of increasing heat loss to the tube walls is reflected by a decrease in burning rate as the tube diameter becomes smaller. Presumably the burning rate would drop to zero at the quenching diameter. The burning rate approaches a nearly constant value for tube diameters above 6 mm. This is probably the true burning rate for the system under the conditions of combustion. Also, Fig. 2 shows that for larger tubes consumption and burning rate are not significantly different. The slight "hump" in the burning rate curve at 3.5 mm. appears to be real. Repeated measurements at this tube diameter indicated that the high value was not due to experimental error. Tube wall effects such as possible catalysis at the walls may cause the burning rate to be too high. These effects become relatively less important as the tube size increases. Thus the hump in the burning rate curve may arise from the fact that the rates were corrected for surface areas, but not for additional effects due to the tube walls.

Table II

Effect of Igniter Energy on Consumption Rate of System 2-Nitropropane–97% Nitric Acid

Energy of igniter, j.	Consumption rate (cm./sec.) First interval	Second interval	Third interval
		(55.4 atm.)	
25	0.650	0.648	0.582
70	0.592	0.592	0.632
71	0.660	0.650	0.632
159	0.612	0.572	0.681
172	0.600	0.594	0.602
		(89.4 atm.)	
35	6.76	6.76	6.60
35	6.35	6.35	7.26
69	6.60	6.50	6.60
69	7.07	7.07	7.16
146	5.97	6.35	6.35
165	5.52	5.23	5.41

Although a similar study in the turbulent burning region is not possible some data were obtained and are presented in Table III. These data show that consumption rate increases as tube diameter increases which is the opposite of the result obtained in the smooth burning region. Moreover, they show that the rate increases very rapidly as tube diameter increases. The reason for this is not clear. High-speed photographs showed that as the tube diameter increased the turbulence appeared to become more violent and more droplets were thrown from the surface into the flame. Thus, the burning surface increased as tube diameter increased. In a system showing this behavior explosions would be expected to occur if somewhat larger tube diameters or somewhat higher pressure were used. Some explosions were observed, but they cannot be produced at will.

Effect of Tube Material.—Rate measurements in tubes of Pyrex, quartz and Kel-F were the same within the accuracy of the determination. Tubes of bakelite and similar materials gave higher con-

TABLE III

EFFECT OF TUBE DIAMETER ON CONSUMPTION RATE DURING TURBULENT COMBUSTION OF THE SYSTEM 2-NITROPROPANE–95% HNO_3

Inside diameter, mm.	Consumption Rate (cm./sec.) Pressure (atm.) 89.4	109.8	137
0.5[a]	1.24	2.74	5.77
1.2[a]	1.70	5.21	10.49
1.8[a]	3.71	8.53	14.33
2.5[b]	6.12	11.68	17.32
3.5[b]	6.22	12.87	23.34
4.0[b]	7.19	13.13	
5.0[b]	8.48	14.91	
6.0[b]	10.13	21.18	
7.0[b]	11.66	24.79	
8.0[b]	12.95		
9.0[b]	19.66		

[a] Capillary tubing. [b] Standard tubing.

sumption rates than those obtained in Pyrex. During the time required to fill these tubes and carry out the combustion, a portion of the tube would dissolve in the mixture. Thus, data obtained in these tubes were not considered valid because essentially a different mix was being burned. As an example of high thermal conductivity material aluminum tubes were tried. Frequently the fuse wires would come in contact with the tube and short out prematurely; but some valid data were obtained from these tubes. The consumption rate in these tubes was two to three times higher than that obtained in Pyrex. This seemed quite reasonable since heat could be conducted down the tube wall and heat up the liquid. Therefore, the liquid would be burning at an effectively higher ambient temperature. However, for this system this large increase in consumption rate would have to be due to the liquid burning at an effective ambient temperature of something like 390°. It has been shown that the surface temperature of this system is approximately 190°[2]; hence, it is unreasonable to say that heat conducted down the aluminum tube walls was able to heat the liquid to a sufficiently high temperature to produce the observed increase in consumption rate. Perhaps, some of the aluminum was dissolved and the salts produced had a catalytic effect on the burning process.

A search was made for tubes that would burn down as fast as the liquid was consumed. Many different combustible materials were tried but none seemed to work satisfactorily. For example, ballistite tubes, approximately the same dimensions as the Pyrex tubes, were prepared and an inhibitor was applied to the inside and outside surfaces of the tube. This prevented the liquid from being absorbed into the ballistite and prevented the ballistite from dissolving in the liquid to produce effects similar to those obtained with bakelite tubes. The rate obtained with ballistite tubes was an intermediate between the ballistite burning rate alone and the rate of the liquid in Pyrex tubes. Since ballistite alone has a burning rate in the low pressure region greater than that of the liquid this result was quite reasonable for the rate is a compromise on burning surface. The ballistite tube simply burns down ahead of the liquid, but the liquid flows over the edge of the ballistite tube and tends to increase its own burning surface and decrease the burning surface of the ballistite. In the turbulent region where the liquid burns faster than the ballistite, results were similar to those obtained in Pyrex tubes. To be successful, it would be necessary to use a solid whose burning rate is slightly less than that of the liquid at all pressures and the pressure coefficient for the solid and the liquid would have to be very nearly the same, so that there would be no cross over in the burning rate curves of the two materials. From these studies, it appears that tubes of an inert substance will give the correct consumption rate but combustible tubes or tubes that react with the system being burned will very likely give spurious consumption rate values.

NUCLEAR SPIN CONTRIBUTION TO THE LOW TEMPERATURE THERMODYNAMIC PROPERTIES OF IODINE, BROMINE AND CHLORINE

BY H. W. DODGEN AND J. L. RAGLE

Contribution from the Department of Chemistry, The State College of Washington, Pullman, Washington

Received December 12, 1955

It is pointed out that sufficient data exist for exact calculation of nuclear spin contributions to the thermodynamic properties of some substances. At low temperatures these contributions form the major part of such properties. Sample calculations have been made from existing data for the cases of solid iodine, bromine and chlorine.

In 1924, two years before Uhlenbeck and Goudsmit postulated the existence of electron spin, Pauli suggested that the nucleus itself might possess a spin angular momentum. Following this, Gibson and Heitler[1] carried out a detailed statistical calculation, including possible nuclear spin effects, of the thermodynamic equilibrium constant for reactions typified by the dissociation of gaseous iodine. Giauque,[2] in 1931, from consideration of existing heat capacity data for solid iodine, concluded that even at temperatures slightly below 10°K. the populations of possible spin states had already reached the high temperature equilibrium distribution. This implied that the spacing of any such levels was much less than thermal energy at this temperature in solid iodine.

(1) G. E. Gibson and W. Heitler, *Z. Physik*, **49**, 465 (1928).

(2) W. F. Giauque, *J. Am. Chem. Soc.*, **53**, 507 (1931).

In the absence of external fields, the nuclear spin energy levels are $2I + 1$ fold degenerate, where I is the nuclear spin. This degeneracy may be partially or completely removed by external electric or magnetic fields. Nuclei with spin greater than $^1/_2$ may possess an electric quadrupole moment and the electric field at such a nucleus in a solid substance caused by valence electrons and/or the crystalline electric field may cause partial lifting of this degeneracy and hence splitting into several levels whose number and spacing depend on the magnitude of the nuclear spin, the magnitude of the nuclear quadrupole moment, and the gradient of the electric field at the nucleus.[3,4]

Transitions between the levels thus produced were first observed about 5 years ago and have since been observed in several nuclear species and many different solid compounds. Those observed so far lie in the short-wave region of the radio frequency spectrum. It is the purpose of this paper to call attention to the fact that nuclear spin contributes to the equilibrium thermodynamic properties of many substances in an accessible temperature range. In this respect, R. V. Pound has pointed out that significant nuclear alignment of I^{127} should occur in ICl at accessible temperatures.

In the case of solid iodine ($I = 5/2$) the electric field at the nucleus causes splitting into three levels: $m_I = \pm 1/2, \pm 3/2, \pm 5/2$, giving two absorption lines in accord with the selection rule $\Delta m_I = \pm 1$. The pure nuclear quadrupole spectrum of iodine has been observed by both Dehmelt[5] and Pound.[6] At 4°K. Pound found lines at 642.8 and 334.0 mcps., corresponding to the transitions $m_I = \pm 5/2 \leftrightarrow \pm 3/2$ and $\pm 3/2 \leftrightarrow \pm 1/2$, respectively. Pure quadrupole spectra have also been observed in solid bromine[7] and chlorine.[8] Both of these nuclei have spin 3/2, but natural samples contain two isotopic species, and therefore two lines are observed in each case. In bromine the observed frequencies are 382.43 and 319.46 mcps. for Br^{79} and Br^{81}, while in chlorine, lines are observed at 54.248 and 42.756 mcps. for Cl^{35} and Cl^{37}, respectively.

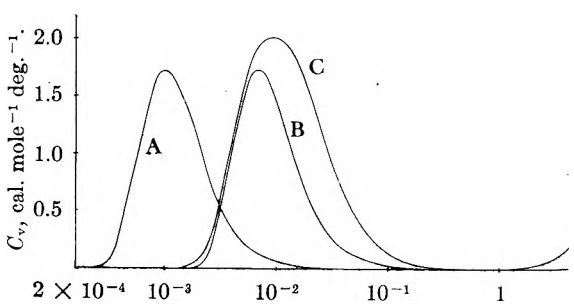

Fig. 1.—A, Cl_2; B, Br_2; C, I_2.

It is known that the nuclei in these cases should approximate assemblies of independent localized systems quite well.[9] Because of the small number of possible energy levels, the nuclear partition functions have simple forms, greatly facilitating numerical work. Straightforward calculations yield the following results for the nuclear contributions to the heat capacities of these substances

Iodine:

$$C_v = \frac{2R}{T^2}\left\{\frac{[h^2\nu_1^2 e^{-h\nu_1/kT} + h^2(\nu_1+\nu_2)^2 e^{-h(\nu_1+\nu_2)/kT}]}{[1 + e^{-h\nu_1/kT} + e^{-h(\nu_1+\nu_2)/kT}]} - \frac{[h\nu_1 e^{-h\nu_1/kT} + h(\nu_1+\nu_2)e^{-h(\nu_1+\nu_2)/kT}]^2}{[1 + e^{-h\nu_1/kT} + e^{-h(\nu_1+\nu_2)/kT}]^2}\right\}$$

Bromine:

$$C_v = \frac{R}{T^2}\left\{\frac{1.010h^2\nu_{79}^2 e^{-h\nu_{79}/kT}}{[1 + e^{-h\nu_{79}/kT}]^2} + \frac{0.990h^2\nu_{81}^2 e^{-h\nu_{81}/kT}}{[1 + e^{-h\nu_{81}/kT}]^2}\right\}$$

Chlorine:

$$C_v = \frac{R}{2T^2}\left\{\frac{3.016h^2\nu_{35}^2 e^{h\nu_{35}/kT}}{[1 + e^{h\nu_{35}/kT}]^2} + \frac{0.9840h^2\nu_{37}^2 e^{h\nu_{37}/kT}}{[1 + e^{h\nu_{37}/kT}]^2}\right\}$$

(For bromine and chlorine the calculations are corrected for the naturally occurring isotopic compositions.) The form of these curves is shown in Fig. 1.

Since $dS = C_v/T\ dT$, by inspection of the figure one can see at what temperature nuclear contributions to the entropy become important. In the case of iodine an extrapolation of the experimental heat capacity data indicates a minimum at approximately 1°K., or within the region of practical experimental work. Pound has measured the thermal relaxation time of iodine nuclei in solid iodine at 4°K. and finds it to be of the order of seconds. Thus it is possible that at lower temperatures the attainment of thermal equilibrium would be a problem in any actual experimental work.

Since the relative populations of these levels in iodine become strong functions of temperature below 0.1°K., measurement of the relative intensities of the two absorption lines might serve as a temperature measuring device in this region, providing that the experimental difficulties could be worked out. In other iodine compounds, where the splitting may not be so great, the population change with temperature would become important only at lower temperatures, and thus by using different compounds of iodine, this scheme could be applied in different temperature regions below 0.1°K. The region of usefulness for crystalline iodine would be between about 4×10^{-3}°K. and 0.1°K.

Acknowledgment.—The authors would like to express their appreciation to Dr. J. H. Wagner, who carried out some of the numerical calculations for iodine.

(3) W. Gordy, W. V. Smith and R. F. Trambarulo, "Microwave Spectroscopy," John Wiley and Sons, Inc., New York, N. Y., 1953, p. 269 ff.

(4) C. H. Townes and B. P. Dailey, *J. Chem. Phys.*, **20**, 35 (1952).

(5) H. G. Dehmelt, *Naturwiss.*, **17**, 398 (1950).

(6) R. V. Pound, *Phys. Rev.*, **82**, 343 (1951).

(7) H. G. Dehmelt, *Z. Physik*, **130**, 480 (1951).

(8) R. Livingston, *J. Chem. Phys.*, **19**, 803 (1951).

(9) For instance, it can be shown that nuclear magnetic dipole-dipole interactions only become important in iodine at temperatures much lower than those considered here.

VAPOR PRESSURE AND DIELECTRIC CONSTANT OF DIBORANE[1]

BY HENRY E. WIRTH AND EMIEL D. PALMER

Department of Chemistry, Syracuse University, Syracuse, N. Y.

Received December 7, 1955

The vapor pressure of diborane is represented by the equation $\log_{10} p_{mm} = 6.9681 - 674.82/(T - 15.02)$, ($108°K. < T < 150°K.$) and $\log_{10} p_{mm} = 6.61885 - 583.120/(T - 24.63)$, ($150°K. < T < 181°K.$). The boiling point of diborane is 180.63 ± 0.02°K., and the heat of vaporization at the boiling point, as calculated from the vapor pressure equation, is 3,413 cal./mole. Two melting points were found for diborane: 108.14 ± 0.02°K. and 108.30 ± 0.02°K. The first value is probably that of a metastable phase. No phase transitions were observed in the solid. Diborane is non-polar, and the dielectric constant of the liquid is represented by the equation $\epsilon = 2.3721 - 0.002765_2 T$.

Introduction

The vapor pressures of diborane previously published[2-4] are reported with an accuracy of 1%. The present work was undertaken to obtain precise values for the vapor pressure of diborane, and to investigate the use of dielectric constant measurements in establishing phase transitions in the solid state.

Experimental

Apparatus.—The dielectric constant–vapor pressure cell (Fig. 1) was constructed from a cylindrical copper block (A) 6.4 cm. in diameter by 19 cm. long. In the center of the block a hole 1.07 cm. in diameter contained the cell proper. The cell consisted of a copper cylinder (C) (12.2 cm. long, 0.92 cm. o.d. and 0.80 cm. i.d.) supported by glass spacers on a copper rod (B) 0.63 cm. in diameter. The wire (D) to the "hot" cylinder passed through insulated terminals (E) and out of the cell. The inner surfaces of the cell were silver plated and polished before assembly. Approximately 6 ml. of liquid was required to fill the cell to the point where addition of more liquid did not change the capacitance.

The cell was mounted in an assembly similar to that used in a Nernst type calorimeter including an upper block with shield and an auxiliary block through which all heater and thermocouple leads passed. The assembly was placed in a Collins helium cryostat, enabling measurements to be made at any temperature between 8°K. and room temperature.

The sample inlet tube was connected to a gas handling system, to a vacuum system, and to a manometer made of 2.2 cm. precision bore tubing maintained at 30 ± 0.1°.

The temperature of the cell was determined with copper–constantan thermocouples[5] which had been calibrated against the Ohio State helium thermometer. A Schering type bridge (General Radio Type 716-C) was used to determine capacitance and dissipation factor. Measurements were made in the frequency range 1–200 kilocycles.

Calibration of the Capacitance Cell.—The capacitance of the cell was found to be 82.11 μμF. at room temperature, using benzene ($\epsilon = 2.2747$ at 25°)[6] as a standard.

The capacitance of a condenser consisting of two coaxial cylinders is given by the relation

$$C = \frac{0.2416l}{\log_{10} r_1/r_2}$$

where l is the length of the cylinders and r_1 and r_2 are their radii. Therefore the only effect of temperature on the capacitance would be due to the change in length of the cylinders. With the cell used, which is made up of two such simple condensers, the length of the central cylinder is the determining factor. Taking the average linear coefficient of expansion of copper as 12.6×10^{-6} per degree between 0 and 300°K., and as 15.9×10^{-6} per degree between 80 and 300°K.,[7] the calculated capacitance of the empty cell was 81.83 μμF. at 20°K., and 81.85 μμF. at 80°K. The cell capacitance was assumed to vary linearly with temperature above 80°K.

The dielectric constant of liquid and solid oxygen was determined to check the cell calibration and the sensitivity of the dielectric constant method for the detection of phase transitions.

The oxygen was prepared by electrolysis between platinum electrodes of 20% KOH solution. The evolved oxygen was passed through tubes containing KOH pellets, CuO at 450°, amalgamated Cu turnings, and $Mg(ClO_4)_2$. It was collected in a trap cooled with liquid N_2, and then distilled into the dielectric constant cell which was held at 60°K. About one ml. more oxygen than that required to give a constant capacitance reading was condensed in the cell. On cooling, the oxygen usually first formed a glass,[8] then abruptly crystallized at about 40°K. The cell was then warmed to the melting point of oxygen to permit liquid to fill the voids produced when the glass crystallized. After cooling to 10°K., measurements were made as the temperature was increased.

Breaks in the dielectric constant–temperature curve were observed at temperatures corresponding to the two known solid–solid phase transitions of oxygen and at the melting point. The transition temperatures observed were $\alpha \rightarrow \beta$ 23.68 ± 0.02°K., $\beta - \gamma$ 43.81 ± 0.02°K., and $\gamma \rightarrow$ liquid, 54.38 ± 0.02°K., in excellent agreement with those reported by Giauque and Johnston.[9] There are large errors in the absolute magnitudes of the dielectric constants obtained as this type of cell could not be completely filled with solid. However, abrupt changes in the dielectric constant were always observed at temperatures corresponding to the phase transitions.

The empirical equation

$$\epsilon = 1.6751 - 1.698 \times 10^{-3} T - 4.00 \times 10^{-6} T^2 \quad (1)$$

fits the ten observations between 54.4 and 89.9°K. made on liquid oxygen with an average deviation of ±0.0002. These values average 0.0032 unit higher than those reported by Werner and Keesom[10] on oxygen containing 2.4% nitrogen. After correcting for the error due to the nitrogen, our values are 0.005 unit higher.

A sample of tank electrolytic hydrogen was liquefied, distilled, and the middle fraction retained for use.

The empirical equation

$$\epsilon = 1.2688 + 3.96 \times 10^{-4} T - 1.12_5 \times 10^{-4} T^2 \quad (2)$$

fits the eight observations between 13.8 and 20°K. made of the dielectric constant of liquid hydrogen with an average deviation of ±0.0003. These values agree with those reported by Werner and Keesom[11] with an average deviation of ±0.0008 unit, but are 0.0025 unit higher than those reported by Guillien.[12]

It is possible that our values for $\epsilon - 1$ may be high by as much as 1%. Since Werner and Keesom used the same cell for their measurements on both oxygen and hydrogen, and since the oxygen used by them was known to be impure, we

(1) Presented at the New York meeting of the American Chemical Society, September, 1954.

(2) A. Stock and E. Kuss, *Ber.*, **56**, 789 (1923).

(3) John T. Clarke, E. B. Rifkin and H. L. Johnston, *J. Am. Chem. Soc.*, **75**, 781 (1953).

(4) E. B. Rifkin, E. C. Kerr and H. L. Johnston, *ibid.*, **75**, 785 (1953).

(5) The thermocouples were supplied by the Cryogenic Laboratory of The Ohio State University through the courtesy of Professor T. R. Rubin.

(6) A. S. Brown and E. W. Abrahamson, *J. Chem. Phys.*, **19**, 1226 (1951).

(7) M. Wolfke and H. K. Onnes, Leiden Comm., 171b.

(8) W. Wahl, *Proc. Roy. Soc.* (*London*), **A88**, 61 (1913).

(9) W. F. Giauque and H. L. Johnston, *J. Am. Chem. Soc.*, **51**, 2300 (1929).

(10) W. Werner and W. H. Keesom, Leiden Comm., 178c.

(11) W. Werner and W. H. Keesom, *ibid.*, 178a.

(12) R. Guillien, *Rev. sci.*, **77**, 575 (1939).

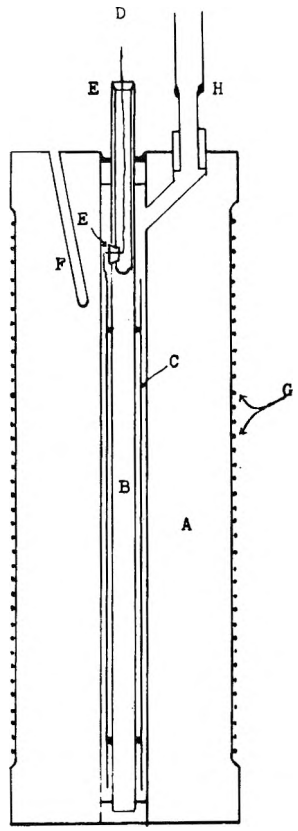

Fig. 1.—Dielectric constant–vapor pressure cell: A, copper block; B, copper rod; C, copper cylinder; D, "hot" lead; E, insulated terminals; F, thermocouple well; G, heating wires; H, Kovar-glass seal.

do not feel justified in correcting the cell calibration on the basis of the results obtained.

The temperature scale was checked further by observation of the vapor pressure of hydrogen and oxygen and the sublimation pressure of carbon dioxide. Above 20°K., the observed and calculated temperatures did not differ by more than ±0.02°K.

Preparation of Diborane.—Diborane was prepared by the reaction of lithium aluminum hydride with boron trifluoride etherate in ethyl ether, using the method described by Shapiro, Weiss, Schmich, Skolnik and Smith.[13] The diborane prepared in this way appeared to be contaminated with small amounts of ethyl ether which were not removed by simple fractionation. The procedure was revised to use boron trifluoride tetrahydrofuranate with tetrahydrofuran as the solvent. While much lower yields were obtained, the diborane was purer. In the first trial (Series I), approximately 5 ml. of liquid diborane was prepared, which was sufficient for vapor pressure measurement, but was not enough to fill the cell for dielectric constant work. The second trial (Series II) gave 11 ml. of liquid diborane and the middle fraction of 6.5 ml. was used for the measurements.

Results

Melting Point of Diborane.—The melting point (Series I) was 108.28°K., and the temperature at which half the solid was melted was 108.26°K. This gave 108.30°K. as the melting point of pure diborane, and a sample purity of 99.9 mole per cent. Since there is a 10% decrease in the dielectric constant of diborane in going from solid to liquid, the fraction melted could be readily obtained from the change in cell capacitance, even though the cell was not completely filled. Of fifteen determinations of the melting point on the second sample (Series II), only one agreed with the value found previously. The other measurements gave a sharp melting point at 108.14°K. The indicated purity was 99.95 mole per cent., based on the fraction melted *vs.* temperature curves. It is believed that diborane can exist in two solid phases, a stable phase melting at 108.30°K., (in agreement with the value reported by Clarke, Rifkin and Johnston[3]) and a metastable phase melting at 108.14°K. Attempts to determine the conditions by which metastable phase could always be converted to the stable phase were unsuccessful. No indications of phase transitions in the solid diborane were observed.

Vapor Pressure of Diborane.—The vapor pressure results are reported in Table I. The data of

TABLE I

VAPOR PRESSURE OF DIBORANE

Temp., °K.	Series	P_{obsd}	P_{calcd}*	$P_{obsd} - P_{calcd}$
*$\log_{10} p_{mm} = 6.9681 - 674.82/(T - 15.02)$ (3)				
108.22	I	0.53	0.53	...
108.37	II	0.54	0.55	−0.01
108.76	I	0.58	0.59	−0.01
113.07	I	1.25	1.22	+0.03
115.10	II	1.68	1.68	...
117.89	I	2.59	2.56	+0.03
119.90	II	3.46	3.42	+0.04
124.40	I	6.34	6.29	+0.05
125.02	II	6.76	6.81	−0.05
130.12	II	12.74	12.74	...
131.81	I	15.66	15.49	+0.17
135.12	II	22.39	22.35	+0.04
140.00	I	37.38	37.04	+0.34
140.11	II	37.55	37.45	+0.10
145.03	II	60.04	59.93	+0.11
147.00	I	71.99	71.63	+0.36
*$\log_{10} p_{mm} = 6.61885 - 583.120/(T - 24.63)$ (4)				
150.03	II	93.28	93.28	...
154.07	I	130.49	129.99	+0.50
155.40	II	144.46	144.45	+0.01
160.00	II	204.82	204.76	+0.06
160.42	I	211.62	211.14	+0.48
165.14	II	294.55	294.33	+0.22
166.90	I	331.61	331.26	+0.35
170.01	II	405.89	405.36	+0.53
172.90	I	485.47	485.31	+0.16
175.04	II	552.40	552.05	+0.35
178.87	I	688.25	689.05	−0.80
179.94	II	732.04	731.63	+0.41
180.66	II	761.83	761.42	+0.41

Series II were used to determine the constants in the equations

$$\log_{10} p_{mm} = 6.9681 - \frac{674.82}{T - 15.02} \quad (108°K. < T < 150°K.) \quad (3)$$

and

$$\log_{10} p_{mm} = 6.61885 - \frac{583.120}{T - 24.63} \quad (150°K. < T < 181°K.) \quad (4)$$

A single equation of this type did not fit the data accurately over the entire temperature range. Other types of equations were tried but they gave

(13) I. Shapiro, H. G. Weiss, M. Schmich, Sol Skolnik and G. B. L. Smith, *J. Am. Chem. Soc.*, **74**, 901 (1952).

less satisfactory agreement with the data than the one used above.

At 180°K., dp/dT = 42 mm. per degree, so an error of ±0.01° in temperature gives rise to an error of 0.84 mm. in the vapor pressure. With a few exceptions, all the data obtained can be represented by the equations given to the accuracy with which the temperature had been determined.

In determining the vapor pressure of diborane, the diborane in the manifold and manometer system was frozen out with liquid nitrogen several times during the course of a series of measurements and the residual pressure measured. The observed pressure was corrected for this residual pressure due to the decomposition of the diborane. In no case did the correction exceed the experimental error due to errors in the measurement of temperature.

The values are about 2.5 mm. higher (at 185°K.) than those reported by Clarke, Rifkin and Johnston,[3] and 9 mm. lower (at 180°K.) than those reported by Rifkin, Kerr and Johnston.[4] They agree with the results of Stock and Kuss[2] to within the experimental error of their temperature measurement.

Boiling Point and Heat of Vaporization of Diborane.—The calculated boiling point is 180.63 ± 0.02°K. This compared to the value 180.32°K. reported by Clarke, Rifkin and Johnston[3] and 180.6 ± 0.2°K. reported by Rifkin, Kerr and Johnston[4] based on vapor pressure data good to 1%. The boiling point is given as 180.63°K. by Rossini.[14]

The heat of vaporization of diborane was calculated using the equation

$$\Delta H = RT^2 \frac{\mathrm{d} \ln p}{\mathrm{d}T}\left[1 + \frac{9PT_c}{128P_cT}\left(1 - \frac{6T_c^2}{T^2}\right) - \frac{PV_{liq}}{RT}\right] \quad (5)$$

with values for T_c = 16.7°C. and P_c = 581 p.s.i.a. as given by Newkirk.[15] The heat of vaporization at 180.63° was calculated to be 3,413 cal./mole, in excellent agreement with the observed value reported by Clarke, Rifkin and Johnston.[3] Two values (3412 and 3422 cal./mole) were quoted in this article.

Dielectric Constant of Diborane.—The dielectric constant of liquid diborane is given for various temperatures in Table II, and can be represented by the equation

$$\epsilon = 2.3721 - 0.002765_3T \quad (6)$$

with an average deviation of ±0.05%. The Clausius–Mosotti function $(\epsilon - 1)/(\epsilon + 2)\ (1/d)$ was calculated using the values for the density of diborane given by Stock, Wiberg and Mathing[16] for

$$d = 0.4371 + 1.0115 \times 10^{-3}(180.6 - T)$$
$$(165°\mathrm{K.} < T < 180°\mathrm{K.}) \quad (7)$$

the temperature range 165–168°K. and by Laubengayer, Ferguson and Newkirk[17] for the temperature

$$d = 0.3140 - 0.001296t°\mathrm{C.};$$
$$(145°\mathrm{K.} < T < 170°\mathrm{K.}) \quad (8)$$

range 140–170°K. Since diborane is non-polar, it is expected that the Clausius–Mosotti function would be a constant. The function is constant through the temperature range where Stock's density equation is valid (average value, 0.5160) but apparently decreases with decreasing temperature through the temperature range where Laubengayer's density data were used. Although the two sets of data agree well where they overlap, it is suspected that the lower temperature density data of Laubengayer may be in error by a little over 1%.

The molar polarization is 14.29 cc.

TABLE II

DIELECTRIC CONSTANT OF LIQUID DIBORANE

Temp., °K.	ϵ_{obsd}	ϵ_{calcd}[a]	Density(d)	$\frac{\epsilon - 1}{\epsilon + 2}\frac{1}{d}$
108.26	2.0735	2.0727		
108.37	2.0724	2.0724		
115.10	2.0529	2.0538		
119.90	2.0397	2.0405		
120.12	2.0400	2.0399		
125.02	2.0255	2.0264		
129.96	2.0131	2.0127		
130.12	2.0118	2.0123		
135.12	1.9978	1.9985		
139.80	1.9866	1.9855		
140.11	1.9841	1.9847		
145.03	1.9705	1.9710	0.4800(L)[17]	0.5089
149.89	1.9587	1.9576	.4736(L)	.5114
150.03	1.9567	1.9572	.4736(L)	.5105
155.40	1.9418	1.9424	.4666(L)	.5120
160.00	1.9307	1.9297	.4606(L)	.5141
160.00	1.9291	1.9297	.4606(L)	.5134
165.14	1.9157	1.9154	.4540(L)	.5151
			.4527(S)[16]	.5166
170.01	1.9013	1.9020	.4477(L)	.5160
			.4477(S)	.5160
170.26	1.9020	1.9013	.4474(L)	.5167
			.4475(S)	.5166
175.04	1.8879	1.8881	.4427(S)	.5159
179.94	1.8741	1.8745	.4377(S)	.5155
180.66	1.8725	1.8725	.4370(S)	.5156

[a] From equation 6.

(14) F. D. Rossini, "Selected Values of Chemical Thermodynamic Properties," Natl. Bureau of Stds. Circular 500, p. 721.

(15) A. E. Newkirk, *J. Am. Chem. Soc.*, **70**, 1978 (1948).

(16) Equation of A. Stock, E. Wiberg and W. Mathing, *Ber.*, **69**, 2811 (1936).

(17) Equation of A. W. Laubengayer, R. P. Ferguson and A. E. Newkirk, *J. Am. Chem. Soc.*, **63**, 559 (1941).

DIELECTRIC CONSTANT AND VAPOR PRESSURE OF PENTABORANE[1]

BY HENRY E. WIRTH AND EMIEL D. PALMER

Department of Chemistry, Syracuse University, Syracuse, N. Y.

Received December 7, 1955

The melting point of pentaborane is 226.41 ± 0.02°K. Liquid pentaborane has a high dielectric constant ranging from 21 at room temperature to 53.1 at the melting point. Pentaborane is a highly polar substance, with an apparent dipole moment varying between 3.37 debyes at room temperature to 4.54 debyes at the melting point. In the temperature range 130–140°K. there is a sluggish solid–solid transition which may be accompanied by the onset of free rotation in the solid. The vapor pressure of pentaborane is given by the equation $\log_{10} p_{mm} = 9.96491 - (1951.14)/T - 0.003688_4 T$ in the temperature range 226–298°K.

Introduction

Dulmage and Lipscomb[2] estimated the dipole moment of pentaborane to be 0.6 debye unit. Later calculations by Eberhardt, Crawford and Lipscomb[3] gave 5.23 debyes as the maximum value, and 1.7–2.0 debyes as the more probable value of the dipole moment. An experimental value of 2.13 debyes in the gas phase was reported by Hrostowski, Myers and Pimental[4] from measurements in the microwave region.

These results indicated that liquid pentaborane would have a high dielectric constant. The apparatus previously developed[5] was therefore used to investigate this substance.

Experimental

Apparatus.—The apparatus described previously[5] was used without modification, except that in some cases it was necessary to place a standard capacitance in series with the experimental cell in order to bring the measured capacitance within the range of the bridge. This reduced the precision of the dielectric constant measurements to ±2%.

Purification of Pentaborane.—Pentaborane was frozen in a trap cooled with Dry Ice–acetone mixture and was maintained under vacuum for 18 hours to remove volatile impurities. A middle fraction of 6.5 ml. from a total sample of 15 ml. was used for the measurements reported.

Results

Melting Point of Pentaborane.—The melting point was found to be 226.41 ± 0.02°K., and the purity as determined from fraction melted *vs.* temperature curves was 99.9+ mole per cent. Johnston, Kerr, Clarke and Hallett[6] found the melting point to be 226.34°K., and Rossini[7] quotes a value of 226.3°K.

Dielectric Constant of Liquid Pentaborane.—The observed values of the dielectric constant for pentaborane are given in Table I. The dielectric constant at room temperature is 21 (compared to 25 for ethyl alcohol, 34 for methyl alcohol, and 81 for water) and increases rapidly with decreasing temperature to a maximum value of 53.1 at the melting point. The values reported are the averages of observations made at 200, 100 and 50 kc. The individual values did not differ by more than 2%. The specific resistance, as calculated from the observed dissipation factor at 50 kc., varied from 2×10^6 ohm cm. at 297°K. to 4×10^6 ohm cm. at 226.4°K. The Onsager[8] equation

$$\frac{(\epsilon - n^2)(2\epsilon + n^2)}{\epsilon(n^2 + 2)^2} = \frac{4\pi N \mu_0^2}{9kT} \qquad (2)$$

(where ϵ is the dielectric constant, n is the "internal refractive index," N is the number of molecules per cc., μ_0 is the permanent electric moment, k is Boltzmann's constant, and T is the absolute temperature) permits the calculation of the dipole moment from measurements made on a liquid. Böttcher[10] and Phadke, Gokhale, Phalnikar and Bhide[11] have shown that application of this equation to unassociated liquids gives results in excellent agreement with measurements made with dilute solutions or gases. The ordinary refractive index (n_D) was used by these authors. With associated liquids (water and alcohols) the values obtained were uniformly higher than obtained by other methods.

TABLE I

DIELECTRIC CONSTANT OF LIQUID PENTABORANE

Temp., °K.	Series	ϵ (obsd.)	Density,[9] g./cc.	p'	$\frac{\epsilon - 1}{\epsilon + 2}\frac{1}{d}$
226.4	I	53.1	0.682	9.33	1.386
226.4	II	53.1	.682	9.33	1.386
230.0	II	50.0	.678	8.85	1.390
237.0	I	45.5	.673	8.13	1.393
240.0	II	42.6	.670	7.61	1.393
247.0	I	39.2	.665	7.11	1.394
254.0	I	35.7	.659	6.55	1.397
261.0	I	32.6	.653	6.06	1.399
268.0	I	29.7	.648	5.57	1.396
273.0	I	28.0	.644	5.30	1.398
278.0	I	26.4	.639	5.04	1.400
280.6	II	25.1	.637	4.82	1.396
283.0	I	24.9	.635	4.80	1.399
288.0	I	23.6	.631	4.59	1.399
288.3	II	22.9	.631	4.46	1.394
292.0	I	22.6	.628	4.42	1.397
292.3	II	22.0	.628	4.31	1.392
296.0	I	21.6	.625	4.25	1.397
297.1	II	20.9	.624	4.13	1.392
298.0	I	21.1	.623	4.17	1.397

(1) Presented in part at the New York meeting of the American Chemical Society, September, 1954.

(2) W. J. Dulmage and W. N. Lipscomb, *J. Am. Chem. Soc.*, **73**, 3539 (1951).

(3) W. H. Eberhardt, B. Crawford, Jr., and W. N. Lipscomb, *J. Chem. Phys.*, **22**, 989 (1954).

(4) H. J. Hrostowski, R. J. Myers and G. C. Pimental, *ibid.*, **20**, 518 (1952).

(5) H. E. Wirth and E. D. Palmer, THIS JOURNAL, **60**, 911 (1956).

(6) H. L. Johnston, E. C. Kerr, J. T. Clarke and N. C. Hallett, *ibid.*, **60**, in press (1956). (An advance copy of this publication was supplied the authors through the courtesy of Prof. H. L. Johnston).

(7) F. D. Rossini, Natl. Bureau of Standards Circular 500, p. 721.

(8) L. Onsager, *J. Am. Chem. Soc.*, **58**, 1486 (1936).

(9) Calculated from the equation

$$d = 0.8674 - 0.00082T \qquad (1)$$

given by S. H. Smith, Jr., and R. R. Miller, *ibid.*, **72**, 1452 (1950).

(10) C. J. F. Böttcher, *Physica*, **6**, 59 (1939).

(11) S. R. Phadke, S. D. Gokhale, N. L. Phalnikar and B. V. Bhide, *J. Indian Chem. Soc.*, **22**, 235 (1945).

The apparent dipole moment of pentaborane, calculated from the measured dielectric constant and index of refraction at 24° (n_D = 1.4445) is 3.41 debye units.

Wyman[12] showed that if the polarization per gram, defined by the relation

$$p' = (\epsilon + 1)/8.5d \qquad (3)$$

is plotted against the reciprocal of the absolute temperature, a straight line should be obtained. From the slope of this line the dipole moment may be obtained

$$\mu = 0.0127 \sqrt{M \frac{dp'}{d\ k/T}} \text{ debyes} \qquad (4)$$

where M is the molecular weight. The intercept on the ordinate axis is the sum of the atomic and electronic polarizations, which can also be obtained from the index of refraction.

Values of p' are given in Table I and are plotted in Fig. 1 against the reciprocal of the absolute temperature. It is evident that p' is not a linear function of $1/T$, and that a considerable curvature is required if the intersection on the ordinate axis is to equal the polarization as obtained from the index of refraction. The slope of the line A, drawn from p' corresponding to the highest temperature (298°K.) to the intercept, gives a calculated value of 3.37 debyes for the dipole moment, which agrees, as it must, with the value calculated by use of the Onsager equation. The slope of line B, drawn through p' corresponding to the lowest temperature (226.4°K.), gives an apparent dipole moment of 4.54 debyes. Line C is drawn with a slope corresponding to the dipole moment of 2.13 debyes found in the gas phase.

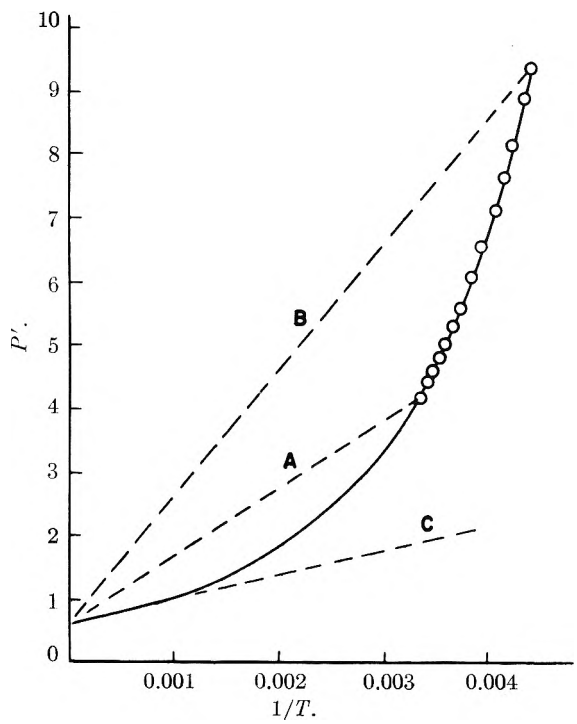

Fig. 1.—Polarization per gram of liquid pentaborane *vs.* reciprocal of the absolute temperature.

(12) J. Wyman, Jr., *J. Am. Chem. Soc.*, **58**, 1482 (1936).

The Clausius–Mosotti function, $(\epsilon - 1)/(\epsilon + 2)(1/d)$, given in Table I is unexpectedly constant. The average value (1.395) gives a molecular polarization of 88.0 cc. for the liquid, as compared to a molar refraction of 26.9 cc. calculated from the index of refraction.

Dielectric Constant of Solid Pentaborane, and the Solid Phases.—On freezing pentaborane the dielectric constant drops rapidly, and becomes approximately 3 at 200°K. In Fig. 2 the dielectric constant of solid pentaborane is given as a function of the frequency for several temperatures. Below 130°K. the dielectric constant is independent of frequency.

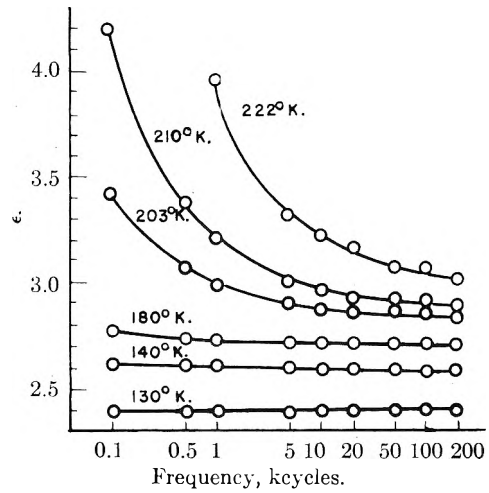

Fig. 2.—Dielectric constant of solid pentaborane at various temperatures as a function of the frequency.

The behavior in the temperature range 130–140°K. is shown in Fig. 3. Curve I was obtained on slowly cooling the solid pentaborane. Dotted lines indicate that the sample was held at constant temperature for the time shown on the graph. Curve II was obtained on warming the sample. At 137.0°K. there are indications of a slow change; at 137.7°K. the change is much faster. Curve III was obtained on continuous heating at a rate of 3° per hour.

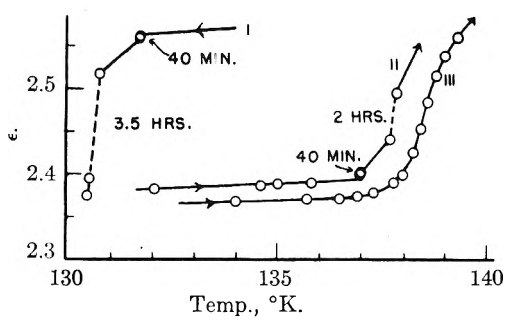

Fig. 3.—Dielectric constant of solid pentaborane in the temperature range 130–140°K.

Johnston, Kerr, Clarke and Hallett[6] reported similar effects in the heat capacity of pentaborane in the temperature range 130–140°. The cooling curve was normal down to 131°K. At this temperature, if the calorimeter was isolated, the temperature rose rapidly to 132°, and reached 132.84°K. after 11 hours. The temperature could

be then increased to 136.7° without evidence of any transition. At 136.7° a transition of the order-disorder type occurred. This behavior is attributed to the onset of free rotation.

Dulmage and Lipscomb[13] give the structure of the high temperature (140–226°K.) form of pentaborane as body centered tetragonal (C^9_{4v} – I4 mm.), a = 7.16 Å., c = 5.38 Å., with two molecules per unit cell and a calculated density of 0.761 g./cc. King and Russell[14] of this Laboratory have found that below 130°K. the X-ray powder pattern agrees with that of a simple tetragonal cell with a = 10.33 Å., c = 10.11 Å., having eight molecules per unit cell and a calculated density of 0.778 g./cc. They have observed that if one considers the high temperature form in its face centered tetragonal orientation (a = 10.13 Å., c = 5.38 Å.) the c-axis of the low temperature form is slightly less than double that of the high temperature form, and the a-axis is slightly larger. This, they suggest, indicates that the transition may involve a decrease in rotation which imposes the observed change in the symmetry.

From this it may be concluded that the observed behavior in the temperature range 130–140°K. can be explained on the basis of a sluggish first-order transition. In the low temperature form there is no free rotation, but in the high temperature form some free rotation is possible. The most convincing evidence for the onset of free rotation is the increase in dielectric constant on going from the low temperature form to the high temperature form despite the density decrease which accompanies this transition. Since there is only a slight shift in molecular positions involved in the transition, it is possible that the heat of transition is small, and the heat effects observed by Johnston, Kerr, Clarke and Hallett[6] are due primarily to the entropy increase associated with the onset of free rotation in the high temperature form.

The dispersion in the dielectric constant of solid pentaborane above 140°K. is in agreement with the observations of Errera[15] who found that solids consisting of polar molecules show this anomalous dispersion. Wintsch[16] determined the dielectric constant and angle of dielectric loss for ice in the temperature range −50 to −6°. While the effects he found for the dielectric constant were much greater (*i.e.*, at −6° and 1000 cycles the dielectric constant of ice is 90% of the liquid value), the general shape of his curves is the same as was found for pentaborane (Fig. 2).

On the other hand, the loss angle is quite different in the two cases. Wintsch found an increase of loss angle with increasing frequency for ice at −6, −10 and −20°, and a maximum around one kilocycle at −40 and −50°. In pentaborane a *minimum* in the dissipation factor (tangent of loss angle) at about one kilocycle was found at low temperatures; this minimum was displaced toward higher frequencies as the temperature was increased so that at temperatures just below the melting point the dissipation factor decreased with increasing frequency throughout the frequency range studied.

An attempt was made to interpret the behavior of solid pentaborane by the method of Debye[17] in terms of a relaxation time (τ) which would be much greater for a solid than for a liquid, but no value of τ could be found which would represent the data at a single temperature, and its variation with temperature was not as great as would be expected.

A key to an interpretation might be the observed abrupt changes in dissipation factor and dielectric constant observed in scanning the frequency spectrum. The dissipation factor varied by as much as a factor of two with small changes in frequency. These "blips" were observed at all temperatures and at frequencies above fifteen kilocycles, but became increasingly evident as the melting point was approached. Since the frequency is much too low to affect molecules, the absorption might be due to large groups of molecules rotating under the influence of the applied field (domain structure).

Vapor Pressure of Pentaborane.—The vapor pressure of pentaborane in the temperature range 226.4–298°K. is given in Table II, and can be represented by the equation

$$\log_{10} p_{mm} = 9.96491 - \frac{1951.14}{T} - 0.0036884T \quad (5)$$

The values are in excellent agreement with those reported by Johnston, Kerr, Clarke and Hallett.[6]

TABLE II

VAPOR PRESSURE OF LIQUID PENTABORANE

Temp., °K.	p_{mm} Obsd.	Calcd.[a]	$P_{obsd} - P_{calcd}$ (mm.)
226.41 (m.p.)	3.26	3.25	+0.01
237.02	7.19	7.22	−0.03
247.03	14.31	14.30	+0.01
254.07	22.28	22.37	−0.09
261.04	33.72	33.70	+0.02
267.97	49.74	49.58	+0.16
272.99	64.77	64.67	+0.10
278.08	83.57	83.71	−0.16
283.05	106.39	106.57	−0.18
287.98	134.10	134.11	−0.01
288.27[b]	135.77	135.90	−0.13
292.00	160.68	160.66	+0.02
292.16[b]	161.96	161.80	+0.16
293.73	173.55	173.34	+0.21
296.04	191.19	191.51	−0.32
297.84	206.85	206.72	+0.13

[a] Calculated from equation 5. [b] Check values on a separate sample.

(13) W. J. Dulmage and W. N. Lipscomb, *Acta Cryst.*, **5**, 260 (1952).

(14) A. J. King and V. Russell, private communication.

(15) J. Errera, *J. phys.*, [6] **5**, 304 (1924).

(16) H. Wintsch, *Helv. Phys. Acta.*, **5**, 126 (1932).

(17) P. Debye, "Polar Molecules," Dover Publications, New York, N. Y., 1945, p. 105.

LOW TEMPERATURE HEAT CAPACITY OF PALMITIC ACID AND METHYL PALMITATE

BY HENRY E. WIRTH,[1] JOHN W. DROEGE AND JOHN H. WOOD

Contribution from the Cryogenic Laboratory and the Department of Chemistry, The Ohio State University, Columbus, Ohio

Received December 17, 1955

Heat capacity measurements were made on methyl palmitate and on palmitic acid in the temperature range 14 to 300°K. The calculated entropies at 298.16°K. were 118.33 ± 0.35 and 108.12 ± 0.22 cal. (mole degree)$^{-1}$, respectively.

Introduction

The polymorphism of soaps and other long-chain compounds is one of their most distinctive characteristics. As part of a program designed to study the phase relationships of palmitic acid, methyl palmitate and sodium palmitate, it seemed advisable to determine the heat capacities and entropies. This paper presents the results for palmitic acid and methyl palmitate.

Materials and Procedure

A mixture of methyl esters containing primarily palmitate and stearate was prepared by methylating Procter and Gamble Triple Pressed Stearic Acid. The esters were hydrogenated at 180°, using Raney nickel catalyst. The iodine number was found to be less than 0.2. The esters were fractionated in a four-foot column patterned after the design of Weitkamp and Brunstrum.[2] A low pressure drop was achieved by the use of Stedman packing. Contamination of the product by stopcock grease was minimized. A closely regulated manostat kept the pressure nearly constant at 2 mm. The take-off assembly was designed so that small samples could be collected and characterized. The product used was the best fraction of the third successive distillation. The setting point, the highest temperature reached upon slow solidification of the melt, was found to be 29.59°. The purity of this sample is believed to have been about 99.7%.

Sodium palmitate was prepared by saponification of the previously purified methyl palmitate with an excess of sodium hydroxide. The soap was extracted with ether and converted to palmitic acid by treatment with 20% H_2SO_4. The palmitic acid was washed until neutral and dried under high vacuum. The purity was tested by a procedure similar to that described by Taylor and Rossini.[3] The freezing point was found to be 62.65° and the purity, 99.8%. The results gave 62.68° as the freezing point of pure palmitic acid. The impurity probably was predominantly stearic acid.

The apparatus and procedure have been described previously.[4] Samples were loaded into a copper calorimeter given the laboratory designation Solid Calorimeter No. 5.

The weight of the palmitic acid sample was 43.282 g. The sample was obtained by crystallization from the melt and was therefore of the form called phase "C" by Francis and Piper.[5] X-Ray analysis confirmed the identification of phase. The molecular weight was taken to be 256.42. The methyl palmitate was melted into the calorimeter. Its weight was 59.822 g. The molecular weight was taken to be 270.44. Electrical energy in terms of International Volts and Ohms was converted to Defined Calories by dividing by 4.1833. All weights were reduced to vacuum.

Results

The first series of measurements on methyl palmitate was made ten days after solidifying the sample. The second series was made 26 days later. The last series, beginning at 280°K., was made after ten more days. Results are given in Table I. Thermodynamic functions derived on the basis of a smooth curve are shown in Table II. The extrapolation to 0°K. was carried out by use of the function C_p/T.

TABLE I

HEAT CAPACITY OF METHYL PALMITATE

Mean temp., °K.	Heat capacity, cal. (mole deg.)$^{-1}$	Mean temp., °K.	Heat capacity, cal. (mole deg.)$^{-1}$
Series I		Series II	
66.67	33.31	13.80	2.76
74.54	37.43	15.49	3.30
82.83	41.17	18.32	4.64
91.60	44.64	21.30	6.26
101.27	47.96	23.53	7.54
111.95	54.80	25.61	8.77
122.55	54.72	27.98	10.18
133.31	57.76	30.99	12.17
144.05	60.68	34.15	14.29
151.86	62.58	37.15	16.32
164.91	66.26	40.52	18.32
176.37	69.12	44.47	20.80
186.77	71.94	48.88	23.50
196.27	74.63	53.54	26.41
205.27	77.29	59.75	30.08
215.17	79.97	65.72	32.85
224.46	82.91	100.50	47.58
233.67	86.44	107.90	50.04
244.82	88.86	115.51	52.47
253.56	93.12	Series III	
263.29	97.39	280.36	104.54
272.56	102.01	285.86	107.26
281.31	105.79	291.34	110.58
		296.66	112.86

The palmitic acid results are shown in Table III. Thermodynamic functions based on a smooth curve are shown in Table IV.

The heat capacity results in the liquid hydrogen range may be in error by as much as 2%. In the range 80 to 200°K. the error is probably about 0.2%, increasing to about 0.5% near room temperature. These uncertainties contribute to the entropy at 298.16°K., an error of about 0.3% in the case of methyl palmitate and about 0.2% for palmitic acid.

Our data are about one calorie per degree mole lower than those of Parks and Kelley.[6]

Some difficulty was encountered in drawing the curve through the palmitic acid points in the region

(1) Department of Chemistry, Syracuse University, Syracuse, N. Y.

(2) A. W. Weitkamp and L. C. Brunstrum, *Oil and Soap*, **18**, 47 (1941).

(3) W. J. Taylor and F. D. Rossini, *J. Research Natl. Bur. Standards*, **32**, 197 (1944).

(4) (a) H. L. Johnston, F. T. Clarke, E. B. Rifkin and E. C. Kerr, *J. Am. Chem. Soc.*, **72**, 3933 (1950); (b) H. L. Johnston and E. C. Kerr, *ibid.*, **72**, 4733 (1950).

(5) F. Francis and S. H. Piper, *ibid.*, **61**, 577 (1939).

(6) G. S. Parks and K. K. Kelley, *ibid.*, **47**, 2089 (1925).

TABLE II

THERMODYNAMIC FUNCTIONS FOR METHYL PALMITATE

T, °K.	C_p, cal. (mole deg.)$^{-1}$	$S° - S_0°$, cal. (mole deg.)$^{-1}$	$H° - H_0°$, cal. (mole)$^{-1}$	$-(F° - H_0°)/T$, cal. (mole deg.)$^{-1}$
20	5.49	2.91	38.2	1.00
40	17.99	10.46	270.5	3.70
60	30.09	20.11	754.2	7.54
80	39.92	30.16	1457.8	11.94
100	47.56	39.91	2334.6	16.56
120	53.96	49.14	3349.9	21.22
140	59.59	57.88	4485.7	25.84
160	64.93	66.18	5729.4	30.37
180	70.14	74.12	7080.1	34.79
200	75.66	81.80	8537.4	39.11
220	81.74	89.29	10110	43.33
240	88.26	96.67	11809	47.47
260	96.05	104.04	13650	51.54
273.16	101.80	108.92	14952	54.18
280	104.88	111.47	15658	55.55
298.16	113.40	118.33	17639	59.17
300	114.27	119.03	17849	59.53

TABLE III

HEAT CAPACITY OF PALMITIC ACID

Mean temp., °K.	Heat capacity, cal. (mole deg.)$^{-1}$	Mean temp., °K.	Heat capacity, cal. (mole deg.)$^{-1}$
Series II		Series III	
74.83	34.75	64.27	30.26
79.52	36.99	68.84	32.19
84.71	39.02	74.38	34.71
89.39	40.54	81.58	37.60
94.56	42.00	89.04	40.23
99.62	43.79	95.99	42.53
101.80	44.24	102.42	44.44
106.82	45.67	108.88	46.53
112.28	47.42	116.69	48.76
117.79	48.86		
124.18	50.43	Series IV	
130.84	52.28	14.91	1.94
136.99	53.77	16.59	2.68
137.71	54.04	18.59	3.36
144.14	55.78	21.32	4.56
150.65	57.67	24.51	6.43
157.71	59.59	28.03	8.62
164.99	61.26	32.09	11.15
172.22	62.66	36.60	14.04
179.98	64.71	41.86	17.39
187.98	66.95	47.37	20.72
196.09	68.94	52.92	24.00
196.22	69.16	58.94	27.68
204.55	71.69	65.57	31.13
213.00	74.10	Series VII	
221.74	76.34	264.14	91.78
230.32	79.10	271.46	95.74
239.12	82.08	277.64	98.52
247.22	84.87	283.01	101.12
254.62	87.67	289.41	104.51
255.16	87.71	295.80	108.40
263.08	91.53	301.60	111.89
271.69	95.62		
280.19	100.97		
287.47	103.77		
295.56	108.62		
302.12	113.12		

TABLE IV

THERMODYNAMIC FUNCTIONS FOR PALMITIC ACID

T, °K.	C_p, cal. (mole deg.)$^{-1}$	$S° - S_0°$, cal. (mole deg.)$^{-1}$	$H° - H_0°$, cal. (mole)$^{-1}$	$-(F° - H_0°)/T$, cal. (mole deg.)$^{-1}$
20	4.00	1.69	23.6	0.51
40	16.19	8.04	221.2	2.51
60	27.97	16.89	665.6	5.80
80	36.96	26.24	1319.8	9.74
100	43.72	35.24	2129.1	13.95
120	49.39	43.73	3062.0	18.11
140	54.68	51.74	4102.3	22.44
160	59.81	59.38	5247.9	26.58
180	64.82	66.71	6493.6	30.63
200	70.27	73.82	7843.7	34.60
220	75.91	80.78	9305	38.48
240	82.27	87.64	10885	42.29
260	89.96	94.52	12604	46.04
273.16	96.25	99.12	13828	48.50
280	99.78	101.54	14499	49.76
298.16	110.10	108.12	16401	53.11
300	111.28	108.80	16604	53.45

140 to 180°K. Several points lie slightly above the smooth curve, which might indicate a very small anomaly. The maximum effect involved is about 12.5 cal./mole. It seemed more likely, however, that this irregularity is to be ascribed to experimental error, and the best smooth curve was drawn through the points. Both curves show upward inflections at about 170°K. This is very probably due to the gradual onset of molecular rotational freedom. A similar effect has been observed in normal hydrocarbons by Finke, Gross, Waddington and Huffman.[7] Plots of the specific heat of methyl palmitate and palmitic acid *vs.* the reduced temperature (actual temperature divided by the melting temperature) are practically identical with the similar plot for *n*-hexadecane given by these authors. The onset of the increase in slopes of these curves occurs at a value of the specific heat of about 0.3 cal. deg.$^{-1}$ g.$^{-1}$, and at a reduced temperature of 0.7.

The lower members of the fatty acid series are known to form hydrogen bonds. It seems probable that hydrogen bonding occurs also in palmitic acid. Crystal structure data indicate that palmitic acid forms monoclinic crystals, made up of double layers of molecules with the carboxyl groups in juxtaposition.[8] The data are not sufficient to show the orientation of the carboxyl groups with respect to one another. It may be that two molecules dimerize through the formation of two hydrogen bonds. If this is the case, there are two possible positions for each dimer with respect to its neighbors. It seems likely that such disorder would persist to the lowest temperature and would contribute R ln 2 to the entropy of a mole of dimer. This would represent an entropy of $^1/_2 R$ ln 2, or 0.69 cal. degree^{-1} mole^{-1} of palmitic acid in addition to the entropy found experimentally. There are other possible ways in which the molecules may be hydrogen bonded, leading to smaller entropy contributions.

(7) H. L. Finke, M. E. Gross, Guy Waddington and H. M. Huffman, *J. Am. Chem. Soc.*, **76**, 333 (1954).

(8) A. Müller and G. Shearer, *J. Chem. Soc.*, **123**, 3156 (1923).

Acknowledgment.—The authors wish to express their sincere gratitude to Dr. Herrick L. Johnston for his full coöperation in the use of facilities of the Cryogenic Laboratory, and to Procter and Gamble Co. for a fellowship which partially supported this work.

DIELECTRIC CONSTANT OF HYDROUS SODIUM PALMITATE

BY HENRY E. WIRTH[1] AND WILLIAM W. WELLMAN

Contribution from the Department of Chemistry, The Ohio State University, Columbus, Ohio

Received December 17, 1955

The dielectric constant of hydrous β- and δ-sodium palmitate is practically constant for water contents between 0 and 3%. Above 3% water the dielectric constant increases rapidly with increasing water content, and becomes frequency dependent. This increase in dielectric constant is far greater than would be expected from a simple mixture, and is attributed to presence of mobile sodium ions in the water which is weakly adsorbed by the soap.

On the basis of vapor pressure and dilatometric studies, McBain, Vold and Johnston[2] concluded that curd sodium palmitate and sodium oleate can contain up to nearly one mole of combined water per mole of soap at 25°. McBain and Lee[3] found that at 90° anhydrous sodium palmitate takes up 1–2% of water by physical absorption and then suddenly forms a hemihydrate which again takes up water until another phase forms. Ferguson, Rosevear and Nordsieck[4] found a sharp break in the vapor pressure over hydrous β-sodium palmitate at 2.5% water content at 27°.[5] Below this water content the vapor pressure decreased to practically zero at 0.2% water. Since there was no "flat" indicating equilibrium between a hydrate and anhydrous soap, and since the X-ray patterns showed only minor and continuous variation through the range 0.2–2.5% water, it was concluded that in this range water is present in interstitial solid solution in the β-phase. Milligan, Bushey and Draper,[6] on the basis of dehydration isobars, found that α-sodium palmitate is a hemihydrate in agreement with the results of Buerger,[7] whereas the beta, delta and omega crystalline phases of sodium palmitate are not definite hydrates.[8] Vold, Grandine and Schott[9] state that the nature of the changes in the X-ray diffraction pattern found for water contents below 3% suggest that the water is present in solid solution rather than as a stoichiometric hydrate.

The present work was undertaken to see if dielectric studies on sodium palmitate of low moisture content would reveal anything of the nature of the binding of the water present.

(1) Department of Chemistry, Syracuse University, Syracuse, New York.

(2) J. W. McBain, M. J. Vold and S. A. Johnston, *J. Am. Chem. Soc.*, **63**, 1000 (1941).

(3) J. W. McBain and W. W. Lee, *Ind. Eng. Chem.*, **35**, 784 (1942).

(4) R. H. Ferguson, F. B. Rosevear and H. Nordsieck, *J. Am. Chem. Soc.*, **69**, 141 (1947).

(5) It is now believed that the method used for water analysis (weight loss in 45 min. at 150°) gives low results. Private communication from F. B. Rosevear.

(6) W. O. Milligan, G. L. Bushey and A. L. Draper, THIS JOURNAL, **55**, 44 (1951).

(7) M. J. Buerger, *Proc. Natl. Acad. Sci., U. S.*, **28**, 529 (1942); M. J. Buerger, L. B. Smith, A. DeBretteville, Jr., and F. V. Ryer, *ibid.*, **28**, 526 (1942).

(8) The phase designations used by Milligan, and also in this paper, are those of R. H. Ferguson, F. B. Rosevear and R. C. Stillman, *Ind. Eng. Chem.*, **35**, 1005 (1943).

(9) R. D. Vold, Joseph D. Grandine, 2nd, and Hans Schott, THIS JOURNAL, **56**, 128 (1952).

Experimental

Materials.—β-Sodium palmitate was supplied by the Procter and Gamble Co. It was prepared by cooling a homogeneous neat soap containing 30% H_2O to 70°, tempering at 70° for 24 hr., cooling to room temperature and air drying. This material was extracted with ether to remove non-saponifiable material and excess palmitic acid. The extracted material contained about 3% H_2O. Palmitic acid regenerated from the sample melted at 62.38°, compared with the calculated melting point (Rossini's method) of 62.68° for pure palmitic acid obtained in this Laboratory.[10] The calculated purity is 98%. Samples with water content greater than 3% were prepared by rehydrating the extracted material. Lower moisture contents were obtained by dehydration in a vacuum desiccator, or by extraction with ether over sodium.

δ-Sodium palmitate was obtained by cooling a 4% solution of the sodium palmitate quickly from 100 to 0°. The gel obtained was dehydrated at room temperature to the desired water content. X-Ray powder patterns of representative samples were taken and interpreted for us by Dr. F. B. Rosevear of the Procter and Gamble Co.

Preparation of Cakes for Dielectric Constant Measurements.—The powdered samples were allowed to equilibrate for at least a week, and usually for several months, before being pressed into cakes. The powdered sample was placed in a stainless steel die 2 in. in diameter. Prior to introduction of the sample, tin foil (0.0005 in. thick) was attached to the inner face of each piston by means of a thin layer of petrolatum. The die was placed in a hydraulic press, and a pressure of 16,000 p.s.i. was applied. A vacuum of *ca.* 1 mm. of mercury was maintained on the sample in the die before applying the pressure in order to eliminate air pockets. Cakes of uniform thickness (±0.0025 in.), having firmly adhering tin foil top and bottom surfaces were obtained. The cakes were allowed to stand for at least a week before measurements were made.

Determination of Dielectric Constant.—A Schering bridge (General Radio Type 716-C) was used to make the capacitance measurements. The cell was patterned after one designed by Hartshorn and Ward[11] and modified by Venable and Kinn,[12] and had plates 2 in. in diameter. The cell was maintained at a temperature of 30.0 ± 0.1°. The capacitance of the system was determined for frequencies between 0.1 and 200 kilocycles with the cake in the cell. The cake was removed and the upper plate adjusted by means of a micrometer to give a plate separation equal to the average thickness of the cake (excluding the tin foil). The capacitance was then redetermined. From these data, and the calculated capacitance of the empty cell, the dielectric constant of the sample was obtained. The dielectric constants so obtained are in error by less than 1% for cakes containing less than 3% water, as estimated from the variation in ob-

(10) H. E. Wirth, J. R. Droege and J. H. Wood, *ibid.*, **60**, 917 (1956).

(11) L. Hartshorn and W. H. Ward, *J. Inst. Elect. Eng.*, **79**, 597 (1936).

(12) D. Venable and T. P. Kinn, "Industrial Electronics Reference Book, Westinghouse Electric Corp.," John Wiley and Sons, New York, N. Y., 1948, pp. 409–410.

served dielectric constant using cakes of the same moisture content but of different thicknesses.

After measurement, each cake was analyzed for water content by drying at 108° for 20–50 hours. This method checked against dehydration at 110° under 10^{-6} mm. mercury pressure within ±0.02%.

Results and Discussion

The results obtained are given in Fig. 1. The dielectric constant of β-sodium palmitate is constant (2.61 ± 0.02) for moisture contents between 1.38 and 3.00%, and is independent of the frequency between 0.1 and 100 kilocycles. The dielectric constant of δ-sodium palmitate increases from 2.51 at 0.15% H_2O to 2.60 at 2.95% moisture content, and is also frequency independent. In both cases, above 2.95 (±0.05) % water, the dielectric constant increases rapidly with increasing moisture content, and becomes frequency dependent. The curves for the frequency dependence of beta sodium palmitate are given in Fig. 2. A similar set of curves was obtained for δ-sodium palmitate. It was observed that the angle of dielectric loss was also strongly frequency dependent (tan δ = 0.9 at 200 cycles, 0.02 at 200 kilocycles in the sample of β-sodium palmitate with 4.10% H_2O, as compared to tan δ = 0.02 at 100 cycles and 0.004 at 200 kilocycles for 2.87% H_2O).

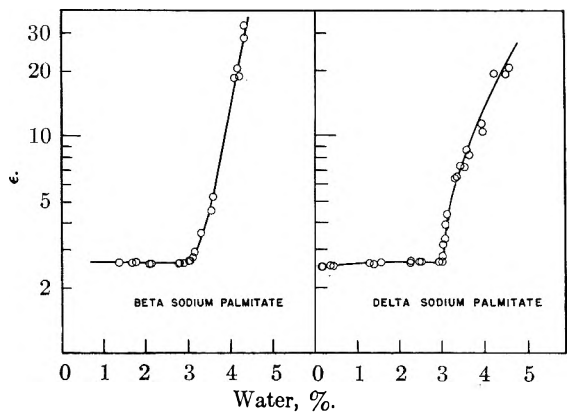

Fig. 1.—Dielectric constant of β- and δ-sodium palmitate as a function of water content.

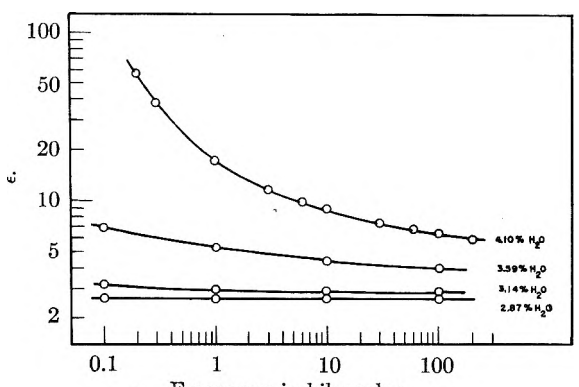

Fig. 2.—Dielectric constant of β-sodium palmitate as a function of frequency for various water contents.

Between 0 and 3% water content, the water is firmly bound to the sodium palmitate, and makes no contribution to the dielectric constant. Vorakso, Grudkova and Mischenko[13] showed that addition of water to crystalline salts of strong electrolytes did not change the dielectric constant of salts forming hydrates, whereas a marked change was observed even at low moisture contents when non-hydrate forming salts were used. The upper limit of the constant value of ε is very close to the theoretical composition of the hemihydrate (3.14% H_2O), so it is possible that the hemihydrate does exist. Other interpretations, such as strongly adsorbed water, or solid solution of water in the soap crystal, are not excluded.[14]

An increase in dielectric constant with increase in water content similar to that found here above 3% water has been observed with gelatin,[15] leather,[16] proteins and amino acids,[17] lac[18] and with plastics and solid dielectrics.

The most satisfactory explanation of these effects was made by Murphy and Lowry,[19] who postulate the existence of adsorbed ions on crystallites which in the presence of adsorbed water move on the surface of the crystallite when a field is applied, but cannot move from one crystallite to another. The effect observed can be interpreted readily on this basis. Above 3% water content, the water is weakly adsorbed by the soap,[14] and provides a medium in which the sodium ions are free to move under the influence of an applied field. Since the soap supplies its own ions, the effect is much larger than when due to foreign ions that may be accidentally introduced into the system. The relatively free movement of the sodium ions in the weakly adsorbed water makes a large contribution to the dielectric constant of the bulk material, particularly at low frequencies. The relatively long time of transit results in a phase lag in the a.c. conduction current, accounting for the large angles of dielectric loss observed at low frequencies. As the frequency of the field is increased, the ions move shorter distances, and the apparent dielectric constant will decrease.

Acknowledgment.—We wish to thank the Procter and Gamble Company for a fellowship which supported this work, and for generously providing samples.

(13) Kh. I. Vorakso, L. I. Grudkova and K. P. Mischenko, *J. Appl. Chem.* (*U.S.S.R.*), **12**, 981 (1939).

(14) For a further discussion, see: H. E. Wirth and W. L. Kosiba, THIS JOURNAL, **60**, 923 (1956).

(15) M. Fricke and E. Parker, *ibid.*, **44**, 716 (1940).

(16) E. C. Compton, *J. Am. Leather Chem. Assn.*, **39**, 74 (1944); C. E. Weir, *J. Research Natl. Bur. Standards*, **48**, 349 (1952).

(17) S. T. Bayley, *Trans. Faraday Soc.*, **47**, 509 (1951).

(18) G. N. Bhattacharya, *Current Sci.* (*India*), **16**, 117 (1947).

(19) R. J. Murphy and H. H. Lowry, THIS JOURNAL, **34**, 598 (1930).

PHASE TRANSITIONS IN SODIUM PALMITATE BY DIELECTRIC CONSTANT MEASUREMENTS

BY HENRY E. WIRTH[1] AND WILLIAM W. WELLMAN

Contribution from the Department of Chemistry, The Ohio State University, Columbus, Ohio

Received December 17, 1955

The first-order "genotypic" transition in sodium palmitate, first reported by Thiessen and co-workers, has been shown to be due to the presence of palmitic acid impurity in their samples. Definite changes in dielectric constant are associated with the crystal-subwaxy, subwaxy-waxy, waxy-superwaxy, and superwaxy-subneat transitions in anhydrous sodium palmitate. The temperatures at which these transitions occur are 117.8, 137, 162 and 206°, respectively.

Thiessen and Ehrlich[2] first reported a transition (the "genotypic" transition) in NaP and in NaSt[3] at temperatures close to the melting point of the parent fatty acid. Dilatometric curves for NaP and NaSt showed abrupt changes in slope, and certain lines in the X-ray pattern of NaP disappeared between 62 and 80°. Later, Thiessen and v. Klenck[4] found an abrupt change in dielectric constant (see Fig. 2 (1)) and a change in the optical double refraction of NaP. Heat effects of the order of 200 calories per mole were found for NaMy, NaP and NaSt, indicating a definite first-order transition. Vold[5] was unable to detect any heat effect in anhydrous NaP, NaMy, NaL, NaSt and NaOl at the genotypic temperature. Later Vold[6] found a change in slope of the dilatometric and differential calorimetric curves at 71°, and concludes that the genotypic point is a transition of the second order. Gallay and Puddington[7] were unable to detect a genotypic effect by differential thermal analysis, but did find some evidence of a change in slope of the dilatometric curve. Sutton[3] was unable to find the genotypic effect in NaSt in a calorimetric study, but did find a discontinuity in the heat capacity just below 70° in an impure sample containing pyrolysis products. Chesley[9] detected a transition in NaP at 67° by X-ray methods. Rosevear[10] states that in low moisture content β-NaP, the outermost ring of the group of five strong short spacing rings gradually weakens above 45–50°, and disappears at 60–65°.

It was of interest to restudy the dielectric behavior of low moisture content of NaP to see if Thiessen's data could be reproduced, and also to see what could be learned of other phase transitions of the anhydrous NaP by means of dielectric measurements.[11]

Experimental

Hydrous β-sodium palmitate was prepared as described in a previous paper.[12] Anhydrous ω-sodium palmitate was prepared by drying the hydrous β-phase at 120°, and cooling.

The cakes for the experiment on the genotypic transition were prepared as described in the previous paper, except that a thin layer of rubber cement was placed on the inner surface of the tin foil, and dried, before being pressed on the soap cake. The tin foil was found to separate from the soap cake during temperature cycling unless this was done. It was shown that the layer of cement did not affect the observed dielectric constant. For the higher temperature observations on anhydrous ω-sodium palmitate tin foil was not used, but the pressed cakes were sprayed on each side with silver conducting paint and baked at 120° for 24 hours to remove the paint solvent.

Cell.—The cell for the dielectric constant measurements is shown in Fig. 1. It was designed to give good contact with the soap cake, and was immersed in a silicone oil-bath whose temperature could be maintained constant to within ±0.01° in the range 25–200°.

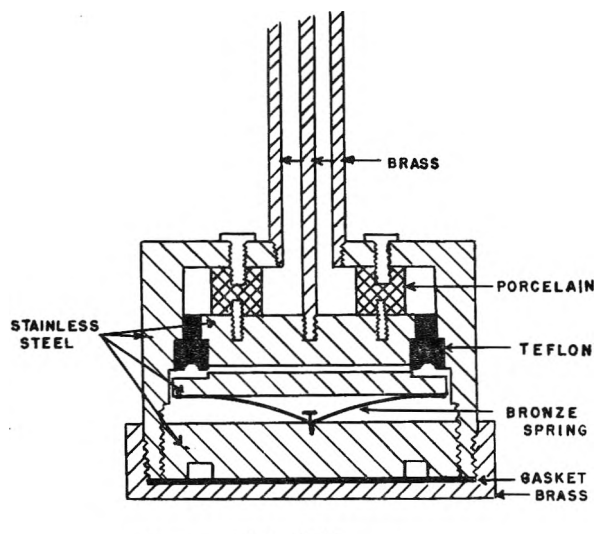

Fig. 1.—Cell used for dielectric constant measurement on sodium palmitate.

Capacitance Measurements.—For these experiments, the heterodyne beat method was used. The circuit developed by Hudson and Hobbs[13] was used without change. The frequency was controlled by a quartz crystal, frequency

(1) Department of Chemistry, Syracuse University, Syracuse, New York.

(2) P. A. Thiessen and E. Ehrlich, *Z. physik. Chem.*, **B19**, 299 (1932).

(3) P = palmitate, St = stearate, My = myristate, L = laurate, Ol = oleate.

(4) P. A. Thiessen and J. v. Klenck, *Z. physik. Chem.*, **A174**, 335 (1935).

(5) R. D. Vold, *J. Am. Chem. Soc.*, **63**, 2915 (1941).

(6) R. D. Vold, THIS JOURNAL, **49**, 315 (1945).

(7) W. Gallay and I. E. Puddington, *Can. J. Research*, **B21**, 202 (1943).

(8) J. W. Sutton, Ph.D. thesis, Stanford University, 1948.

(9) F. O. Chesley, *J. Chem. Phys.*, **8**, 642 (1940).

(10) F. B. Rosevear, private communication.

(11) The various high temperature phases of anhydrous NaP, and their transition temperatures observed by previous workers are
Crystal-Subwaxy: 125° (a), 117° (b), 117° (c), 117° (d), 114° (e)
Subwaxy-Waxy: 135° (b), 135° (c), 138° (d), 135° (e)
Waxy-Superwaxy: 172° (c)
Superwaxy-Subneat: 195° (a), 208° (b), 208° (c), 205° (d), 209° (e)
Subneat-Neat: 255° (a), 253° (b), 253° (c), 257° (d), 237° (e)
Neat-Nigre: 297° (a), 292° (b), 295° (c), 290° (d), 292° (e).
(a) R. D. Vold, F. B. Rosevear and R. H. Ferguson, *Oil and Soap*, **16**, 48 (1939); (b) R. D. Vold and M. J. Vold, *J. Am. Chem. Soc.*, **61**, 808 (1939); (c) R. D. Vold, *Soap and Sanitary Chemicals*, June (1946); M. J. Vold, *J. Am. Chem. Soc.*, **63**, 160 (1941); (d) Chesley (ref. 9); (e) Vold (ref. 5).

(12) H. E. Wirth and W. W. Wellman, THIS JOURNAL, **60**, 921 (1956).

(13) B. E. Hudson, Jr., and M. E. Hobbs, *Rev. Sci. Instruments*, **13**, 140 (1942).

498.8 kilocycles. A General Radio standard condenser (Type 722-D) was used. All components except the measuring cell were enclosed in an air thermostat maintained at 35 ± 0.5°. The cell was mounted rigidly to a support on the thermostat enclosing the measuring apparatus.

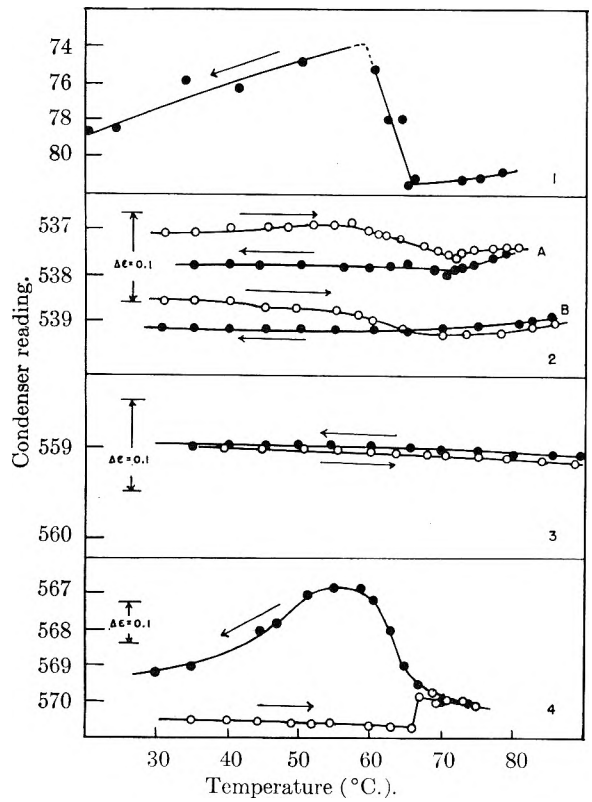

Fig. 2.—Changes in the dielectric constant of sodium palmitate as a function of temperature. Decrease in condenser reading corresponds to an increase in dielectric constant. (1) Results of Thiessen and v. Klenck[4]; (2A) β-sodium palmitate originally containing 3.07% H_2O (heating period 8 days, cooling period 11 days); (2B) β-sodium palmitate originally containing 2.85% H_2O (heating period 7 days, cooling period 7 days); (3) anhydrous ω-sodium palmitate (heating period 2 days, cooling period 2 days); (4) β-sodium palmitate plus 5% palmitic acid (3% H_2O) (heating period 6 days, cooling period 11 days).

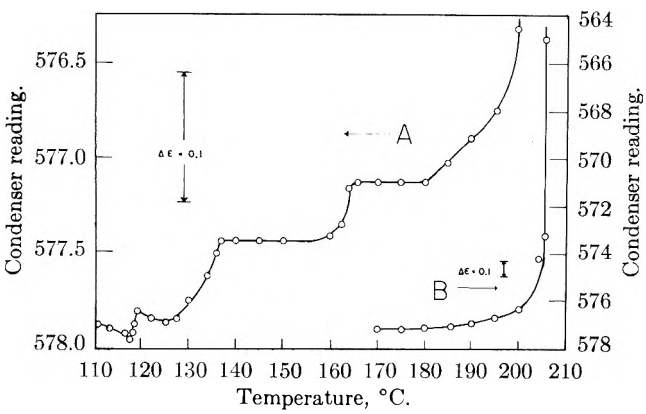

Fig. 3.—Changes in the dielectric constant of anhydrous sodium palmitate as a function of temperature. Decrease in condenser reading corresponds to an increase in dielectric constant.

Results and Discussion

There is no information as to the phase or moisture content of the sodium palmitate sample used by Thiessen and v. Klenck[4] so two samples of β-sodium palmitate (3.07 and 2.85% H_2O) and one sample of anhydrous ω-sodium palmitate were investigated in the temperature range 30–85°. While the exact magnitude of the change reported by Thiessen and v. Klenck[4] is in doubt, as condenser readings only are reported, it was felt that the effect must have been large, as the apparatus used was not of high sensitivity.

Our results (Fig. 2 (2,3)) show slight variations in dielectric constant on heating in the case of the hydrous β-samples, but relatively little change on cooling. No effect was observed with anhydrous ω-sodium palmitate. The small changes observed with the hydrous samples may be due to a slight dehydration on heating, which could not be prevented, or may accompany the variation in X-ray pattern observed by Rosevear.[10] In any case, there is no evidence for a first-order transition of the type reported by Thiessen and v. Klenck.[4]

It has been observed in this Laboratory[14] that the dielectric constant of palmitic acid shows an increase at the freezing point on cooling from the melt. It was suspected that the sample used by Thiessen may have been contaminated, so a sample of sodium palmitate containing 5% of palmitic acid was made up. Water was added to bring the water content up to 35%, the mixture was annealed at 70° for 25 hours and then air-dried to give 3% H_2O. This treatment gave the beta phase.

TABLE I

Phase	Transition temp., °C.	Order of transition
Crystal		
	117.8	First order (?)
Subwaxy		
	137	?
Waxy		
	162	First
Superwaxy		
	206	First
Subneat		

On heating this sample (Fig. 2 (4)) an increase in dielectric constant was observed at 66–67°, and a curve very similar to that of Thiessen and v. Klenck was obtained on cooling. It is therefore concluded that the first-order "genotypic" transition is due to the presence of palmitic acid as an impurity in the samples. On the basis of the heat effects observed by Thiessen and v. Klenck[4] (230 cal./mole), it was calculated that the effects observed by him could be due to the presence of 1.5% palmitic acid as an impurity.

The results of capacitance measurements on anhydrous sodium palmitate in the temperature range 110–210° are given in Fig. 3. The observed transition temperatures are summarized in Table I.

While the temperature at which the crystal phase transforms to the subwaxy is quite distinct, inability to obtain definite drift-free values for the dielectric constant in the subwaxy region makes it impossible to state definitely whether this transition is first or second order. The exact temperature and order of the subwaxy-waxy transition is in doubt for the same reason. The waxy state is characterized by a very steady

(14) G. W. Mays, Ph.D. Thesis, The Ohio State University, 1953.

dielectric constant. The waxy-superwaxy transition is relatively sharp and therefore first order. The temperature is somewhat lower than that observed by Vold[11c] (172 ± 2°) using the Bernal hot wire technique. In present work 5 days were taken to follow the temperature interval 159–166°, so it is felt that the lower value is more reliable.

The superwaxy-subneat transition is very striking when examined by this technique. The lattice starts to loosen at 180°, which accounts for the range of values (195–209°) reported by other workers.[11] The temperature was assigned to this transition by approaching the transition point from both sides. This transition is accompanied by a marked change in the X-ray pattern.[15]

It was experimentally impossible to follow the measurements above 207°, as oscillations ceased in the variable frequency oscillator.

(15) H. Nordsieck, F. B. Rosevear and R. H. Ferguson, *J. Chem. Phys.*, **16**, 175 (1948).

ISOTHERMAL DEHYDRATION OF HYDROUS SODIUM PALMITATE[1a]

By Henry E. Wirth[1b] and Walter L. Kosiba

Contribution from the Department of Chemistry, The Ohio State University, Columbus, Ohio

Received December 17, 1955

Isothermal dehydration curves were obtained for α-sodium palmitate at 29.9 and 40.4°, and for δ- and ε-sodium palmitate at 29.9, 35.3, 40.4 and 45.6°. The samples had not been dehydrated previously. These phases showed sharp breaks in equilibrium pressure of water at water contents of 3.14 ± 0.05%. With ω-sodium palmitate a gradual reduction in equilibrium water pressure was exhibited between 1.8 and 2.5% water. The heat of interaction between liquid water and the soap phase below 3% water content was 3200–3900 cal./mole of water for ε-sodium palmitate and 2700–3100 cal./mole for the delta phase. Above 3% H_2O, the heat of interaction is 0–400 cal./mole of water. The results may be interpreted in terms of hydrate formation, strong adsorption, or solid solution of water in the anhydrous soap phase. A physical picture of the nature of the binding of water in low moisture soap phases is presented.

In a previous paper[2] it was shown by dielectric constant measurements that the β- and δ-phases of sodium palmitate contain up to 3% of strongly bound water.

The conflicting views as to the nature of the role of water in the low moisture phases of sodium palmitate, and the differences between the results of Ferguson, Rosevear and Nordsieck[3] and those of Milligan and Draper[4] on the equilibrium pressure of water over hydrous soap systems has led to a reinvestigation of the behavior on dehydration of such systems, using hydrous soap samples which had not previously been dehydrated.

Apparatus and Materials

The apparatus consisted of a McBain–Bakr[5] quartz spring balance and a mercury manometer which could be immersed in a thermostat. The quartz coils had sensitivities of 1.5 cm./100 mg. to 2.1 cm./100 mg. and bore a maximum load of 1 g. A two-tiered nickel bucket held 500–700 mg. of sample. After assembly, the system was evacuated to a pressure of 10^{-4} mm., while the sample was held at liquid air temperature. The Dewar of liquid air was removed and the sample allowed to thaw gradually. The evacuated apparatus was then detached from the vacuum system, transferred to the constant temperature bath, and rejoined to the vacuum system. A cathetometer was used to measure the pressure in the system and the extension of the quartz coil.

A small amount of water vapor was removed from the system, and the measurements were repeated. At the conclusion of a run the sample was completely dehydrated by direct evacuation.

All runs were single dehydrations with the exception of two series at 40.4° where water was added after partial, and again after complete dehydration. β-Sodium palmitate,[6] prepared by cooling a homogeneous neat soap containing 30% H_2O to 70°, tempering at 70° for 24 hr., and then cooling to room temperature, was supplied by the Procter and Gamble Co. This material was extracted with ether to remove non-saponifiable matter and any excess palmitic acid. The palmitic acid regenerated from this sample melted at 62.38°. This compares with a calculated freezing point of 62.68° for pure palmitic acid obtained in this Laboratory[7] and indicates a purity of 98%.

On cooling to liquid air temperatures, β-sodium palmitate containing 8–9% H_2O was found to convert to the ε-modification first reported by Buerger and co-workers.[6b] This phase was therefore the starting material for the dehydration studies.

The α-phase was prepared by precipitation of sodium palmitate from a 10% solution in 50% alcohol. X-Ray powder patterns showed it to be contaminated with an estimated 5–10% of δ-phase. δ-Phase was prepared by partial drying of the curd precipitated from a 3% aqueous solution. No contamination by other phases was detected. The ω-phase was prepared by heating dehydrated ω-phase to 150° under vacuum for one hour. Water was sprayed onto this material and it was allowed to stand for several weeks in an attempt to form a hydrous ω-phase. The product was found to be contaminated with some α-phase, which was unexpected since alpha had been previously obtained only by precipitation from alcoholic solution.

(1a) Presented at the Buffalo meeting of the American Chemical Society, March, 1952.

(1b) Department of Chemistry, Syracuse University, Syracuse 10, N. Y.

(2) H. E. Wirth and W. W. Wellman, This Journal, **60**, 921 (1956). (References to other work bearing on the nature of water in low moisture soap systems are given in this article.)

(3) R. H. Ferguson, F. B. Rosevear and H. Nordsieck, *J. Am. Chem. Soc.*, **69**, 141 (1947).

(4) W. O. Milligan and A. L. Draper, This Journal, **56**, 123 (1952).

(5) J. W. McBain and A. M. Bakr, *J. Am. Chem. Soc.*, **48**, 690 (1926).

(6) The designations α, β, δ and ω for the phases of sodium palmitate used in this paper are those of R. H. Ferguson, F. B. Rosevear and R. C. Stillman [(a) *Ind. Eng. Chem.*, **35**, 1005 (1943)]. Other designations have been used by M. J. Buerger, L. B. Smith, F. V. Ryer and J. E. Spike, Jr. [(b) *Proc. Natl. Acad. Sci., U. S.*, **31**, 226 (1945)], and by R. D. Vold, J. D. Grandine, 2nd, and H. Schott [(c) This Journal, **56**, 128 (1952)]. The methods used in preparation of the various phases are given in sufficient detail to provide adequate identification of the phases used in this work. In addition, X-ray powder patterns of the initial phases, and final dehydration products were made and interpreted for us by Dr. F. B. Rosevear of the Procter and Gamble Co.

(7) H. E. Wirth, J. W. Droege and J. H. Wood, This Journal, **60**, 917 (1956).

Results

Dehydration curves (pressure *vs.* water content) were obtained for α- and ω-sodium palmitate at 29.9 and 40.4°, and for ϵ- and δ-sodium palmitate at 29.9, 35.3, 40.4 and 45.6°. Typical curves at 40.4° are given in Figs. 1–4.

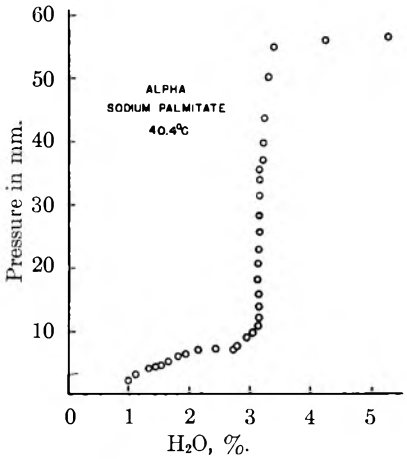

Fig. 1.—Dehydration curve for α-sodium palmitate (40.4°): starting material, alpha containing 5–10% of δ-sodium palmitate; dehydrated product, low moisture beta containing 5–10% of delta.

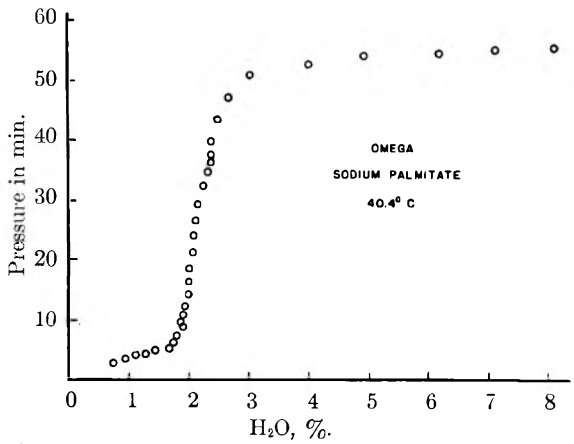

Fig. 2.—Dehydration curve for ω-sodium palmitate (40.0°): starting material, omega containing some alpha; dehydrated product, omega containing some low moisture beta.

From the curves for ϵ- and δ-sodium palmitate, values of the pressure at 4.00, 3.5, 3.14, 3.00, 2.50 and 2% H_2O were estimated, and from plots of log p *vs.* $1/T$ the heat corresponding to the reaction

$$\infty(NaP\cdot xH_2O)_s \longrightarrow \infty(NaP\cdot xH_2O)_s + H_2O(g) \quad (1)$$

was calculated. From these, the heats of wetting

$$\infty(NaP\cdot xH_2O)_s + H_2O(l) \longrightarrow \infty(NaP\cdot xH_2O)_s \quad (2)$$

were obtained (Table I), assuming an average value of −10,400 cal./mole for the heat of liquefaction of water in this range.

TABLE I

% H_2O	ΔH_1, cal./mole (reaction 1)	ΔH_2, cal./mole (reaction 2)	ΔH_1, cal./mole (reaction 1)	ΔH_2, cal./mole (reaction 2)
	ϵ-Sodium Palmitate		δ-Sodium Palmitate	
4.00	10,800	− 400	10,400	0
3.50	10,700	− 300	10,400	0
3.14	14,300	−3,900	13,100	−2,700
3.00	13,900	−3,500	13,500	−3,100
2.50	13,600	−3,200	13,200	−2,800
2.00	14,100	−3,700	13,200	−2,800

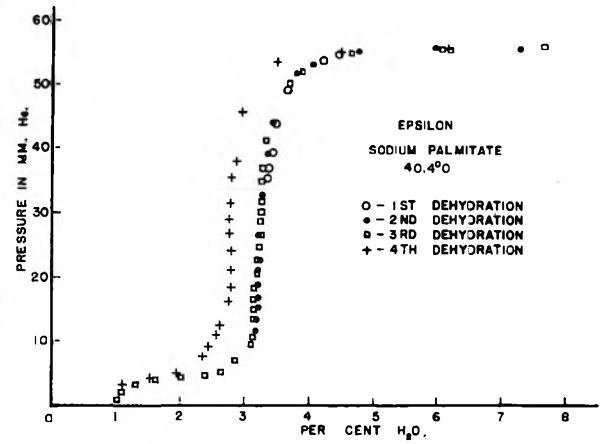

Fig. 3.—Dehydration curve for ϵ-sodium palmitate (40.4°): starting material, hydrous epsilon; dehydration product, anhydrous epsilon (?). (The X-ray pattern of the anhydrous phase has an additional short spacing at d/n = 3.5 Å., and a short spacing at d/n = 3.75 Å. present in the hydrous sample has disappeared.) The first series started with a sample containing 4.45% H_2O; water was added to the system after the water content had been reduced to 3.34% to give the starting material for the second series; water was added after the water content was reduced to 3.16% to give the starting material for the third series; and water was added after complete dehydration to give the starting material for the fourth series.

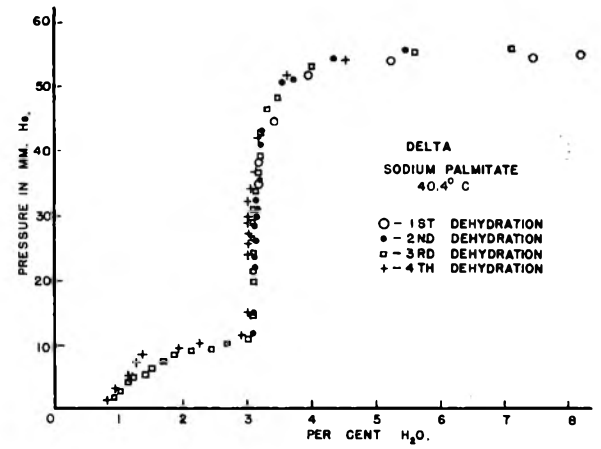

Fig. 4.—Dehydration curve for δ-sodium palmitate (40.4°): starting material, hydrous delta; dehydration product, anhydrous delta. The first series started with a sample containing 9.0% H_2O; water was added to the system after the water content had been reduced to 3.17% to give the starting material for the second series; water was added after the water content was reduced to 3.08% to give the starting material for the third series; and water was added after complete dehydration to give the starting material for the fourth series.

Discussion

By X-ray analysis of single crystals, Buerger[8] has shown that the α-phase of sodium stearate and of sodium palmitate is a hemihydrate. This was confirmed by the isobaric dehydration experiments of Milligan, Bushey and Draper[9] and by the iso-

(8) M. J. Buerger, (a) *Proc. Nat. Acad. Sci., U. S.*, **28**, 529 (1942); (b) *Amer. Mineralogist*, **30**, 551 (1945).

(9) W. O. Milligan, G. L. Bushey and A. L. Draper, THIS JOURNAL, **55**, 44 (1951).

thermal dehydration results reported here (Fig. 1). The α-phase does not exhibit normal phase behavior by giving an anhydrous phase in equilibrium with the hydrate for water contents between 0 and 3%, but decomposes into a low moisture β phase. Below about 2.5% H_2O, the dehydration curve (Fig. 1) represents the further dehydration of the low moisture beta phase. The α-phase does not reform reversibly on simply increasing the moisture content above 3%, although Buerger, *et al.*,[6a] have carried out the conversion by heating in a sealed tube at 47°.

The β-, δ-, ϵ- and ω-phases have not been prepared as single crystals, so the powerful method developed by Buerger[6b] cannot be used to solve the problem of the nature of the water present in these phases. Other methods must be used to indicate possible solutions for the problem.

The isothermal dehydration curve for δ-sodium palmitate (Fig. 2) is very similar to that obtained with the α-phase, in that the equilibrium pressure of water over the system changes abruptly as the water content approaches 3.14%. Below this water content, the equilibrium pressure decreases, but no phase transition takes place, and the dehydrated material retains the X-ray powder pattern characteristic of the δ-phase. In the curves obtained at 29.9, 35.3 and 45.6°, the abrupt change in the equilibrium pressure of water also came at 3.14 ± 0.05% H_2O, indicating no shift in this characteristic composition with temperature. Similar desorption isotherms were obtained by Milligan and Draper[4] for the δ-phase at 12 and 2°, except that the abrupt change came at higher moisture contents (approx. 3.3 and 3.7% H_2O, resp.). The heats of adsorption calculated by Milligan and Draper are much higher than were found here (Table I). The sorption isotherms of Milligan and Draper showed considerable hysteresis for moisture contents below the sharp break.

The dehydration curve for ϵ-sodium palmitate at 40° (Fig. 3) shows the same abrupt change in equilibrium pressure of water over the system as the water content nears 3.14%. The break occurs at the same water content for observations made at 29.9, 35.3 and 45.6°. The change in X-ray pattern is more pronounced on complete dehydration, and the dehydration curve obtained on the rehydrated material after complete dehydration may be due to lack of complete reversibility of this change.

The dehydration curve for the ω-phase (Fig. 4) is similar to that obtained by Milligan and Draper.[4] The decrease in equilibrium water pressure is more gradual, and occurs at a lower water content.

There are three interpretations of the nature of the water present in low moisture soap phases: the water is present in a hydrate, the water is strongly adsorbed on the soap, or the water is in solid solution.

The hydrate theory is supported by the results presented here on the dehydration of the δ- and ϵ-phases. A sharp break in the equilibrium water pressure over the system, the same as obtained in the case of the known alpha hydrate, is observed at a water content that agrees with the composition $NaC_{16}H_{31}O_2 \cdot {}^1/_2H_2O$ within the experimental error. The heat effects observed below 3% H_2O (Table I) are of the magnitude that would be expected for hydrate formation. The dielectric constants of beta and δ-phases[2] also show abrupt changes at this water content. However, the expected behavior of a constant equilibrium pressure at compositions between that of the hydrate and the anhydrous material is not observed, and the X-ray pattern of intermediate compositions show continuous variation through this region, as was shown by Ferguson, Rosevear and Nordsieck[3] for the β-phase, and by Vold, Grandine and Schott[6c] for other phases. These facts can be reconciled only by the rather strained hypothesis that in each case the anhydrous and hydrate phases are very similar in crystal structure, and the intermediate compositions represent solid solution of the two phases present.

Milligan and Draper[4] have interpreted their results in terms of strong adsorption on plate-like crystals. They believe that there is some chemisorption, and calculated pore radii which they felt too small to be significant. This interpretation does not account for the abrupt change in dielectric constant and equilibrium pressure at 3% water.

Vold, Grandine and Schott[6c] postulate solid solution of water in the anhydrous phase to account for continuous variation in X-ray pattern up to 3% water. It would be necessary to assume that the upper limit of this solid solution always corresponds to the hemihydrate composition to explain our results.

Whatever words are used, it is believed that a clear physical picture of the nature of water present in soap phases can be developed. A crystalline soap phase formed in the presence of excess water will have one molecule of water held, probably by hydrogen bonding, to the polar ends of two soap molecules. This water will be present in the crystal planes containing the polar groups. For the α-phase, the crystal is considered to be true hydrate, but in the absence of single crystal X-ray data the other hydrous phases may be considered to have the water present as hydrate, in solid solution, or strongly adsorbed without altering the real picture. Water over and above 3% will be weakly adsorbed by the soap.

As water is removed from the soap systems, the weakly adsorbed water is given up first, and then water is removed from the interior polar planes of the crystal. This may result in a complete breakdown of the crystal, as with the α-phase, or in a slight change in cell dimensions as with the other phases. Once the water has been removed, reintroduction of the water may not be easy, as the crystal must expand to accommodate the water molecules. This would explain the hysteresis effects observed by Milligan and Draper, and the fact that some of his phases did not strongly resorb 3% of water. This would also explain the behavior of the ω-phase, which can be prepared only by heating anhydrous soap above 120°. The crystal formed on cooling may be stronger than those formed in the presence of

water, and it is impossible for water molecules to expand the lattice enough for the full quota of water to be taken up.

Acknowledgment.—We wish to express our appreciation to the Procter and Gamble Company for the samples used in this work, and to Dr. F. B. Rosevear for taking and interpreting powder X-ray diagrams.

THE CONVERSION OF FIBRINOGEN TO FIBRIN. XVIII. LIGHT SCATTERING STUDIES OF THE EFFECT OF HEXAMETHYLENE GLYCOL ON THERMODYNAMIC INTERACTIONS IN FIBRINOGEN SOLUTIONS[1]

BY EDWARD F. CASASSA

Contribution from the Department of Chemistry, University of Wisconsin, Madison, Wisconsin

Received December 27, 1955

Light scattering studies of bovine fibrinogen at *p*H 6.2 in phosphate buffered sodium chloride solutions of ionic strength 0.45 show that the addition of 0.5 *M* hexamethylene glycol to the solvent composition is attended by effects undetected in earlier work. An apparent increase in molecular weight by about 7% is attributed to binding, in a thermodynamic sense, of glycol or other solvent components by the protein; while increases in the molecular length and in the second virial coefficient appear to be related to swelling of the protein molecule. The virial coefficient in the presence of the glycol agrees with that calculated for impenetrable molecules having the dimensions of fibrinogen. At *p*H 9.5 in salt–glycine buffer, even in the absence of thrombin, fibrinogen undergoes an aggregation reaction reversible, at least in part, by addition of hexamethylene glycol or by dilution. The assumption made in some earlier work, that the specific refractive index increment of a protein in aqueous solution is independent of concentration of salt and other components, is unsatisfactory; thus it is suggested that small changes in the increment with variations in solvent composition be determined from an appropriate form of the Gladstone–Dale mixture rule if accurate experimental data are not available.

I. Introduction

As one aspect of the interest attaching to fibrinogen in its singular role in the blood clotting process, fairly extensive studies of solutions of bovine fibrinogen by Rayleigh scattering have been carried out in this[2] and other[3,4] laboratories. The present investigation represents an extension of the earlier studies in that the scattering measurements comprehend a wider range of solute concentrations, sufficient for ascertaining deviations from thermodynamic ideality. In this regard it was considered of interest to determine the effect, as reflected in thermodynamic quantities and molecular dimensions, of the addition to fibrinogen solutions of hexamethylene glycol since this substance has been used to prevent the thrombin-catalyzed polymerization of fibrinogen from going to completion.[5,6] Most of the previous work was carried out with solutions at *p*H in the vicinity of 6; and similar conditions were employed in the polymerization studies.[6] Recently, however, the polymerization reaction occurring at *p*H 9.5 has been investigated by light scattering[7,8] and sedimentation[8,9]; and it was thus thought desirable to extend the earlier work on monomeric fibrinogen to this *p*H.

(1) This investigation was supported by the Office of Naval Research, United States Navy, under Contract N7onr-28509.

(2) S. Katz, K. Gutfreund, S. Shulman and J. D. Ferry, *J. Am. Chem. Soc.*, **74**, 5706 (1952).

(3) C. S. Hocking, M. Laskowski, Jr., and H. A. Scheraga, *ibid.*, **74**, 775 (1952).

(4) R. F. Steiner and K. Laki, *ibid.*, **73**, 882 (1951); *Arch. Biochem. Biophys.*, **34**, 24 (1951).

(5) S. Shulman and J. D. Ferry, THIS JOURNAL, **55**, 135 (1951).

(6) J. D. Ferry, S. Shulman, K. Gutfreund and S. Katz, *J. Am. Chem. Soc.*, **74**, 5709 (1952).

(7) E. F. Casassa, *J. Chem. Phys.*, **23**, 596 (1955).

(8) E. F. Casassa and I. H. Billick, to be published.

(9) I. Tinoco, Jr., and J. D. Ferry, *Arch. Biochem. Biophys.*, **48**, 7 (1954).

II. Experimental Procedures

Materials.—The fibrinogen used in this work was refractionated from two samples, designated Lot 128-163 and Lot 210, of Armour Bovine Fraction I. The final fractionation was carried out by methods adapted from that of Laki.[10]

Procedure I as follows was employed for Lot 128-163. Fraction I was dissolved in 0.051 *M* phosphate buffer[11] at about *p*H 6.2, 100 cc. of buffer being used for each gram of material. The solution was filtered, then stored for about 12 hours at 2–4°. After filtration at the same temperature to remove the precipitate formed, the solution was warmed quickly to 23–25° and precipitation of fibrinogen was carried out by slow addition, with stirring, of saturated (at the precipitation temperature) ammonium sulfate. Addition of precipitant was discontinued when the *p*H fell to 5.90, but in no case was more than 0.30 volume of ammonium sulfate added to one volume of protein solution. The fibrinogen was washed several times with buffer of the same composition as the solvent at the completion of precipitation and then dissolved and dialyzed against whatever buffer was desired for further experiments.

Procedure II, used with fibrinogen from Lot 210, and in one instance with Lot 128-163, was the same as Procedure I except that 0.030 *M* phosphate was used in the initial step.

In some cases two fibrinogen fractions were obtained in the course of the precipitation by ammonium sulfate. The first fraction, containing very roughly 10 to 20% of the total protein thrown down, was separated by allowing the solution to stand for 5 to 10 minutes after the first permanent appearance of precipitate. At this stage the precipitated fibrinogen was highly swollen; it coagulated readily and the bulk of it could be collected easily on the stirring rod.

Both fractionation procedures usually yielded fibrinogen preparations at least 90% clottable by the customary gravimetric assay.[12] However, Procedure I applied to Lot 210 gave unsatisfactory products only 70 to 85% clottable. Difficulties in obtaining adequately pure fibrinogen from

(10) K. Laki, *ibid.*, **32**, 317 (1951).

(11) The phosphate buffer used here and in Procedure II below is conveniently prepared by appropriate dilution of a stock solution containing 0.203 *M* NaH_2PO_4 and 0.101 *M* Na_2HPO_4.

(12) J. D. Ferry and P. R. Morrison, *J. Am. Chem. Soc.*, **69**, 388 (1947).

certain samples of Fraction I have also been reported by other workers.[13]

The clot for the assay was formed at *p*H *ca.* 6.3 in buffer of 0.15 ionic strength. Stock solutions assayed were always sufficiently concentrated that dilution of one or two cc. of the stock with 20 cc. of *p*H 6.2 buffer brought the concentration and the *p*H, even for the stock solutions in *p*H 9.5 buffer, into the proper range for formation of the "coarse" clot[12] required for the assay technique. Total protein was determined by absorption of ultraviolet light at 2780 Å. in the Beckman Model DU spectrophotometer with slit opening less than 0.5 mm. The relation between optical density D and protein concentration c in g./cc., $c \times 10^5 = 669D$, was established by the Kjeldahl nitrogen analysis and dry weight determinations.

For all experiments discussed in this paper, refractionated fibrinogen was dissolved in buffers of 0.450 total molar ionic strength. The *p*H 6.2 buffer was made up as 0.01014 M in NaH_2PO_4, 0.01007 M in Na_2HPO_4 and 0.400 M in NaCl. Alkaline buffer at *p*H 9.5 was prepared as 0.100 M in glycine, 0.0500 M in NaOH and 0.400 M in NaCl. All the inorganic materials were of analytical reagent quality while the glycine was Eastman Kodak white label grade. In some of the experiments buffers of the compositions given above contained in addition hexamethylene glycol at a concentration of 0.500 M. The glycol, obtained through the generosity of E. I. du Pont de Nemours and Co., was distilled at reduced pressure before use. When the glycol was added to salt-buffer solvent, some cloudiness usually developed; but this was removed entirely by filtration through an "ultrafine" sintered glass disk.

Light Scattering Technique.—In preparation for light scattering studies, fibrinogen stock solutions were clarified by a preliminary filtration through asbestos pads, previously freed of traces of calcium by thorough washing with sodium citrate solution. Final removal of dust particles or other suspended matter was accomplished by centrifuging solutions and solvent for two hours at 20,000 *g* in a "Servall" Model SS-2 vacuum centrifuge. In order to avoid subjecting the protein to any temperature above 25° during centrifugation, the rotor was cooled to 5° before use. At *p*H 9.5 fibrinogen is quite unstable at moderately elevated temperatures; at 35° solutions rapidly lose clotting power and gradually increase in turbidity.[14]

The light scattering photometer used in this work has been described earlier.[15] The only important modification introduced was a thermostat[16] to maintain the temperature of the protein solution at 25.0 ± 0.2°. The range of scattering angles covered by the experiments, 25–140° relative to the direction of the incident beam, was limited by the aperture of the window of this thermostat. All measurements were made with hand blown conical cells,[16] not entirely free from optical irregularities. Although the fact that the cells were immersed in water in the thermostat minimized errors from this source, the media both within and without the cells having then approximately the same refractive index, any residual error was compensated for by determining the observed intensity, in each cell, of fluorescence scattering alone in dilute fluorescein solution.[16] Since the fluorescence must be independent of scattering angle, the observed variations of intensity with angle could depend only on optical flaws in the cell or thermostat window, reflections of scattered light and geometrical factors, of which the most important is the very nearly proportional dependence of the illuminated volume viewed by the detector upon the cosecant of the angle. To correct scattering data on fibrinogen for these effects and to reduce readings to a common basis, the measured intensity at any angle was divided by the ratio of apparent fluorescence intensities at that angle and at right angles.

In studying the scattering from a particular fibrinogen sample as a function of concentration, all measurements were made in a single cell in order that errors in the calibration constants for each cell relating measured photocurrents to absolute light intensity might not obscure the rather small deviation of solute scattering from direct proportionality to concentration. For the same reason, measurements to determine the small effect of added hexamethylene glycol on scattering from the protein solutions were also made in a single cell.

Unpolarized incident light of wave length 4358 Å., isolated by the appropriate Corning filters from the radiation of an AH-3 (Westinghouse Co.) or H85-A3 (General Electric Co.) mercury arc, was used in all the scattering measurements.

Routine conversion of intensity measurements, in arbitrary units as galvanometer scale readings, to absolute intensities was accomplished by the working standard method of Brice, Halwer and Speiser[17]; but the ultimate reference was a 7.50 g./l. solution of a certain polystyrene sample in butanone for which the reduced intensity (or Rayleigh's ratio) for scattering at right angles due to solute was assumed to be 17.20×10^{-4} at 4358 Å. for unpolarized light as determined by Carr and Zimm.[18]

III. Treatment and Interpretation of Data

Light Scattering.—The experimental data were evaluated in the manner advocated by Zimm[19]: graphs of the familiar reciprocal intensity function $Kc/R(\theta)$ against concentration c and $\sin^2(\theta/2)$, θ being the scattering angle, were combined on a single plot, and a double extrapolation was performed to infinite dilution and zero angle. The limiting relations

$$Kc/R(0) = (1/M + 2A_2c + 3A_3c^2 + \cdots)/\omega^2 \quad (1)$$
$$= 1/M' + 2A_2'c + 3A_3'c^2 + \cdots$$

and

$$\frac{Kc}{R(\theta)_{c=0}} = \frac{1}{M'}\left[1 + \frac{1}{9}\left(\frac{2\pi L}{\lambda'}\right)^2 \sin^2\frac{\theta}{2} + \cdots\right] \quad (2)$$

were used to obtain the molecular length, and apparent molecular weight M' and virial coefficients A', A'. In all cases but one, however, measurements did not cover a wide enough concentration range to justify retention of the quadratic term of equation 1. Numerical results for A_2 and A_2 reported below are consistent with c expressed as grams of protein component per cc. of solution. The quantity ω, as is indicated by equation 8 below, may differ from unity only in systems of more than two components. In equation 2, the coefficient of $\sin^2(\theta/2)$ has been written explicitly in the form corresponding to the assumption that the fibrinogen molecule is a cylindrical rod of length L and of thickness much less than the wave length of light λ' in the medium. As expressed here, the reduced scattered intensity from solute $R(\theta)$ (corrected for the Thomson scattering factor $1 + \cos^2\theta$ arising with unpolarized incident light) determines the same angular intensity distribution, within experimental error, as is obtained with vertically polarized incident radiation since the depolarization of scattering at right angles is much too small to necessitate the inclusion of a Cabannes factor[18,20] in equations 1 and 2. The quantities collected in the constant $K = 2\pi^2n^2(dn/dc)^2/N\lambda^4$ have the customary significance with N Avogadro's number, λ the wave length of light *in vacuo*, and n the refractive index of the solution.

Protein Concentration.—The fibrinogen concentrations used in calculating the results presented in this paper represent total protein rather than

(13) J. M. Sturtevant, M. Laskowski, Jr., T. H. Donnelly and H. A. Scheraga, *J. Am. Chem. Soc.*, **77**, 6168 (1955).

(14) E. F. Casassa, unpublished results.

(15) S. Katz, *J. Am. Chem. Soc.*, **74**, 2238 (1952).

(16) E. F. Casassa and S. Katz, *J. Polymer Sci.*, **14**, 385 (1954).

(17) B. A. Brice, M. Halwer and R. Speiser, *J. Optical Soc. Am.*, **40**, 768 (1950).

(18) C. I. Carr and B. H. Zimm, *J. Chem. Phys.*, **18**, 1616 (1950).

(19) B. H. Zimm, *ibid.*, **16**, 1099 (1948).

(20) J. Cabannes and Y. Rocard, "La diffusion moléculaire de la lumière," Les Presses Universitaires de France, Paris, 1929.

clottable protein. If the concentration of clottable protein had been used, the molecular weights from equation 1 would, of course, have been higher than those reported. The choice as to which measure of protein concentration should be used is necessarily rather arbitrary. If the non-clotting material is of very low molecular weight compared to fibrinogen, the scattered intensity is almost entirely due to fibrinogen; and in that case calculation on the basis of clottable protein yields a molecular weight nearly that of the fibrinogen component. There is, however, no *a priori* reason for assuming the impurities to be of low molecular weight. It is evident in the results of Katz, Gutfreund, Shulman and Ferry[2] that the molecular weights calculated by them on the basis of clottable protein are generally highest for those preparations containing the most non-clottable material. The molecular weights obtained from their results on the basis of total protein show greater uniformity though the same trend persists. In any case, calculations on the basis of total protein concentration measured by ultraviolet light absorption give the weight average molecular weight of the system as a whole, provided the non-clotting fraction has the same extinction coefficient as fibrinogen.

Specific Refractive Index Increment.—Since the constant K in equations 1 and 2 contains the square of the specific refractive index increment dn/dc, it is important that it be known accurately. In earlier publications from this Laboratory[2,6] the specific refractive index increment of fibrinogen was assumed to be the same in all the solvents utilized. This assumption, even over the small refractive index range encountered with the buffers used in these studies, is rather unsatisfactory; and moreover it can easily be replaced by an approximation considerably less in error.

If we assume the refractive index of a binary mixture to be a linear function of the composition by volume,[21] we may write

$$n = n_1\bar{v}_1c_1 + n_2\bar{v}_2c_2 = \bar{v}_2c_2(n_2 - n_1) + n_1 \qquad (3)$$

in which n_1, n_2, $\bar{v}_1$, $\bar{v}_2$, c_1, c_2, are, respectively, the refractive indices, partial specific volumes, and concentrations (in grams per cc. of solution) of the two components. For the present purpose we consider only mixtures dilute in component 2, chosen as the solute; and we need not require n_2 to be identical with the refractive index of pure component 2, but simply a constant defined by equation 3. Letting $c_2 = c$, we obtain for the refractive index increment

$$\frac{dn}{dc} = (n_2 - n_1)\bar{v}_2 + c\frac{d\bar{v}_2}{dc}$$

For the protein solutions employed in this work $c(d\bar{v}_2/dc)$ is surely very small compared to $\bar{v}_2$, and this expression can be simplified

$$\frac{dn}{dc} = \bar{v}_2(n_2 - n_1) \qquad (4)$$

If the refractive index increment $[dn/dc]_a$ is known for a particular solvent of refractive index n_a, equation 4 can be used to calculate $[dn/dc]_x$ for a solvent of index n_x provided that $\bar{v}_2$ and n_2 are the same in both solvents; that is

$$\left[\frac{dn}{dc}\right]_x = \left[\frac{dn}{dc}\right]_a - \bar{v}_2(n_x - n_a) \qquad (5)$$

Equation 5 is an adaptation of the Gladstone–Dale empirical rule for the refractive index of mixtures in a form similar to that which has been used for solutions of high polymers in organic solvents.[22]

In considering the refractive index increment for systems of more than two components it is necessary to define precisely the process involved in changing solute concentration. For a three component mixture—protein, salt, water, for example—the refractive increment of the protein to which equation 4 applies is evidently that referring to change of protein concentration at constant molality of the salt. In other words, the concentration of protein component, which may be defined to include salt ions, is changed by removal or addition of salt solution of fixed composition. We may apply similar reasoning to a system of any number of components and state equation 4 in the more general form

$$\left(\frac{\partial n}{\partial c}\right)_m = \bar{v}_2(n_2 - n_s) \qquad (6)$$

where, as before, c and $\bar{v}_2$ refer to the solute while n_s is the refractive index of the system of the other components, the mixed solvent. (The dilution process described here was that used in varying protein concentration for the light scattering measurements discussed in this paper.)

The value of the refractive index increment for bovine fibrinogen used by Katz, *et al.*,[2] 0.197 at 4358 Å., was derived from measurements at 5890 Å. in 0.3 M sodium chloride by Armstrong, Budka, Morrison and Hasson[23] and the dispersion data of Perlmann and Longsworth.[24] With this result and the partial specific volume[25] taken as 0.71, we have used refractive indices and dispersion data at 5890 Å. and 25° determined with the Abbe refractometer to calculate the refractive index increments at 4358 Å. in the solvents of interest in connection with light scattering studies. Whether or not the originally derived value of 0.197 for dn/dc is correct, the calculated refractive increments and corresponding values of the light scattering constant K, as given in Table I, are probably reasonably reliable in relation to one another. Indeed, the differences between these figures may well be accurate within the experimental error in measurement of dn/dc with commercially available equipment for differential refractometry.

Thermodynamic Interpretation of the Light Scattering Equation.—To establish the precise significance of the parameters appearing in equation 1, it is necessary to consider the fact that the systems of interest in the present study contain several components. The statistical fluctuation theory of

(21) More elaborate mixture rules, both theoretical and empirical, have been proposed. Some of these are discussed by W. Heller, *Phys. Rev.*, **68**, 5 (1945).

(22) P. Outer, C. I. Carr and B. H. Zimm, *J. Chem. Phys.*, **18**, 830 (1950).

(23) S. H. Armstrong, Jr., M. J. E. Budka, K. C. Morrison and M. Hasson, *J. Am. Chem. Soc.*, **69**, 1747 (1947).

(24) G. E. Perlmann and L. G. Longsworth, *J. Am. Chem. Soc.*, **70**, 2719 (1948).

(25) V. L. Koenig, *Arch. Biochem.*, **25**, 241 (1950); K. Bailey and F. Sanger, *Ann. Rev. Biochem.*, **20**, 103 (1951).

TABLE I

CALCULATED SPECIFIC REFRACTIVE INDEX INCREMENT OF BOVINE FIBRINOGEN IN VARIOUS SOLVENTS

Solvent	n (4358 Å.)	$(dn/dc)_m$	$K \times 10^7$
0.3 *M* NaCl	1.3435	0.1970	6.362
Phosphate buffer; Γ/2, 0.45	1.3459	.1953	6.275
Phosphate buffer; Γ/2, 0.45; 0.5 *M* HMG[a]	1.3530	.1903	6.021
Glycine buffer; Γ/2, 0.45	1.3465	.1949	6.255
Glycine buffer; Γ/2, 0.45; 0.5 *M* HMG	1.3537	.1898	5.996

[a] Hexamethylene glycol.

Rayleigh scattering in multicomponent solutions[26] leads to the following approximate expression for the excess scattering (the intensity scattered from solution less that from the solvent) for a system consisting of a macromolecular solute and other components which it is convenient to designate collectively as solvent

$$R(0) = \frac{2\pi^2 n^2 V \psi_2^2}{N\lambda^4}\left(\frac{\omega^2 m_2}{1 + m_2(\partial\beta_2'/\partial m_2)_\mu}\right) \quad (7)$$

in which

$$\omega = \sum_K \frac{\psi_K}{\psi_2}\left(\frac{\partial m_K}{\partial m_2}\right)_\mu \qquad \psi_K = (\partial n/\partial m_K)_m \quad (8)$$

We allow the subscripts K to take on the values 2 (protein component), 3 (designating the sum of terms involving the salt–buffer components, which we do not attempt to consider separately) and 5 (hexamethylene glycol).[27] The concentrations m_K are referred to a fixed mass of component 1 (conveniently the principal solvent, water) contained in a volume V of solution. It is appropriate therefore to regard them as weight molalities and define the chemical potentials μ_K accordingly[28]; *i.e.*, for the protein component

$$\mu_2/RT = \mu_2^\circ/RT + \ln m_2 + \Sigma_i \nu_{2i} \ln m_i + \beta_2$$
$$= \mu_2^\circ/RT + \ln m_2 + \beta_2' \quad (9)$$

where $RT\beta_2$ is the excess chemical potential taken as zero in the reference state at infinite dilution of component 2. The quantities ν_{2i} are the numbers of moles of species i (which in this case we take as the ions composing the components 3) included in the definition of a mole of component 2, and the m_i are the total concentrations of these species. The ν_{2i} are subject to the requirement that component 2 be electrically neutral as is each of the other components. Subscript μ indicates differentiation with all potentials except μ_2 and μ_1 held fixed, while m subscribed to derivatives has the usual significance of denoting constancy of all concentrations except that involved in differentiation. Pressure and temperature are held constant in all differentiations.

The requirement of electrical neutrality for all components amounts, physically, to limiting possible concentration fluctuations to those resulting in no net charge in any volume element of dimensions comparable with the wave length of light. This restriction,[29] which is necessary for the application of equation 7 to be valid, is satisfied at the high ionic strength we have employed. Equation 7 is analogous to equation 3.5 of Stockmayer[26b] for three components and involves the same approximations.

It will be observed that the refractive increments and the concentrations of equation 7 are defined differently from those of equation 1. In terms of the concentration c of protein component in g./cc. and the specific refractive index increment $(\partial n/\partial c)_m$ defined in the preceding section, equation 7 may be rearranged to give

$$\frac{Kc}{R(0)} = \frac{1}{M\omega^2(1 - c\bar{v}_2)^2} + \frac{1000fc}{M^2\omega^2(1 - c\bar{v}_2)^3}\left(\frac{\partial\beta_2'}{\partial m_2}\right)_\mu \quad (10)$$
$$= \frac{1}{M\omega^2} + 2c\left[\frac{\bar{v}_2}{M\omega^2} + \frac{500f}{M^2\omega^2}\left(\frac{\partial\beta_2'}{\partial m_2}\right)_\mu\right] + \ldots$$

correct to terms in c. The molecular weight of the protein component is $M = M'/\omega^2$ and $f = \bar{v}_1 + w_3\bar{v}_3 + w_5\bar{v}_5$.[30] The quantities $\bar{v}_1$, $\bar{v}_2$, $\bar{v}_3$, $\bar{v}_5$ are partial specific volumes, respectively, of water, protein and the other components while w_3, w_5 are concentrations in grams per gram water. In general $(\partial\beta_2'/\partial m_2)_\mu$ will depend on m_2: but the limiting value, as $c \to 0$, of the quantity in brackets in the last equality of equation 10 is the coefficient A_2' of equation 1, and we may define a second virial coefficient A_2^w consistent with solute concentration in grams per gram of the principal solvent by

$$A_2^w = \frac{500}{M^2}\left[\lim_{c\to 0}\left(\frac{\partial\beta_2'}{\partial m_2}\right)_\mu\right] = \frac{1}{f}\left(A_2 - \frac{\bar{v}_2}{M}\right) \quad (11)$$

The molecular weight M of component 2 and the thermodynamic quantities appearing in equations 7 and 10 obviously depend on the definition of that component. Any suitable definition is applicable to equation 10 provided that the concentration c and the refractive index increment $(\partial n/\partial c)_m$ are both consistent with it. For the purposes of this paper we shall assume that the specifications of protein component, concentration and refractive increment are self-consistent and that the protein component is so defined as to contain any excess (or deficiency) of small ions required to make the "binding" parameter ω equal unity in systems at *p*H 6.2 *containing no hexamethylene glycol*. These precise distinctions are not of practical importance in determining experimentally the molecular weight of fibrinogen—the molecular weight corresponding to isoionic protein in the absence of salt would presumably not differ appreciably from that defined here—but they do come into question in discussing the differential effect of the addition of hexamethylene glycol to the solvent composition.

(26) (a) H. C. Brinkman and J. J. Hermans, *J. Chem. Phys.*, **17**, 574 (1949); J. G. Kirkwood and R. J. Goldberg, *ibid.*, **18**, 54 (1950); (b) W. H. Stockmayer, *ibid.*, **18**, 58 (1950).

(27) Here we adopt the procedure of Scatchard[28] in assigning even numbers to macromolecular components and odd numbers to low molecular weight components. It must be noted that by the formalism used here any effects of the neutralization reaction of protein and buffer are implicitly included in the interactions between protein and the components 3.

(28) G. Scatchard, *J. Am. Chem. Soc.*, **68**, 2315 (1946).

(29) J. J. Hermans, *Rec. trav. chim.*, **68**, 859 (1949).

(30) For calculations, f was estimated from density measurements to be 1.07 and 1.01, respectively, in the solutions with and without hexamethylene glycol.

TABLE II

LIGHT SCATTERING FROM BOVINE FIBRINOGEN

Expt.[a]	Protein source and fractionation[a]	Clottable fibrinogen, %	Solvent[b]	$M' \times 10^5$	$L \times 10^8$ (cm.)	$M/L \times 10^{10}$	$A_2' \times 10^5$	$\frac{A_2^w}{\omega^2} \times 10^5$
P46	210 II	91.8	*p*H 6.2	4.04	620	6.5	−0.1	−0.3
P50	210 II	91.2	*p*H 6.22	4.79	700	6.8	0.6	0.4
			*p*H 6.2 HMG	5.14	800	6.0	3.2	2.9
P51	210 II	91.5	*p*H 6.2	4.73	670	7.1	0.8	0.7
			*p*H 6.2 HMG	5.08	740	6.4	3.4	3.1
P52	128–163 II	91.5	*p*H 6.2	4.69	640	7.3	0.8	0.6
			*p*H 6.2 HMG	5.07	720	6.5	2.7	2.4
$P53_1$	210 II_1	88.6	*p*H 6.2	3.96	550	7.2		
$P53_2$	210 II_2	93.0	*p*H 6.2	3.73	570	6.5		
P54	210 II_2	86.2	*p*H 6.20	4.07	620	6.6	1.1	1.0
			*p*H 6.25 HMG	4.35	700	5.8	2.0	1.7
P55	128–163 I_2	87.2	*p*H 6.21	4.29	600	7.2	1.2	1.0
			*p*H 6.26 HMG	4.24	640	6.7	3.3	2.9
P57	128–163 I_2	92.0	*p*H 6.2	3.99	580	6.9	0.9	0.7
			*p*H 6.17 HMG	4.14	660	6.0	3.2	2.9
G42	210 II	94.8	*p*H 9.5 HMG	4.35	630		1.7	1.5
G45	210 II	92.9	*p*H 9.5 HMG	4.28	700		1.9	1.6

[a] The roman numerals designate fractionation procedures described in the text. Subscripts 1 and 2 denote the first and second fractions in those cases in which the precipitated fibrinogen was collected in two parts. Expts. $P53_1$ and $P53_2$ concern the two fractions of a single preparation. [b] HMG indicates presence of 0.5 *M* hexamethylene glycol. Buffer compositions are as given in the text.

IV. Discussion of Results

Fibrinogen Solutions at *p*H 6.2 Containing no Hexamethylene Glycol.—Results obtained from the foregoing analysis of light scattering data are shown in Table II.

Assuming that the best molecular weight and length of fibrinogen in the systems at *p*H 6.2 without glycol are given by the lowest results from protein containing the least amount of non-clotting material, we average the results of experiments P46, $P53_2$, P57 to obtain 392,000 for the molecular weight and 590 Å. for the length based on the thin cylinder molecular model.[31] The experiments in solutions at *p*H 6.2 are listed in chronological order in Table II, each code number in the first column serving to identify light scattering studies carried out with a particular lot of refractionated fibrinogen. It is evident that three successive preparations (P50 through P52) yielded material with both molecular weight and length about 20% greater than the value quoted above. This behavior has not been explained but it does suggest that the character of the material retained in the fractionation procedure may depend critically upon some of the conditions of the protein precipitation or possibly upon traces of impurity in the reagents used.

Our results for molecular weight and length are definitely higher than those reported by Katz, *et al.*,[2] who took as the best estimates from their light scattering data[32] 340,000 and 520 Å.; however, the ratio of molecular weight to length from our data, 6.6×10^{10} g./cm. agrees with theirs within experimental error. The molecular weight difference appears to be significant experimentally since the same procedure and reference standard were used in the two light scattering studies to relate phototube response to absolute light intensity; but it would probably be futile to speculate on the cause as the magnitude of the difference is only about half the unexplained discrepancy in molecular weights of different preparations found in the course of our work. Since the best of the fibrinogen used by Katz, *et al.*, contained somewhat less non-clotting material than ours, their results for molecular weight and size may well be the more reliable. Our molecular weight of 392,000 is close to that of 407,000 found by Hocking, Laskowski, and Scheraga[3] but still much smaller than 540,000 given by Steiner and Laki.[4]

In column 8 of Table II are listed the experimental values of the virial coefficient A_2 (with $\omega = 1$, $A' = A_2$) which determines, to a linear approximation in protein concentration, the deviation from thermodynamically ideal behavior of the protein component. Averaging all the results for solutions at *p*H 6.2 without glycol we obtain 0.8×10^{-5} cc. mole g.$^{-2}$; but as there is some indication in the data that A_2 may be smallest for protein preparations containing the least non-clottable matter, the correct figure for pure fibrinogen may possibly be somewhat less. The variation of the individual measurements is fairly large and definitely beyond experimental uncertainty, which we estimate to be about $\pm 0.2 \times 10^{-5}$. In establishing the magnitude of A_2 in these systems, we do not contradict the earlier assertion of Katz, *et al.*, that this coefficient is zero within experimental error; for their studies of the concentration dependence of scattering involved only concentrations between

(31) Calculations on the basis of thin prolate ellipsoids give molecular lengths about 25% greater. When small, as in the present case, the angular dependence of scattered light intensity determines only the radius of gyration of the molecule; calculation of actual molecular dimensions must therefore depend upon an assumed model.

(32) The molecular weight of 340,000 reported by Katz, *et al.*, was calculated on the basis of concentrations as clottable protein with the refractive index increment taken as 0.197. The two corrections we apply to express the result in terms of the total protein concentration and of a better choice of dn/dc compensate in this particular case and the result remains unchanged.

0.3 and 2.3 g./l., which is too restricted a range for measurement of concentration effects this small. Most of our experiments involved a concentration range at least threefold greater.

For the systems without glycol the last column of Table II gives the second virial coefficient A_2^w related by equation 11 to the concentration scale of equation 7. The average of the results is 0.6×10^{-5}; thus the difference between A_2 and A_2^w is not of great importance in this particular case. Although neglect of this distinction, as Ehrlich[33] observes, cannot be considered permissible, *a priori*, for any system whatsoever, the necessity of justifying such an approximation has perhaps not always been appreciated.

It is of interest to compare the experimental A_2 with the interaction to be expected in a system of simple molecular models possibly representative of the size and shape of fibrinogen. For rigid impenetrable cylindrical rods of diameter d in a continuous medium the virial coefficient[34] is $N\pi dL^2/4M^2$. Substituting in this expression the molecular weight and length for fibrinogen and the diameter consistent with the molecular volume determined by the partial specific volume 0.71, we obtain 3.4×10^{-5}, a result larger than the measured value.[35] Hence the effective mutually excluded volume for a pair of solute molecules is smaller than the model requires.

Effect of Hexamethylene Glycol at *p*H 6.2.—The pairs of experiments denoted by the same code numbers in Table II were designed to elucidate the effect of adding hexamethylene glycol to protein–salt–buffer systems. The two sets of solutions used in light scattering measurements were made up from a single fibrinogen stock solution and were of identical protein concentration; both solvents were of the same molar composition except for the presence in one case of 0.5 *M* hexamethylene glycol (added to the protein by dilution with a 1 *M* solution in the salt–buffer). These solvents were chosen for investigation because they represent the conditions used in some of the studies in this series, by light scattering[6] and other methods, of the polymerization of fibrinogen through the enzymatic action of thrombin.

It is seen from the tabulated results that in every case but one the apparent molecular weight is greater in solutions containing glycol. Averaging the individual ratios (with the exception of P55) we find the ratio of apparent molecular weights with and without glycol to be 1.07 ± 0.01. The deviation of this value from unity appears to be experimentally significant although it is small and depends critically on the calculated difference between refractive index increments in the two systems; but our conclusion on this point must remain somewhat speculative. As the apparent molecular weight is increased by the presence of glycol, the molecular length calculated from equation 2 also becomes greater by a factor of 1.12 ± 0.04 averaged over all the results. It should be remarked that these effects would be completely masked, through lack of reproducibility in molecular weight and length, were comparison attempted between pairs of experiments in which different preparations of purified fibrinogen had been used.

One conceivable explanation of these findings would be aggregation of a small part of the fibrinogen present. The possibly greater increase in the molecular length than in the weight could then arise naturally from the heterogeneity of the solute: the molecular weight calculated from light scattering in a heterogeneous system is the weight average $\Sigma_j M_j w_j$, the w_j representing weight fractions of the various solute species j, while the average length represented by L in equation 2 is $(\Sigma_j M_j w_j L_j^2/\Sigma_j M_j w_j)^{1/2}$, an average more heavily weighted in favor of large aggregates. The experimental data could then be explained by assuming that 7% of the fibrinogen monomer is converted to rod-like dimer particles 1.5 times the length of the monomeric unit; therefore a partial overlapping,[36,37] such as may occur in the enzymatic polymerization of fibrinogen, would be indicated. This hypothesis of aggregation induced by the glycol appears unattractive, however, when it is considered that hexamethylene glycol is an effective inhibitor for at least the final stage of the polymerization steps leading to the formation of fibrin clots[5,6]; but even more pertinent to this particular question is the fact that the glycol also inhibits a partial aggregation of fibrinogen, discussed below, occurring at high *p*H in the absence of thrombin.

If, then, polymerization of fibrinogen can be excluded as the cause of the apparently increased molecular weight in the presence of hexamethylene glycol, the effect must be attributed to an increased value of the quantity ω; *i.e.*, to positive binding (*in the purely thermodynamic sense of equation 7*) of a solvent component or components to the protein component. Since the systems under consideration have more than one solvent component in addition to the principal one, it is impossible without special assumptions to determine uniquely from the molecular weight data which components are responsible for the binding. It is useful, however, in illustrating the order of magnitude involved to compute the binding required if only glycol or sodium chloride is concerned. Taking the molal refractive increment ratio ψ_5/ψ_2 as roughly 1.8×10^{-4} (derived from the dn/dc already given for fibrinogen and the refractive indices of the solvents) we could account for the experimental result of 1.07 for ω^2 by a value of about 200 for $(\partial m_5/\partial m_2)_\mu$.

(33) G. Ehrlich, THIS JOURNAL, **58**, 769 (1954).

(34) B. H. Zimm, *J. Chem. Phys.*, **14**, 164 (1946).

(35) The divergence between experiment and theory is more apparent when it is considered that the calculated molecular volume represents a minimum value; the dissolved molecule undoubtedly imbibes solvent and effectively occupies a volume larger than that determined by the partial molal volume. Therefore, the calculated virial coefficient probably also represents a minimum. Aside from this question, agreement with experiment would not, of course, prove that the model is in every respect adequate. The virial coefficient involves an integral over space of a distribution function[34] specifying molecular density and configuration relative to the center of a reference molecule. An infinity of arbitrary distribution functions could be devised to yield the same integral. None the less it is frequently useful to replace the actual molecule under consideration by an "equivalent" simple model. It may be remarked that for the molecular model used here, the virial coefficient arises entirely from the entropy of dilution. We do not wish to imply, however, that the enthalpy of dilution is necessarily zero in the fibrinogen solutions.

(36) J. D. Ferry, *Proc. Nat. Acad. Sci.*, **38**, 566 (1952).

(37) J. D. Ferry, S. Katz and I. Tinoco, Jr., *J. Polymer Sci.*, **12**, 509 (1954).

Since the refractive increment is not far different for sodium chloride, a like number of moles of salt would serve, as would any combination of both components giving an algebraic sum of 200. An unambiguous calculation would be possible were the equilibrium distribution[28] across a membrane impermeable to component 2 known for the low molecular weight components. It would therefore be of interest to compare results from light scattering and equilibrium dialysis measurements, preferably for systems without the complication of buffers.

If binding is accepted as the cause of the apparent molecular weight change, it becomes necessary to explain the observed increase of 12% in the molecular length without invoking aggregation. The only possible explanation appears to be an actual expansion of the molecule; and one independent indication that this may occur is the fact that the second virial coefficient is decidedly more positive in the solvent containing glycol than in that without, the average difference in A_2 for the pairs of experiments at *p*H 6.2 in Table II being 2.1×10^{-5}. An increase in A_2 signifies an increased effective volume of mutual exclusion for interaction between molecular pairs, *i.e.*, a greater net intermolecular repulsion. Furthermore it is probable that the intermolecular repulsion is associated with intramolecular repulsion between parts of the same molecule. In the statistical thermodynamic treatment of solutions of uncharged flexible chain molecules, for example, the intermolecular interaction is considered the resultant of segment–segment interactions which individually in no wise differ from the interactions occurring between segments within a single molecule. Experimentally it is well known that a large positive virial coefficient in such solutions is correlated with a highly expanded molecular configuration. Although protein solutions are scarcely to be described adequately in terms of like conceptual simplicity, it appears that such ideas are qualitatively applicable provided long range electrostatic forces are suppressed as at high ionic strength. Since it is generally accepted that protein molecules can undergo considerable swelling in solution, there is no difficulty in assuming that the fibrinogen structure is sufficiently deformable to permit the requisite change in length.

The average value of A_2 in the systems containing glycol is 3.1×10^{-5}, in excellent agreement with the value calculated above for impenetrable rods.[35]

The thermodynamic quantities appearing in equations 7 and 10 may be expressed in terms of the more familiar derivatives[28,38] $\beta_{KJ} = (\partial\beta_K/\partial m_J)_m = (\partial\beta_J/\partial m_K)_m$ by use of the relation[26b] $(\partial\mu_2/\partial m_K)_\mu = |a_{KJ}|/A_{2K}$ in which A_{2K} is the cofactor of the element $a_{2K} = (\partial\mu_2/\partial m_K)_m$ of the determinant $|a_{KJ}|$, the subscripts including all components except component 1. Since the virial coefficient and binding parameter ω refer to limiting behavior as m_2 approaches zero, the β_{KJ} for $K, J \neq 2$ may be determined from solutions not containing the protein. Then, the changes in apparent molecular weight and in A_2^w caused by addition of glycol to the solvent medium provide two independent relations among the quantities β_{2K} in the two systems in question. From the form of the equations it may be seen that for plausible values[39] of the β_{KJ} ($K, J \neq 2$), the increases found experimentally in both ω and A_2^w are consistent only if β_{22} becomes more positive in the presence of glycol.

Fibrinogen Solutions at *p*H 9.5.—Results from two light scattering experiments at *p*H 9.5 on fibrinogen in the salt-glycine-glycol solvent are shown in Table II. The average molecular weight M' for these experiments is 432,000 while A_2' is 1.8×10^{-5}, a somewhat smaller value than was found in the comparable solutions of the same ionic strength and glycol content buffered by phosphate at *p*H 6.2. Since the fibrinogen ion already carries an effective negative charge at *p*H 6.2 in the solvent systems used in this work, as is shown by the electrophoretic mobility,[40] it would be expected to carry a greater negative charge in the more basic solution. But an increase in the charge, in the absence of other effects, would be reflected in an increased virial coefficient, although in our experiments the ionic strength was so high that a large effect could not be anticipated.[41] The considerable decrease in A_2' we have observed may arise from the neutralization reaction between the buffer and protein.

The sole instance in which it appeared justified to retain the term in c^2 in equation 1 (expt. G42) involved data at concentrations up to 15 g./l. The curvature of the plot was reasonably well accounted for by a positive third coefficient A_3' of 1.3×10^{-4}. From this and the results given in Table II we find that $A'/(A_2')^2M' = A_3/A_2^2M = 1.0$. We make no claim as to the experimental significance of this figure but only note for comparison that the value of this quantity is $^5/_8$ for the interactions of hard spheres of equal size, less for "soft" spherical models,[42] and very small for extremely asymmetric shapes such as thin rods.[43]

Comparisons of the type discussed in the preceding section between systems at *p*H 9.5 with and without hexamethylene glycol could not be made since in the glycine buffer fibrinogen was found to form aggregates which broke down, at least in part, upon dilution or upon addition of the glycol. The Zimm plots shown in Fig. 1 constitute evidence for this assertion: plot B for the solution containing glycol is normal in appearance for a solute with positive second virial coefficient while plot A for the system without glycol shows a non-linear increase in $Kc/R(\theta)$ as c approaches zero, the behavior expected for a solute containing aggregates dissociable upon dilution. The solutions used to obtain both plots

(38) J. T. Edsall, H. Edelhoch, H. Lontie and P. R. Morrison, *J. Am. Chem. Soc.*, **72**, 4641 (1950).

(39) From freezing point measurements and the interionic attraction theory, we estimate β_{33}, β_{35} and β_{55} to be -0.3, $+0.4$ and -0.2, respectively, in the three component system containing 0.49 molal sodium chloride (3) and 0.54 molal hexamethylene glycol (5).

(40) E. M. Zaiser, private communication.

(41) A very extensive investigation by light scattering of the effect of the charge of a macroion in solutions of bovine serum albumin has been made by Edsall, *et al.*[38] An increase in virial coefficient with charge is clearly demonstrated in their results as is the gradual suppression of the effect at increasing salt concentration. An analogous effect is, of course, obtained with the osmotic pressure.[28]

(42) W. H. Stockmayer and E. F. Casassa, *J. Chem. Phys.*, **20**, 1560 (1952).

(43) L. Onsager, *Ann. N. Y. Acad. Sci.*, **51**, 627 (1949).

were prepared from the same fibrinogen stock solution, which had been dialyzed against glycine buffer.

While no systematic study of the appearance of polymers in alkaline fibrinogen solutions was undertaken, further evidence for aggregation was obtained from the clotting behavior of stock solutions held over a period of time under storage conditions normally constituting part of our experimental procedures. A sample of crude fibrinogen, Lot 210, was refractionated by procedure II described above, then divided into two parts, one being dialyzed against phosphate buffer at *p*H 6.2, the other against glycine buffer at *p*H 9.5. During dialysis and afterward the solutions were kept at 5°. Periodically, over a week's time, portions were withdrawn and assayed for clottable fibrinogen with the results presented in Table III.

TABLE III

ASSAY OF FIBRINOGEN SOLUTIONS HELD AT 5°

Buffer	Total protein concn., g./l.	% clottable 35 hr.[a]	72 hr.	119 hr.	170 hr.
Phosphate, *p*H 6.2	26.8	90.1	91.9	90.1	90.4
Glycine, *p*H 9.5	25.7	90.4	85.7	77.9	76.0

[a] Time is measured from the beginning of dialysis against the buffer.

It is clear that the clottability decreased steadily with the passage of time[44] at *p*H 9.5 though not at *p*H 6.2. However, this change in the alkaline medium was evidently associated with an aggregation reaction, for the sample eventually became visibly turbid and its viscosity increased. After 170 hours, a blank assay was run on the alkaline solution; that is, the assay method was followed except that thrombin was not added to the solution. As soon as the concentrated stock was diluted with *p*H 6.3 buffer, in accordance with the normal assay procedure, gel-like material began to form which could be synerized easily. The "clot" obtained in this way was found to contain 29% of the total protein. This substance resembled normal fibrin to the extent that it was insoluble in the original glycine buffer but did dissolve readily in 6 *M* urea.

V. Conclusion

The studies described here show that the addition of hexamethylene glycol to fibrinogen solutions induces effects which are reflected in altered thermodynamic interactions between protein molecules and between protein and the low molecular weight

(44) The clottable fibrinogen content reported as a criterion of purity of the various preparations in this study and the other publications of this series represents the condition of the protein between 24 and 48 hours after the completion of the fractionation procedure and the beginning of dialysis against the buffer.

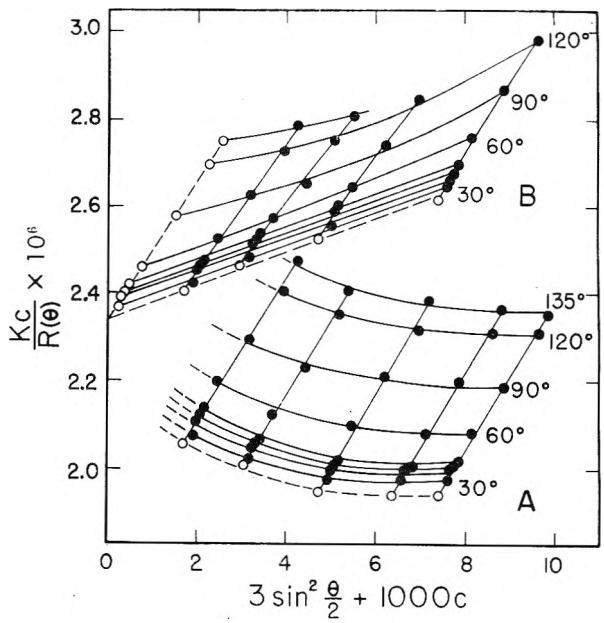

Fig. 1.—Light scattering from fibrinogen (expt. G45): plot A, in glycine buffer at *p*H 9.5 ionic strength 0.45; plot B, in same solvent with 0.50 *M* hexamethylene glycol added.

constituents of the solvent medium. Although these experiments concern fibrinogen, not the activated form resulting from the action of thrombin, it may be expected that the general nature of the changes caused by the glycol applies as well in the case of the activated species—which could not be studied under the conditions employed here—and hence that our observations bear a relation to the inhibitory influence of the glycol on the polymerization of activated fibrinogen to fibrin. The results are at least consistent with earlier speculations[45] that hexamethylene glycol may cause steric interferences to the clotting process in being bound to particular sites on the protein. Similarly, steric effects may arise in connection with the observed expansion of the fibrinogen molecule. Very recently Sturtevant, Laskowski, Donnelly and Scheraga[13] have reported evidence that the clotting reaction involves the formation of intermolecular hydrogen bonds. In this view, the binding of glycol would interfere with the formation of such bonds, possibly by participation of the glycol hydroxyl groups in hydrogen bonding at some of the sites involved in fibrin formation.

We are greatly indebted to Dr. Ethel M. Zaiser and Dr. Irwin H. Billick who aided materially in some of the experimental work and to Professor John D. Ferry who contributed many helpful suggestions in the course of discussions.

(45) J. D. Ferry and S. Shulman, *J. Am. Chem. Soc.*, **71**, 3198 (1949).

VANADYL CHELATES OF TETRAPHENYLPORPHINE AND ITS *PARA*-SUBSTITUTED DERIVATIVES[1]

BY KEIHEI UENO[2] AND ARTHUR E. MARTELL

Contribution of the Department of Chemistry of Clark University, Worcester, Mass.

Received December 27, 1955

The preparation of the vanadyl chelates of tetraphenylporphine, and its *p*-methyl, *p*-methoxy and *p*-chloro derivatives are described, and a study of their ultraviolet, visible and infrared spectra are reported. The ultraviolet and visible spectra are found to resemble those of the Cu(II), Co(II), Ni(II) and Ag(II) chelates of tetraphenylporphine. Infrared frequencies are assigned to bond or group vibrations, and a comparison is made with the corresponding frequencies of chelates of various divalent metals with other ligands. Two bands at 1337 and 535–528 cm.$^{-1}$ are tentatively assigned to V–O stretching and bending vibrations, respectively, and two bands at 1000 and 465–435 cm.$^{-1}$ are tentatively assigned to metal–nitrogen in-plane and out-of-plane vibrations, respectively.

In the course of a general investigation of metal chelate compounds related to the natural and synthetic oxygen carriers, tetraphenylporphine and a number of its *para*-substituted derivatives[3] have previously been synthesized in these laboratories. It was thought of interest to prepare and study the corresponding vanadyl chelates of these compounds, because the presence of a single strongly-bound oxygen atom would provide a comparison with the weaker metal–oxygen bonds of the oxygen carriers. Although the ultraviolet spectra of a number of divalent metal chelates of tetraphenylporphine have been reported,[4] the preparation of the vanadyl chelates of the parent ligand and of its derivatives have not been described. However, a number of vanadyl chelates of β-diketones[5–7] and of the tetradentate ligand bissalicylaldehydeethylenediimine[8,9] have been reported. The ligands kindly made available for this research by Mr. D. W. Thomas are indicated by formula I.

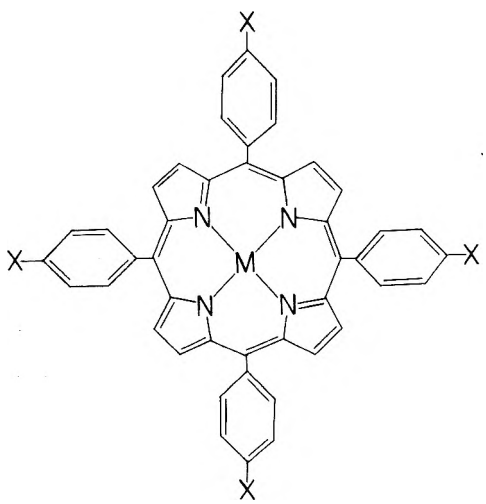

I, *para*-Substituted tetraphenylporphines
X = —H, —CH_3, —OCH_3, and —Cl.

(1) This research was supported by the National Institutes of Health, U. S. Public Health Service, under grant #G3819(C2).

(2) Postdoctoral Research Fellow, Clark University, 1953–55; present address, Dojindo & Co., Kumamoto-shi, Japan.

(3) D. W. Thomas and Arthur E. Martell, *J. Am. Chem. Soc.*, **78**, 1335 (1956).

(4) G. D. Dorough, J. R. Miller and F. M. Huennekens, *ibid.*, **73**, 4315 (1951).

(5) G. T. Morgan and H. W. Moss, *J. Chem. Soc.*, 78 (1914).

(6) A. Rosenheim and H. Y. Mong, *Z. anorg. Chem.*, **148**, 34 (1925).

(7) M. M. Jones, *J. Am. Chem. Soc.*, **76**, 5995 (1954).

(8) P. Pfeiffer, T. Hesse, H. Pfitzner, W. Scholl and H. Thielert, *J. prakt. Chem.*, **149**, 217 (1937).

(9) H. J. Bielig and E. Bayer, *Ann.*, **580**, 135 (1953).

Experimental

Vanadyl Tetraphenylporphines.—A finely-powdered mixture of 300 mg. of tetraphenylporphine and 300 mg. of vanadyl acetate was heated for 48 hours at 190–200° in 100 ml. of glacial acetic acid. The reaction mixture which was green at the beginning changed to brown near the end of the reaction. It was dispersed in water, extracted with benzene, and the benzene extract was evaporated to dryness. The crude product was dissolved in trichloroethylene, filtered and chromatographed on a talc column. Development with additional trichloroethylene resulted in the formation of a cherry-red band which passed through the column, while a green band remained behind. Evaporation of the effluent gave a dark violet solid, which was recrystallized from chloroform–methanol to yield 210 mg. (63%) of dark violet crystals. The green band which remained on the column was eluted with acetone and found by absorption measurements to be tetraphenylporphine.

The vanadyl chelates of the *para*-substituted tetraphenylporphines were synthesized in a similar manner, but differences in the solubilities of each compound in benzene and in trichloroethylene necessitated slight changes in the standard procedure described above. The order of solubility of the vanadyl chelates in the organic solvents employed is *p*-methyl-TPP > TPP > *p*-chloro-TPP > *p*-methoxy-TPP. The individual procedures and yields are listed in Table I.

TABLE I

PREPARATION OF VANADYL TETRAPHENYLPORPHINES

Ligand	Chromatographic solvent	Crystallization medium	Yield,[a] %
TPP[b]	Trichloroethylene	Methanol	63.4
p-Methyl-TPP	Trichloroethylene	Methanol–water	61.7
p-Methoxy-TPP	Trichlroethylene–chloroform	Methanol	65.8
p-Chloro-TPP	Trichloroethylene	Methanol	67.8

[a] Based on tetraphenylporphine. [b] TPP represents tetraphenylporphine.

The Cu(II) and Co(II) chelates of tetraphenylporphine were prepared by the method of Dorough, *et al.*,[4] and purified by the method described above.

Absorption Spectra.—Ultraviolet and visible spectra were measured with a Beckman DU spectrophotometer equipped with a photomultiplier attachment. Spectroscopic grade benzene was used as a solvent.

Infrared absorption spectra were measured with a Perkin–Elmer Model 21 double-beam recording spectrophotometer. Sodium chloride optics were used in the region from 4000 to 650 cm.$^{-1}$, and an interchangeable potassium bromide prism assembly was substituted in order to make measurements in the 650 to 400 cm.$^{-1}$ region. Since the potassium bromide pellet method did not give good resolution for tetraphenylporphines, Nujol and hexachlorobutadiene mulls were employed. The significant spectral bands found for the compounds studied are reported in Table II, together with the assignments which were possible in each case.

Discussion

Although other metal chelates of tetraphenylporphine are best prepared by heating the ligand and metal acetate in glacial acetic acid, various attempts to prepare the vanadyl chelate by this

TABLE II

INFRARED ABSORPTION SPECTRA OF VANADYL CHELATES OF TETRAPHENYLPORPHINES AND ITS *para*-SUBSTITUTED DERIVATIVES

TPP				*p*-CH_3		*p*-OCH_3		*p*-Cl		
Ligand	Cu(II)	Co(II)	VO(II)	Ligand	VO(II)	Ligand	VO(II)	Ligand	VO(II)	Assignments
1597m	1596s	1599s	1599s	1600m	1603s	1610m	1602vs	1595m	1595m	C:C & phenyl
1575m	1575w	1575w	1580[a] w 1575 w	1582m	1582w	1575m	1571m	1582m	1580w	Conjugated phenyl
1560m	1563w	1559w		1560m		1563w	1560w	1565m	1562w	
1545w	1545w	1541w		1543w		1547w		1548w		
	1537w		1533w		1530w		1525m		1530m	
	1525w	1525w								
1512vw	1510w	1508w	1511w	1510w	1506m			1512w	1510w	
						1512vs	1510vs			
								1503w		
1497m	1487m	1490m	1490m	1487m	1485m	1497m	1494vs	1490m	1487vs	Phenyl
1477m				1470m		1475m		1473m		C:N?
			1461w		1460w		1465m		1462w	
								1463m		
								1455w		
				1452m	1453m					$-CH_3$ deformation
1444m	1441s	1442s	1443s	1438w	1443w	1442m	1440m	1443w	1442w	C–H deformation of pyrrole rings
							1410w			
1403m				1400w		1405w		1396m		
	1382w	1363w	1394w						1395m	
				1375m	1378s					$-CH_3$ deformation
1362m				1363m				1367m		
1350m				1347m		1350m		1347m		
	1345s	1348s	1345s							C–N stretching
			1337s		1338s		1337s		1337s	V–O stretching
1325w				1320w				1332m		
1310vw	1307w	1306m	1311w	1307vw	1301w	1303m	1300w	1285vw	1300w	
1286vw	1272w	1278w	1274w	1270w	1270w	1288m	1285s			
1250w		1250w		1245w	1252w			1255w		
						1247vs	1245vs			C–O stretching in methoxy group
		1235w							1235w	
1222w				1224m		1231m		1222m		
1213w				1226m		1214w		1213w		
	1202m	1204m	1204s		1206m		1203m		1206m	
				1198w						
1188m				1183w		1184m		1186w		
1176m	1173s	1175w	1175vs	1168w	1178m			1174m	1178m	
						1173vs	1175vs			$-OCH_3$?
1155m	1156m	1152m	1157w	1150m	1165m	1153m		1155w		Phenyl & *p*-subst. phenyl
				1105w	1104w	1105m	1105m	1100m	1110w	*p*-Subst. phenyl
1080m				1092m	1090m					
								1088s	1089vs	
1070m				1070w				1072m		
	1070s	1075s	1069vs		1066s		1070m			
		1065s								
1055w				1050w				1056w		
1030m				1036w		1034m				
					1033m		1029s			
		1018m		1018w		1010w		1013m		
	1000s	1002s	1001vs		1001vs		1015vs		1002vs	Metal-ligand vibration
999m				997m		989m		990m		
	987s	995s					995vs			
978m				977m		980m		980m		
963s				969s		964s		963m		
							956w		960w	
								941m	937w	C–Cl?
		927w	919w		920m		927m			
		920w		908m						
		898w								

TABLE II (*Continued*)

TPP				*p*-CH_3		*p*-OCH_3		*p*-Cl		
Ligand	Cu(II)	Co(II)	VO(II)	Ligand	VO(II)	Ligand	VO(II)	Ligand	VO(II)	Assignments
873m				883m	883m	875w	882w	872w	880m	
							861w			
								851m	845m	C–Cl stretching
847m		845m		838w		837m		837m		
	830m	830m	832m				847m			
825w				825w		818w		818w		
809m				812m				800s		
795vs	799s	792s	804vs	799vs	805vs	803s	806vs	790vs	803vs	Phenyl
	795s			793s	800vs					
783m				786vs		782s	786m	784s		
				772vs	774vs					
757s	747s	747s	748vs							Monosubst. phenyl
				750w	753w	759m	750w		745w	
744s		720s					738m			
727s		711s	724m	723vs	723s	734s	729s	725s	724s	
720s		705s								Monosubst. phenyl
702s	698s	699s	702s	706s	703m	704w		702m	707m	
694s				697m				699m		
654m	662m	668w	661m	655w	662m	666w	667w	665w	665w	
						644w				
637w				633w		635w	638w	635w	631w	
								629w		
						597s	603s			
559w						554m	561m	556w	570w	
						538m	542m			
			528m				532m		535w	V–O bending.
								505s	502vs	
								492m		
	444w	465w	455s		456w		440w		435w	Metal-ligand vibration
				444m	442m					
419vw			419vw	417w	418w	419w	419w	418w	418w	

[a] A broad band between the frequency regions indicated.

procedure, as outlined by Dorough, *et al.*,[4] were unsuccessful. After a study of the influence of the variation of starting material, temperature and reaction time, it was found that satisfactory yields are obtained by heating the free base and vanadyl acetate in glacial acetic acid in a sealed tube at about 200° for 48 hours. Chromatographic separation and spectrophotometric study of the reaction products revealed the presence of only a small amount of unchanged tetraphenylporphine in addition to the main reaction product.

The absorption spectrum of vanadyl tetraphenylporphine, illustrated in Fig. 1, is quite similar to those of the corresponding copper(II), nickel(II), cobalt(II) and silver(II) chelates described by Dorough, *et al.*[4] The visible and ultraviolet absorption spectra of the *p*-substituted tetraphenylporphine free bases have been noted to be quite similar to those of the parent compound,[3] with slight shifts in the positions of the bands as the result of substitution in the benzene rings. The change in the absorption spectra of the *para*-substituted porphines which occurs on coördination with the vanadyl ion, was found to be almost the same as occurs in tetraphenylporphine. The characteristics of the absorption bands of the metal chelates are listed in Table III.

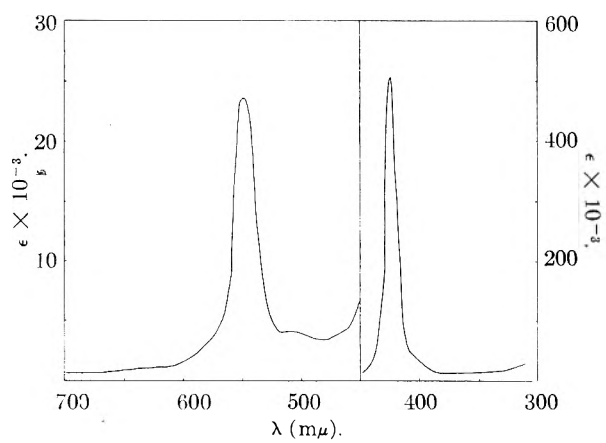

Fig. 1.—Visible and ultraviolet absorption spectra of tetraphenylporphine-VO(IV) in benzene.

TABLE III

VISIBLE AND ULTRAVIOLET ABSORPTION BANDS OF VANADYL *para*-SUBSTITUTED TETRAPHENYLPORPHINES IN BENZENE

Ligand	Molarity × 10^5	λ_{1max}, mμ	ϵ_1 × 10^3	Molarity × 10^5	λ_{2max}, mμ	ϵ_2 × 10^3
TPP	1.40	548	23.6	0.28	424	509
p-Methyl-TPP	0.99	548	23.3	.198	425	530
p-Methoxy-TPP[a]	1.17	548	21.5	.117	429	441
p-Chloro-TPP	0.86	548	26.2	.172	425	564

[a] Additional weak absorptions were observed at 590 mμ (ϵ 4.6 × 10^3), 512 mμ (ϵ 3.6 × 10^3) and 48[illegible] mμ (ϵ 3.0 × 10^3).

The electronic configuration in the outer orbitals of vanadium in the vanadyl porphine complexes may be illustrated schematically as

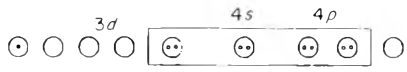

The strong binding of the metal by the tetradentate ligand is probably covalent, as it is with the other transition metals. Thus, a set of dsp^2 orbitals of the metal, which correspond to a square-planar arrangement of covalent bonds, would be filled by four electron pairs donated by the ligand. If it is assumed that the V–O bond (Fig. 2) is ionic, a configuration with one unpaired electron would be expected. The only evidence for the covalent character of the metal–ligand bonds comes from the absorption spectra which fall in the same class as the spectra of the nickel(II) and cobalt(II) tetraphenylporphines, which have been shown by magnetic measurements to be covalent. In the observed visible spectra of tetraphenylporphine–VO(IV), illustrated in Fig. 1, any possible weak absorption bands arising from forbidden d-orbital transitions have been completely masked by the very intense K-type band at 548 mμ.

Infrared study of the *para*-substituted derivatives of the tetraphenylporphine free bases has been reported elsewhere,[3] and the following discussion will be limited to the interpretation of absorption spectra of the metal porphine chelates. However, the study of the spectra of the metal derivatives has resulted in the assignment of a vibration in the free bases. The weak absorption of tetraphenylporphine and its derivatives near 3350 cm.$^{-1}$ was found to be absent in all metal chelates. This absorption is therefore assigned to the hydrogen bonded N–H stretching vibration of the porphines, since, in the metal chelates, both hydrogens are replaced by the metal ion.

The main absorption bands of the metal chelates, which appear at around 1600 cm.$^{-1}$, and at lower frequencies, are listed in Table II.

Since both phenyl rings and C=C bonds are present, strong absorption bands would be expected in the double bond region. Thus, the first absorption at 1595–1610 cm.$^{-1}$, which is fairly constant in position, is due to both C=C and aromatic C=C stretching vibrations. Another absorption band at 1575–1582 cm.$^{-1}$, which is also stable in its position, is assigned to conjugated C=C vibrations in the phenyl rings. It is interesting to note that the first absorption, which has medium intensity in the free base, increases in intensity on metal chelation; however, the second band decreases in intensity.

It would be expected that absorption bands would be found which correspond to C=N stretch and N–H deformation for the ligand, and to C=N stretch for the metal chelate. However, the two or three absorptions occurring between 1560 and 1510 cm.$^{-1}$ cannot be assigned to these modes of vibrations with any degree of certainty. The bands of the free bases shift or split into several bands and also undergo a change of intensity when the hydrogens are replaced by a metal ion.

Another absorption of intermediate intensity at 1497–1485 cm.$^{-1}$, which undergoes little change of position on metal chelation, is assigned to the skeletal vibration of the phenyl rings. The next

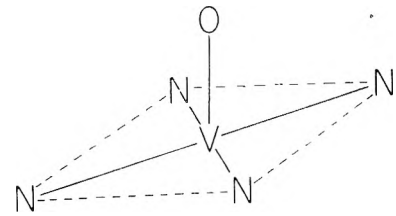

Fig. 2.—Steric configuration of VO in tetraphenylporphine-VO(IV).

band at 1444–1438 cm.$^{-1}$ which does not shift appreciably when the metal chelate is formed from the free base, is assigned to C–H deformation vibration of the porphine ring.

Carbon–hydrogen deformation vibrations of phenyl rings also should give rise to absorptions in the frequency range of 1225–650 cm.$^{-1}$. Thus an absorption band at around 1155 cm.$^{-1}$ is assigned to phenyl ring deformation, and an additional band at around 1105 cm.$^{-1}$ in the spectra of the *para*-substituted derivatives is assigned to a *para*-disubstituted phenyl ring deformation vibration. Another set of bands of very strong intensity at around 800–780 cm.$^{-1}$ are also assigned to a C–H deformation vibration of the phenyl rings.

In *para*-substituted derivatives, there are some additional absorptions which can be assigned to each substituent. Two bands at 1453–1452 cm.$^{-1}$ and 1378–1375 cm.$^{-1}$ of the *para*-methyl derivative are assigned to a $-CH_3$ deformation vibration; very strong absorptions at 1247–1245 cm.$^{-1}$ and at 1173–1175 cm.$^{-1}$ of the *para*-methoxy derivative are assigned to the $-OCH_3$ group; and an absorption at 851–845 cm.$^{-1}$ and probably another band at 941–937 cm.$^{-1}$ of the *para*-chloro derivative are assigned to C–Cl stretching vibrations.

There are additional groups of bands which are characteristic of the ligands or the metal chelates, and the latter group may be subdivided further into two groups, one of which contains absorption bands characteristic of the vanadyl chelates, while the other includes a number of bands which seem to be common to the other divalent metal chelates. An absorption band which appears at 1477–1470 cm.$^{-1}$, is observed only in the free bases, and not in the metal chelates. In the vanadyl chelates, a new band occurs in a slightly lower frequency region. The frequency of this band in the ligands is probably too low to be assigned to N–H deformation. The band is probably associated with the stretching vibration of conjugated C=N bonds, which probably undergo a change of bond order and mode of vibration when the ligand is coördinated with a metal ion.

The three absorptions observed at around 1400, 1360 and 1350 cm.$^{-1}$ are characteristic of the ligands. In the metal chelates of tetraphenylporphine, a new band of strong intensity is found at around 1345 cm.$^{-1}$, which is, however, absent in the metal chelates of the *para*-substituted ligands. These bands are tentatively assigned to C=N vibrations.

The absorption found at 1338–1337 cm.$^{-1}$ is characteristic of all vanadyl chelates, and cannot be found either in the ligands nor in the chelates of copper and cobalt. This absorption is rather

strong and is tentatively assigned to the V–O stretching vibration.

The steric configuration of five-coördinated vanadyl chelates have been discussed previously.[7] For the purposes of discussion in the present work, it is considered permissible to assume the structure to be that shown in Fig. 2. Such a structure is also supported by some preliminary measurements which indicate a significantly large dipole moment for vanadyl tetraphenylporphine.[10] This dipole moment must be due to the asymmetrical configuration of the V–O bond, which is normal to the plane of the porphine ring. The ligand is symmetrical and should not contribute to the dipole moment.

It is possible to estimate roughly the force constant of the V–O bond by the use of the simple equation[11] where ν is the absorption frequency in

$$\nu = 1307\sqrt{k/\mu}$$

wave numbers, k is the force constant for the stretching vibration and μ is the reduced mass which can be calculated from the masses of two bodies by $\mu = m_1m_2/(m_1 + m_2)$. The calculated value is 12.65×10^5 dyne/cm., which is about the same as the value of the C=O stretching force constant ($k_{C=O}$ (acetone) $= 12 \times 10^5$ dyne/cm.). The value obtained for the V–O bond is rather high in comparison with the value 7.54×10^5 dyne/cm., determined by Raman spectra,[12] for the force constant of the V–O stretching vibration in $VOCl_3$. However, the oxidation states, and the arrangement of electrons in the metal orbitals are different, and a difference in the bonding force of vanadium to oxygen would therefore also be expected.

The strong sharp band at 1015–1000 cm.$^{-1}$ is specific for all metal chelate compounds studied, while all ligands have a band of medium intensity at slightly lower frequency. The bands found for the metal chelates are unusually strong in comparison with the band of the ligand. Since this band is found not only in the vanadyl chelates but also in the copper and cobalt chelates, it cannot be due to an absorption related to the V–O vibration. The modes of vibration of the central metal ion in the metallo-porphines are both in-the-plane and out-of-the-plane of the porphine ring. Both modes of vibration result in changes of dipole moment and are, therefore, infrared active. Very few assignments of metal-ligand vibrations have been reported in the literatures. Several absorption bands below 700 cm.$^{-1}$ in the metal chelates of acetylacetone[13] and of bis-acetylacetone-ethylenediimine and related compounds[14] were assigned to metal–ligand vibrations. The extraordinary stability of the metalloporphines, however, indicates that the metal–ligand bonds are much stronger in metalloporphines than in the metal chelates of acetylacetone and bis-acetylacetone-ethylenediimine. This stabilization can be explained on the basis of the strong resonance effect of the porphine ring, which imparts more double bond nature to the metal–ligand bonds than would be true of the metal chelates formed from other ligands.

Since one can expect, therefore, that the metal–ligand absorptions would occur in a higher frequency region, the strong absorption gand at 1015–1000 cm.$^{-1}$ is assigned to the in-the-plane metal–ligand vibration, which should appear at higher frequency than the out-of-the-plane vibration.

In the lower frequency region another group of absorptions are found which are characteristic of all metal porphine chelates The frequency of these bands shifts considerably as one passes from one metal to another, and the intensity of the bands also varies from strong to weak. In the case of copper and cobalt chelates of tetraphenylporphine and of the vanadyl chelate of *p*-methyltetraphenylporphine, one band is missing; however, all of these bands are characterized by the fact that no corresponding bands can be found in the ligands. Similar bands in this region were observed in the metal chelates of bis-acetylacetone-ethylenediimine and its analogous compounds, and were also assigned to metal–ligand vibrations.[13] Thus the absorption bands in the 535–528 cm.$^{-1}$ region of all the vanadyl tetraphenylporphines with the exception of the *p*-methyl derivative, and an absorption which is observed in all metal porphine chelates in the region of 465–435 cm.$^{-1}$, are assigned to metal–ligand vibrations. Although it is not possible to assign each band to a specific mode of vibration, all of these bands correspond to a relatively feeble elastic force. One might tentatively assign the band at 535–528 cm.$^{-1}$ to the V–O bending vibration, and the band at 465–435 cm.$^{-1}$ to the out-of-plane deformation vibration of metal–nitrogen bonds.

(10) K. Ueno and A. E. Martell, unpublished results.

(11) L. N. Ferguson, "Electronic Structures of Organic Molecules," Prentice-Hall, Inc., New York, N. Y., 1952, p. 231.

(12) H. J. Eichhoff and F. Weigel, *Z. anorg. allgem. Chem.*, **275**, 267 (1954).

(13) J. Lecomte, *Disc. Faraday Soc.*, **9**, 108 (1950); C. Duval, R. Freymann and J. Lecomte, *Bull. soc. chim., France*, 106 (1952).

(14) K. Ueno and A. E. Martell, THIS JOURNAL, **59**, 998 (1955).

A PHASE RULE STUDY OF THE SYSTEM ZINC OXIDE–CHROMIUM TRIOXIDE–WATER AT 25°[1]

BY A. E. WOODWARD,[2] E. R. ALLEN AND R. H. ANDERSON

Contribution from the School of Chemistry, Rutgers University, New Brunswick, New Jersey

Received January 3, 1956

A phase diagram study at 25° has provided evidence for the existence of four compounds: $2ZnO \cdot CrO_3 \cdot H_2O$, $1.5ZnO \cdot CrO_3 \cdot 3H_2O$, $ZnO \cdot CrO_3 \cdot 2H_2O$ and $ZnO \cdot 2CrO_3 \cdot 2H_2O$ which have the same $ZnO:CrO_3$ molar ratios as those reported previously.[3-6] A series of solid solutions was indicated between the $ZnO:CrO_3:H_2O$ molar ratios of 4.7:1.0:3.7 to 3.4:1.0:2.6. Chromium trioxide was found to be the solid in equilibrium with the final portion of the liquidus curve.

Introduction

Among the variety of inorganic pigments used in protective coating formulations, certain $ZnO–CrO_3–H_2O$ compositions have become increasingly important and have been found to be especially useful as corrosion inhibitors for metals exposed to unfavorable environments such as sea water. The $ZnO–CrO_3$ compositions of interest, reported as compounds at 25°, have been those of low water solubility and high ZnO content such as zinc tetroxy chromate $5ZnO \cdot CrO_3 \cdot 4H_2O$,[7] zinc trioxychromate $4ZnO \cdot CrO_3 \cdot 3H_2O$[3] and zinc dioxychromate $3ZnO \cdot CrO_3 \cdot 2H_2O$.[3]

Although the chromates of zinc have great commercial interest, little has been published until very recently to show the existence of compounds in these systems. The only phase rule study at 25° of the $ZnO–CrO_3–H_2O$ system reported up to this time is that of Gröger.[3] That investigation did not include the entire range of liquid–solid equilibrium mixtures nor did it show the existence of zinc tetroxy chromate as a compound. Therefore to elucidate further the phase relations in this system and to obtain a more complete phase diagram at 25°, the investigation to be reported herein was carried out. In the first phase of this study mixtures of zinc oxide, chromium trioxide and water were made and the liquid and paste samples were analyzed for zinc and chromium; in one area of the phase diagram it was also necessary to analyze dried samples prepared independently of the other ones. To confirm the results found in the first part of this work, the region of low solubility was further investigated independently using improved methods of mixing and analysis; in this part the paste samples were taken to dryness and then analysed in conjunction with the liquid phases.

Experimental Procedures

In the first part of this study reagent grade zinc oxide, reagent grade chromium trioxide and distilled water were brought together to give mixtures of five to ten grams of solids in 100 g. of solution in one of the following ways: 1. To a "slurry" of zinc oxide in water a solution of chromium trioxide was added. 2. A saturated solution of zinc oxide and chromium trioxide was added to a zinc oxide "slurry" in a water bath at 25°. 3. To a zinc oxide "slurry" in an ice-bath a saturated solution of zinc oxide and chromium trioxide plus solid chromium trioxide was added. 4. Solid zinc oxide was added to a saturated chromium trioxide solution plus solid chromium trioxide in an ice-bath.

After the initial mixing operation, the solid phase and a portion of the liquid phase were ground to a smooth paste in a mortar; this was found to hasten greatly the attainment of equilibrium. The mixtures were transferred to 125-ml. erlenmeyer flasks fitted with ground-glass stoppers, completely immersed in a water-bath at 25 ± 0.5°, and slowly rotated until equilibrium conditions were believed to have been approached. The time necessary for the mixtures to approach equilibrium was determined by analysis of the liquid phase and paste, as described below, of a number of mixtures, chosen to represent the complete liquid–solid range, at 3 to 4 day intervals after a minimum time of 3 to 4 days.

Samples of the liquid phase and the paste were obtained by one of the following methods:

A. The mixture was subjected to vacuum filtration, a liquid sample taken, and the paste pressed between pieces of filter paper to further remove the liquid phase. The complete operation required 5 to 10 minutes.

B. The mixture was allowed to stand immersed in the bath for two to five hours and then a sample of the liquid phase was drawn off. After removal of the excess liquid by decantation, the paste was pressed between pieces of filter paper. The latter operation was not used for mixtures with a high chromium trioxide content since they were believed to attack the paper.

The liquid and paste samples were then weighed, the paste dissolved in the least amount of 6 *N* sulfuric acid and the samples diluted to a given volume. Since known volumes of the liquid phase were taken as samples, a measure of the density was obtained. However, in regions of high solubility these measurements would be subject to a "drainage error."

The iodometric method of Brizzolara, Denslow and Rumbel[8] was used to analyze for chromate. Zinc was precipitated from a basic solution with 8-hydroxyquinoline essentially according to the procedure given for magnesium by Kolthoff and Sandell[9]; the precipitate was dissolved and determined volumetrically with standard $KBrO_3$ and $Na_2S_2O_3$ by the procedure given by the same authors.[10] For zinc oxide samples of 35 mg., analysis by this method gave an error of ±0.7%. Reagent grade materials were used in the analytical procedures.

To determine certain portions of the solidus curve, dry powders were prepared from pastes obtained by the methods given above. As a check on the drying conditions, in some cases, two samples from the same mixture were dried at different temperatures; essentially the same result was found for a given sample whether dried at 25° for 11 days or for 13–20 hours at 100°.

(1) This work was carried out under the sponsorship of the Office of Naval Research as a part of a larger research program under contract Nonr 404(06). Reproduction in whole or in part is permitted for any purpose of the United States Government.

(2) Department of Chemistry, The Pennsylvania State University, University Park, Pennsylvania.

(3) M. Gröger, *Z. anorg. Chem.*, **70**, 135 (1911).

(4) M. Gröger, *ibid.*, **66**, 7 (1910).

(5) E. Hayek, H. Hatzl and H. Schmid, *Monatsh.*, **85**, 92 (1954).

(6) W. Feitknecht and L. Hugi-Carmes, *Helv. Chim. Acta*, **37**, 2093, 2107 (1954).

(7) R. W. Leisy, U. S. Patent 2,251,846 (August 5, 1941); British Patent 547,859 (September 15, 1942); W. H. Kittelberger, *Ind. Eng. Chem.*, **34**, 363 (1942).

(8) A. A. Brizzolara, R. R. Denslow and S. W. Rumbel, *Ind. Eng. Chem.*, **29**, 656 (1937).

(9) I. M. Kolthoff and E. B. Sandell, "Textbook of Quantitative Inorganic Analysis," 3rd Ed., The Macmillan Co., New York, N. Y., 1952, pp. 362–363.

(10) Ref. 9, pp. 607–608.

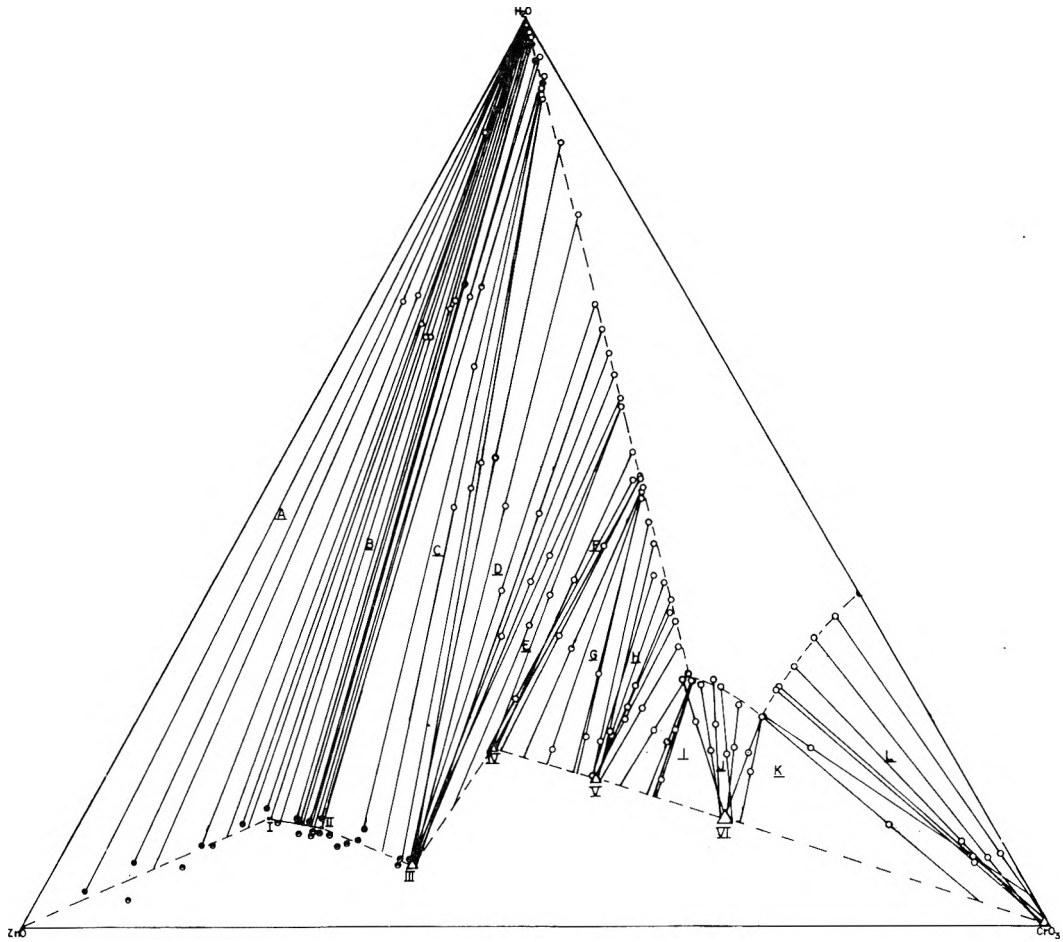

Fig. 1.—Phase rule diagram of the $ZnO-CrO_3-H_2O$ system at 25°: liquid-paste analyses (○); powder analyses (◓); and liquid-powder analyses (●).

In the second phase of this investigation,[11] to a smooth paste of zinc oxide in water, formed by using a Vibratory Mixer,[12] a solution of chromium trioxide was added slowly while stirring or vibromixing. The samples were placed in 4-ounce wide-mouth bottles with screw tops and 1/16 inch polyethylene liners, then immersed and rotated as given above in a water-bath at 24.9 ± 0.1°. Upon removal of the sample bottles from the bath, the liquid phase was filtered off under vacuum, the paste being pressed with a rubber dam to force liquid from it. The paste was weighed and dried to constant weight at 105–115°. The dried sample was pulverized and thoroughly mixed, then dissolved in 6 *N* H_2SO_4 and analyzed as given above.

Experimental Results

The results of the liquid–paste analyses are listed in Table I along with the density of the liquid phase, the time the mixture was in the bath and the section of the phase diagram these data define. The values for % ZnO and % CrO_3 are the mean of two determinations which for values of 10% by weight and above agreed within 0.2 weight % and below 10% by 0.02 weight %. The results of the experiments to determine when equilibrium was established under the conditions of this study showed that after 6 to 8 days there were no appreciable changes in the compositions of the liquid or solid phases. The differences in % ZnO or % CrO_3 for samples removed after 3 to 4 days in the bath and those removed after 6 to 7 days were not found to exceed 0.1; although the magnitude of this change is large with respect to the liquid phase values in the region of low solubility, it is within the error in plotting the data and should not affect appreciably the determination of the solid phase composition.

To check the results of the liquid–paste and dried powder analyses in the range of low solubility, additional studies were conducted independently using a refined method of sample mixing (see Experimental Procedures). Table II summarizes the results of these liquid–powder analyses. Results of duplicate titrations for numbers 14, 15, 16 and 17 showed agreement for % CrO_3 within ±0.001 weight % for the liquid phases, while for the solids it was within ±0.2 to 0.3 for % ZnO and ±0.02 for % CrO_3. In four cases the composition of the solid has been corrected for the amount of liquid present when drying of the paste was started.

The data given in Tables I and II along with the values found by analyses of dried powders, to supplement the data in Table I, are shown plotted on a triangular diagram in Fig. 1.

The data in area B of the phase diagram indicate that a series of solid solutions exists from 69.8% ZnO, 18.2% CrO_3 (I) to 65.3% ZnO, 23.7% CrO_3 (II). The liquid compositions with which the solid solutions are in equilibrium have the invariant points at <0.01% ZnO, 0.004% CrO_3 and 2.4 ± 0.4% ZnO, 5.4 ± 0.4% CrO_3 as limits. The molar

(11) Carried out by R. H. Anderson.

(12) Purchased from A. G. für Chemie, Apparatebau, Zurich.

TABLE I

ANALYTICAL RESULTS OF LIQUID PHASE AND PASTE ANALYSIS AT 25°

Time in bath at 25°, days	Density, g./ml.	Liquid phase: % ZnO by wt.	Liquid phase: % CrO_3 by wt.	Paste: % ZnO by wt.	Paste: % CrO_3 by wt.	Section of phase diagram[a]
5	...	<0.01	<0.01	27.9	3.20	$A^{1,5}$
5	...	<0.01	<0.01	26.0	4.30	$A^{1,5}$
3	...	<0.01	<0.01	10.4	2.08	$A^{1,5}$
3	0.998	<0.01	<0.01	27.3	6.15	$A^{1,5}$
3	...	0.04	0.08	27.6	7.41	$B^{1,5}$
5	1.000	0.21	0.34	27.1	7.79	$B^{1,5}$
5	1.002	0.47	0.90	23.7	8.18	$B^{1,5}$
6	...	0.74	1.37	22.7	8.26	$B^{1,5}$
6	1.016	0.95	1.89	20.8	8.32	$B^{1,5}$
7	1.032	1.36	3.40	21.0	9.47	$B^{1,5}$
11	1.052	1.62	4.75	19.4	10.10	$B, C^{1,5}$
4	1.063	2.88	5.54	24.5	13.7	$C^{1,5}$
5	1.056	2.45	5.20	34.3	19.4	$C^{1,5}$
6	1.066	2.60	5.72	31.7	20.0	$C^{1,5}$
6	1.073	2.85	6.01	29.2	19.6	$C, D^{1,5}$
4	1.132	3.73	10.0	27.6	20.7	$D^{1,6}$
4	1.216	6.00	15.5	29.3	24.2	$D^{1,6}$
5	1.323	9.45	22.0	34.4	28.4	$D^{1,6}$
4	1.354	10.1	24.1	26.6	27.8	$D^{1,6}$
4	1.390	10.8	26.0	37.0	30.9	$D^{1,6}$
5	1.429	11.5	27.7	31.2	30.8	$D^{1,6}$
3	...	12.2	29.5	27.9	31.2	$D^{1,6}$
4	1.490	12.6	30.1	33.6	33.0	$E^{2,6}$
5	...	12.6	29.9	30.0	33.4	E, F
3	1.550	14.1	33.6	26.8	34.9	$F^{2,6}$
4	1.588	15.7	35.1	39.1	35.7	$F^{2,6}$
11	...	14.8	35.8	22.1	35.9	$F^{2,6}$
3	1.602	14.6	35.7	31.4	36.5	$F^{2,6}$
4	1.598	15.0	36.6	30.8	38.3	$G^{2,6}$
6	1.608	15.4	36.7	38.3	42.0	$G^{2,6}$
11	...	15.8	37.0	29.2	42.4	$G^{2,6}$
6	1.620	15.4	36.5	34.4	44.5	$G^{2,6}$
7	1.688	16.4	39.0	33.3	46.2	$H^{3,6}$
7	1.742	17.1	40.7	31.8	46.6	$H^{3,6}$
5	1.738	18.9	42.4	35.9	47.4	$H^{3,6}$
5	1.793	18.3	43.8	31.9	47.0	$H^{3,6}$
5	1.878	18.6	45.4	26.8	46.7	$H^{3,5}$
5	...	19.4	46.0	28.7	47.0	$H^{3,5}$
7	1.865	19.4	47.0	29.6	47.4	$H^{3,6}$
4	...	20.5	48.7	27.4	48.5	$H^{3,6}$
4	1.925	21.1	51.0	27.5	50.7	$I^{3,6}$
8	...	21.1	51.7	26.9	52.7	$I^{3,6}$
5	...	21.1	52.0	25.4	52.8	$I^{3,6}$
4	...	21.0	52.0	29.5	54.2	$I^{3,6}$
4	...	21.9	50.8	23.0	54.4	$I, J^{4,6}$
5	2.07	20.4	52.9	23.2	57.4	$J^{4,6}$
5	1.965	18.8	53.8	21.2	56.5	$J^{4,6}$
13	2.07	18.6	55.0	21.8	59.1	$J^{4,6}$
13	...	17.9	57.6	20.7	59.5	$J^{4,6}$
7	1.970	16.3	60.6	19.6	61.2	$J, K^{4,6}$
5	2.13	16.5	60.7	20.5	62.4	$K^{4,6}$
6	...	16.4	60.5	10.0	78.7	$K^{4,6}$
5	2.06	16.0	60.8	13.3	67.0	$K, L^{4,6}$
4	...	13.4	60.5	3.9	89.0	$L^{4,6}$
5	...	12.5	60.6	3.7	88.6	$L^{4,6}$
4	...	10.3	61.0	3.9	86.6	$L^{4,6}$
4	...	6.9	61.4	2.3	90.0	$L^{4,6}$
4	...	3.6	62.3	0.78	91.0	$L^{4,6}$
1	...	...	63.4	...	...	L^{6}

[a] Superscripts [1], mixtures prepared by method 1, [2], mixtures prepared by method 2, [3], mixtures prepared by method 3, [4], mixtures prepared by method 4, [5], liquid and paste samples obtained by method A, [6], liquid and paste samples obtained by method B.

TABLE II

ANALYSIS OF LIQUID AND SOLID PHASES

Mixture no.	Time in bath, days	Liquid phase: % ZnO by wt.	Liquid phase: % CrO_3 by wt.	Solid phase[a]: % ZnO by wt.	Solid phase[a]: % CrO_3 by wt.	Section of phase diagram
14	0	<0.01	0.004	91.84	4.25	A
15	0	< .01	.006	85.39	7.51	A
16	0	< .01	.005	77.77	13.16	A
17	6	< .01	.002	72.70	16.00	A
18	7	< .01	.003	69.38	17.40	A
19	5.5	.288	.555	67.14[b]	20.91[b]	B
20	5.25	.979	2.047	66.02[b]	22.33[b]	B
21	10	1.442	2.198	64.70[b]	23.40[b]	B
22	9	2.191	5.003	61.12[b]	27.95[b]	C

[a] Dried at 105–115° to constant weight. [b] Value corrected for liquid adhering to solid.

ratios of $ZnO:CrO_3:H_2O$ for the two limiting solid solutions are 4.7:1.0:3.7 and 3.4:1.0:2.6. The end-points of the three solidus regions bounding portions A, B and C were taken as the points of intersection of the solidus lines determined by drawing the best line through the points found by powder analysis; these intersections are found to be consistent with the available liquid–paste and liquid–powder data. The values for the two sets of dried samples when plotted in Fig. 1, although showing differences in the % H_2O of 1 to 2% are considered to be in satisfactory agreement to give approximate solidus lines. The differences found in Sections B and C are probably due to the corrections made in the data from Table II. It can be seen that the two sets of data, obtained by independent investigators, separately indicate solid solutions in this region and also are in close agreement concerning the composition of the liquid phase.

In area D of the diagram liquid compositions from the invariant points at 2.4% ZnO, 5.4% CrO_3 to another at 12.6 ± 0.0% ZnO, 30.0 ± 0.1% CrO_3 are in equilibrium with a solid containing 58.4% ZnO and 34.6% CrO_3 (III) corresponding to a $ZnO:CrO_3:H_2O$ molar ratio of 2.0:1.0:1.1 indicative of the compound $2ZnO\cdot CrO_3\cdot H_2O$.

The solid in equilibrium with liquid phases containing from 12.6% ZnO, 30.0% CrO_3 to the next invariant point at 15.4 ± 0.2% and 36.7 ± 0.2% CrO_3 (area F) contains 43.7% ZnO and 36.3% CrO_3 (IV) or a $ZnO:CrO_3:H_2O$ molar ratio of 1.5:1.0:3.1. The compound $1.5\ ZnO\cdot CrO_3\cdot 3H_2O$ is therefore indicated; due to the uncertainty in this point of intersection, the number of moles of water reported here is only approximate and may vary from 2.5 to 3.5.

A third compound found to occur as a stable solid phase (Section H) has 35.7% ZnO, 47.9% CrO_3 (V) giving a $ZnO:CrO_3:H_2O$ molar ratio of 0.9:1.0:1.9. The compound $ZnO\cdot CrO_3\cdot 2H_2O$ is therefore found as the solid which appears to be existing in equilibrium with liquid compositions ranging from 15.4% ZnO, 36.7% CrO_3 to another invariant point at 21.3 ± 0.3% ZnO, 51.5 ± 0.5% CrO_3. As can be seen in Fig. 1, tie-lines are not given connecting either of the invariant points to the point of inter-

section; therefore, there is some possibility of a series of solid solutions occurring in either of these areas accompanied by invariant points.

The existence of a final ZnO–CrO_3 compound under the conditions of this study is shown by the tie-lines defining section J; the % ZnO is 25.5 and the % CrO_3 62.5 (VI) giving a $ZnO:CrO_3:H_2O$ molar ratio of 1.0:2.0:2.1 indicative of the compound $ZnO \cdot 2CrO_3 \cdot 2H_2O$. As can be seen from the figure the % H_2O is doubtful and could vary from 1.5 to 2.5. Although two separate points of intersecting appear to be present in this region, this behavior is probably due to non-equilibrium conditions in some of the samples. The final invariant point contains 16.3 ± 0.2% ZnO and 60.7 ± 0.1% CrO_3.

In the last section of the diagram, CrO_3 is found to be the solid in equilibrium with the final portion of the liquidus curve.

Over the range of composition from <0.01% ZnO, 0.004% CrO_3 to 2.4% ZnO, 5.4% CrO_3 in the liquid phase, the molar ratio of CrO_3:ZnO, although showing a rather large variance in some cases, is found to increase from a value of approximately 1 to 2. From this second invariant point to a composition of 21.3% ZnO, 51.5% CrO_3 the CrO_3:ZnO molar ratio has an apparently constant value of 1.96 ± 0.06. Over the remaining range to the liquid containing only chromium trioxide, the ratio is variable and increases.

Discussion

Although compounds with a zinc oxide content greater than $2ZnO:CrO_3$ have been reported by a number of investigators,[3,5-7] none were shown to exist in ZnO–CrO_3–H_2O equilibrium mixtures at 25° in this investigation. From a phase rule study at 25° Gröger[3] claimed the existence of two compounds in this region, $4ZnO \cdot CrO_3 \cdot 3H_2O$ and $3ZnO \cdot CrO_3 \cdot 2H_2O$. Another compound believed to occur at 25° in this range of low solubility is zinc tetroxy chromate,[7] $5ZnO \cdot CrO_3 \cdot 4H_2O$. The more recent work of Hayek, Hatzl and Schmid,[5] which included conductivity data and X-ray powder diagrams as well as analytical determinations of various liquid–solid equilibrium mixtures at 35°, indicated the presence of the compound $3.5ZnO \cdot CrO_3 \cdot 2.5H_2O$ whereas the compounds reported by Gröger were not found. A more basic compound believed to be identical with zinc tetroxy chromate was also reported by these authors, although the conductivity data did not support their claim. Feitknecht and Hugi-Carmes[6] investigated ZnO–CrO_3–H_2O equilibrium mixtures at 20° by using the Schreinemakers residue method along with special techniques for determining the moles of water also reported the $3.5ZnO \cdot CrO_3 \cdot 2.5H_2O$ compound and another hydrate. By the controlled precipitation from a zinc dichromate solution with standard alkali, the more basic composition $4\text{-}5ZnO \cdot CrO_3 \cdot 3\text{-}4H_2O$ was also obtained; it was found that along with the change in $ZnO:CrO_3$ ratio given above, the composition of the liquid phase in equilibrium changed also indicative of a series of solid solutions. Determinations of the configuration of the solid materials from the composition and X-ray powder diagram led to the proposal that this change is accompanied by a continuous replacement of chromate by hydroxyl ions.[6] The present investigation gives evidence that a series of solid solutions is also present in this area of the phase diagram at 25°; in this case the limiting $ZnO:CrO_3:H_2O$ molar ratios were found to be 4.7:1.0:3.7 and 3.4:1.0:2.6. Although there is some apparent convergence of two tie lines in the region of $3.5ZnO \cdot CrO_3 \cdot 2.5H_2O$ (see Fig. 1), the liquid compositions which could possibly be in equilibrium with this solid are limited to a range containing concentrations of zinc oxide and chromium trioxide of 0.18 and 0.33, respectively, to 0.33 and 0.59 mole/liter. As in the case of the $3.5ZnO:CrO_3$ compound the data present here do not completely rule out the existence of zinc tetroxy chromate as a compound at 25°, but they do greatly limit the range of compositions over which liquid–solid mixtures would contain it as a stable solid phase.

From this investigation the following five compounds are believed to occur as stable solid phases in ZnO–CrO_3–H_2O mixtures at 25°: $2ZnO \cdot CrO_3 \cdot H_2O$, $1.5ZnO \cdot CrO_3 \cdot 3H_2O$, $ZnO \cdot CrO_3 \cdot 2H_2O$, $ZnO \cdot 2CrO_3 \cdot 2H_2O$ and CrO_3. The first of these has been found by other investigators[5,6] at 20 and 35°; Gröger[3] gave 1.5 as the number of moles of water in this compound. Gröger also reported the compounds $1.5ZnO \cdot CrO_3 \cdot {}^1/_2H_2O$ and $ZnO \cdot CrO_3 \cdot H_2O$. Although there is considerable uncertainty in the number of moles of water reported in this study for the $1.5ZnO:CrO_3$ compound, the amount of water is 2 to 3 moles higher than that found by Gröger. Previously published investigations did not include the remaining range of still higher solubility, but the preparations of $ZnO \cdot 2CrO_3 \cdot 3H_2O$ and $ZnO \cdot 2CrO_3$ have been given in another paper.[4] The present study, however, indicates the presence of two molecules of water in this compound, although again there is considerable uncertainty in this figure. The compound $ZnO \cdot 3CrO_3 \cdot 3H_2O$ prepared by Groger[4] was not found.

The molar ratios of CrO_3:ZnO in the liquid phase at 25° as described in the preceding section are in agreement with those obtained at 20 and 35°[5,6] over the region of the solid solutions and the compound $2ZnO \cdot CrO_3 \cdot H_2O$, the range covered by those investigators. The steady increase of this ratio from 2:3 at the point of lowest solubility to 2:1 as that in equilibrium with the $ZnO:CrO_3$ compound at 25° as reported earlier[3] was not found. Concerning the temperature dependence of the solubility, preliminary experiments have indicated that the amount of soluble material, at least in the range of the solid solutions and the next lower invariant point (areas B and C in Fig. 1), decreases with a rise in temperature, the precipitate formed dissolving by lowering the temperature back to 25°. If this is true the limiting ZnO and CrO_3 concentrations should decrease with a rise in temperature. There is some indication of this when the data given here and obtained at 35°[5] are compared for the $2ZnO \cdot CrO_3 \cdot H_2O$ compound. Other comparisons with that study are not possible due to the different results reported for the solid phase. However, comparison with the data obtained at 20°[6] also shows a decrease in both the ZnO and CrO_3 molar concentrations with decreasing temperature. It appears

therefore that further investigations are necessary to resolve this problem.

From the phase diagram it can be seen that the compound $ZnO \cdot 2CrO_3 \cdot 2H_2O$ is completely soluble at 25° after the total amount of water exceeds approximately 28% by weight. However upon addition of greater amounts of water the solution still exists as a saturated one. When water is added to the compounds $ZnO \cdot CrO_3 \cdot 2H_2O$, $1.5ZnO \cdot CrO_3 \cdot 3H_2O$, and $2ZnO \cdot CrO_3 \cdot H_2O$, the solid undergoes a change in composition to a compound, a solid solution, a mixture of compounds or a mixture of a solid solution and a compound containing $ZnO:CrO_3$ molar ratios dependent on the total composition of the final liquid-solid mixture. The amount of soluble material, which can be calculated from the data plotted in Fig. 1, will depend on the final composition, the solubility increasing with the $\%H_2O$ present.

The range of solid compositions of greatest use as corrosion inhibitors for metals is probably the series of solid solutions which show a relatively low solubility. Along with the continuous change of composition which occurs when going from one limiting solid solution to the other a corresponding change in physical and chemical properties should occur.

THE EQUILIBRIA BETWEEN DI-*n*-DECYLAMINE AND SULFURIC ACID

BY KENNETH A. ALLEN

Oak Ridge National Laboratory, Oak Ridge, Tennessee

Received January 9, 1956

Benzene solutions of di-*n*-decylamine have been equilibrated with aqueous sulfuric acid at 25°. The amine salts remain in the organic phase, and the data are interpreted on the basis of association of these species. Equilibrium constants for the formation of colloidally dispersed amine sulfate and for sulfate–bisulfate exchange within the colloid are evaluated. The precipitation of pure di-*n*-decylamine bisulfate at a given acid activity independent of total amine concentration is attributed to a maximum bisulfate content for a stable colloidal dispersion corresponding to approximately equal moles of sulfate and bisulfate.

I. Introduction

High molecular weight amines in organic diluents have been shown to extract a wide variety of substances from aqueous solutions. Some of these extractions are useful in analytical procedures[1] and others show promise of possible application to industrial purifications.[2] The fundamental processes underlying this behavior of the long chain amines are therefore of some interest.

Solubility and extraction data obtained in the systematic studies have provided considerable evidence indicative of association of the amine salts in the organic phases.[2] Titrations of benzene solutions of di-*n*-decylamine (hereinafter this amine will be referred to as DDA) with sulfuric acid have been shown by Baes to support this view, and the extraction of iron by DDA sulfate has been interpreted from this standpoint.[3] The mole per cent. of amine bisulfate formed by DDA in the solvent Amsco G was found by Horner to be a very nearly linear function of the *p*H of half molar sulfate aqueous phases containing sulfuric acid and sodium sulfate.[2]

The present investigation was undertaken with the object of obtaining more evidence as to the nature of the equilibria involved in these reactions. In a previous paper it was shown that the sulfuric acid extraction behavior of tri-*n*-octylamine was consistent with a quantitative treatment based on partial aggregation of the sulfate species.[4] The present results are in accord with those of the earlier work, and the treatment is along the lines of that found applicable in the case of the tertiary amine, although specific differences in behavior between the two amines have been observed.

II. Experimental

Materials.—The di-*n*-decylamine used in this work was prepared in the following way.[5] Armeen 10D (a mixture of 8, 10 and 12 carbon straight chain saturated primary amines, principally *n*-decylamine) was fractionated in a Podbielniak-type still; 900 g. of product with a boiling range of 216–217° at 725 mm. was collected. This material was heated in a reaction vessel under argon with about 200 g. of Raney nickel and 400 ml. of ethyl alcohol. The alcohol was allowed to evaporate slowly without reflux. Rapid ammonia evolution commenced at 140°, continuing until the temperature of the reaction mixture reached 150° over a period of about ten minutes. Further heating for 20–30 minutes raised the temperature to 220° with markedly decreased ammonia evolution. The cooled partially solidified mixture was taken up with chloroform and filtered. Fractional distillation resulted in a center cut of 450 g. of DDA in the boiling range 195–196° at 5.0 ± 0.1 mm.

This material was subjected to both total and differential titrations.[6] The resulting apparent molecular weight was 298.6 (theoretical for DDA 297.6). The primary amine content was found to be less than 0.5%, and the tertiary 3 ± 1%, using the methods referred to. Titration curves constructed from the sulfuric acid equilibration data given in the following section showed inflection points at 98.0 ± 0.5% of theoretical for DDA concentrations in benzene ranging from 0.05 to 0.5 *M*. Assuming tertiary amine to be the only impurity, and that its behavior is similar to that of tri-

(1) E. L. Smith and J. E. Page, *J. Soc. Chem. Ind. (London)*, **67**, 48 (1949); J. Y. Ellenburg, G. W. Leddicotte and F. L. Moore, *Anal. Chem.*, **26**, 1045 (1954); H. A. Mahlman, G. W. Leddicotte and F. L. Moore, *ibid.*, **26**, 1939 (1954).

(2) K. B. Brown, C. F. Coleman, D. J. Crouse, J. O. Denis and J. G. Moore, Classified Report ORNL-1734, May 27, 1954; D. J. Crouse and J. O. Denis, Classified Report ORNL-1859, February 1, 1955; J. G. Moore, K. B. Brown and C. F. Coleman, Classified Report ORNL-1922, June 24, 1955.

(3) C. F. Baes, Jr., unpublished work; Classified Report ORNL-1930, July 25, 1955.

(4) K. A. Allen, THIS JOURNAL, **60**, 239 (1956).

(5) The preparation, purification and analyses of this amine were carried out by W. J. McDowell of this Laboratory.

(6) C. D. Wagner, R. H. Brown and E. D. Peters, *J. Am. Chem. Soc.*, **69**, 2609 (1947); 2611 (1947); C. E. Pifer, E. G. Wollish and M. Schmall, *Anal. Chem.*, **25**, 310 (1953).

n-octylamine, inspection of the comparative titration curves for the latter and DDA (Fig. 1) shows that at the inflection point for DDA only a negligible amount of acid will have been consumed by the tertiary impurity. On this basis the sulfuric acid equilibrations indicate a tertiary amine content of 2.0 ± 0.5%, in agreement, within experimental error, with the value obtained by differential analysis. Free amine concentrations below the equivalence point were therefore calculated from 98.0% of the concentrations given below (*e.g.*, in this range, the 0.05 *M* solution was treated as being 0.0490, the 0.1 *M* solution as 0.0980, etc.).

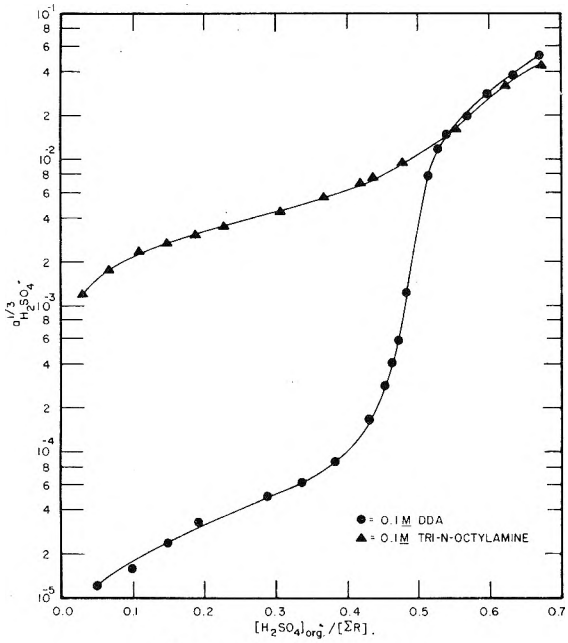

Fig. 1.—Titration curves.

Above the equivalence point the salt forms of DDA and tri-*n*-octylamine behave very similarly, as is shown by Fig. 1. Consequently, in the bisulfate range the tertiary impurity was ignored and all calculations were based on the total concentrations shown. The 0.5 *M* solution was prepared on a weight basis, using the apparent molecular weight obtained by analysis. The other solutions were obtained by dilution from the half molar stock. These benzene solutions were prepared at 25° and stored in a 25.00 ± 0.05° thermostat throughout their period of use. The other materials were of the usual reagent grade furnished by the large chemical supply houses.

Procedure and Analyses.—The apparatus and technique employed for the equilibrations were the same as those described for tri-*n*-octylamine.[4] A series of preliminary rate studies showed that equilibrium was attained by all the DDA solutions *vs.* widely varying amounts of sulfuric acid in at most 30 minutes. The data reported below are based on shaking times of one hour or more at 25.0 ± 0.1°. Aqueous acid concentrations greater than 10^{-3} *M* were determined volumetrically with standard base. The lower sulfuric acid molarities reported were obtained by *p*H measurement, using a Beckman Model G meter and an experimentally determined calibration curve. These results are shown with two and three significant figures, but it should be pointed out that they may be in error by as much as ±10%, and possibly more in the very low range. This source of error, together with the known impurity of the amine, is considered to account for the scatter observed in the points calculated for the data below the equivalence point. The reliability of the data above this point is comparable to that encountered in the case of tri-*n*-octylamine.[4]

Sulfuric acid absorbed into the organic phases was measured by titration with standard sodium ethoxide.[7] When necessary free amine was then determined in the same sample by potentiometric titration with perchloric acid in dioxane.

(7) J. S. Fritz, "Acid–Base Titrations in Non-aqueous Solvents," G. Frederick Smith Chemical Co., Columbus, Ohio, 1952.

III. Results and Discussion

The aqueous sulfuric acid activities used in the graphs and equilibrium constant expressions given below were obtained from Harned and Owen[8] using the graphical method described previously.[4] For brevity and convenience in the following discussion reacting sulfuric acid is written in the undissociated form and the symbol R is used to denote the amine molecule $(C_{10}H_{21})_2NH$. The reaction for normal sulfate formation is

$$H_2SO_4 + 2R = R_2H_2SO_4 \qquad (1)$$

and the corresponding equilibrium constant, assuming true solution behavior and unit activity coefficients for the benzene soluble species, should be

$$K' = \frac{[R_2H_2SO_4]}{a_{H_2SO_4}[R]^2} \qquad (2)$$

Plots of log $a_{H_2SO_4}$ *vs.* log $[R_2H_2SO_4]/[R]^2$ calculated from data obtained below the equivalence point for 0.05, 0.1, 0.2 and 0.5 *M* DDA did not conform to the behavior predicted by (2). The points for the different concentrations exhibited widely separated lines, and there was no indication of any tendency for these lines to approach coincidence at low organic sulfate levels, as was the case with tri-*n*-octylamine. It was therefore tentatively concluded that with DDA aggregation occurs immediately on the formation of the first amine sulfate.

On this basis (2) may be rearranged, giving

$$a_{H_2SO_4}[R]^2 = \frac{[R_2H_2SO_4]_c}{K'} \qquad (3)$$

where the subscript c denotes the colloidal salt of constant activity. The right-hand side of (3) should be a constant, and we write

$$K'' = a_{H_2SO_4}[R]^2 \qquad (4)$$

again assuming unit activity coefficient for the free amine. In Fig. 2 log $a^{1/3}_{H_2SO_4}$ is plotted against log [R].[9] Although the points on this plot exhibit serious scatter, there is no evidence of any systematic departure from the line shown as a function of total amine concentration. There is some indication of a general, and possibly real, curvature toward the theoretical slope at high activities. Along the line, the apparent amine sulfate concentrations vary appreciably (*e.g.*, at [R] = 0.04, the ratio between $[R_2H_2SO_4]$ for the 0.5 *M* data and that for the 0.05 *M* data is *ca.* 45), and it may be concluded, within the experimental error indicated by the observed scatter, that below the equivalence point the relationship between acid activity and free amine con-

(8) H. S. Harned and B. B. Owen, "The Physical Chemistry of Electrolytic Solutions," 2nd Ed., Reinhold Publ. Corp., New York, N. Y., 1952.

(9) As in the case of tri-*n*-oetylamine, bisulfate corrections were found necessary for the low [R] values at high acid activities. These corrections were much smaller here, however, because of the greater basicity of DDA. Free amine concentrations were calculated from the material balance relation

$$[R] = [\Sigma R] - 2[\Sigma S]\frac{1}{1 + X} \qquad (5)$$

where $[\Sigma R]$ and $[\Sigma S]$ denote, respectively, total amine and total organic sulfate in moles per liter, and the equivalent fraction X of bisulfate was obtained from

$$K_2 = \frac{X^2}{a_{H_2SO_4}(1 - X)} = 2600 \text{ (see below).}$$

centration is independent of the amount of salt present.

The line of Fig. 2, being of slope -1 instead of $-3/2$ as predicted by equation 4, leads to an empirical constant of the form

$$K_1 = a_{H_2SO_4}[R]^3 \sim 6 \times 10^{-18}\ (\text{moles/liter})^6 \quad (6)$$

which is consistent with an activity coefficient for the free amine in benzene $\gamma_R \propto [R]^{1/2}$. Tri-*n*-octylamine was found to obey (4) in this region after correcting for a hypothesized distribution of free amine between solvent and colloid, implying at least a constant activity coefficient.

The data from equilibrations in the bisulfate range were treated as in the previous paper[4]; the formation of amine bisulfate is regarded as an exchange reaction, *viz.*

$$2HSO_4^- + R_2H_2SO_4 = 2RH_2SO_4 + SO_4^- \quad (7)$$

The sulfate and bisulfate species are considered to form a series of ideal solutions within the aggregate, and their activities are taken equal to their respective equivalent fractions.[10] Accordingly

$$K_2' = \frac{a_{SO_4} = X^2_{RH_2SO_4}}{a^2_{HSO_4} - X_{R_2H_2SO_4}} \quad (8)$$

Here, for brevity, we put $X = X_{RH_2SO_4} = [RH_2SO_4]/[\Sigma R]$, and since it is apparent from K_1 that in this region only negligible quantities of amine remain uncombined, $X_{R_2H_2SO_4} = 1 - X$. The aqueous ion activity ratio readily can be shown to be proportional to $1/a_{H_2SO_4}$, and we obtain the simpler equivalent expression

$$K_2 = \frac{X^2}{a_{H_2SO_4}(1 - X)} \quad (9)$$

In Fig. 3 $\log X^2/(1 - X)$ is plotted against $\log a_{H_2SO_4}$. Here the 0.05 and 0.1 *M* data are superimposed on a straight line of the slope (unity) required by (9), but systematic departures are evidenced by the data for the two higher concentrations. These departures are in the direction which would be expected for true solution behavior, although their magnitude is by no means sufficient for any actual correlation on this basis. It seems more reasonable to attribute them to failure of the activity relationship assumed for the colloidal species and expressed in (8) as equivalent fractions. The line shown leads to a value for K_2 of 2600 ± 400 $(\text{moles/liter})^{-3}$, with the restrictions that this constant holds only for total amine concentrations between 0.05 and 0.1 *M* and for equivalent fractions of bisulfate less than 0.25.[11] Bisulfate formation in 0.1 *M* DDA equilibrated with half molar sulfate solutions of varying acid activity was found by Baes[3] to be several per cent. less than is shown here in the range over which K_2 is valid. On the plot of Fig. 3, his data would fall between the line and the points for the 0.2 *M* solution; this difference may in part be attributed to uncertainty in the values of $a_{H_2SO_4}$ for the half molar sulfate solutions. Unpublished data obtained with one molar sulfate indicate that this trend continues in at least a qualitatively consistent manner.[12]

(10) A. P. Vanselow, *Soil Sci.*, **22**, 95 (1932); G. E. Boyd, J. Schubert and A. W. Adamson, *J. Am. Chem. Soc.*, **69**, 2818 (1947).

(11) The bisulfate data obtained by Horner[2] for DDA and dilaurylamine in aromatic mineral spirits at about 35° lead to a value for K_2 (as defined by equation 9) of *ca.* 600.

(12) W. J. McDowell, private communication.

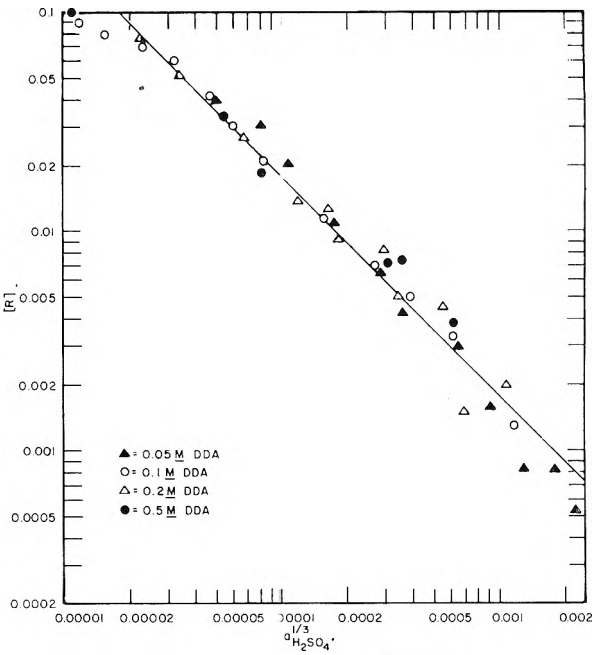

Fig. 2.—Free amine *vs.* $a^{1/3}_{H_2SO_4}$.

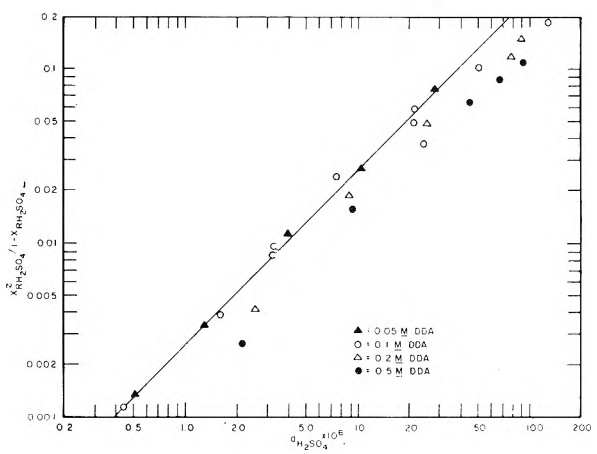

Fig. 3.—Bisulfate equilibria.

The curvature away from the line exhibited by the three more concentrated solutions at higher activities is apparently real, and may be taken as an indication of a gradually decreasing tendency for the salt to absorb more bisulfate. Increasing the aqueous sulfuric acid concentration to still higher levels resulted in the appearance of a precipitate at an acid activity of *ca.* $.6 \times 10^{-4}$. This solid was found to be the pure bisulfate both from direct analysis[12] and material balance differences (see Table I). A rough estimate of the upper limit of its solubility in benzene at 25° was made by contacting successively diluted DDA solutions with large volumes of half molar sulfuric acid. This experiment limited the solubility of the bisulfate to less than 0.001 *M*, by visual inspection of the equilibrated organic phases.

In another series of equilibrations 0.05, 0.1, 0.2 and 0.5 *M* DDA solutions were contacted with successively increasing aqueous concentrations at 25°. Favorably large aqueous/organic phase ratios were used, and at each acid level a sufficient number of

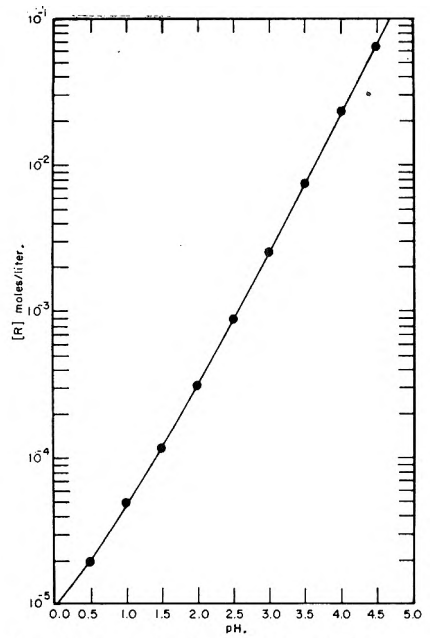

Fig. 4.—Free di-*n*-decylamine molarity in benzene *vs.* *p*H of aqueous sulfuric acid at 25°.

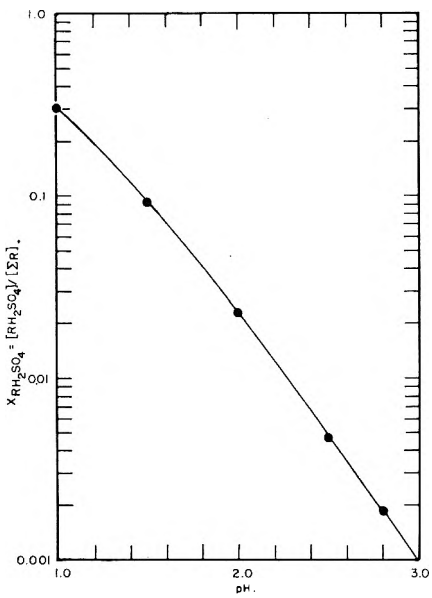

Fig. 5.—Colloid composition as equivalent fraction of di-*n*-decylamine in bisulfate form *vs.* *p*H of aqueous sulfuric acid at 25°. Total amine molarity in benzene must not exceed 0.1 *M*.

equilibrations were made to ensure equilibrium at a known acid activity. By visual inspection, again, it was shown that in all four amine solutions precipitation occurred between $a_{H_2SO_4} = 1.6 \times 10^{-4}$ and $a_{H_2SO_4} = 1.8 \times 10^{-4}$. In the range of amine molarities used it is therefore concluded that this effect is essentially independent of total amine concentration.

The data shown in Table I were obtained in order to further elucidate this phenomenon, with particular emphasis in this case on the composition of the species remaining in solution after an appreciable fraction of the amine has been precipitated. The mole ratios of sulfate to amine in the species remaining dispersed are very close to two thirds, with slight increases for the 0.1 and 0.2 *M* solutions at the higher acid concentrations shown. This ratio corresponds to the composition $(R_2H_2SO_4 \cdot RH_2SO_4)_n$ for the aggregate, and is considered to represent an approximate value for an upper limit of bisulfate content consistent with colloidal stability. In contrast to this behavior of DDA, the bisulfate salt of tri-*n*-octylamine was found to be appreciably soluble in benzene.[4]

TABLE I

EQUILIBRATION DATA WITH PRECIPITATED BISULFATE

		Solution		
[ΣR]	$[H_2SO_4]_{aq}$	[R]	$[H_2SO_4]_{org}$	$[H_2SO_4]_{org}/[R]$
0.1	0.273	0.0212	0.0306	0.69
.1	.365	.0130	.0177	.73
.2	.196	.0766	.111	.69
.2	.297	.0282	.0397	.71
.5	.198	.0550	.0816	.67

		Precipitate		
[ΣR]	$[H_2SO_4]_{aq}$	R(mmoles)	H_2SO_4 (mmoles)	H_2SO_4/R
0.1	0.273	1.388	1.385	1.00
.2	.196	1.778	1.811	1.02
.5	.198	8.368	8.160	0.97

The plots shown in Figs. 4 and 5 are included as a means of presenting the significant results of this investigation in an easily interpreted form. The points were calculated from the equilibrium constants given in the text. Sulfuric acid activities were converted to molarity and then to *p*H graphically, using an experimentally determined calibration curve for the latter conversion. In the case of the bisulfate plot (Fig. 5) the total di-*n*-decylamine molarity in benzene should not exceed 0.1 *M*, although readings at moderately higher concentrations (less than 0.2 *M*) will not be in serious error. Bisulfate precipitation commences at a *p*H of about 0.9. The relationships depicted in Fig. 4 are independent of total amine concentration.

GASEOUS MOLYBDENUM OXYCHLORIDE

BY NEILEN HULTGREN AND LEO BREWER

Radiation Laboratory and Department of Chemistry and Chemical Engineering, University of California, Berkeley, California

Received January 13, 1956

The reaction of MoO_3 with HCl was studied and the formation of the gaseous molecule MoO_2Cl_2 demonstrated. This molecule is probably responsible for the anomalous earlier observations of the reaction of molybdenum metal with hydrogen chloride gas.

N. L. Lofgren[1] ran flow experiments in which a mixture of H_2 and HCl gases was passed over solid molybdenum metal at 1200°K. in a silica system. Assuming a reaction of the form $Mo(s) + xHCl = MoCl_x(g) + x/2\ H_2$, Lofgren found that $x = 4$ satisfied the observed HCl and H_2 pressure dependences. The calculated ΔS for the reaction $Mo(s) + 4HCl(g) = MoCl_4(g) + 2H_2(g)$ gave a ΔS of formation for $MoCl_4(g)$ of +22 e.u. This was in marked disagreement with an estimated value of −15 e.u. and indicated that the proposed reaction was not the correct net reaction.

In the present work it was found that about 10^{-4} atm. of $H_2O(g)$ could suffice to cause the observed volatility of Mo if the reaction were $Mo(s) + 2H_2O(g) + 2HCl(g) = MoO_2Cl_2(g) + 3H_2(g)$. The calculated and estimated entropy values for this reaction are in good agreement. If the formation of molybdenum halides from the reaction of molybdenum with hydrogen chloride gas is to be studied, it will require a very dry non-oxide system to prevent formation of MoO_2Cl_2 gas.

Experimental

(1) **Flow Method.**—HCl was passed over heated MoO_3 and collected in a liquid nitrogen trap. The flow and pressure of HCl were controlled by a series of capillary tubes. After a given time the amount of HCl collected and the weight loss of the MoO_3 were measured. Temperatures were about 480°K. Reproducible results could not be obtained, even when the flow was as low as 9 cc./min.

(2) **Click Gage.**—MoO_3 and HCl were heated in a sealed tube. The pressure was measured with a quartz "click" gage accurate to better than 1 mm. of pressure for several series between 90 and 290°. Between 105 and 290° no deviations from the ideal gas law were noted in the pressure as shown by a typical run presented in Fig. 1. The numbers given for each point indicate the order of taking the measurements. The reaction $MoO_3(s) + 2HCl(g) = MoO_2Cl_2(g) + H_2O(g)$ would show no pressure change. Also, a reaction forming MoO_2OHCl gas would show no pressure change. A reaction such as $MoO_3(s) + 2HCl(g) = MoO(OH)_2Cl_2(g)$ would deviate from the ideal gas law by about 35 mm. of Hg at 250° if the equilibrium constants obtained below are correct. At temperatures below 100° the pressures became too low, indicating formation of the known $MoO_3 \cdot 2HCl$ solid.

Figure 2 presents the results of heating $MoO_3 \cdot 2HCl$ with HCl gas in a sealed tube. The order of the observations is indicated in Fig. 2. Upon initial heating no deviations from perfect gas law were observed up to 100°. As the volatility of molybdenum species is very small at these temperatures, no reactions of any type have taken place. Upon heating above 115° at 475 mm. HCl, dissociation of $MoO_3 \cdot 2HCl$ solid to MoO_3 solid and HCl commenced. The steeply rising portion of the curve represents the HCl pressure in equilibrium with the two solid phases $MoO_3 \cdot 2HCl$ and MoO_3. Upon cooling, the system returned to perfect gas behavior at a higher HCl pressure, indicating that the surface MoO_3 had been reconverted to $MoO_3 \cdot 2HCl$ without reconverting the underlying MoO_3. Figures 1 and 2 correspond to two portions of a pressure *versus* temperature curve at constant volume such as is given in Fig. 3, where the portion corresponding to the univariant three-phase region is independent of volume and amounts of material while the slopes of the straight-line sections depend upon the amounts of material as well as the volume of the

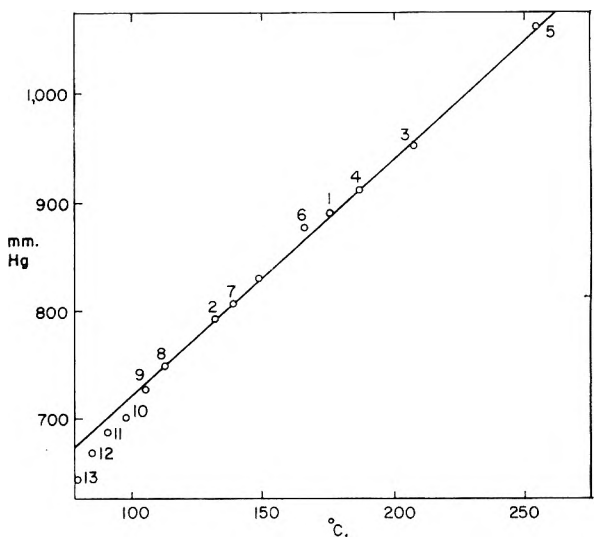

Fig. 1.—Total pressure of constant volume system starting with solid MoO_3 and gaseous HCl.

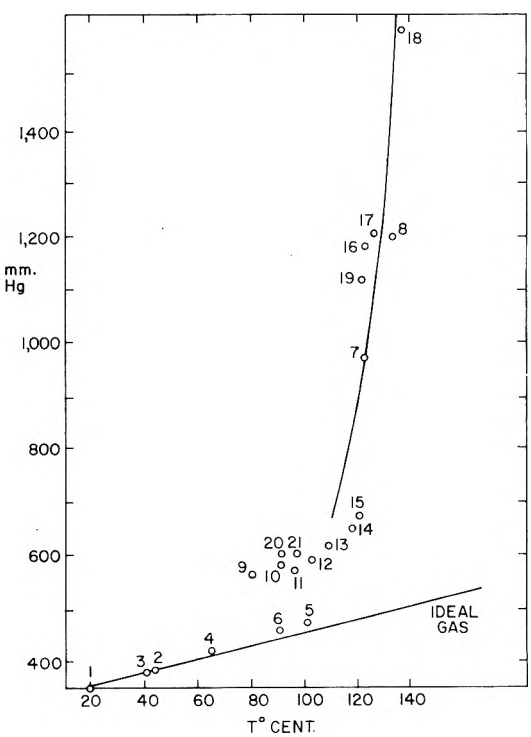

Fig. 2.—Total pressure of constant volume system starting with solid $MoO_3 \cdot 2HCl$ and gaseous HCl.

(1) N. L. Lofgren, "Gaseous Molybdenum Chlorides in HCl and H_2 Atmospheres," unpublished work, University of California, 1948.

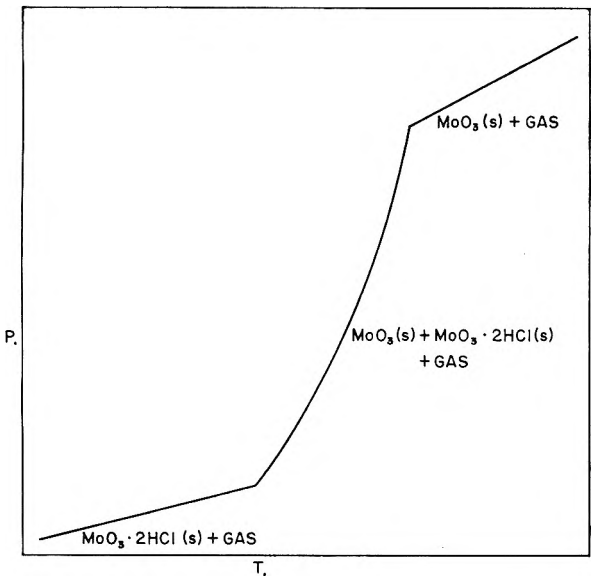

Fig. 3.—Pressure *versus* temperature behavior for constant volume system with MoO_3 and HCl components.

system. Thus the intersections of the three curves can be changed by changing the volume of the system or the amounts of material as in the above two experiments.

(3) **Quartz Fiber.**—MoO_3 was placed in a quartz pan located at the end of a 20-cm. quartz fiber sealed in a glass tube. The weight of the MoO_3 could be calculated from the amount of deflection of the fiber as observed through a cathetometer. HCl was added and the tube was heated in an oven. Air was circulated by means of a fan. Two different series of runs using different temperatures gave fairly consistent results. At high temperatures there was some condensation of greenish crystals on the glass tube. In the third run water was added. All the data are presented in Table I. The weight loss of the MoO_3 was vastly diminished by addition of water. The only reaction considered plausible which shows no volume change and which produces water is $MoO_3(s) + 2HCl(g) = MoO_2Cl_2(g) + H_2O(g)$. After a run the formerly pale yellow MoO_3 on the tray was bluish black. The greenish crystals which condensed on cooling turned dark blue on exposure to air. As even minute reduction of hexavalent molybdenum compounds often causes deeply blue colors, the color changes appear to be due to a slight reduction caused by reducing impurities or slight loss of oxygen.

Results

The HCl pressure at each temperature can be calculated from the pressure at room temperature, the amount removed due to reaction with MoO_3, and the perfect gas law.

From 400–600°, ΔC_p for the reaction $MoO_3(s) + 2HCl(g) = MoO_2Cl_2(g) + H_2O(g)$ was estimated to be −6 cal./mole. A "Σ" diagram was plotted against $1/T$ where $\Sigma = -R \ln K + \Delta C_p \ln T = \Delta H_0/T + I$. The slope of the curve gives ΔH_0 and the intercept gives I.

From the graph it is found that $\Delta H_0 = 24{,}800 \pm 2{,}000$ cal./mole and $I = -72.2$. Hence for the reaction $MoO_3(s) + 2HCl(g) = MoO_2Cl(g) + H_2O(g)$, $\Delta F = 24{,}800 + 13.8\,T \log T - 72.2T$ and $\Delta S = -d\Delta F/dT = -13.8 \log T + 66.2$.

At a temperature of 500°K., $\Delta S = 28.9$ e.u. This gives an entropy of formation for $MoO_2Cl_2(g)$ of −15 e.u., which is in very good agreement with an estimated value of −15 e.u.

Using the above data, it is found that the reaction $Mo(s) + 2HCl(g) + 2H_2O(g) = MoO_2Cl_2(g) + 3H_2(g)$ would account for the volatility of Mo observed at 1200°K. by Lofgren if 10^{-4} atm. of water were present in his vacuum line. He states that the H_2O pressure is less than 10^{-3} atm. in his line.

James Kane[2] passed HCl, H_2 and $H_2O(g)$ over solid Mo in a short series of experiments yielding the data shown in Table II. The approximate extrapolated K for these temperatures (adding the equations $MoO_3 + 2HCl = MoO_2Cl_2 + H_2O$ and $3H_2O + Mo = MoO_3 + 3H_2$) is 0.02. The MoO_3 and H_2O data were obtained from Coughlin.[3] The uncertainties are large for both the high temperature determinations and the extrapolated value of the equilibrium constant for the reaction $Mo(s) + 2H_2O(g) + 2HCl(g) = MoO_2Cl_2(g) + 3H_2(g)$. The difference may be due to experimental errors but under the condition of large water pressures the possibility of the formation of other molybdenum compounds should be considered. Reactions

TABLE I

$MoO_3(s) + 2HCl(g) = MoO_2(g) + H_2O(g)$

The P_{HCl} values given at room temperature are the pressures of HCl(g) in atm. introduced into the glass tube at room temperature. The value given for P_{H_2O} was calculated from the weight of introduced water. W_{Mo} is the weight loss, in milligrams, of the MoO_3 on the pan. The volume of the system was 234 cc.

T, °K.	P_{H_2O}, atm.	W_{Mo}, mg.	K	$-R \ln K$	$\Delta C_p \ln T$	Σ	$10^3/T$
			Run no. 1 (P_{HCl} = 0.192 atm. at 293°K.)				
511	..	6.7	6.80×10^{-4}	14.49	−37.38	−22.89	1.957
544	..	15.6	4.29×10^{-3}	10.83	−37.75	−26.92	1.838
558	..	19.2	6.96×10^{-3}	9.87	−37.90	−28.02	1.792
584	..	26.8	.0156	8.27	−38.18	−29.91	1.712
611	..	36.8	.0548	6.62	−38.45	−31.83	1.637
			Run no. 2 (P_{HCl} = 0.518 atm. at 296°K.)				
480	..	10.5	2.26×10^{-4}	16.68	−37.00	−20.32	2.083
529	..	19.5	8.2×10^{-4}	14.12	−37.58	−23.46	1.890
572	..	60.5	0.00367	11.14	−38.05	−26.91	1.748
609	..	96.5	0.0348	6.672	−38.43	−31.76	1.642
637	..	168	0.194	3.298	−38.70	−35.44	1.570
			Run no. 3 (with water) (P_{HCl} = 0.141 atm. at 297°K. and 0.255 atm. at 535°K.)				
535	1.04	.1	2.78×10^{-3}	11.69	−37.65	−25.96	2.083

(2) J. S. Kane, unpublished work, University of California, 1954.

(3) J. P. Coughlin, *Bur. of Mines Bull.*, 542 (1954).

such as $Mo(s) + 3H_2O(g) + HCl(g) = MoO_2OHCl(g) + 3H_2$ may account for the large volatility observed by Kane.

TABLE II

VOLATILITY OF MOLYBDENUM METAL IN HCl, H_2, H_2O GASEOUS MIXTURES

T, °K.	P_{Mo} species atm. × 10^6	P_{HCl}, atm.	P_{H_2O}, atm. × 10^3	P_{H_2}, atm.	K
1156	20.3	0.307	5.3	0.652	2.0
1177	2.0	.303	5.3	.646	0.2
1175	8.7	.303	5.3	.650	0.9

It is clear from these results that the study of the reaction $Mo(s) + 4HCl(g) = MoCl_4(g) + 2H_2(g)$ cannot be carried out in an oxide system due to the formation of MoO_2Cl_2 gas and possibly other oxy- and hydroxy-chlorides of Mo at high temperatures and a completely metallic system will be necessary.

This work was performed under the auspices of the U. S. Atomic Energy Commission.

THE ENTROPY OF SOLUTION OF BROMINE IN PERFLUORO-*n*-HEPTANE

BY L. W. REEVES AND J. H. HILDEBRAND

Department of Chemistry and Chemical Engineering, University of California, Berkeley, California

Received January 14, 1956

The solubility of Br_2 in n-C_7F_{16} between −5 and 25° conforms closely with the equation: $\log_{10} x_2 = 1.5398 - 849.58/T$. x_2 denotes mole fraction of Br_2. At 25°, $x_2 = 0.0490$. The mole fraction of C_7F_{16} in Br_2 is of the order of 5×10^{-5}. The partial molal volume of Br_2 in C_7F_{16} at saturation is 72 cc., an enormous expansion over its molal volume, 51.5 cc. Its partial molal entropy of sclution is 13.05 cal. deg.$^{-1}$, whereas the entropy of dilution according to Raoult's law would be only 6.0 e.u. The discrepancy can be accounted for by considering the entropy that would accompany (a) an expansion of the solvent by 20.5 cc., (b) the resultant increase in the free volume available to the Br_2, (c) a "Flory–Huggins" entropy for mixing at constant volume, and (d) a small decrease in molecular order of C_7F_{16} molecules adjacent to Br_2 molecules.

In order to test the validity of any theory based upon a model, it is proper to select cases that subject it to considerable strain. It is for this reason that we have carefully studied solutions of iodine in f-heptane, where its activity coefficient is 1400, as to conformity with the theory of regular solutions.[1] There is one respect, however, in which that system is not altogether satisfactory. In that theory, the standard state chosen for both components is the pure liquid, and a wide extrapolation below the melting point of iodine is required to obtain the essential properties of liquid iodine at ordinary temperatures. The pair bromine and f-heptane, on the other hand, are both liquid above −7.7°; both have zero dipole moment; they are chemically inert toward each other, and the difference between their solubility parameters is very large. These considerations led us to undertake the study here reported.

Materials.—The f-heptane was from the stock purified by Glew and Reeves.[2] The bromine was "analytical grade" from Baker and Mallinckrodt, density 3.10235 g. ml.$^{-1}$ at 25°. Precautions were taken to keep it dry.

Solubility of Br_2 in C_7F_{16}.—f-Heptane was saturated with bromine for periods of 8 to 24 hours in the apparatus described by Glew and Hildebrand[1] at temperatures constant to 0.002°. Portions were drawn off into a solution of KI and titrated with $N/20$ thiosulfate from a microburet. The equilibrium temperatures selected were all below room temperature, in order to avoid loss of bromine during the withdrawal of each sample. The results are given in Table I. x_2 denotes the mole fraction of Br_2.

Log x_2 plotted against $1/T$ gives a straight line whose equation is $\log_{10} x_2 = 1.5398 - 849.58/T$. The values in the last column were calculated by this equation.

TABLE I

SOLUBILITY OF BROMINE IN f-HEPTANE, MOLE FRACTION

t, °C.	$100\,x_2$, obsd.	$100\,x_2$, calcd.
−11.93	1.766 (solid)	...
− 4.97	2.343	2.345
− 0.12	2.693	2.690
4.41	3.019	3.013
9.84	3.453	3.456
14.78	3.887	3.882
19.94	4.366	4.377
25.00	...	4.898

Solubility of C_7F_{16} in Br_2.—This was determined from the diminution in volume of a small globule of f-heptane after equilibrating with a large volume of bromine.

The apparatus consists of a glass bulb to which are attached two tubes, one a calibrated capillary, both with stopcocks near their outer ends, lubricated with fluorocarbon grease. The apparatus is filled with bromine through the larger tube. A small amount of f-heptane is added at the top of the capillary, and its volume measured with a cathetometer. The bromine wets the glass preferentially, therefore the f-heptane is a well-defined globule. The apparatus is then tilted so that the globule runs out of the capillary into the bulb and the apparatus is rocked so that the globule rolls around in contact with the bromine. After at least 24 hours rocking, the capillary is raised to a vertical position, whereupon the globule runs up to the top where its volume is again measured.

The solubility is extremely small, therefore the results, shown in Table II, show considerable percentage fluctuation. They could not be improved by using a much smaller capillary, because then the bromine would not displace the fluorocarbon. We can assert only that the mole fraction of f-heptane in bromine at 25° is approximately 5×10^{-5}.

Partial Molal Volume of Br_2 in C_7F_{16}.—The densities of pure C_7F_{16} and of solutions of Br_2 therein, were determined, using a graduated, double stem pycnometer, having a volume of 28 cc. The mole fraction of Br_2 in each solution was determined by titration. The density of the C_7F_{16} was 1.72004 ± 0.00005 at 25°. The results are given in Table III. $\bar{v}_2$ is the partial molal volume and v_2° is the molal volume.

(1) H. A. Benesi and J. H. Hildebrand, *J. Am. Chem. Soc.*, **70**, 3978 (1948); J. H. Hildebrand, H. A. Benesi and L. M. Mower, *ibid.*, **72**, 1017 (1950); D. N. Glew and J. H. Hildebrand, THIS JOURNAL, **60**, 616 (1956); J. H. Hildebrand and D. N. Glew, *ibid.*, **60**, 618 (1956).

(2) D. N. Glew and L. W. Reeves, *ibid.*, **60**, 615 (1956).

TABLE II

SOLUBILITY OF f-HEPTANE IN BROMINE

t, °C.	Capillary, cc./cm.	Mole % Br_2
25	0.06	0.0052
31	.06	.0041
36	.06	.0078
25	.031	.0036

TABLE III

PARTIAL MOLAL VOLUME OF Br_2 IN n-C_7F_{16}, 25°

Density of soln.	100 x_2	$\bar{v}_2$	$(\bar{v}_2 - v_2^\circ)/\phi_1^2$
1.72277	1.692	72.0	21.0
1.72358	2.228	72.4	21.6
1.72405	2.441	71.6	20.8
1.72842	4.918	71.5	21.6
		Av.	21.3

The molal volume of Br_2 at 25°, v_2°, is 51.5 cc. The change of $\bar{v}_2 - v_2^\circ$ with the composition of the solution at these high dilutions is almost masked by the experimental fluctuations, but the values obtained can be extrapolated to $x_2 = 0$ by the relation, $\bar{v}_2 - v_2^\circ = k\phi_1^2$, where ϕ_1 is the volume fraction of C_7F_{16}. The average of the figures in the last column may be taken as the limiting value of $\bar{v}_2 - v_2^\circ$. It will be noted that this expansion is enormous, compared with the known cases, where it seldom exceeds 1 or 2%, except in the case of iodine, recently reported,[1] where we found an expansion from 59 to 100 cc.

The entropy of solution of Br_2 in C_7F_{16} can be determined by aid of the pure thermodynamic relation already employed,[3]

$$\bar{s}_2 - s_2^\circ = R\left(\frac{\partial \ln a_2}{\partial \ln x_2}\right)_T\left(\frac{\partial \ln x_2}{\partial \ln T}\right)_{sat} \qquad (1)$$

a_2 denotes activity. From a plot of the figures in Table I, we obtain $R(\partial \ln x_2/\partial \ln T) = 14.08$. The Henry's law factor, $\partial \ln a_2/\partial \ln x_2$, is not far from unity in so dilute a solution. It can be estimated closely enough for our purpose by aid of the approximate relation, $\ln a_2 = \ln x_2 + B\phi_1^2$. The data in this case give $B = 3.015$ and $\partial \ln a_2/\partial \ln x_2 = 0.927$, whence $\bar{s}_2 - s_2^\circ = 13.05$ e.u.

Let us see what theoretical inferences we can draw from this figure. The contribution of expansion to the entropy of mixing we determine by expanding x_1/x_2 moles of f-heptane by $\bar{v}_2 - v_2^\circ$ cc. before introducing the bromine. The entropy of expansion is given by the expression

$$\Delta S_1^{ex.} = (\bar{v}_2 - v_2^\circ)(\partial P/\partial T)_V \qquad (2)$$

In this case, $\bar{v}_2 - v_2^\circ = 20.5$ cc. The solution is so dilute in bromine that we may use the value of $(\partial P/\partial T)_V$ for pure f-heptane,[4] 6.75 atm. deg.$^{-1}$. This gives $\Delta S_1^{ex.} = 3.45$ cal. deg.$^{-1}$

Next, we add 1 mole of bromine to a large amount of solution containing x_1/x_2 moles of f-heptane. The ideal entropy for this dilution would be 6.0 e.u., but because of the very different molal volumes of these components, we use the Flory–Huggins expression for the athermal mixing of liquids having unequal molal volumes

$$\bar{s}_2 - s_2^\circ = -R\left[\ln \phi_2 + \phi_1\left(1 - \frac{v_2}{\bar{v}_1}\right)\right] \qquad (3)$$

This gives $\bar{s}_2 - s_2^\circ = 7.32$ e.u. Adding this to the entropy of expansion gives 10.8 e.u., considerably less than the experimental value above. The most obvious explanation of the discrepancy seems to be that the Flory–Huggins expression is not strictly applicable to a solution such as this. An athermal solution is ordinarily formed with little or no change in volume, but the expansion in this case is enormous, being exceeded only by iodine in the same solvent.

The senior author[5] derived an expression for the entropy of mixing in terms of free volumes

$$-\Delta S^M/R = N_1 \ln \frac{N_1 v_1^f}{N_1 v_1^f + N_2 v_2^f} + N_2 \ln \frac{N_2 v_2^f}{N_1 v_1^f + N_2 v_2^f} \qquad (4)$$

It reduces to equation 3 if the free volumes are proportional to molal volumes. This, however, is far from true for components of such different molecular sizes and degrees of expansion as in this case. But it is not yet clear which of the possible definitions of free volume is the one to use to obtain the proper values to substitute in equation 4. Bondi[6] has distinguished "empty volume," "expansion volume" and "fluctuation volume." The model used in deriving equation 4 corresponded to "expansion volume." We are now engaged in obtaining accurate values of the entropy of solution and the partial molal volume of gases whose molecules differ considerably in size, in order to throw light upon this important problem. In the meantime, we merely suggest a possible line of treatment.

In breaking down the mixing as above, the bromine is added to $x_1/x_2 = 20.15$ moles of f-heptane that has been expanded by 20.2 cc. The entropy of vaporization of f-heptane at 25° is 26.2 e.u. per mole. Computing the fluctuation free volume in this liquid by the equation $\Delta s_1^{vap.} = R \ln (v_1^g/v_1^f)$ gives $v_1^f = 0.42$ cc. mole^{-1}. If the same free volume is available to dissolved bromine, as yet only an hypothesis, the total in 20.15 moles amounts to 8.5 cc. But if the bromine is introduced into f-heptane under tension, expanded by 20.5 cc., the free volume becomes 29 cc. The additional entropy gained by adding the bromine to the expanded f-heptane may be expressed in terms of the ratio of these two free volumes, $R \ln 29/8.5 = 1.6$ e.u. If this is added to the two contributions previously considered, the sum becomes 12.4 e.u., reducing the discrepancy in the total calculated measured and calculated partial molal entropy of solution of bromine to 0.65 e.u., not a serious difference.

We see only one possible, though small, contribution to the entropy of solution. The molecules of f-heptane are not very flexible, and there is evidence of some quasi-parallel order in the liquid[7] that would doubtless diminish among the molecules adjacent to a molecule of bromine.

It has become increasingly apparent that the considerable success that has been achieved in calculating isothermal solubility in terms of an ideal or

(3) J. H. Hildebrand and R. L. Scott, *J. Chem. Phys.*, **20**, 1520 (1952).

(4) B. J. Alder, E. W. Haycock, J. H. Hildebrand and H. Watts, *ibid.*, **22**, 1060 (1954).

(5) (a) J. H. Hildebrand, *ibid.*, **15**, 225 (1947). See also (b) J. H. Hildebrand and R. L. Scott, "Solubility of Non-electrolytes," Reinhold Publ. Corp., New York, N. Y., 1950, p. 108.

(6) A. Bondi, THIS JOURNAL, **58**, 929 (1954).

(7) J. H. Hildebrand and G. J. Rotariu, *J. Am. Chem. Soc.*, **74**, 4455 (1952).

a Flory–Huggins entropy combined with an enthalpy expressed by $v_2\phi_1^2(\delta_2 - \delta_1)^2$ is in part due to the fact that any unrecognized factor contributing to entropy would involve a corresponding contribution to enthalpy. Expansion on mixing, for example, is accompanied by absorption of heat. But the neglect of a factor in the formulation of entropy leads to a wrong temperature coefficient of solubility. The inadequacy in this respect of the simple equations used for regular solutions became evident long ago in the solubility of iodine[8] in carbon tetrachloride over a wide range of temperature. The values of $\delta_2 - \delta_1$ calculated from the solubility decrease from 5.68 at 0° to 5.28 at 50°, although as calculated from heats of vaporization and molal volumes it is nearly constant at 5.5.

When Hildebrand and Scott[5] computed a figure for the partial molal entropy of solution of iodine in carbon tetrachloride, they used a figure for the entropy of expanding liquid iodine from v° to $\bar{v}$ before adding it to the solution. This involves an expansion of 6.8 cc. per mole, or 11.5%. However, to expand liquid iodine by 41 cc. per mole, or nearly 70%, as would be necessary, according to the recent findings of Glew and Hildebrand, in order to introduce it at constant volume into its solution in f-heptane at 1 atmosphere, would require a quite unrealizable state of the liquid, where even an extrapolated value of $(\partial P/\partial T)_v$ as a function of volume would be highly uncertain. In that case as in this we have first expanded the f-heptane and then added the solute. This is an expansion of only 1%, in which the change of $\partial P/\partial T$ is negligible.

The reader may properly ask, however, whether this entropy of expanding 20.15 moles of f-heptane is equivalent to the partial molal entropy of expansion of bromine by 20 cc. The entropy of forming a mole of mixture may be expected to be proportional approximately to the product of the volume fractions, $\phi_1\phi_2$, and have the general form, for these components, shown in Fig. 1. The tangent to the curve at low values of x_2 intercepts the ordinate at $x_2 = 1.00$ at a point corresponding to the value of $\bar{s}_2 - s_2^\circ$. This graphic relation between partial and total quantities is explained by Hildebrand and Scott.[9] The maximum of the curve for this system should lie near $x_2 = 0.9$, and the portion between zero and 0.049 is practically linear, hence, by the similar triangles, $\Delta s^M/x_2 = (\bar{s}_2 - s_2^\circ)/1$. Since Δs^M is the entropy of forming a mole of mixture, $\Delta s^M/x_2$ is the entropy of forming a mixture containing 1 mole of bromine and 20.5 moles of f-heptane, for which $\partial P/\partial T$ cannot differ significantly from its value for pure f-heptane.

The simple regular solution equation with ideal entropy is

$$RT \ln a_2 = RT \ln x_2 + v_2\phi_1^2(\delta_2 - \delta_1)^2 \qquad (5)$$

For Br_2 in C_7F_{16}, $a_2 \cong 1$. Substituting the observed value of x_2 and ϕ_2, with $v_2 = 225.5$, one gets $\delta_2 - \delta_1 = 6.0$. This is reasonably close to the difference between the solubility parameters obtained from the energy of vaporization per cc., $11.5 - 5.7 = 5.8$, despite the fact that the actual entropy is far from ideal, the reason being that the expansion on mixing increases both the entropy and the enthalpy.

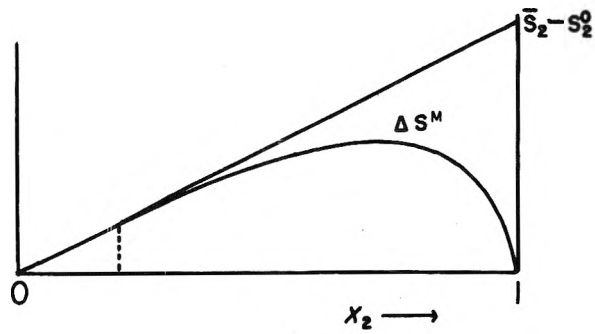

Fig. 1.

The same equation also explains the extremely small solubility of C_7F_{13} in Br_2. With $v_1 = 225.5$, $a_1 \cong 1$, $\phi_2^2 \cong 0.98$, and $\delta_2 - \delta_1 = 6.0$, we get $x_1 \cong 0.3 \times 10^{-5}$.

The Calculation of Volume Changes.—This system serves well to emphasize the necessity of taking account of volume changes in order to improve the theory of regular solutions. Their neglect is not extremely serious in dealing with the free energy, or isothermal solubility, but it introduces large errors in the entropy and enthalpy, and therefore into the change of solubility with temperature. To be able to calculate volume changes becomes therefore a matter of great importance.

We acquainted R. L. Scott with our remarkable findings for the expansion when iodine and bromine are dissolved in f-heptane, and he presented at the meeting of the American Chemical Society in Minneapolis a theoretical calculation of $\bar{v}_2 - v_2^\circ$ in fair agreement with our experimental results. He will include it in a paper he is now preparing on the general subject of volume changes on mixing liquids. By common understanding, we give a summary of it here.

It is based upon the thermodynamic relation for the excess total change of volume on mixing

$$\Delta v^M = \left(\frac{\partial \Delta F^M}{\partial P}\right)_{T,P=P_0}$$

This yields for the partial molal expansion[10]

$$\bar{v}_2 - v_2^\circ = \beta RT \ln \gamma_2 \qquad (6)$$

where β is the compressibility of the solution and γ_2 the activity coefficient. Scott has now added a factor, $n = (\partial E/\partial v)_T/(-E/v)$. For C_7F_{16}, $n = 1.35$ and $\beta = 2.38 \times 10^{-4}$ atm.$^{-1}$. This gives the partial molal expansions of I_2 and Br_2 in C_7F_{16} shown in Table IV, with the measured values for comparison. The agreement is good in the case of Br_2, and not bad in the case of I_2 in view of the extrapolated value for v_2°.

TABLE IV

PARTIAL MOLAL EXPANSION OF I_2 AND Br_2 DISSOLVED IN C_7F_{16}

	γ_2	$\bar{v}_2 - v_2^\circ$ Calcd.	Obsd.
I_2	1430	57	41
Br_2	20.4	25	21

The ultimate goal must be to construct a theory of solutions that rests solely upon the properties of

(8) J. H. Hildebrand, *J. Am. Chem. Soc.*, **59**, 2083 (1937).

(9) Ref. 5(b), p. 40.

(10) See Ref. 5b, page 7 ff.

the pure components, and we do not reach it by calculating expansion from an activity coefficient. This approach is, however, not altogether unsatisfactory, because free energy, and hence γ, can be calculated with fair approximation because of the cancelling of uncertainties in entropy and enthalpy, noted above.

We thank Dr. Berni J. Alder and Professor R. L. Scott for their criticisms, and the Atomic Energy Commission for its support of this work.

THE CONTORTIONAL ENERGY REQUIREMENT IN THE SPREADING OF LARGE DROPS

BY S. G. BANKOFF[1]

Argonne National Laboratory, Lemont, Ill.

Received January 16, 1956

The equation of the surface of a semi-infinite sheet of liquid spreading uni-directionally on a solid is deduced. For a particular liquid at a given temperature, a single curve describes all possible surface configurations, regardless of contact angle. The reversible free energy change for a sheet of liquid climbing a barrier is then calculated. This is shown to be a measure of the energy barrier, and corresponds roughly to Good's concept of "contortional energy," which has, however, serious inconsistencies. For semi-infinite sheets on any surface, or for finite sheets on perfectly smooth surfaces, there is no hysteresis of the contact angle upon advancing the barrier into the line of contact, if the surface energies are assumed to be time-independent. For finite sheets on rough surfaces, the hysteresis of the contact angle depends upon the predominant orientation of the surface roughnesses, since Young's Equation must hold microscopically everywhere. This is partially confirmed by Bartell and Shepard's observations.

Introduction

Wenzel[2] has formulated an expression which describes the contact angle in the spreading of a liquid drop over a rough surface. However, this expression is strictly valid only for very small drops (which are not appreciably flattened by gravity) resting on a surface whose roughnesses are very minute. Numerous metastable equilibrium states are possible, and for macroscopic roughnesses the energy barrier in passing from metastable to stable equilibrium may become controlling, as indicated by the data of Bartell and Shepard.[3] Bikerman,[4] in discussing the motion of a drop front over a rough surface, has pointed out that the climbing of a drop front over a ridge requires "contortion (*i.e.*, extension) of the liquid–air interface," and consequently an increase in the energy of the system. Good[5] has related this contortional energy to the observed contact angle hysteresis, and suggested that it could, in principle, be calculated for simple barrier configurations. As a preliminary to this calculation, the two-dimensional equation for the surface of a semi-infinite sheet of liquid spreading uni-directionally over a solid surface is derived. A very interesting result is obtained, in that the resulting equilibrium equation contains only one parameter, which is a function only of the liquid properties. Hence, a single equation serves to define the surface contour of a particular liquid at a particular temperature, regardless of the contact angle, surface properties or surface configuration. This result should have interest for applications other than the one at hand.

The reversible free energy for a sheet of liquid climbing a sharp, plane barrier of arbitrary height and inclination is then calculated. If the horizontal surface and barrier are perfectly smooth, and if time-dependent effects are excluded,[6] it is shown that there will be no contact angle hysteresis. This will be true also if the surface is microscopically rough, but the liquid is semi-infinite in extent. For the usual case of a microscopically rough surface and a liquid of finite extent, the contact angle will increase as the volume of liquid is increased until the energy increment exceeds the "contortional energy," when the liquid rapidly climbs the barrier. It is shown that the reversible free energy change is a rough measure of the contortional energy requirement for a drop front to advance over a ridge. These considerations lead to a simple relationship between the advancing and receding contact angles, which was, in fact, observed by Bartell and Shepard.[3]

Surface of a Semi-infinite Sheet of Liquid.—In order to compute the energy change for a large drop in climbing over a ridge, we must first obtain the equation for the equilibrium free liquid surface. We may consider the drop to be axially symmetrical, and if we consider a really large drop, the problem reduces itself to a semi-infinite sheet of liquid spreading unidirectionally against a normal, plane barrier. Our first task is then to derive the equation for the free liquid surface under equilibrium conditions. Referring to Fig. 1, the horizontal asymptote to the free liquid surface will be chosen as the x-axis. The location of the z-axis is arbitrary. One principal radius of curvature of the liquid surface is everywhere infinite, and both principal radii of curvature are infinite at $x = \infty$. The Gibbs condition for equilibrium of a curved interface[7] reduces to

$$(\rho_g - \rho_l)\, gz = \frac{\gamma}{R} \qquad (1)$$

where ρ_g and ρ_l are the gas and liquid densities, g the local acceleration due to gravity, γ the sur-

(1) Rose Polytechnic Institute, Terre Haute, Ind.

(2) R. N. Wenzel, *Ind. Eng. Chem.*, **28**, 988 (1936).

(3) J. W. Shepard and F. E. Bartell, THIS JOURNAL, **57**, 458 (1953).

(4) J. J. Bikerman, *ibid.*, **54**, 653 (1950).

(5) R. J. Good, *J. Am. Chem. Soc.*, **74**, 5041 (1952).

(6) The expression "time-dependent effects" is used herein to include adsorption and any other surface altering effects.

(7) J. W. Gibbs, "Collected Works," Vol. I., Yale Univ. Press, New Haven, Conn., 1948, p. 282.

face tension, and R the radius of curvature of the liquid surface. R can be eliminated by

$$ds = -R\,d\alpha \qquad (2)$$

where s is arc length, and α is the angle of inclination of the tangent with the horizontal. Equations 1 and 2 can be readily solved to give

$$-B\cos\alpha = \frac{z^2}{2} + \text{const.} \qquad (3)$$

where

$$B = \frac{\gamma}{(\rho_1 - \rho_g)g}$$

When $z = 0$, $\alpha = 0$, for a sheet of liquid advancing to the left and hence eq. 3 becomes

$$B(1 - \cos\alpha) = \frac{z^2}{2} \qquad (4)$$

A similar result was obtained by Coghill and Anderson[8] in their consideration of the "edge effect."

α can be eliminated from eq. 4 to give

$$\frac{dz}{dx} = \pm\sqrt{\frac{1}{\left(1 - \frac{z^2}{2B}\right)^2} - 1} \qquad (5)$$

corresponding to convex and concave menisci. This is easily solved, with the substitution

$$\cos w = 1 - \frac{z^2}{2B} \quad 0 \le w \le 2\pi \qquad (6)$$

giving

$$x = B^{1/2}\left(\log\tan\frac{w}{4} + 2\cos\frac{w}{2}\right) + \text{const.} \qquad (7)$$

For $z = 0$, w may be 0 or 2π, resulting in $x = -\infty$ or $+\infty$. These correspond to a semi-infinite sheet advancing to the right or to the left, respectively. If we choose the latter case by limiting w between π and 2π, eq. 7 yields, upon elimination of w

$$x = B^{1/2}\log\left[-\frac{2B^{1/2}}{z}\left(\sqrt{1 - \frac{z^2}{4B}} + 1\right)\right] - 2B^{1/2}\sqrt{1 - \frac{z^2}{4B}} + \text{const.} \qquad (8)$$

The signs in front of the square root terms would be reversed for a sheet advancing to the right. If we choose our coördinate system such that $x = 0$ when $z = 2B^{1/2}$, the constant in eq. 8 vanishes identically. A plot of eq. 8 for water at 25 and 100°, and for carbon tetrachloride at its normal boiling point, is given in Fig. 1. It should be noted that, for a particular liquid at a particular temperature, a single curve describes all possible surface configurations, regardless of contact angle, since B is the only parameter in eq. 8.

This result should be of significance for applications other than the one at hand. For instance, it is expected to be of value in computing the dimensions of a surface cavity of given shape which will just barely entrap gas as the liquid drop spreads over it.

The Climbing of a Barrier by a Sheet of Liquid.— Having obtained an expression for the equilibrium free surface of a large sheet of liquid, we now take up the problem of the energy change in climbing a barrier. For simplification, the roughness element is supposed to be a plane wall lying parallel to the line of contact. In practice, it makes a difference whether we consider that the wall and the horizontal surface area are perfectly smooth, or minutely rough, *i.e.*, whether the roughnesses have roughnesses.

(8) W. H. Coghill and C. O. Anderson, U. S. Bur. Mines Tech. Paper 262, 47 (1923).

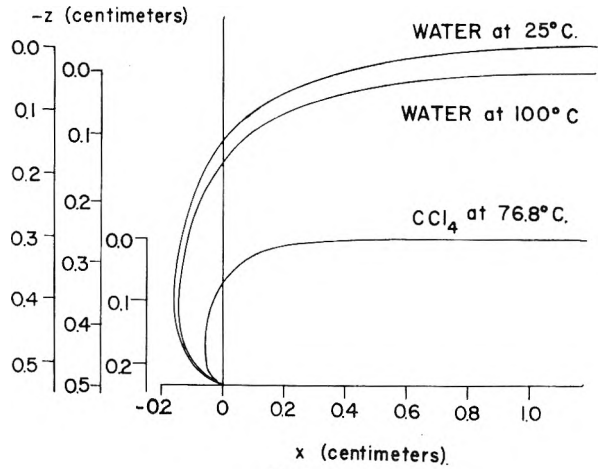

Fig. 1.

Consider a sheet of liquid advancing to the left against a wall inclined at an angle ϕ with the horizontal (Fig. 2). We take the location of the line of contact as x_1, z_1 and assume that the liquid extends for a distance L behind the line of contact. We shall assume first of all that the horizontal surface and the barrier are very smooth, so that all surface planes offered to the line of contact are parallel to the direction of the surface itself. Then, by the principle of a microscopic force balance, the contact angle through the liquid, θ, is fixed when the liquid is at rest, and is the same whether the line of contact is resting against the horizontal surface or the wall. Since L and α_1 are fixed by the system chosen, eq. 4 and 8 fix the surface contour, and the volume of liquid at equilibrium. The free energy in this case is given by

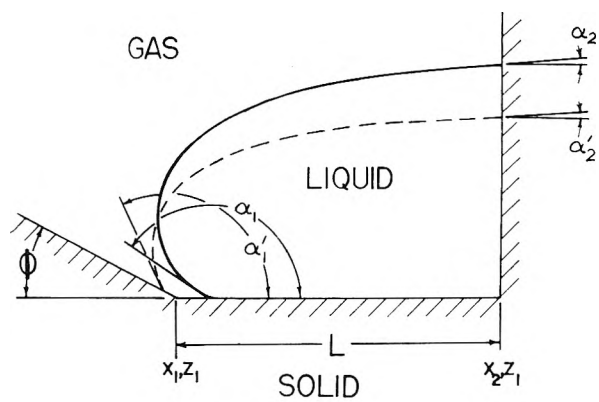

Fig. 2.

$$F = M\bar{h} + \gamma_{23}s + \gamma_{13}L + \gamma_{12}L' \qquad (9)$$

where, for unit width of sheet, s is the arc length of the liquid surface, L' is an arbitrary length of the wall, M the weight of liquid and $\bar{h}$ is the height of the center of gravity of the liquid above the horizontal surface. The subscripts 1, 2 and 3 refer to the solid, gaseous and liquid phases.

If the liquid were in equilibrium at the base of the wall (shown as the dotted in line Fig. 2), the free energy in this case would be

$$F' = M'\bar{h}' + \gamma_{23}s' + \gamma_{13}L + \gamma_{12}L' \quad (10)$$

and the decrement would be

$$\Delta F = F' - F = (s' - s)\gamma_{23} + (\bar{h}'M' - \bar{h}M) \quad (11)$$

From eq. 1 and 2 it can be shown that

$$s = B^{1/2} \log \left(\frac{\tan \alpha_1/4}{\tan \alpha_2/4} \right) \quad (12)$$

where α_1 and α_2 are the angles of inclination with the horizontal of the tangents to the surface at $x = x_1$ and $x = x_1 - L$. Similarly

$$s' - s = B^{1/2} \log \left(\frac{\tan \frac{\alpha_2}{4} \tan \frac{\alpha'_1}{4}}{\tan \frac{\alpha_1}{4} \tan \frac{\alpha'_2}{4}} \right) \quad (13)$$

The fact that the arc lengths s and s' are segments of the same curve, as pointed out previously, has some interesting consequences. As L approaches infinity, $s' - s$ approaches a constant value. This may also be seen from eq. 13, where $\alpha'_2 \rightarrow x_2$ as $L \rightarrow \infty$. Also, $\bar{h}' < \bar{h}$, and $M' < M$, so that

$$\bar{h}M - \bar{h}'M' = (h - h')M' + h(M - M') \rightarrow \infty$$

as $L \rightarrow \infty$. Hence $-\Delta F$ is infinite for a semi-infinite sheet. This means that if a barrier, at any inclination, ϕ, were advanced into a semi-infinite sheet of liquid, the liquid would immediately begin to climb the barrier, with no hysteresis of contact angle, even if the surface roughness were such that some variation in the apparent contact angle were possible.

We now consider the case of finite L. The gravitational potential energy change is

$$\bar{h}'M' - \bar{h}M = \bar{z}M - \bar{z}'M' = \frac{\rho}{2} \int_{x_1 - L}^{x_1} (z^2 - z'^2)\, dx \quad (14)$$

where

$$z' = z + b \quad (15)$$

since the effect of changing α at the line of contact is simply to translate the z-axis. This displacement may be shown to be

$$b = 2B^{1/2} \left(\sin \frac{\alpha_1}{2} - \sin \frac{\alpha_1'}{2} \right) \quad (16)$$

From eq. 14 and 15 one can derive

$$\bar{h}'M' - \bar{h}M = -b\rho \left[z_2 \sqrt{B - \frac{z_2^2}{4}} - z_1 \sqrt{B - \frac{z_1^2}{4}} + \frac{bL}{2} \right] \quad (17)$$

Equations 13, 16 and 17, when substituted into eq. 11, constitute a solution for the equilibrium free energy change upon beginning to climb the barrier. This quantity would superficially appear to correspond to the "contortional energy" proposed by several writers.[4,5] However, the concept is not simple, and deserves careful analysis.

Good,[5] in a treatment valid only for drops small enough to have spherical surfaces, shows that

$$\frac{\partial F}{\partial A_{13}} = \gamma_{23}(\cos \theta_{obsd} - \cos \theta_{eq}) = \gamma_{23} \Delta \cos \theta \quad (18)$$

He then defines a "contortional energy," F_c, due to the extension of the liquid-air interface in climbing over a ridge such that the drop will cease to change its shape when

$$\frac{\partial F}{\partial A_{12}} = |\gamma_{23} \Delta \cos \theta| \leqq F_c \quad (19)$$

This is, on the face of it, open to at least two objections. First, $\partial F/\partial A_{13}$ must be negative in order for the drop to spread at all, and not positive, as implied by eq. 19. Secondly, the energy term, F_c, is not dimensionally consistent with the other terms, whose units are energy per unit area. The meaning of eq. 19 is therefore not clear, and it seems better to state that the drop will cease to spread simply when

$$\frac{\partial F}{\partial A_{13}} \geq 0 \quad (20)$$

which is, of course, the Gibbs condition.

The situation is complicated by the fact that the climbing of the barrier is normally not a reversible process. For the system shown in Fig. 2, the retaining wall at $x_1 - L$ may be considered to be a piston, which is reversibly retracted until the liquid assumes the dotted line configuration. The piston is then reversibly returned to its original position, the liquid simultaneously climbing the wall. Since the liquid surface is now always more flat than it was initially, the center of gravity will be lower, and the net work of the liquid on the surroundings will be positive. This, however, is not the actual path, which is highly irreversible. If the piston is returned to its original position, while, at the same time, restraining the liquid from climbing the wall, the work input, which is equal to $-\Delta F$ of eq. 11, is a measure of the departure from equilibrium. ΔF is therefore a measure of the energy input required to cause the liquid to leave its equilibrium state at the base of the wall. It is probably higher than the actual energy input, despite the irreversibility of the process. This is because the liquid surface can assume dynamic non-equilibrium shapes which limit the energy changes principally to the region near the line of contact.

Returning to our model of a perfectly flat horizontal surface and wall, a small displacement of the piston to the left from its initial position will immediately cause the liquid to climb the barrier until it reaches a new position of equilibrium some distance away. This is because L, α_1 and M are fixed for a smooth surface, leaving no degrees of freedom. Hence, the equilibrium is unstable for a piston displacement in this direction only. Good[5] considers $\gamma_{23} \Delta \cos \theta$ to be a driving force which determines the ability of the liquid to climb a ridge. In the above case $\Delta \cos \theta$ is zero, and yet the smallest displacement causes the liquid to climb a finite distance. It is apparent, therefore, that the displacement of the cosine of the contact angle from the equilibrium value is not adequate, *per se*, as a measure of the driving force.

If we now consider that both the horizontal surface and the wall have numerous minute surface ridges, it is possible for the microscopic force balances to be satisfied with a change in the apparent contact angle for a differential movement of the

piston to the right. This will continue until the line of contact, by small movements, is no longer able to find a sufficient number of planes of proper orientation to provide the apparent contact angle demanded by the relationships of eq. 4 and 8. At that point, the equilibrium becomes unstable, and the liquid climbs the wall. The contact angle hysteresis is determined, therefore, not by the inclination or height of the barrier (within reasonable limits), but by the predominant orientation of the surface roughnesses. If the roughnesses consist of a series of ridges whose sides are inclined to the horizontal by an angle, ϕ, we would expect

$$\theta_a = \theta_{eq} + \varphi \qquad (21)$$

This relationship was in fact, observed by Bartell and Shepard[3] for liquids of high surface tension spreading over blocks of paraffin whose surfaces had been ruled to give asperities of known inclination. Eliminating runs in which large amounts of air were obviously entrapped, it was found that the height of the asperities had little effect, and that eq. 21 was obeyed, if $\theta_{eq.}$ is taken as θ_r, instead of $(\theta_a + \theta_r)/2$, as is usually done, for want of more precise knowledge. The situation is complicated here by the fact that their surfaces were ruled in two directions, so that spreading within the valleys, as climbing over the ridges, was an important mode of advance and recession. For this reason, presumably, their data for liquids of low surface energy do not follow eq. 21 so well (Table I).

TABLE I

ADVANCING AND RECEDING CONTACT ANGLES IN THE SPREADING OF LIQUID DROPS OVER MACHINED PARAFFIN SURFACES (DATA OF SHEPARD AND BARTELL[3])

Liquid	γ, dynes/cm.	Smooth surface θ_a	Smooth surface θ_r	ϕ = 30° θ_a	ϕ = 30° θ_r	ϕ = 45° θ_a	ϕ = 45° θ_r	ϕ = 60° θ_a	ϕ = 60° θ_r
Water	72	110°	99°	129°	99°	142°	94°	160°	96°
3 *M* $CaCl_2$	84.5	119	109	136	114	149	115	174	125
Glycerol	63.2	97	90	115	92	127	83	145	68
Ethylene glycol	47.5	81	74	93	65	102	49	120	17
Methyl cellosolve	30	62	42	76	12	82	0	93	0
Methanol	22.6	42	27	58	0	50	0	0	0

Conclusions

(1) A semi-infinite sheet of liquid would be expected to display no time-independent hysteresis of contact angle, *i.e.*, hysteresis attributable to surface roughness.

(2) A method is given for calculating the reversible free energy change of a finite sheet of liquid upon climbing a barrier of known height and inclination. This corresponds roughly to the "contortional energy," and hence gives a measure of the contact angle hysteresis to be expected on advancing over a surface whose roughnesses have random inclinations and orientations. If, however, the roughnesses have a predominant inclination, this will tend to determine the contact angle hysteresis, in accordance with eq. 21.

DEGREE OF HYDRATION OF PARTICLES OF COLLOIDAL SILICA IN AQUEOUS SOLUTION

BY R. K. ILER AND R. L. DALTON

Grasselli Chemicals Department, Experimental Station, E. I. du Pont de Nemours and Company, Inc.

Received January 16, 1956

The viscosity of colloidal dispersions of silica has been studied, with the objective of determining the amount of water bound to the surface of the discrete, spherical amorphous particles. By applying the Mooney equation for the viscosity of a dispersion of spheres in a liquid medium, it is calculated from the viscosity data that there is a monomolecular layer of water molecules immobilized, probably through hydrogen bonding, at the hydroxylated surface of the silica particles.

The degree to which the molecules in water are immobilized at the surface of a highly polar solid apparently varies with the nature of the surface. For example, Bertil Jacobson[1] concluded that near the surface of molecules of sodium desoxyribonucleate, water molecules are oriented to form an immobilized lattice-oriented layer similar to ice. On the other hand, Vand[2] has concluded that the viscosity of an aqueous solution of sucrose is consistent with the assumption that there is approximately a single layer of water molecules hydrogen bonded to the hydroxyl groups of the sugar molecule. It was of interest to determine whether the surface of amorphous silica immobilizes or otherwise binds water molecules. The viscosity of colloidal dispersions of amorphous silica has therefore been studied with the objective of determining the amount of water bound to the surface.

Vand[3] and Mooney[4] have developed equations for a dispersion of spheres in a liquid, relating the relative viscosity of the dispersion to the volume fraction of the dispersed phase. The dispersed phase includes the volume of the solid particle plus any part of the medium which is bound to the surface of the particles. With spheres larger than 100 mμ diameter, the presence of a single molecular layer of solvent bound to the surface of the particle would have little effect on the volume fraction of the dispersed phase. However, in the case of spherical particles smaller than 10 or 20 mμ in diameter, one or two molecular layers of solvent attached to the surface would appreciably increase the volume of the dispersed phase. This would have a marked influence on the viscosity. In the case of particles 5 mμ in diameter, for example, the presence of two molecular layers of water, having a thickness of the

(1) B. Jacobson, *J. Am. Chem. Soc.*, **77**, 2919 (1955).
(2) V. Vand, THIS JOURNAL, **52**, 314 (1948).
(3) V. Vand, *ibid.*, **52**, 277, 300 (1948).
(4) M. Mooney, *J. Colloid Sci.*, **6**, 162 (1951).

order of 0.5 mμ would increase the over-all diameter of the dispersed unit to about 6 mμ. This would increase the volume fraction of the dispersed phase by about 70%.

Assuming the above equations to be applicable to spheres of very small diameter, it is thus possible to calculate from the viscosity the degree to which spherical silica particles are "hydrated." On this basis, our results, described below, indicate that uncharged particles of amorphous silica in suspension in water at *p*H 2 are associated with only a monomolecular layer of water molecules, probably hydrogen bonded to the silanol (–SiOH) groups which make up the surface of the particles.

Experimental

Preparation of Sols.—A series of silica sols containing discrete, non-aggregated particles having specific surface areas of 400 to 800 square meters per gram of SiO_2, corresponding to average particle diameters of about 7 to 3.5 mμ, were prepared for viscosity studies. That the particles are discrete and not aggregated in solution was shown by examining electron micrographs taken of deposits on a supporting film from sols at high dilution. In these micrographs the discrete particles lie as a single layer on the supporting film with very few aggregates which are deposited less regularly and form darker clumps more than one particle deep on the film.

It is possible to prepare sols of discrete particles free from aggregates by slow deionization of a dilute solution of sodium silicate (3% SiO_2), while maintaining the *p*H above 7, at elevated temperature. The specific surface area of the product may be varied by changing the temperature and rate of deionization while maintaining the *p*H between 11 and 9.[5] For example, a dilute solution of sodium silicate (SiO_2:Na_2O weight ratio 3.25) containing 3% SiO_2 was maintained at 47°, and "Nalcite" HCR, a sulfonic type cation-exchange resin in the hydrogen form, was added slowly over a 13-min. period, lowering the *p*H from 11.3 to 9.1. The *p*H was then maintained at *ca.* 9.0 by careful addition of resin. Samples were removed after 1 and 3 hours, cooled and filtered. The second sample was further deionized to *p*H 8.6 and again filtered. Additional sols were prepared by varying the time and temperature of deionization, as shown in Table I.

Table I

Preparation and Characterization of Silica Sols

	Time required for preparation, hr.	Temp. of preparation, °C.	*p*H of final sol	Molar ratio SiO_2:Na_2O	A,[a] m.²/g.	S, %[b]	n[c]
A,	1	47	9.07	38	827	79	0.9
B,	3	47	8.57	80	717	84	0.6
C,	2	64	8.86	67	690	81	0.9
D,	1	64	9.4	28	705	81	0.9
E,	2	64	7.9	113	612	83	0.9
F,	1	90	8.9	100	615	82	0.8
G,	6.5	90	9.12	100	478	85	1.1
H,	23.8	90	9.34	100	406	89	0.8
I.	50	90	9.27	100	360	89	1.0
						Av.	0.9

[a] A, specific surface area of the silica. [b] S, per cent. by weight of anhydrous silica in the "dispersed phase." [c] n, calculated number of molecular layers of water held at the silanol surface of the particles.

For the preparation of samples C and D, the deionization was carried out still more slowly, initial samples of the sodium silicate solution being treated with ion-exchange resin to remove sodium over a period of 30 minutes, to lower the *p*H to 9.1, and then maintaining the *p*H at this value for 1 and 2 hours, respectively. Similarly, by aging these sols at about *p*H 9 for 1 and 6.5 hours at 90°, samples F to I were prepared.

(5) R. K. Iler and F. J. Wolter, U. S. Patent 2,631,134 (E. I. du Pont de Nemours & Co., Inc., 1953).

Characterization of Sols.—The specific surface area of the particles, A, was determined by a titration method described by G. W. Sears.[6] The per cent. by weight of silica in the dispersed phase, S, was calculated from the relative viscosity of the sols and the densities of water and silica.

In order to avoid electroviscous effects, the viscosity of the colloidal solution was measured at *p*H 2, where the charge on the silica particles is at a minimum.[7] The solution of the freshly prepared colloidal silica is alkaline and the particles are negatively charged. However, just before measuring the viscosity, the *p*H must be reduced to about 2, in order to minimize the charge on the particles. This is done by adding wet, freshly regenerated "Nalcite" HCR resin, in the hydrogen form, in sufficient quantity to remove all the sodium ions, filtering and then adding sufficient 1 *N* HCl to lower the *p*H to about 2.0. The concentration of SiO_2 in the solution is then determined, either gravimetrically, or by measuring accurately the specific gravity of the solution. The viscosity of the solution was then measured at 25° with an Ostwald pipet, and the relative viscosity calculated from the following expression

$$N_r = \frac{dt}{d_w t_w}$$

where d and t are the density and the time of flow of the silica sol, and d_w and t_w are the density and time of flow of water, respectively.

On the assumption that the solution contains dispersed spherical particles, the relative volume fraction of the dispersed phase is then calculated from the viscosity data, using the Mooney equation[4]

$$\ln N_r = \frac{2.5c}{1 - 1.43c}$$

where c is the volume-fraction of the "dispersed phase." At concentrations of silica employed in this study, the Mooney and Vand equations give essentially the same value for c.

The "dispersed phase" consists of particles of anhydrous SiO_2 together with any water which is immobilized at the surface of the particles.

The relation between c and S, the per cent. by weight of silica in the dispersed phase, in a sol containing P per cent. by weight of silica, may be calculated as follows.

Assume 100 g. of sol containing P g. of silica. Since the volumes of silica and water in the system are additive,[8] the volume of the sol is $(P/2.3 + 100 - P)$ ml.

The dispersed phase thus has a volume of $c(P/2.3 + 100 - P)$ ml. The dispersed phase thus consists of $P/2.3$ ml. of silica and

$$c\left[\frac{P}{2.3} + 100 - P\right] - \frac{P}{2.3} \text{ ml. of water}$$

Then

$$\frac{S}{100} = \frac{P}{P + c\left[\frac{P}{2.3} + 100 - P\right] - \frac{P}{2.3}}$$

$$\text{whence } S = \frac{P}{0.00566P + c(1 - 0.00566P)}$$

The values of S for the sols in Table I were calculated from this equation, using the values of c calculated from viscosity data.

Effects of *p*H, Salts and Aggregation.—The viscosity of an acidic sol is relatively independent of *p*H. For example, a 7.6% sol at *p*H 2.0 and 3.2 exhibited viscosities of 1.239 and 1.250. In alkaline solution, a change in *p*H from 8.0 to 9.0, produced a viscosity change from 1.478 to 1.580.

The value of S as measured by viscosity, is unchanged when the viscosity is measured over a two-fold concentration of silica. Thus, at *p*H 2, increasing the concentration of silica from 3.77 to 6.63%, increased the viscosity from 1.149 to 1.295 but the calculated value for S was 53% in both cases.

(6) G. W. Sears, paper to be submitted for publication.

(7) N. E. Gordon, Colloid Symposium Monograph, Vol. II, Chemical Publishing Co., New York, N. Y., 1925, pp. 114–125.

(8) It was verified experimentally that the density of a colloidal dispersion of silica in water can be calculated from the composition and densities of amorphous silica (2.3 g./ml.) and of water (1.0 g./ml.).

At *p*H 2, where there is little charge on the particles, the addition of an electrolyte has very little effect. In the aforementioned sols containing 3.77 and 6.63% silica, addition of 1.5% of sodium sulfate did not change the viscosity.

It is necessary to measure the viscosity promptly when the *p*H of the sol has been reduced to 2, even though the rate of gelling of colloidal silica is a minimum at about this point.[9] Over a period of several days at 25°, aggregation of the particles occurs, and eventually the solution will form either a precipitate or gel. However, during the first hour or so, at ordinary temperature, colloidal solutions at the indicated concentrations increase very little in viscosity.

It should be pointed out that the volume fraction of the dispersed phase, c, may be increased not only by the amount of water associated with the surface of the individual silica particles, but also by the degree of aggregation of the particles. If a number of particles were joined together to form a porous aggregate, the water within the pores would be essentially immobilized from a hydrodynamic standpoint, so that the "dispersed phase" would include more water than if the particles were not aggregated. Thus aggregation decreases the value of S. This effect of aggregation accounts for the low value of S (*i.e.*, 53%) for the sols mentioned above. However, since the sols referred to in Table I are not aggregated, the relationship between viscosity and surface area can be accounted for by the hydration of the surface, as shown below.

Calculation of the Composition of the "Dispersed Phase."—It is known that the hydrated surface of amorphous silica is covered with silanol groups (–SiOH).[10] The composition of discrete spherical particles, in terms of SiO_2 and H_2O present as hydroxyl groups, can be calculated from the specific surface area. Thus

$$A = 2720/\mathbf{d}$$

where A = specific surface area of the particles in square meters per gram and $\mathbf{d}$ = average particle diameter in millimicrons. The particle composition[9] has been calculated as

$$x = \frac{22\pi}{6}\,\mathbf{d}^3 \text{ and } y = \frac{\pi}{2}\,(2.80\mathbf{d})^2$$

where the composition is represented as $(SiO_2)_x(H_2O)_y$.

(9) R. K. Iler, "The Colloid Chemistry of Silica and Silicates," The Cornell Press, Ithaca, N. Y., 1955, p. 45.

(10) Ref. 9, pp. 99, 103, 234.

Let us now assume that in addition to the chemically bound layer of silanol groups, there are n layers of water molecules adsorbed or fixed in some way to the surface as far as their hydrodynamic behavior is concerned. The association of hydrogen-bonded water molecules with the silanol layer, in view of the large volume of the oxygen atom relative to hydrogen, suggests that in the first layer there may be one water molecule associated with each underlying silanol group.[11] Since the hydrogen atoms of two silanol groups are equivalent to one molecule of water reacted with one unit of anhydrous SiO_2, the composition of the "dispersed phase" may be represented as

$$(SiO_2)_x(H_2O)_y(H_2O)_{n(2y)}$$

Thus for every molecule of water present in the silanol layer there would be two water molecules in each physically bound water layer.

From the above formula, using the formula weights for SiO_2 and H_2O, the dispersed phase has the composition, by weight

$$\frac{S}{100} = \frac{60x}{60x + y(2n+1)18}$$

Substituting for x, y and d from the above relationships

$$n = \frac{1}{2}\left[\frac{8480(100 - S)}{SA} - 1\right]$$

Degree of Hydration.—Applying this formula to the values of S and the specific surface area, A, in Table I, the values of n for each sol were calculated. For example, for sol E having a specific surface area of 612 m.²/g. and a viscosity corresponding to a value of S of 83%, n was calculated to be 0.9. For n to have been 0 or 2, the required value of S would have been about 94 or 74%, respectively. Such values are well outside the range of experimental error in determining viscosity.

Thus, for discrete silica particles ranging in size from 3.3 mμ diameter in sol A to 7.5 mμ in sol I, the value of n remains constant at a value of about unity. It therefore appears that there is about a monomolecular layer of water molecules immobilized at the hydroxylated surface of the silica particles.

(11) Ref. 9, p. 240.

APPLICATION OF THE ABSOLUTE RATE THEORY TO ADHESION*

By Marshall R. Hatfield and George B. Rathmann

Contribution No. 95, Central Research Department, Minnesota Mining & Manufacturing Company, St. Paul 1, Minnesota

Received January 19, 1956

Attempts to treat adhesion of a deformable adhesive to a rigid surface in terms of a simple fuse model for the bond are shown to be inadequate for explaining the time dependence of adhesion failure. Modification of this model to include the effects of a time dependent modulus of elasticity for the adhesive does not appear to be a satisfactory solution. The application of the absolute rate theory is based upon the assumption that bonding and debonding are rate processes and do not occur instantaneously which automatically results in a time dependent failure. The general implications of the theory are that: (1) loads below a critical force will never produce failure, (2) the work of adhesion will have a profound effect on the time to breakage for a given load, although it represents a small fraction of the energy expended, and (3) the free energy of activation for viscoelastic flow of the adhesive also has a profound effect on the time to breakage for a given load. Precise and simplified forms of the rate equation are given for adhesion failure of a bond under tensional load. For comparison of similar systems, the simplified form may be adequate. In addition, proper use of the simplified form may permit some information concerning work of adhesion to be derived from experimental adhesion data.

Introduction

Adhesion, as discussed in this paper will be restricted to the bonding together of two solids, one soft and deformable (adhesive) and the other rigid and non-deformable (adherend). The primary purpose is to demonstrate that the rate theory offers a plausible mechanism for the direct approach to the failure of such an adhesive bond under tensional stress. The fact that small variations in the applied stress have a pronounced effect on the time required for bond failure is well established experimentally. The introduction of the rate theory provides a natural explanation for this time-dependency. Other explanations, which consider the adhesive bond as a fuse, introduce time-dependency through the viscoelastic properties of the adhesive

* Presented at the 128th National American Chemical Society Meeting, Cincinnati, Ohio, April, 1955.

which are known to be time dependent. Such explanations will be grouped as the fuse theory of adhesion.

The Fuse Theory.—Consider a rigid solid attached to an elastomeric solid by adhesive bonds at the interface. If the applied force exceeds the product of the number of bonds and the force required to break each bond, instantaneous failure results. The analogy to a fuse in electrical circuits is obvious. This picture clearly needs alteration to introduce time-dependency since failure would occur immediately at forces above a critical value and never at forces below this value. A superficially attractive modification incorporates the modulus behavior of the elastomeric adhesive. If a constant load is applied to the system such that the stress (load per unit cross-section) at the interface is not sufficient to break the bonds, failure does not occur immediately. Creep of the adhesive and the resulting smaller cross-section will result in higher stresses within the elastomer. Sufficiently high stresses are developed, it may be argued, to break the adhesive bonds. Actually, however, only the time-dependency of cohesive failure could be accounted for in this way, since there is no change in the cross-section of the interface. A further modification of the theory postulates changes in geometry in the stretching adhesive to account for a stress build-up at the interface. A precise formulation of the stress build-up resulting from geometry changes would be, at best, complicated. Distributions of bond energies and more elaborate mechanisms for developing high interfacial stress as a result of increasing stress within the adhesive offer no substantial improvement.

One modification of the fuse theory introduces the concept of tensional fluctuation. Even for forces insufficient to break the bonds instantly, statistical fluctuations in tension will result in random rupturing of the bonds. As the bonds fail, the stress at the interface increases and complete failure eventually occurs. Such an approach is mathematically as complicated as the application of the absolute rate theory, and does not offer any advantages. The rate theory by focusing attention upon the interface where failure is known to occur, provides a means of examining bond formation as well as bond failure.[1]

The Rate Theory.—Instead of considering bonds as fuses it will be assumed that the formation and failure of bonds involves the passage over a free energy barrier. Molecules at the interface must be thermally activated before passing into the unbonded state. The time to failure is, then, the time required for all the bonded molecules to acquire sufficient energy by thermal fluctuations to pass over the barrier. Following Eyring[2] a free energy profile can be drawn as in Fig. 1.

Here, the difference in free energy of the bonded and unbonded states, W, is the free energy of adhesion per bond. It is assumed that in the unbonded

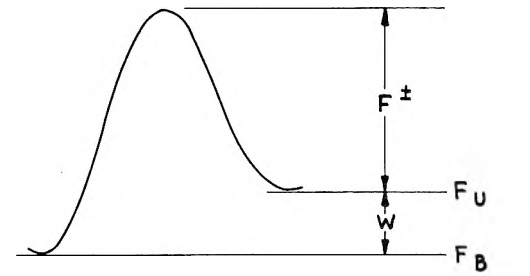

Fig. 1.—Free energy profile–adhesion system: F_U, energy min.-unbounded molecules; F_B, energy min.-bonded molecules; W, energy of adhesion bond; $F^{\pm}$, free energy of activation.

state, the bonding areas of the adhesive as well as those of the rigid solid are bonded to the surrounding medium. Obviously, W depends upon the medium surrounding the system. Henceforth, bond failure will be assumed to be occurring in air and W_A is then the work of adhesion in air per bonding site.[3]

$F^{\ddagger}$, the free energy of activation per bond will be assumed to depend only on the free energy of activation for deformation of the adhesive. Let

N_B = no. of molecules in the bonded state
N_U = no. of molecules in the unbonded state
$N_0 = N_B + N_U$ = total no. of molecules available for adhesion

At equilibrium, the rate of passage of molecules from bonded to unbonded state (forward) is equal to the rate in the reverse direction. Thus at equilibrium

$$N_B \exp [-(F^{\ddagger} + W_A/kT)] = N_U \exp [-F^{\ddagger}/kT] \quad (1)$$

where k is the Boltzmann constant and T is the absolute temperature.

Solving equation 1 for N_B, the number of molecules in the bonded state at equilibrium, gives

$$\frac{N_B}{N_U} = \exp (+ W_A/kT) \quad (2)$$

$$N_0 = N_B + N_U \quad (3)$$

$$N_B = \frac{N_0}{1 + \exp (-W_A/kT)} \quad (4)$$

If a small load is applied as pure tension to the elastomer–solid system the equilibrium given by equation 4 will be shifted slightly to favor the unbonded state. It is assumed that the energy supplied to each bonded molecule by the load, F, is small compared to $F^{\ddagger}$. Furthermore, it is assumed that the only direct effect is to raise the energy level of the bonded state and lower the level of the unbonded state by equal amounts. Figure 2 is a diagram of the system under load. The constant, λ, represents the distance the adhesive molecules move when passing from the bonded to the unbonded state. It seems apparent that the shift in energy levels will cause molecules to pass over the energy barrier from bonded to unbonded state until equilibrium is once more established. It should be noted, however, that at constant load, F, any decrease in the number of molecules in the bonded state, N_B,

(1) W. M. Bright, Paper presented at Case Institute Symposium on Adhesion, Cleveland, 1952. "Adhesion and Adhesives, Fundamentals and Practice," Editors Clark, Rutzler, and Savage, John Wiley Sons, New York, N. Y., 1954, p. 130.

(2) S. Glasstone, K. Laidler and H. Eyring, "The Theory of Rate Processes," McGraw-Hill Book Co., New York, N. Y., 1941.

(3) A more precise approach would be to consider a vacuum as the medium surrounding the system. Then no error would be introduced in the event that a bond failed somewhere in the system such that air was not available, *i.e.*, a failing bond completely surrounded by other bonded sites.

will cause an immediate increase in the quantity $F\lambda/2N_B$.

Thus, addition of a load may either (a) cause total bond failure or (b) shift the equilibrium without resulting in failure.

The net rate $-dN_B/dt$ of bond rupture is given by equation 5 and 8 where R_1 is the rate in the forward direction and R_2 the rate in the reverse direction. C is the frequency factor which can be calculated from the theory of absolute reaction rates to be kT/h.

$$\frac{-dN_B}{dt} = R_1 - R_2 \tag{5}$$

$$R_1 = CN_B \exp\left[-\frac{(F^\ddagger + W_A - F\lambda/2N_B}{kT}\right] \tag{6}$$

$$R_2 = CN_U \exp\left[\frac{-(F^\ddagger + F\lambda/2N_B}{kT}\right] \tag{7}$$

$$\frac{-dN_B}{dt} = CN_B \exp\left[\frac{-F^\ddagger - W_A + F\lambda/2N_B}{kT}\right]$$

$$(CN_0 - N_B) \exp\left[\frac{-F^\ddagger - F\lambda/2N_B}{kT}\right] \tag{8}$$

Equation 8 represents the net rate of passage over the barrier at time t, as a function of the number of molecules, $N_B(t)$, remaining in the bonded state. Integration to determine the relationship between break time and the various parameters is not possible. Two alternative ways to use equation 8 will be described.

The initial rate can be shown to be

$$-\left(\frac{dN_B}{dt}\right)_{t=0} = \left[CN_B \exp\left(\frac{-(F^\ddagger + W_A)}{kT}\right)\right]\left[\exp\left(\frac{F\lambda}{2N_B kT}\right) - \exp\left(\frac{-F\lambda}{2N_B kT}\right)\right] \tag{9}$$

since from equation 1 $N_B \exp(-W_A/kT) = N_U$. If it is assumed that the initial rate remains unchanged until failure, then the time to failure, t_B, can be derived.

$$t_B = \frac{N_B}{-(dN_B/dt)_{t=0}} \tag{10}$$

Substituting into (8) gives

$$\frac{1}{t_B} = C \exp\left[\frac{-(F^\ddagger + W_A)}{kT}\right]\left[\exp\left(\frac{F\lambda}{2N_B kT}\right) - \exp\left(\frac{-F\lambda}{2N_B kT}\right)\right] \tag{11}$$

or

$$\frac{1}{t_B} = A[\exp(BF) - \exp(-BF)] \tag{12}$$

where

$$A = C \exp\left[\frac{-(F^\ddagger + W_A)}{kT}\right] = \frac{kT}{h} \exp\left[\frac{-(F^\ddagger + W_A)}{kT}\right] \tag{13}$$

and

$$B = \frac{\lambda}{2N_B kT} = \frac{\lambda[1 + \exp(-W_A/kT)]}{2N_0 kT} \tag{14}$$

Equation 12 might be tested experimentally by comparing the time to failure of two systems for which either $F^\ddagger$ or W_A are the same. Certain plasticizers will decrease $F^\ddagger$ while probably not affecting W_A. Immersion in a suitable liquid will change W_A without affecting $F^\ddagger$. It must be established, of course, that N_0 and λ are the same for the two systems.

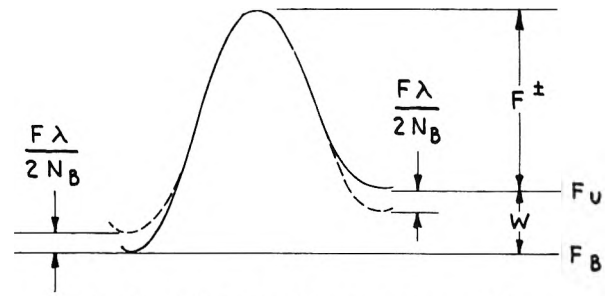

Fig. 2.—Effect of load on free energy profile.

A precision device was not available for testing equation 12. The apparatus used for a rough check is depicted in Fig. 3. The electromagnet and weight assembly (A) was constructed for the sole purpose of application of the adherend plunger (B) to the film of adhesive to be tested (C). The applied or "breaking" tensional load is added to the balance pan at (D).

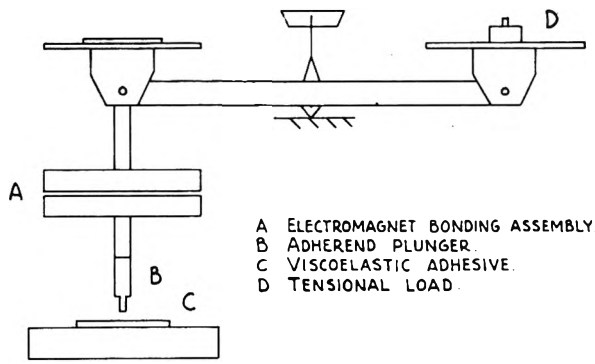

Fig. 3.—Tensional adhesion apparatus.

Data obtained with this instrument for polymethylmethacrylate (Lucite) bonded to polyisobutylene (Vistanex) are given as experimental points in Fig. 4. Note that reproducibility is poor. For comparison, the hyperbolic sine curve predicted by equation 12 is also plotted.

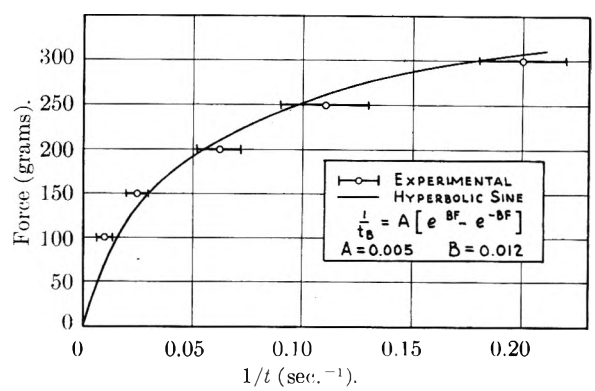

Fig. 4.—Comparison of experimental–theoretical adhesion curves.

Another approach involves extracting as much information as possible from equation 8. First, it is possible to examine the conditions under which $-dN_B/dt = 0$, or a dynamic equilibrium exists between bonded and unbonded state. At equilibrium with force F

$$\exp\left(\frac{F\lambda}{N_B kT}\right) = \frac{(N_0 - N_B)}{N_B}\exp(W_A/kT) \quad (15)$$

$$F\lambda = N_B kT \ln\frac{N_0 - N_B}{N_B} + N_B W_A \quad (16)$$

Clearly (for all values of W_A) $F\lambda = 0$ at $N_B = 0$. For large N_B, $F\lambda$ becomes negative, yet the initial slope of $F\lambda$ at $N_B = 0$ is positive. Consequently, $F\lambda$ must pass through a maximum. Values of $F\lambda$ in excess of this maximum produce failure. Differentiating equation 16 with respect to N_B and determining N_B^c, the value of N_B when $F\lambda$ is a maximum, in terms of W_A/kT

$$\frac{dF\lambda}{dN_B} = 0 = kT\ln\frac{N_0 - N_B^c}{N_B^c} - \frac{N_0 kT}{N_0 - N_B} + W_A \quad (17)$$

$$\frac{N_0}{N_0 - N_B^c} = \ln\frac{N_0 - N_B^c}{N_B^c} + \frac{W_A}{kT} \quad (18)$$

If W_A and N_0 are known, it is possible to calculate the minimum force necessary to produce failure, or "critical force," from equations 16 and 18.

To obtain a comparison between the simplified rate expression, equation 12 and the general expression, equation 8, it is necessary to assume arbitrary values of the several parameters appearing in the rate expressions. For purposes of calculation, let

$W_A = 3kT = 3 \times 10^{-21}$ cal./molecule
$N_0 = 1 \times 10^{12}$ molecules
$F^\ddagger = 30kT = 30 \times 10^{-21}$ cal./molecule
$\lambda = 100$ Å. $= 1 \times 10^{-6}$ cm.

Note that W_A was assumed to be roughly equal to the energy of van der Waals bonds. The value for $F^\ddagger$ was chosen to be equal to the activation energy for viscoelastic deformation of polyisobutylene. The 100 Å. value chosen for λ was quite arbitrary. The value for N_0, also quite arbitrary, was chosen by dividing the cross-sectional area of the adherend plunger in the experimental apparatus (see Fig. 3) by an estimated area for each bonding site, *i.e.*, 10^{-1} cm.$^2/10^{-13}$ cm.^{2}.

The constant C in equations 8 and 13 is equal to kT/h or 6.33×10^{12} sec.$^{-1}$. Using the above values for $F^\ddagger$ and W_A gives a value of 0.032 for A in equation 13. The A obtained by fitting an hyperbolic sine function to experimental data is 0.005 (see Fig. 4). If $F^\ddagger$ had been chosen as $31.8kT$, instead of $30kT$, the calculated value of A would then have been 0.005. For purposes of calculation, the assumed value of $30kT$ for $F^\ddagger$ will be changed to $31.8kT$ so that the value of A in the simplified expression will agree with experiment.

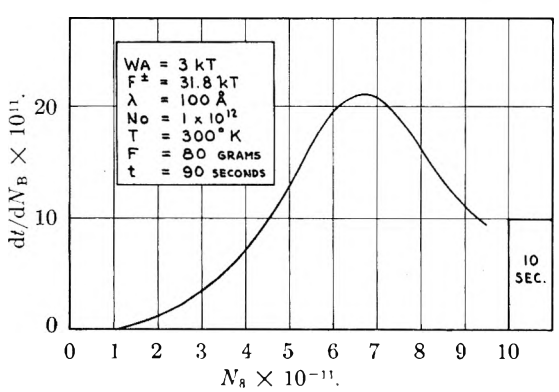

Fig. 5.—Plot for graphical integration of general rate equation.

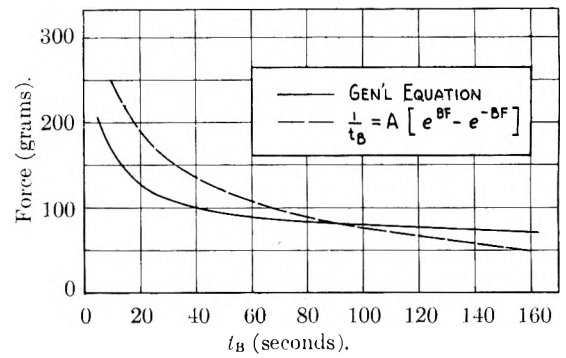

Fig. 6.—Comparison simplified—general rate expressions.

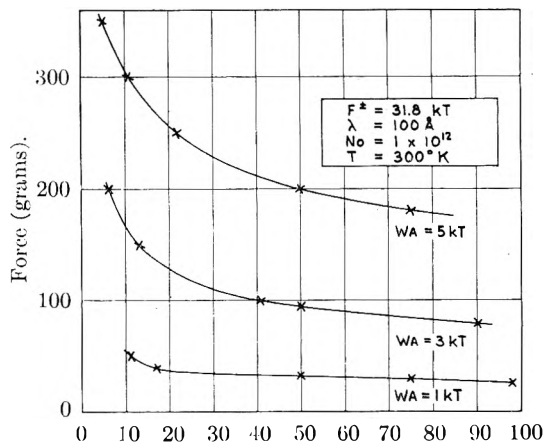

Fig. 7.—Effect of work on adhesion on tensional adhesion (calculated).

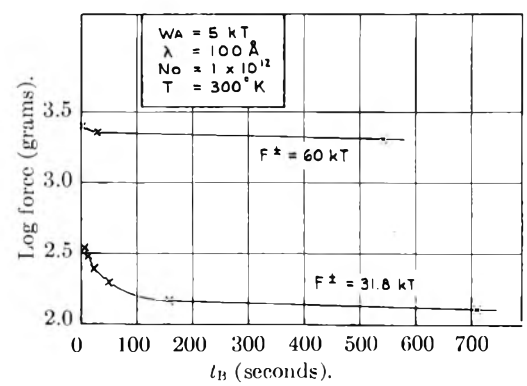

Fig. 8.—Effect of free energy of activation on tensional adhesion (calculated).

Thus

$$N_B^\circ \text{ (equil., no load)} = \frac{N_0}{1 + \exp\left(\frac{-W_A}{kT}\right)} = \frac{N_0}{2.05}$$

$$= 9.5 \times 10^{11} \text{ molecules}$$

$$A = C\exp[-(F^\ddagger + W_A/kT)] = 0.005$$

$$B = \frac{\lambda}{2N_B^\circ kT} = \frac{1 \times 10^{-6} \times 2.3 \times 10^{-5}}{2 \times 9.5 \times 10^{-11} \times 1 \times 10^{-21}} = 0.012 \text{ g.}^{-1} \text{ molecules}^{-1}$$

NOTE: If F is in grams and λ is cm. then $F\lambda$ must be multiplied by 2.3×10^{-5} to get calories—or kT divided by 2.3×10^{-5} to get gram cm.

Equations 8 and 12 can now be compared. For equation 12 F is plotted *versus* $1/t_B$. For equation 8 dt/dN_B is plotted as a function of N_B at constant F. Integrating graphically from $N_B = (N_B)_{t=0}$ to $N_B = 0$, gives t_B for each F (see Fig. 5). A comparison of the simplified and general expressions is given in Fig. 6. The curves have a similar shape except for an important distinction. The simplified equation 12 suggests no critical force, while the more precise equation 8 predicts a critical force at 67.5 g.

A rough indication of the effect of the variables W_A and $F^\ddagger$ on the apparent bond strength can be obtained by calculation. Figures 7 and 8 show the results. Note that work of adhesion has a profound effect on time to breakage for a given load, although it represents a small fraction of the energy expended. The free energy of activation for viscoelastic flow of the adhesive also has a marked effect.

Although, admittedly, experimental confirmation is lacking, it is felt that the absolute rate theory affords a new point of view for examining adhesion and may suggest experiments which could lead to a true understanding of the effect of the variables governing the process.

SURFACE TENSION AT ELEVATED TEMPERATURES. III. EFFECT OF Cr, In, Sn AND Ti ON LIQUID NICKEL SURFACE TENSION AND INTERFACIAL ENERGY WITH Al_2O_3

BY C. R. KURKJIAN AND W. D. KINGERY

Ceramics Division,[1] Department of Metallurgy, Massachusetts Institute of Technology, Cambridge, Massachusetts

Received January 20, 1956

The sessile drop method has been employed to study the surface tension and interface energy of dilute solutions of indium, tin, chromium and titanium in nickel for the system Ni(l)–Al_2O_3(s). The surface tension of pure liquid nickel was found to be 1725 dyne cm.$^{-1}$. Indium and tin concentrate at the liquid–gas interface, lowering the surface tension; chromium and titanium concentrate at the solid–liquid interface, lowering the interface energy. Adsorption at the solid–liquid interface is closely related to the free energy of metal–oxygen bond formation.

Introduction

Although the importance of surface and interface energies in determining wetting behavior, in studying joining phenomena, and in determining equilibrium microstructure of polyphase systems is well known,[2,3] there have been few quantitative measurements at elevated temperatures. It has previously been reported that small amounts of oxygen and sulfur are markedly surface active in liquid iron.[4] In the present paper, the surface and interface energy of the solutions in liquid nickel of indium and tin, which have low surface tensions, large atomic size and might be expected to be surface active, and of chromium and titanium, which are known to enhance wetting behavior, are reported.

Data previously reported for the surface tension of liquid nickel give values from 1505–1760 dynes/cm. under various atmospheres and in contact with various supports.[5] The higher value would be expected to be closest to the value for pure nickel, lower values being due to various sources of minor contamination.[4] No data are available in the literature for solutions of other constituents in nickel.

Experimental

The sessile drop method which previously has been described in detail[4,5] was employed to simultaneously determine liquid surface tension and contact angle of the liquid in contact with aluminum oxide. The maximum experimental deviations in measured values for a given composition varied between 1 and 3%. Interface energies were calculated from the following relation between the liquid–solid, solid–vapor and liquid–vapor interface energies and the contact angle, θ taking a value of 930 erg/cm.^{2} for

$$\gamma_{LS} = \gamma_{SV} - \gamma_{LV} \cos \theta \qquad (1)$$

the solid surface energy of Al_2O_3 at 1475°.[6] An error in this value, or a change due to the presence of liquid nickel, will shift the absolute value of interfacial energy reported, but will not affect the slope of the curves or the calculation of interfacial adsorption if it can be assumed that small solute additions have no effect on the solid surface energy.

High-purity vacuum-melted nickel (Vacuum Metals Corporation) was employed as the base material for all compositions prepared. This material has the following impurities: 0.004% C, 0.0043 O, 0.000042 N, 0.0023 S, 0.002 Cu, 0.025 Fe, 0.01 Mg, 0.009 Si. Compositions were prepared by vacuum melting this material with various additions of high-purity tin, indium, chromium and titanium hydride. From these ingots, samples were prepared with hemispherical bases to ensure a uniform advancing contact angle. Sessile drops were melted on Al_2O_3 plaques prepared from calcined aluminum oxide (J. T. Baker, reagent grade), sintered *in vacuo* at 1830°, and polished.

Indium–nickel and tin–nickel compositions were studied in a purified helium atmosphere; chromium–nickel and titanium–nickel compositions were heated in pure dry hydrogen and then melted *in vacuo* (0.005 μ). No differences in liquid surface tension were found between measurements in hydrogen, helium, or *vacuo*, indicating that previous variations in different atmospheres[5] (which gave lower surface tension values than reported here) must be attributed to small amounts or impurities.

In view of the known effects of small amounts on metal surface tension,[4] all compositions were analyzed for oxygen as well as for the added constituent. Results of experimental surface tension measurements, contact angles, and interface energies calculated from equation 1 are listed in Table I.

(1) With funds from the United States Atomic Energy Commission under Contract No. AT(30-1)-1192.

(2) C. S. Smith, *Trans. A.I.M.E.*, Tech. Paper No. 2387 (1948).

(3) A. Bondi, *Chem. Revs.*, **52**, 417 (1953).

(4) F. A. Halden and W. D. Kingery, THIS JOURNAL, **59**, 557 (1955).

(5) W. D. Kingery and M. Humenik, Jr., *ibid.*, **57**, 359 (1953).

(6) W. D. Kingery, *J. Am. Cer. Soc.*, **37**, 42(1954).

TABLE I

SURFACE TENSION AND CONTACT ANGLE MEASUREMENTS AT 1475°

Wt. % added constituent	Wt. % oxygen	Surface tension, dyne cm.$^{-1}$	Contact angle, degree	Interface energy, erg cm.$^{-2}$
0.05 In	0.0048	1510	136.7	2030
0.53 In	.0044	1329	140.9	1960
0.90 In	.0060	1277	141.8	1935
3.32 In	.0037	1251	143.1	1930
0.007 Sn	.005	1627	141.1	2196
0.047 Sn	.005	1540	145.8	2202
0.56 Sn	.003	1494	145.4	2160
1.86 Sn	.002	1422	148.8	2136
0.027 Cr	.006	1725	136.1	2171
0.14 Cr	.007	1725	135.2	2156
0.89 Cr	.0006	1725	135.2	2155
3.61 Cr	.003	1725	118.2	1746
8.72 Cr	.0075	1725	108.8	1485
0.004 Ti	.002	1725	137.8	2205
0.015 Ti	.001	1725	125.1	1920
0.025 Ti	.001	1725	123.6	1885
0.051 Ti	.001	1725	121.3	1450
0.87 Ti	< .0001	1725	90.0	930

Discussion

A. Liquid Surface Tension.—In two component systems, the relation between surface tension and composition for ideal mixtures is given by

$$\gamma = \gamma_1 + \frac{RT}{\epsilon_1} \ln \frac{X^s_1}{X^b_1} = \gamma_2 + \frac{RT}{\epsilon_2} \ln \frac{X^s_2}{X^b_2} \qquad (2)$$

where γ_1 and γ_2 are the surface tensions of the pure components ϵ_1 and ϵ_2 are the molal surface areas, and X^s and X^b are the surface and bulk mole fractions, respectively.[7-9] If solutions are not ideal, an additional term must be included in equation 2 to take into account the mutual interaction of the two components. Surface adsorption of the solute is favored by positive deviations from Raoult's law as well as by a lowering of the surface tension.[7-9]

As indicated in Table I, small additions of chromium and titanium have no appreciable effect on the surface tension of nickel. This is not unexpected, since various empirical correlations[3,10,11] indicate that the surface tensions of titanium and chromium should be similar to that of nickel.

The surface tension of nickel is markedly lowered by small additions of indium and tin. These effects have been calculated from equation 2. The measured density (8.0 g./cc.) and surface tension (1725 dyne/cm.) were employed for liquid nickel in these calculations, taking surface area as equal to the (molal volume)$^{2/3}$. The density of tin is known[12] at 1475° (6.18 g./cc.), giving a surface area of 10.0×10^{-16} cm.^{2}/atom. A linear extrapolation of the molar volume *vs.* temperature for indium[13] gives a surface area of 10×10^{-16} cm.^{2}/atom at 1475°. Crude extrapolations of surface tension data from much lower temperatures give estimates of 400 dyne/cm. for the surface tension of tin and 150 dyne/cm. for the surface tension of indium at 1475°.

Results of these calculations are shown as solid lines in Fig. 1 together with measured surface tensions. Tin shows negative deviations from ideal solution behavior,[14] so that a smaller surface activity is expected than that calculated. Deviations of Ni–In solutions from ideal solution behavior are not known. Additions above 0.5% show surface tensions of the magnitude to be expected, with deviations for tin occurring in the right direction to be accounted for by deviations from ideality. The lower concentrations show surface tensions which are considerably lower than can be accounted for by ideal solution behavior, and can hardly be accounted for by deviations from ideality since they deviate in the opposite directions from higher concentrations. We have no satisfactory explanation of these results for low concentrations. They are probably in part, and may be completely, due to the 0.005% oxygen present. About this same amount of oxygen is present in the Ni–Cr and Ni–Ti solutions, but would have a lower activity there.

The surface tension of pure nickel may be taken from these results as equal to 1725 dyne/cm. at 1475°. This value is close to the value of 1720 dyne/cm. at 1570° previously reported for pure liquid iron.[4]

B. Interfacial Energy with Al_2O_3.—The interfacial energies of the compositions studied are shown in Fig. 2, plotted against log weight per cent. addition. Over the range of compositions studied, additions of tin and or indium have little effect on the interface energy. In contrast, both titanium and chromium markedly lower the interface energy. The excess surface concentrations can be derived from the Gibbs isotherm

$$\Gamma = -\frac{d\gamma}{RT\, d \ln a} \qquad (3)$$

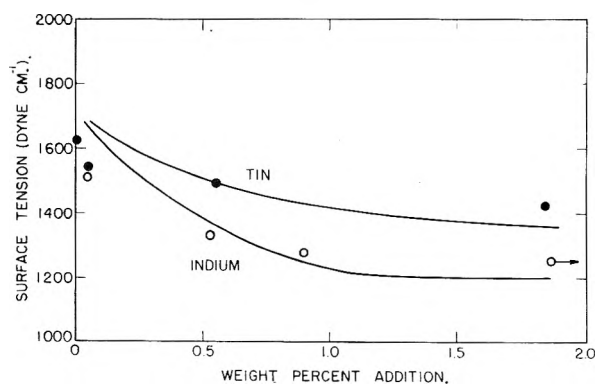

Fig. 1.—Effect of tin and indium on the surface tension of liquid nickel at 1475°.

(7) R. Defay and I. Prigogine, *Trans. Faraday Soc.*, **46**, 199 (1950).

(8) J. H. Hildebrand and R. L. Scott, "Solubility of Non-Electrolytes," Reinhold Publ. Corp., New York, N. Y., 1950.

(9) E. A. Guggenheim, "Mixtures," Oxford Univ. Press, Cambridge, 1952.

(10) C. J. Leadbeater, "Selected Gov't. Res. Rept., Powder Metallurgy," Ministry of Supply, 1951.

(11) K. Huang and R. Wyllie, *Proc. Phys. Soc.*, **A62**, 180 (1949).

(12) A. L. Day and R. B. Sosman and J. C. Hostetter, *Am. J. Sci.*, **37**, 1 (1914).

(13) R. N. Lyon, Ed., "Liquid Metals Handbook," Atomic Energy Commission and Bureau of Ships, 1952.

(14) C. Wagner, "Thermodynamics of Alloys," Addison-Wesley Press, Cambridge, Mass., 1952.

and indicate that a monolayer of adsorbed titanium (12×10^{14} atoms/cm.^{2}) is found at about 0.01 weight % concentrations. A monolayer of adsorbed chromium (13×10^{14} atoms/cm.^{2}) is formed at about 1.0 weight % chromium. Since there are 15.3×10^{14} atoms/cm.^{2} in the plane of densest packing of oxygen atoms in Al_2O_3,[15] and the surfaces used were randomly oriented and small grained, this corresponds to about one excess metal atom for each oxygen ion at the surface.

The solid curves in Fig. 2 have been drawn in conformance with the Langmuir adsorption equation,[8,9] *i.e.*

$$\Gamma = \sigma \frac{c}{c + c_0} \qquad (4)$$

$$\gamma = \gamma_0 - \sigma kT \ln \left(1 + \frac{c}{c_0}\right) \qquad (5)$$

where σ and c_0 are experimentally determined constants. These curves fit the experimental data reasonably well. Without information as to activities, speculation regarding deviations seems pointless.

These results and other measurements of interface energies of metals on oxide systems[4-6] indicate that the oxide surface is dominated by large oxygen anions, and that there is little attraction between an oxide surface and an inert metal. It is only highly electropositive constituents (such as chromium and titanium) which tend to concentrate at the interface. This transfer to the interface layer is a chemisorption process and may be represented as

(15) W. L. Bragg, "Atomic Structure of Minerals," Cornell Univ. Press, Ithaca, N. Y., 1937, p. 93.

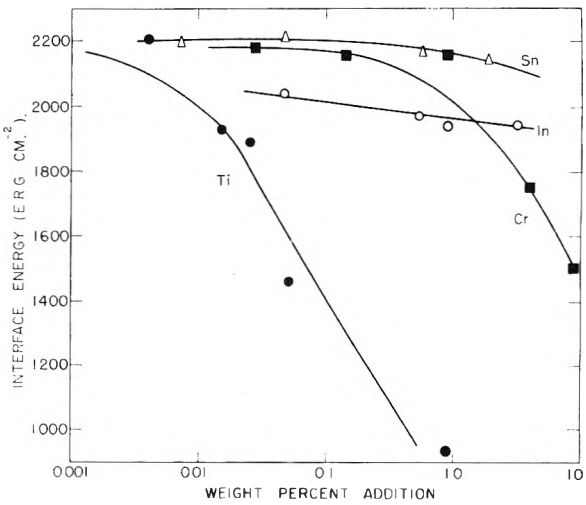

Fig. 2.—Effect of Sn, Ti, In and Cr on the Ni(l)–Al_2O_3(s) interfacial energy at 1475°.

$$M_1(\text{solute}) + M_2\text{–O(surface)} = M_1\text{–O(surface)} + M_2(\text{solvent}) \qquad (6)$$

with the free energy change for this process directly related to the standard free energies of formation of the oxides. Materials forming more stable oxides (Cr, Ti, Si[6]) than the solvent (Ni, Fe[6]) are adsorbed at the oxide surface while solutes forming less stable oxides (In, Sn) show little interfacial adsorption. The concentration at which essentially complete surface coverage is obtained (1, 0.1, and 0.01 for Cr, Si and Ti) decreases with increasing oxide stability ($\Delta F^\circ_{TiO} = -117$ kcal./mole; $\Delta F^\circ_{1/2SiO_2} = -110$; $\Delta F^\circ_{1/3Cr_2O_3} = -96$).

BINARY FREEZING POINT DIAGRAMS FOR 2-AMINOPYRIDINE WITH SATURATED AND UNSATURATED LONG CHAIN FATTY ACIDS

BY ROBERT R. MOD AND EVALD L. SKAU

Southern Regional Research Laboratory,[1] *New Orleans, Louisiana*

Received January 21, 1956

Binary freezing point data have been obtained for 2-aminopyridine with lauric, myristic, palmitic, stearic, oleic, elaidic and α- and β-eleostearic acids. The binary diagrams prove the existence of two congruently-melting, crystalline, molecular compounds in each case. For the saturated acid systems, the compounds had the compositions $RCOOH \cdot NC_5H_4NH_2$ and $4RCOOH \cdot NC_5H_4NH_2$, and for the unsaturated acid systems, $R'COOH \cdot NC_5H_4NH_2$ and $2R'COOH \cdot NC_5H_4NH_2$. If the deviation from ideal freezing point depression can be attributed to molecular compound formation alone the data show that the degree of dissociation of the acid–amine compound in the molten state varies with the chain length and the degree of unsaturation. For the saturated acids dissociation is greater the longer the chain length of the acid. For the C_{18} acids the dissociation is greater the less the degree of unsaturation.

Though amine salts of mixtures of long chain fatty acids have long been used as soaps, emulsifiers and detergents very little effort has been made toward the isolation and characterization of the pure individual compounds. Ramsay and Patterson[2] isolated an equimolecular compound of 2-aminopyridine with stearic acid in connection with the use of this amine in the separation of homologous fatty acids by partition chromatography. In previous publications[3-6] from this Laboratory it was shown by binary freezing point measurements that acetamide forms a similar 1:1 compound with stearic acid but that the corresponding C_{18}, mono-unsaturated oleic and elaidic compounds have incongruent melting points and the more highly unsaturated eleostearic acids form no crystalline molecular

(1) One of the laboratories of the Southern Utilization Research Branch, Agricultural Research Service, U. S. Department of Agriculture.

(2) L. L. Ramsay and W. I. Patterson, *J. Assoc. Off. Agr. Chemists*, **31**, 139 (1948).

(3) F. C. Magne and E. L. Skau, *J. Am. Chem. Soc.*, **74**, 2628 (1952).

(4) R. R. Mod and E. L. Skau, THIS JOURNAL, **56**, 1016 (1952).

(5) R. R. Mod, E. L. Skau and R. W. Planck, *J. Am. Oil Chem. Soc.*, **30**, 368 (1953).

(6) R. T. O'Connor, R. R. Mod, M. D. Murray and E. L. Skau, *J. Am. Chem. Soc.*, **77**, 892 (1955).

compounds. The binary freezing point diagrams for 2-aminopyridine with a number of saturated and unsaturated fatty acids reported below show that two crystalline compounds form in each case—an equimolecular compound and a compound consisting of 2 or 4 molecules of acid per molecule of amine depending upon whether the acid is unsaturated or saturated.

Experimental

The fatty acids were purified by the procedures previously described.[3-5] The pure 2-aminopyridine, f.p. 58.0°, was obtained by repeated recrystallization from benzene. The freezing point determinations were made with a probable accuracy of ±0.2° by the thermostatic synthetic procedure,[3] which involves finding two temperatures a few tenths of a degree apart at which, in one case, liquefaction is complete and, in the other, a few crystals persist after a long period with agitation at constant temperature.

Results and Discussion

The data for the complete binary freezing point diagrams are given in Table I and are represented graphically for the saturated acids in Fig. 1 and for the various unsaturated acids in Fig. 2. For the oleic acid system only two points were obtained in equilibrium with the stable modification of the acid; the metastable equilibria are represented by the broken lines in Fig. 2. In all of the eight systems two molecular compounds form, each having a congruent melting point.

TABLE I

BINARY FREEZING POINT DATA FOR 2-AMINOPYRIDINE WITH VARIOUS ACIDS[a]

Mole % 2-amino-pyridine	F.p., °C.	Mole % 2-amino-pyridine	F.p., °C.	Mole % 2-amino-pyridine	F.p., °C.
Lauric acid		Myristic acid		Palmitic acid	
0.00	43.9	0.00	53.9	0.00	62.5
6.23	41.8	12.27	50.2	6.56	61.3
12.41	39.2	16.68	47.6	12.50	59.4
16.00	36.5	(17.7)[b]	(46.8)[b]	17.28	57.2
17.61	35.0	(20.00)[c]	(47.2)[c]	(18.0)[b]	(56.6)[b]
(18.5)[b]	(33.8)[b]	21.06	47.2	18.47	56.7
19.23	33.9	30.68	44.5	18.93	56.9
(20.00)[c]	(33.9)[c]	(33.20)[b]	(43.2)[b]	(20.00)[c]	(57.0)[c]
21.29	33.9	35.88	46.1	20.58	57.0
26.15	32.9	(50.00)[c]	(51.3)[c]	23.15	56.9
30.10	32.1	51.33	51.3	26.11	56.5
(32.4)[b]	(31.6)[b]	68.62	46.8	29.17	55.6
35.08	34.6	(73.2)[b]	(44.4)[b]	31.47	54.1
39.07	38.2	79.43	48.9	(33.4)[b]	(52.6)[b]
45.56	41.3	89.71	54.2	34.64	53.5
(50.00)[c]	(41.6)[c]	100.00	58.0	37.16	55.2
50.15	41.6			41.71	57.3
54.51	41.4			44.90	58.2
59.78	40.1			(50.00)[c]	(58.8)[c]
64.84	38.1			50.67	58.8
(67.4)[b]	(36.8)[b]			54.64	58.4
70.21	40.0			59.86	57.3
74.88	44.3			69.30	54.5
79.51	47.7			73.69	53.0
84.67	50.8			75.27	52.4
94.77	55.6			(80.00)[b]	(50.5)[b]
100.00	58.0			80.00	50.5
				82.11	51.4
				89.71	54.4
				100.00	58.0

Mole % 2-amino-pyridine	F.p., °C.	Mole % 2-amino-pyridine	F.p., °C.	Mole % 2-amino-pyridine	F.p., °C.
Stearic acid		α-Eleostearic acid		β-Eleostearic acid	
0.00	69.3	0.00	48.4	0.00	70.5
12.40	66.8	14.58	43.4	12.28	67.2
15.77	65.5	16.11	42.3	17.83	64.7
(18.0)[b]	(64.5)[b]	17.82	41.4	19.87	63.6
(20.00)[c]	(65.0)[c]	21.61	38.1	24.36	60.7
22.07	65.0	29.81	28.9	28.51	57.4
31.95	62.8	31.42	26.9	(28.5)[b]	(57.4)[b]
(35.2)[b]	(60.3)[b]	(31.6)[b]	(26.4)[b]	(33.33)[c]	(58.7)[c]
37.44	61.3	(33.33)[c]	(26.5)[c]	33.59	58.7
(50.00)[c]	(64.7)[c]	34.68	26.5	36.31	58.4
50.69	64.7	35.26	26.4	(40.0)[b]	(57.0)[b]
65.34	62.1	37.72	26.5	40.19	57.1
79.90	57.3	42.19	24.6	43.42	58.4
85.88	54.9	(42.2)[b]	(24.6)[b]	48.31	59.3
(87.40)[b]	(54.2)[b]	46.76	27.3	(50.00)[c]	(59.4)[c]
90.26	55.2	47.91	27.6	53.05	59.4
94.45	56.5	49.96	27.9	58.54	58.1
100.00	58.0	(50.00)[c]	(27.9)[c]	63.56	56.3
		54.89	27.2	71.93	53.1
		58.35	26.3	75.88	50.8
		60.56	25.6	79.76	48.9
		(62.4)[b]	(24.6)[b]	(80.80)[b]	(48.4)[b]
		63.93	29.0	85.03	51.0
		67.11	35.3	87.99	52.5
		88.15	52.3	100.00	58.0
		100.00	58.0		
Elaidic acid		Oleic acid			
0.00	43.8	0.00	16.3, *13.5*[d]		
13.58	40.6	4.44	15.8, *12.8*		
19.71	37.6	8.20	*11.6*		
21.89	36.3	14.27	*8.7*		
22.34	36.0	(19.1)[b]	*(5.9)*[b]		
(24.0)[b]	(34.8)[b]	22.17	8.6		
27.05	35.6	26.68	11.8		
30.50	36.4	32.72	13.7		
33.17	36.7	(33.33)[c]	(13.8)[c]		
(33.33)[c]	(36.7)[c]	36.40	13.4		
34.24	36.6	41.61	11.1		
35.05	36.5	(45.5)[b]	(8.9)[b]		
(36.6)[b]	(36.0)[b]	47.56	9.4		
36.85	36.1	49.66	9.8		
37.12	36.3	(50.00)[c]	(9.8)[c]		
43.56	39.3	51.17	9.8		
(50.00)[c]	(40.2)[c]	51.85	9.9		
50.77	40.1	(53.6)[b]	(9.5)[b]		
62.06	38.2	54.65	12.9		
(65.9)[b]	(36.7)[b]	56.80	19.4		
65.93	36.7	61.41	29.9		
67.85	39.9	71.38	43.4		
74.58	46.0	80.50	49.9		
85.85	52.8	100.00	58.0		
100.00	58.0				

[a] The values in parentheses were obtained by graphical interpolation. [b] Eutectic. [c] Freezing point of compound. [d] Values in italics are for metastable equilibria.

For the saturated fatty acids these compounds have the compositions $RCOOH \cdot NC_5H_4NH_2$ and $4RCOOH \cdot NC_5H_4NH_2$. The freezing points of the 4:1 and 1:1 compounds for stearic acid are nearly identical, about 4.3 and 4.6°, respectively, below that of the acid. As the number of carbon atoms in the acid decreases from 18 to 12 the difference

between the freezing points of the acid and the 4:1 compound increases from 4.3 to 10.0° while the corresponding difference for the 1:1 compound decreases from 4.6 to 2.3°. As a result, the freezing point of the 4:1 compound in the stearic acid system is 0.3° higher than that of the 1:1 compound, but for palmitic, myristic and lauric acids it is 1.8, 4.1 and 7.7° lower, respectively.

Since all of the molecular compounds melt congruently there are three eutectics, *viz.*, between the acid and the 4:1 compound, between the 4:1 and 1:1 compounds, and between the 1:1 compound and the amine. For stearic acid these eutectic compositions are 18.0, 35.2 and 87.4 mole % of amine, respectively. As the number of carbon atoms in the acid molecule decreases the first of these eutectic compositions remains virtually unchanged and the others change gradually so that the eutectic compositions for the lauric acid system are 18.5, 32.4 and 67.4 mole % of amine, respectively.

In contrast to the behavior of the saturated acids, the molecular compounds formed by the C_{18} unsaturated fatty acids have the compositions $RCOOH{\cdot}NC_5H_4NH_2$ and $2RCOOH{\cdot}NC_5H_4NH_2$. The 1:1 compound of elaidic (*trans*) acid has a higher freezing point than the 2:1 compound, and for the oleic (*cis*) acid the reverse is true. For the (*cis-trans-trans*) α- and (*trans-trans-trans*) β-eleostearic acids the 1:1 compound has a slightly higher freezing point than the 2:1 in both cases.

It is apparent from the amine side of Fig. 1 that the lowering of the freezing point of 2-aminopyridine by a given mole % of saturated fatty acid is greater the shorter the chain length of the acid. This can be construed as meaning that the degree of dissociation of the molten molecular compounds into free acid and amine decreases with a decrease in the length of the fatty acid molecule, as was previously[3] found to be true for the molecular compounds between acetamide and these acids. According to the same reasoning the degrees of dissociation of the acid–amine compounds for the oleic, elaidic and myristic acids are practically identical; that for the β-eleostearic acid is about the same as lauric acid; and that for the α-eleostearic acid is the lowest of all. This would indicate that for the C_{18} acids the degree of dissociation of the acid–amine compound decreases as the degree of unsaturation increases.

For the saturated acids the relative degrees of dissociation of the acid–amine compounds can also be deduced from the data on the acid side of Fig. 1; *i.e.*, from the freezing point depression of the acid by the amine. Since the heats of fusion of the individual saturated fatty acids are known, the ideal freezing point lowering can be calculated. In the range of concentrations where the acid is the solid phase the experimental freezing points fall below the calculated values and the deviation increases as the chain length of the acid decreases. If the deviation is attributed entirely to compound formation the data show that, at the temperature in question, the proportion of free acid present in the molten acid–amine compound is lowest for the short chain acids. This is consistent with the above conclusion that the degree of dissociation of the saturated acid–amine compounds increases as the length of the acid molecule increases.

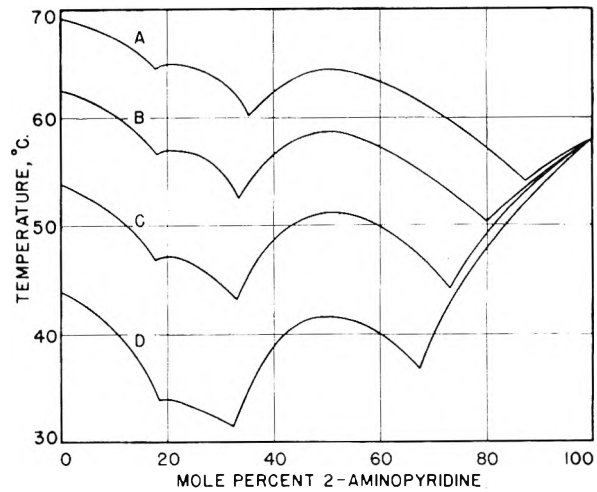

Fig. 1.—Binary freezing point diagrams for 2-aminopyridine with: A, stearic acid; B, palmitic acid; C, myristic acid; D, lauric acid.

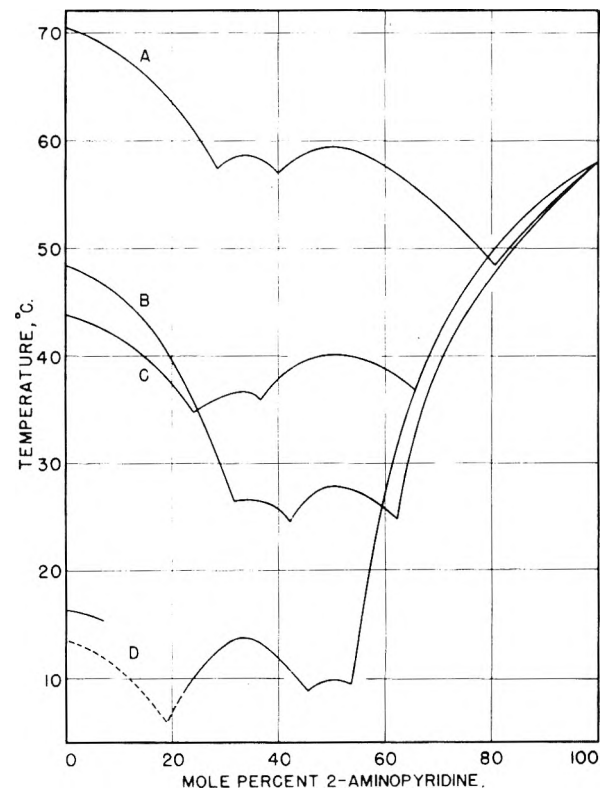

Fig. 2.—Binary freezing-point diagrams for 2-aminopyridine with: A, β-eleostearic acid; B, α-eleostearic acid; C, elaidic acid; D, oleic acid. Broken lines represent metastable equilibria.

Acknowledgment.—The authors are indebted to Ralph W. Planck for supplying the purified α- and β-eleostearic acids.

APPROXIMATIONS IN THE KINETICS OF CONSECUTIVE REACTIONS

BY DARL H. MCDANIEL AND CHARLES R. SMOOT

Contribution from the Departments of Chemistry of the University of Pittsburgh, Pittsburgh, Pa., and Purdue University, Lafayette, Ind.

Received January 25, 1956

A general approximation for the kinetics of the reaction $A \rightleftarrows B \rightarrow C$ has been developed. The limits of the approximation and the relation between the approximation and the exact solution are established. Comparison of the results of this approximation with other approximations in current use is made.

The increasingly frequent use of steady-state and equilibrium treatment approximations for the kinetic treatment of complex reactions warrants a fresh look at the assumptions involved. Such a look leads to a more general approximation than has been used previously. Consider the reaction

$$A \underset{k_2}{\overset{k_1}{\rightleftarrows}} B \xrightarrow{k_3} C \qquad (1)$$

Here

$$\frac{d[A]}{dt} = k_2[B] - k_1[A] \qquad (2)$$

$$\frac{d[B]}{dt} = k_1[A] - k_2[B] - k_3[B] \qquad (3)$$

$$\frac{d[C]}{dt} = k_3[B] \qquad (4)$$

And if we set

$$[A] + [B] + [C] = A^\circ \qquad (5)$$

Then

$$\frac{d[A]}{dt} + \frac{d[B]}{dt} + \frac{d[C]}{dt} = 0 \qquad (6)$$

The exact solution of this set of equations is known[1,2] and will be discussed in a later section of the paper.

One variation of the equilibrium treatment[3] makes use of equations 4 and 6 and the two approximations that

(a) $[B] = K_{eq}[A] = \frac{k_1}{k_2}[A]$

(b) $\frac{d[B]}{dt}$ is negligible in equation 6

This gives

$$-\frac{d[A]}{dt} = \frac{d[C]}{dt} = \frac{k_1k_3[A]}{k_2} \qquad (7)$$

Alternatively, and more rigorously, an expression for $d[B]/dt$ may be obtained from the first approximation (a) and used in equation 6, giving

$$-\frac{d[A]}{dt} = \frac{k_1k_3}{k_1 + k_2}[A] \qquad (8)$$

In this paper equation 7 will be termed the equilibrium approximation and equation 8 the rigorous equilibrium approximation.

The steady-state treatment[3] makes use of equations 3, 4, and 6 and the approximation that $d[B]/dt$ is negligible in equations 3 and 6. This gives

$$[B] = \frac{k_1}{k_2 + k_3}[A]$$

and

$$-\frac{d[A]}{dt} = \frac{d[C]}{dt} = \frac{k_1k_3}{k_2 + k_3}[A] \qquad (9)$$

The treatment developed here makes use of equations 3, 4 and 6 and the first approximation that $d[B]/dt$ is negligible in equation 3. As in the case of the steady-state treatment this assumption and equation 3 yield

$$[B] = \frac{k_1}{k_2 + k_3}[A] \qquad (10)$$

A second approximation for $d[B]/dt$ may be obtained by differentiating the above equation with respect to t, *i.e.*

$$\frac{d[B]}{dt} = \frac{k_1}{k_2 + k_3}\frac{d[A]}{dt} \qquad (11)$$

If this second approximation for $d[B]/dt$ is used in equation 6, and (10) with (4), then

$$-\frac{d[A]}{dt} - \frac{k_1}{k_2 + k_3}\frac{d[A]}{dt} = \frac{d[C]}{dt} = \frac{k_1k_3}{k_2 + k_3}[A]$$

which rearranges to

$$-\frac{d[A]}{dt} = \frac{k_1k_3}{k_1 + k_2 + k_3}[A] \qquad (12)$$

Equation 12 may be termed the improved steady-state approximation. Inspection of equations 7, 8 and 9 shows that the equilibrium treatment, the rigorous equilibrium treatment, and the steady-state treatment may all be considered to hold as special cases of (12) where the terms k_1 and k_3, k_3, and k_1, respectively, are negligible terms in the denominator.

Limits of the Approximation.—The limits of the improved steady state approximation may be roughly set by a third approximation, *i.e.*, (3) and (11) may be equated and $d[A]/dt$ replaced by $k_2[B] - k_1[A]$, *i.e.* (2) giving

$$[B] = \frac{k_1(k_1 + k_2 + k_3)[A]}{k_2(k_1 + k_2 + k_3) + k_3(k_2 + k_3)}$$

This reduces to

$$[B] = \frac{k_1}{k_3 + k_2}[A]$$

when $k_1 << k_2 + k_3$, *i.e.*, the intermediate is unstable *or* when $k_3 << k_2$, *i.e.*, the rate of product formation is so slow that an equilibrium does exist between the reactant and intermediate. Either condition is sufficient for the approximation to hold for the calculation of [A] and [B]. Furthermore, we are pleasantly surprised to find that due to the symmetry of the exact solution for [C] with regard

(1) T. M. Lowry and W. T. Johns, *J. Chem. Soc.*, **97**, 2634 (1910).

(2) See also A. A. Frost and R. G. Pearson, "Kinetics and Mechanism," John Wiley and Sons, Inc., New York, N. Y., 1953, pp. 160–164. The treatment given in these references is for a more general case involving an additional rate constant, k_4, as a return reaction of C yielding B. The solution for (1) is then a specific case where $k_4 = 0$ in the solution given in references 1 and 2.

(3) See, for example, ref. 2, pp. 179–183.

to interchange of k_1 and k_3 the approximation breaks down for [C] only as k_1 and k_3 approach each other and k_2 becomes less than k_1 or k_3.

The limits may be found more rigorously by a comparison with an exact solution. The exact solution[1,2] of

$$A \underset{k_2}{\overset{k_1}{\rightleftharpoons}} B \xrightarrow{k_3} C$$

has the form

$$[A], [B] \text{ or } [C] = C_1 + C_2 \exp\{-\lambda_2 t\} + C_3 \exp\{-\lambda_3 t\}$$

The coefficients C_1, C_2 and C_3 are constants which are functions of the rate constants and are different for [A], [B] and [C]. The values of λ_2 and λ_3 are also functions of the rate constants, but are the same for [A], [B] and [C]. The exponential term which controls the equation at large values of t is given by

$$\lambda_3 = 1/2\{k_1 + k_2 + k_3 - \sqrt{(k_1 + k_2 + k_3)^2 - 4k_1k_3}\}$$

A binomial expansion of the expression for λ_3 gives

$$\lambda_3 = \frac{k_1k_3}{k_1 + k_2 + k_3} + \frac{(k_1k_3)^2}{(k_1 + k_2 + k_3)^3} + \frac{2(k_1k_3)^3}{(k_1 + k_2 + k_3)^5} + \frac{5(k_1k_3)^4}{(k_1 + k_2 + k_3)^7} + \cdots$$

The first term of this series is seen to be identical with our approximation for the over-all rate constant. The necessary condition for the first term to adequately represent the series is that $4k_1k_3/(k_1 + k_2 + k_3)^2$ be small compared to one. This condition is fulfilled under any of the following circumstances

(a) $k_2 \gg k_3$ (c) $k_3 \gg k_1$
(b) $k_2 \gg k_1$ (d) $k_1 \gg k_3$

The Integrated Form of the Approximation.—Equation 12 may be integrated to give

$$[A] = \text{Const. exp.}\left\{-\frac{k_1k_3}{k_1 + k_2 + k_3}t\right\}$$

Since the approximation holds only after a transient equilibrium has been established, the boundary condition of $[A] = A^\circ$ at $t = 0$ is not useful. Instead an extrapolated boundary at $t = 0$ of $[B] = [k_1/(k_2 + k_3)]\,[A]$ and $[A] + [B] = A^\circ$ has been used here and gives

$$[A] = \left\{1 - \frac{k_1}{k_1 + k_2 + k_3}\right\} A^\circ \exp.\left\{-\frac{k_1k_3}{k_1 + k_2 + k_3}t\right\} \quad (13)$$

and

$$[B] = \frac{k_1}{k_1 + k_2 + k_3} A^\circ \exp.\left\{-\frac{k_1k_3}{k_1 + k_2 + k_3}t\right\} \quad (14)$$

and by difference

$$[C] = A^\circ\left\{1 - \exp.\left(-\frac{k_1k_3}{k_1 + k_2 + k_2}t\right)\right\} \quad (15)$$

The integrated form[4] of the equilibrium approximation (7) may be taken as

$$[C] = A^\circ\left\{1 - \exp.\left(-\frac{k_1k_3}{k_2}t\right)\right\} \quad (16)$$

and of the rigorous equilibrium treatment (8) as

$$[C] = A^\circ\left\{1 - \exp.\left(-\frac{k_1k_3}{k_1 + k_2}t\right)\right\} \quad (17)$$

and of the steady state approximation (9) as

$$[C] = A^\circ\left\{1 - \exp.\left(-\frac{k_1k_3}{k_2 + k_3}t\right)\right\} \quad (18)$$

Comparison of the Results of the Approximations with the Exact Solution.—Figure 1 shows the

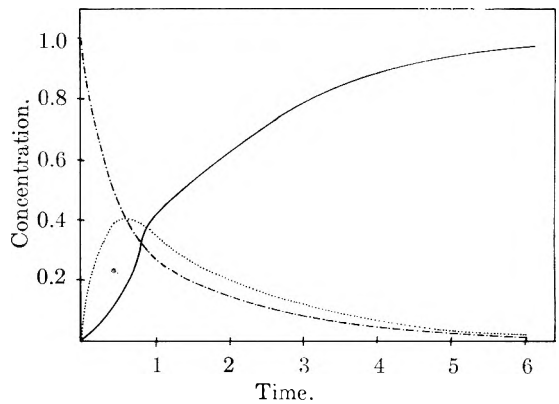

Fig. 1.—Variation of concentrations with time for a first-order consecutive reaction with $k_1 = 2$, $k_2 = 1$, $k_3 = 1$ (see eq. 1). Solid line denotes [C], dotted line denotes [B], and the dot-dashed line denotes [A]. Concentrations are expressed as fractions of A°. The induction period is 1.25 time units.

variation of the concentrations of A, B and C with time calculated from the exact solution[1,2,5] for the values $k_1 = 2$, $k_2 = 1$ and $k_3 = 1$.[6] It may be noted that a period of time is required before [B] assumes a constant relation with respect to [A]. Until [B] has attained a constant relationship to [A], none of the approximations, (15), (16), (17) and (18) may be expected to hold. This period of time has been termed the induction period. We have taken the point of inflection in the curve of [B] *versus* t as a criterion for the length of the induction period, *i.e.*

$$t = \frac{2}{\lambda_2 - \lambda_3} \ln \frac{\lambda_2}{\lambda_3}$$

Figure 2 shows the variation of [C] *versus* t calculated for $k_1 = 1$, $k_2 = 100$, $k_3 = 1$ by the approximations and the exact solution. It is expected here that all approximations will be about equally satisfactory since both k_1 and k_3 are small compared to k_2.

Figure 3a shows [C] *versus* t for $k_1 = 1$, $k_2 = 100$ and $k_3 = 100$. Here it is expected that the equilibrium treatments will be unsatisfactory since k_3 may not be ignored. The steady-state treatment will be about as satisfactory as the improved steady state treatment since k_1 is small compared to $k_2 + k_3$.

Figure 3b shows [C] *versus* t for $k_1 = 100$, $k_2 = 100$ and $k_3 = 1$. In this case neither the non-rigorous equilibrium nor the steady-state treatment are expected to be satisfactory since k_1 is not small compared to $k_2 + k_3$. The rigorous equilibrium

(4) It may be noted that [C] is not particularly affected by the boundary conditions used as long as [C] = 0 at $t = 0$.

(5) The values of λ may be evaluated readily by means of a table prepared by S. W. Benson, *J. Chem. Phys.*, **20**, 1605 (1952). He has tabulated z_1 and z_2 which are the roots of $z^2 - (1 + K_1 + K_3)z + K_1K_3$ where $K_1 = k_1/k_2$ and $K_3 = k_3/k_2$. From these $\lambda_2 = k_2z_1$ and $\lambda_3 = k_2z_2$.

(6) The numerical values of the rate constants in the examples given were arbitrarily selected for ease of calculation and only the relative magnitudes are important.

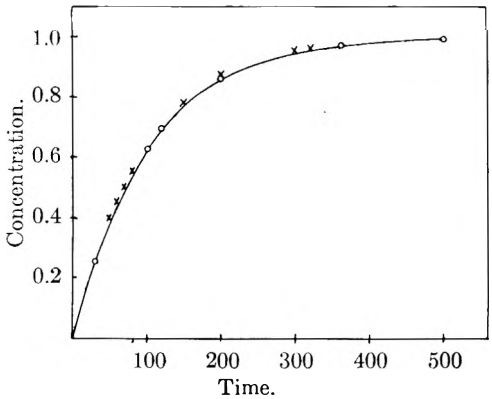

Fig. 2.—Variation of [C] with time for $k_1 = 1$, $k_2 = 100$, $k_3 = 1$ (see eq. 1) comparing the approximations with the exact solution. The solid line denotes the exact solution and (within the limits of the graph) the improved steady-state approximation, eq. 15. The x's denote points calculated by the equilibrium approximation, eq. 16, and the circles denote points calculated by the rigorous equilibrium approximation, eq. 17, and by the steady-state approximation, eq. 18. The induction period is 0.18 time unit.

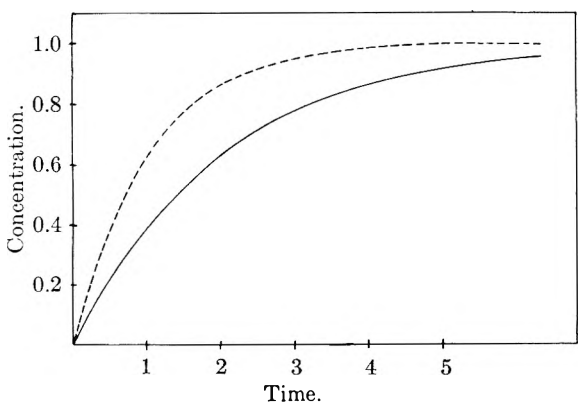

Fig. 3a.—Variation of [C] with time for $k_1 = 1$, $k_2 = 100$, $k_3 = 100$ (see eq. 1) comparing the approximations with the exact solution. The solid line denotes (within the limits of the graph) the exact solution, the improved steady-state approximation, and the steady-state approximation. The broken line denotes the equilibrium approximations, eq. 16 and 17. The induction period is 0.06 time unit.

3b. Variation of [C] with time for $k_1 = 100$, $k_2 = 100$, $k_3 = 1$ (see eq. 1) comparing the approximations with the exact solution. Within the limits of the graph the solid line denotes the exact solution, the improved steady-state approximation, and the rigorous equilibrium approximation. The broken line denotes the equilibrium approximation and the steady-state approximation. The induction period is 0.06 time unit.

treatment will be about as satisfactory as the improved steady-state treatment since k_3 is small compared to $k_1 + k_2$.

In the three examples which were given (Figs. 2 and 3) it was found that the improved steady-state approximation was the only approximation which was satisfactory in all cases. Furthermore, this approximation exceeded the accuracy of the next best approximation although this difference was too small to represent graphically. This difference is greatly magnified in the cases where the improved steady-state approximation itself begins to deviate noticeably from the exact solution. Figure 4 shows [C] *versus* t for $k_1 = 1$, $k_2 = 1$ and $k_3 = 1$. After the induction period, which covers 40% of

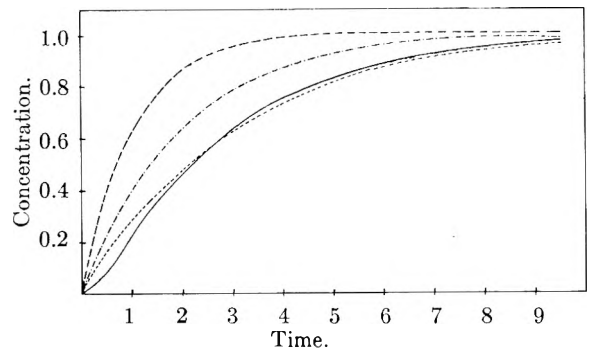

Fig. 4.—Variation of [C] with time for $k_1 = 1$, $k_2 = 1$, $k_3 = 1$ (see eq. 1) comparing the approximations with the exact solution. The solid line denotes the exact solution, the short dashes denote the improved steady-state approximation, the dot-dashed line denotes both the rigorous equilibrium approximation and the steady-state approximation, and the long dashes denote the equilibrium approximation. The induction period is 1.74 time units.

the reaction, the improved steady-state treatment gives results within 10% of the exact solution whereas the rigorous equilibrium treatment and the steady-state treatment have a maximum error of 40%. For example, at $t = 4$ time units the value of [C] in terms of A° is 0.747 by the exact solution, 0.735 by the improved steady-state approximation, 0.87 by the rigorous equilibrium and steady-state approximations, and 0.98 by the equilibrium approximation.

Finally, the case where $k_2 = 0$ and k_1 and k_3 become equal may be considered. This is the case where the improved steady-state treatment is expected to behave most poorly. Figure 5 illustrates

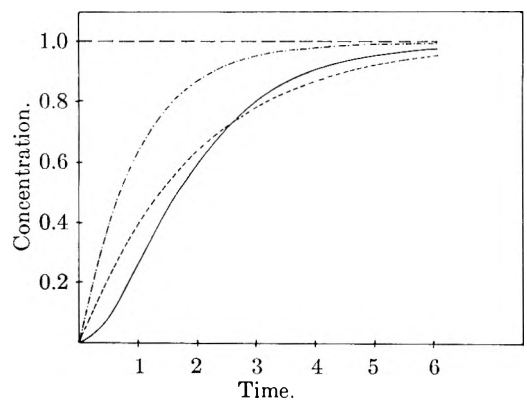

Fig. 5.—Variation of [C] with time for $k_1 = 1$, $k_2 = 0$, $k_3 = 1$ (see eq. 1) comparing the approximations with the exact solution. The solid line denotes the exact solution, the short dashes denote the improved steady-state approximation, the dot-dashed line denotes both the rigorous equilibrium approximation and the steady-state approximation, and the long dashes denote the equilibrium approximation. The induction period is 2.00 time units.

this case. Here the induction period takes up 61% of the reaction. Yet after the induction period is over the improved steady-state treatment gives values for [C] within 5% of the values calculated by an exact treatment. The rigorous equilibrium treatment and the steady-state treatment again have maximum errors of about 40%. For example at $t = 3$ time units the value of [C] in terms of A° is 0.80 by the exact solution, 0.78 by the improved steady-state approximation, 0.95 by the rigorous

equilibrium and steady-state approximations, and 1.00 by the equilibrium approximation.

Approximations for the Kinetics of Higher Order Reactions.—The degree of success of equation 15 in approximating the exact solution prompts us to look at higher order reactions where an exact solution has not yet been found and one must resort to an approximation. For the general case

$$nA \underset{k_2}{\overset{k_1}{\rightleftharpoons}} B \xrightarrow{k_3} C$$

both the non-rigorous equilibrium and steady-state treatments yield the same form of the rate constant as in the previous case whereas our approximation yields[7]

$$\frac{dA}{dt} = \frac{nk_1k_3[A]^n}{n^2k_1[A]^{n-1} + k_2 + k_3}$$

We are currently investigating these higher order reactions as well as studying the implications of these results on the calculation of equilibrium constants from the forward and reverse rate constants of complex reactions.

NOTE ADDED IN PROOF.—Equation 15 may be derived in a somewhat different manner than has been used here; see K. J. Laidler, *Can. J. Chem.*, **33**, 1614 (1955).

(7) The rate constants refer to production or disappearance of B.

THE REACTION BETWEEN AQUO FERROUS IRON AND CUMENE HYDROPEROXIDE[1]

BY W. L. REYNOLDS[2] AND I. M. KOLTHOFF

Contribution from the School of Chemistry, University of Minnesota, Minneapolis, Minnesota

Received February 1, 1956

The rate constants of the reaction between ferrous iron and cumene hydroperoxide have been found to be $3.53 \times 10^8 \exp(-9970/RT)$ and $9.25 \times 10^8 \exp(-10840/RT)$ liter mole^{-1} sec.$^{-1}$ in H_2O and D_2O media, respectively. The main products of the reaction are ferric iron, acetophenone and ethane. A reaction mechanism is postulated and discussed. The possible nature of the rate-determining reaction step is also briefly discussed.

The ability of hydroperoxides to furnish free radicals upon reduction with a suitable reducing agent has led to their widespread use as initiating agents for polymerization.[3] It has been observed that different hydroperoxides yield widely different rates of polymerization in emulsion polymerization systems. Differences in the rates of polymerization with different hydroperoxides may result from differences in the rates of reaction of the hydroperoxides with a given reductant, from differences in the reactivity of the free radicals produced in the reduction of the hydroperoxides, and from differences in the distribution of hydroperoxide between the aqueous and organic layers. Since an iron(II) species frequently is used as the reducing agent for the hydroperoxide a study of the kinetics of the reactions between various hydroperoxides and various iron(II) species will provide information whether this factor is responsible for the different behavior of the hydroperoxides as initiating agents. Kolthoff and Medalia,[4] Fordham and Williams,[5] Orr and Williams[6] and Kolthoff and Reynolds[7] have reported results of kinetic studies on rates of reaction between aquo ferrous iron and various hydroperoxides. Wise and Twigg[8] have investigated the stoichiometry of the reaction between aquo ferrous iron and cumene hydroperoxide (CHP) and determined some of the products formed. In this report the results of a more thorough study of the kinetics and mechanism of the latter system are presented. The reaction was also studied in D_2O since it was hoped that the results might provide information about the mechanism of the rate-determining step of the reaction.

Experimental

Determination of Rate Constants.—The method by which the reaction between aquo ferrous iron and CHP was followed and by which the rate constant was determined already has been described.[7] When the rate of reaction in D_2O was determined, rate measurements were made alternatively in D_2O and H_2O media to eliminate the possibility that the D_2O results were affected by incorrect functioning of the rotated platinum wire electrode. The electrolysis cell employed for D_2O media had a capacity of 10 ml. but otherwise was similar in construction to the cell used for H_2O media. The D_2O was obtained from Norsk Hydroelectrisk Kvaelstofaktieselskab and was used both without further treatment and after distillation from alkaline permanganate and dilute sulfuric acid, similar results being obtained with both samples.

Determination of Stoichiometry.—Reaction ratios were determined by polarographic methods. When excess CHP was used a dropping mercury electrode (DME) was employed. Known quantities of air-free ferrous iron were injected into an electrolysis cell containing a known quantity of CHP in air-free reaction medium. The sum of the CHP and ferric iron diffusion currents was measured at -0.8 v. *vs.* saturated calomel electrode (SCE) after completion of the reaction. It was established that in a mixture of ferric iron and CHP the sum of the diffusion currents of both species was equal to the predicted value. This indicates that under the experimental conditions a kinetic current caused by reaction between ferrous iron produced at the surface of the electrode and CHP is negligible. The i_d/C

(1) This work was carried out under the sponsorship of the Federal Facilities Corporation, Office of Synthetic Rubber, in connection with the Synthetic Rubber Program of the United States Government.

(2) Abstracted from the thesis of W. L. Reynolds presented to the Graduate School of the University of Minnesota in partial fulfillment of the requirements for the Ph.D. degree, 1955.

(3) I. M. Kolthoff, E. J. Meehan, F. Bovey and A. I. Medalia, "High Polymers," Vol. IX, Interscience Publishers, Inc., New York, N. Y.

(4) I. M. Kolthoff and A. I. Medalia, *J. Am. Chem. Soc.*, **71**, 3789 (1949).

(5) J. W. L. Fordham and H. L. Williams, *ibid.*, **73**, 1634 (1951).

(6) R. J. Orr and H. L. Williams, THIS JOURNAL, **57**, 925 (1953).

(7) I. M. Kolthoff and W. L. Reynolds, *Disc. Faraday Soc.*, No. 17, 167 (1954).

(8) W. S. Wise and G. H. Twigg, *J. Chem. Soc.*, 2172 (1953).

values for CHP and ferric iron were determined separately in each medium in which the reaction ratio was determined and thus the residual CHP concentration could be calculated. Acetophenone is one of the reaction products between ferrous iron and CHP and gives a well defined polarographic wave in alkaline medium. Sufficient air-free sodium hydroxide was added to the reaction mixture to give a hydroxide concentration of 0.1 *M*. The sum of the CHP and acetophenone (AP) diffusion currents was measured at −1.8 v. *vs.* SCE. The CHP diffusion current at −1.8 v. *vs.* SCE was calculated from its value at −0.8 v. *vs.* SCE and the known drop times of the electrode at the two potentials. The i_d/c value of AP was determined separately in each reaction medium. The concentration of AP formed by reaction could thus be determined. The reliability of the method was checked by polarographic analysis of mixtures of ferric iron, CHP and acetophenone of known composition.

When ferrous iron was used in excess over CHP a rotated platinum wire electrode was employed to measure the concentration of ferrous iron before and after the reaction. The AP formed was determined with a DME after making the reaction medium alkaline as described above.

Determination of Methyl Alcohol.—Methanol was determined by a modification of the method recommended by Jacobs[9] and by Feigl.[10] One milliliter of solution to be tested was placed in a test-tube. One drop of 3.2 *M* phosphoric acid and one drop of 5% potassium permanganate was added. The oxidation of methanol was allowed to proceed for 1 to 5 minutes at room temperature; the time of oxidation was not critical. The solution was decolorized with 5% sodium bisulfite and 5 ml. of a chromotropic acid solution consisting of 1.5 g. of chromotropic acid in 200 ml. of 75% sulfuric acid was added. The resulting solution was heated for 10 minutes at 100° in a water-bath, cooled and diluted to volume with 75% sulfuric acid in a 10-ml. volumetric flask. The absorbance was measured at 570 mμ against a reagent blank. Since AP and alcohols of molecular weight higher than *n*-propyl alcohol interfere in this test,[11] the methanol content of a reaction solution was determined in the following manner. One hundred milliliters of reaction mixture was prepared; the initial ferrous and CHP concentrations were each 0.005 *M*. This solution was divided into four equal parts and methanol was added to give a concentration of 0, 1, 2 and 3 m*M*, respectively. Each part was extracted four times with 10-ml. portions of benzene; the methanol extracted was negligible. The aqueous solution was made alkaline to remove iron which interferes in the test and filtered. The chromotropic acid test described above was applied to each filtrate. From a plot of absorbance *vs.* added methanol concentration and from the known dilutions the methanol concentration of the reaction mixture could be calculated. The precision of the method with a given reaction mixture was of the order of ±2%. A plot of absorbance *vs.* methanol concentration in a series of blank experiments gave a straight line relationship up to approximately 10 m*M* methanol. Acrylonitrile interferes with the test.

Determination of Gas Evolved.—High concentrations of reactants were used to secure gas evolution. The reaction medium was flushed with helium instead of nitrogen since nitrogen interferes with the mass spectrometric analysis of the gas evolved. The evolved gas was collected over the reaction mixture and its volume determined. Since the main gaseous component was ethane, the small amount of water vapor present did not interfere with the analysis.

Results

Kinetics.—The reaction was found to be first order with respect to both aquo-ferrous iron and CHP in H_2O, in D_2O,[12] and in the presence and absence of acrylonitrile (AcN) at the *p*H values investigated. Values of the second-order rate constant, *k*, obtained at various temperatures in 0.1 *N* sulfuric acid in the presence and absence of AcN are given in Table I.

Table I

Fe^{++}–CHP Rate Measurements in 0.05 *M* H_2SO_4 in H_2O

t, °C.	$(CHP)_0 \times 10^4$, *M*	$(Fe^{++})_0 \times 10^4$, *M*	(AcN), *M*	*k*, l. mole^{-1} sec.$^{-1}$
25.0	19.9	1.99	0.10	15.7[a]
	9.95	1.25	.10	16.2[a]
	9.95	2.48	.10	16.5[a]
	20.0	2.00	...	15.7[b]
	20.0	2.00	.10	16.2[b]
	10.5	2.12	.10	17.1[b]
	4.58	2.16	.10	18.0[a]
	19.2	1.00	.10	16.9[c]
	24.3	1.00	.10	16.8[c]
	24.3	1.00	.10	16.1[c]
	24.3	1.00	.10	16.3[c]
	22.5	1.00	.10	16.4[c]
	20.0	1.00	...	14.1[d]
13.9	22.5	1.00	.10	7.73[c]
	22.5	1.00	.10	8.37[c]
12.9	22.5	1.00	.10	7.96[c]
5.4	22.5	1.00	.10	4.99[c]
0.0	10.0	1.00	.10	3.43[a]
	10.0	1.00	.10	3.52[a]
	10.0	1.00	.10	3.51[a]

[a] CHP of 85.9% purity. [b] Sodium salt of CHP of 61.8% purity. [c] CHP of 88.67 ± 0.01% purity. These results were obtained in the 5 ml. electrolysis cell employed for the reactions in D_2O. [d] 0.025 *M* Fe^{+++} added initially.

Table I also shows that the initial presence of a large excess of aquo ferric ion decreases the value of *k* slightly. The rate constant *k* was found independent of *p*H from *p*H 0 to *p*H 3 in the presence of AcN whereas in the absence of AcN the rate constant decreased somewhat with increasing *p*H in this range as shown in Table II.

Table II

Effect of *p*H in the Presence and Absence of AcN, 25.0 ± 0.1°

*p*H	$(CHP)_0 \times 10^4$, *M*	$(Fe^{++})_0 \times 10^4$, *M*	(AcN), *M*	*k*, l. mole^{-1} sec.$^{-1}$
0	20.0	1.00	0.1	17.6
	6.06	22.0	..	16.0
	6.06	15.8	..	18.1
1.2	...	...	0.1	16.2[a]
	20.0	2.00	..	15.7[b]
2.1	20.0	1.00	0.1	16.6
	20.0	1.00	..	14.4
3.0	20.0	1.00	0.1	15.3
	20.0	1.00	..	12.8

[a] Average of the values for *k* in the presence of 0.1 *M* AcN from Table I. [b] This value is from Table I.

From Table III it is seen that *k* is independent of ionic strength, μ, over the range $0.01 \leq \mu \leq 1.07$ in the presence of AcN. Sodium perchlorate was used to adjust μ where necessary. Values of *k* obtained at various temperatures in 0.05 *M* sulfuric acid in D_2O in the presence of AcN are given in Table IV.

(9) M. B. Jacobs, "The Analytical Chemistry of Industrial Poisons, Hazards, and Solvents," Interscience Publishers, Inc., New York, N. Y., 2nd ed., p. 616.

(10) F. Feigl, "Spot Tests," Elsevier Publishing Co., New York, N. Y., 4th ed., Vol. II, p. 245.

(11) C. E. Bricker and H. R. Johnson, *Ind. Eng. Chem.* (*Anal. Ed.*), **17**, 400 (1945).

(12) The authors wish to thank Professor R. W. Lumry of this University for furnishing the D_2O for this work and for discussions pertaining to the significance of results obtained in this medium.

TABLE III

EFFECT OF VARIATION OF IONIC STRENGTH

0.1 M AcN; 25.0 ± 0.1°

pH	μ	$(CHP)_0 \times 10^4$, M	$(Fe^{++})_0 \times 10^4$, M	k, l. mole^{-1} sec.$^{-1}$
1.2	0.067	...	..	16.2[a]
	0.23	19.0	2.0	16.1
	1.07	20.0	1.0	18.5
2.1	0.01	20.0	1.0	16.6[b]

[a] Average value of all rate constants in Table I with the exception of the one obtained in the initial presence of ferric iron. [b] Increasing the pH from 1.2 to 2.1 keeping μ constant did not affect the rate constant.

TABLE IV

Fe^{++}–CHP RATE MEASUREMENTS IN 0.05 M H_2SO_4 IN D_2O, (AcN) = 0.1 M

t, °C.	$(CHP)_0 \times 10^4$, M	$(Fe^{++})_0 \times 10^4$, M	k, l. mole^{-1} sec.$^{-1}$
25.0	21.8	1.00	10.1[a]
	21.8	1.00	11.7[a]
	21.8	1.00	10.7[a]
	23.3	1.00	10.4[b]
14.5	23.3	1.00	5.07[b]
13.3	25.5	1.00	4.68[b]
5.5	21.8	1.00	3.03[a]
5.0	21.8	1.00	2.79[a]
4.5	25.5	1.00	2.86[a]

[a] These measurements were made in the D_2O as received. [b] These measurements were made after distillation from alkaline permanganate and then from dilute sulfuric acid.

As functions of temperature the rate constants for H_2O and D_2O may be written $k = 3.53 \times 10^8 \exp(-9970/RT)$ l. mole^{-1} sec.$^{-1}$ and $k = 9.25 \times 10^8 \exp(-10{,}840/RT)$ l. mole^{-1} sec.$^{-1}$, respectively. The frequency factors and activation energies were evaluated by a least squares calculation. The standard deviations in the activation energies in H_2O and D_2O were 120 and 380 cal./mole, respectively.

Stoichiometry.—In Table V are presented the values of the reaction ratio, R, determined in 0.1 N sulfuric acid in the presence and absence of AcN. R is defined as the number of moles of ferrous iron oxidized per mole of CHP reduced. In the presence of AcN, $R = 1.00 \pm 0.03$ and in the absence of AcN, $R = 0.95 \pm 0.01$ omitting the values of very high initial ferrous concentration. Values of R determined at various pH values in the presence and absence of AcN are presented in Table VI. It is seen that in the absence of AcN R tends to increase with decreasing pH. Also included in Tables V and VI are the results of the polarographic determinations of the concentration of acetophenone (AP) formed in the reaction. It will be noted that the CHP which was reduced was converted to AP in high yield.

With the initial concentrations $(Fe^{++})_0 = (CHP)_0 = 0.005$ M, the methanol concentration was found to be 18, 4.5 and 10% of the initial amount of CHP at pH 0, 1.2 and 3.0, respectively; no monomer was used in these experiments because it interferes with the methanol determination. When H_3PO_4–$H_2PO_4^-$ buffer of pH 4 was used the ferric iron precipitated as it was formed and no methanol was found. When 0.1 M ferric iron and

TABLE V

REACTION RATIO IN THE ABSENCE OF OXYGEN AND IN THE PRESENCE AND ABSENCE OF AcN

0.1 N H_2SO_4; pH 1.2; 25.0 ± 0.1°

$(CHP)_0 \times 10^3$, mole/l.	$(Fe^{++})_0 \times 10^3$, mole/l.	(AcN), mole/l.	$\frac{(Fe^{++})_0}{(CHP)_0}$	$(AP)_0 \times 10^3$, mole/l.	$R = \frac{\Delta(Fe^{++})}{\Delta(CHP)}$
2.00	0.395	0.1	0.20	0.41	0.93
1.50	.395	0.1	.27	.45	0.97
1.05	.392	0.1	.37	.35	1.08
2.00	1.50	0.1	.75	1.98	1.00
2.00	0.790	1.0	.40	0.76	1.07
1.16	.780	1.0	.67	.70	1.10
2.00	.395	1.0	.20	.40	0.92
1.50	.395	1.0	.27	.44	.95
3.72	.372	..	.10	.40	.94
2.00	.50	..	.25	.59	.95
2.00	1.00	..	.50	1.14	.94
2.00	1.50	..	.75	1.58	.99
1.00	0.90	..	.90	1.09	.92
0.50	1.00	..	2.00	0.46	1.00
0.25	1.00	..	4.00	0.19	0.92
50.00	50.0	..	1.00	35.1	0.95
1.16	1000	..	860	0.40	1.17
0.06[b]	1000	..	16700	...	1.09
0.06[b]	1000	..	16700	0.40	1.10

[a] (AP) designates the concentration of acetophenone formed. [b] 0.10 ml. increments of 0.030 M CHP added every minute to 50.0 ml. of 1 M $FeSO_4$ until 2.00 ml. of CHP had been added in all.

the above concentrations of ferrous iron and CHP were used at pH 1.2 the methanol formed corresponded to 8% of the amount of CHP consumed. Increasing the initial concentrations of ferrous iron and CHP to 0.05 M in the absence of AcN at pH 1.2 resulted in the formation of 10% methanol based on the amount of CHP consumed.

The initial concentration of $(Fe^{++})_0$ was 0.0300 M, of $(CHP)_0$ 0.0228 M, and the volume of reaction mixture was 120 ml. when the amount of gas evolved was measured. The reaction ratio was found to be 0.98. Determination of acetophenone and methanol showed that CHP was 83% converted to acetophenone and 10% to methanol. Analysis of the gas with a mass spectrometer showed that the gas evolved was composed of approximately 90% ethane and 10% methane; the gas contained no oxygen and no carbon dioxide.

The observed volume of gas evolved was 21.5 ml. corrected for the solubilities of methane and ethane in the reaction solution. A material balance calculation may be made as follows: 2.75 millimole of CHP was reduced by Fe^{++}, 2.28 millimole of acetophenone was produced and 2.28 millimole of $CH_3\cdot$ free radical was formed assuming that the amount of $CH_3\cdot$ free radical produced was equal to acetophenone formed. The molal volume of a gas at the temperature and atmospheric pressure of the laboratory assuming ideal gas behavior is 24.4 liter. Since 21.5 ml. of gas was formed the number of millimole of gas formed was 0.88, of which 0.09 mmole was methane and 0.79 mmole was ethane. Since 10% methanol (based on the amount of CHP reduced) was formed the total $CH_3\cdot$ free radical found was (0.09 + 1.58 + 0.28) or 1.95 mmoles as compared to 2.28 mmoles assumed to be formed if $CH_3\cdot$ formed is equal to acetophenone found.

Table VI

Reaction Ratio at Various *p*H Values in the Presence and Absence of AcN; 25.0 ± 0.1°

*p*H	$(CHP)_0$ × 10^3, mole/l.	$(Fe^{++})_0$ × 10^3, mole/l.	(AcN), mole/l.	$(AP)^a$ × 10^3, mole/l.	$R = \frac{\Delta(Fe^{++})}{\Delta(CHP)}$
0[b]	2.00	1.50	..	1.32	1.06
	0.61	2.18	..	0.55	1.00
	2.00	1.50	0.1	1.46	1.05
	5.00	5.00	..	...	1.09
1.2[c]	...	...	0.1	...	1.00[d]
	...	...	..	...	0.95[d]
3.0[e]	2.00	1.50	..	1.50	0.88
	0.50	1.00	..	0.48	0.90
	5.00	5.00	..	4.09	0.85
	2.00	1.50	0.1	1.53	1.05

[a] (AP) designates the concentration of acetophenone formed. [b] 1 *M* H_2SO_4, $\mu = 1.02$. [c] 0.05 *M* H_2SO_4. [d] These values are the average of the values of *R* in Table V for 0.1 *M* AcN and for the absence of AcN (excluding the measurements at high initial Fe^{++} concentration). [e] $HSO_4^- - SO_4^-$ buffer of $\mu = 1.03$.

This difference is greater than can be accounted for by experimental error and may be partly due to side reactions discussed below.

Discussion

In view of the facts that the reaction ratio was about 1 ± 0.1 over a wide range of experimental conditions, that acetophenone was produced in about 80–100% yield from reacted CHP both in presence and absence of AcN, that ethane was produced in the absence of AcN in about 85–90% yield as compared to the amount of acetophenone formed, and that the rate constant was only slightly affected by presence or absence of AcN, it is proposed that the main reactions involved are

$$Fe^{++} + ROOH \xrightarrow{k_1} Fe^{+++} + RO\cdot + OH^- \quad (1)$$

$$RO\cdot \longrightarrow C_6H_5(CO)CH_3 + CH_3\cdot \quad (2)$$

$$2CH_3\cdot \longrightarrow C_2H_6 \quad (3)$$

This mechanism is very different from that postulated by Wise and Twigg.[8] Firstly, their mechanism predicts that reacted CHP will produce 46% acetophenone, 46% methanol and 54% 2-phenyl-2-propanol over the concentration range where they found the reaction ratio to be 1.08. In our investigation, under similar reaction conditions, a much higher yield of acetophenone and a much lower yield of methanol was found. Secondly, their mechanism predicts the rate of ferrous iron disappearance to be $2k_1(Fe^{++})(ROOH)$ in the absence of acrylonitrile and $k_1(Fe^{++})(ROOH)$ in the presence of acrylonitrile considering that Baxendale, Evans and Park[13] have shown that OH· free radical does not react with Fe^{++} or ROOH in the presence of 0.1 *M* AcN. Actually we found that the rate of ferrous iron disappearance in 0.1 *N* sulfuric acid (the medium used by Wise and Twigg) was unaffected by the presence or absence of AcN (see Table I). Thirdly, their mechanism does not provide for gas formation.

Although the proposed mechanism is considered as the major one it is necessary to consider the occurrence of some side reactions to account for all the analytical results reported in the previous sections. In the first place reaction (4)

$$Fe(III) + CH_3\cdot + H_2O \longrightarrow Fe^{++} + CH_3OH + H^+ \quad (4)$$

may contribute to some extent to methanol formation. The evidence in support of reaction (4) is as follows. When ferric iron is added initially to the reaction mixture at *p*H 1.2 the observed rate constant for the disappearance of ferrous iron is decreased (Table I). At *p*H 1.2 the reaction ratio is equal to 0.95 and 4.5% of methanol, based on the amount of CHP consumed, was formed. Since equal amounts of Fe^{++} and methanol are formed by reaction (4) the reaction ratio would be decreased by 5% as observed. At *p*H 3.0 the reaction ratio was equal to 0.88, 10% methanol was formed and the observed rate constant for the disappearance of ferrous iron was decreased (in the absence of AcN). The increase in methanol content at *p*H 3, as compared to that at *p*H 1.2, is probably due to $FeOH^{++}$ being more effective in producing methanol than Fe^{+3}. At *p*H 3 ferric iron is chiefly present as $FeOH^{++}$ whereas at *p*H 1.2 Fe^{+3} is the predominant form.[14] Furthermore no methanol was formed when the reaction was conducted at *p*H 4 where ferric iron (but not ferrous) was precipitated. However, reaction (4) does not account for the increase in methanol content at *p*H 0 as compared to *p*H 1.2. It would appear that a second, *p*H dependent reaction could lead to methanol formation. If this reaction was dependent upon the first power of the hydrogen ion concentration its rate at *p*H 1.2 would be only 0.06 of that at *p*H 0 and hence would contribute to a minor extent at *p*H 1.2. Reaction (5)

$$CH_3\cdot + ROOH \longrightarrow CH_3OH + RO\cdot \quad (5)$$

proposed by Wise and Twigg,[8] is not considered likely as it leads to a chain decomposition of CHP. The constancy of the reaction ratio under a wide range of experimental conditions indicates that such a mechanism for chain decomposition of CHP need not be considered. Also reaction (5) does not account for the *p*H dependence observed for methanol formation.

At the low concentration level of reactants where CHP was virtually quantitatively converted to acetophenone (see Table V) the reaction

$$Fe^{++} + RO\cdot + H^+ \longrightarrow Fe^{+3} + ROH$$

is not important since this reaction would reduce the yield of acetophenone. Furthermore when ferrous iron was present in great excess (Table V) the reaction ratio was but little greater than unity. In this respect our results differ from those of Wise and Twigg[8] who found that as the initial concentration of ferrous iron was increased the reaction ratio approached the value of two. At these high concentration levels of ferrous iron the figures given for the initial concentration ratio have no exact significance since the reaction occurs in the locality where one reagent is added to the other before complete mixing can occur.

The formation of methane at the high concentration level used in the gas evolution experiments

(13) J. H. Baxendale, M. G. Evans and G. S. Park, *Trans. Faraday Soc.*, **42**, 155 (1946).

(14) R. M. Milburn and W. C. Vosburgh, *J. Am. Chem. Soc.*, **77**, 1352 (1955).

may be the result of reaction with ferrous iron

$$Fe^{++} + CH_3\cdot + H^+ \longrightarrow Fe^{+++} + CH_4 \quad (6)$$

or of H-atom extraction from CHP or acetophenone.

$$CH_3\cdot + RH \longrightarrow R\cdot + CH_4 \quad (7)$$

If CHP is involved in reaction (7) it is believed that a C–H bond rather than an O–H bond would be broken since the bond energy of the former is considerably lower than the bond energy of the latter. Since the reaction ratio in the gas evolution experiment was 0.98, reaction (6) does not appear too likely because the ferric iron production would have to be exactly counterbalanced by a reaction consuming CHP or a side reaction which produces ferrous iron, like reaction (4). It should be noted in the experiment under discussion CHP was 83% converted to acetophenone and that a discrepancy of 15% was found in the values of the amount of $CH_3\cdot$ formed in the acetophenone formation reaction and the amount of $CH_3\cdot$ found in the form of methanol, methane and ethane. (See section on gas evolution in section Results.) If reaction (8) were assumed

$$RO\cdot + \cdot CH_3 \longrightarrow ROCH_3 \text{ (an ether)} \quad (8)$$

the observed figures could be accounted for quantitatively.

The effect of AcN upon ethane formation was not studied but in the reactions of ferrous Versenate and ferrous pyrophosphate (to be reported in a subsequent paper) with CHP, where acetophenone and ethane are also produced in high yield in absence of AcN, the presence of AcN decreased the amount of ethane formed but not the amount of acetophenone. This observation raises the question of whether $CH_3\cdot$ or $RO\cdot$ is responsible for the bulk of the initiation reaction. Experiments with CHP containing labeled methyl groups could be used to answer this question.

At this point a short discussion of the nature of the rate-determining step, equation 1, is relevant. The data of Cahill and Taube[15] on the measurement of O^{18} fractionation factors show definitely that the O–O bond of hydrogen peroxide is partly broken in the transition state for the reduction of hydrogen peroxide by ferrous iron. The data of Orr and Williams[6] on reactions between ferrous iron and substituted cumene hydroperoxides show that the O–O bond of hydroperoxides is partially broken in the transition state of the reactions typified by equation 1. For example, the activation enthalpies are 13.1, 12.0, 10.18 and 9.9 kcal./mole and the activation entropies are −10.8, −14.9, −16.5 and −18.3 cal./mole degree for the reaction of ferrous iron with *p*-nitrocumene, cumene, *p*-isopropylcumene and *p*-*t*-butylcumene hydroperoxides, respectively.[6] If the $RO\cdot$ free radical is formed in the rate determining step with ferrous iron by the breaking of the O–O bond then the activation energies of these reactions should decrease in the order given above because the bond dissociation energies, D(RO–OH), of the RO–OH bonds decrease in this order. This may be seen as follows. The resonance structures can be written for the $RO\cdot$ free radicals. Depending on the nature of

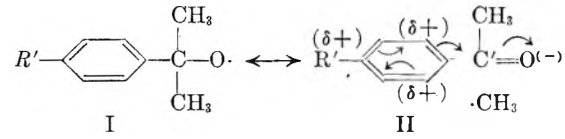

I II

the R′ groups other resonance structures can be written giving greater or less stabilization to the ketone than exists for acetophenone, the product formed from the cumyl free radical (R′ = H). Any change in R′ so as to increase the resonance energy of form II will decrease the bond dissociation energy, D(RO–OH). In the *p*-nitrocumyl free radical the resonance effects of the nitro group and the carbonyl group are in opposite directions and this radical will be less stabilized by resonance than the cumyl free radical. Similar considerations for the *p*-isopropylcumyl and *p*-*t*-butylcumyl free radicals show that D(RO–OH), and hence the activation energies, should decrease in the order *p*-nitrocumene, cumene, *p*-isopropylcumene and *p*-*t*-butylcumene hydroperoxide as observed.[6] The entropy of activation should decrease in the same order because as the amount of resonance in form II increases the rotational entropies of the R′ and

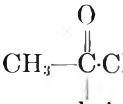

groups decrease as a result of the increased rigidity of form II. Hence it is concluded that the transition state in reaction (1) contains a partially broken RO–OH bond and that it is the differences in D(RO–OH) which cause the differences in the enthalpies of activation for the different hydroperoxides.

The experiments in D_2O were run in the hope of establishing whether reaction (1) for the oxidation of ferrous iron was a direct electron transfer from the iron to the hydroperoxide molecule or a H-atom transfer as in reaction (9).

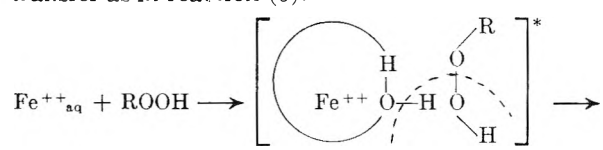

$$Fe^{++}{}_{aq} + ROOH \longrightarrow [\ldots]^* \longrightarrow FeOH^{++}{}_{aq}\cdot + RO\cdot + H_2O \quad (9)$$

In reaction (13) the circle about the iron represents other water molecules in the hydration sphere of Fe^{++} and the asterisk represents the transition state. In this reaction an O–H bond is broken. The increase of activation energy observed in D_2O medium as compared to H_2O medium suggests that an O–H bond may be broken in the reaction. However, if reaction (1) involves replacement of an inner shell H_2O molecule by a hydroperoxide molecule followed by direct transfer of the electron from ferrous iron to hydroperoxide, the increase of activation energy observed in D_2O may be the result of increased heat of hydration of ferrous iron in D_2O as compared to H_2O. The heat of hydration of ferrous iron in D_2O is not known. LaMer[16] has stated that the dipole moments and dielectric constants of H_2O and D_2O are equal within the experimental error of about 1%. If these two quantities are equal for H_2O and D_2O then the heats of hydration of ferrous ion for the two media will be

(15) A. E. Cahill and H. Taube, *J. Am. Chem. Soc.*, **74**, 2312 (1952).

(16) V. K. LaMer, *Chem. Revs.*, **19**, 363 (1936).

equal. If the two quantities are greater by about 1% for D_2O than for H_2O then the heat of hydration of ferrous ion will be greater by about 6 kcal./mole[17] in D_2O than in H_2O or by 1 kcal./mole for each water molecule if it is assumed that there are six water molecules in the first hydration shell of ferrous ion. Thus the activation energy would be 1 kcal./mole greater in D_2O than in H_2O for the electron transfer mechanism. Unfortunately the observed increase of activation energy does not permit a choice to be made between the two possible mechanisms.

(17) W. M. Latimer, "Oxidation Potentials," Prentice-Hall, Inc., New York, N. Y., 1952, 2nd edition.

THE STANDARD POTENTIAL OF THE SILVER–SILVER HALIDE ELECTRODES IN ETHANOL AND THE FREE ENERGY CHANGE IN THE TRANSFER OF HCl, HBr AND HI FROM ETHANOL TO WATER

BY L. M. MUKHERJEE

Department of Chemistry, University College of Science and Technology, Calcutta 9, India

Received February 3, 1956

According to the Born equation: $\Delta F = -\epsilon^2/2r(1/D_2 - 1/D_1)$ the free energy change in the transfer of ions from one solvent to another should vary linearly with respect to the reciprocal of the radius of the ions. Previous observations with cells involving transfer of the chlorides of Li^+, Na^+ and K^+ ions from methanol to water show that the free energy change decreases in the order KCl > NaCl > LiCl contrary to the order expected from the radii of the ions, *viz.*, $Li^+ < Na^+ < K^+$. It is suggested[1] that the discrepancy may be due to some order/disorder changes associated with the process. The present communication is a report of the results derived regarding the free energy change in the transfer of electrolytes such as HCl, HBr and HI from ethanol to water, based on the difference in the corrected value of the standard potentials of the corresponding Ag/Ag halide electrodes in the two media. It is seen that the magnitudes of the free energy change are fairly linear with the reciprocal of the crystal radii of the anions and are in the order $Cl^- > Br^- > I^-$.

Introduction

Direct measurement of e.m.f.'s of cells of the type

$$Ag/AgCl:MCl_{aq};\ M_{Hg}^{Hg}M;\ MCl_{non-aq};\ AgCl/Ag$$

composed of 2 cells placed back to back gives, on extrapolation to ∞ dilution of both the solutions and reducing the difference in the "cratic" term to zero by proper correction to equal mole-fraction, the free-energy change attending the transfer of ions of the electrolytes, from one medium to another. The theoretical estimate of this quantity, however, can be made from a knowledge of the extent of the shift in equilibrium constant for the cell process, *viz.*

$$AgCl + M \rightleftharpoons Ag + M^+ + Cl^-$$

with change in dielectric constant which is related by

$$\Delta \ln K = -\frac{\epsilon^2}{2kT}\left(\frac{1}{r_{M^+}} + \frac{1}{r_{Cl^-}}\right)\Delta\left(\frac{1}{D}\right)$$

derived on the basis of the Born equation,[9] *viz.*

$$\Delta F = -\frac{\epsilon^2}{2D}\left(\frac{1}{r_{M^+}} + \frac{1}{r_{Cl^-}}\right)$$

It appears that $\Delta \ln K$ or ΔF will vary linearly with the reciprocal of the radius of the ions involved in the transfer. Thus, in the case of KCl, NaCl and LiCl, *i.e.*, a series of electrolytes with cations of varying radius, the expected relative magnitudes of the free energy change in transfer should decrease in order Li^+, Na^+, K^+. However, actual measurements with these electrolytes in methanol and methanol–water mixtures show that the relative magnitudes of the difference in free energy changes for the alkali chlorides are linear with $1/D$ as expected, but that the magnitudes of ΔF are in the order KCl > NaCl > LiCl, contrary to what is demanded by theory.

A similar trend is also observed in the plot of ΔH against $1/D$ for these systems, where it is found that for a value of about 0.6 mole fraction of methanol the heat of solution of NaCl has the same value as in pure water; in other words, the heat of transferring the ion from water to the methanol–water mixture is zero. Thus, the simple electrostatic theory seems to be inadequate for explaining the observed facts and it is therefore suggested by Gurney[1] that probably the inequality of entropy of the ions transferred becomes so predominant that the final e.m.f. of the cells fails to correspond to the simple electrostatic relation.

The present paper summarizes the results obtained with HCl, HBr and HI, a series in which the dimension of the anions increases in the order shown. In these cases the more reliable hydrogen electrode can be used in combination with the corresponding Ag/Ag halide electrode as shown below

$$Pt, H_2;\ HCl(Br \text{ or } I)_{aq};\ Ag/AgCl(Br \text{ or } I)$$

$$(Br \text{ or } I)\ AgCl/Ag;\ HCl(Br \text{ or } I)_{EtOH};\ H_2,Pt$$

$E^0 = E^0_{H_2O} - E^0_{EtOH}$, where E^0 is the e.m.f. of the whole cell at ∞ dilution of both the aqueous and ethanol solutions; $E^0_{H_2O}$ and E^0_{EtOH} represent the standard reduction potentials of the respective Ag/Ag halide electrode relative to H-electrode as zero, in aqueous and ethanol solutions.

Evaluation of E^0 thus requires a knowledge of the standard potentials of the Ag/Ag halide electrodes in water and ethanol. Since sufficiently accurate data are available for the aqueous solutions, the main problem is to ascertain the standard po-

(1) R. W. Gurney, "Ionic Processes in Solution," McGraw-Hill Book Co., New York, N. Y., 1953.

tentials of the Ag/Ag halide electrodes in ethanol, for which the following cell was set up.

$$\text{Pt, } H_2;\ HX_{EtOH};\ Ag/AgX \text{ (where X = Cl, Br or I)}$$

$$E_{obs} = E^0 - \frac{2RT}{F} \ln a_{\pm HX}$$

Experimental

The ethanol used was of the same standard of purity and dryness, as characterized by ultraviolet spectrophotometry.[2]

The preparation of the Ag/AgCl electrode, together with details of its standardization in ethanol, has been discussed separately in a previous communication.[3]

The hydrogen electrode assembly consisted of a freshly platinized Pt-foil in equilibrium with electrolytic H_2 gas ($p \sim 1$ atm.) purified through the usual train of purifiers, *e.g.*, concd. H_2SO_4, heated Cu gauze, lead acetate solution, concd. NaOH solution, concd. H_2SO_4 and, lastly, ethanol.

The Ag/AgBr electrode was of the thermal type, as was used by Keston[4] in methanol. The Ag/AgI electrode was of the thermal electrolytic type, prepared by liberating iodine from aqueous KI solution in a separate anode compartment on a stout Pt helix fused at the end of a Pyrex glass tube and previously coated with Ag by electrolysis of $KAg(CN)_2$ and later, by decomposition of a freshly prepared alkali-free Ag_2O paste at 450–500°. Before and after experiment, the electrodes were checked in aqueous solutions of KBr and KI of known halide ion activity. Before use, the electrodes were washed thoroughly with ethanol.

Dry gaseous HBr and HI were obtained by allowing pure, dry H_2 and the halogens to react over heated pumice stone or platinum catalyst. Before absorption in ethanol the gases were led through a number of vessels containing red phosphorus and kept immersed in a freezing mixture, whereby the free halogen, if any, was completely removed. The stock solutions of HBr and HI in ethanol thus obtained were kept in a refrigerator in sealed black Jena glass containers to prevent possible decomposition of the acids and subsequent interaction with ethanol. The solution of HBr in ethanol was standardized by taking aliquot portions of the stock solution in an excess of aqueous KI solution and titrating the acid against standard KOH solution using phenolphthalein as indicator. The HI solution was taken in water to which a drop or two of very dilute $Na_2S_2O_3$ solution was added to discharge the color of the liberated iodine, if any, and then titrated against standard KOH as above. In view of the more or less unstable nature of the solutions, the preparation of the stock and the working solutions and the actual measurement of e.m.f. were completed within 24 hours. Compared to the solution of HBr, the HI solution was very unstable and required caution and checking up. However, no appreciable change in concentration could be noted within 24 hours, before which time the entire measurements were completed. The concentration of the solutions has been calculated in terms of molarity.

The e.m.f.'s were noted at intervals of 30 minutes for about 3–4 hours at 35 ± 0.25° with the help of a Leeds & Northrup type-K potentiometer and a Hartmann–Braun galvanometer till the values were constant within ±0.0001 volt.

Results and Discussion

The table below presents the e.m.f.'s observed for the above cells for different concentrations of HBr and HI solutions in ethanol and the extrapolated[5,6] values of the standard reduction potentials, E^0 (relative to H_2 electrode), of the Ag/AgBr and Ag/AgI electrodes, respectively. The values of the a^0 parameter and other relevant quantities are also given in the table for reference. The ΔF^0 values indicate the amount of free energy change in the transfer of one mole of HBr or HI at equal mole fraction from ethanol to water. The observed values of ΔF^0 for HCl used in Fig. 2 have been derived from the difference in standard potential of Ag/AgCl electrode in water and ethanol as reported earlier.[7]

TABLE I

$AgBr + {}^1/_2 H_2 \rightleftarrows Ag + H^+_{EtOH} + Br^-_{EtOH}$ $a^0_{HBr} = 6$ Å.		$AgI + {}^1/_2 H_2 \rightleftarrows Ag + H^+_{EtOH} + I^-_{EtOH}$ $a^0_{HI} = 6$ Å.	
Concn. of HBr, *M*	E.m.f.$_{obsd}$ $(v.)_{cor}$ to 1 atm. H_2 press.	Concn. of HI, *M*	E.m.f.$_{obsd}$ $(v.)_{cor}$ to 1 atm. H_2 press.
0.011033	0.18285	0.020597	−0.50140
.005516	.21400	.010301	− .53565
.004597	.22245	.005463	.04425
.002207	.25805	.001906	.09365
.001204	.28595	.001565	.10135
.001103	.29010	.001184	.11475
.000602	.31950	.000900	.12890
.000216	.37085	.000440	.16395
.000110	.40600		
$E^0_{Ag/AgBr} = -0.08155$ v. in molar scale, *i.e.*, −0.06895 v. in molal scale		$E^0_{Ag/AgI} = -0.25305$ v. in molar scale, *i.e.*, −0.24047 v. in molal scale	
$\Delta F^0_{EtOH \rightarrow H_2O} = -0.5232 \times 10^{23}$ e.v.		$\Delta F^0_{EtOH \rightarrow H_2O} = -0.2146 \times 10^{23}$ e.v.	

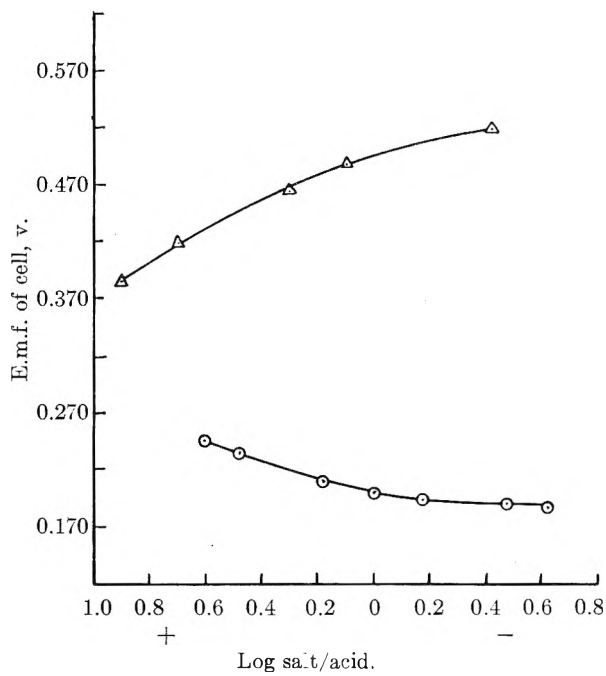

Fig. 1.—△, 0.0103 *N* HI/EtOH titrated with 0.1040 *N* NaOEt/EtOH by quinhydrone electrode; ⊙, 0.01104 *N* HBr/EtOH titrated with 0.08387 *N* NaOEt/EtOH by H-electrode.

The plots of E against log $x/(1-x)$ (Fig. 1) where x = fraction of the acid neutralized do not exhibit linearity. This failure of the Henderson equation was considered as the basis for regarding HBr and HI as completely dissociated. Deyrup,[8] from a study of the kinetics of acetal formation, also concluded that HCl, HBr and HI behave as strong acids in ethanol.

The magnitudes of the free energy change (see Fig. 2) associated with the transfer of the ions of

(2) L. M. Mukherjee, *Science & Culture (India)*, **19**, 314 (1953).
(3) L. M. Mukherjee, THIS JOURNAL, **58**, 1042 (1954).
(4) A. S. Keston, *J. Am. Chem. Soc.*, **57**, 1671 (1935).
(5) H. S. Harned, *ibid.*, **60**, 336 (1938).
(6) T. H. Gronwall, V. K. LaMer and K. Sandved, *Physik. Z.*, **29**, 358 (1928).
(7) L. M. Mukherjee, *Naturwissenschaften*, **41**, 228 (1954).
(8) A. J. Deyrup, *J. Am. Chem. Soc.*, **56**, 60 (1934).

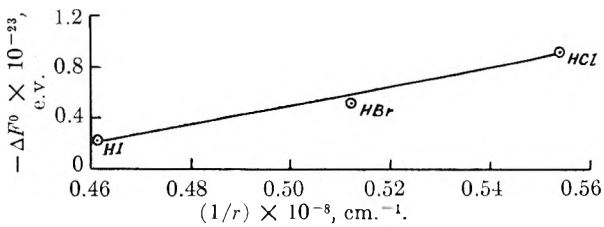

Fig. 2.

HCl, HBr and HI are in the order HCl > HBr > HI which is also the increasing order of the dimensions of the halide ions. Moreover, the free energy changes when plotted against the reciprocal of the crystal radius of the corresponding ions, *viz.*, Cl^-, Br^- and I^- ions, give a straight line. Although no quantitative agreement was sought for, it is suggestive that these results are in conformity with the view[9] that in the field of a small ion *in vacuo* there is initially more energy to lose and consequently when the ion is plunged into a solvent, more energy is lost and the energy loss is greater the smaller the size of the ion.

Acknowledgment.—My grateful thanks are due to Dr. S. K. Mukherjee, D.Sc., Department of Applied Chemistry, University College of Science & Technology, Calcutta, and to Dr. A. K. Ganguly, D.Sc., for their valuable suggestions and helpful criticism of the work.

(9) M. Born, *Z. Physik.*, **1**, 45 (1920).

THE TRANSFERENCE NUMBERS OF IODIC ACID AND THE LIMITING MOBILITY OF THE IODATE ION IN AQUEOUS SOLUTION AT 25°

BY M. SPIRO[1]

Department of Chemistry, University of Toronto, Toronto 5, Ontario, Canada

Received February 8, 1956

The transference numbers of iodic acid in aqueous solution at 25° have been determined for concentrations from 0.01 to 0.08 *N* by the direct moving boundary method. Both the hydrogen and the iodate ion constituent transference numbers were measured and their sum was unity to within a few units in the fourth decimal place. Above a certain low current range the iodate transference numbers increased with increasing current. The Longsworth function t_H^0' varied linearly with concentration and an extrapolation gave a value of 40.54 for the limiting mobility of the iodate ion. A re-examination of recent conductance data on KIO_3 indicated that the conductances below 0.0015 *N* were not reliable but that the values above this concentration were in good agreement with the present work and led to a dissociation constant for KIO_3 of 1.7_6 mol. l.$^{-1}$.

Within the last 30 years, the conductances of many strong and weak electrolytes, and the transference numbers of several strong electrolytes, have been measured in aqueous solution with a precision of a few hundredths of 1%. No accurate transference determinations have been made on any simple, incompletely dissociated electrolyte, despite the fact that such information would be helpful in interpreting moving boundary work with buffer systems,[2] as well as the transference data of salts in non-aqueous of solvents low dielectric constant. Moving boundary transference measurements were therefore done on iodic acid, the latter being chosen because it is monobasic, its dissociation constant is known (0.167 mole l.$^{-1}$),[3] and it is stable and easily purified. KIO_3 and H_3PO_4 were suitable indicators for the determination of the hydrogen and the iodate ion constituent transference numbers, respectively, both giving stable, falling boundaries.

Experimental

The tube in the falling boundary cell had an internal diameter of 2.4 mm., and was calibrated with the KCl/LiCl system, taking $t_K^{KCl} = 0.4900_0$ at 0.04 *N*.[4,5] The current, controlled by a semi-constant current device,[6] was measured in absolute amperes by means of calibrated resistances and a Rubicon precision potentiometer. Time readings were made to the nearest half-second with a metronome clicking at 2 beats a second in conjunction with a Hamilton chronometer watch, which was checked periodically against the Dominion Observatory official time signal. The faraday was taken as 96500 absolute coulombs. The average reproducibility of the runs, in terms of the average deviation from the mean, was 1 in 6000 for the calibration runs, 1 in 5400 for the HIO_3/KIO_3 runs, and 1 in 2600 for the HIO_3/H_3PO_4 runs. The boundaries in the HIO_3/H_3PO_4 system looked much "thicker" than those in the HIO_3/KIO_3 system.

Chemicals.—The "equilibrium" conductivity water used for all solutions and purifications had a specific conductance of 0.8×10^{-6} ohm^{-1} cm.$^{-1}$ and a *p*H of 6.0. For the solvent corrections in the HIO_3 solutions, the contribution to the conductance due to the ionization of carbonic acid ($0.4_0 \times 10^{-6}$ ohm^{-1} cm.$^{-1}$) was subtracted and $0.1_7 \times 10^{-6}$ ohm^{-1} cm.$^{-1}$ added[7] to take account of contamination in the cell.

A strong, aqueous solution of Merck reagent iodic anhydride was filtered through a sintered glass frit, and the iodic acid twice recrystallized by slow evaporation in a vacuum desiccator. A stock solution was made up and analyzed in an atmosphere of purified nitrogen by weight titration with NaOH solution, using either brom thymol blue or B.D.H. universal indicator. The NaOH solution was prepared by diluting a saturated solution of Merck reagent NaOH, and the carbonate remaining was decomposed by boiling the titrated solution twice just before the end-point. A reproducibility of 1 in 8000 was attained. The primary standard was constant boiling HCl.[8]

Mallinckrodt analytical reagent 85% orthophosphoric acid was twice recrystallized as $H_3PO_4 \cdot {}^1/_2H_2O$. Seed crys-

(1) Chemistry Department, University of Melbourne, Carlton, N.3, Victoria, Australia.

(2) E. B. Dismukes and R. A. Alberty, *J. Am. Chem. Soc.*, **76**, 191 (1954), and earlier papers; I. Brattsten and H. Svensson, *Acta Chem. Scand.*, **3**, 359 (1949), and earlier papers.

(3) O. Redlich, *Chem. Revs.*, **39**, 333 (1946); N. C. C. Li and Ying-Tu Lo, *J. Am. Chem. Soc.*, **63**, 397 (1941).

(4) R. W. Allgood, D. J. Le Roy and A. R. Gordon, *J. Chem. Phys.*, **8**, 418 (1940).

(5) L. G. Longsworth, *J. Am. Chem. Soc.*, **54**, 2741 (1932).

(6) D. J. Le Roy and A. R. Gordon, *J. Chem. Phys.*, **6**, 398 (1938).

(7) D. R. Muir, J. E. Graham and A. R. Gordon, *J. Am. Chem. Soc.*, **76**, 2157 (1954).

(8) A. I. Vogel, "Quantitative Inorganic Analysis," Longmans, Green and Co., London, 1939, p. 279.

tals were obtained by cooling a few cc. in a Dry Ice–acetone bath, and their introduction into 85% acid at 11° gave a mass of fine, white crystals that was collected by filtration through a sintered glass frit. Analysis by flame photometry showed that the two recrystallizations had reduced the Na content by ⅔ to 0.015 mole %, while the K content was unaltered at 0.010 mole %. These were the chief impurities, and their presence caused no error as they migrated away from the HIO_3/H_3PO_4 boundary. A stock solution of phosphoric acid was analyzed as above with brom cresol green or methyl orange as indicator; the precision was much lower than for the HIO_3 titrations.

The crystallized B.D.H. Analar potassium iodate was dried under vacuum. The preparations of KCl[4] and LiCl[9] have been described.

All solutions were made up by weight, and all weights had been calibrated. In converting from mass to volume concentrations, all weights were corrected to vacuum, and literature density data[10b] were employed. All solutions were partially degassed at ½ atm. immediately before a run.

Electrodes and Volume Corrections.—In the HIO_3/KIO_3 runs, a Cd rod served as anode and a Pt wire as cathode. To prevent gassing at the anode in the more concentrated solutions, a KCl solution was placed around the rod and the KIO_3 solution slowly and carefully added to prevent undue mixing. It was noticed that a light grey deposit, insoluble in water but soluble in dilute HCl, formed on the rod, and was attributed to Cd(OH)Cl.[11] The anode was weighed before and after the run to determine the extent of this side reaction, which ranged from 0–48 mole % of the total electrode reaction. Although this percentage was quite reproducible under given conditions, no specific trend with any variable was found other than a decrease with increasing current.

The volume corrections are given by $-c_{HIO_3}(\Delta V/1000)$, where c is the normality and V the volume in cm.^{3}, and where, with t representing transference number

$$\Delta V_1 = -\tfrac{1}{2}V_{Cd} - t_H^{HIO_3}\bar{V}_{HIO_3}^{HIO_3} + -\tfrac{1}{2}\bar{V}_{Cd(IO_3)_2}^{KIO_3} = -13.2 \quad \text{(no KCl)}$$

$$\Delta V_2 = -\tfrac{1}{2}V_{Cd} - t_H^{HIO_3}\bar{V}_{HIO_3}^{HIO_3} + -\tfrac{1}{2}\bar{V}_{CdCl_2}^{KCl} + \bar{V}_{KIO_3}^{KIO_3} - \bar{V}_{KCl}^{KCl} = -12.7 - 0.7\sqrt{c_{KCl}} \quad \text{(KCl, no deposit)}$$

$$\Delta V_3 = -\tfrac{1}{2}V_{Cd} - t_H^{HIO_3}\bar{V}_{HIO_3}^{HIO_3} + -\tfrac{1}{2}V_{Cd(OH)Cl} + \bar{V}_{KIO_3}^{KIO_3} - \bar{V}_{KCl}^{KCl} + -\tfrac{1}{2}\bar{V}_{HCl}^{KCl} - -\tfrac{1}{2}V_{H_2O} = -6.3 - 2.6\sqrt{c_{KCl}} \quad \text{(KCl, Cd(OH)Cl deposit)}$$

When KCl was used, ΔV_2 and ΔV_3 were weighted according to the experimentally found proportion of the side reaction. Numerical values not listed by Longsworth[6] were computed from the somewhat discordant literature density data to give $\bar{V}_{HIO_3} = 28 \pm 2$,[10b,12–14] $\bar{V}_{KIO_3} = 34 \pm 2$,[10b,13,14] $\bar{V}_{Cd(IO_3)_2} = 37$,[14] and $\bar{V}_{Cd(OH)Cl} = 36.2$.[10a,11]

In the HIO_3/H_3PO_4 runs, a Pt wire served as anode and a thermally prepared AgBr electrode as the non-gassing cathode (Ag_3PO_4 did not precipitate under the experimental conditions). A large cathode compartment of about 40-ml. capacity was used to prevent bromide ions reaching the boundary. In the first run with a freshly prepared electrode the current readings were often erratic, and at times a viscous streaming effect was noticed that slowly turned the solution around the electrode cloudy and gave a deposit at the bottom of the electrode compartment. The latter disturbance was probably caused by finely dispersed AgBr or Ag; both effects disappeared after the first run.

The volume corrections are given by $-c_{HIO_3}(\Delta V_4/1000)$, where

$$\Delta V_4 = V_{Ag} - V_{AgBr} - t_{IO_3}^{HIO_3}\bar{V}_{HIO_3}^{HIO_3} + \bar{V}_{HBr}^{H_3PO_4} = + 3.4 + 0.5\sqrt{\mu_{H_3PO_4}}$$

μ is the ionic strength. The numerical values used were $V_{Ag} = 10.3$,[5] $V_{AgBr} = 29.0$,[10a] $\bar{V}_{HBr} = 24.9 + 0.5\sqrt{\mu}$.[10b,14,15]

Results and Discussion

The Effects of Current and Indicator Concentration.—The values of t_H were independent of current at all currents used and showed no variation when the indicator concentration was changed from the Kohlrausch value to one 6% below it. When a wider range of indicator concentrations was tested at 0.02 N, t_H was not appreciably altered even when the KIO_3 concentration was 18% below the Kohlrausch figure, as had been expected.[16]

In the HIO_3/H_3PO_4 runs t_{IO_3} increased with increasing current. At any given current, t_{IO_3} was not affected by a change in the indicator strength from the Kohlrausch concentration to one 6% lower. At 0.02 N, where a greater range of indicator concentrations was investigated, an increase in the H_3PO_4 concentration to 6% above the Kohlrausch value did not influence t_{IO_3}, but a decrease to 17% below this figure gave somewhat lower transference numbers. A comparison of all the results indicated that

$$t_{IO_3}(I = 1) - t_{IO_3}(I = 0) - f(I/\alpha c) \qquad (1)$$

where α is the degree of dissociation in a c normal solution of iodic acid and I is the current. The function is approximately proportional to $(I/\alpha c)$.[2,7] Figure 1 shows how well this empirical relationship

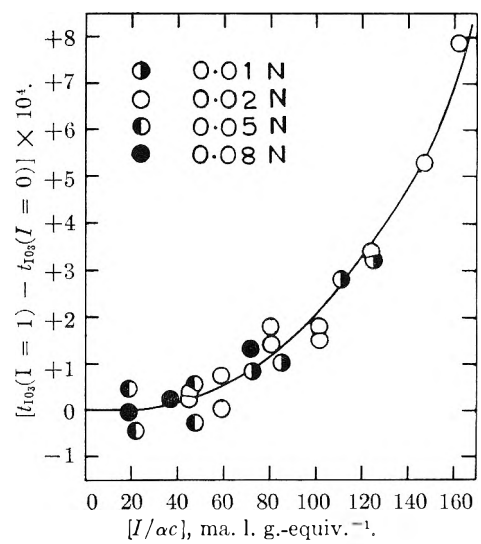

Fig. 1.—Variation of t_{IO_3} with current I at different ionic strengths αc.

holds. No explanation of this phenomenon is offered, but it should be pointed out that some moving boundary measurements with strong electrolytes in the past have indicated that transference numbers are subject to change when the current becomes too high.[17] It may well be that this current variation depends upon the cell design,[16] and it is possible that weak electrolyte systems are more sensitive to such an effect. Whatever the cause, it introduces no uncertainty exceeding $\pm 2 \times 10^{-5}$ into the t_{IO_3} values at zero current in Table I.

(9) R. E. Jervis, D. R. Muir, J. P. Butler and A. R. Gordon, *J. Am. Chem. Soc.*, **75**, 2855 (1953).

(10) "International Critical Tables." McGraw-Hill Book Co. Inc., New York, N. Y., (a) Vol. I, 1926; (b) Vol. III, 1928.

(11) J. W. Mellor, "A Comprehensive Treatise on Inorganic and Theoretical Chemistry," Vol. IV, Longmans, Green and Co., London, 1922, p. 546.

(12) R. Lühdemann, *Z. physik. Chem.*, **B29**, 133 (1935).

(13) M. Randall and M. D. Taylor, THIS JOURNAL, **45**, 959 (1941).

(14) K. Fajans and O. Johnson, *J. Am. Chem. Soc.*, **64**, 668 (1942).

(15) K. Fajans, *J. Chem. Phys.*, **9**, 283 (1941).

(16) A. R. Gordon and R. L. Kay, *J. Chem. Phys.*, **21**, 131 (1953).

(17) H. P. Cady and L. G. Longsworth, *J. Am. Chem. Soc.*, **51**, 1656 (1929); A. R. Gordon, private communication.

TABLE I

SUMMARY OF TRANSFERENCE MEASUREMENTS AT 25.00 ± 0.02°

c_{HIO_3}[a]	$\mu = \alpha c$	t_H current range, ma.	t_H[b]	t_{IO_3} current range, ma.	t_{IO_3}[c]	$t_H + t_{IO_3}$	"Best" t_{IO_3}	At rounded[d] concn.
0.01000	0.00955	0.23–0.45	0.9013	0.69–1.19	0.09831	0.9996	0.09835	0.09835
.01966	.01815	.33–0.57	.9034	.81–2.93	.09648	0.9999	.09649	.09644
.04989	.04247	.57–1.46	.9065	.82–1.98	.09363	1.0001	.09361	.09360
.07997	.06407	.82–1.72	.9074	1.20–4.62	.09222	0.9996	.09226	.09226

[a] The average of several closely agreeing concentrations, gram equivalents per liter of solution. [b] The average of between 4 and 9 runs, with solvent and volume corrections added. [c] Based on between 4 and 23 runs, with solvent and volume corrections added. The values at the two lowest concentrations were subject to a small extrapolation based on eq. 1, since the boundaries were too faint for observation at lower currents. [d] "Best" values of t_{IO_3} at 0.01, 0.02, 0.05 and 0.08 N, respectively.

Best Values and the Variation with Concentration.—The experimental values are given in Table I. α was computed by taking the dissociation constant K as 0.167 mole $l.^{-1}$[13] and by using the Davies activity coefficient expression[18]

$$\log_{10} f_{\pm} = [-0.50\sqrt{\alpha c}/(1 + \sqrt{\alpha c})] + 0.1\,\alpha c \quad (2)$$

The sum of t_H and t_{IO_3} is close to unity, thus providing a check on the results. If the small deviations from 1 can be ascribed to uncertainties in the concentrations or to any other factors (such as the tube calibrations or the solvent corrections) common to both sets of measurements, then "best" values will be obtained by multiplying both transference numbers by $1/(t + t_{IO_3})$. This has been done in Table I. In the past, the "best" value of the transference number of a given ion constituent was usually obtained by averaging this number as measured and the difference between 1 and the measured transference number of the other ion constituent. The latter procedure implies that both numbers are subject to the same absolute rather than the same relative uncertainty, and while essentially the same "best" values are given by both methods when the transference numbers are close to 0.5, they differ when one transference number is much larger than the other, as in the present case. The values in the last two columns of Table I are probably accurate to about 1 in 1300; the last figure will, however, be retained in subsequent calculations.

The variation of the best values with concentration could be accounted for by any of the following three modifications of the equation Longsworth[5] proposed for strong electrolytes.

$$t^{\circ\prime}_{IO_3} = 0.10386 + 0.0662c \quad (3)$$

$$t^{\circ\prime}_{IO_3} = 0.10386 + 0.0584(\alpha c) + 0.0953(\alpha c)^{3/2} \quad (4)$$

$$t^{\circ\prime}_{IO_3} = 0.10386 + 0.0674(\alpha c) + 0.237(\alpha c)^2 \quad (5)$$

$$= 0.10386 + 0.0662\,[1.018(\alpha c) + 3.58(\alpha c)^2 \quad (5')$$

where

$$t^{\circ\prime}_{IO_3} = (t_{IO_3}\Lambda' + \sigma\sqrt{\alpha c})/(\Lambda' + 2\sigma\sqrt{\alpha c})$$

and

$$\Lambda' = \Lambda^\circ - (\theta\Lambda^\circ + 2\sigma)\sqrt{\alpha c}$$

The Onsager constants θ and σ were taken as 0.2289 and 30.09, respectively, and Λ°, the conductance of HIO_3 at infinite dilution, as 390.37. A change of 0.2 unit in Λ° changes $t^{\circ\prime}_{IO_3}$ by no more than 1×10^{-5}. The average difference between the best transference number and that calculated by equation 3, 4 or 5 is 1×10^{-5}.

(18) C. W. Davies, *J. Chem. Soc.*, 2093 (1938).

Nearly all the existing data for strong electrolytes show that $t^{\circ\prime}$ varies, as a first approximation, linearly with concentration. Equations 4 and 5 show that $t^{\circ\prime}$ of the partially associated iodic acid varies in an analogous manner with αc, as would have been expected. There is no theoretical reason for preferring either of these equations to the other or to any combination of them. It was surprising to find, however, that eq. 3 also fitted the results for iodic acid. A possible explanation may be found by comparing 3, 5′, and the mass action equation in the form $c = (\alpha c) + [f^2_{\pm}(\alpha c)^2/K]$, and noting that $f^2_{\pm}/K$ changes little with concentration and is 3.88 at the highest ionic strength where the term in $(\alpha c)^2$ is relatively most important. The linear variation of $t^{\circ\prime}_{IO_3}$ with c, rather than with αc, may therefore be fortuitous. Alternatively, since $c = \alpha c + (1 - \alpha)c$, it is possible to explain eq. 3 on the basis of a medium effect caused by the undissociated iodic acid.

In terms of the individual ionic mobilities (λ)

$$t^{HIO_3}_{IO_3} = \frac{[IO_3^-]\lambda_{IO_3^-}}{[IO_3^-]\lambda_{IO_3^-} + [H^+]\lambda_{H^+}} = \frac{\lambda_{IO_3^-}}{\lambda_{IO_3^-} + \lambda_{H^+}} \quad (6)$$

if the mobility of the undissociated iodic acid is assumed to be zero, and where the square brackets denote concentrations. Equations 3, 4 and 5 show that the iodate transference number at infinite dilution is 0.10386, and if $\lambda^\circ_{H^+} = 349.83$,[19,20a] $\lambda^\circ_{IO_3} = 40.54 \pm 0.03$. This value is based on a fairly small extrapolation. The transference method employing weak acid/weak acid boundaries seems promising as a means of determining limiting anion mobilities, particularly since this method yields limiting mobilities that are much less sensitive to either experimental errors or any uncertainty in $\lambda^\circ_{H^+}$ than are the values derived by the traditional conductance procedure in which the limiting anion mobility appears as the relatively small difference between two large quantities, Λ° and $\lambda^\circ_{H^+}$.

Values of the limiting mobility of the iodate ion derived from KIO_3 conductance data are discussed in detail below.

The Conductance of Potassium Iodate Solutions.—Krieger and Kilpatrick,[21] who did measurements from 0.00013 to 0.10 N, showed that several modifications of the Onsager equation fitted their points above 0.0015 N with an average devia-

(19) R. A. Robinson and R. H. Stokes, "Electrolyte Solutions," Butterworths Scientific Publications, London, 1955, p. 452.

(20) H. S. Harned and B. B. Owen, "The Physical Chemistry of Electrolytic Solutions," Reinhold Publ. Corp., New York, N. Y., 2nd ed., 1950 (a) p. 591; (b) pp. 537–8, 590.

(21) K. A. Krieger and M. Kilpatrick, *J. Am. Chem. Soc.*, **64**, 7 (1942).

tion of 0.06 in Λ and led to $\Lambda^{\circ}_{KIO_3} = 114.00$. If $\lambda^{\circ}_{K^+} = 73.50$[19,20a], then $\lambda^{\circ}_{IO_3^-} = 40.50$, in good agreement with the present value.

Monk[22] redetermined the conductances from 0.00018 to 0.0039 N, and concluded that $\Lambda^{\circ}_{KIO_3} = 114.27 \pm 0.02$, which gives $\lambda^{\circ}_{IO_3^-} = 40.77 \pm 0.02$. He mentioned that in dilute solutions the resistance readings drifted steadily even in a fused quartz cell, though he considered that this difficulty was overcome by taking readings rapidly after shaking the cell. An additional drift was found in a borosilicate cell. Monk calculated a dissociation constant for KIO_3 of 1.7 mole $l.^{-1}$ from his 5 most dilute points by means of the method which Davies[23] had used for 2:2 electrolytes. This assumes that the limiting Onsager equation

$$\Lambda_\epsilon = \Lambda^\circ - (\theta\Lambda^\circ + 2\sigma)\sqrt{\alpha c} \qquad (7)$$

applies, and $\alpha = \Lambda/\Lambda_\epsilon$, where Λ is the observed conductance at normality c. However, he used an arithmetically incorrect slope of 87.29; the correct figure of 86.29, together with his own limiting conductance, gives dissociation constants that increase with increasing concentration, with a mean value of 1.0 for the 5 lowest points. It has been shown since[24-26] that the conductance is represented more exactly by a modified relation which includes a term in the ionic strength whose numerical coefficient is approximately the same as the limiting slope. If it is assumed that Λ_ϵ, the hypothetical conductance of completely dissociated KIO_3 at an ionic strength of αc, is given by

$$\Lambda_\epsilon = \Lambda^\circ - (\theta\Lambda^\circ + 2\sigma)\sqrt{\alpha c} + (\theta\Lambda^\circ + 2\sigma)\,\alpha c \qquad (8)$$

then the dissociation constants still show a concentration trend, with a mean value of 0.6 mole $l.^{-1}$ for the 5 lowest points. Davies[23] derived a dissociation constant of about 2.0 mole $l.^{-1}$ in the range 0.01 to 0.10 N by applying an empirical conductance relationship to older conductance figures at 18°.

The situation is not very satisfactory, and both recent sets of conductances were therefore reexamined with the aid of the present results, in the absence of data for a completely ionized iodate. From eq. 6 and the assumption of independent ionic migration

$$\Lambda_\epsilon = \lambda_{K^+} + \lambda_{IO_3^-} = \lambda_{K^+} - \lambda_{H^+} + \lambda_{H^+}/t_H^{HIO_3}$$
$$= t_K^{KCl}\Lambda_{KCl} - t_H^{HCl}\Lambda_{HCl} + t_H^{HCl}\Lambda_{HCl}/(1 - t_{IO_3}^{HIO_3}) \qquad (9)$$

This way of combining the data minimizes the effect of undissociated HIO_3 on $\lambda_{IO_3^-}$. The KCl and HCl data listed by Harned and Owen[20b] were expressed analytically in terms of the ionic strength μ (in moles per liter of solution) and combined with eq. 5 to give

$$\Lambda_\epsilon = 114.045 - 86.29\,\mu^{1/2} - 89.04\,\mu - 31.36\,\mu^{3/2} + 11\text{?}.4\mu^2 - 34\,\mu^{5/2} + 50\,\mu^3 \qquad (10)$$

If the assumption of independent ionic migration does not break down at the higher ionic strengths, eq. 10 should hold over the range in which the experimental figures are known, μ = 0.01–0.06.

When μ was replaced by c in eq. 10, the values obtained were all larger than the corresponding observed values of Λ, except below 0.0015 N. This indicated that KIO_3 is incompletely dissociated, and degrees of dissociation α were then computed by the usual method[27] of successive approximations until $\alpha = \mu/c = \Lambda/\Lambda_\epsilon$. The thermodynamic dissociation constant of KIO_3, K, was found from

$$K = \alpha^2 c f_\pm^2/(1 - \alpha) \qquad (11)$$

where $f_\pm$ was given by eq. 2. The results fell into 3 groups: (1) the K values obtained from the 13 points between 0.002 and 0.06 N were independent of concentration, with a mean of 1.76 mole $l.^{-1}$ and an average deviation from the mean of 0.06; (2) the K values from the 2 points between 0.0015 and 0.002 N were 2.8 and 2.3 mole $l.^{-1}$, but owing to the small differences between Λ and Λ_ϵ in this range an error of only 0.02 in Λ would bring them into agreement with those in group (1); (3) the K values from the 7 points below 0.0015 N were, with one exception, negative, *i.e.*, $\Lambda > \Lambda_\epsilon$.

Between 0.0015 and 0.06 N, eq. 10 and the experimental data on which it is based, and the conductances of KIO_3, are therefore consistent with each other and with the assumption of incomplete dissociation in KIO_3 solutions. It would be surprising if eq. 10, having proved its worth in this range, should suddenly break down below 0.0015 N, and it seems more likely that the results in group (3) are caused by errors in the conductances. This explanation is supported both by Monk's report[22] of the experimental difficulties encountered in the resistance measurements in the most dilute solutions, and by the fact that the conductance solvent corrections in this region are several times greater than the differences needed to bring the observed conductances into line with those in the stronger solutions.

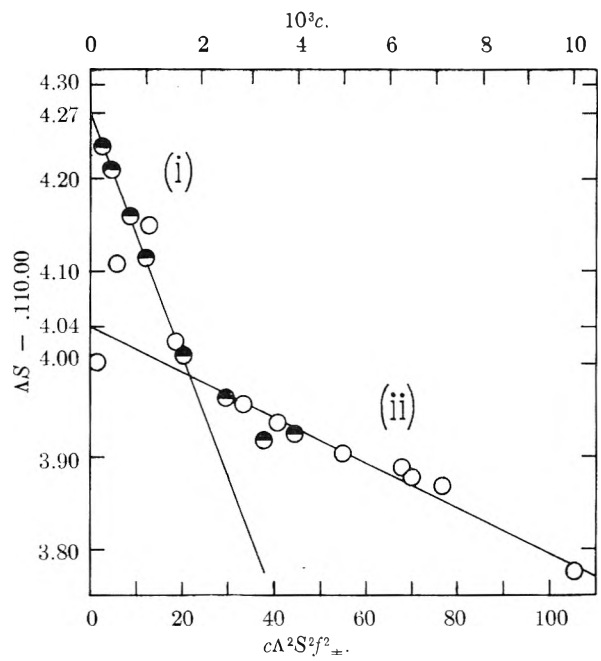

Fig. 2.—Shedlovsky "combination" equation plot of KIO_3 conductances: ○, Krieger and Kilpatrick[21]; ◓, Monk.[22]

(22) C. B. Monk, *J. Am. Chem. Soc.*, **70**, 3281 (1948).
(23) C. W. Davies, *Trans. Faraday Soc.*, **23**, 351 (1927).
(24) T. Shedlovsky, *J. Am. Chem. Soc.*, **54**, 1405 (1932).
(25) R. A. Robinson and C. W. Davies, *J. Chem. Soc.*, 574 (1937).
(26) R. A. Robinson and R. H. Stokes, *J. Am. Chem. Soc.*, **76**, 1991 (1954).
(27) D. A. MacInnes and T. Shedlovsky, *J. Am. Chem. Soc.*, **54**, 1429 (1932).

The divergence between the experimental conductances at low and at moderate concentrations is brought out by Fig. 2, in which the KIO_3 conductances have been plotted by means of the Shedlovsky[28,29] "combination" equation

$$\Lambda S = \Lambda^\circ - [c\Lambda^2 S^2 f_\pm^2/K\Lambda^\circ] \quad (12)$$

which combines eq. 11 with the Shedlovsky conductance equation[28]

$$\Lambda = \alpha\Lambda^\circ - [(\theta\Lambda^\circ + 2\sigma)\Lambda\sqrt{\alpha c}/\Lambda^\circ] \text{ (cond. eq. S)} \quad (13)$$

Here c, α, Λ and K again refer to KIO_3, S is the Shedlovsky function,[30] and $f_\pm$ was calculated from the Guggenheim approximation

$$\log_{10} f_\pm = -0.5092\sqrt{\alpha c}/(1 + \sqrt{\alpha c}) \quad (14)$$

The corresponding concentrations are shown at the top of Fig. 2; above 0.01 N the equation would not be expected to hold.[28] No straight line fits all the points, but the latter can easily be grouped along the two lines shown. The conductances below 0.002 N extrapolate to $\Lambda^\circ = 114.27$, as given by Monk,[22] but the data above 0.0015 N can be extrapolated to 114.04, in accord with the limiting iodate mobility found in the present work and the accepted limiting mobility of K^+.[19,20a]

From the slopes of lines (i) and (ii) and eq. 12, dissociation constants of 0.67 and 3.53 mole $l.^{-1}$, respectively, can be calculated. Another activity coefficient expression in place of eq. 14, such as eq. 2 or the limiting Debye–Hückel equation, would change these values (but not the intercepts) by a few per cent. only, and would not account for the difference between either figure and that of 1.76 mole $l.^{-1}$ found above. However, it has been shown[29] that for a fairly strong electrolyte the dissociation constant obtained depends upon whether the Onsager limiting law or the Shedlovsky equation 13 is applied in deriving a "combination" equation such as 12. The sensitivity of K to the theoretical relation employed can be quantitatively generalized by writing a general conductance equation in the polynomial form

$$\Lambda/\beta' = \Lambda^\circ - (\theta\Lambda^\circ + 2\sigma)(\beta' c)^{1/2} + A\beta' c + A'(\beta' c)^{3/2} + \ldots \text{ (cond. eq. G)} \quad (15)$$

as compared with the limiting Onsager law

$$\Lambda/\beta = \Lambda^\circ - (\theta\Lambda^\circ + 2\sigma)(\beta c)^{1/2} \text{ (cond. eq. L)} \quad (16)$$

where β' and β are the degrees of dissociation calculated from the respective equations. If $\beta' = \beta(1 - \delta)$

$$\frac{}{1-\delta} = \frac{\beta}{\beta'} = \frac{\Lambda^\circ - (\theta\Lambda^\circ + 2\sigma)(\beta c)^{1/2}(1-\delta)^{1/2} + A\beta c(1-\delta) + A'(\beta c)^{3/2}(1-\delta)^{3/2} + \ldots}{\Lambda^\circ - (\theta\Lambda^\circ + 2\sigma)(\beta c)^{1/2}}$$

The binomial theorem enables this relation to be expressed as a polynomial in δ, and in very dilute solutions, where $c \ll 1$ and $\beta \approx 1$, all terms higher than δ^1 and c^1 can be dropped to give

$$\delta = Ac/\Lambda^\circ \quad (17)$$

Under the same conditions, eq. 11 approximates to $K^{-1} = (1 - \alpha)/c$, hence

$$K_G^{-1} - K_L^{-1} = [(1 - \beta')/c] - [(1 - \beta)/c] = (\beta - \beta')/c \approx \delta/c$$

where the subscript on K refers to the conductance equation used. Thus

$$K_G^{-1} - K_L^{-1} = A/\Lambda^\circ \quad (18)$$

An expansion of eq. 13 in the form of eq. 15 gives $A_S = (\theta\Lambda^0 + 2\sigma)^2/\Lambda^\circ$, so that

$$K_S^{-1} - K_L^{-1} = (\theta\Lambda^\circ + 2\sigma)^2/\Lambda^{\circ 2} \quad (19)$$

which is identical with the relation derived earlier[29] by another method. Combination of eq. 18 and 19 gives

$$K_G^{-1} - K_S^{-1} = [A/\Lambda^\circ] - [(\theta\Lambda^\circ + 2\sigma)/\Lambda^\circ]^2 \quad (20)$$

In the case of KIO_3, it seems reasonable to suppose that a dissociation constant of 1.76 would have been obtained from a plot such as Fig. 2 if eq. 12 had been based, not on the Shedlovsky conductance equation 13, but on the general equation 15 with the value of A appropriate to KIO_3. This hypothesis provides another test for distinguishing between lines (i) and (ii). According to eq. 20, if $K_G = 1.76$, then

if $K_S = 0.67$ [line (i)], $A = -40$
if $K_S = 3.53$ [line (ii)], $A = +98$

On theoretical grounds A should be positive, while experiment shows[24,25] that A is usually around $(\theta\Lambda^\circ + 2\sigma)$, here equal to 86.29. Moreover, eq. 10, based on work with other electrolytes, predicts that A should be 89.04, although the numerical coefficients in eq. 10 (but not Λ_c) depend to some extent on the analytical expressions chosen to represent the experimental data.

Again, if the Robinson and Stokes[26] conductance equation is written in the form of eq. 15, $A_{RS} = (\theta\Lambda^\circ + 2\sigma)B\mathring{a}$, where $B = 0.3286$ in aqueous solution at 25° and $\mathring{a}$ is the "distance of closest approach" of the ions. According to this equation, line (i) gives the unlikely $\mathring{a}$ value of -1.4 Å, while line (ii) gives a reasonable distance of $+3.5$ Å.

In conclusion, it appears that the experimental conductances of KIO_3 below 0.0015 N are not reliable, while the conductances above this concentration are compatible with a limiting iodate mobility of 40.54 and a dissociation constant for KIO_3 of 1.76.

Acknowledgments.—The author is deeply indebted to Professor A. R. Gordon for suggesting this work and for much helpful advice and numerous illuminating discussions. He also wishes to express his gratitude to the National Research Council of Canada for the award of a University Post-doctorate Fellowship.

(28) T. Shedlovsky, *J. Franklin Inst.*, **225**, 739 (1938).
(29) R. M. Fuoss and T. Shedlovsky, *J. Am. Chem. Soc.*, **71**, 1496 (1949).
(30) H. M. Daggett, Jr., *ibid.*, **73**, 4977 (1951).

STREAMING POTENTIAL STUDIES ON QUARTZ IN SOLUTIONS OF AMINIUM ACETATES IN RELATION TO THE FORMATION OF HEMI-MICELLES AT THE QUARTZ–SOLUTION INTERFACE

BY D. W. FUERSTENAU

Department of Metallurgy, Massachusetts Institute of Technology, Cambridge, Mass.

Received February 10, 1956

By streaming potential techniques, the zeta potential of quartz has been measured as a function of the concentration of various aminium acetates. These experiments indicate that adsorption of aminium ions takes place as individual aminium ions until a certain critical concentration is reached within the double layer, at which point the adsorbed aminium ions begin to associate into patches of ions, called hemi-micelles. At neutral *p*H, the bulk concentration required for hemi-micelle formation is dependent upon the length of the hydrocarbon chain. The effect of competition between sodium ions and dodecylammonium ions for the surface and the effect of *p*H on hemi-micelle formation has been investigated.

At low concentrations dodecylammonium ions affect the zeta potential of quartz in nearly the same manner as do sodium ions, but at a certain concentration, these long-chained ions make enormous electrokinetic changes at the quartz–solution interface.[1,2] Electrokinetic experiments have shown that monovalent inorganic counterions cannot change the sign of the zeta potential, ζ, but only cause it to approach zero at high concentrations, whereas multivalent inorganic counter ions are able to change the sign of ζ.[1,3] If ζ is plotted as a function of the logarithm of the concentration of dodecylammonium chloride (ζ *vs.* log C curve), the resulting curve is similar to that obtained for sodium chloride in dilute solutions, but at a certain concentration of dodecylammonium chloride, the zeta potential changes sign quite abruptly. It was concluded that in dilute solutions, dodecylammonium ions are adsorbed as individual ions, but once the adsorbed ions reach a certain critical concentration at the solid–liquid interface, they begin to associate into patches of ions at the solid–solution interface in much the same way they associate to form micelles in bulk solutions.[1,2] The forces causing ionic association at the surface will be the same as those operating in the bulk except that coulombic attraction for the surface will aid the association. Because of the high surface charge, the adsorbed aminium ions in the Stern layer (the layer of counterions adjacent to the solid surface) must necessarily be oriented with the charged heads toward the surface and with the tails sticking out into the liquid. If the adsorbed aminium ions associate tightly in this manner through van der Waals attraction between hydrocarbon chains, a minimum surface area of hydrocarbon chain will be in contact with water. Because of the proposed appearance of these adsorbed aminium ions, Gaudin and Fuerstenau have termed these patches of associated ions *hemi-micelles*.[2]

The total double layer potential ψ_0 at the quartz surface depends upon the *p*H of the solution since hydrogen and hydroxyl ions are potential-determining ions for quartz.[1,3] If the *p*H is increased, the surface will become more negatively charged and the adsorption of counterions increases. As the solution *p*H is increased, experiments indicate that the bulk concentration at which hemi-micelles form is lowered.[1,2] This points to the probability that a certain critical concentration must be reached in the Stern layer before the adsorbed aminium ions begin to associate.

In the investigation reported in this paper, streaming potential techniques were used to study the influence of the length of the hydrocarbon chain on the zeta potential at neutral *p*H, the competition between sodium and dodecylammonium ions for the surface, and the effect of solution *p*H on the formation of hemi-micelles.

The bulk critical micelle concentration depends greatly on the length of the hydrocarbon chain. For the acetate salts of primary aminium ions, the critical micelle concentration depends on the number of carbon atoms in the hydrocarbon chains as follows[4]: C 18, 0.0003 *M*; C 16, 0.0008 *M*; C 14, 0.004 *M*; C 12, 0.013 *M*; C 10, 0.04 *M*; C 8, very high. If adsorbed aminium ions associate into hemi-micelles adjacent to the surface through van der Waals attraction between hydrocarbon chains, the length of the hydrocarbon chain should have a marked effect on hemi-micelle formation.

Since both sodium ions and dodecylammonium ions appear to act as indifferent counterions until hemi-micelles form with long-chained aminium ions, it seems reasonable that they should compete for positions in the double layer on the basis of the ratio of their bulk concentrations. After hemi-micelle formation has set in, adsorption of the long-chained aminium ions would be favored because of the added attractive force between hydrocarbon chains. To study this experimentally, the zeta potential of quartz was measured as a function of the concentration of dodecylammonium acetate in water and in sodium chloride solutions.

The influence of *p*H on hemi-micelle formation was investigated further. It seems that if the concentration of dodecylammonium acetate is maintained somewhat below that necessary to form hemi-micelles at neutral *p*H, raising the *p*H of the solution should bring about the formation of hemi-micelles at the surface because of the increased adsorption.

Experimental Method and Materials

The method depends on the interrelation of mechanical

(1) D. W. Fuerstenau, Sc.D. thesis, Massachusetts Institute of Technology, 1953.

(2) A. M. Gaudin and D. W. Fuerstenau, *Trans. A.I.M.E.*, **202**, 958 (1955).

(3) A. M. Gaudin and D. W. Fuerstenau, *ibid.*, **202**, 66 (1955).

(4) A. W. Ralston, "Fatty Acids and Their Derivatives," John Wiley and Sons, Inc. New York, N. Y., 1948, Chap. 8.

and electrical phenomena at solid–liquid interfaces. Streaming potentials are determined by measuring the potential difference between the ends of a porous plug of particles when liquid is forced through the plug. The zeta potential is calculated from streaming potential data by the following equation[1,5]

$$\zeta = \frac{4\pi\eta}{\epsilon} \times \frac{E\lambda}{P} \qquad (1)$$

in which η is the viscosity, ϵ the dielectric constant, λ the specific conductivity, E the streaming potential and P the applied pressure difference. In aqueous solutions at 25°, the equation becomes

$$\zeta = 9.69 \times 10^4 \frac{E\lambda}{P} \text{ mv.} \qquad (2)$$

with E, P and λ being, respectively, the streaming potential in millivolts, the driving pressure in cm. of mercury, and the specific conductance of the solution within the plug in ohms^{-1} cm.$^{-1}$. To calculate ζ, these three variables have to be measured experimentally. The apparatus for measuring streaming potentials has been described in detail recently.[6] Briefly, the streaming potential apparatus consists of a cell assembly in which quartz particles are packed between two porous platinum electrodes, a source of purified nitrogen for driving solution through the plug of particles, manometers and an electrical circuit for measuring E and λ. For E, the electrical circuit consists of a potentiometer with a vibrating reed electrometer as a null point instrument. For resistances less than one megohm, the specific conductances are determined with a Wheatstone bridge utilizing 1000-cycle a.c., while for resistances greater than one megohm, a d.c. bridge is used. The experimental quantities can be measured with these pieces of equipment with a total error less than 0.5%. However, measurement of streaming potentials with a plug of particles has been shown by Overbeek and Wijga[7] to yield low values in dilute solutions because of surface conductance within the plug. Surface conductance results from the double layer's contributing substantially to the total conductance within the plug. Since the data yield low results in dilute solutions, the zeta potential appears to increase with increasing concentration of electrolyte, although ζ may actually be decreasing. With the present experimental setup, the zeta potential of quartz always calculates to be −70 mv. in conductivity water and increases with the concentration of an indifferent electrolyte, such as sodium chloride, to a maximum value of about −100 mv. in 6×10^{-5} molar solutions before decreasing to zero at high concentrations. This hump in the ζ–log C curves is unreal. Actually the zeta potential should be more like −150 mv. than the calculated value of −70 mv. which is obtained from data on quartz plugs in conductivity water. At concentrations greater than 6×10^{-5} molar, the value of ζ determined with plugs is nearly correct. However, keeping the effect of surface conductance in mind, the data still can be interpreted satisfactorily.

The quartz used in this research was the 48/65-mesh fraction (208/295 microns) obtained from crushing selected quartz crystals. The crushed product was leached repeatedly in boiling concentrated hydrochloric acid until no discoloration of the acid by dissolved iron was observed. The quartz was washed with distilled water until the filtrate showed no trace of chloride ion. Finally the material was washed with and stored under conductivity water. Only water with a specific conductance less than 7×10^{-7} ohms^{-1} cm.$^{-1}$ was used to make the solutions. All experiments were conducted in the absence of carbon dioxide.

All inorganic chemicals were of reagent grade. High purity octylammonium, decylammonium, dodecylammonium, tetradecylammonium and hexadecylammonium acetates were supplied through the courtesy of Dr. H. J. Harwood of Armour and Company, Chicago, Illinois.

Experimental Data

Effect of Chain Length on the Zeta Potential.—Using streaming potential techniques, the zeta potential of quartz was measured as a function of the concentration of hexadecylammonium acetate, tetradecylammonium acetate, dodecylammonium acetate, decylammonium acetate, octylammonium acetate and ammonium acetate. In Fig. 1 these

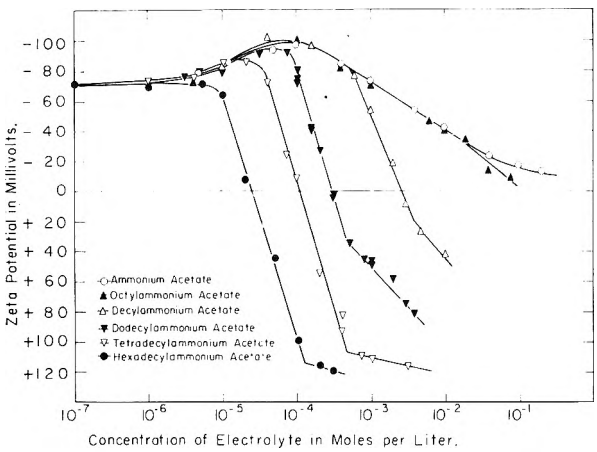

Fig. 1.—Effect of hydrocarbon chain length on the zeta potential of quartz in solutions of aminium acetates.

data are presented graphically. The calculated value of ζ for quartz in water is −70 mv. In solutions of ammonium acetate, ζ reaches a maximum value of about −100 mv. in solutions containing 6×10^{-5} mole per liter and approaches zero as a limit upon further increase in the concentration of ammonium acetate. The zeta potential does not change sign. However, for long-chained aminium acetates, there are sharp breaks in the ζ–log C curves with the zeta potential becoming positive, and these breaks are dependent upon the chain length of the aminium ion. As the chain is increased in length, the breaks occur in more dilute solutions. Note that octylammonium acetate behaves nearly identically to ammonium acetate.

Effect of Sodium Chloride on the Zeta Potential in Solutions of Dodecylammonium Acetate.—Two different experiments were conducted with sodium chloride and dodecylammonium acetate to study the double layer about quartz. In one experiment, the concentration of dodecylammonium acetate was held constant at 10^{-4} mole per liter and sodium chloride was added to the system. The experimental data are presented in Fig. 2. In this experiment ζ remains constant until the concentration of sodium chloride exceeds about 6×10^{-5} mole per liter and thereafter it is reduced to zero as a limit. The slope of the ζ–log C curve over the straight line portion is 29 mv. per tenfold increase in sodium chloride concentration.

In the other experiment the concentration of sodium chloride is held constant at 10^{-3} mole per liter while the concentration of dodecylammonium acetate in solution is increased. The experimental data are also presented in Fig. 2. In the millimolar sodium chloride solutions, the sharp break in the ζ–log C curve does not occur until the solution concentration of dodecylammonium acetate is about 6×10^{-4} mole per liter, whereas in conductivity water the sharp break occurs when the concentration of dodecylammonium acetate is about 1×10^{-4} mole per liter. For comparative

(5) H. R. Kruyt, "Colloid Science," Vol. I, Elsevier Publishing Co., New York, N. Y., 1952, Chap. 4 and 5.

(6) D. W. Fuerstenau, to be published in *Mining Eng.*

(7) J. Th. G. Overbeek and P. W. O. Wijga, *Rec. trav. chim.*, **65**, 556 (1946).

purposes, in Fig. 2 the zeta potential of quartz is also plotted as a function of the concentration of dodecylammonium acetate in conductivity water.

Effect of *p*H on the Zeta Potential in Solutions Containing 4×10^{-5} Mole of Dodecylammonium Acetate per Liter.—In this series of experiments, 4×10^{-5} mole of dodecylammonium acetate per liter was added to the solution initially and the *p*H of the solution was changed with either hydrochloric acid or sodium hydroxide. A Beckman *p*H meter was used to measure the *p*H of the solutions. In Fig. 3 the zeta potential of quartz is plotted as a function of *p*H of these solutions. From a *p*H of about 3.7, the zeta potential increases from zero to a maximum value of about −115 mv. at *p*H 9. Between *p*H 9 and 10, ζ changes from −115 mv. to about +10 mv. Further increase in *p*H causes ζ to become negative again.

Discussion of Results

Surface-inactive indifferent electrolytes reduce the value of ζ by compression of the double layer. The zeta potential cannot change sign by the addition of such an electrolyte but only approaches zero at infinite concentration. If the counterions are attracted to the surface by specific forces in addition to simple electrostatic forces between the ions and the surface charge, they can reverse the sign of ζ and are called surface-active indifferent electrolytes. As has been mentioned earlier, hydrogen and hydroxyl ions are potential-determining ions for quartz and are responsible for the existence of the electrical double layer around the quartz surface.

Since the zeta potential only approaches zero as a limit at high concentrations of ammonium acetate, it can be concluded that ammonium ions function only as surface-inactive counter ions.

However, the ζ–log C curves for long-chained aminium acetates differ from the curve for ammonium acetate and these differences depend upon the length of the hydrocarbon chain of the aminium ion. The ζ–log C curves for aminium acetates possess three distinct segments: (1) a portion which follows the curve for surface-inactive indifferent electrolytes, (2) a portion where the curve breaks sharply and ζ becomes positive, and (3) a portion where the slope decreases again. These three segments have been interpreted in the following manner[1,2]: In dilute solutions, long-chained aminium ions are adsorbed as individual ions. However, as the concentration of aminium ions is increased in solution, the number of ions in the Stern layer next to the surface is increased and once these ions get close enough together, van der Waals attraction between hydrocarbon chains causes them to associate into hemi-micelles. The third segment in the curves at higher concentrations appears to be the onset of multilayer adsorption. Possibly, since the second layer would not be held by coulombic forces, these ions are stripped off by the streaming liquid and have a less pronounced effect on ζ. This second break in the curve for dodecylammonium acetate corresponds approximately to monolayer coverage found by de Bruyn using tracer and B.E.T. techniques.[8]

(8) P. L. de Bruyn, *Trans. A. I. M. E.*, **202**, 191 (1955).

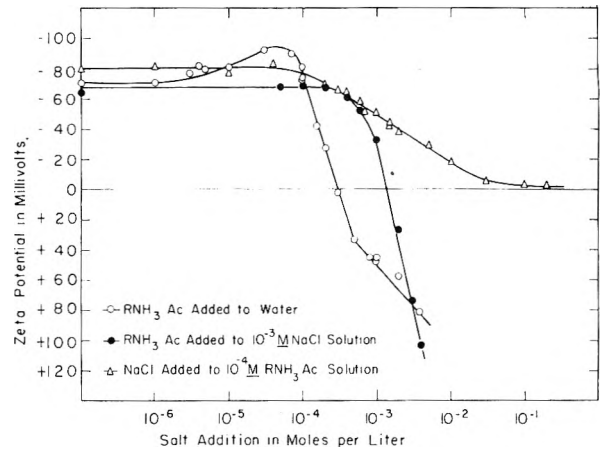

Fig. 2.—Effect of competition between dodecylammonium ions and sodium ions for the surface on the zeta potential of quartz.

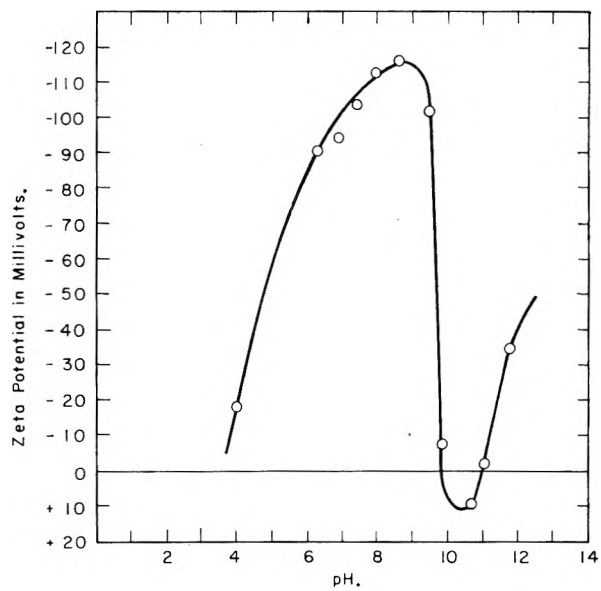

Fig. 3.—Effect of *p*H on the zeta potential of quartz in solutions containing 4×10^{-5} mole of dodecylammonium acetate per liter.

If the forces causing association of aminium ions adjacent to the surface are the same as those causing association of aminium ions in bulk solutions, the bulk concentration which is necessary to give a surface concentration great enough for hemi-micelle formation at neutral *p*H should be proportional to the bulk critical micelle concentration. The bulk concentration at which hemi-micelle formation begins is taken as the point on the ζ–log C curve where the slope changes markedly from the curve for ammonium acetate. With data obtained on plugs of particles where surface conductance affects the results, it is difficult to ascertain exactly where the slope changes. Table I shows the proportionality between the bulk critical micelle concentration of the different aminium acetates and the bulk concentration required before hemi-micelles form adjacent to the surface.

From this table it can be seen that there is a rough proportionality between the bulk critical micelle concentration and the concentration re-

TABLE I

PROPORTIONALITY BETWEEN THE BULK CRITICAL MICELLE CONCENTRATION AND THE BULK CONCENTRATION AT WHICH HEMI-MICELLES BEGIN TO FORM NEXT TO THE SURFACE AT NEUTRAL *p*H

No. of carbon atoms in the aminium ion	Bulk critical micelle concn. moles/l.	Bulk concn. necessary for hemi-micelle formation, *M*	Ratio of bulk C.M.C. to hemi-micelle bulk critical concn.
16	3×10^{-4}	8×10^{-6}	100
14	4×10^{-3}	3×10^{-5}	130
12	1.3×10^{-2}	1×10^{-4}	130
10	4×10^{-2}	6×10^{-4}	70
8	Very High	...	..

quired for hemi-micelle formation at the quartz–solution interface. Before this hypothesis can be tested more exactly, experiments will have to be conducted with a capillary where surface conductance effects are absent.

When there are only ten carbon atoms in the aminium-ion chain, the tendency for hemi-micelle formation is a little less than one would predict; and for eight carbon aminium ions, the tendency to form hemi-micelles at neutral *p*H seems to have disappeared. Before the hydrocarbon chain can play a role in adsorption, it apparently must contain more than eight carbon atoms.

Increasing the ionic strength of the solution increases the charge at the solid surface.[5] In one series of experiments sodium chloride was added to a solution containing 10^{-4} mole of dodecylammonium acetate per liter (Fig. 2). After sufficient sodium chloride had been added to increase the ionic strength of the solution, ζ was then reduced to zero at infinite concentration. Since the surface charge is increased under these conditions, the adsorption of counterions increases accordingly. If dodecylammonium ions have any special affinity for the surface, the adsorption of dodecylammonium ions would have increased. Since 10^{-4} mole of dodecylammonium acetate is just at the concentration required for hemi-micelle formation at neutral *p*H, this would have resulted in a marked change in ζ because of the formation of hemi-micelles. Therefore, the experiment indicates that sodium ions and not dodecylammonium ions are adsorbed to compensate the increase in charge and that dodecylammonium ions have no special affinity for the surface in the absence of hemi-micelle formation.

The reverse experiment is interesting. In this series of experiments, the concentration of sodium chloride was held constant at 10^{-3} mole per liter, and dodecylammonium acetate was added to the system (Fig. 2). In this experiment, the ζ–log C curve does not break sharply until the concentration of aminium salt reaches about 6×10^{-4} mole per liter. This can be interpreted on the basis of competition between sodium and dodecylammonium ions for sites in the double layer. If the concentration of aminium ions in the Stern layer must reach a certain value before the aminium ions associate into hemi-micelles, the presence of excess sodium ions competing with the dodecylammonium ions for sites within the double layer would keep the concentration of dodecylammonium ions within the double layer below the minimum concentration required for association into hemi-micelles. Hence, the bulk concentration of dodecylammonium acetate must be increased before enough dodecylammonium ions are adsorbed for hemi-micelle formation to take place.

The solution *p*H has been shown to play an important part in the adsorption of dodecylammonium ions at the quartz–solution interface. If the addition of dodecylammonium acetate is held constant at 4×10^{-5} mole per liter (below hemi-micelle formation at neutral *p*H) and the *p*H is changed with hydrochloric acid or sodium hydroxide, the zeta potential changes markedly (Fig. 3). As the *p*H is lowered below 7 with hydrochloric acid, ζ decreases because of the reduction in the total double layer potential ψ_0. As the *p*H is increased above 7 with sodium hydroxide, ζ increases because ψ_0 is increased. With the increase in ψ_0, increased adsorption of counterions takes place to compensate the increase in negative charge at the surface. Most of the counterions will be dodecylammonium ions until the *p*H reaches nearly 10 since dodecylammonium ions will be the most abundant cations in solution. Because of the increased adsorption, sufficient dodecylammonium ions go into the Stern layer to permit them to associate into hemi-micelles when the *p*H reaches 9 and change the sign of ζ to positive. Further increase in *p*H causes ζ to become negative again because of two factors: (1) competition between sodium and dodecylammonium ions for the surface, and (2) the formation of free amine at high *p*H. The ratio of the concentration of free amine to that of dodecylammonium ions can be calculated as a function of *p*H by equation 2.[4]

$$RNH_3^+ + OH^- = RNH_2 + H_2O;\ K = 4.3 \times 10^{-4} \quad (2)$$

The solubility of dodecylamine is 2×10^{-5} mole per liter.[8] In Table II the ratio of the concentration of dodecylammonium ions to the concentration of sodium ions is presented as a function of the solution *p*H.

TABLE II

COMPARISON OF THE CONCENTRATION OF SODIUM IONS AND DODECYLAMMONIUM IONS IN SOLUTIONS TO WHICH 4×10^{-5} MOLE OF DODECYLAMMONIUM ACETATE HAD BEEN ADDED INITIALLY

*p*H	RNH_2, moles/l.	RNH_3^+, moles/l.	Na^+ moles/l.	RNH_3^+/Na^+ ratio
8	9.3×10^{-8}	4×10^{-5}	1×10^{-6}	40
9	9.1×10^{-7}	4×10^{-5}	1×10^{-5}	4
10	7.6×10^{-6}	3.2×10^{-5}	1.1×10^{-4}	0.3
11	2×10^{-5}	8.6×10^{-6}	1.0×10^{-3}	0.008
12	2×10^{-5}	8.6×10^{-7}	1.0×10^{-2}	0.00009

Summary and Conclusions

Aminium salts in sub-micellar bulk concentrations make enormous electrokinetic changes at the quartz–solution interface, depending upon the length of the hydrocarbon chain. The adsorption of these ions seems to take place as individual aminium ions until a certain critical concentration is reached within the double layer. At this critical concentration, it seems that the adsorbed ions begin to associate into hemi-micelles adjacent to the

surface. The bulk concentration required to form hemi-micelles adjacent to the surface is roughly proportional to the bulk critical micelle concentration for the different aminium acetates. Aminium ions containing eight or less carbon atoms act as surface-inactive counter ions, similar to ammonium and sodium ions.

In the presence of a large amount of sodium ions, hemi-micelles do not form until the bulk concentration of aminium ions is considerably greater than the concentration required to form them in conductivity water. This is the reverse of the effect of a high concentration of sodium chloride on the bulk critical micelle concentration, in which case the bulk critical micelle concentration is lowered and not raised. At the quartz surface, competition between aminium and sodium ions keeps aminium ions out of the double layer until the bulk concentration of aminium ions approaches that of the sodium ions.

Solution *p*H plays an important role in the formation of hemi-micelles because hydrogen and hydroxyl ions are potential-determining ions for quartz. An increase in *p*H aids hemi-micelle formation because it increases the adsorption of counter ions.

Acknowledgments.—The author wishes to acknowledge the thought-provoking discussions he had with Professor A. M. Gaudin (M.I.T.), Professor J. Th. G. Overbeek (University of Utrecht, Netherlands), Professor P. L. de Bruyn (M.I.T.), and Mr. F. F. Aplan (M.I.T.) on this subject. The author is indebted to Dr. H. J. Harwood (Armour and Company, Chicago) for the samples of aminium acetates. The work was sponsored by the United States Atomic Energy Commission.

CONDUCTANCES OF CONCENTRATED AQUEOUS SODIUM AND POTASSIUM CHLORIDE SOLUTIONS AT 25°

BY J. F. CHAMBERS,[1] JEAN M. STOKES[2] AND R. H. STOKES[2]

Chemistry Department, University of Western Australia, Nedlands, Australia

Received February 13, 1956

Precise conductance measurements are reported for aqueous potassium and sodium chloride solutions in the region from 0.1 *N* to saturation at 25°, and values at round concentrations are tabulated.

Introduction

Since the development of the interionic attraction theory of electrolyte solutions, a tremendous amount of careful work has been devoted to the conductance of dilute solutions, especially in the region below 0.1 mole $l.^{-1}$, but more concentrated solutions have been relatively neglected. Thus the literature contains no data of modern accuracy for even such common salts as potassium chloride and sodium chloride at 25° above about 0.2 mole $l.^{-1}$, with the exception of Jones'[3] absolute determination of the specific conductance of one-demal potassium chloride. Since recent theoretical developments[4,5] offer promise of supplying an adequate theory for concentrated solutions, we are studying the conductances of some simple salts over a wide range of concentration and temperature, the first results being now reported.

Experimental

Sodium chloride was of analytical reagent quality, dried for 24 hours at 400°. Part of the material was further purified by precipitation with hydrogen chloride gas; the product however gave results indistinguishable from those for the original material. **Potassium chloride** was analytical reagent material purified by recrystallization from conductance water and similarly dried; fusion was also tried but gave results identical with the more convenient drying at 400°. **Conductance water** was redistilled through Pyrex glass from the laboratory distilled water supply and stored in polyethylene bottles; at equilibrium with the laboratory air it had a specific conductance of 1.2×10^{-6} ohm^{-1} $cm.^{-1}$. Solutions were prepared by weight, usually in amounts of about 150 g. so that the final weight was within the capacity of an analytical balance. For occasional larger batches of solution, the salts were weighed on analytical balance and the final solution on a large balance of sensitivity ~5 mg. The amount of salt taken was always such that its weight was determinable within 0.005%; where more dilute solutions were required, these were prepared by weight-dilution of more concentrated stocks. Vacuum-corrections were applied throughout, and the densities given in the International Critical Tables[6] were used to compute the concentrations in moles per liter given in Tables I and II. Conductance cells having cell constants from 0.5 to 80 $cm.^{-1}$ were employed. They were of Pyrex glass, the platinum-to-Pyrex seals being rendered completely tight by a layer of "Araldite" thermosetting resin on the side remote from the solution. The electrode-leads were of silver, well separated from each other and from the cell filling tubes. The cells were calibrated at 25° using the Jones and Bradshaw 1, 0.1 and 0.01 *D* potassium chloride standards,[2] retaining the International ohm units in which these standards are expressed. The cells were used in an oil-thermostat controlled to better than ±0.003° as indicated by a Beckmann thermometer; the actual temperature was thus constant within these limits throughout the work, but may have been as much as 0.02° different from the true 25°, this being the accuracy of the standard thermometer used. However, since the temperature coefficients for the solutions are very similar to those of the calibration standards, a negligible error should arise from this uncertainty. Two measuring bridges were used, the earlier one being built up from a calibrated post-office box, while later a Leeds and Northrup Jones conductivity bridge became available. Both salts were studied with both

(1) Electrolytic Zinc Company Research Fellow, 1955.

(2) Chemistry Department, University of New England, Armidale, N.S.W., Australia.

(3) G. Jones and B. C. Bradshaw, *J. Am. Chem. Soc.*, **55**, 1780 (1933).

(4) H. Falkenhagen, M. Leist and G. Kelbg, *Ann. Physik*, [6] **11**, 51 (1952); H. Falkenhagen and M. Leist, *Naturwiss.*, **41**, 570 (1954); R. M. Fuoss and L. Onsager, *Proc. Natl. Acad. Sci., U. S.*, **41**, 274 (1955).

(5) B. F. Wishaw and R. H. Stokes, *J. Am. Chem. Soc.*, **76**, 1991 (1954).

(6) "International Critical Tables," Vol. III, McGraw-Hill Book Co., Inc., New York, N. Y.

bridges, the results (Table I) being in excellent agreement, though those from the Jones bridge are of somewhat higher precision. All measurements were made at 500,100 and 2000 c./s.

Results

The experimental concentrations and equivalent conductances are reported in Table I. Large-scale graphs of deviation-functions of the form $x = \Lambda + A\sqrt{c}$ were prepared, where the constant A is arbitrarily chosen to make the range of variation of x only a few units of equivalent conductance. Suitable values were $A = 20$ for KCl and $A = 29$ for NaCl. These deviation functions are of course without theoretical significance. From the graphs, equivalent conductances at rounded concentrations were obtained (Table II). Errors in the tabulated values are unlikely to exceed 0.03%.

TABLE I

EQUIVALENT CONDUCTANCES OF POTASSIUM AND SODIUM CHLORIDE SOLUTIONS AT 25°

c = concn. of soln.; Λ = equiv. conductance.

Potassium chloride		Sodium chloride	
c, mole l.$^{-1}$	Λ, Int. ohm^{-1} mole^{-1} cm.^{2}	c, mole l.$^{-1}$	Λ, Int. ohm^{-1} mole^{-1} cm.^{2}
A. Results using P.O. box bridge (J.M.S. and R.H.S.)			
0.14075	126.64	0.15621	103.66
.19141	124.43	.20998	101.36
.28307	121.51	.24584	100.02
.36417	119.71	.33998	97.29
1.5329	108.08	.49935	93.66
2.0000	105.29	.68703	90.26
2.6082	101.72	1.05142	85.12
3.0645	99.08	1.3948	81.02
3.6951	95.37	1.5193	79.65
4.0000	93.46	1.9279	75.41
		2.3793	71.14
		2.7439	67.82
		3.1431	64.36
		3.5037	61.30
		4.5199	53.13
		5.3540	46.83
B. Results using Jones bridge (J.F.C.)			
0.12004	127.67	0.11300	105.91
.14968	126.13	.12452	105.24
.18588	124.58	.18776	102.19
.24678	122.53	.26492	99.41
.32330	120.54	.36091	96.71
.40698	118.81	.46914	94.25
.53211	116.79	.60766	91.60
.66460	115.10	.66232	90.65
.76142	114.03	.74528	89.34
.93485	112.41	.86366	87.58
1.1934	110.35	1.2312	82.87
1.5642	107.87	1.4647	80.215
1.9155	105.74	1.8416	76.277
2.3789	103.07	2.6739	68.445
2.6188	101.70	3.1723	64.088
3.4686	96.72	3.8769	58.228
3.7046	95.29	4.3281	54.622
		4.8114	50.882

Comparison with Previous Results.—The data of Stearn,[7] after adjusting to the Jones and Bradshaw standards, show considerable scatter about the present results. The results of Shedlovsky[8] in the region 0.10–0.22 N NaCl and 0.10–0.12 N KCl are in good agreement with our results, and were included in the deviation-function graphs from which Table II was prepared. The standard values of Jones and Bradshaw[3] for 0.1 and 1 demal potassium chloride correspond to $\Lambda = 128.96$ for 0.099692 N KCl and $\Lambda = 111.915$ for 0.99488 N KCl, and were also used in preparing Table II.

TABLE II

EQUIVALENT CONDUCTANCES OF POTASSIUM AND SODIUM CHLORIDE SOLUTIONS AT ROUND CONCENTRATIONS AT 25°

c	Λ_{KCl}	Λ_{NaCl}	c	Λ_{KCl}	Λ_{NaCl}
0.1	128.96	106.74	1.0	111.87	85.76
.125	127.40	105.21	1.2	110.30	83.26
.15	126.11	103.92	1.4	108.92	80.95
.175	125.01	102.74	1.6	107.64	78.77
.2	124.08	101.71	1.8	106.43	76.70
.25	122.43	99.89	2.0	105.23	74.71
.3	121.09	98.37	2.5	102.38	70.02
.4	118.96	95.77	3.0	99.46	65.57
.5	117.27	93.62	3.5	96.54	61.33
.6	115.88	91.73	4.0	93.46	57.23
.7	114.69	90.04	4.5	...	53.28
.8	113.65	88.51	5.0	...	49.46
.9	112.72	87.09	5.350	...	46.86

Theoretical discussion of the results will be postponed until data for other salts and temperatures are obtained.

Acknowledgment.—The results reported in Table IB were obtained by J. F. C. during the tenure of an Electrolytic Zinc Company Research Fellowship, for which our thanks are expressed.

(7) A. E. Stearn, *J. Am. Chem. Soc.*, **44**, 670 (1922).

(8) T. Shedlovsky, A. S. Brown and D. A. MacInnes, *Trans. Electrochem. Soc.*, **66**, 165 (1934).

THE EXCHANGE OF HYDROGEN BY DEUTERIUM IN HYDROXYLS OF KAOLINITE

BY L. A. ROMO[1]

Department of Geochemistry, The Pennsylvania State University, University Park, Pennsylvania

Received February 27, 1956

Kaolinite treated hydrothermally at 300° and 10,000 p.s.i. in the presence of D_2O exchanges hydrogen of hydroxyl groups with deuterium as is shown by infrared spectroscopy. The rate of exchange appears to be characterized by two steps: one in which the exchange takes place predominantly on the surface hydroxyls. In the other one, a process of diffusion is involved to effect exchange in the intralattice hydroxyls.

Introduction

Since the advent of the concept of "hydrogen bonding" considerable attention has been paid to the study of the O–H–O group. Further understanding of the hydrogen bond is important especially in inorganic structures where very little is known about its behavior. As a matter of fact, most of the information gained on this bond by means of infrared methods has been the result of investigations with organic compounds.

It is an established fact that the frequency of absorption spectra depends on the distances between the interacting atoms and their masses in the particular group. Thus, when hydrogen is substituted by deuterium shifts in the frequencies of infrared absorption spectra are recorded.

This investigation was carried out with the purpose of determining whether or not deuterium exchanges for hydrogen in Kaolinite and, if so, what is the nature of the shift in frequency of absorption of the O–H–O groups.

It has been shown[2,3] that the infrared absorption pattern of this silicate has absorption bands due to hydroxyl groups, thus investigations of the exchange of hydrogen by deuterium in the hydroxyl groups may also provide further information on the nature of this bond. Previously, this problem has been partially investigated by indirect procedures.[4,5]

Experimental

Materials and Methods.—The <2 μ fraction of Kaolinite (A. P. I. 4) was separated by the standard sedimentation procedure. The relative purity of this mineral was established by means of X-ray diffraction. It was also found that it gave strong infrared absorption bands characteristic of hydroxyl groups.

Small samples of the oven-dried powder mineral were packed in envelopes made of silver foil. These envelopes were then placed into a small Morey[6] bomb containing a given volume of D_2O (purity 99.5%) calculated to yield a pressure of 10,000 p.s.i. at 300°. The closed bomb was placed in a furnace with a suitable temperature control, and heated at 300 ± 5° for times varying from 3 to 92 hours. In all the runs, the D_2O concentration, temperature and pressure were kept constant; the time of reaction being the only variable. At the end of each run the bomb was quenched. The deuterated materials were dried at 110° for three days.

In order to record the infrared spectra of deuterated Kaolinite, potassium bromide discs containing known amounts of this material were prepared. From 1.000-g. mixtures of finely powdered KBr containing 10 mg. of sample, 0.200-g. portions were withdrawn to prepare the discs. The infrared spectrum was recorded using the Perkin–Elmer double beam spectrometer, Model 21 equipped with a CaF_2 prism at a slow speed using a slit width of 8.4 μ.

Results

Exchange of Hydrogen by Deuterium in Kaolinite.—The infrared spectra of the samples which had been treated hydrothermally with D_2O showed the absorption bands: 3.67, 3.78, and 3.73μ (Fig. 1).

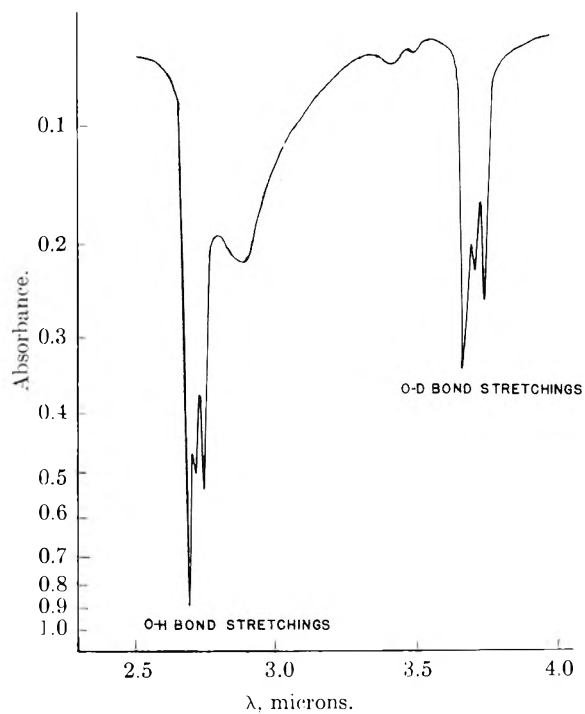

Fig. 1.—O–H and O–D bands of kaolinite treated hydrothermally with D_2O at 300° and 10,000 p.s.i.

To obtain evidence on the nature of the O–D bond, the polarized infrared spectra of oriented samples was obtained. To do this, AgCl plates containing a thin layer of Kaolinite[7] deposited from suspensions made with methanol were placed tilted at an angle of 45° with respect to the polarized beam. The spectra of the O–H and O–D region were then recorded having the electrical vector (E) parallel and then perpendicular to the planes of vibration of these bonds. The spectra shown in Fig. 2 indicate clearly that by having rotated the plane of polarization 90° (from $\parallel$ to $\perp$) one has effected a significant change in the absorbances of

(1) Pigments Department, du Pont de Nemours, Wilmington, Delaware.

(2) H. Adler, A. P. I. Res. Report 49 (1950).

(3) M. Hunt, M. P. Wisherd and L. C. Bonham, *Anal. Chem.*, **22**, 1478 (1950).

(4) C. D. McAuliffe, L. A. Dean and S. B. Hendricks, *Proc. Soil Sci. Soc., Am.*, **12**, 119 (1947).

(5) J. A. Faucher and H. C. Thomas, THIS JOURNAL, **59**, 189 (1955).

(6) G. W. Morey, *Am. Min.*, **22**, 1121 (1937).

(7) The X-ray diffraction patterns showed only the presence of 001 reflections.

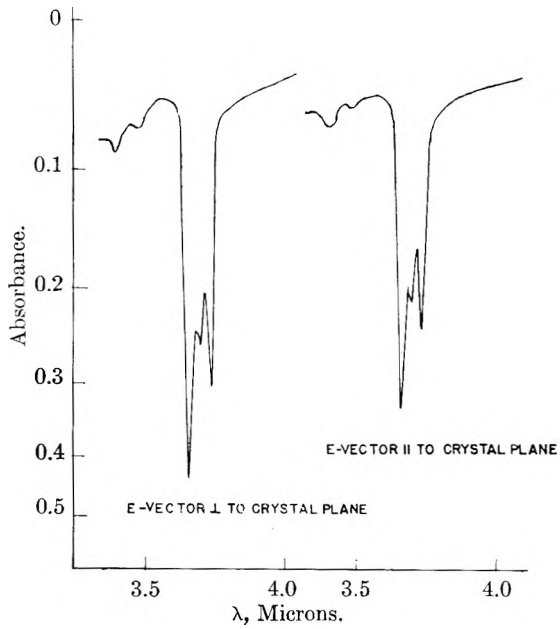

Fig. 2.—Polarized spectra of the O–D bond stretching region of deuterated kaolinite.

the various O–H and O–D bond stretchings. This variation in absorbances arises as a result of the preferred orientation of the O–D and O–H bonds which are obviously along the direction of maximum absorbance (*i.e.*, the O–H, O–D bonds vibrate ⊥ to the *c*-planes). In case all the O–H and O–D groups were situated at random in the structure, there would be no variations in the absorbances of the patterns recorded with the use of polarized infrared radiation.[8] The ratio of absorbances of OH/OD bands obtained with polarized light beamed parallel and perpendicular to the planes of vibration were found to be the same in both cases.

Although the absorbance of the O–H absorption bands decreased as the exchange of hydrogen by deuterium increased, it was found that the increase in absorbance of the O–D bands was greater than the small decrease in absorbance of the O–H band. This rather unexpected result complicated the calculation of absolute changes in concentration. Although the relation of absorbances of the O–H, O–D bands in this case is not known it was found convenient to plot the ratio of integrated areas of the absorptions peaks of the O–H/OD *versus* time. The validity of this is justified on the following grounds: (a) the spectra of all runs were scanned using the same base line, (b) all of them were adjusted to give zero absorption at the zero of the scale and (c) particle size and scattering were the same in all runs.

The curve in Fig. 3 shows that the hydrogen–deuterium exchange increased gradually as the time of hydrothermal treatment was increased up to 28 hours. Therefrom, the rate decreased considerably as is indicated by the marked change in slope of the curve.

Discussion

The results of this investigation indicate that

(8) To eliminate any adsorbed D_2O the samples of deuterated Kaolinite were dried in the oven at 250° overnight. No changes either in the intensity or the shape of the O–H and O–D bands were observed.

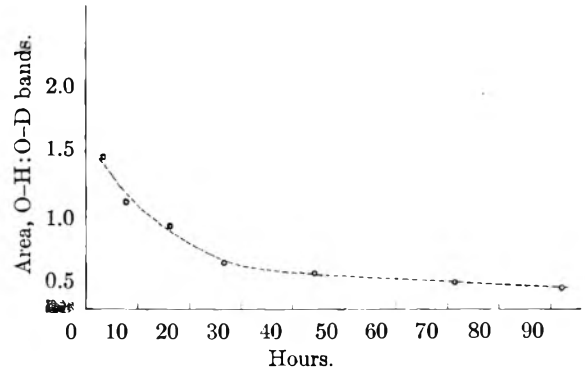

Fig. 3.—The rate of exchange of hydrogen by deuterium in kaolinite treated hydrothermally with D_2C at 300° and 10,000 p.s.i.

hydrogens from the hydroxyl groups are replaced partially by deuterium. This finding was established by the appearance of absorption bands with peaks at 3.67, 3.70 and 3.73 μ which increased in intensity as the time of hydrothermal reaction was increased.

The improved resolution obtained with the use of CaF_2 prism allows one to definitely identify O–H bond stretchings corresponding to three types of hydroxyls with frequencies corresponding to 2.70, 2.73 and 2.76 μ. The shifts in wave length effected by the replacement of hydrogen by deuterium in the three types of hydroxyls is, in every case, 0.97 μ.

The studies of the O–H and O–D regions with polarized infrared radiation show that the vibrational positions of the O–H bands have not changed as a result of the exchange of hydrogens by deuterium in the various hydroxyl groups. This fact is evidenced by the constancy of the ratio of the absorbances of the O–H and O–D bands of the oriented specimens of Kaolinite when they were examined with the polarized beam ∥ and ⊥ with respect to the planes of vibration.

It has been shown that in Kaolinite the replacement of hydrogen by deuterium takes place gradually. The exchange increases as the time of hydrothermal treatment is increased although the rate decreases considerably as a function of time. These results indicate also that the exchange of the three types of hydroxyls follows a definite pattern. At present, any quantitative analysis of rates of exchange of each one of these groups is not possible because of the tendency to degeneracy of the bands recorded at 2.73 and 3.70 μ, respectively, and thus only parametric estimates (Fig. 2) of the over-all rates can be made. The fact that the rate of exchange decreases considerably as the time of reaction becomes longer can be explained as follows: (a) most of the relatively rapid rate of exchange is effected by surface or exposed hydroxyls as is shown by the segment of the curve from 0 to 28 hours, and (b) the slower rate of exchange recorded after 28 hours of reaction is due presumably to a process in which the hydrogens of the intralattice hydroxyls are exchanged by deuterium by means of diffusion.

Acknowledgment.—This work was carried out while I was a Research Associate in the Depart-

ment of Geochemistry, The Pennsylvania State University, University Park, Pennsylvania. I wish to thank Dr. R. Roy for his help with some phases of the experimental work.

THE AMPLITUDE OF VIBRATION OF AEROSOL DROPLETS IN A SONIC FIELD[1]

BY FRANK T. GUCKER AND GEORGE J. DOYLE[2]

Contribution No. 791 from the Chemical Laboratory of Indiana University, Bloomington, Indiana

Received March 5, 1956

We have determined the amplitudes of vibration of droplets of the non-volatile plasticizers Flexol DOP (bis-2-ethylhexyl phthalate) and Flexol 3GH (di-2-ethylbutyrate triethylene glycol) at the displacement antinode of a standing sonic field. The sonic generator was of the type developed by H. W. St. Clair, employing an electromagnetically-driven bar. The measurements were made photomicrographically, covering a range of droplet radii between 0.8 and 3.9 μ, at a sound frequency of 4.85 kc./sec. The size of the particles was determined by applying the Stokes–Cunningham law to rate-of-fall measurements also determined photomicrographically. The dependence of vibration amplitude on particle radius is given within the accuracy of our experiments by the theoretical equation of Sewell, based on an approximate hydrodynamic treatment. In the range of our work this equation is nearly the same as that derived by Brandt, Freund and Hiedemann, on the basis of a simple interaction between sound field and particle derived from Stokes's law. These results may prove useful to those wishing to apply sonic fields in the study of aerosols, since they show that measurements of particle amplitude may be used to determine particle size.

Introduction

The motion of small particles in a sonic field has been of interest for many years. Theoretical studies have been made by König,[3] Sewell[4,5] and Brandt, Freund and Hiedemann.[6] Most experimental work has been confined to the use of small particles in determining the intensity, wave form or other property of sound[7–12] or to the verification of a particular theory of particle motion[13]; but recently considerable interest has arisen in the application of sonic fields to the study and technology of aerosols.[6,14–26]

In 1946 English started with the senior author to investigate the possibility of studying size distribution in aerosols by measuring the amplitude of vibration of the particles in a sound field. Since we could find no experimental data in the literature sufficiently precise to allow an evaluation of the method, and the theories[3–6] for the behavior of small particles in a sound field are not exact, the junior author in 1947 undertook an experimental investigation of the dependence of particle amplitude on particle size. A brief description of our apparatus was given earlier by one of us.[27] Recently Cassel and Schultz[26] have reported preliminary experiments using a considerably different technique to determine the sizes of larger particles at lower sound frequencies than we employ.

The theoretical expression most appropriate for small particles in the sound field of a viscous compressible fluid was obtained by Sewell[4,5] from the linearized Stokes–Navier partial differential equation of hydrodynamics, assuming that the fluid is isotropic and that the only dissipative mechanism is shear viscosity. Although other dissipative mechanisms have been discussed by Markham and his collaborators,[28,29] *e.g.*, heat conductivity and lack of thermal equilibrium between translational and internal degrees of freedom of the gas molecules, they are negligible under our experimental conditions, although not necessarily for other gases or other frequencies. Sewell's complicated equation for the amplitude and phase of the particle relative to that of the unperturbed sound wave need not be reproduced here. However, under certain circumstances it becomes equivalent to that which Brandt, Freund and Hiedemann[6] derived by the use of Stokes' law

$$\frac{X_p}{X_g} = \left[1 + i\frac{2d\omega r^2}{9\eta}\right]^{-1} \qquad (1)$$

Here X_p, X_g are, respectively, the amplitude of the particle and of the unperturbed sound wave, i =

(1) This paper is based upon a thesis submitted to the Faculty of the Graduate School of Indiana University by George J. Doyle in partial fulfillment of the requirements for the degree, Doctor of Philosophy, 1952. Further details may be found in this thesis.

(2) Manuscript originally received January 21, 1955.

(3) W. König, *Ann. Physik*, [3] **42**, 353, 549 (1891).

(4) C. J. T. Sewell, *Trans. Roy. Soc. (London)*, **A210**, 239 (1910).

(5) H. Lamb, "Hydrodynamics," 6th ed., Dover Publ., New York, N. Y., 1945, pp. 659–661.

(6) O. Brandt, H. Freund and E. Hiedemann, *Z. Physik*, **104**, 511 (1937).

(7) E. P. Lewis and L. P. Farris, *Phys. Rev.*, [2] **6**, 491 (1915).

(8) K. Gehlhoff, *Z. Physik*, **3**, 330 (1920).

(9) E. N. da C. Andrade, *Proc. Roy. Soc. (London)*, **A134**, 445 (1931).

(10) E. N. da C. Andrade and R. C. Parker, *ibid.*, **A169**, 507 (1937).

(11) R. A. Scott, *ibid.*, **A183**, 296 (1945).

(12) L. L. Beranek, "Acoustic Measurements," John Wiley and Sons, Inc., New York, N. Y., 1949, p. 159–61.

(13) M. Wagenschein, *Ann. Physik*, [4] **65**, 461 (1921).

(14) O. Brandt and E. Hiedemann, *Trans. Faraday Soc.*, **32**, 1101 (1936).

(15) E. N. da C. Andrade, *ibid.*, **32**, 1111 (1936).

(16) R. C. Parker, *ibid.*, **32**, 1115 (1936).

(17) O. Brandt and E. Hiedemann, *Kolloid-Z.*, **75**, 129 (1936).

(18) O. Brandt, *ibid.*, **76**, 272 (1936).

(19) O. Brandt, H. Freund and E. Hiedemann, *ibid.*, **77**, 103 (1936).

(20) E. Hiedemann, *ibid.*, **77**, 168 (1936).

(21) H. W. St. Clair, U. S. Bureau of Mines Report of Investigations No. 3400, p. 51–64 (1938).

(22) H. W. St. Clair, M. J. Spendlove and E. V. Potter, ref. 21, No. 4218 (1948).

(23) H. W. St. Clair, *Ind. Eng. Chem.*, **41**, 2434 (1949).

(24) H. W. St. Clair, Chapter 24 in "Proceedings of the United States Technical Conference on Air Pollution," (ed. L. C. McCabe), McGraw–Hill Book Co., New York, N. Y., 1952, pp. 382–387.

(25) E. P. Neumann, C. R. Senderberg, Jr., and A. A. Fowle, ref. 24, Chapter 45, pp. 388–393.

(26) H. M. Cassel and H. Schultz, ref. 24, Chapter 76, pp. 634–642.

(27) F. T. Gucker, Jr., Proc. 1st Nat. Air Pollution Symp., Stanford Research Institute, Los Angeles, California, November, 1949, p. 23–5.

(28) J. J. Markham, *Phys. Rev.*, [2] **86**, 497 (1952).

(29) J. J. Markham, R. T. Beyer and R. B. Lindsay, *Rev. Mod. Phys.*, **23**, 353 (1952).

$\sqrt{-1}$, d the density of the particle, ω the angular frequency of the sound wave, r the radius of the particle, and η the coefficient of viscosity of the fluid. The absolute magnitude of the amplitude ratio is that of the complex number in equation 1, and the phase angle of the particle relative to the unperturbed sound wave is $\delta = -\tan^{-1}(2d\omega r^2/9\eta)$.

Sewell's equation reduces to equation 1 when the following are much less than unity: (1) the absolute magnitude of the product of the wave number and the radius of the particle, (2) the ratio of the density of the fluid to that of the particle, and (3) the ratio of twice the kinematic shear viscosity to the product of the angular frequency and the square of the particle radius. In the region of rapid variation of X_p/X_g for aerosols, the first two conditions are satisfied in general and the third for small values of r. As r increases so does the deviation of equation 1 from that of Sewell, the difference being about 10% for particles 5 μ in radius, under our experimental conditions.

When equation 1 is used for small particles, Cunningham's correction[30] must be applied to account for viscous slip,[31] dividing the viscosity by the quantity $[1 + (AL/r)]$ where A is a constant and L the mean free path of the gas molecules. Instead of correcting Sewell's equation by introducing slip into the boundary conditions of his derivation, we followed the simpler alternative of applying Cunningham's correction here also. We used the value of $A = 1.23$, corresponding to Millikan's famous watch oil in air with Chapman's formula for L.[32] Values of the amplitude ratio and phase angle for Flexol 3GH particles in nitrogen at several different frequencies, calculated from equation 1 with the Cunningham correction, are plotted in Figs. 1 and 2.

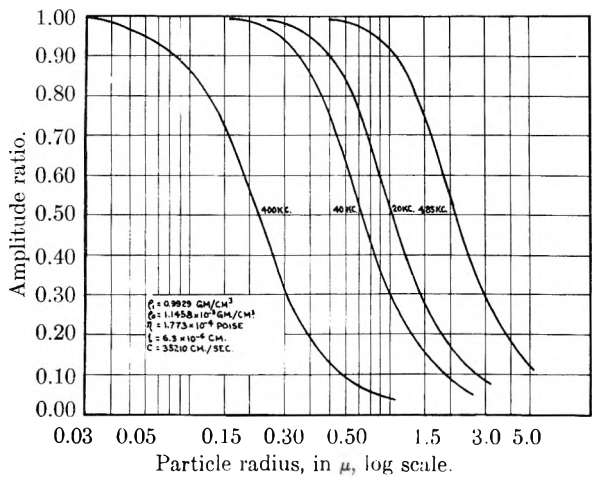

Fig. 1.—Amplitude ratio *vs.* particle radius for several sonic frequencies according to Sewell's theory with Cunningham's correction for Flexol 3GH particles in nitrogen at 25° and atmospheric pressure.

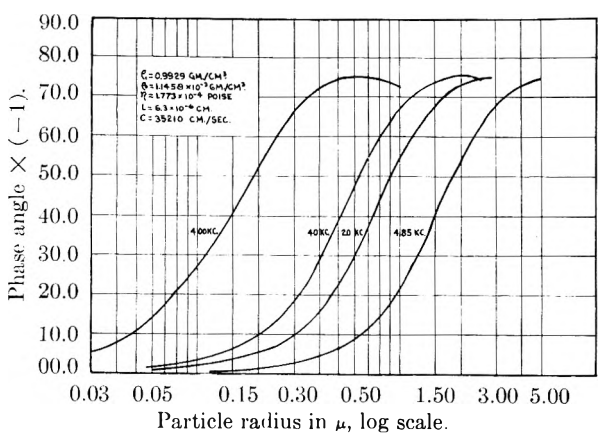

Fig. 2.—Phase angle *vs.* particle radius for several sonic frequencies according to Sewell's theory with Cunningham's correction for Flexol 3GH particles in nitrogen at 25° and atmospheric pressure.

Experimental

Our measurements required a sonic apparatus to determine the amplitude ratio, a rate-of-fall apparatus to measure particle size, and an aerosol generator to produce homogeneous aerosols over a considerable range of particle size.

Sonic Amplitude Measurements.—Particle amplitudes were determined by measuring photomicrograph tracks of aerosol particles at the displacement antinode of a standing sound wave, where they are symmetrically affected by sound pressure and a given amplitude is obtained with minimum sonic energy. Sonic amplitudes were determined by measuring tracks of very small particles which presumably oscillate with the full amplitude of the sound.

Figure 3 shows the schematic cross-section of the apparatus, mounted rigidly on an L-shaped optical bench. The sonic generator A is connected through a horn K to a thin observation cell M where an intense stationary sound field is set up. The aerosol is illuminated by a dark-field optical system Q, L_1, R, L_2, mounted on one arm of the bench, while the particles are viewed or photographed through the microscope J at the bottom.

Intense illumination from a 4-ampere carbon arc, Q, overloaded 50%, is collected by means of a Watson-Conrady achromatized aplanat L_1,[33] with liquid silicone between the lens elements to withstand the heat. A tube R of 1% cupric chloride, 76 mm. long, acts as a heat filter. Using the Kohler method of illumination an enlarged image of the lamp crater fills the entrance pupil of the microscope condenser, L_2, which forms a reduced image of the exit pupil of the lamp condenser at the region under observation. To ensure rigid alignment, the components are mounted upon a Bausch and Lomb ultramicroscope optical bench provided with a special microscope mount.

To take advantage of the intense small angle light scattering of isotropic dielectric spheres, we used an Abbe condenser L_2 of 1.25 NA (with oil) and a dark-field patch stop to give hollow-cone dark-field illumination. Its working distance of about 1 mm. in air allows observation farther from the cell window than the distance of about 0.03 mm. necessary under our experimental conditions[34,35] to avoid serious wall effects upon the motion of the observed particles.[36] The microscope J used a Spencer 20× Apochromatic objective of 8 mm. focal length with a Leitz Periplan 10× Ocular. A Leitz Micro-Ibso photomicrographic attachment (not shown in the figure), with a beam splitter to allow visual observation, was modified to use a Rapax Synchromatic shutter giving exposures down to 1/400 sec. Such short exposures, necessary to avoid blurring the image, required the use of Eastman Kodak Company's very fast Linagraph Pan film.

The observation cell M, 1.8 mm. wide, 12 mm. high and 5 to 10 cm. long, is closed by the plane face of the snugly-

(30) E. Cunningham, *Proc. Roy. Soc. (London)*, **A83**, 357 (1910).

(31) E. H. Kennard, "Kinetic Theory of Gases," McGraw-Hill Book Co., New York, N. Y., 1938, pp. 292–311, especially pp. 309–11.

(32) E. H. Kennard, ref. 31, p. 147.

(33) Furnished by W. Watson and Sons, Ltd., 313 High Holburn, London, W.C., England.

(34) H. Lamb, ref. 5, p. 620.

(35) P. M. Morse, "Vibration and Sound," 1st ed., McGraw-Hill Book Co., New York, N. Y., 1936, p. 213.

(36) After our apparatus was designed and built for the Abbe condenser, which probably utilizes less than 20% of the incident light, the superior Leitz D-0.80 dark-field condenser became available, designed for observations in air at a working distance of 4 mm.

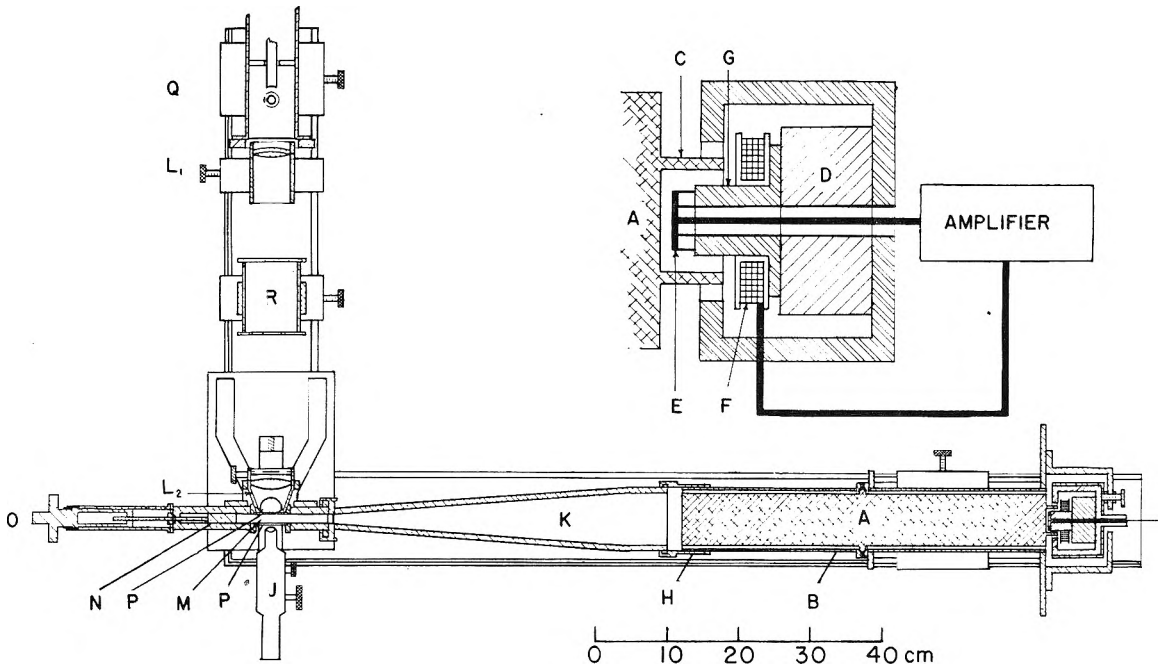

Fig. 3.—Schematic cross-section of apparatus for determination of amplitude ratio.

fitting rectangular piston N, adjustable by the threaded knob O to a position an odd number of quarter wave lengths from the center of the field of the microscope J. The generator can be moved horizontally within a telescoping adapter H, by means of an adjusting screw, to establish a standing wave system with an antinodal plane in the center of the microscope field. Two circular ports, P, P, in opposite sides of the viewing cell are closed with discs of No. 1 slide cover glass sealed flush with the cell wall. The cell length allows $^1/_2$ wave length (3.5 cm.) to the right of the observation ports and somewhat more than $^3/_4$ wave length to the left. Its cross-section is determined by the working distance and size of the microscope objective and condenser.

The observation cell is connected to the sonic generator by a pyramidal horn tapering rapidly from the round cross-section of the vibrator to that of an inscribed square, and then more gradually to the rectangular cross section of the cell. Calculations show that this horn is about 3.6 times more efficient than a simple constriction in transmitting sonic energy from the generator to the cell. A special valve near the viewing ports, closing flush with the cell wall, allows rapid introduction of the aerosol sample, while a light gravity-loaded relief valve incorporated in the horn provides an exhaust port. A solenoid-operated gate in front of the bar prevents sound from entering the cell until shortly before the film is exposed, thus avoiding unnecessary sonic coagulation.

Preliminary experiments showed that a Hartmann jet ultrasonic generator[37] was difficult to control and did not give a pure sine wave. A sonic generator of the type developed by St. Clair[38] was then chosen for its ease of control, low harmonic distortion and relatively high energy output. The vibrating member is a duraluminum bar A, 51 cm. long and 3.5 cm. in diameter, with a V-shaped ring projecting from its center, held inside a horizontal cylindrical case B in a rubber mount to reduce mechanical damping. On the right end of the bar is machined a thin coaxial ring C which, as shown in the enlarged detail, floats free in the magnetic field of an Alnico dynamic-speaker magnet D. As the bar vibrates in its fundamental longitudinal mode, a signal is picked up capacitatively by the insulated disk C of thin sheet copper, slit along a radius. This signal is fed into an amplifier, the output of which passes through coil F wound on the magnetic pole piece G and induces a much larger current in the cylindrical ring C which acts as the secondary of a step-down transformer. The alternating current reacts with the magnetic field to drive the bar at its natural frequency.

An idealized analysis of the electrical driving system of the sonic generator and coupling horn shows that it supplies about 7% of the total electrical power to the bar and at most 0.4% to the associated air load in an infinite tube of equal cross section. Although the efficiency might be increased somewhat by various refinements, we estimate that it could not exceed about 1% at the frequency we used.

The electronic circuits of the sonic generator are shown schematically in Fig. 4. The signal from the capacitative pickup is fed through shielded cable to the input circuit and

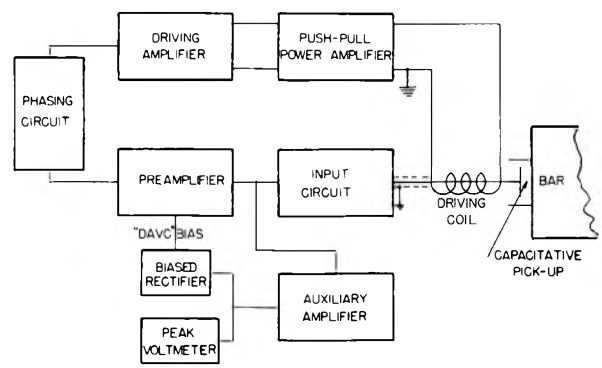

Fig. 4.—Block diagram of sonic generator.

thence to the preamplifier and auxiliary amplifier. The latter operates the peak-reading voltmeter which indicates the amplitude of vibration of the bar, and the biased rectifier comprising the DAVC (delayed automatic volume control) circuit. Whenever the peak output voltage from the preamplifier exceeds the manually adjustable rectifier bias, the difference is applied as a negative grid bias to the remote cut-off stages of the preamplifier, thus reducing the gain and stabilizing the amplitude of vibration of the bar.

Manual adjustment of the phasing circuit brings the power from the driving coil to the bar in phase with its motion. The driving amplifier converts the 1-sided signal to a 2-sided one necessary to drive the class AB$_1$ push-pull power amplifier, coupled through an output transformer to the coil.

The detailed electronic circuit is shown in Fig. 5. The input circuit consists of a 1-megohm resistor R1 attached

(37) J. Hartmann and B. Trolle, *J. Sci. Instruments*, **4**, 101 (1927).
(38) H. W. St. Clair, *Rev. Sci. Inst.*, **12**, 250 (1941).

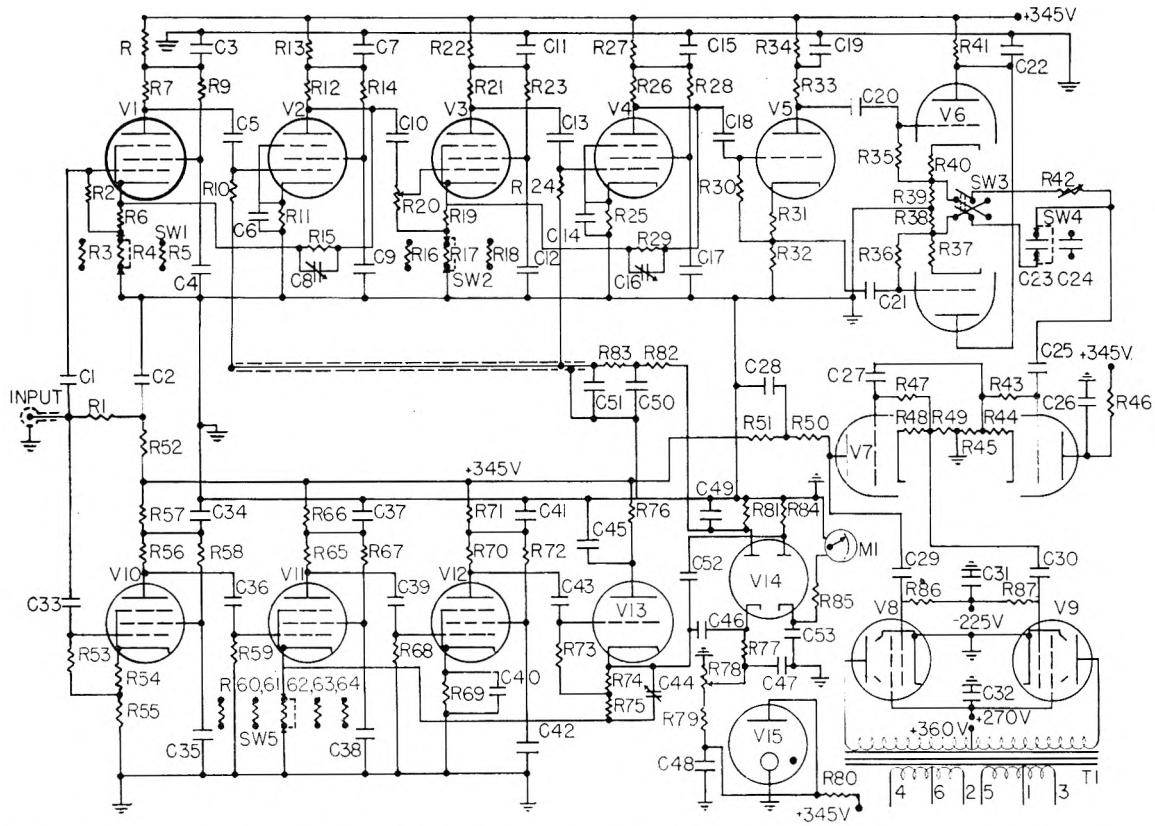

Fig. 5.—Diagram of Electronic Circuit for Sonic Generator—The values of the components are listed below: capacities in microfarads unless designated $\mu\mu$F (micro-microfarad) and resistors in ohms unless designated K(kilohm) or M(megohm) Resistors are $^1/_2$ watt carbon unless otherwise designated, *e.g.*, 10w(watt), ww(wire wound).

C1—0.01	C12—0.02	C23—100$\mu\mu$F	C33—0.01	C43—0.01
C2,C3—4	C13—0.01	C24—30$\mu\mu$F	C34—4	C44—5-25$\mu\mu$F
C4—0.02	C14,C15—4	C25—0.01	C35—0.02	C45—4
C5—0.01	C16—5-25$\mu\mu$F	C26—4	C36—0.01	C46—0.01
C6,C7—4	C17—0.02	C27—0.01	C37—4	C47—0.02
C8—5-25$\mu\mu$F	C18—0.001	C28—4	C38—0.02	C48—4
C9—0.02	C19—4	C29,C30—0.01	C39—0.01	C49,C50,C51—0.1
C10—0.001	C20,C21—0.001	C31—50	C40,C41—4	C52—0.01
C11—4	C22—4	C32—4	C42—0.02	C53—0.05
R1—1M	R17—1.2K	R34—6.8K, 2w	R52—15K, 2w	R69—150
R2—270K	R18—1.5K	R35,R36—270K	R53—270K	R70,R71—15K, 1w
R3—150	R19—100, 1w	R37—470	R54—150	R72—68K
R4—1.5K	R20—250K (Pot.)	R38,R39—27K, 1w	R55—1.5K	R73—270K
R5—3.9K, 1w	R21,R22—15K, 1w	R40—470	R56,R57—15K, 1w	R74—470
R6—100, 1w	R23—68K	R41—12K, 2w	R58—68K	R75,R76—10K, 1w
R7,R8—15K, 1w	R24—270K	R42—500K (Rheo.), 1w	R59—270K	R77—100K
R9—68K	R25—68, 1w, ww	R43—1M	R60—47, 1w, ww	R78—50K (Pot.), 4w, ww
R10—270K	R26—4.8K, 2w	R44—1K	R61—56, 1w, ww	R79—15K
R11—68K, 1w, ww	R27—5K, 10w, ww	R45—22K	R62—75, 1w, ww	R80—10K, 10w, ww
R12—4.8K, 2w	R28—39K	R46—10K	R63—114, 1w, ww	R81—500K
R13—5K, 10w, ww	R29—27K, 2w	R47—270K	R64—238, 1w, ww	R82,R83—100K
R14—39K	R30—270K	R48—560	R65,R66—15K, 1w	R84—270K
R15—27K, 2w	R31—150	R49,R50—22K	R67—68K, 1w	R85—500K
R16—150	R32,R33—4.7K, 1w	R51—4.7K	R68—270K	R86,R87—270K
V1—6SH7	V4—6AB7	V7—6SL7	V10,V11,	V14—6H6
V2—6AB7	V5—6J5	V8,V9—5881	V12—6SH7	V15—0C3
V3—6SH7	V6—6SN7		V13—6J5	

M1—0-50 microamperes.
T1—Custom-built ultrasonic output transformer (1-60 Kc.) to load: 50, 125, 200, 250, 333, and 500 ohms input impedances.

through a decoupling network, R52, C2, to the B+ supply. The input signal from the capacitative pickup appears across resistor R1 which is RC coupled to the input tubes V1 and V10, of the preamplifier and auxiliary amplifier, respectively, both with very flat gain curves from 2 to more than 50 kc./sec.

The preamplifier consists of two 2-pentode feedback loops, V1-V2, and V3-V4, each consisting of a 6SH7 sharp cut-off pentode RC coupled to a 6AB7 remote cut-off pentode, the grid of which is connected to the DAVC bias. The feedback path is from the plate of the 6AB7 to the cathode of the 6SH7. Two 3-position switches, SW1, SW2, in the cathode circuits, allow a choice of nine gain settings, while potentiometer R20 permits continuous intermediate variation. Later study showed that the elimination of the negative feedback used to stabilize the preamplifier would have increased greatly the sensitivity of the DAVC circuit.

The input stage of the auxiliary amplifier employs pentode V10 with large cathode degeneration to minimize the effect of tube characteristics upon the gain. It is RC coupled to a

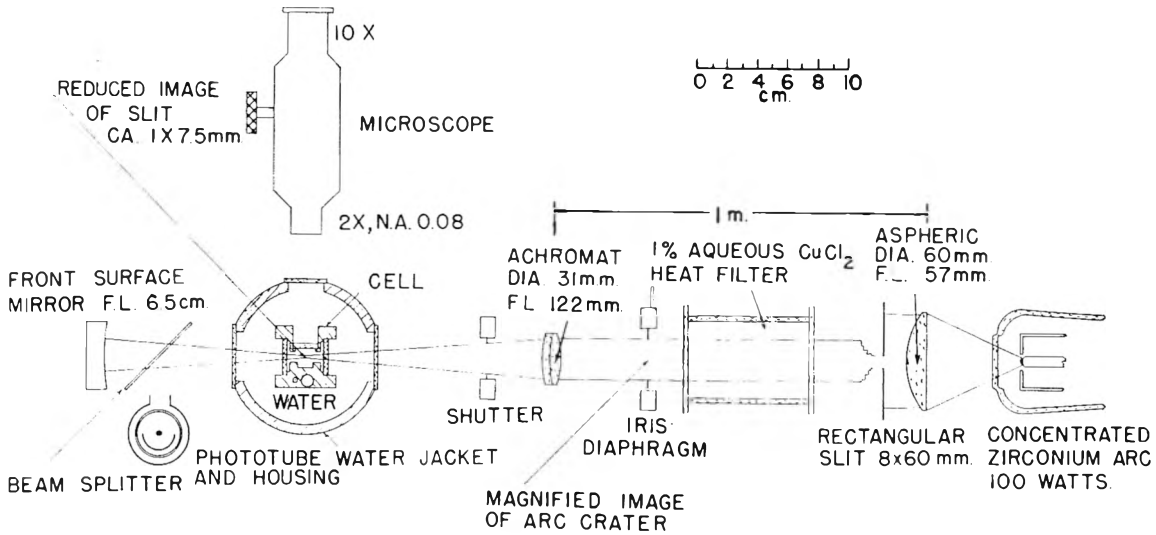

Fig. 6.—Schematic diagram of optical system of rate-of-fall apparatus.

3-tube loop V11–V12–V13, with feedback from the cathode of the final cathode-follower V13 to that of the V11, and various feedback ratios provided by switch SW5 with resistors R60 to R64. This particular loop was designed to provide the very low impedances necessary to drive the nonlinear load of the biased rectifier.

The biased rectifier is one half of the double diode V14. An adjustable positive bias is applied to its cathode through the voltage divider R78–R79 connected to the VR tube, V15. The difference between this bias and the negative peak output voltage of the auxiliary amplifier appears by rectification $^1/_6$ across R77 and $^5/_6$ across R81, this fraction passing through the RC filters, R81-C49, R82-C50, R83-C51 to appear as negative grid bias on the remote cut-off stages of the preamplifier. Theoretically a 10% change in the air load of the bar would cause less than 1% change in the amplitude of its vibration under all experimental conditions.

The peak-reading voltmeter utilizes the second half of the tube V14. A d.c. voltage equal to the peak positive output of the auxiliary amplifier appears across R84-M1-R85. The deflection of meter M1 therefore serves to monitor the generator.

The phasing circuit consists of a phase-inverting tube V5, driving a double cathode follower V6, the low output impedances of which act as two arms of the phasing bridge, of which R42 and C23 or C24 are the others. The switch SW3 provides an additional 180° phase shift.

The two-stage driving amplifier utilizes the double triode V7. The first is a cathode follower with a high input impedance which produces minimum interference on the phasing circuit which feeds it, and the second a standard phase-inverter connected to the push-pull power amplifier, utilizing two 6L6 or 5881 tubes, V8 and V9, in class AB_1 operation. This combination, with a suitable output transformer, can furnish up to 20 w. of electrical energy to the bar.

Rate-of-fall Apparatus.—In order to study many particles, we took photomicrographs of a relatively large field under dark-field illumination for a known time and calculated the velocity from the track lengths. The apparatus is shown in Fig. 6. Using Kohler illumination, a 1 × 8 mm. image of the rectangular slit is formed in the center of the observation cell, to match the field of view of the microscope objective. The concave mirror beyond the cell refocuses the light upon the slit image to increase its illumination.

The observation cell, 6 × 19 mm. in cross section and 19 cm. long, is water-jacketed like the differential settler of LaMer and Sinclair.[39] Three circular ports 51 mm. from the bottom are closed with $^1/_{16}$ in. (1.6 mm.) glass windows. The two illumination ports are 22 mm. in diameter and the viewing port, 16 mm. in diameter, is perpendicular to the others and faces a cylindrical light trap, 3 mm. deep. A brass inlet tube entering the top and an outlet tube extending to the bottom of the cell are closed at the lower ends by spring-loaded needle valves operated by wires passing through small tubes. The inlet tube supports the cell inside a covered water jacket 83 mm. in diameter, with matching windows. A glass propeller drives water down toward the bottom of the jacket and circulates it vigorously enough to ensure temperature equilibrium and reduce convection currents to less than 10 μ/sec. The cell is mounted on a plywood heat insulator backed by a brass plate with three leveling screws carried on the optical bench supporting the microscope. To minimize stray light the cell and the interior of the jacket are painted with optical black lacquer, protected from the water with a coat of clear Tygon plastic varnish which does not reflect light since its index of refraction is very near that of water. The photomicrographic system has a total magnification of 6.7 ×.

Originally, a manually-actuated electric timer with a ten-second sweep dial was used to measure the time the camera shutter was open, hence the time of fall. Later, a more accurate photoelectrically-actuated counting chronograph was used to measure the time the shutter in the illuminating light beam was open. Light from the beam splitter falls onto a phototube which controls a Model 1000 Berkeley scaler. The exposure time in milliseconds is obtained by counting the cycles from a Hewlett-Packard Model 200C audio oscillator set at 1.000 kc./sec., by comparison with the 600 c.p.s. modulation of station WWV's carrier wave. Stokes's law with Cunningham's correction is used to determine the radius of the aerosol droplets from the velocity v and other quantities previously defined, by the equation

$$r = r_S[\sqrt{1 + x^2} - x] \qquad (2)$$

where the Stokes radius $r_S = 9\eta v/2g(d - d_a)$, and $x = AL/2r_S$. Actually

$$r \doteq r_S\,[1 - (AL/2r_S)] = r_S - AL/2 = r_S - 0.038\,\mu \qquad (3)$$

The chief sources of error in the measurement of particle size are: (1) convection currents in the observation cell, which are minimized by its design, and (2) evaporation of the droplets when the aerosol is diluted about 40-fold before being injected into the cell, which depends upon the vapor pressure of the aerosol material and the dilution ratio. Assuming that the vapor behaves ideally and equilibrium conditions are maintained

$$\frac{r}{r_0} = \left[1 - \left(\frac{1}{n} - \frac{1}{n_0}\right)\frac{3MP}{4\pi r_0^3 dRT}\right]^{1/3} \qquad (4)$$

where r_0, r, n_0, n are, respectively, the radii and number of particles per cc. before and after dilution, M is the molecular weight of the vapor, d the density of the particle, p its vapor pressure at absolute temperature T, and R the gas constant.

We used two aerosol materials: bis-2-ethylhexyl phthalate (Union Carbide and Carbon Corporation "Flexol" plas-

(39) D. Sinclair, Chapter 8 in "Handbook on Aerosols," Publ. U. S. Atomic Energy Commission, Washington, D. C., 1950, pp. 102–6.

ticizer DOP), and di-2-ethyl butyrate triethylene glycol ("Flexol" plasticizer 3GH). Application of the Clausius–Clapeyron equation to vapor pressure data for pure bis-2-ethylhexyl phthalate (Octoil) at low pressures,[40] gives at 25° a vapor pressure of 1.48×10^{-7} mm. (95% confidence limits estimated $1.02–2.14 \times 10^{-7}$), agreeing with extrapolated values found in the literature.[41] For Flexol 3GH, extrapolation from recorded boiling points under reduced pressure gives at 25° a vapor pressure of 2×10^{-5} mm. (95% confidence limits estimated 6×10^{-7} to 5×10^{-4}). Taking the upper limits for the vapor pressures at 25°, initial concentrations of 5×10^6 particles per cc., and a 40-fold dilution, we find that aerosols of DOP must exceed 0.03 μ, and those of Flexol 3GH about 0.4 μ radius to avoid more than 5% decrease in radius on dilution. Evaporation probably caused some erratic results in preliminary experiments with small aerosols of 3 GH. In later work this material was used only for particles of 1.5 μ radius or larger, and DOP was used for all smaller ones.

Aerosol Generator.—To obtain homogeneous aerosols for several hours at a time in the range 0.5 to 5.0 μ, we built a LaMer–Sinclair generator[42,43] of Pyrex glass, modified to minimize heat loss, prevent local overheating, and allow accurate temperature control. Preheated air passes through a sintered glass bubbler near the bottom of a cylindrical saturator tube, the temperature of which is regulated by means of a thermocouple connected to a Brown circular-chart recorder and controller. Eight other iron–constantan thermocouples monitor the temperature at various points. Nuclei are supplied by sintered sodium chloride on a coil of platinum wire, heated by a carefully adjusted current. The concentrated aerosol stream from the generator is diluted with gas in a venturi orifice, beyond which large radii of curvature and moderate flow velocities reduce the loss of particles through impingement. Positive pressure is maintained within the generator, and the outlet streams are connected to a rotary suction pump to maintain a regular flow.

The generator, originally designed to produce 8 l. per min. of sulfur aerosol containing a million particles per cc., each 5 μ in radius, easily handled the more volatile aerosol materials used in this research. Our first attempt to produce concentrated aerosols larger than 1 μ radius showed that materials like DOP and oleic acid decompose extensively in air, hence we substituted filtered nitrogen, except in the aerosol diluting stream. Later we found "Flexol" 3GH available in 98.5 + % purity and satisfactorily stable. From distribution curves given in a progress report by LaMer, *et al.*,[44] we estimated the standard deviation of the output of his improved generator at 16% of the radius for a 0.45μ DOP smoke, which is about that measured during the course of this work for much larger aerosols.

Procedure.—Initially, the image of the slit was centered within the observation cell of the rate-of-fall apparatus, which was leveled to make the focal plane of the microscope vertical and bring the region of sharp focus completely within the illuminated volume. Few readjustments were necessary. The apparatus was brought to a steady state over a period of 1.5 to 2 hr. while the generator was adjusted, by varying the flows and particularly the temperature, to produce particles of the desired radius at a concentration of about 5 million per cc. Approximate radii were determined by timing with the manually-operated clock the fall of several particles across a slit in the focal plane of the ocular in the rate-of-fall microscope. The amplifier gain of the sonic generator was set at about twice that required to maintain oscillation at optimum phasing, and the DAVC potential was adjusted to maintain the output meter at a point where tobacco smoke particles showed a sonic amplitude of 50μ.

During a typical experiment a five-foot strip of film was exposed in the following sequence: two rate-of-fall frames; two of tobacco smoke in the sound field; sequences of four samples of the aerosol and one of tobacco smoke in the sound field; two frames of tobacco smoke in the sound field; and finally two rate-of-fall frames. The film was developed in a standard manner, with EKC D-19, immersed for one minute in EKC stop-bath SB-5 to minimize swelling of the gelatin, and finally rinsed for one minute in EKC Photoflow before drying. The film was placed in a Recordak film reader and the tracks measured with a rule graduated in mm. The scale of amplitudes was arbitrary, since only ratios were needed; but the optics of the rate-of-fall apparatus were calibrated by photographing a slide micrometer scale placed in the object space, and projecting this photograph on the Recordak screen. The data consist of the initial and final samples of the radius distribution, with intermediate samples of the amplitude distribution and spot checks of the sound amplitude from the photographs of tobacco smoke.

Results and Conclusions

Consideration of experimental errors (including track length, film and optical resolution, Brownian movement and measurement of time with the counting chronograph) led us to estimate the standard deviation in the radius as about 1% from 5 to 1 μ, increasing to 2% at 0.5 μ; and that in the amplitude as about 2% near 2 μ, rising steeply to 5% at 1 μ, and more gradually to the same value at 4.6 μ. The sonic amplitude is extremely sensitive to small changes in the acoustic characteristics of the gas if the vibrator is at a displacement node, but a series of alternate photographs of tobacco smoke in air and very fine Flexol 3GH particles in nitrogen showed no appreciable difference in amplitude in these two media. Sonic coagulation should be negligible at a sonic energy so far below that used for coagulation[22]; so also should be any systematic error due to the temperature rise of about 0.5° due to adiabatic compression, since the temperature antinodes are one-quarter wave length from the displacement antinodes, with little time available for heat transfer to the aerosol particles.

We could not study the vibration amplitude and rate of fall of the same aerosol particles or even of samples taken simultaneously from the generator; hence we measured many particles in each case, and correlated their average behavior. We investigated some of the rate-of-fall data, which supplied far larger samples than the amplitude ratios, using the chi-square statistical test[45] to see if the distribution of radii was normal according to r or r^2. The latter might be expected from the prediction of Howard Reiss[46] that the rate of change of r^2 is a function of time alone for the growth of uniform colloids. The chi-square test slightly favored the normal distribution of r^2, but the standard deviation is so small that the distribution is approximately normal according to r. For convenience we assumed this distribution and used appropriate small-sample statistics. We calculated the means and variances of the four rate-of-fall frames and rejected ten of the final twenty-one experiments in which the second and third of these gave values of F and Student's t falling outside the region of 95% probability. For all satisfactory experiments, we determined the means of the two rate-of-fall sam-

(40) P. A. Small, K. W. Small and P. Cowley, *Trans. Faraday Soc.*, **44**, 810 (1948).

(41) S. Dushman, "Scientific Foundations of Vacuum Technique," John Wiley and Sons, Inc., New York, N. Y., 1949, p. 222.

(42) D. Sinclair and V. K. LaMer, *Chem. Revs.*, **44**, 245 (1949).

(43) V. K. LaMer and S. Hochberg, *ibid.*, **44**, 341 (1949).

(44) J. Benedict and G. G. Goyer, "Investigation of Particle Size by Differential Settling," Part B, Progress Report No. 5 by Central Aerosol Laboratories, Columbia University, to Air Force Materiel Command for Contract AF-19(122)-164 (Director: Prof. V. K. LaMer), 1 December 1950–28 February 1951, Curve A, Fig. 4.

(45) M. G. Kendall, "The Advanced Theory of Statistics," 3rd ed., Vol. 1, Charles Griffin, London, 1947, Chapter 12, "Chi-Squared Distribution."

(46) H. Reiss, *J. Chem. Phys.*, **19**, 482 (1951).

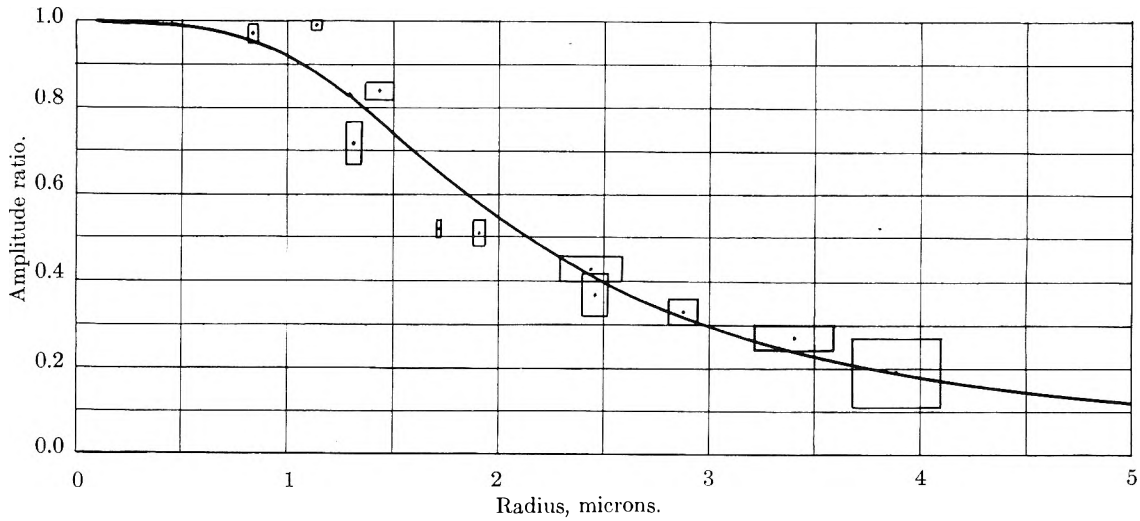

Fig. 7.—Graph showing fit of correlated means to Sewell's theory with Cunningham's correction, the rectangles indicating 95% confidence intervals.

ples and of all the amplitude ratios, and calculated 95% confidence intervals for each variable. Figure 7 is a plot of the correlated means enclosed with rectangles indicating these confidence intervals. The solid curve represents Sewell's expression with Cunningham's correction for the amplitude ratio as a function of radius.

Table I compares the mean observed amplitude ratios with those calculated from the mean rate-of-fall particle radii. A least-squares solution gave as the best linear equation for the experimental ratio as a function of the theoretical

$$\left|\frac{X_p}{X_g}\right|_{\text{expt.}} = -0.01 + 1.00\left|\frac{X_p}{X_g}\right|_{\text{th.}} \qquad (5)$$

A graph of these results is shown in Fig. 8. Since the 95% confidence limits of the intercept and slope are, respectively, ±0.15 and ±0.22, these results fit Sewell's expression within the limit of accuracy of the experiments. The value of 0.074 for the standard deviation of the experimental points from the straight line indicates the operation of random factors not included in the estimate of errors measured by the 95% confidence limits. Although nearly half of the final experiments were discarded because of changes in the generator output, we

TABLE I

CORRELATION OF EXPERIMENTAL AND THEORETICAL AMPLITUDE RATIOS[a]

Experiment no.	Mean radius obsd.	Mean amplitude ratio Obsd.	Calcd.
85	0.84(±0.02)	0.97(±0.02)	0.95
87	1.14(±0.03)	.99(±0.01)	.89
88	1.32(±0.04)	.72(±0.05)	.83
105	1.44(±0.07)	.84(±0.02)	.78
107	1.72(±0.01)	.52(±0.02)	.65
95	1.91(±0.04)	.51(±0.03)	.58
96	2.44(±0.15)	.43(±0.03)	.47
97	2.46(±0.06)	.37(±0.05)	.46
99	2.88(±0.07)	.33(±0.03)	.31
100	3.41(±0.18)	.32(±0.03)	.24
102	3.89(±0.21)	.19(±0.08)	.19

[a] The figures within parentheses define the 95% confidence interval.

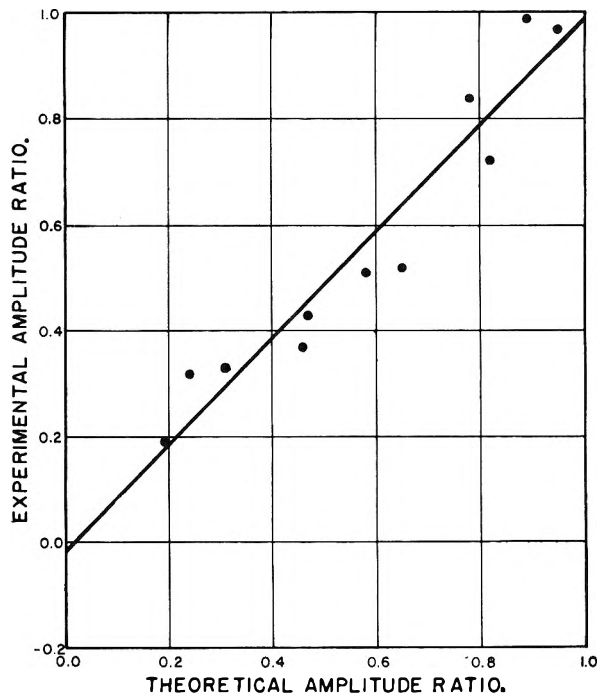

Fig. 8.—Graph showing fit of our data to a least-square linear equation connecting experimental and theoretical amplitude ratios.

suspect that these irregularities are chiefly responsible for the spread of the results. The behavior of the generator might be improved by better temperature control of the bubbler and nucleator, or some method of reducing the thermal decomposition of the bulk aerosol material, by feeding it slowly into the generator.

This work shows that the measurement of sonic amplitude may be applied to the study of aerosol particle size. The severest restriction of the present apparatus is the small number of particles photographed per exposure, due to the extremely small volume, about 10^{-6} cc., under observation in the cell. Also, much time is required to process the film, read and interpret the data. Further experi-

mental development is under consideration in our laboratory. Measurements might be made more rapidly in an aerosol stream which flowed through the cell without disturbing the sound field; *e.g.*, through quarter-wave stubs terminating in low acoustic impedances in the inlet and outlet stream. By putting in the optical path a neutral light filter of linear gradient to vary the illumination along the direction of sonic motion, a phototube which viewed a particle moving rapidly across the cell would deliver an output signal of sonic frequency, with an amplitude proportional to that of the particle. A narrow band-pass amplifier to enhance the signal-to-noise ratio could be used in conjunction with a rapid electronic circuit to obtain combined particle count and size distribution, while the phase lag of the particle also could be studied with a rapid electronic phase meter, and correlated with the amplitude ratio as a further test of Sewell's theory and another method for determining particle size.

Acknowledgments.—It is a pleasure to acknowledge our indebtedness to the Research Committee of the Indiana University Foundation for a grant-in-aid of this work; to E. Eugenia Schmidt for making the numerical calculations of the theoretical amplitude ratios and phase angles given in Figs. 1 and 2; and to Jack Baird and Maurice Williams for the construction of the apparatus in the machine shop.

THE REACTIONS OF FERROUS VERSENATE AND FERROUS PYROPHOSPHATE WITH CUMENE HYDROPEROXIDE[1]

BY W. L. REYNOLDS[2] AND I. M. KOLTHOFF

School of Chemistry, University of Minnesota, Minneapolis, Minnesota

Received March 5, 1956

The rate constants of the reactions between cumene hydroperoxide and ferrous Versenate and ferrous pyrophosphate have been determined under various experimental conditions. The rate constant of the former reaction was $5.0 \times 10^{10} \exp(-10{,}400/RT)$ liter mole^{-1} sec.$^{-1}$ and was independent of *p*H over the range 3.7 to 10.3. The rate constant of the latter reaction was $2.0 \times 10^{8} \exp(-8200/RT)$, $2.7 \times 10^{9} \exp(-8900/RT)$, and $1.6 \times 10^{9} \exp(-8400/RT)$ liter mole^{-1} sec.$^{-1}$ at *p*H 4.8, 6.8 and 8.8, respectively. The stoichiometry observed in the presence and absence of acrylonitrile suggests that a termination reaction between polymer free radicals and the ferrous complex can occur at low concentrations of reactants. In the presence of monomer the main products of reaction at low reactant concentrations are the ferric complex, acetophenone and polymer.

Although the reactions between aquo ferrous iron and various organic hydroperoxides have received some attention very few investigations have been made of the reactions between complexed ferrous iron and organic hydroperoxides. Orr and Williams[3] have studied the reactions between polyethylenepolyamine complexes of ferrous iron and cumene and *p*-butylcumene hydroperoxides. Boardman[4] has reported on the reaction between potassium ferrocyanide and cumene hydroperoxide. From a polymerization viewpoint a knowledge of the kinetics and mechanisms of the reactions of ferrous Versenate and ferrous pyrophosphate with organic hydroperoxides is important since these reactions are frequently employed to supply free radicals for the initiation of polymerization in emulsion polymerization systems.

Experimental

Determination of Rate Constants.—The rate of disappearance of the ferrous complex was determined by measuring its diffusion current at a rotated platinum wire electrode during the course of the reaction. This diffusion current was found proportional to the concentration of the ferrous complex. The diffusion current of the complex iron(II) was measured at a potential where a film of oxide is formed on the electrode.[5] When the current voltage curve is measured with a self registering apparatus the film formation is characterized by a wave with an apparent limiting current (see curve 1 of Fig. 1). Film formation is also responsible for the distorted shape of the current–voltage curve of the complexed ferrous iron (curve 2, Fig. 1) when measured with a polarograph. Upon subtraction of the residual current a diffusion current plateau was observed as is evident from curve 3 in Fig. 1. Film formation did not interfere with the kinetic measurements when a potential was applied at which the film was formed and the limiting current of iron(II) was measured. The current caused by film formation rapidly decays with time.[5] Thus upon measuring a current–time curve the current is found to decrease rapidly to the value of the diffusion current of iron(II).

The apparatus employed has been described elsewhere.[6] Complexing agent was added to the buffer solution in the electrolysis cell, the solution deaerated, a known quantity of ferrous iron added and a potential of +0.7 v. *vs.* the saturated calomel electrode (S.C.E.) applied to the electrode. After the limiting current had decreased to a constant value (the diffusion current of the iron(II)) a known quantity of air-free standard cumene hydroperoxide(CHP) solution was injected into the electrolysis cell. A typical current–time curve obtained after addition of CHP is shown in Fig. 2.

From the value of the Fe(II) diffusion current before CHP addition and the known concentration of the ferrous complex the value of i_d/c for the electrode could be calculated. An excess of ferrous iron was always used and from the value of the Fe(II) diffusion current at the end of the reaction the final Fe(II) was calculated. Hence the stoichiometry of the reaction was readily determined.

The rate equation

$$\frac{dx}{dt} = k_0((\mathrm{Fe})_0 - n.x)(R_0 - x) \qquad (1)$$

(1) This work was carried out under the sponsorship of the Federal Facilities Corporation, Office of Synthetic Rubber, in connection with the Synthetic Rubber Program of the United States Government.

(2) From a thesis submitted by W. Reynolds to the University of Minnesota in partial fulfillment of the requirements for the degree of Doctor of Philosophy, June, 1955.

(3) (a) R. J. Orr and H. L. Williams, *Disc. Faraday Soc.*, No. 14, 170 (1953); (b) *J. Am. Chem. Soc.*, **76**, 3321 (1954).

(4) H. Boardman, *ibid.*, **75**, 4268 (1953).

(5) I. M. Kolthoff and N. Tanaka, *Anal. Chem.*, **26**, 632 (1954).

(6) I. M. Kolthoff and W. L. Reynolds, *Disc. Faraday Soc.*, No. 17, 167 (1954).

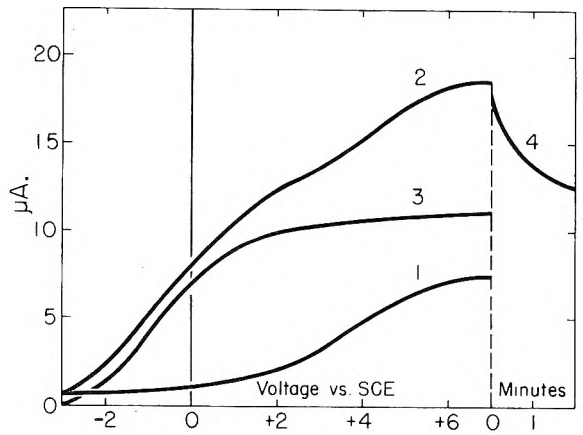

Fig. 1.—1, residual current of reaction medium; *p*H 9.2; 2, limiting current of 1.00×10^{-4} *M* ferrous Versenate; 3, diffusion current of ferrous Versenate; 4, limiting current at constant potential.

was tentatively adopted. In equation 1 $(Fe)_0$ is the initial total concentration of Fe(II), R_0 is the initial concentration of CHP, x is the decrease in CHP concentration at time t, k_0 is the observed rate constant, and n is the stoichiometric factor and was found equal to unity or two depending upon the experimental conditions. At the concentration levels employed for the measurement of k_0, n was equal to two in the ferrous Versenate–CHP and ferrous pyrophosphate–CHP reactions when acrylonitrile (AcN) was present and in the ferrous pyrophosphate–CHP reaction when monomer was absent. Rate measurements were not made for the ferrous Versenate–CHP reaction in the absence of monomer. In the ferrous pyrophosphate–CHP reaction n was approximately unity when methyl methacrylate (MMAc) was present. Integration of equation 1 and substitution of

$$((Fe)_0 - nx) = (Fe(II)) = Ki_d \text{ where } K = (Fe)_0/(i_d)_0,$$
$$x = ((Fe)_0 - Ki_d)/n$$

and

$$((Fe)_0 - nR_0) = K(i_d)_\infty$$

gives equation 2

$$k_0 t = \frac{2.30}{K(i_d)_\infty}\left\{\log \frac{i_d}{i_d - (i_d)_\infty} + \log \frac{nR_0}{(Fe)_0}\right\} \quad (2)$$

where i_d designates a diffusion current. A plot of log $[i_d/i_d - (i_d)_\infty]$ *vs.* t as in Fig. 3 gave a straight line in all cases, the slope, s, of the line being $k_0K(i_d)_\infty/2.30$. The observed intercept in all cases was in good agreement with the calculated value of log $((Fe)_0/nR_0)$. Therefore equation 2 was found to be valid and the rate constant, k_0, was calculated from $k_0 = 2.30s/K(i_d)_\infty$.

Determination of Stoichiometry.—Since the final concentration of iron was determined as described and the initial CHP concentration was known the stoichiometry was readily determined.

Determination of Acetophenone.—Acetophenone is one of the reaction products formed. When the concentrations of the reactants were sufficiently high (*ca.* 10^{-3} *M*) the acetophenone formed from the CHP was determined polarographically with a dropping mercury electrode in alkaline medium. The total current measured at -1.7 v. *vs.* S.C.E. was corrected for residual current and the diffusion current of the ferric complex to yield the diffusion current of acetophenone. By adding known quantities of acetophenone to the electrolysis cell and measuring the increase of diffusion current the concentration of acetophenone in the reaction mixture could be calculated.

When the initial concentration of CHP was too low (*ca.* 3×10^{-5}*M*) to permit direct determination of the acetophenone concentration in the reaction mixture with a dropping mercury electrode two other methods of analysis were employed. One method, applicable when monomer was absent, consisted of the extraction of acetophenone with spectrophotometric grade isoöctane followed by spectrophotometric determination of the extracted acetophenone. One hundred ml. of reaction mixture was taken; the initial Fe(II) and CHP concentrations were 10 and 2.5×10^{-5} *M*, respectively. This solution was divided into four equal parts and acetophenone was added to increase its concentration by 0, 2.5, 5.0 and 7.5×10^{-6} *M*, respectively. Each part was extracted thrice with 12.5-ml. portions of isoöctane and the three portions combined. The absorbances of the resulting four isoöctane solutions were measured with respect to the pure solvent at 238 mμ in quartz cells with a Beckman DU spectrophotometer. These absorbances were corrected for the absorbance of a blank obtained by extracting a reaction mixture containing no acetophenone. The absorbance–acetophenone concentration plot gave a straight line. Hence the acetophenone concentration in the reaction mixture could be calculated. Appropriate blank experiments showed that acetophenone was completely extracted from simulated mixtures by the above procedure. The other method, applicable when acrylonitrile was present, consisted of the extraction of acetophenone with benzene so as to concentrate the acetophenone followed by the polarographic determination of the acetophenone in a non-aqueous solution. Three hundred ml. of reaction mixture was prepared. The initial concentrations of Fe(II), CHP and AcN were 1.17×10^{-4}, 4.90×10^{-5} and 0.01 *M*, respectively. This solution was extracted twice with 15-ml. portions of benzene

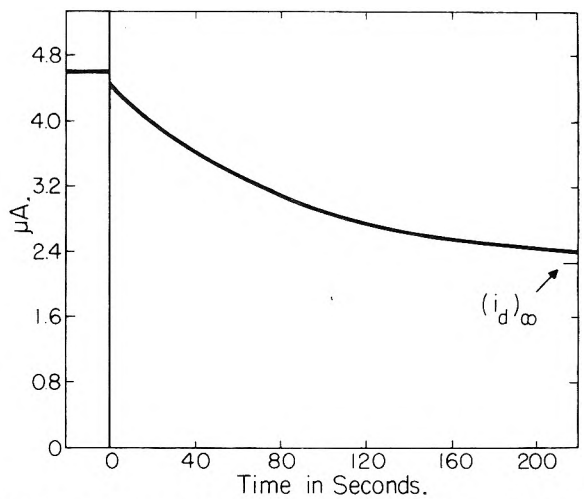

Fig. 2.—$(Fe)_0 = 9.9 \times 10^{-5}$ *M*; $R_0 = 2.47 \times 10^{-5}$ *M*; AcN = 0.15 *M*; *p*H 10.0, 0.0°.

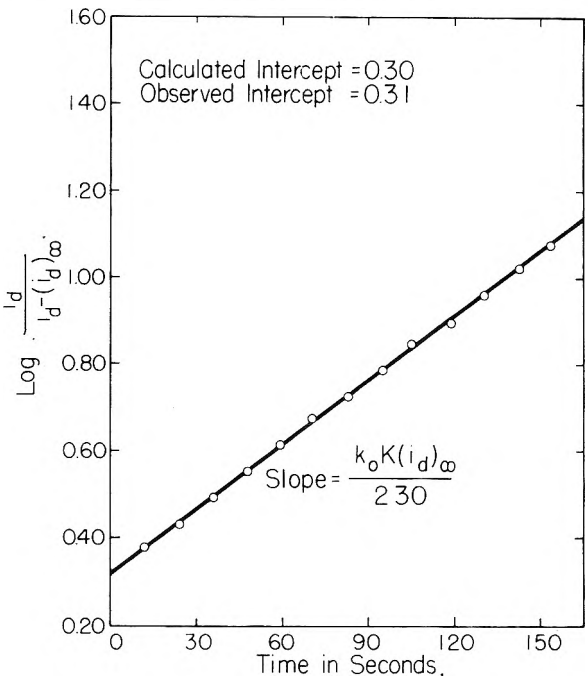

Fig. 3.—$(Fe)_0 = 9.90 \times 10^{-5}$ *M*; $R_0 = 2.47 \times 10^{-5}$ *M*; AcN = 0.15 *M*; *p*H 10.0; 0.0°.

by vigorous shaking for 15 minutes, separation of phases with a centrifuge and collection of the organic layer in a small separatory funnel. The two benzene portions were combined, 15 ml. added to 15 ml. of absolute ethanol containing 0.2 *M* tetraethylammonium chloride and 0.005% gelatin in an electrolysis cell and the current–voltage curve determined. In this medium the diffusion current region of acetophenone began at about −1.84 v. *vs.* SCE. The diffusion current was determined at −1.9 v. *vs.* S.C.E. The error in the analysis was at least ±10% since, in the presence of AcN, a large reduction current began at about −1.9 v. *vs.* S.C.E. and interfered with the determination. The residual current at −1.9 v. *vs.* S.C.E. was determined by extracting a simulated reaction mixture without acetophenone present and determining the current–voltage curve after addition of organic phase to ethanol as described above. Appropriate blank experiments in the absence of AcN showed that the acetophenone in simulated reaction mixtures was about 100 ± 10% recovered by this method.

Determination of Methanol.—One hundred ml. of reaction mixture containing 0.070 *M* Fe(II) and 0.018 *M* CHP initially was extracted with three 25-ml. portions of benzene to eliminate acetophenone. Sufficient sodium hydroxide was added to give an alkali concentration of approximately 0.1 *M*. This solution was divided into four equal parts and methanol was added to give a concentration of 0, 0.5, 1.0, and 1.5 m*M*, respectively. Each part was separately distilled to dryness under reduced pressure, the distillate diluted to volume in a 25-ml. volumetric flask, and tested for methanol by a procedure which already has been described.[7] The absorbance, measured at 570 mμ against a reagent blank, was plotted *vs.* added methanol concentration. The result was a straight line which passed through the origin showing no measurable quantity of methanol present in the reaction mixture. Thus, methanol was not a reaction product in the above experiment. Appropriate blank experiments showed that methanol was not measurably extracted from simulated reaction mixtures by the benzene extraction.

Determination of Gas Evolution.—High concentrations (*ca.* 0.05 *M*) of reactants were used to secure gas evolution. Helium was used for deaeration purposes since nitrogen interfered in the mass spectrometric analysis for ethane in the gas evolved. The gas was collected over the reaction mixture and its volume determined. Since the main gaseous component was ethane the small amount of water vapor present did not interfere with the analysis.

Results

Stoichiometry.—The results of determinations of stoichiometry of the ferrous Versenate–CHP reaction at different *p*H and temperature values in the presence of AcN are given in Table I. It is seen that the reaction ratio, *R*, defined as the number of moles of ferrous Versenate oxidized per mole of CHP reduced, is approximately equal to two in all cases. In Table II the effect of varying the type and concentration of monomer and the effect of high concentrations of reactants is shown.

Table I

The Reaction Ratio of the Ferrous Versenate–CHP Reaction as a Function of *p*H and Temperature

0.1 *M* AcN present in all cases; $\mu = 0.1$.

*p*H	*t*°,C.	$(CHP)_0 \times 10^5$, *M*	$(FeY^-)_0 \times 10^5$, *M*	$R = \Delta(FeY^-)/\Delta(CHP)$	*n*[a]
3.72	25.0	1.3–2.5	2.5–10	2.00 ± 0.13	8
5.36	25.0	1.3–5.0	2.3–10	1.98 ± 0.15	11
5.36	0.0	2.4	4.5–10	1.92 ± 0.12	6
8.40	25.0	2.4	4.5–10	1.87 ± 0.09	10
8.80	25.0	2.4	4.5–10	1.98	2
9.18	25.0	2.4	4.5–10	1.95 ± 0.07	6
10.0	25.0	2.4	4.5–10	1.86	4
10.0	0.0	2.4	4.5–10	1.90 ± 0.05	6
10.3	25.0	2.4	4.5–10	1.85	2

[a] *n* is the number of measurements.

Table II

*p*H 5.4; $\mu = 0.1$; 25°

Monomer	(Monomer), *M*	$(CHP)_0 \times 10^5$, *M*	$(FeY^-)_0 \times 10^5$, *M*	*R*
...	...	3060	5820	1.2
...	...	40	100	1.0
...	...	2.5	10	0.84
AcN[a]	1.0	2170	4800	1.2
	1.0	40	100	1.7
	0.1	25	100	1.5
	0.1	3.5	10	1.9
	0.01	2.5	10	1.6
	6×10^{-4}	2.5	10	1.4
AcA[b]	0.1	2.5	10	1.9
	0.01	2.5	10	1.8
	0.001	2.5	10	1.2
AA[c]	0.17	2.5	10	1.6
	0.10	2.4	10	1.1
	0.01	2.4	10	0.8

[a] Acrylonitrile. [b] Acrylic acid. [c] Allyl acetate.

In the absence of monomer the reaction ratio increased somewhat as the concentrations of reactants were increased. With a fixed concentration of a given monomer the reaction ratio increased as the concentrations of reactants were decreased. With fixed concentrations of reactants and with a given monomer the reaction ratio approached the value of two as the monomer concentration was increased. Allyl acetate was less efficient in increasing the reaction ratio than either acrylonitrile or acrylic acid; the latter two are quite similar in behavior in this respect.

In Table III are some results obtained by varying *p*H, temperature, the type of monomer, and the initial concentrations of reactants in the ferrous pyrophosphate–CHP reaction. At *p*H 8.8 in the absence of monomer and in the presence of AcN the reaction ratio, *R*, was about 2 in the lowest concentration range of reactants and decreased to about 1.6 in the presence of AcN and to about unity in the absence of monomer as the concentrations of the reactants were increased. At *p*H 6.6 the reaction ratio was also equal to 2 in the absence of monomer and in the presence of AcN at the lowest concentration level of reactants and decreased as the concentrations of reactants were increased above this level. At *p*H 4.8 the reaction ratio was somewhat less in the absence of monomer than in the presence of AcN but the difference is not significant. At all three *p*H values methacrylate (MMAc) as monomer gave a reaction ratio only slightly greater than unity. An important difference between the ferrous Versenate and ferrous pyrophosphate reactions with CHP is that, at the low concentrations of reactants where the rate constants were determined, the reaction ratio of the former reaction is less than unity whereas the reaction ratio of the latter reaction is equal to two in the absence of monomer.

It is seen from Table III that the change of temperature does not affect the reaction ratio.

Formation of Acetophenone.—The results of analyses for acetophenone are presented in Table

(7) W. L. Reynolds and I. M. Kolthoff, This Journal, **60**, 969 (1956).

TABLE III

THE REACTION RATIO, R, OF THE FERROUS PYROPHOSPHATE–CHP REACTION AS A FUNCTION OF pH, TEMPERATURE, TYPE OF MONOMER AND INITIAL CONCENTRATION OF REACTANTS; $\mu = 0.1$

pH	t, °C.	(Monomer), M[b]	$(CHP)_0$ × 10^5, M	$(Fe(II))_0$ × 10^5, M	R	n[a]
8.8	0	0.5 AcN	1.3–2.6	4.4–20	2.08 ± 0.15	9
	25	0.5 AcN	1.2–2.6	2.5–20	2.08 ± 0.15	13
		1.0 AcN	40	100	1.65	1
		1.0 AcN	1750	7000	1.56	1
		1.0 MMAc	40	100	1.00	1
			2.5	10	2.2	1
			40	100	1.2	1
			2910	7000	1.1	1
6.8	0		2.5–5.0	7.0–10	1.97	4
	25		0.6–4.0	2.2–20	1.98 ± 0.09	6
			10	20–40	1.76 ± .09	6
		0.2 AcN	0.6–4.0	2.2–20	2.02 ± .14	10
		0.2 AcN	10	20–40	1.79	2
		0.4 MMAc	1.2–3.4	4.0–15	1.22	3
		0.2 MMAc	10	20–40	1.17	2
4.8	0	0.5 AcN	24	50–75	1.93	2
			24	50–75	1.82	2
		0.2 MMAc	24	40	1.15	1
4.8	25	0.5 AcN	4.0–7.0	13–18	1.97	3
			6.0	14–17	1.75	2
		0.2 MMAc	4.0–11.0	9–16	1.18	3

[a] n is the number of measurements. [b] AcN and MMAc designate acrylonitrile and methyl methacrylate, respectively.

IV. In the presence of 1 M AcN or MMAc a large reduction current began at such potentials as to seriously interfere with the acetophenone determination and hence the corresponding analyses for acetophenone were rather inaccurate. In the ferrous pyrophosphate–CHP reaction, CHP was quantitatively converted to acetophenone within the accuracy of the measurements at all concentration levels. In the ferrous Versenate–CHP reaction CHP was 80–100% converted to acetophenone at the lowest concentration level and less than 50% at the high concentration levels.

TABLE IV

Reaction	(AcN), M	$(Fe(II))_0$ × 10^4, M	$(CHP)_0$ × 10^4, M	% AP[a]	R
Ferrous Versenate–CHP		10	4.0	80	1.0
		582	306	45	1.2
	0.1	10	4.0	108	1.1
Ferrous Pyrophosphate–CHP		1.0	0.25	108	2.2
		10	4.0	98	1.2
		700	291	96	1.1
	0.01	1.2	0.49	100	2.0
	1.0	10	4.0	120[b]	1.7
	1.0	700	175	101[b]	1.6
	1.0[c]	10	4.0	High	1.0

[a] AP designates acetophenone. [b] AcN interfered seriously in the acetophenone determination. [c] MMAc. Presence of monomer interfered so that an approximate determination of acetophenone could not be made. However, the acetophenone wave was evident on the polarogram.

Formation of Gas.—In the ferrous Versenate–CHP reaction when the initial concentrations of ferrous Versenate, CHP and AcN were 0.0480, 0.0217 and 1 M, respectively, insufficient gas was evolved to saturate the solution and form a gas phase. With initial concentrations of ferrous Versenate and CHP of 0.0582 and 0.0306 M, respectively, in 103 ml. of solution in the absence of monomer 0.70 millimole of gas, consisting of 10 ± 5% methane and 90 ± 5% ethane, was formed. Thus the gas phase accounted for 1.33 ± 0.04 millimole of methyl free radical. The amount of CHP consumed was 3.15 millimoles and the amount of acetophenone formed was 1.41 millimoles (45% conversion of CHP to acetophenone). Methanol was not found. Thus the amount of methyl free radical produced, within the experimental error, is equal to the amount of acetophenone formed.

In the ferrous pyrophosphate–CHP reaction when the initial concentrations of ferrous pyrophosphate and CHP were 0.0700 and 0.0291 M, respectively, in the absence of monomer 1.23 millimoles of gas, consisting of 10 ± 5% methane and 90 ± 5% ethane, was formed. Thus the gas phase accounted for 2.34 millimoles of methyl free radical. The amount of CHP used was 3.31 millimoles. CHP was 96% converted to acetophenone, so that 3.18 millimoles of acetophenone was formed. Methanol was not found in the reaction mixture. If the amount of CH_3 radical again were equal to the amount of acetophenone the difference between the observed and calculated quantities of methyl free radical was 26%. This difference may be due to both experimental error and the occurrence of side reactions. With the initial concentrations of ferrous pyrophosphate, CHP and AcN of 0.0700, 0.0175 and 1 M, respectively, a small amount of gas (0.33 millimole) was formed. Thus the amount of gas evolved was considerably decreased by the presence of AcN in both reactions.

Rate Constants.—The results of determinations of the second-order rate constant of the ferrous Versenate–CHP reaction are given in Table V for 0 and 25° and for various pH values. The standard deviation of a single measurement was approximately 13%. The observed second-order rate constant did not change significantly over the pH range investigated. Substitution of acrylic acid for acrylonitrile did not affect the observed rate constant. Changing the buffer constituents at constant pH and ionic strength did not affect the observed rate constant either. As a function of temperature the rate constant of this reaction may be written $k_0 = 5.0 \times 10^{10} \exp(-10{,}400/RT)$ liter mole^{-1} sec.$^{-1}$.

TABLE V

SUMMARY OF FERROUS VERSENATE–CHP RATE MEASUREMENTS

$\mu = 0.1$; $\Delta(Fe(II))/\Delta(CHP) = 2$; (AcN) = 0.1 M

t, °C.	pH	$(CHP)_0$ × 10^5, M	$(Fe(II))_0$ × 10^5, M	k_0, l. mole^{-1} sec.$^{-1}$	n
25.0 ± 0.1	3.72	1.30–2.53	2.30–10.1	1370 ± 216	6
	5.36	1.25–2.47	2.30–10.0	1200 ± 157	10
		2.44	4.98–9.95	1270	2[a]
	8.40	2.44	4.95–9.90	1140 ± 157	9
	8.80	2.44	4.86–9.90	1000	2
	9.18	2.44	4.95–9.90	1050 ± 146	6
	10.0	2.44	4.95–9.90	1100 ± 182	4
	10.3	2.25	4.95–9.90	1170	2
0.0 ± 0.2	5.36	2.45	4.95–9.90	240 ± 33	6
	10.0	2.45	4.95–9.90	240 ± 38	6

[a] 0.1 M acrylic acid was employed instead of acrylonitrile.

Values of the second-order rate constant of the ferrous pyrophosphate–CHP reaction are given in Table VI for three pH values at 0 and 25°. The rate constants were determined at the low concentration levels where the reaction ratio was equal to two in the absence of monomer and in the

TABLE VI

SUMMARY OF FERROUS PYROPHOSPHATE–CHP RATE MEASUREMENTS

t, °C.	pH	$(CHP)_0 \times 10^5$, M	$(Fe(II))_0 \times 10^5$, M	(Monomer), M	k_0	n
25 ± 0.1	4.82	3.89–11.1	9.15–17.7		227	2
				0.5 AcN	211	3
				0.2 MMAc	197	3
		Av. k_0 = 209 ± 22 l. mole^{-1} sec.$^{-1}$				
	6.78	0.60–1.98	1.45–4.08		837	6
		0.47–1.95	1.45–4.10	0.2 AcN	825	11
		1.20	4.00	0.2 MMAc	780	1
		Av. k_0 = 830 ± 114 l. mole^{-1} sec.$^{-1}$				
	8.80	1.21–2.45	2.46–14.1	0.5 AcN	1200 ± 200	8
0.0 ± 0.2	4.82	24.4	54.9–69.6		55.2	2
		24.0	57.9	0.5 AcN	60.0	2
		44.4	77.0	0.2 MMAc	66.3	1
		Av. k_0 = 59 ± 7 l. mole^{-1} sec.$^{-1}$				
	6.78	2.66–5.16	7.35–10.9	0.2 AcN	201	3
		2.66	7.35		240	1
		Av. k_0 = 210 ± 26 l. mole^{-1} sec.$^{-1}$				
	8.80	1.30–2.60	4.06–18.7	0.5 AcN	300 ± 38	10

presence of AcN. In the presence of MMac the reaction ratio had the values indicated in Table III. To obtain good agreement between calculated and observed values of log $((Fe)_0/nR_0)$ (see Experimental section) the observed value (not the value of unity) of n had to be used in calculating the log term. However, the value of the rate constant does not depend upon the value of n employed so long as n is constant throughout the reaction. It is very important to note that, within the experimental error, the value of the rate constant is independent of the presence or absence of monomer and of whether the monomer yields a reaction ratio of two or unity. At pH 6.78 the rate constant was independent of a variation of ionic strength over the range 0.091 to 1.35 and of pyrophosphate concentration as long as the latter was in considerable excess over the iron. However, the experimental error was sufficiently large to prevent the detection of a small effect. The observed rate constant was dependent on pH and increased with increasing pH. In terms of temperature the rate constants at pH 4.82, 6.78 and 8.80 were $2.0 \times 10^8 \exp(-8200/RT)$, $2.7 \times 10^9 \exp(-8900/RT)$, and $1.6 \times 10^9 \exp(-8400/RT)$ liter mole^{-1}sec.$^{-1}$, respectively.

Discussion

The complex ions FeY^{-2} and FeY^- are stable in the pH range 3.5 to 6.5.[8] At pH values greater than 6.5 the equilibria[9]

$$FeY^{-2} + OH^- \rightleftharpoons Fe(OH)Y^{-3};\ K = 7.4 \times 10^4$$
$$Fe(OH)Y^{-3} + OH^- \rightleftharpoons Fe(OH)_2Y^{-4};\ K = 1.3 \times 10^4$$

have to be considered for the ferrous species. Since the rate of reaction between ferrous Versenate and CHP was found to be independent of pH the rate of reaction was not dependent upon the exact composition of the ferrous Versenate species. The formulas of the ferrous pyrophosphate species at various pH values are not known. The reaction of these species with CHP was found to be dependent on pH. All ferrous Versenate and ferrous pyrophosphate species were electroactive at the electrode used.

In view of the facts that, in the ferrous Versenate–CHP reaction at low concentration levels, the reaction ratio was equal to two in the presence of AcN, unity (or less) in the absence of monomer, and approached the value of two as monomer concentration was increased, that CHP was converted to acetophenone in high yield in the presence and absence of monomer, that all three ferrous Versenate species reacted with CHP at the same rate, and that the rate constant was not affected by a change of monomer the following mechanism is proposed. The reaction $RO\cdot + FeY^{-2} \rightarrow RO^- +$

$$Fe(OH)_mY^{-2-m} + ROOH \xrightarrow{k_1} Fe(OH)_mY^{-1-m} + RO\cdot + OH^-;\ m = 0, 1, 2 \quad (1)$$

$$RO\cdot \xrightarrow{k_2} C_6H_5(CO)CH_3 + CH_3\cdot \quad (2)$$

$$CH_3\cdot + M \xrightarrow{k_i} M_1\cdot \text{ (initiation)} \quad (3)$$

$$M_1\cdot + M \xrightarrow{k_p} M_2\cdot \text{ (propagation)} \quad (4)$$

$$M_{n-1}\cdot + M \xrightarrow{k_p} M_n\cdot$$

$$Fe(OH)_mY^{-2-m} + M_n\cdot \xrightarrow{k_{t,m}} Fe(OH)_mY^{-1-m} + M_n^-,\ m = 0, 1, 2 \quad (5)$$

$$M_n^- + H^+ \longrightarrow M_nH \quad (6)$$

FeY^- was omitted since in the absence of monomer the reaction ratio was less than unity at the low concentrations of interest in measuring the rate constant. This reaction may be important in the absence of monomer at the higher concentration levels of reactants employed since the reaction ratio increased somewhat and the acetophenone concentration decreased with increasing reactant concentrations.

Termination reaction (5) has been written as reduction of the polymer free radical by a ferrous

(8) I. M. Kolthoff and C. Auerbach, *J. Am. Chem. Soc.*, **74**, 1452 (1952).

(9) G. Schwarzenbach, *Helv. Chim. Acta*, **34**, 576 (1951).

Versenate species because of the observations made concerning the reaction ratio in presence and absence of monomer and because the reaction ratio decreased when monomer concentration decreased. Although ethane formation occurred at high reactant concentrations it cannot contribute significantly at low reactant concentrations and high monomer concentration because the termination reaction $2CH_3\cdot \rightarrow C_2H_6$ would lead to a reaction ratio less than two. As monomer concentration is decreased this termination reaction may become important and so result in a reaction ratio of less than two. Termination by combination of two polymer free radicals must also be excluded under the conditions where the reaction ratio was equal to two. Termination by disproportionation results in a double bond in one of the two polymer molecules formed. It is hardly possible that this double bond is reduced by iron(II). Termination by chain transfer can occur since one polymer free radical is replaced by another until one eventually reacts with iron(II). According to the proposed mechanism the methyl free radicals must be 100% efficient in initiating polymerization when the reaction ratio is two. It must be emphasized that the analyses for acetophenone were not sufficiently accurate to determine whether a few per cent. of RO· initiated polymerization also.

The reaction ratio of less than unity in the absence of monomer may be the result of some decomposition of CHP by a free radical formed by H-atom extraction from the Versene molecule by the methyl free radical. The reaction $CH_3\cdot$ + ROOH $\rightarrow$ CH_3OH + RO· cannot be proposed to account for this since methanol was not found and since this reaction was not found to occur in the reaction of aquo ferrous iron with CHP.[7] Considering that ferrous Versenate is such a strong reducing agent it does not seem likely that reduction of ferric Versenate by some intermediate is responsible for this low reaction ratio.

Making the usual assumption about the steady states of free radicals and the assumption that the propagation rate constants are all equal, the rate of decrease of total ferrous iron is found to be

$$-\frac{d(Fe(II))}{dt} = 2k_1(ROOH)(Fe(II))$$

or

$$\frac{dx}{dt} = k_1(ROOH)(Fe(II))$$

since (Fe(II)), the total iron(II) concentration at time t, was equal to $(Fe)_0 - 2x$ (see Experimental). The observed rate constant, k_0, given in Table V, is equal to k_1, the rate constant of the reaction between CHP and ferrous Versenate. In the absence of monomer the CH_3 free radicals formed in reaction (2) combine to form ethane.

For the reaction between ferrous pyrophosphate and CHP in the presence of AcN a mechanism similar to that for the ferrous Versenate–CHP reaction may be postulated. Since the formulas of the ferrous pyrophosphate species present at various pH values are not known a rate equation cannot be derived to give the observed rate constant as a function of hydrogen ion concentration. Although polymer formation was not observed in the ferrous Versenate–CHP reaction considerable polymer formation was observed in the ferrous pyrophosphate–CHP reaction in the presence of both AcN and MMAc. Since, in the latter reaction, the reaction ratio was equal to two in the absence of monomer at the low concentrations where the rate constants were determined the methyl free radical, or a free radical derived from it, must oxidize a second mole of ferrous pyrophosphate by a reaction such as

$$Fe(II) + CH_3\cdot + H^+ \longrightarrow Fe(III) + CH_4\cdot$$

At very high concentrations of reactants ethane is formed but the reaction ratio under these conditions is 1.1 (see Table IV). When the ferrous pyrophosphate–CHP reaction occurred in the presence of MMAc the reactions ratio was about 1.15. In this system polymer formation was observed. Termination must occur mainly by reactions not involving iron(II). Since the observed rate constant was the same when monomer was absent as when either AcN or MMAc was present the rate determining steps must be the reactions of the ferrous pyrophosphate species with CHP.

In conclusion it is interesting to note that the two ferrous species under our experimental conditions can act as polymerization termination agents as well as part of the initiation system.

THE ADSORPTION AND HEAT OF IMMERSION STUDIES OF IRON OXIDE

By F. H. Healey, J. J. Chessick and A. V. Fraioli

Contribution from the Surface Chemistry Department, Lehigh University, Bethlehem, Penna.

Received March 6, 1956

The surface of an iron oxide powder was investigated by water adsorption and calorimetric measurements. Two thirds of the surface was found to physically adsorb water in the region of relative pressure where monolayer coverage is normally encountered. The remainder of the surface chemisorbed water which could be released only by activation at temperatures up to 450°. The average heat of hydration of the chemisorbed water was calculated to be about −24 kcal./mole H_2O. Evidence for the release of internal water and other gases at elevated temperatures was found. In addition, thermodynamic calculations revealed that the water physically adsorbed at 25° on iron oxide had the properties of ice in the first layer.

Introduction

The adsorption of water vapor on porous iron oxide samples was measured previously by Foster[1] and Rao.[2] Here, a systematic study of the surface characteristics of a non-porous iron oxide has been made using adsorption and heat of immer-

(1) A. G. Foster, *J. Chem. Soc.*, 360 (1945).

(2) K. S. Rao, This Journal, **45**, 500 (1941).

sional wetting measurements. A knowledge of the nature of such a surface is vital in the fields of lubrication and corrosion inhibition since even the cleanest structural metals are known to have a surface oxide film.

Experimental

Apparatus.—An all-glass volumetric adsorption apparatus was used in this investigation. Mercury cut-offs were employed to prevent contact with stopcock grease when the adsorbate was an organic vapor. Float valves limited the height of the cut-offs to three inches. A gold wool trap isolated the sample from mercury vapor. Degassing was accomplished by use of a single-stage mercury diffusion pump in conjunction with a Welch Duo-Seal fore-pump. The final pressure produced by this combination was lower than 10^{-6} cm. pressure as read by the McLeod gage.

Dosing and equilibrium pressures were measured with a gage[3] in the pressure range from 0.0001 to 0.75 cm. pressure; higher pressures were read on a simple mercury manometer. The Puddington gage was constructed of precision-bore glass tubing supplied by the Fisher–Porter Co., Hatboro, Pa. A novel feature of the gage was a three-way stopcock below the wide-bore manometer section with a finely drawn-out capillary in one of the arms. This capillary permitted precise setting of the mercury at the reference marks without operator strain. The multiplying factor of the gage was 112.4. The limiting precision of the instrument was about 1 μ. In practice consecutive readings of the same pressure would vary from two to four microns. The system was calibrated for temperature dependence of the zero-reading, and the correction applied to all pressure measurements.

Materials.—The ferric oxide was Baker and Adamson Reagent Grade Ferric Oxide Powder, Lot J 153, with the following maximum impurities: Insoluble in HCl, 0.25%; $SO^{=}_{4}$, 0.25%; Cu, 0.005%; Zn, 0.005%; not precipitated by NH_4OH, 0.20%. The oxide was prepared by controlled oxidation of FeS. This process was followed by a washing and grinding operation to remove soluble impurities. Purification of the adsorbate was carried out by placing *ca.* 10 cc. in one of two inter-connected storage tubes and pumping to remove gaseous impurities. The water was twice distilled from one tube into another, while pumping, using liquid nitrogen as a coolant. A portion of the liquid was distilled into the gas thermometer tube, where its vapor pressure was measured at 25° and was found to agree with the tabular value within the limit of precision of the mercury manometer.

Adsorption Studies.—Adsorption data for water on ferric oxide was measured only in the range from 0.1 to 0.4 relative pressure for samples activated at 100, 150 and 450°. For the sample activated at 25°, low equilibrium pressures were also measured. Equilibrium at low pressures was attained in about 24 hours. Above 0.1 relative pressure, adsorption equilibrium was attained within one hour. Nitrogen adsorption was measured at −195°. The cross-sectional areas of 10.8 and 16.2 A.^{2} were used for the water and nitrogen molecules, respectively.

Desorption Measurements.—Volume analyses of gases evolved from iron oxide samples at 100, 150 and 450°, respectively, were carried out. This was accomplished by condensing the gases in the cold-finger tube of a known volume system. An oil manometer containing Apiezon "B" oil was employed to measure pressures. The samples were first outgassed overnight at 26° and a final vacuum of 10^{-5} mm. to remove physically adsorbed water. The desorption system was then isolated from the pumps and the temperature of the sample was raised with an electric furnace already at the desired temperature. The sample was maintained at this temperature for two hours. The gases were completely condensed on a cold finger at −195°. A stopcock was then closed to the sample, the condensate allowed to evaporate into the system of known volume, and the pressure was measured. After the cold bath was removed the pressure rose in two distinct steps. At first the pressure built up rapidly and continuously. After a momentary halt, the pressure rose slowly to its final value. It was further established that the more volatile gas did not condense at pressures up to 2.070 cm. at −78.5°. This gas was completely absorbed by ascarite and was assumed to be CO_2. The second fraction was believed to be water vapor. Mass spectrometer analyses by Consolidated Electrodynamics, Pasadena, California, showed that the major constituents of the desorbed gas were, indeed, CO_2 and water vapor.

During the desorption studies carried out at 450°, evidence for the presence of a permanent gas was noted initially. This gas, however, was evidently converted to a condensable vapor during the two-hour period of activation. The nature and source of this gas will be discussed below.

Immersional Calorimetry.—The heats of immersional wetting of iron oxide samples in water were measured at 25°. The apparatus and techniques were previously described.[4] Measurements were made with samples evacuated at 25, 100, 150 and 450° before immersion. In addition heat values were obtained for samples initially evacuated at 25° which contained known and increasing amounts of preadsorbed water.

Results and Discussion

The results of the adsorption and desorption experiments are listed in Table I. The agreement in nitrogen areas for samples evacuated at 25 and 450° showed that no appreciable sintering of the oxide occurred at the higher temperature. However, the amount of water adsorbed was appreciably lower than expected on the basis of the external area of the oxide, particularly at the lower evacuation temperatures. Since the amount of water adsorbed increased with increasing activation temperature, this increase was taken as a measure of the sites uncovered by the high temperature activation. The good agreement between the calculated water area and that obtained from nitrogen adsorption after the 450° activation suggested that hydrated portions of the surface could not physically adsorb water.

The difference in V_m's obtained from adsorption data for a sample evacuated at 25° and at an elevated temperature was assumed a good measure of the amount of chemisorbed water desorbed at the higher temperature. Consequently, it was expected that desorption studies with fresh iron oxide samples at elevated temperatures after removal of physically adsorbed water would also measure the amount of chemisorbed water, and be in at least qualitative agreement with the adsorption results. This agreement was not found. The amount of water evolved by desorption of fresh samples was greater than could be accounted for by the difference in V_m's. The discrepancy between the amount of water chemisorbed calculated from adsorption and desorption data was not large after the 100 or 150° activation; slightly more water was evolved by desorption as shown in Table I. Undoubtedly, a small part of this water could not be returned to the sample by adsorption at 25° and might well be internal water which diffused through the sample at the elevated temperature of activation.

The amount of water evolved by desorption at 450°, exclusive of that physically adsorbed, was more than twice that chemisorbed at 25°. In addition a large volume of another gas was also desorbed as shown in Table I. This gas will be discussed below. The adsorption–desorption results indicated that the water desorbed at 450° was partly chemisorbed surface water and partly in-

(3) I. E. Puddington, *Rev. Sci. Instr.*, **19**, 577 (1948).

(4) A. C. Zettlemoyer, G. J. Young, J. J. Chessick and F. H. Healey, THIS JOURNAL, **57**, 649 (1953).

TABLE I

ADSORPTION AND DESORPTION STUDIES OF IRON OXIDE

$V_{m_{10}} - V_{m_{250}}$

Evacuation Time, hr.	Temp., °C.	ΣN_2, m.²/g.	ΣH_2O, m.²/g.	ml. H_2O (STP)/g.	H_2O desorbed, ml./g.	CO_2 desorbed, ml./g.	ΔH hydration Ads.	kcal./mole Desorp.
18	25	10.8	7.2					
2	100		7.8	0.21	0.32 ± 0.03	Negligible	−27.6	−18.1
2	150		8.5	0.44	0.58 ± .03	Negligible	−18.7	−14.2
2	450	10.8	10.5	1.16	2.76 ± .63	1.78 ± .73	−26.3	−11.1
							av. −24.2 ± 3.6	

ternal water. The large and erratic volumes of gases released at this temperature also suggested sudden rupture and release of internal gases along grain boundaries rather than by slow diffusion which may occur at lower activation temperatures.

Independent gravimetric adsorption measurements on an 80-g. sample of oxide were used to demonstrate that diffusion of water into bulk oxide does not occur at 25°. After removing the internal and external water by activation at 450° for 2 hours, the sample was weighed, then exposed to water vapor at its saturation pressure at 25° until condensation occurred and finally outgassed at 25° and reweighed. The amount of water which could chemisorb on the external surface was calculated to be 1.16 ml. (STP)/g.; the experimental amount adsorbed was found to be 1.10 ml. (STP)/g. It does not appear that internal water removed at elevated temperatures can be readmitted to the sample by an adsorption or immersion process at 25°.

At least part of the CO_2 evolved at 450° activation comes from methane, no doubt incorporated into the sample during preparation. The presence of this gas was established by the mass spectrometer analysis. Furthermore, it was pointed out in the experimental section that during the 450° activation a gas non-condensable at −195° was initially evolved. This gas converted with time into a condensable gas. The most likely explanation is that initially methane evolved and was oxidized by the surface oxide to CO_2 and H_2O.

The difference in the heat of immersion values for samples evacuated at two different temperatures represents the wetting of additional sites freed of chemisorbed water at the higher activation temperature. Heats of hydration of the surface sites can be calculated from these heat values and a knowledge of the amount of water necessary to cover the new sites. Two series of heats of hydration were calculated and are listed in Table I. In the first series, the heats of hydration were calculated using the differences in V_m's from adsorption data as a direct measure of the amount of chemisorbed water. In the second series, the amounts of chemisorbed water obtained directly from desorption were used. The fact that the heats of hydration calculated from adsorption data are higher and more consistent supports their acceptance and also indicates that internal water is not returned to sample either by adsorption or immersion at 25°.

The possibility that surface water reacts to form the hydroxide according to the equation

$$Fe_2O_3 + 3H_2O \rightleftharpoons 2Fe(OH)_3$$

is unlikely. An endothermic heat of hydration of 2.5 kcal./mole H_2O was calculated for this process from heat of formation data.[5] Haber suggested that failure to isolate crystalline ferric hydroxide may be due to the very high vapor pressure of this compound.[6] However, evidence has been presented for the formation of mono and higher hydrates with Fe_2O_3 in the presence of liquid water.[7]

The heats of immersion of Fe_2O_3 evacuated at 25° are shown plotted in Fig. 1 as a function of the

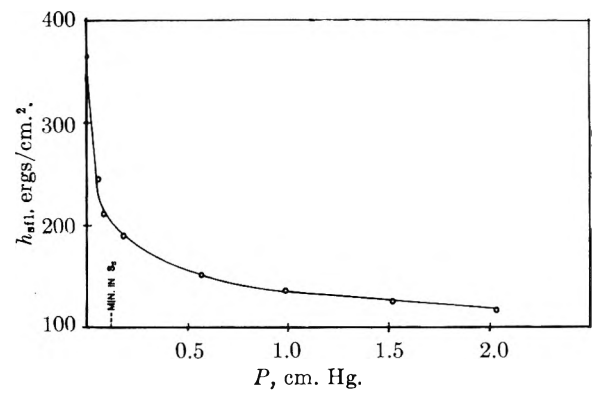

Fig. 1.—Heat of immersion of iron oxide with known amounts of pre-adsorbed water at 25° as a function of the equilibrium pressure of the adsorbed film.

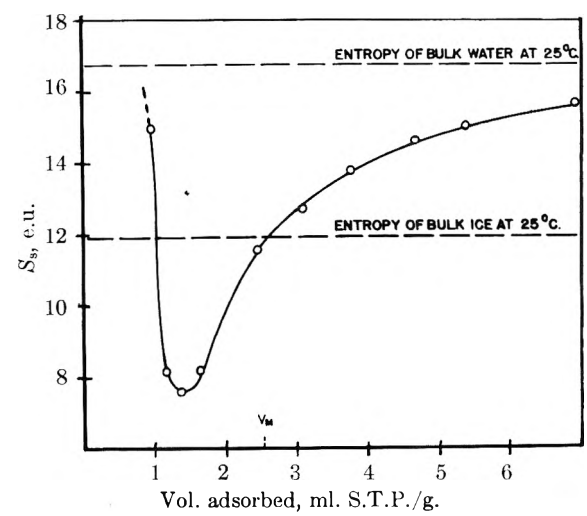

Fig. 2.—Absolute entropy of the adsorbed film as a function of the volume adsorbed.

equilibrium pressure of the water vapor pre-adsorbed on the surface prior to immersion. The

(5) F. D. Rossini, "Selected Values of Chemical Thermodynamics," N. B. S. Circular No. 500, 1952.

(6) F. Haber, *Naturwissenschaften*, **13**, 1007 (1925).

(7) L. A. Welo and O. Baudisch, *Phys. Rev.*, **55**, 1143 (1941).

entropy of the adsorbed state was calculated from the equation

$$T(S_S - S_L) = \frac{h_{SfL} - h_{SL}}{N_S} + \varphi/\Gamma - kT \ln X$$

as developed by Jura and Hill.[8] In this equation S_S refers to the absolute entropy of the adsorbed state, S_L, the entropy of the liquid adsorbate, $h_{SfL} - h_{SL}$ is the difference in the heat of wetting between the clean solid, h_{SL}, and the film coated solid, h_{SfL}. The symbol φ represents the spreading pressure, Γ the surface concentration and X is the relative equilibrium pressure of the vapor and adsorbed water film. The calculated entropy values, S_S, are shown plotted in Fig. 2 as a function of the volume of water adsorbed. Curves of similar shape are now unknown.[9,10] However, two interesting features are apparent: entropy values lower than that of ice were found, and the minimum in the entropy curve occurs at about half coverage, whereas normally this minimum occurs near $\theta = 1$ for physical adsorption. The reason for this shift of the minimum to the left is not clear, although Hill states that the occurrence of a minimum shifted in this direction could be expected in systems where there is strong binding of the adsorbate to the adsorbent. Heat of immersion and adsorption data also showed that the position of the minimum corresponds to the completion of adsorption on the most energetic portion of the surface.

Acknowledgment.—The authors wish to express their appreciation for the financial support provided by the Office of Ordnance Research, Ordnance Project No. TB2-0001 (457), Contract No. DA-36-034-ORD-935.

(8) G. Jura and T. L. Hill, *J. Am. Chem. Soc.*, **74**, 1598 (1952).
(9) T. L. Hill, P. H. Emmett and L. G. Joyner, *ibid.*, **73**, 5101 (1951).
(10) F. H. Healey and G. J. Young, THIS JOURNAL **58**, 885 (1954).

KINETICS OF THE THERMAL DECOMPOSITION OF PHENYLTRIMETHYLAMMONIUM HYDROXIDE IN SOLUTION[1]

BY MARK D. BAELOR, DENNIS BARNUM AND GEORGE GORIN[2]

Contribution from the Department of Chemistry, University of Oregon, Eugene, Oregon

Received March 12, 1956

The second-order rate constants for the thermal decomposition of 0.05 *M* phenyltrimethylammonium hydroxide in 60% *n*-propanol–water at 100, 110 and 120° are 2.88, 9.0 and 23.7 × 10^{-4} liter $mole^{-1}$ $sec.^{-1}$, respectively, and the energy of activation is 30.6 kcal. $mole^{-1}$. At this concentration, the effect of ionic strength on the rate constant is quite small but in *qualitative* agreement with Brønsted's theory of salt effects. The ultraviolet absorption spectrum of phenyltrimethylammonium hydroxide is reported.

Quaternary ammonium hydroxides are decomposed by heat in two ways

$$R_4N^+ + OH^- \begin{cases} \xrightarrow{a} R'CH{=}CH_2 + R_3N + H_2O \\ \xrightarrow{b} ROH + R_3N \end{cases}$$

The R groups may be the same or different, and may be aliphatic, aromatic or mixed. The reaction proceeds according to equation a if one of the R groups is capable of forming an olefin, and much information is available concerning the course of this reaction with various groups.[3]

On the other hand, reaction b is not well understood. Hughes, Ingold and Patel[4] measured the rate of decomposition of neopentyltrimethylammonium hydroxide and benzyltrimethylammonium hydroxide and concluded that the reaction may proceed, in different circumstances, by a bimolecular mechanism, a monomolecular mechanism, or by both simultaneously. In order to clarify the characteristics of this reaction an investigation of the thermal decomposition of phenyltrimethylammonium hydroxide was undertaken. Rate constants were determined, various kinetic parameters were calculated, and the effect of ionic strength was studied.

Conditions for Reaction.—Prolonged heating of a 0.1 *M* solution at 120° was necessary in order to effect appreciable decomposition in water. The rate constant at this temperature is 3.2 × 10^{-5} l. $mole^{-1}$ $sec.^{-1}$, which corresponds to a half-life of about 86 hours. For the purposes of systematic study, it would be convenient to deal with a faster reaction, and use of 60% *n*-propanol–water as a medium serves to make the rate of decomposition more conveniently measurable at 100–120°. The reaction was carried out in sealed tubes of alkali-resistant glass and the rate was measured by titrating the hydroxide ion remaining at various times with standard acid.

Stoichiometry of the Reaction.—Claus and Rautenberg[5] reported that phenyltrimethylammonium hydroxide decomposes into methanol and dimethylaniline. This was confirmed by comparing the absorption spectra of the hydroxide and of dimethylaniline with that of the reaction mixture after about 75% decomposition. The results are shown in Fig. 1; curve A represents the spectrum of phenyltrimethylammonium hydroxide, curve C that of dimethylaniline, and curve B that of the reaction product. If the last two spectra were identical, curves B and C would be parallel,

(1) Presented in part at the 124th national meeting, American Chemical Society, Chicago, Ill., Sept. 7–12 (1953).
(2) To whom inquiries concerning this paper should be sent. Department of Chemistry, Oklahoma A. and M. College, Stillwater.
(3) C. K. Ingold, "Structure and Mechanism in Organic Chemistry," Cornell University Press, Ithaca, N.Y., 1953, pp. 420, 427.
(4) C. K. Ingold and C. S. Petel, *J. Chem. Soc.*, 67 (1933); E. D. Hughes and C. K. Ingold, *ibid.*, 63 (1933).
(5) A. Claus and P. Rautenberg, *Ber.*, **14**, 620 (1881).

and it is seen that they are very nearly so; curve B bulges a little in the region where the residual phenyltrimethylammonium hydroxide contributes appreciably to the total absorption. Other aromatic products, if produced in substantial quantities, would stand clearly revealed. As an additional check, a 0.25 M solution of phenyltrimethylammonium hydroxide in water was allowed to decompose at 120–130° for 24 hr., and a nearly quantitative recovery of dimethylaniline was effected by extraction and precipitation as the picrate.

Kinetic Order and Rate Constants.—A plot of $1/c$, where c is the concentration of phenyltrimethylammonium hydroxide at any time, against time gave straight lines, in conformity with the requirements of second-order kinetics. Two typical plots are shown in Fig. 2.

Several runs were made at each temperature, with the initial concentration always close to 0.05 M. The rate constants, measured by the slope of the lines, were 2.88 ($\times 10^{-4}$ l. mole^{-1} sec.$^{-1}$) at 100°, 9.0 at 110°, and 23.7 at 120°. Application to these data of the equations of Arrhenius and of Eyring[6]

$$k = Ae^{-E/RT} = \frac{kT}{h} e^{\Delta S^{\ddagger}/R} e^{-\Delta H^{\ddagger}/RT} \qquad (1)$$

gives 30.6 kcal. mole^{-1} for the experimental energy of activation, E, 29.8 kcal. mole^{-1} for $\Delta H^{\ddagger}$, and about 7 cal. deg.$^{-1}$ mole^{-1} for $\Delta S^{\ddagger}$.

Effect of Ionic Strength on the Rate Constants.—According to Brønsted,[7] the rate constant for a reaction between two ions A and B is given by the expression

$$k = k_0 \frac{f_A f_B}{f_{AB}^*} \qquad (2)$$

where k_0 is the rate constant at infinite dilution and f_A, f_B, and f_{AB}^* are the activity coefficients of the ions A and B and of the activated complex AB*, respectively. If the Debye–Hückel limiting law is used to estimate the activity coefficients, one obtains for the case of interest here, where the charges on the ions and the activated complex are +1, −1 and zero, respectively

$$\log k = \log k_0 - 2Q\sqrt{\mu} \qquad (3)$$

where Q is the usual coefficient in the Debye–Hückel limiting equation and μ is the ionic strength.

According to equations 2 and 3, the rate constant should increase as the ionic strength decreases; when phenyltrimethylammonium hydroxide alone makes up the ionic atmosphere, then, the rate constant should increase as the reaction proceeds and the reagent is used up. Actually, as was pointed out in the preceding section, the data conform to a simple second-order rate equation over the first half-life period. When measurements were extended further, as in curve A of Fig. 2, some upward curvature became apparent; but the nature of the function is such that small variations in k are not made evident.

(6) S. Glasstone, K. J. Laidler and H. Eyring, "The Theory of Rate Processes," McGraw–Hill Book Co., New York, N. Y., 1941, pp. 196–199.

(7) J. N. Brønsted, *Z. physik. Chem.*, **102**, 169 (1922); **115**, 337 (1925).

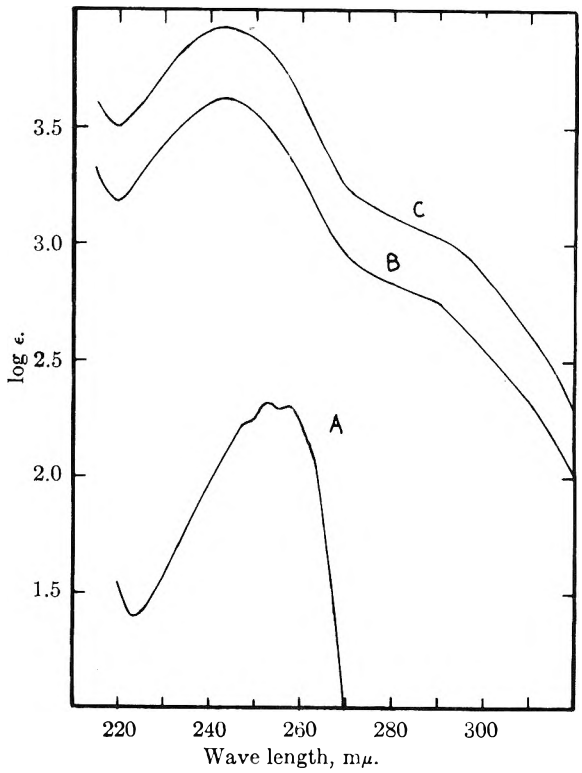

Fig. 1.—Ultraviolet absorption spectra: A, $PhMe_3NOH$; B, reaction product (arbitrary ordinate scale); C, $PhNMe_2$.

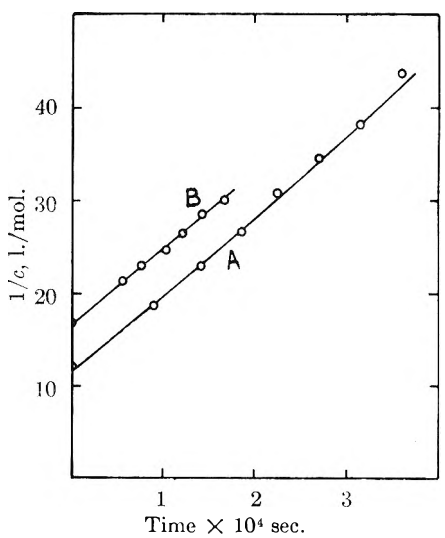

Fig. 2.—Decomposition velocity of phenyltrimethylammonium hydroxide; two representative runs.

In order to test the influence of ionic strength more effectively, the initial concentration of reagent was varied, and, also, two neutral salts were added, sodium chloride and sodium sulfate. In each instance, the reaction was allowed to proceed for about one half-life period, and the value of k was estimated graphically, using the simple second-order kinetic relationship. The results are plotted in Fig. 3, against the square root of the initial ionic strength.

It can be seen by inspection that the rate constant decreases with increasing ionic strength, but that the decrease is quite small in the range of

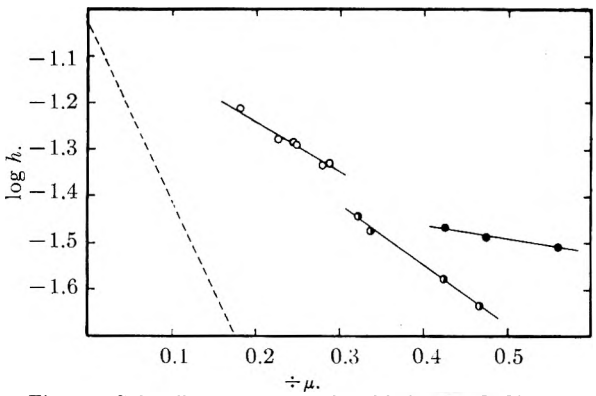

Fig. 3.—Salt effects: ○, no salt added; ◑, NaCl added; ●, Na_2SO_4 added. Dashed line indicates the slope predicted by the Debye–Hückel limiting law (dielectric constant = 25.2[10]).

concentrations examined; in the range of concentration encompassed by an average run the variation to be expected was, in fact, not much larger than the experimental error. It is for this reason that the calculation of rate constant was made from a simple second-order expression; the accuracy of the data does not warrant more laborious refinements.[8]

The decrease in rate constant with increasing ionic strength is qualitatively in agreement with the Brønsted theory of salt effects. However, equation 3, which results from combining this theory with the Debye–Hückel limiting law, predicts, quantitatively, a much larger effect, indicated in Fig. 3 by the dashed line. Clearly, the experimental points, to which short, linear segments have been fitted, are far removed from the limiting slope.

It was, of course, to be expected that the Debye–Hückel limiting law would fail to apply quantitatively to the system under study; but it had been hoped that the deviations would nevertheless prove instructive with respect to the applicability of the Brønsted theory. However, the data do not discriminate among the various factors involved, and it did not seem profitable to attempt a separation of these factors by further study of the system at hand.

Although the theory of salt effects requires more extensive experimental testing and theoretical elaboration, it seems to the writers that this development requires very numerous and fairly accurate data; from the practical standpoint this demands, in turn, examination of systems which react more rapidly and can be measured more conveniently than the one discussed here. It may be appropriate to mention, in passing, that the more reactive *m*-nitro derivative was investigated briefly with these considerations in mind. However, the reaction in this case is stoichiometrically complex, and the proposed study was not pursued for this reason.[9]

Experimental

Phenyltrimethylammonium iodide was prepared by allowing dimethylaniline to stand with a 25% excess of methyl iodide for several hours at room temperature. It was decolorized with activated carbon and crystallized three times from 2:1 (by vol.) isopropyl alcohol–water. The yield of crude product was about 90%. The purified compound sublimed at 218–219°, and two preparations gave 48.20 and 48.25% iodine (calcd. 48.23%).

***n*-Propanol** was distilled through an efficient column and the middle eight-tenths retained for use; b.p. 96.9–97.2°.

Preparation of Quaternary Hydroxide Solution.—Carbonate-free sodium hydroxide was mixed with a slight excess of silver nitrate with vigorous mechanical stirring. The precipitate was filtered and washed until free of silver ions. The freshly prepared silver oxide was added in 25% excess to a solution of phenyltrimethylammonium iodide, shaken vigorously, allowed to stand for half an hour, filtered into a 100-ml. volumetric flask containing 60.0 ml. of *n*-propanol, and diluted to the mark with water. No carbonate, silver or iodide ions were detected in the solutions.

Isolation of Dimethylaniline as the Picrate.—Forty milliliters of 0.26 *M* dimethylaniline in water was extracted with four 7-ml. portions of ether. The ether extract was dried over anhydrous sodium sulfate, evaporated, and the residue treated with a 50% excess of picric acid in 20 ml. of absolute alcohol. The picrate was obtained in 89% yield; m.p. 161–162°. Forty milliliters of 0.264 *M* phenyltrimethylammonium hydroxide in water was heated at 120–130° for 24 hours, at the end of which time the concentration of undecomposed hydroxide, determined by titration, was 0.179 *M*. The solution was treated in the same way as described above, and the amount of picrate obtained amounted to 90% of that calculated from the amount of hydroxide decomposed. Since the recovery is the same as in the control experiment, the conversion of the quaternary hydroxide into dimethylaniline may be considered to have been quantitative. The product melted at 161–161.5° and after one recrystallization from propanol–methanol, at 162–163°. It showed no depression upon admixture with the authentic picrate.

Spectrophotometric Measurements.—All spectrophotometric measurements were made with a Beckman DU spectrophotometer using 1.00 cm. silica cells.

(A) **Phenyltrimethylammonium Hydroxide.**—An aqueous solution was prepared as described above, the concentration of hydroxide determined by titration, and the solution diluted to approximately 0.01 *M*. Three independently prepared samples were employed and the results averaged.

(B) **Dimethylaniline.**—Eastman "white label" dimethylaniline was distilled through a 4-ft. helices-packed column and the distillate collected at 193° and 771 mm. It was dissolved in 60% *n*-propanol–water and diluted 200–500 times with water quantitatively to give a 0.001 *M* solution, which was measured against water as the blank.

(C) **Decomposition Product.**—A 1.00-ml. sample was withdrawn from a 60% *n*-propanol–water mixture which had been heated at 101° for about two half-lives and diluted to 500 ml. In this case, log ϵ is diminished by an arbitrary constant, in order that the curve may be compared with

TABLE I

SECOND-ORDER REACTION RATE CONSTANTS FOR THE DECOMPOSITION OF PHENYLTRIMETHYLAMMONIUM HYDROXIDE IN 60% *n*-PROPANOL–WATER SOLUTIONS AT 110.0°

Initial concn. of $PhMe_3NOH$	Added salts	Initial μ	10^4 k/l. mole^{-1} sec.$^{-1}$
0.08303	None	0.08303	7.83
.07821	None	.07821	7.82
.06271	None	.06271	8.60
.06066	None	.06066	8.68
.05212	None	.05212	8.80
.03263	None	.03263	10.3
0.07339	0.03 *M* NaCl	0.1034	6.05
.06437	.05 *M* NaCl	.1144	5.63
.07973	.10 *M* NaCl	.1797	4.45
.06795	.15 *M* NaCl	.2180	3.85
0.09191	0.03 *M* Na_2SO_4	0.1819	5.73
.07463	.05 *M* Na_2SO_4	.2246	5.47
.08461	.07 *M* Na_2SO_4	.2964	5.22

(8) G. Scatchard, *J. Am. Chem. Soc.*, **52**, 52 (1930).

(9) D. Barnum, M. A. Thesis, University of Oregon, 1954.

(10) Estimated from the data of G. Åkerlöf, *J. Am. Chem. Soc.*, **54**, 4125 (1932).

curve c without overlapping it; identical spectra would give perfectly parallel curves.

Kinetic Measurements.—The reaction was carried out in sealed tubes of Corning No. 728 alkali-resistant glass. It was demonstrated in the early stages of this work that Pyrex glass was attacked by the strongly alkaline solutions and non-reproducible rate constants were obtained.

Several filled tubes were sealed, plunged into the constant temperature bath simultaneously, and two minutes was allowed for the bath to regain temperature equilibrium. Then the first tube was withdrawn, plunged into cold running water, and the time started. The remaining tubes were withdrawn from the bath at appropriate intervals and the reaction quenched. After allowing sufficient time for each sample to reach room temperature the tube was opened and a 10.00-ml. aliquot was titrated potentiometrically with standard acid.

Rate constants were corrected for expansion of the solvent since the concentration of the reactants is different at temperatures other than 25°. Thus, values of k obtained at 100° were corrected by multiplying k by 1.04, at 110° by 1.05, and at 120° by 1.05.

Temperature Control.—The thermometer was calibrated against a platinum resistance thermometer which had been checked recently by the National Bureau of Standards. The temperature was controlled within ±0.2°.

EFFECT OF pH ON POLYMERIZATION OF SILICIC ACID

By Katsumi Goto

Faculty of Engineering, Hokkaido University, Sappor, Japan

Received March 13, 1956

In view of discordant results reported by earlier investigators, the effect of pH on the polymerization of silicic acid has been further studied. The reaction rate constant at various pH values in the range from 7 to 10 was calculated from the rate of disappearance of molecularly dispersed silica, on the assumption that the polymerization reaction is third order with respect to the concentration of molecular silica. The value of the calculated constant increased linearly with pH, indicating that the polymerization occurred more rapidly at higher pH. The time required for complete depolymerization of the particles of colloidal silica formed at various pH's, indicated that larger particles are formed at higher pH.

Many workers[1-8] have reported the effect of pH on the polymerization of silicic acid in water, but their conclusions are not identical. Iwasaki, *et al.*,[1] have stated recently that the polymerization is most rapid at the neutral point. Similar conclusions have been drawn from measurements of gel time.[2-4] On the other hand, Brady[6] has concluded from light scattering measurements that the optimum pH for polymerization is about 8, while Greenberg and Sinclair[7] on the basis of similar experiments, have reported a maximum rate of polymerization at pH 8.6.

It is our belief that the above disagreement arises from the tacit assumption in each case that the polymerization proceeds to the same equilibrium state regardless of pH. This assumption seems to be incorrect when it is considered that the solubility of amorphous silica changes with pH, as has been described in the previous paper.[9]

The present investigation was carried out to obtain a clear picture of the effect of pH on the rate of polymerization of silicic acid, and also to determine whether the equilibrium state of polymerization has been affected by pH.

Experimental

I. Changes in Concentration of Molecularly Dispersed Silica.—These changes were measured at various pH's in a manner similar to that reported in the previous paper.[9] Adjustment of pH was carried out by rapid mixing of sodium silicate solution with the silicic acid solution prepared by the ion-exchange method. The latter also contained a large amount of molecularly dispersed silica.

To simplify presentation of data, the following equation was assumed to be applicable to the polymerization of silicic acid

$$-\frac{dC}{dt} = k(C - S)^3$$

where C is the concentration of molecularly dispersed silica at time t; S, the solubility of amorphous silica; and k is a constant.

Values of k for the polymerization at various pH's are plotted on a logarithmic scale in Fig. 1, which clearly shows the greater polymerization rate at higher pH. Polymerization may be a reaction too complex to be fully dealt with by such a simple assumption. Nevertheless, the results indicated in Fig. 1 still show at least qualitatively the effect of pH.

II. Depolymerization Time.—The measurements of depolymerization time were carried out to determine whether there were any differences in the polymers formed at different pH's.

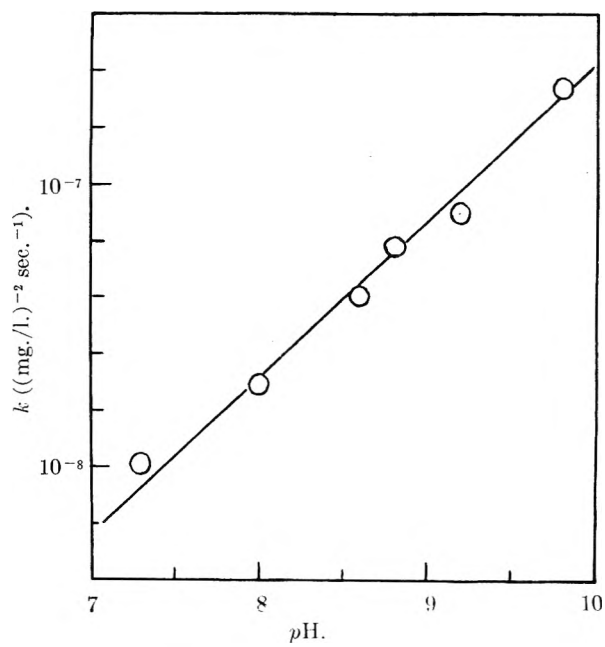

Fig. 1.—Values of k at various pH's.

(1) I. Iwasaki, T. Tarutani, T. Katsura and H. Arino, *J. Chem. Soc. Jap., Pure Chem. Sec.*, **75**, 856 (1954).

(2) R. C. Merrill and R. W. Spencer, This Journal, **54**, 806 (1950).

(3) I. A. Heald, K. B. Coates and J. E. Edwards, *J. Appl. Chem.*, **5**, 425 (1955).

(4) R. K. Iler, This Journal, **57**, 604 (1953).

(5) C. B. Hurd and H. A. Letteron, *ibid.*, **36**, 605 (1932).

(6) A. P. Brady, A. G. Brown and H. Huff, *J. Coll. Sci.*, **8**, 252 (1953).

(7) S. A. Greenberg and D. Sinclair, This Journal, **59**, 435 (1955).

(8) G. B. Alexander, *J. Am. Chem. Soc.*, **76**, 2094 (1954).

(9) K. Goto, *J. Chem. Soc., Pure Chem. Sec.*, **76**, 1364 (1955).

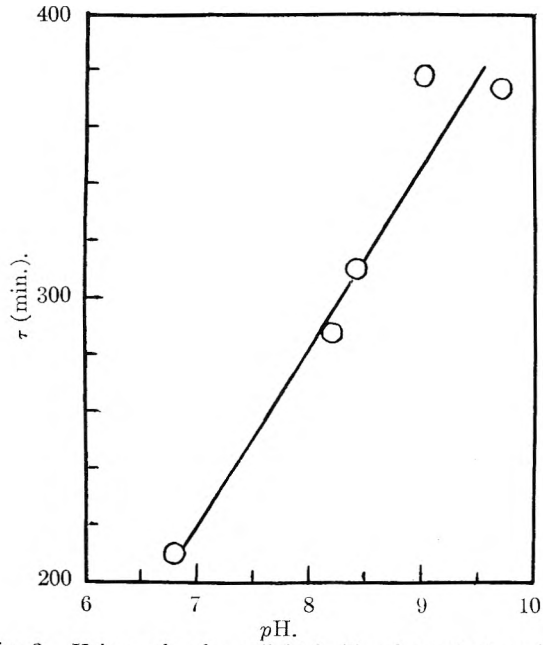

Fig. 2.—Values of τ for colloidal silica formed at various pH's.

Suito, *et al.*,[10] have derived the following equations for the dissolution of fine particles, assuming the dissolution rate to be proportional to the surface area of the particles.

$$n^{1/3} M^{1/3} = K(\tau - t)$$

$$\tau = b\, v_0$$

where M is the total weight of particles at time t; τ, the time necessary for complete dissolution (in the present study τ means the time necessary for complete depolymerization); v_0, the initial radius of particle; n, the number of particles; and b and K are proportionality constants.

Therefore, the $M^{1/3}$ *versus* t plot becomes a straight line for monodisperse systems, and τ can be obtained by extrapolating this straight line to the point where $M^{1/3} = 0$.

By applying these procedures to depolymerization of colloidal silica, values of τ have been obtained for colloidal silica formed at various pH's. They are shown in Fig. 2 and indicate that larger particles are formed at higher pH. Depolymerization experiments were carried out by diluting one volume of colloidal silica solution with 100 volumes of the solution containing 1 g./l. Na_2CO_3 (pH 10.8). The colloidal silica solutions used in these experiments were prepared by aging at various pH's for 6 days and contained 2 g. of SiO_2 per liter.

(10) E. Suito, N. Hirai and K. Taki, *J. Chem. Soc.*, **72**, 713 (1951).

Discussion

In no case has polymerization reached true equilibrium, since in this case the system, at infinite time, would consist of water containing a single large particle of amorphous silica. After aging the colloidal solutions for only 6 days, surely only a pseudo-equilibrium is established. It might therefore be postulated that as the monomer disappeared to form colloidal particles, these colloidal particles further polymerize, or at least increase in particle weight, and this rate of increase in particle size is also a function of pH, since the largest particles are formed at highest pH.

From the foregoing evidence, it is clear that hydroxyl ions promote the polymerization of silicic acid over a pH range wider than that reported by previous workers. It is very interesting to note that the polymerization takes place more rapidly at higher pH, where colloidal silica particles are highly charged and depolymerize very rapidly. This might be evidence for the fact that the same mechanism is involved both in polymerization and in depolymerization.

Acknowledgment.—The author is indebted to Prof. Y. Uzumasa, Prof. G. Okamoto and Assist. Prof. T. Okura for their valuable advice and encouragement.

CHARACTERISTICS OF ADSORPTION OF COMPLEX METAL-AMMINES AND OTHER COMPLEX IONS OF ZINC, COPPER, COBALT, NICKEL AND SILVER ON SILICA GEL[1]

BY GRANT W. SMITH AND HOWARD W. JACOBSON

Contribution from the College of Chemistry and Physics, The Pennsylvania State University, University Park, Pa.

Received April 18, 1956

The adsorption isotherms for complex metal ammines, ethylenediamine-metal complexes, and diethylenetriamine-metal complexes on silica gel are shown. The extremely complex nature of the adsorption of metal ammines is demonstrated for the nickel and copper ammines. Metal ammines are adsorbed in the following decreasing order, in millimoles adsorbed per gram of silica gel: zinc, copper, cobalt, nickel, silver. For diethylenetriamine complexes, those with higher formation constants were more highly adsorbed. For ethylenediamine complexes studied, six-coördinate systems were more highly adsorbed than four-coördinate. An interpretation of the adsorption process in terms of hydrogen bonding of ligand to silica surface is presented. Complex copper ammines, copper ethylenediamines and copper diethylenetriamines dissociate during adsorption on silica gel. This is shown by a comparison of the absorption spectra of solutions of the complex metal ions before and after adsorption. The ratio, ammonia:copper ion adsorbed is higher than that of the complex species originally in solution. The more stable a given complex ion, the closer the ratio for the adsorbate agrees with that of the species initially in solution.

Introduction

This study was undertaken to correlate the relative adsorption of complex metal ammines and other metal complexes in which ethylenediamine (abbreviated en) and diethylenetriamine (abbreviated dien) are the ligands, with the structure and stability of the complex entities. The unusually strong adsorption of complex metal ammines on silica gel was first reported by Smith and Reyerson.[2] Complex metal ammines adsorbed on the surface

(1) This paper is based on part of a thesis submitted by Howard Wayne Jacobson in partial fulfillment of the requirements for the degree of Doctor of Philosophy at The Pennsylvania State University, August, 1953.

(2) G. W. Smith and L. H. Reyerson, *J. Am. Chem. Soc.*, **52**, 2584 (1930).

of silica gel form a quite stable system. Ordinary electrodialysis fails to remove the adsorbed ions to any extent, but changes do take place after considerable time. This indicates that a surface disintegration of the gel with its adsorbed ions has occurred.[3] Studies of the adsorption of copper ammine on silica gel have shown that final equilibrium is reached only after very prolonged shaking, and that the composition of the copper ammine ion undergoes continuous change during the process.[4]

Experimental

The silica gel was a commercial product of 6–12 mesh size, obtained from the Davison Chemical Corporation. It was cleaned by treating with 6 *M* nitric acid for 12 hours to remove impurities and was then washed with frequent changes of distilled water over a period of one week. It was then dried at 120° for 24 hours and finally at 300° for four hours. The silica gel used throughout the entire study came from the same lot.

Stock solutions of the complex metal ammines were prepared by placing the desired quantity of metal nitrate in a liter volumetric flask and adding concentrated ammonium hydroxide until the precipitate formed just dissolved. At this point an excess of 10 ml. of concentrated ammonium hydroxide was added. The solutions were then diluted to the correct volume. Solutions of the complex metal ammines of lower concentrations were prepared by diluting these stock solutions. The cobalt–ammine solution required 25 ml. more of concentrated ammonium hydroxide per liter than the other metal ammines.

Stock solutions of the complex metal ions, in which ethylenediamine and diethylenetriamine were the ligands, were prepared in a manner similar to the complex metal ammines. In both cases an excess of 10 ml. of concentrated reagent was added per liter of final solution.

Solutions of the ligands alone—ammonia, ethylenediamine and diethylenetriamine—were prepared for adsorption by diluting the concentrated reagents.

The samples were prepared for the adsorption study as follows: 10.00 g. of silica gel was weighed into 125-ml. polyethylene bottles and then 75 ml. of solution was added. Duplicate samples were run in all cases. The bottles were capped and mounted on a shaker in a 25.0° water-bath and rotated at a rate of 25 revolutions per minute for a period of 72 hours. Two special series were run with the copper- and nickel–ammines. In the first of these, the volume of the metal ammine solution was 50 ml. and the weight of silica gel was 5 g. In the second, the volume of the metal ammine solution was 50 ml. and the weight of the silica gel was 2 g. At the end of the shaking period the bottles were removed and the solutions were analyzed for the metal ions in the case of the series of metal complexes, and for ammonia, ethylenediamine or diethylenetriamine in studies of ligand adsorption.

The following analytical methods were employed.

(1) **Silver**: precipitated as silver chloride and weighed in sintered glass crucibles.

(2) **Nickel**: precipitated as nickel dimethylglyoxime and weighed in sintered glass crucibles. The precipitation was effected by the hydrolysis of urea from homogeneous solution

(3) **Copper**: iodometric titration in sulfuric acid solution. with sodium thiosulfate which had been previously standardized with freshly recrystallized potassium iodate.

(4) **Zinc**: precipitated as zinc ammonium phosphate and ignited to the pyrophosphate and weighed as such.

(5) **Cobalt**: electrolytically deposited on platinum electrodes.

(6) **Ammonia, ethylenediamine, diethylenetriamine**: titrated with sulfuric acid previously standardized with sodium carbonate.

The silver complexes involving ethylenediamine and diethylenetriamine were not studied because they did not form stable systems. A considerable amount of insoluble hydroxide and oxide formed in these cases which could not be dissolved by the addition of excess ethylenediamine or diethylenetriamine.

To exhibit the extent to which complex copper–amines, copper–ethylenediamines and copper–diethylenetriamines dissociate during adsorption, solutions of the complex metal ions were prepared in which the ligand:metal ion ratio was varied in integral steps from one to the maximum coördination number of the metal ions. Ammonium nitrate was added to stabilize these systems with respect to insoluble hydroxide formation. The minimum amount of ammonium nitrate required to prevent hydroxide formation in the least stable member of a series was used throughout that entire series. Immediately after the 72-hour shaking period with silica gel, the solutions were subjected to quantitative and spectrophotometric analysis. A Beckman Model DU Photoelectric Quartz Spectrophotometer was used to take the absorption spectra before and after adsorption. In using the spectrophotometer, minimum slit width and maximum sensitivity were employed. To obtain the absorption data, the solutions of the complex metal ions were compared to an ammonium nitrate solution whose concentration was equal to the ammonium nitrate concentration present in the complex metal ion solution in question. The ammonium nitrate was 6.0 *M* in the copper–ammine series, 3.0 *M* in the copper–ethylenediamine series and 2.0 *M* in the copper–diethylenetriamine series.

The *p*H of each solution was measured both before and after adsorption with a Model G Beckman *p*H Meter.

Results

Figures 1–6 show the adsorption isotherms of indicated systems on silica gel. They were obtained by plotting the equilibrium concentrations of the solutions against the number of millimoles of complex ion adsorbed per gram of silica gel.

Discussion

The ordinary hydrated metal ions are not significantly adsorbed on silica gel, but the replacement of the bound water molecules by ammonia, ethylenediamine or diethylenetriamine results in considerable adsorption of the metal ions. Figure 1 shows that ammonia, ethylenediamine and diethylenetriamine all exhibit a high affinity for the surface of silica gel.

The surface of silica gel can be considered to be made up primarily of oxygen atoms since the silicon atom is quite small. It seems conceivable to account for the strong adsorption of the complex metal ions on silica gel by considering hydrogen bonds to be formed between the oxygen atoms in the surface of silica gel and the nitrogen-containing ligands which in turn are coördinated to the metal ion. In the case of the aquated metal ions, a similar bonding could be considered to exist between the hydrogens of water and the surface oxygen atoms, but the water–metal ion bond is not of sufficient strength to hold the metal ion to the surface. Water itself is adsorbed to a considerable extent on silica gel.

The structure of the complex entity in solution should be one of the important factors governing the amount of metal complex adsorbed. For the complex metal ammines, a maximum of six hydrogen atoms could lie on a flat surface for tetrahedral structure. For a planar ammine, a maximum of eight hydrogens could attach to a flat surface if the entity were on its face and four if on an edge. In an octahedral structure, the maximum is six, while for the linear type it is four. The structures of the metal ammines involved in this study are generally thought to be as follows: zinc–ammine, tetrahedral; copper–ammine, planar; cobalt–ammine, octahedral; nickel–tetraamine, tetrahedral; and silver–

(3) L. H. Ryerson and R. E. Clark, THIS JOURNAL, **40**, 1055 (1936).

(4) I. M. Kolthoff and V. Stenger, *ibid.*, **38**, 475 (1934).

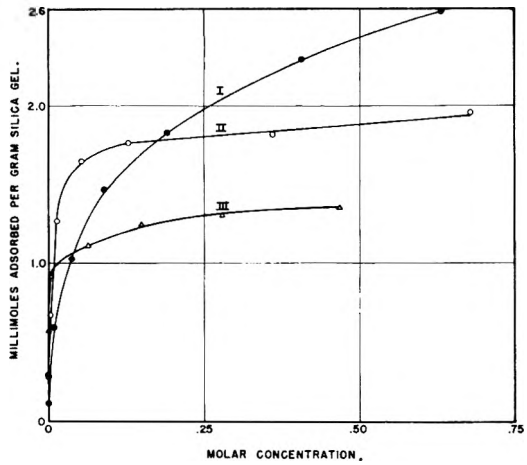

Fig. 1.—Adsorption of ligands by silica gel: I, ammonia; II, ethylenediamine; III, diethylenetriamine.

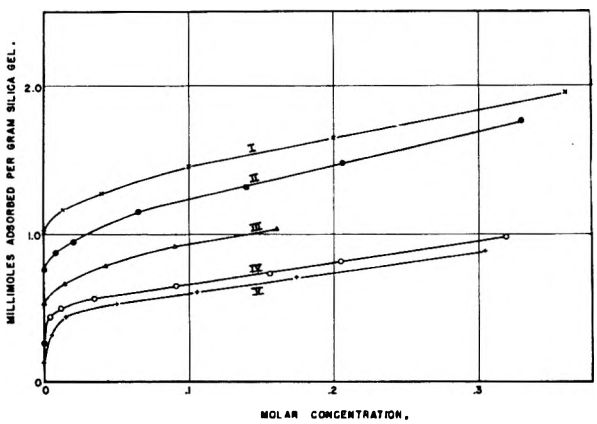

Fig. 2.—Adsorption of metal ammines by silica gel: I, zinc–ammine; II, copper–ammine; III, cobalt–ammine; IV, nickel–ammine; V, silver–ammine.

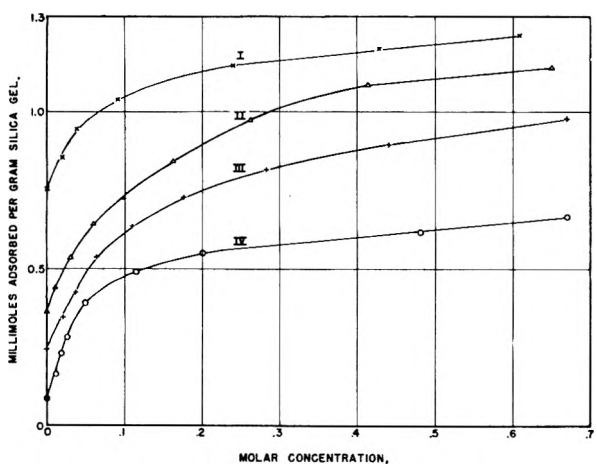

Fig. 3.—Adsorption of ethylenediamine complexes by silica gel: I, zinc–ethylenediamine; II, cobalt–ethylenediamine; III, nickel–ethylenediamine; IV, copper–ethylenediamine.

ammine, linear. The latter has been determined in the form of silver ammine sulfate.[5] The other structures are based on the electronic configuration of the metal ions, magnetic measurements, and by comparison to known structures of other derivatives of the metal ions.[6] Considering the adsorption of metal ammines on silica gel on the basis of millimoles per gram adsorbent, the following decreasing order is observed: zinc, copper, cobalt, nickel and silver. In terms of structure, that would be tetrahedral, planar, octahedral, tetrahedral and linear.

No reliable correlation between the geometry of the species and adsorbability is evident from the

(5) A. F. Wells, "Structural Inorganic Chemistry," Clarendon Press, Oxford, 1950, p. 120.

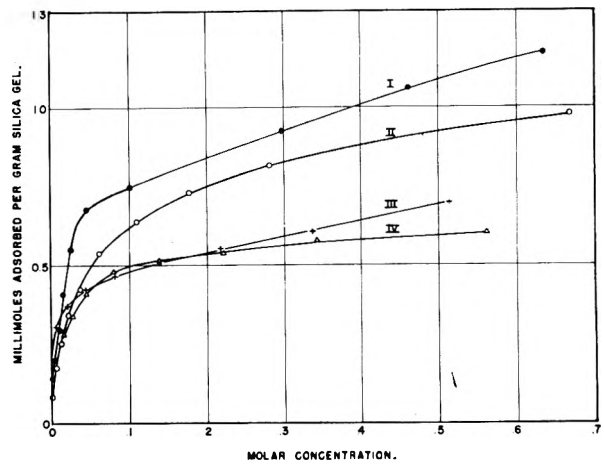

Fig. 4.—Adsorption of diethylenetriamine complexes by silica gel: I, copper–ethylenetriamine; II, nickel–diethylenetriamine; III, zinc–diethylenetriamine; IV, cobalt–diethylenetriamine.

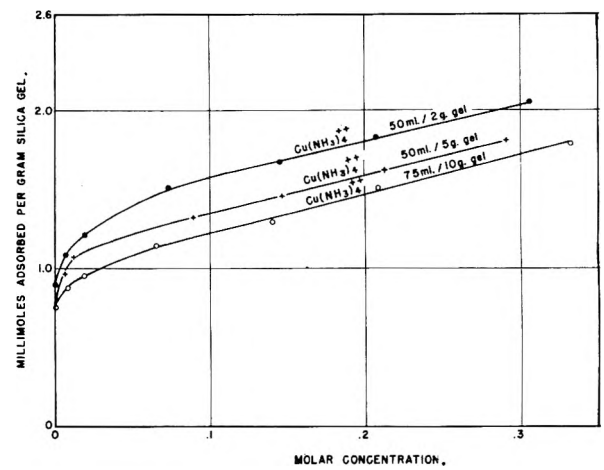

Fig. 5.—Adsorption of copper–ammine solutions by silica gel.

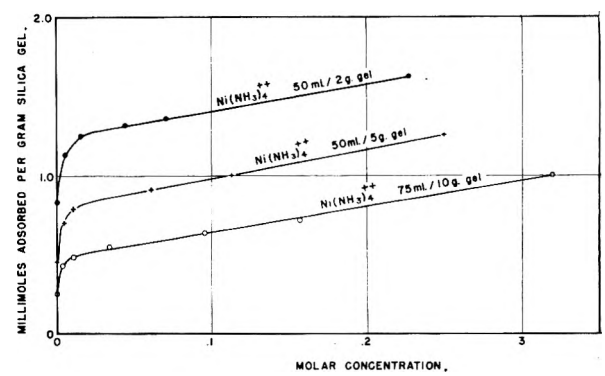

Fig. 6.—Adsorption of nickel–ammine solutions by silica gel.

(6) Ref. 5, pp. 316.

TABLE I

TABLE OF FORMATION CONSTANTS

Metal ion	log k_1	log k_2	log k_3	log k_4	log k_5	log k_6	Ref.
Ammonia complexes							
Zinc	2.18	2.25	2.31	1.96			7
Copper	3.99	3.34	2.76	1.97			7
Cobalt	1.99	1.51	0.93	0.64	0.06	−0.74	7
Nickel	2.67	2.12	1.61	1.07	0.63	−0.09	7
Silver	3.23	3.83					
Ethylenediamine complexes							
Zinc	5.92	5.15	1.86				8
Cobalt	5.93	4.73	3.03				9
Nickel	7.60	6.48	5.03				10
Copper	10.76	9.37					10
Diethylenetriamine complexes							0
Copper	16.0	5.3					11
Nickel	10.7	8.3					11
Zinc	8.9	5.5					11
Cobalt	8.1	6.0					11

zinc, cobalt and nickel, have three values shown for the formation constants indicating six-coördinate systems. Only two values for the copper complex indicates a four-coördinate system. In this series the six-coördinate systems are all adsorbed to a greater extent than the four-coördinate copper ion.

For diethylenetriamine complexes there seems to be a fair correlation, *i.e.*, the greater the stability (as indicated by higher formation constants), the higher the adsorption. This trend seems to be reversed for the ethylenediamine series, however, and no correlation is evident for the series of ammonia complexes.

For a simple adsorption system, one can change the amount of adsorbent or the amount of solution in contact with an adsorbent and still get points falling on one adsorption isotherm. The curves of Figs. 5 and 6 show that for the adsorption of copper and nickel ammines on silica gel, this is not the case. It appears that variations in the ligand: metal ion ratio adsorbed were such that one reaches a different equilibrium state when the amount of

TABLE II

Empirical composition	Wave length of peak Before ads.	Wave length of peak After ads.	E Before ads.	E After ads.	Ligand/metal ion ratio ads.[a] A	Ligand/metal ion ratio ads.[a] B	pH Before ads.	pH After ads.	Molar concn. after adsorption[b]
Cu^{++}	815	815	14.80	14.80	..	..	2.60	2.60	0.0400
$Cu(NH_3)_1^{++}$	755	765	21.75	19.60	3.9	6.3	4.48	4.43	.0378
$Cu(NH_3)_2^{++}$	700	715	30.50	26.00	3.5	4.9	5.23	5.02	.0339
$Cu(NH_3)_3^{++}$	655	675	40.00	33.00	4.1	4.8	5.95	5.45	.0282
$Cu(NH_3)_4^{++}$	600	645	50.00	39.70	5.7	6.1	6.70	5.95	.0267
$Cu(en)_1^{++}$	655	665	30.50	28.60	3.0	4.9	4.95	4.76	.0388
$Cu(en)_2^{++}$	555	560	60.00	49.25	2.3	4.3	6.51	5.46	.0345
$Cu(dien)_1^{++}$	610	610	52.95	64.80	1.0	..	5.33	4.67	.0383
$Cu(dien)_2^{++}$	580	580	81.00	89.75	2.0	..	7.96	6.43	.0211

[a] Column A, calculated from shift in wave length; column B, calculated from decrease in E. [b] Concentration before adsorption was 0.0400 M.

data. However, there is considerable doubt that the nickel tetraamine is tetrahedral. If it is actually octahedral, the position of this ammine in the adsorbability series appears reasonable. In this case, the other two positions in the octahedral arrangement would be occupied by water molecules, and the relatively lower adsorption of the nickel ammine would be satisfactorily accounted for.

The way a complex ion is oriented on the silica surface probably depends not only upon its shape but also upon the inter-atomic spacings. If the hydrogen-bonding theory applies, the number of hydrogens able to make contact with a "flat" surface is probably of less importance than the number of hydrogens spaced properly to form good hydrogen bonds with the surface oxygen atoms.

The stability of the entity should also be an important factor controlling the amount of metal complex adsorbed. Table I shows the logarithms of the stepwise formation constants of the indicated complex ions. The ethylenediamine complexes of solution or the amount of silica gel were changed. The copper–ammine adsorption curves are somewhat closer together than those of the nickel–ammines. This no doubt is due to the fact that the copper–ammine complex is more stable than the nickel–ammine complex. This is indicated by the formation constants. There must be some dissociation of the complex entities during adsorption in order to reach a different equilibrium state by varying the weight of adsorbent or volume of solution.

By comparing the absorption spectra of the copper complex solutions after contact with silica gel with those of the original solutions, changes undergone in the complex ions during adsorption are revealed. In the case of the copper ammines, the adsorption process causes the maximum absorption peak to be shifted to higher wave lengths and the maximum absorption value to decrease. This indicates that the ammonia:copper ion ratio adsorbed is somewhat higher than that of the primary complex species initially in solution. Dissociation of the complex metal ion has apparently occurred while in contact with the silica gel. Whether the dissociation of the complex ion has taken place at the surface of the silica gel or in the bulk solution is not revealed, but it is probably a combination of both.

Table II shows the changes in wave length and molar extinction coefficient E during the adsorption process along with an empirical value of the ratio of

(7) J. Bjerrum, "Metal Ammine Formation in Aqueous Solution," P. Haase and Son, Copenhagen, 1941, p. 289.

(8) J. Bjerrum and P. Anderson, *Kgl. Danske Vikenskab. Math-Fys Medd.*, **11**, No. 582 (1931).

(9) L. J. Edwards, Doctors Dissertation, University of Michigan, 1950.

(10) F. Basolo and R. K. Murmann, *J. Am. Chem. Soc.*, **74**, 2373 (1952).

(11) J. E. Prue and Schwarzenbach, *Helv. Chim. Acta*, **33**, 963 (1950).

the ligand:metal ion adsorbed. These ratios were calculated by linear interpolation by considering shifts in the wave lengths and also by considering changes in the molar extinction coefficients during adsorption. These two methods give quite different values in some cases, but when one considers that for most of these systems, the absorption maximum is not too sharply defined, some differences would be expected.

The values calculated using the shift in wave length method were made by observing the change in the maximum absorption peak with reference to the center of the peak before and after adsorption. The first value for the copper–ammine and ethylenediamine complexes is somewhat out of line with the other values since the absorption maximum of the aquated copper ion is very poorly defined. The more stable a given complex ion (Table I), the nearer this ratio approaches the value of the primary complex species initially in solution.

The increase in the molar extinction coefficient after adsorption for the copper diethylenetriamine series is unexpected. There is also a widening of the entire absorption maximum.

The *p*H values show that in all cases there is a lowering of *p*H with adsorption, but the extent of this lowering follows no simple relationship. The *p*H of the solutions would not be expected to change much since a rather large quantity of ammonium nitrate is present in the systems.

INTERMEDIATE ORDER HETEROGENEOUS CATALYSIS AND HEATS OF ADSORPTION

BY JOHN FOSS

Department of Chemistry, University of Utah, Salt Lake City, Utah

Received February 23, 1956

An explicit relationship, based on a simple model, is developed between the heat of adsorption of a reactant on a surface and the experimental energy of activation for the unimolecular reaction on that surface. Numerical values are calculated for the decomposition of ammonia on tungsten.

Introduction

In the literature of heterogeneous catalysis there appears to be no simple discussion concerning the relationship between experimental heats of adsorption and catalysis other than for the limiting cases of first and zero order reactions.[1] For the former the experimental energy of activation is usually stated as being equal in magnitude to the difference in energy between the activated state and the gaseous reactant. For the latter it is this same quantity, plus the heat of adsorption of the reactant at full surface coverage. However, actual catalytic studies will in general not take place in one of these limiting regions but rather in an intermediate order region. In this paper the relationships between experimental heats of adsorption and activation energies are presented in a form simple enough to permit use. The present paper is limited to unimolecular reactions.

On the assumption that the rate-controlling step is the reaction of the adsorbed species on the surface we have, from absolute reaction rate theory for a simple unimolecular reaction[2]

$$v = \frac{kt}{h} c_a \frac{f^{\ddagger}}{f_a} e^{-(\epsilon_0 + \epsilon)/kT} \backsimeq \frac{kt}{h} c_a e^{-(\epsilon_0 + \epsilon)/kT}$$

where

c_a = concn. of adsorbed molecules in no. per square cm.
f = partition function for the transition state per square cm.
$f_a{}^{\ddagger}$ = partition function for the adsorbed gas per square cm.
ϵ_0 = height of the highest energy barrier above the ground state of the initial gaseous reactant
ϵ = the heat of adsorption of the reactant

(1) K. J. Laidler, "Catalysis," Vol. I, ed. by P. H. Emmett, Reinhold Publ. Corp., New York, N. Y., p. 135.

(2) S. Glasstone, K. J. Laidler and H. Eyring, "The Theory of Rate Processes," McGraw-Hill Book Co., New York, N. Y.

Now $c_a = L\theta$ where L is the number of sites per square centimeter on the uncovered surface (around 10^{15}) and θ is the fraction of the surface which is covered. This in turn is given by

$$\theta = \frac{1}{1 + \frac{f_s}{f_a}\frac{F_g}{c_g} e^{-\epsilon/kT}} \backsimeq \frac{1}{1 + \frac{F_g}{c_g} e^{-\epsilon/kT}} \qquad (1)$$

where f_s is the surface partition function, F_g is the partition function per cubic centimeter of gaseous reactant, and c_g is the gas concentration in molecules per cc. We should note that in using this Langmuir type adsorption isotherm we are assuming a homogeneous surface, and are attributing decreases in heat of adsorption with coverage (such as introduced below in equations 4 and 5) to lateral interaction, or changes of the type suggested by Boudart.[3]

Combining our equations we then have

$$v = \frac{kT}{h} L \frac{\frac{c_g}{F_g} e^{-\epsilon_0/kT}}{1 + \frac{c_g}{F_g} e^{\epsilon/kT}} \qquad (1a)$$

The partition function F_g may be approximated by $K_1 T^{m-1}$ where K_1 is a constant dependent only on the mass and moment of inertia of the reactant gas. The gas concentration is given ideally by $K_2\, p/T$. Making these substitutions and taking the logarithm of (1a) gives

$$\ln v = \ln c' - \frac{3}{2}\ln T + \ln p - \frac{\epsilon_0}{kT} - \ln\left(1 + \frac{Kp}{T^m} e^{\epsilon/kT}\right) \qquad (2)$$

(where c' contains temperature independent terms and $K = K_2/K_1$).

(3) M. Boudart, *J. Am. Chem. Soc.*, **74**, 3556 (1952).

The experimental activation energy E, is given by

$$\frac{E}{kT^2} = \left(\frac{\partial \ln v}{\partial T}\right)_p = \left(\frac{\partial \ln v}{\partial T}\right)_{\epsilon,p} + \left(\frac{\partial \ln v}{\partial \epsilon}\right)_{T,p}\left(\frac{d\epsilon}{dT}\right)_p \quad (3)$$

The second term on the right takes into account variations in the heats of adsorption with coverage.

In order to evaluate (3) it is necessary to have some explicit functional relationship between the heat of adsorption and the coverage θ. There are two general equations which will fit a good portion of the experimental data now available, *viz.*

$$\epsilon = \epsilon_1 - S\theta^n \quad (4)$$

and

$$\epsilon = \epsilon_2 - C \ln \theta \quad (5)$$

where S and C are constants of the particular system under consideration and are assumed to be independent of temperature and pressure. ϵ_1 and ϵ_2 are the heats of adsorption at $\theta = 0$ and 1, respectively.

From (1) and (4) after simplification

$$\left(\frac{d\epsilon}{dT}\right)_p = \frac{Sn\theta^n(1-\theta)}{1 + \frac{S}{kT}n\theta^n(1-\theta)}\left[\frac{\epsilon}{kT^2} + \frac{m}{T}\right] \quad (6)$$

while (1) and (5) lead to

$$\left(\frac{d\epsilon}{dT}\right)_p = \frac{C(1-\theta)}{1 + \frac{C}{kT}(1-\theta)}\left[\frac{\epsilon}{kT^2} + \frac{m}{T}\right] \quad (7)$$

Considering first the non-logarithmic case and using (2) to obtain $\left(\frac{\partial \ln v}{\partial T}\right)_{\epsilon,p}$

$$\frac{E}{kT^2} = -\frac{(m-1)}{T} + \frac{\epsilon_0}{kT^2} + \frac{\theta\left(\frac{\epsilon}{kT^2} + \frac{m}{T}\right)}{1 + \frac{S}{kT}n\theta^n(1-\theta)} \quad (8)$$

$$\equiv -\frac{(m-1)}{T} + \frac{\epsilon_0}{kT^2} + g_n\theta\left(\frac{\epsilon}{kT^2} + \frac{m}{T}\right)$$

and

$$E = -(m-1)kT + \epsilon_0 + g_n\theta(\epsilon + mkT) \equiv E_1 + g_n\theta(\epsilon + mkT) \quad (9)$$

where E_1 is the activation energy for the first-order reaction, *i.e.*, the limiting value when θ approaches zero. Similar calculations lead in the case of logarithmic dependence to where λ is defined as

$$E = E_1 + \lambda\theta(\epsilon + mkT) \quad (10)$$

$$\lambda = \frac{1}{1 + \frac{C}{kT}(1-\theta)}$$

The remainder of this paper will be devoted to a consideration of the second term in (9) and (10) which we shall denote by E' for both equations. (That (9) and (10) do give the correct limiting values for first and zero reactions may readily be seen by a direct calculation of the limiting values for equation (1a). The limiting value of E' for the zero order case is $\epsilon + mkT$ and not ϵ as is usually assumed, and mkT is not always negligible.)

Functionally, for the non-logarithmic case $E' = E'(\theta,\epsilon,S,n,m)$. So that for any particular reactant–catalyst system for which (4) is known, m may be estimated and $E' = E'(\theta)$. Then using (1) and an appropriate partition function for the gas the relationship between p and θ may then be used to find $E' = E'(p)$. This will be done later for the case of the decomposition of ammonia on tungsten.

First we shall consider the simplest case of heat of adsorption variation with coverage, *viz.*, no variation. Though this case is probably never observed in practice it is useful because it leads to a method of calculating an approximate $\epsilon(\theta)$ relationship from the observed dependence of the experimental activation energy on pressure. With $\epsilon = \epsilon_1$ and for simplicity, $\epsilon_1 >> mkT$

$$E' = \epsilon_1\theta = \frac{\epsilon_1}{1 + \frac{F_g}{c_g}e^{-\epsilon_1/kT}} \quad (11)$$

Thus for a particular gas at a fixed temperature the dependence of E' on c_g (and therefore on pressure) may be calculated. Because it is inconvenient to require a separate graph for every temperature (11) may be modified and ϵ_1/kT used as a dimensionless parameter, giving

$$\frac{E'}{kT} = \frac{\epsilon_1/kT}{1 + \frac{F_g}{10^{16}p}e^{-\epsilon_1/kT}} \equiv \frac{X_1}{1 + \frac{F_g}{10^{16}p}e^{-x_1}} \quad (12)$$

where c_g is expressed in terms of pressure (mm.) at 900°K. A family of theoretical curves for E'/kT as a function of F_g/p using X as a parameter may be calculated. This is shown in Fig. 1.

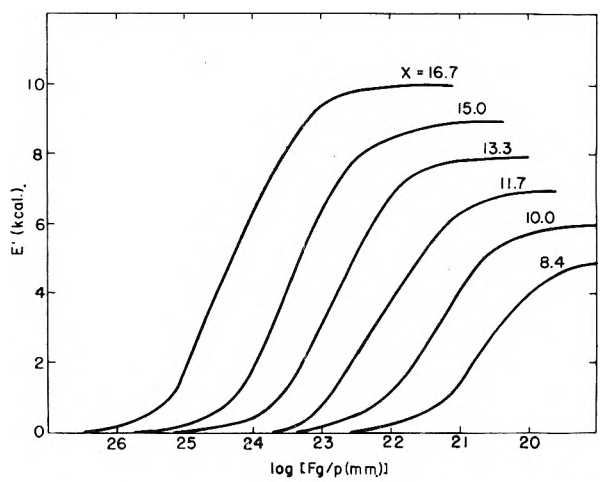

Fig. 1.

Let us consider the use of Fig. 1 for the case of a reactant whose heat of adsorption on the catalytic surface does not change with coverage. From the difference in the zero- and first-order activation energies we may determine ϵ_1/kT using the mean temperature at which the activation energy was determined. Knowing ϵ_1/kT, the variation of the experimental activation energy with F_g/p can be determined from the appropriate curve (and therefore the variation of the experimental activation energy with pressure, except for the additive constant $E_1 = \epsilon_0 + kT$).

For the more realistic case of the heat of adsorption varying with coverage the entire family of curves must be used, rather than just one as in the previous case. Knowing how E' varies with pressure permits calculation directly of how ϵ varies

with F_g/p (and indirectly therefore how it varies with coverage).

There is one final point of minor interest which may be seen from Fig. 1. Normally on increasing the pressure in the intermediate order region the activation energy would be expected to increase with pressure monotonically. However, if the heat of adsorption drops quite rapidly with coverage E' may actually decrease at some point before approaching the zero order activation energy—*i.e.*, there will be a maximum in $E'(p)$.

(A survey of Laidler's recent compilation of data on heterogeneous decompositions[4] showed only one reaction—that of phosphine on tungsten—exhibiting a maximum in $E(p)$. But an examination of the original literature ruled out even this case. However, in view of the small amount of really careful work which has been done in the field of heterogeneous catalysis it is not surprising that maxima of this sort have not as yet been observed. If such maxima are observable it will probably be for those systems where the heat of adsorption falls off very rapidly, *e.g.*, as log θ.)

Rather than use the somewhat awkward and indirect method described above to calculate $E'(p)$ from heat of adsorption data, we may return to the direct use of (9) and (10).

Since

$$\theta = \frac{1}{1 + \frac{F_g}{C_g} e^{-\epsilon/kT}} = \frac{\epsilon_1 - \epsilon}{\epsilon_1 - \epsilon_2} \equiv \frac{\epsilon_1 - \epsilon}{S} \qquad (13)$$

E' is of the form

$$E' = E'(T, \epsilon, p, F_g, S)$$

(where ϵ rather than θ has been chosen as the independent variable). Then with ϵ (θ) data for any particular gas (*i.e.*, F_g and S fixed) isotherms of E'-(p) can be plotted. (The simplest way to do this is to choose a range of heats and calculate the resulting pressures.)

The Ammonia-Tungsten System.—Using the ideas developed above let us consider the case of the ammonia decomposition on tungsten and see what predictions would be made from heat adsorption data.

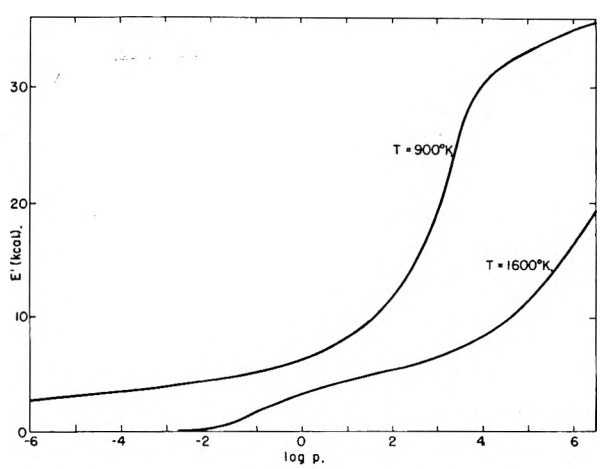

Fig. 2.

(4) K. J. Laidler, ref. 1, Chapter IV.

Wahba and Kemball[5] have measured the differential heat of adsorption at 21° of ammonia on evaporated tungsten films. The heat varies from 72.6 to 33.4 kcal. in going from zero to full coverage and may be fitted by a straight line to a very good approximation. Assuming that the heat of adsorption is relatively independent of temperature these data may be used for the high temperature decomposition on tungsten. (Differential heats of adsorption are known to be independent of temperature in at least some cases, *e.g.*, Beeck.[6])

With these data $E'(p)$ has been calculated at two temperatures, as shown in Fig. 2. All of the experimental work done has been carried out between these temperatures and in a pressure range of approximately 0.001 to 265 mm.

From Fig. 2 the following observations may be made

1. It appears that all of the work done on the ammonia decomposition was in the intermediate order region. The discrepancy between this conclusion and the experimental reports of approximately zero-order dependence can be explained in terms of a "compensated zero-order reaction" which will be discussed below.

2. The measured energy of activation for any given pressure should decrease with increasing temperature.

3. This difference between low and high temperature activation energies should increase with pressure, though not markedly in the pressure range studied. It should increase to as much as 8.5 kcal. in the highest pressure range experimentally studied.

Because of the wide variations in activation energies reported in the literature it is difficult to make comparisons with the predictions of Fig. 2. What can be said is that there are no disagreements with the qualitative predictions, except perhaps with point 1. And, in some cases there is some interesting, though very likely fortuitous, agreement. For example Kunsman,[7] finds a difference of about 12 kcal. between his low and high temperature activation energies compared with a predicted value of about 8.5 kcal. (at a pressure of 265 mm.).

The disagreement between predicted and observed orders may easily be rationalized by introducing the idea of "compensated zero reactions." Ideally, when a reaction is zero order the rate is completely independent of pressure. However, in actual practice, reactions are said to be zero order when there is only a small dependence of velocity on pressure. For example, Hinshelwood[8] labeled the ammonia decomposition on tungsten as zero order because a fourfold pressure increase (50–200 mm.) led to only a one third increase in the reaction velocity.

The velocity of a surface reaction will be proportional to the coverage. But in the intermediate order region θ is often not too sensitive to pressure.

(5) M. Wahba and C. Kemball, *Trans. Faraday Soc.*, **49**, 1351 (1953).

(6) O. Beeck, *Disc. Faraday Soc.*, **8**, 314 (1950).

(7) C. H. Kunsman, *J. Am. Chem. Soc.*, **50**, 2100 (1928).

(8) C. N. Hinshelwood and R. E. Burk, *J. Chem. Soc.*, **127**, 1105 (1925).

And, in addition, the increased activation energy often compensates for even this increase. For example on the 1600°K. isotherm, in going from 10 to 100 mm. pressure the coverage increases from approximately 0.25 to 0.35. But the activation energy increases from 4 5 to 5.5 kcal. so that the relative ratio of the two velocities will be

$$\frac{v_{100}}{v_{10}} = \frac{0.35e^{-5.5 \times 10^3/1.99 \times 1600}}{0.36e^{-4.5 \times 10^3/1.99 \times 1600}} = 1.02$$

Thus a tenfold pressure increase leads to only a 2% increase in velocity. Of course it is only by chance that the compensation is so complete. In the same pressure region on the 900°K. isotherm a tenfold increase actually leads to an 80% decrease in velocity. This would still probably be considered as an approximately zero-order reaction (though some explanation would very likely be proposed to account for the slight decrease in rate).

From this discussion there are a number of points which should be emphasized. First, it is not true that zero-order kinetics necessarily imply a saturation of the catalytic surface with reactant. In fact, in the author's opinion, there are probably very few cases of thermal decompositions in the 900°K. range where the surface becomes even as much as nine-tenths saturated. And very likely it is more often well under half covered because the heat of adsorption of ammonia at full coverage is as great as the heat of adsorption of many gases at zero coverage.

A second point to be emphasized is that the only way in which one can be reasonably certain of being in a region where the surface is very close to saturation is to measure the activation energy as a function of pressure over as wide a pressure range as feasible. If it remains constant, or approaches a limiting value, the surface is very likely close to saturation.

A third point is the importance of using initial rates rather than "half times" since the activation energy can change significantly as the pressure decreases. This is very important for the model used in the present paper in the 100–10,000 mm. region at 900°K. However, most studies of the ammonia decomposition fail to state what initial pressures were used; and at least one did not even report the temperature interval. Kunsman[7] found 45.3 and 43.2 kcal. activation energies for the reaction by the use of "half" and "quarter times," respectively.

Since the assumption of a surface having sites of uniform activity is probably a poor one, it would be of interest to carry out similar calculations for a heterogeneous surface and see how this affects Fig. 2. At present this is being done for the simple case of a linear variation in activity of the surface sites. In addition the relationship between this work and that of Brunauer, Love and Keenan[9] will be discussed in a future paper.

The author would like to express his appreciation of financial support from the California Research Corporation and acknowledge many helpful discussions with Drs. Antonino Fava and Izumi Higuchi.

(9) S. Brunauer, K. S. Love and R. G. Keenan *J. Am. Chem. Soc.* **64**, 751 (1942).

NOTES

THE Fe(II)–Tl(III) REACTION AT HIGH CHLORIDE CONCENTRATION

By Frederick R. Duke and Bernard Bornong

Contribution No. 402 from the Institute for Atomic Research and Department of Chemistry, Iowa State College, Ames, Iowa[1]

Received October 13, 1955

The reaction between Tl(III) and Fe(II)[2a] has been shown to be retarded by chloride.[2b] This is readily explained in terms of the prior equilibrium[3]

$$Tl(III) + Fe(II) \rightleftharpoons Fe(III) + Tl(II) \qquad (1)$$

followed by the slow reaction

$$Tl(II) + Fe(II) \longrightarrow Fe(III) + Tl(I) \qquad (2)$$

in conjunction with the associated equilibria, $Ti(III) + Cl^- \rightarrow TlCl^{+2}$, $TlCl_2^+$ and higher complexes.[4]

(1) Work was performed in the Ames Laboratory of the Atomic Energy Commission, Iowa State College, Ames, Iowa.

(2) (a) C. E. Johnson, *J. Am. Chem. Soc.*, **74**, 959 (1952); (b) O. L. Forchheimer and R. P. Epple, *ibid.*, **74**, 5772 (1953).

(3) K. G. Ashurst and W. C. E. Higgonson, *J. Chem. Soc.*, 3044 (1953).

(4) R. Benoit, *Bull. soc. chim. France*, **5**, [6] 518 (1949).

However, since chloride is usually a catalyst for such reactions in the absence of a prior equilibrium, it is of interest to determine the effect of high chloride on the rate, particularly in view of the work on the Tl(I)–Tl(III) exchange where chloride has a retarding effect at low concentration and then a catalytic effect at higher concentrations.[5]

Experimental

The Tl(III) and Fe(II) perchlorates were prepared as described by Forchheimer and Epple.[6] C.P. HCl was used, as well as C.P. LiCl, for maintaining ionic strength and acidity. $LiClO_4$ was prepared by dissolving C.P. LiOH in C.P. $HClO_4$.

The appropriate amounts of reagents were added to a volumetric flask in a constant temperature bath (25°) to make the final concentration of Fe(II) = 0.095 *M*, Tl(III) = 0.05 *M*, $[Cl^-]$ varying from 0.2 to 2.0 *M*, $[H^+]$ = 2.50 *M*, and μ = 3.30. The method of analysis used was to measure the absorbancy at 430 mμ, where the ferric chloride complex absorbs. The absorbancy index of the Fe(III) for a particular solution was taken from the "infinite time" value of the absorbancy. Since TiCl precipitates at these

(5) G. Harbottle and R. W. Dodson, *J. Am. Chem. Soc.*, **73**, 2442 (1951).

(6) O. L. Forchheimer and R. P. Epple, *Anal. Chem.*, **23**, 1445 (1951).

concentrations, the solution was filtered just before measuring the absorbancy.

Results and Discussion

Second-order plots, first order in each Tl(III) and Fe(II) yielded straight lines up to 60–65% of complete reaction; presumably the deviation at higher reaction percentages is the result of prior equilibrium (1). The slope of the straight line portions of the second-order plots were compared with the results taken from the graph in the paper by Forchheimer and Epple.[2] The results are presented in Figure 1. It is evident that a minimum in the rate of reaction occurs between chloride concentration of 0.1 and 0.2 *M*. Then the curve rises steeply and levels off between 1.5 and 2 *M* chloride. The conclusion drawn is that Tl(II) must complex chloride for the following reasons:

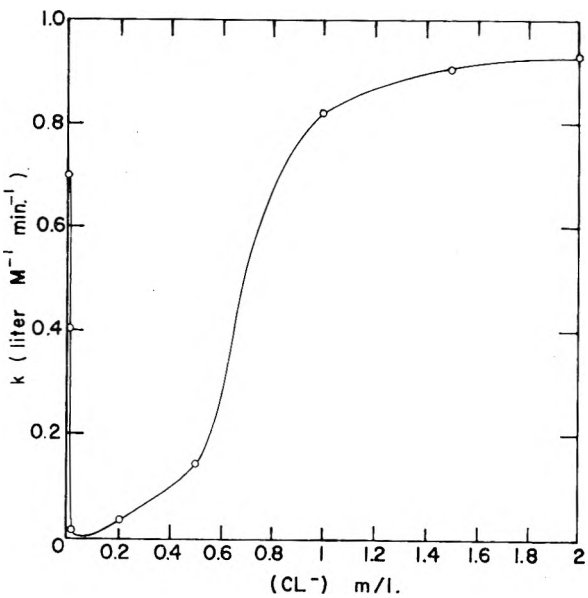

Fig. 1.—Effect of chloride on the second-order rate constant for the Fe(II)–Tl(III) reaction.

1. Fe(III) does not associate with chloride sufficiently to increase the equilibrium concentration of Tl(II) in reaction (1) to the extent indicated by the data in Fig. 1.

2. Reaction (2) does not appear to be strongly catalyzed by free chloride ion, because the leveling off at high chloride ion concentrations would not be expected from participation of chloride merely in the activated complex.

3. The only other alternative is to allow the formation of Tl(II)–Cl^- complexes with a stability somewhat less than that of the Tl(III)–Cl^- complexes.

This interpretation of the data serves to explain the Cl^- effect on the Tl(I)–Tl(III) exchange.[5] Consider the reaction $TlCl^{+2} + Tl^+ \rightleftarrows Tl^{+2} + TlCl^+$. If the dissociation of $TlCl^+$ is slow compared with the reverse of the indicated reaction, the equilibrium would be largely non-exchanging. When the $[Cl^-]$ reaches the point that the reaction is $TlCl_2^+ + Tl^+ \rightleftarrows TlCl^+ + TlCl^+$, the exchange rate should increase, particularly if the slow reaction is Cl^- catalyzed.

THE RELATION OF FORCE CONSTANT TO ELECTRONEGATIVITY AND COVALENT RADIUS

By R. L. Williams

Ministry of Supply, E. R. D. E., Waltham Abbey, England

Received December 13, 1955

Numerous attempts[1] have been made to relate force constants with interatomic distance, of which perhaps the best known are Badger's and Gordy's rules. In the case of the latter, the force constant, k_{AB}, of the bond between the atoms A and B, is given by the equation

$$k_{AB} = aN(x_A x_B/d^2)^{3/4} + b \qquad (1)$$

where a and b are constants, N is the order of the bond between A and B, d, the internuclear distance, and x_A, x_B the electronegativities. This equation is of interest since it involves the electronegativities of atoms A and B. However, it is difficult to understand why the force between two atoms should be a function of the product of electronegativities, when most physical and chemical properties, *e.g.*, dipole moment, have been shown to be related to their difference.

If the logarithm of the electronegativity[2,3] of elements in Groups IV to VII is plotted against the logarithm of the corresponding covalent radius[2,3] divided by the number of its valence electrons, a good straight line is obtained, Fig. 1, corresponding to the equation

$$x_A = 0.761(z_A/r_A)^{0.70} \qquad (2)$$

where r_A is the covalent radius and z_A the number of valence electrons. A similar equation, *viz.*

$$x_A = 0.31(z_A + 1)/r_A + 0.50 \qquad (3)$$

has been derived by Gordy.[3] However, if (2) is used to substitute for electronegativity in Gordy's rule, (1), it is found that

$$k_{AB} = A(z_A z_B)^{0.525} \times d^{-2.525} + 0.30 \qquad (4)$$

where $A = 1.058aN$, provided that

$$(r_A r_B)^{0.525} = (r_A + r_B)/2 = d/2$$

which is a very good approximation for the range of possible values of covalent radii.

It can be seen that (4) is of the form of an equation put forward by Guggenheimer[4]

$$k_{AB} = A'(z_A z_B)^{0.5} \times d^{-2.46}$$

Consequently, Gordy's result that the force constant between two atoms depends on the product of electronegativities, is accidental. The main factors determining the force constant are the covalent radius and the number of valence electrons of each atom. Electronegativity enters the force constant equation only because it is a simple function of both these quantities. It may also be noted that (1) on substitution with Gordy's second equation, (3), does not go over easily into Guggenheimer's equation.

(1) For a recent summary: H. O. Pritchard and H. A. Skinner, *Chem. Revs.*, **55**, 745 (1955).

(2) L. Pauling, "The Nature of the Chemical Bond," 2nd edn., Cornell University Press, Ithaca, N. Y., 1948.

(3) W. Gordy, *Phys. Rev.*, **69**, 604 (1946).

(4) K. M. Guggenheimer, *Proc. Phys. Soc.*, **58**, 346 (1946).

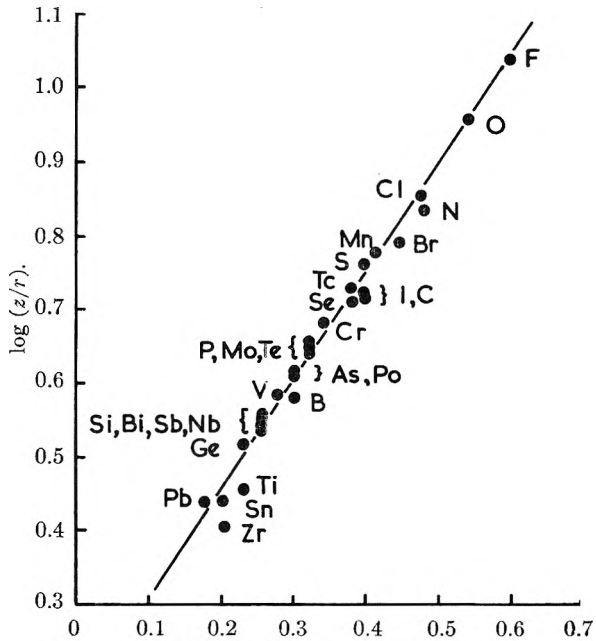

Fig. 1.

The extension of this treatment to the remaining elements is made difficult by the problem of deciding what constitutes the "covalent" radius of these elements. Gordy used Pauling's values[2] of tetrahedral covalent radii to establish (3), but it is doubtful whether these radii are covalent radii in the same sense as those of the more electronegative elements, since the former have been derived from crystal lattice distances.

I acknowledge with gratitude the award of a Senior Research Fellowship from the Ministry of Supply. Thanks are also due to Dr. L. J. Bellamy for several helpful discussions.

NEUTRON EMISSION FROM ACTINIUM FLUORIDE

By K. W. Foster and J. G. Stites, Jr.

Mound Laboratory, Monsanto Chemical Company,[1] Miamisburg, Ohio

Received January 18, 1956

One of the methods developed to prepare the element actinium is the reduction of actinium fluoride with lithium.[2] Since fluorine is an excellent neutron producer when bombarded by α-particles,[3] and since actinium 227 and many of its daughter products are α-emitters, it is to be expected that actinium fluoride would be naturally neutron active. Likewise, it is to be expected that any appreciable fluorine traces in metallic actinium would result in detectable neutron emission. Therefore, a study of the neutron yield from actinium fluoride was made, and from the data obtained in this study a method was developed whereby the purity of actinium samples could be determined by neutron counting techniques.

Pure actinium 227 is only mildly alpha active since 99% of the material decays by β-emission, but the intensity of α-emission grows considerably as the various radioactive daughters accumulate. Accordingly, the intensity of neutron emission from any light element impurity should grow as more and more of the active daughters are formed.

The actinium alpha growth was computed from the available nuclear data.[4] The neutron growth was then determined from this alpha growth and from the fluorine neutron yields at the various α-particle energies in the actinium decay chain.[5,6] A correction for the limited volume of fluorine that is available for nuclear reaction was applied,[7] and it was found that the theoretical neutron emission rate for 17.4 mg. of actinium fluoride (corresponding to one curie of actinium 227) should grow from about 1,000 neutrons per second immediately after separation of the actinium from its daughters to a maximum of 1.07×10^6 neutrons per second after 180 days.

A sample of actinium fluoride, weighing 0.77 mg., was prepared by adding an aliquot of actinium chloride solution to 24% hydrofluoric acid in a special Teflon centrifuge tube. This tube was constructed in such a manner that a small molybdenum cup, pressure sealed to the Teflon, formed the bottom of the tube. The precipitate was centrifuged into this container, and the container and its contents were removed from the centrifuge and dried. The container was then closed with a special lid, and the assembly was sealed by an even coating of nickel which was deposited from the thermal decomposition of nickel carbonyl. The sealed assembly was then neutron counted periodically for approximately four months. During this period the radioactivity content was determined by periodic calorimetric analysis.

The sample was found to contain 0.044 curie of actinium, and it attained a maximum neutron count of 53,400 ± 600 neutrons per second. Thus, the neutron emission rate from actinium fluoride was found to be 1.21×10^6 neutrons per second per curie of actinium in equilibrium with its daughter products. This compares favorably with the theoretical value of 1.07×10^6 neutrons per second per curie.

Both these values are subject to errors which may be quite large. The theoretical value is based on some rather uncertain neutron yields in the higher α-energy range, and the relation that was used to correct for a finite fluorine volume is empirical and has never been determined accurately for fluorine and actinium. The theoretical value may be wrong by as much as a factor of 2.

The experimental value suffers from the fact that the neutron emission rates were determined by comparing the sample with a radium–beryllium standard neutron source. There is no assurance that the actinium–fluorine neutron energy spectrum is sufficiently similar to the radium–beryllium neutron energy spectrum to give the same over-all detector efficiency. In addition, the ab-

(1) Mound Laboratory is operated by Monsanto Chemical Company for the United States Atomic Energy Commission under Contract Number AT-33-1-GEN-53.

(2) J. G. Stites, M. L. Salutsky and B. D. Stone, *J. Am. Chem. Soc.*, **77**, 237 (1955).

(3) H. L. Anderson, "Neutrons from Alpha Emitters," Preliminary Report No. 3, NP-851, December, 1948.

(4) Circular 499, National Bureau of Standards, September 1, 1950.

(5) G. T. Seaborg and I. Perlman, *Revs. Mod. Phys.*, **20**, 585 (1948).

(6) E. Segre and C. Wiegand, "Thick-Target Excitation Functions for Alpha Particles," MDDC-185, September 15, 1944.

(7) O. Sisman, "Development of a Process for Production of Radium-Beryllium Sources," Final Report CNL-17, p. 4, January 28, 1948.

solute value of the standard is not known closer than ± 10%. Therefore, the actinium fluoride neutron emission rate determined experimentally is probably no better than ± 15 to 20%.

However, since the neutron emission from the fluoride sample, and the theoretical growth curve agreed quite closely over the growth period, and since the theoretical and experimental maximum values are of the same order of magnitude, one can conclude that the values that were used for computation are approximately correct, and the neutron yields obtained by extrapolation from data in reference six are not unreasonable. Thus, the use of neutron counting techniques for quantitative detection of trace quantities of fluorine in actinium appears feasible. There seems to be no serious objection to extending the technique to the detection of fluorine or other light elements, such as beryllium or boron, in any of the alpha-active heavy elements.

We wish to acknowledge the assistance of Mr. R. D. Joyner and Mr. S. R. Orr, who found time between their regular duties to prepare the actinium fluoride and to perform the calorimetric assay. We are also grateful to Dr. H. W. Schamp for his assistance with the sealing problem.

THE INFRARED SPECTRA OF THREE ALUMINUM ALKOXIDES

By Donald L. Guertin, Stephen E. Wiberley, Walter H. Bauer and Jerome Goldenson

Contribution from the Walker Laboratory of Rensselaer Polytechnic Institute, Troy, N. Y., and The Chemical and Radiological Laboratories Army Chemical Center, Maryland

Received January 25, 1956

Infrared absorption near 990 cm.$^{-1}$ in aluminum di-soaps was ascribed to the aluminum–oxygen linkage by Scott, *et al.*[1] Ludke, *et al.*,[2] later showed that this band was associated with the aluminum–oxygen–aluminum linkage rather than the aluminum–oxygen–carbon linkage. To verify this correlation, it appeared of value to investigate the infrared spectra of several aluminum alkoxides. The spectra of aluminum isopropoxide has previously been reported[3] but the spectra of the two other alkoxides discussed in this paper are not available. The present work indicates that aluminum–oxygen–carbon linkages give rise to absorption between 1028 to 1070 cm.$^{-1}$.

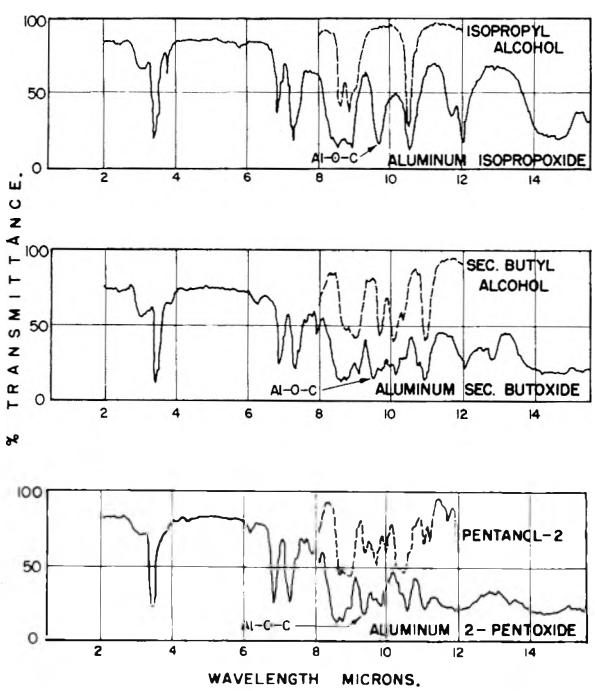

Fig. 1.—Infrared spectra of three aluminum alkoxides.

Experimental

Alcohols.—Alcohols were stored over Drierite for two weeks, filtered and distilled from calcium hydride. The boiling points and infrared spectra agreed with reported data.[4]

Preparation and Analysis of Alkoxides.—The alkoxides were prepared according to directions in Organic Reactions.[5] The boiling points of the alkoxides and analytical results for per cent. aluminum are presented in Table I.

TABLE I

ANALYSIS OF ALUMINUM ALKOXIDES

Alkoxide	B.p., °C. (mm.) Lit.[6]	B.p., °C. (mm.) Found	Al, % Calcd.	Al, % Found
Isopropoxide	140.5 (8)	140 (10)	13.21	13.22
Sec. Butoxide	180–181.5 (8)	160 (10)	10.95	11.03
2-Pentoxide	....	140–150 (10)	9.35	9.20

Infrared Absorbance Measurements.—Infrared spectra were obtained on a Perkin–Elmer Model 21 double beam recording infrared spectrometer equipped with rock salt optics. Alcohols were measured in a demountable liquid cell without a spacer. Liquid alkoxides were measured in a fixed liquid cell with a 0.025 mm. spacer and in a demountable liquid cell without a spacer to resolve strong bands. Nujol mulls of the solid alkoxides were measured in a demountable liquid cell without a spacer. Potassium bromide windows[7] of the solid alkoxides were also prepared, but hydrolysis of the alkoxides occurred in these cases.

Results and Discussion

The infrared spectra of the alkoxides and the spectra of the corresponding alcohol in the region of 8 to 12 μ are shown in Fig. 1. Table II presents the frequencies assigned to the Al–O–C linkage in the alkoxides studied.

TABLE II

FREQUENCIES (CM.$^{-1}$) ASSOCIATED WITH THE Al–O–C LINKAGE IN THREE ALKOXIDES

Alkoxide	Assignment, cm.$^{-1}$
Aluminum isopropoxide	1033
Aluminum *sec*-butoxide	1058
Aluminum 2-pentoxide	1070

(1) F. A. Scott, J. Goldenson, S. E. Wiberley and W. H. Bauer This Journal, **58**, 61 (1954).

(2) W. O. Ludke, S. E. Wiberley, J. Goldenson and W. H. Bauer, *ibid.*, **59**, 222 (1955).

(3) J. V. Bell, J. Heisler, H. Tannenbaum and J. Goldenson, *Anal. Chem.*, **26** 1720 (1953).

(4) Am. Petroleum Inst., Research Project 44, Carnegie Institute of Technology, "Catalog of Infrared Spectral Data," 1950: Spectrograms 428, 431 and 436.

(5) R. Adams, editor-in-chief, "Organic Reactions" Vol. II, John Wiley and Sons, Inc., New York, N. Y., 1944, p. 198.

(6) "Beilsteins Handbuch der organischen Chemie," Band 1, Vierte Auflage, 1943.

(7) M. M. Stimson and M. J. O'Donnell, *J. Am. Chem. Soc.*, **74**, 805 (1952).

As can be noted from Table II the frequency shifts with change in inductive effect of the alkane substituent.

According to Ingold's[8] theory the alkyl groups concerned can be listed in order of electron releasing ability as

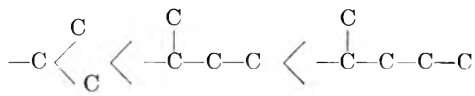

As the oxygen becomes more negative, the Al–O bond strength increases and the frequency increases.

Fichter[9] has assigned the Al–O–Al frequency in hydrated aluminum oxide to the region 945–980 cm.$^{-1}$. In the case of silicon and phosphorus the Si–O–C and P–O–C frequencies are higher than the corresponding Si–O–Si and P–O–P frequencies. It is evident then that the assignment by Ludke, *et al.*,[2] of the band at 990 cm.$^{-1}$ in aluminum soaps to an Al–O–Al type linkage is strengthened further by this study of the alkoxides.

Acknowledgment.—This study was conducted under contract between the Chemical Corps, U. S. Army, and Rensselaer Polytechnic Institute.

(8) C. K. Ingold, "Structure and Mechanism in Organic Chemistry," Cornell Univ. Press, Ithaca, N. Y., 1953.
(9) R. Fichter, *Helv. Phys. Acta*, **19**, 21 (1946).

ON THE DETERMINATION OF THE AUTOPROTOLYSIS CONSTANT OF ETHANOL

By L. M. Mukherjee

Physical Chemistry Laboratory, University College of Science and Technology, Calcutta, India

Received February 3, 1956

The autoprotolysis constant of liquids such as water, ethanol or the like is a significant quantity in so far as the ionization of acids and bases in them is concerned, for the ionization of an acid in such solvents is considered to proceed as

$$HX + H_2O \text{ (or EtOH)} \longrightarrow H_3O^+ \text{ (or } EtOH_2^+) + X^-$$

in which the solvent takes up the proton from the acidic solute, thereby itself acting as a base. Toward a basic solute, on the other hand, such a solvent behaves in a relatively acidic fashion, by parting with the proton available from it. This inherent property of the solvent acts in such a way that, besides the effect of the dielectric constant of the medium, usually a decreased basicity (*i.e.*, basic character) decreases the ionization of the acid but increases the acidity of the solution because the ionization takes place only as a result of the transfer of a proton from a weaker to a firmer binding. The properties of a base should depend upon the acidity (acidic character) of the solvent in an analogous manner. Thus, the range of acidities that may be investigated in a given solvent decreases as the autoprotolysis constant increases.

The present communication is a report of the results derived from the determination of the value for the autoprotolysis constant of ethanol. The purity and dryness of the ethanol was characterized by ultraviolet spectrophotometry.[1] Previous investigations[2] for the purpose of finding out this constant do not indicate the state of purity and dryness of the sample of ethanol used; moreover, some of the assumptions made, such as the consideration of the conductance ratio to give the activity coefficient, cannot be justified. Electrometric procedures had not been designed to eliminate the uncertain junction potential which is found to be present in practically all the measurements so far undertaken. Again, measurement of the conductivity of such liquids, being too sensitive to the presence of impurities, does not appear to be reliable.

The set of measurements outlined below involves titration of HCl solutions in ethanol at two different initial concentrations against NaOEt solution in ethanol, with the help of the cell

$$Pt/H_2;\ HCl/EtOH;\ Ag/AgCl$$

following the method of Hammett and Dietz[3] employed in the determination of the self ionization constant of formic acid, when used as a solvent. The value of the autoprotolysis constant has been calculated from the equation as

$$-\log K = \frac{E_{ab}}{2.303RT/F} - \log C_a \times C_b$$

where K is the autoprotolysis constant of ethanol; C_a, the concentration (molarity) of the unneu-

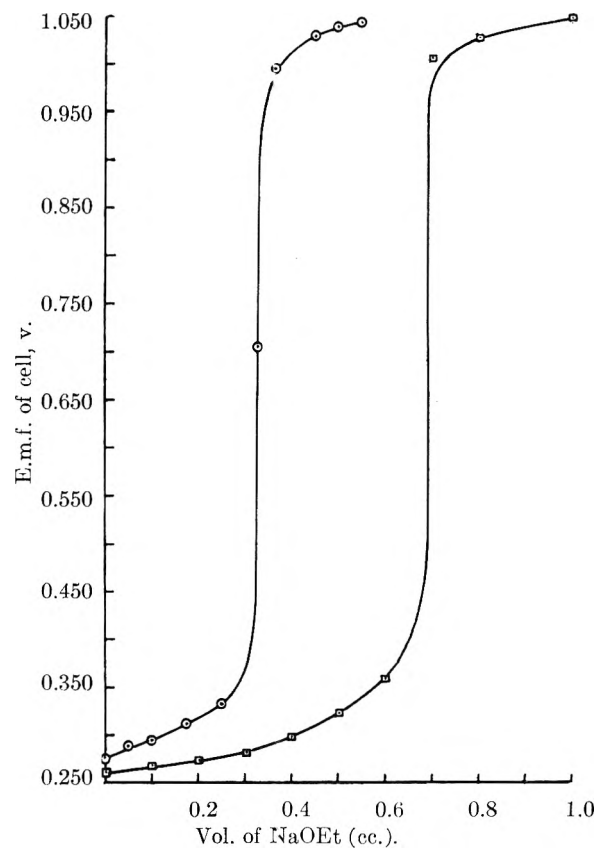

Fig. 1.—⊙, 0.0094 *N* HCl/EtOH titrated with 0.1240 *N* NaOEt/EtOH; ⊡, 0.0164 *N* HCl/EtOH titrated with 0.2525 *N* NaOEt/EtOH.

(1) L. M. Mukherjee, *Science & Culture (India)*, **19**, 314 (1953).
(2) (a) P. S. Danner and J. H. Hildebrand, *J. Am. Chem. Soc.*, **44**, 2824 (1922); (b) P. S. Danner, *ibid.*, **44**, 2832 (1922).
(3) L. P. Hammett and N. Dietz, *ibid.*, **52**, 4795 (1930).

tralized acid; and C_b, the concentration (molarity) of the base, NaOEt, present in excess at two points on the titration curve on either side of the equivalence showing a difference in e.m.f., represented by E_{ab}. The values of the autoprotolysis constant so derived are presented in Table I with the concencentrations of HCl solution used for the measurement. The actual titration curves are also given in the figure for reference.

TABLE I

Concn. of HCl, M	K, the autoprotolysis constant of ethanol
0.0094	1.7378×10^{-17}
0.0164	1.7783×10^{-17}

Thus, by eliminating the limitations of the method of measurement and securing a high state of purity of the sample of ethanol used, the value for the autoprotolysis constant, K, of the solvent is found to be 1.76×10^{-17}, which is, however, not in agreement with those obtained in the previous work[2a,b] consisting of e.m.f. as well as conductivity measurements.

My grateful thanks are due to Dr. S. K. Mukherjee of the Department of Applied Chemistry, University College of Science & Technology, Calcutta, for valuable suggestions and helpful criticism of the work and to Dr. A. K. Ganguly for kindly going through the manuscript.

TRIARYLBORON ANIONS. III. THE DISSOCIATION CONSTANT OF SODIUM TRIMESITYLBORON IN TETRAHYDROFURAN

BY TING LI CHU AND THEODORE J. WEISMANN

Department of Chemistry, Duquesne University, Pittsburgh, Pa.

Received February 13, 1956

The electrolytic conductance of sodium triphenylboron in ether solution has been studied by Bent and Dorfman[1] in the concentration range 10^{-6} to 10^{-3} M. However, the calculation of the dissociation constant of sodium triphenylboron from their conductance data is complicated by the fact that the ion-pairs of this compound associate to complex aggregates in ether solution.[2] On the other hand, sodium trimesitylboron has been shown to be monomeric in tetrahydrofuran solution, having one unpaired electron.[3] We have measured the conductances of a series of sodium trimesitylboron solutions in tetrahydrofuran over the concentration range 2×10^{-6} to 10^{-4} at 20.0 and 35.0° and calculated its dissociation constants by the Fuoss method.[4]

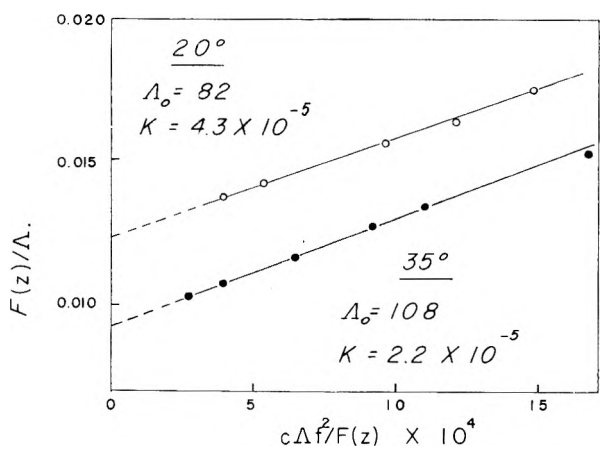

Fig. 1.—Fuoss plot for sodium trimesitylboron in tetrahydrofuran.

The calculation of the dissociation constant from the conductance data requires the dielectric constant and viscosity of the solvent. The dielectric constants of tetrahydrofuran reported as 7.58 and 7.16, respectively, at 20.0 and 35.0° were used.[5] The viscosities of tetrahydrofuran, measured with an Ostwald viscometer, are 5.09×10^{-3} and 4.34×10^{-3} poises at 20.0 and 35.0°, respectively.

The functions F/Λ and $cf^2\Lambda/F$, defined by Fuoss, were computed from the measured conductances and plotted in Fig. 1. In the concentration range studied, the Fuoss plots give linear relations. The extrapolation of these plots yields limiting equivalent conductances 82 and 108 at 20.0 and 35.0°, respectively. The ion-pair dissociation constants calculated from the slopes for

$$C_6H_3(CH_3)_3B^- Na^+ \rightleftharpoons C_6H_3(CH_3)_3B^- + Na^+$$

are 4.3×10^{-5} at 20.0° and 2.2×10^{-5} at 35.0°.

Experimental

The preparation of trimesitylboron and the purification of tetrahydrofuran have been described previously.[3]

Conductance measurements were made at 1000 cycles using a General Radio type 650-A impedance bridge with a Hewlitt-Packard audio oscillator as the source of oscillating current; bridge balance was detected by null point of an oscilloscope trace. Measurements repeated with an Industrial Instruments Model RC-168 conductivity bridge, claimed to be accurate within 1% in the range used, were in good agreement with those made with the more elaborate setup.

The Pyrex conductance cells were cylindrically shaped, about 3.5 cm. in diameter and 8 cm. in height, with 2 cm. diameter bright platinum electrodes of 4 mm. spacing having vacuum tight leads. Cell constants of the two cells used, determined in the usual manner with potassium chloride solutions using the reference values of Benson and Gordon,[6] were 0.08963 and 0.08455 cm.$^{-1}$ No significant change in the cell constants was observed over the temperature range 20.0 to 35.0°. A 25 cm. length of 11 mm. Pyrex tubing with ground joint, connected to the cells, adapted them for use under vacuum. A small tube was attached parallel to the conductance cell above a constriction in the 11 mm. tubing, 23 cm. from the base of the cell.

Solutions for the conductance measurements were prepared in the following manner. An aliquot of a stock solution of TMB in benzene was placed in the conductance cell and a piece of freshly cut sodium in the side tube. The solvent was evaporated on the vacuum line and the residue evacuated for 24 hours. Sodium was distilled into the neck of the conductance cell, slightly below the constriction. A measured amount of predried tetrahydrofuran was distilled into the cell and the latter sealed off. The cell was placed on a mechanical shaker and the resistance of the solution measured intermittently until constant in two successive measurements, when the reaction was considered complete. The cell was immersed in a thermostated oil-bath, which maintained a temperature constant to within

(1) H. E. Bent and M. Dorfman, *J. Am. Chem. Soc.*, **57**, 1924 (1935).

(2) T. L. Chu, *ibid.*, **75**, 1730 (1953).

(3) T. L. Chu and T. J. Weismann, *ibid.*, **78**, 23 (1956).

(4) R. M. Fuoss, *ibid.*, **57**, 488 (1935).

(5) F. E. Critchfield, J. A. Gibson, Jr., and J. L. Hall, *ibid.*, **75**, 6044 (1953).

(6) G. C. Benson and A. R. Gordon, *J. Chem. Phys.*, **13**, 473 (1945).

0.05°, and the resistance measured at 20.0 and 35.0°. The specific conductance of the solvent was negligible in comparison with that of the solution measured. The concentration of the solution was calculated by assuming that the trimesitylboron was converted quantitatively to sodium trimesitylboron, and that the volume of the solution does not differ appreciably from that of the pure solvent.

Acknowledgment.—The authors wish to thank the Research Corporation for the Frederick Gardner Cottrell grants which supported this work.

PHASE EQUILIBRIUM IN THE SYSTEM NiO–H_2O[1]

BY L. A. ROMO[2]

Department of Geochemistry, The Pennsylvania State University, University Park, Pa.

Received March 5, 1956

The isobaric decomposition of $Ni(OH)_2$ has been investigated by Hüttig and Peters at various temperatures.[3] They found that the hydroxide decomposes gradually at a constant pressure of 10 mm. giving a series of hydrates which are converted into NiO at a temperature of 230°. More recently, it has been reported that the complete conversion of the hydroxide into the oxide takes place at a slightly higher temperature.[4]

Since $Ni(OH)_2$ is used as a catalyst[5-7] in reactions at fairly high pressures as well as high temperatures, it is very important that some information be obtained on the phase equilibrium and stability relations of $Ni(OH)_2$ at various pressures and temperatures.

Experimental

The hydrothermal runs were made in "test-tube" bombs which are attachable to a high pressure source of water by means of suitable fittings.[8] They were heated to the desired temperature by means of furnaces provided with a temperature control.

The starting material used in all runs was $Ni(OH)_2$ prepared from $NiNO_3$ in solution by precipitation with 0.1 *N* NaOH. Crystallization of this material was obtained by treating it hydrothermally at 200° and 10,000 p.s.i. for a period of 3 days. Small amounts of the hydroxide were packed in small envelopes made of silver foil. These envelopes were dropped into the "test-tube" bombs which were then joined to the high water pressure pump and heated at the desired temperature at a given pressure. After several trials, it was found that 24-hour runs were adequate. The products obtained on quenching the bombs were examined by means of X-ray diffraction. The readings of temperature and pressure are believed to be accurate within the limits of ±5° and ±1 kg./cm.², respectively.

Results

(a) **Phase Equilibrium.**—In the system NiO–H_2O there are two components and three phases. This according to the phase rule gives a univariant 3-phase equilibrium system. The composition of the two phases is constant depending only on the water vapor pressure, thus, the phase equilibria relations can be represented by the p–t diagram. It is interesting to indicate that in some cases it was possible to determine the p–t values at which both NiO and $Ni(OH)_2$ coexisted in equilibrium with water vapor. This finding indicated that the univariant line represents the equilibrium boundary with a high degree of accuracy. It must be emphasized that in no case a conversion of NiO into $Ni(OH)_2$ was recorded, even in cases where long time (10 days) runs were made.

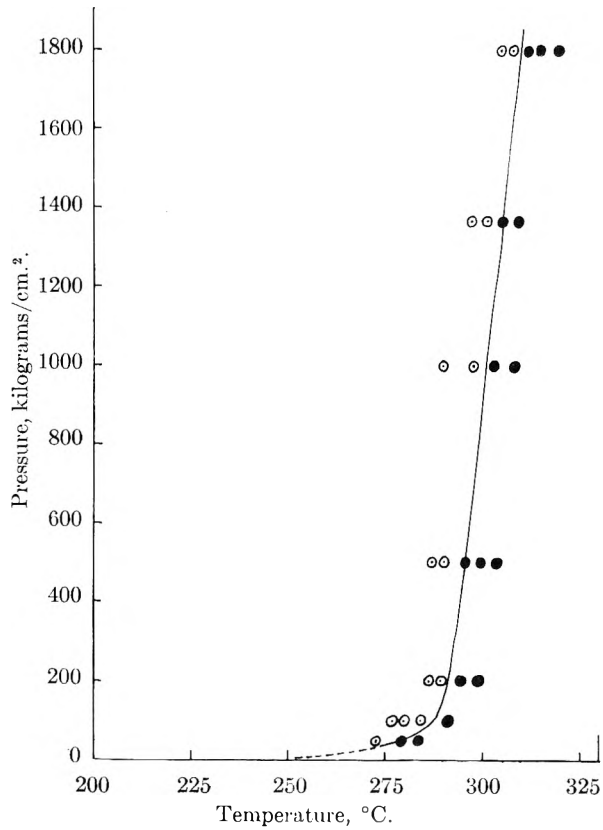

Fig. 1.—Phase equilibrium diagram of the system NiO–H_2O: ⊙, $Na(OH)_2$; ●, NiO.

The temperature of conversion of $Ni(OH)_2$ into NiO in open air as determined by differential thermal analysis is 255 ± 5°.

(b) **Heat of Reaction.**—The ΔH value was calculated by means of the Clapeyron–Clausius equation. The accuracy of the value calculated from this equation depends on two factors: (a) the accuracy of the dp/dT values, *i.e.*, the slope of the univariant curve and (b) the value of ΔV which is the change in molar volumes of the components of the system as a function of pressure and temperature. In this case, it can be stated that the $\Delta p/\Delta T$ at various values is highly accurate, their error being within the magnitude of the error of measurement of temperature and pressure. This is confirmed by the fact that it was possible to record p—t values where both phases coexisted in equilibrium. Changes in volume per gram of NiO and $Ni(OH)_2$ are not known. However, if one considers that the specific volume of H_2O changes considerably as the pressure and temperature are raised, it need not be considered

(1) The experimental work was carried out in the Department of Geochemistry, The Pennsylvania State University, University Park, Pennsylvania.

(2) Pigments Department, du Pont de Nemours, Wilmington, Delaware.

(3) G. F. Hüttig and A. Z. Peters, *Anorg. allgem. Chem.*, **189**, 183 (1930).

(4) A. Merlin and S. Teichner *Compt. rend.*, **236**, 1892 (1953).

(5) S. J. Vles, *Rec. trav. chim. Pays-Bas*, **46**, 743 (1925).

(6) K. Chakravarty and I. Ch. Ghosh, *J. Ind. Chem. Soc.*, **4**, 431 (1927).

(7) A. Quartaroli, *Gazz. chim. ital.*, **57**, 234 (1927).

(8) R. Roy and E. F. Osborn, *Econ. Geol.*, **47**, 717 (1952).

critical the comparatively small changes in specific volume of the solid phases. Values for the molar volumes of water vapor were obtained from the Handbook of Physical Constants (for $P < 100$ atm.)[9], and the tables given by Kennedy[10] (for $P > 100$ atm.). The value of $\Delta\bar{V}$ was defined as

$$\Delta\bar{V} = \bar{V}_{H_2O(g)} + \bar{V}_{NiO(s)} - \bar{V}_{Ni(HO)_2(s)}$$

The ΔH calculated from values of $\Delta p/\Delta T$ taken along a hydrothermal pressure range of 10 to 1800 kg./cm.^{2} with a corresponding temperature change of 250 to 310° is 12.0 ± 1.5 kcal. mole^{-1}.

Acknowledgment.—The author wishes to thank Dr. R. Roy for reading the manuscript.

(9) R. W. Goranson, "Handbook of Physical Constants," Geol. Soc. Am., Section 14, 211–212, 1942.

(10) G. C. Kennedy, *Am. J. Sci.*, **44**, 100 (1950).

NEGATIVE "NET" HEATS OF ADSORPTION[1]

By Donald Graham

Contribution No. 178 from Jackson Laboratory, E. I. du Pont de Nemours and Company, Wilmington, Delaware

Received March 8, 1956

Discussion.—The "net" heat of adsorption of a vapor on a solid is the difference between the heat of adsorption and the latent heat of condensation. The term was first used in the belief that liquefaction was the first step in adsorption.[2] We now know that this belief was incorrect but "net" heats are still widely reported and are useful when correctly interpreted. Negative values for the "net" heat were first observed in the adsorption of the first monolayer of water on charcoal, both by isosteric calculation[3a] and by calorimetry.[3b] Some confusion has arisen in the treatment of such negative "net" heats and a clearer understanding of the relations involved is needed.

Negative "net" heats of adsorption result from a combination of two conditions: (1) An adsorptive vapor with a latent heat of condensation higher than that heat of its adsorption which does not include interaction between adsorbed molecules. (2) Prevention (or at least severe limitation) of interaction between adsorbed molecules.

The widely discussed concept of a BET "*C*" constant less than unity as a criterion of negative "net" heat has failed to meet the test of experiment. Also, the type 3 isotherm associated with a fractional "*C*" constant represents strong lateral interaction. This concept is therefore in direct conflict with the required limitation of lateral interaction.

A second serious obstacle to understanding and general acceptance of negative "net" heats of adsorption has been the accompanying requirement that the entropy of the two-dimensional adsorbed film must be greater than that of the corresponding liquid. A two-dimensional gas model was proposed to explain the high entropy of water adsorbed on carbon with negative "net" heat but was subsequently withdrawn as inadequate for treatment of a localized, hydrogen bonded adsorbate.[4]

Data are now available which permit a roughly quantitative definition of the isolation requirement by determining, from a break-down of the adsorbate entropy, the minimum distance between sites required to prevent interaction of adsorbed molecules. The heat of immersion of Graphon in water combined with an adsorption isotherm at the same temperature yielded a negative "net" heat of adsorption[5] (supporting the results of references 3a and 3b). Application of the BET equation to data for the adsorption of water and of nitrogen on Graphon indicated that only about 1/1500 of the total surface was receptive to water molecules. The authors recognized the implication that the active sites were isolated, preventing the interaction between adsorbed molecules which, when present, contributes strongly to the heat of adsorption. The indicated surface area per active site is about 16,000 Å.^{2} corresponding to an average distance between sites of about 130 Å. It is, therefore, reasonable to conclude that a molecule displaced from any site will re-enter the gas phase with negligible probability of moving directly to another site.

The entropy analysis is made at the coverage of minimum integral molar entropy ($\theta \sim 1$), as this minimizes the error in estimating the configurational contribution. The observed integral entropy at this point was 29.3 e.u. The authors of reference 5 state that heterogeneity precludes any appreciable configurational term. However, the nature of the bond and the shape of the entropy plot indicate that the active sites were much more uniform than they believed and that the effect of configuration must be considered. Ideally, the integral entropy of configuration at $\theta = 1$ would be 0, but in real systems there is a residual contribution at the entropy minimum due to some second layer deposition before the first monolayer is complete. This quantity has been estimated to be about one entropy unit[6] leaving 28.3 e.u. for the degrees of freedom associated with the motion of the adsorbate molecules. The adsorbed molecules can rotate freely in the plane of the surface but there may be some hindrance in the other two coördinates. The barrier is probably small as acetone adsorbed on mercury with a comparable heat apparently retains almost unhindered rotation.[7] Loss of only about 2 units of rotational entropy is therefore assumed, leaving 8.4 e.u. for adsorbate rotation.

Part of the translational entropy of the gas is converted to what may be treated as a weak vibration perpendicular to the adsorbent surface. Kemball[7] has developed a method for estimating this contribution. For water on Graphon at 25°, his method gives a value of 2.6 e.u.

(1) Presented before the Division of Colloid Chemistry, at the 128th National Meeting of the American Chemical Society in Minneapolis, Minnesota, September, 1955.

(2) A. B. Lamb and A. S. Coolidge, *J. Am. Chem. Soc.*, **42**, 1146 (1920).

(3) (a) A. S. Coolidge, *ibid.*, **49**, 708 (1927); (b) F. G. Keyes and M. J. Marshal, *ibid.*, **49**, 156 (1927).

(4) J. H. deBoer, "The Dynamical Character of Adsorption," Oxford University Press, London, 1953, p. 53, 234.

(5) G. J. Young, J. J. Chessick, F. H. Healey and A. C. Zettlemoyer, This Journal, **58**, 313 (1954).

(6) L. E. Drain, *Science Prog.*, **42**, 608 (1954).

(7) C. Kemball, *Proc. Roy. Soc. (London)*, **A190**, 117 (1947).

This entropy breakdown may be summarized as

Obsd. integral adsorbate entropy, e.u.		29.3
Configurational entropy, e.u.	1.0	
Rotational entropy, e.u.	8.4	
Entropy of vibration perpendicular to adsorbent surface, e.u.	2.6	
Total		12.0
Residual entropy assigned to motion in plane of adsorbent surface, e.u.		17.3

The residual 17.3 e.u., assigned to motion in the plane of the surface, determines the separation required for isolation of sites. Since the bond is weak and predominantly electrostatic, an adsorbed water molecule will have very considerable mobility, over the site. This suggests, as a useful approximation, that the motion in the plane parallel to the adsorbent surface be treated as translation instead of vibration. If the adsorbed molecule is assumed to move at random within a circle of which the site is the center, the radius of this circle may be calculated from the residual entropy.

The partition function for isolated translation in two dimensions gives, by the usual methods of statistical mechanics, the following expression for the translation entropy

$$Q_T = \frac{2\pi mkTa}{h^2}$$

$$S_T = R\left[\ln \frac{2\pi mkTa}{h^2} + 1\right]$$

R = gas constant
m = mass of one molecule
k = Boltzmann constant
T = absolute temp.
a = area covered by the oscillation of an adsorbed molecule
h = Planck's constant

Solution for a (from an entropy of 17.3 e.u.) gives a value of 120 Å.^{2} for the area of freedom of an adsorbate molecule. The corresponding radius is 6.2 Å., indicating a necessary separation between sites of roughly 12 Å. It is apparent from this result that the hydrophilic sites on Graphon are much more widely separated than the minimum necessary to prevent interaction between adsorbed molecules. The area normally occupied by an adsorbed water molecule is about 10.8 Å.^{2}.[8] Essentially complete isolation of sites should thus be possible, if the area of the first water monolayer is less than about one-eleventh of the total surface area of the adsorbent and if the sites are not grouped in clusters.

(8) H. K. Livingston, *J. Colloid Sci.*, **4**, 447 (1949).

COMMUNICATION TO THE EDITOR

SECOND EXPLOSION LIMITS OF CARBON MONOXIDE-OXYGEN MIXTURES

Sir:

In a criticism[1] of our recent paper on this subject[2], points were raised which do not clearly reflect the content of our paper. It was claimed that since our results were influenced by surface, no mechanism could be deduced from the experimental results. There is no logical reason for the above criticism if the effect of surface is taken into account.

We have reasons from both experimental and theoretical evidence for the various elementary reactions in our mechanism. We have also discussed and rejected key reactions in previously postulated mechanisms. Where our mechanism might be questioned upon theoretical grounds, we have given detailed justification. Contrary to the statement of Roth, von Elbe and Lewis,[1] the mechanism which we have postulated easily accounts for the effects of composition, surface to volume ratio, and inerts. In addition, this mechanism is consistent with our spectral studies of the CO–O_2 explosion.[3]

Roth, von Elbe, and Lewis[1] claim that they have developed a procedure which effectively suppresses the surface chain branching reaction "over a wide range of *mixture composition* and temperature." However, their published data and curves[4] show that this lack of surface dependence exists only at *one* mixture composition, namely, $1CO:2O_2$. Compositions on either side, $4CO:1O_2$ and $1CO:4O_2$ show a large surface effect.

Von Elbe, Lewis and Roth claim that they lose surface dependence when they heat their vessels for two hours under vacuum at 800–900° (using a $1CO:2O_2$ mix). Using the same mixture, we have previously reported that this treatment did not lessen the effect of surface.

The heating is claimed to remove a strongly adsorbed film of CO_2 which they believe is responsible for the surface effects. We have grave doubts that CO_2 plays such a role because, as discussed above, their loss of surface dependence is for only one composition. Also, both von Elbe, Lewis and Roth, and ourselves report a slow reaction prior to the explosion. Thus, even if the walls were clean at the start they should be covered with CO_2 by the time that the explosion temperature is achieved.

Von Elbe, Lewis and Roth derive Eq. 2 in their paper[4] from the following postulated reactions (using their notation)

$$O + O_2 + M = O_3 + M \quad (I)$$

$$O + CO + M = CO + M \quad (II)$$

(1) W. Roth, G. von Elbe and B. Lewis, THIS JOURNAL **60**, 512 (1956).

(2) A. S. Gordon and R. H. Knipe, *ibid.*, **59**, 1160 (1955).

(3) R. H. Knipe and A. S. Gordon, *J. Chem. Phys.*, **23**, 2097 (1955).

(4) G. von Elbe, B. Lewis and W. Roth, "Fifth Symposium on Combustion," Reinhold Publishing Corp., New York, 1955, p. 610.

$$CO_2^* + O_2 = CO_2 + 2O \qquad (V)$$
$$CO_2^* + O_2 + M = CO_2 + O_2 + M \qquad (VI)$$

Employing the usual technique of setting the rate of chain break reactions equal to the rate of chain branch reactions for the critical situation at the chain branch explosion limit, the following equation is readily derived

$$[M]_e = \frac{k_5}{k_6} \frac{1 - \frac{k_1 f_{O_2}}{k_2 f_{CO}}}{1 + \frac{k_1 f_{O_2}}{k_2 f_{CO}}}$$

Unfortunately, the authors have confused the sign of the numerator and denominator in their derivation and their published Eq. 2 reads

$$[M]_e = \frac{k_5}{k_6} \frac{1 + \frac{k_1 f_{O_2}}{k_2 f_{CO}}}{1 - \frac{k_1 f_{O_2}}{k_2 f_{CO}}}$$

This is not a typographical error, since the authors make the point that their equation predicts an infinite pressure limit at a critical value of mixture composition which is consistent with their data. The correctly derived equation predicts a zero pressure limit at this critical value of the mixture composition. It should be noted that equation 2 is the crux of their discussion.

CHEMISTRY DIVISION ALVIN S. GORDON
U. S. NAVAL ORDNANCE TEST STATION R. H. KNIPE
CHINA LAKE, CALIFORNIA

RECEIVED APRIL 30, 1956

ANNOUNCING

New Rates for Single Copies of Current Issues and Back Numbers, *Effective January 1, 1956*

PUBLICATIONS OF THE AMERICAN CHEMICAL SOCIETY

Journal	Current Year Rate	Back Year Rate	Foreign Postage	Canadian Postage
ANALYTICAL CHEMISTRY				
Vols. 1-4, each issue	.....	$2.00	$0.15	$0.05
Vols. 5-8, each issue	.....	1.25	0.15	0.05
Vols. 9-27, each issue	.....	1.50	0.15	0.05
Vol. 28 et seq., each issue	$1.50[1]	2.00[1]	0.15	0.05
(1) April issue appears in two parts; sold as unit for $2.00 current year or $2.50 back year.				
CHEMICAL AND ENGINEERING NEWS				
Vols. 1-24, each issue	.....	0.25	0.10	.....
Vol. 25 et seq., each issue	0.40	0.50	0.10	.....
INDUSTRIAL AND ENGINEERING CHEMISTRY	1.50[2]	2.00[2]	0.25	0.10
(2) March and September issues in two parts; each sold as a unit for $2.50 current year or $3.00 back year.				
JOURNAL OF AGRICULTURAL AND FOOD CHEMISTRY	1.00	1.50	0.15	0.05
JOURNAL OF THE AMERICAN CHEMICAL SOCIETY				
Vols. 1-31 (Order volumes prior to 32 from Walter J. Johnson, 125 E. 23rd St., New York 10, N. Y.)				
Vols. 32-77, each issue	.....	1.75	0.15	0.05
Vol. 78 et seq., each issue	1.50	1.75	0.15	0.05
THE JOURNAL OF PHYSICAL CHEMISTRY				
Vols. 1-55 (Order volumes prior to 56 from Walter J. Johnson, 125 E. 23rd St., New York 10, N. Y.)				
Vol. 56 et seq., each issue	1.35	1.75	0.15	0.05
THE JOURNAL OF ORGANIC CHEMISTRY				
Vols. 1-16 (Walter J. Johnson)–Vols. 17-19 (Williams & Wilkins Co., Baltimore 2, Md.)				
Vol. 20 et seq., each issue	2.50	3.00	0.15	0.05
CHEMICAL ABSTRACTS				
Vols. 1-10 (Order volumes prior to 10 from Walter J. Johnson, 125 E. 23rd St., New York 10, N. Y.)				
Vols. 11-30				
Numbers 1-22, each issue	.....	1.25	0.15	0.05
Numbers 23 and 24, each	.....	3.00	0.45	0.15
Vols. 31-49				
Numbers 1-22, each issue	.....	2.25	0.15	0.05
Number 23 (Author Index)**	.....	12.00	0.30	0.10
Number 24 (Subject Index)**	.....	24.00	0.60	0.20
THE CHEMICAL ABSTRACTS SERVICE (formerly known as CHEMICAL ABSTRACTS)				
Vol. 50 et seq. Single issues commencing with Volume 50 are sold in accordance with prices listed here until January 1 of the second year following the close of the volume year, after which they will be sold at back issue prices also shown here.				

	Members Personal-Use	Colleges & Universities	All Others			
Numbers 1-22, each	$ 2.00	$ 3.00	$15.00	2.50	0.15	0.05
Author & Patent Index*	5.00	15.00	20.00	15.00	0.30	0.10
Subject & Formula Index*	10.00	35.00	40.00	30.00	0.60	0.20

* Patent Index will be bound with either Subject or Author Index as determined by production schedules.
** A special rate of 50% of these amounts applies to orders from ACS members for personal use.

Rates for Volumes of Back Numbers

Journal	Rate	Foreign Postage	Canadian Postage
ANALYTICAL CHEMISTRY (formerly Analytical Edition)			
Volumes 1-8	$ 7.50	$0.75	$0.25
Volumes 9-27	15.00	0.75	0.25
Volume 28 et seq.	20.00	0.75	0.25
CHEMICAL AND ENGINEERING NEWS			
Volumes 1-24	5.00	2.25	0.75
Volume 25 et seq.	20.00	2.25	0.75
INDUSTRIAL AND ENGINEERING CHEMISTRY			
Volume 1 et seq.	20.00	2.25	0.75
JOURNAL OF AGRICULTURAL AND FOOD CHEMISTRY			
Volume 1 et seq.	15.00	1.50	0.50
JOURNAL OF THE AMERICAN CHEMICAL SOCIETY			
Volumes 1-31 (Order volumes prior to 32 from Walter J. Johnson, 125 E. 23rd St., New York 10, N. Y.)			
Volumes 32-77	20.00	1.50	0.50
Volume 78 et seq.	35.00	1.50	0.50
THE JOURNAL OF PHYSICAL CHEMISTRY			
Volumes 1-55 (Order volumes prior to 56 from Walter J. Johnson, 125 E. 23rd St., New York 10, N. Y.)			
Volumes 56-59	15.00	1.20	0.40
Volume 60 et seq.	18.00	1.20	0.40
THE JOURNAL OF ORGANIC CHEMISTRY			
Vols. 1-16 (Walter J. Johnson)–Vols. 17-19 (Williams & Wilkins Co., Baltimore 2, Md.			
Volume 20 et seq.	30.00	1.50	0.50
CHEMICAL ABSTRACTS			
Volumes 1-10 (Order volumes prior to 11 from Walter J. Johnson, 125 E. 23rd St., New York 10, N. Y.)			
Volumes 11-30	25.00	2.40	0.80
Volumes 31-49	65.00	2.40	0.80
THE CHEMICAL ABSTRACTS SERVICE (formerly CHEMICAL ABSTRACTS). Back volumes commencing with Volume 50 are sold in accordance with prices listed here after January 1 of the second year following the close of the volume year.			
Volume 50 et seq.	80.00	3.00	1.00

AMERICAN CHEMICAL SOCIETY

BACK ISSUE DEPARTMENT

1155 SIXTEENTH STREET, N.W. WASHINGTON 6, D.C.